NATIONAL AERONAUTICS AND SPACE ADMINISTRATION

Technical Memorandum 33-571

Telecommunications Systems Design Techniques Handbook

Edited by
R. E. Edelson

JET PROPULSION LABORATORY
CALIFORNIA INSTITUTE OF TECHNOLOGY
PASADENA, CALIFORNIA

July 15, 1972

NATIONAL AERONAUTICS AND SPACE ADMINISTRATION

Technical Memorandum 33-571

Telecommunications Systems Design Techniques Handbook

Edited by
R. E. Edelson

JET PROPULSION LABORATORY
CALIFORNIA INSTITUTE OF TECHNOLOGY
PASADENA, CALIFORNIA

July 15, 1972

Technical Memorandum 33-571

Prepared Under Contract No. NAS 7-100
National Aeronautics and Space Administration

PREFACE

The work described in this report was performed by the Telecommunications Division of the Jet Propulsion Laboratory.

FOREWORD

The Deep Space Network (DSN), managed by the Jet Propulsion Laboratory for the NASA, increasingly supports deep space missions sponsored and managed by organizations without long experience in its design and operation. This document is intended to provide a reference source of telecommunications information for the design and specification of a DSN-compatible spacecraft. It should serve to acquaint new users with the design techniques available and should summarize for experienced personnel the analyses and data necessary for system design and specification.

This Telecommunications System Design Techniques Handbook makes specific reference to much of the official DSN documentation, particularly the Deep Space Network/Flight Project Interface Design Handbook, DSN Standard Practice 810-5, in order to relate the spacecraft and DSN into a telecommunications system design. However, the information quoted within is representative, not specific, and designers of particular missions should consult the official, up-to-date publications for specific performance measures. This handbook is written as a guideline and information source. There is no intent to present requirements to or constraints on the reader. Where further detail may be useful, references are cited.

A great many members of the Spacecraft Telecommunications Section are represented in the work presented herein. The principal authors were:

R. E. Edelson
J. R. Gilder
G. W. Garrison
A. J. Spear
P. M. Kotani
B. D. Trumpis
B. K. Levitt
C. Hanna
B. Dorsch

We are grateful also to numerous others who helped with discussions and review, particularly J. R. Hall and R. P. Mathison of the Jet Propulsion Laboratory.

For matters of interpretation, questions, or corrections, contact R. E. Edelson, mail station 114-B13, Jet Propulsion Laboratory, Pasadena, California, 91103.

This document was prepared with the support and concurrence of the Office of Tracking and Data Acquisition of the Jet Propulsion Laboratory.

CONTENTS

CONTENTS (Contd)

CONTENTS (Contd)

CONTENTS (Contd)

TABLES

TABLES (Contd)

FIGURES

FIGURES (Contd)

FIGURES (Contd)

FIGURES (Contd)

FIGURES (Contd)

FIGURES (Contd)

FIGURES (Contd)

FIGURES (Contd)

ABSTRACT

The Deep Space Network (DSN), managed by the Jet Propulsion Laboratory for NASA, increasingly supports deep space missions sponsored and managed by organizations without long experience in DSN design and operation. This document is intended as a textbook for those DSN users inexperienced in the design and specification of a DSN-compatible spacecraft telecommunications system. For experienced DSN users, the document provides a reference source of telecommunication information which summarizes knowledge previously available only in a multitude of sources. Extensive references are quoted for those who wish to explore specific areas more deeply.

SECTION I

INTRODUCTION

1.1 PURPOSE OF THE HANDBOOK

In the past few years, the Spacecraft Telecommunications System Section of the Jet Propulsion Laboratory has developed a number of design techniques, procedures, and analyses which have contributed to the success of lunar and deep space missions. Increasingly, the Deep Space Network is supporting deep space missions sponsored by other NASA centers, and deep space missions managed by private contractors. To obtain the maximum scientific return from each mission, the telecommunications system must perform in an efficient and predictable manner. This requires the effective coordination of many technical disciplines both on the ground and on-board the spacecraft. This handbook has been written to:

1) Introduce DSN personnel and DSN users to the system analysis activities, definitions, and methods used to design DSN-compatible telecommunications systems;

2) Describe the telecommunication interfaces between flight projects and the DSN which must be understood and properly managed;

3) Summarize for all DSN users the design techniques and analysis aids developed at JPL which will generally be useful to all flight projects.

1.2 TELECOMMUNICATION SYSTEM ACTIVITIES

Every flight project which utilizes the DSN must perform certain telecommunication systems activites. The responsibility of the telecommunications system analyst is to coordinate the design, implementation, testing, and operation of a telecommunication system which meets the requirements of the mission and is compatible with the DSN. Telecommunications can be thought of as a service provided to the flight project. The flight project must formulate various measures of performance necessary to achieve the mission objectives, such as telemetry data rates, data quality requirements, command

requirements, and radio tracking requirements. Telecommunications system activities must then be performed to assure that the required telecommunication performance is achieved throughout the mission. Some typical activites are:

1) Specify spacecraft hardware parameters
2) Specify spacecraft/DSN interface parameters
3) Generate and maintain radio link Design Control tables and publish a Telecommunications Design Control document
4) Prepare telecommunications system performance predictions necessary for mission operations
5) Provide liaison support between spacecraft subsystem engineers, DSN engineers and other project personnel
6) Perform system level verification tests prior to hardware fabrication
7) Coordinate system level tests and subsystem calibrations of the flight hardware
8) Coordinate testing necessary to guarantee telecommunication compatibility between the spacecraft and the DSN
9) Collect and publish data required by the DSN to successfully track and communicate with the spacecraft
10) Coordinate all telecommunication activities during mission operations.

1.3 SCOPE OF THE HANDBOOK

This handbook contains descriptive and analytical information which should be useful to a flight project in the performance of its telecommunications system activities. A description is presented of a deep space telecommunication system, including the relevant aspects of the DSN. Next, the Design Control Policy of the Jet Propulsion Laboratory is described, along with a description of how that policy is implemented at JPL. A detailed discussion of the design and analysis of the tracking, telemetry, and command

functions is presented; and antenna requirements for deep space vehicles are examined. Considerations involved in selecting operating frequencies and bandwidth are then discussed. The preparation of telecommunications performance predictions used to evaluate the condition of the spacecraft and to make decisions regarding the operation of the spacecraft is presented. Finally, the design, specification, and control of critical telecommunications interfaces are explained in detail.

The analysis leans heavily on experience gained with Mariner-type spacecraft, and is oriented toward a direct communication link between one vehicle and the DSN. The principles developed may be applied to other types of links such as relay links and multiple vehicle communications.

Where it is deemed desirable, derivations are included in appendices. Generally, results are presented without proof, in keeping with a handbook philosophy.

This data should be useful to flight projects in all stages of a mission, from preliminary planning to mission operations. It is intended as a guideline rather than as a constraint and should not be regarded as a controlling document. Further, the intent of this handbook is not to fully document or characterize the DSN, which maintains its own documentation for that purpose.

1.4 REVISION AND CONTROL

This document will be revised when significant amounts of new or refined information becomes available in sufficiently well-defined form to justify a handbook formulation, or, when enough error corrections have accumulated to justify a corrected edition. Errata memos will be distributed when required, between revisions.

Requests for additions, changes, or corrections should be submitted to R. E. Edelson, mail station 114-B13, Jet Propulsion Laboratory, Pasadena, California 91103.

SECTION II

THE TELECOMMUNICATIONS SYSTEM

The Telecommunications System consists of all elements necessary to track, command, and obtain and process telemetry from the spacecraft. Of major importance in describing the Telecommunications System are descriptions of the Deep Space Network systems, the Spacecraft Systems, and the communication channel.

2.1 DEEP SPACE NETWORK SYSTEM DESCRIPTION

The DSN is a facility of the NASA Office of Tracking and Data Acquisition (OTDA) under the management and technical direction of JPL. The DSN provides communications with spacecraft out to interplanetary distances, and provides data handling capabilities to support deep space missions.

The DSN consists of six systems, three of which are of particular interest to the telecommunications system designer.

1) Tracking
2) Telemetry
3) Command

The tracking and telemetry systems provide tracking and telemetry data to project users. The command system generates and transmits commands to the spacecraft.

Three facilities provide operational capability for the DSN systems:

1) The Deep Space Instrumentation Facility (DSIF).
2) The Ground Communication Facility (GCF).
3) The Network Control Center (NCC).

The DSIF consists of a network of 26-meter Deep Space Stations (DSS) and a network of 64-meter Deep Space Stations located around the world approximately 120 degrees apart in longitude. A spacecraft in or near the ecliptic plane will always be in view of at least one station.

The GCF consists of communications equipment necessary to transmit voice and data between deep space stations and the flight project. It uses the NASA Communication System (NASCOM) which is managed by Goddard Space Flight Center (GSFC).

The Network Control Center coordinates and directs the Deep Space Network from its headquarters at the Jet Propulsion Laboratory. It provides the interface by which the flight project makes use of the Deep Space Network.

The DSN documentation system describes and characterizes the DSN; its plans, facilities and systems. DSN Standard Practice document 810-1 defines the documentation system, and itemizes those documents which have been published. Of particular interest to flight project users of the DSN are the following documents:

1) 810-1, DSN Documentation System
2) 801-2, DSN Capabilities and Plans
3) 801-2, Add. 1, CTA-21 Configuration and Capabilities
4) 801-2, Add. 2, DSS-71 Configuration and Capabilities
5) 801-4, DSN Resource Allocation System
6) 810-5, DSN/Flight Project Interface Design Handbook
7) 890-2, CTA-21 Capability Document
8) 890-3, DSS-71 Capability Document

In addition to this abbreviated list of documents which are applicable to all flight projects, the DSN provides a number of project-peculiar documents (the 600 series) for each flight project. These documents are intended to document project support and DSN/flight project interfaces.

2.2 SPACECRAFT SYSTEM DESCRIPTION

The spacecraft telecommunication system includes those elements necessary to receive a signal from a DSS of the DSN, extract command and ranging modulation from the carrier signal, generate a downlink carrier, and transmit to Earth an S-band or X-band signal containing ranging and telemetry modulation.

2.2.1 Spacecraft Telecommunications System Functions

Generally, the flight project will provide the flight hardware subsystems necessary to support the telecommunication functions of tracking, telemetry, and command. Each project must tailor its subsystems to meet the mission requirements. However, the creation of interfaces at advantageous points in the system has led to a series of subsystem definitions that are useful for all projects.

The Radio Frequency Subsystem (RFS) includes those elements necessary to receive and demodulate the uplink rf carrier and those elements necessary to generate, phase modulate, and transmit the downlink rf carrier.

The Flight Command Subsystem (FCS) obtains command modulation from the RFS, detects the command data bits, and decodes the commands.

The Flight Telemetry Subsystem (FTS) obtains spacecraft data and modulates the data onto one or more subcarriers, combines these subcarriers in a summing and level-setting device, and sends a composite telemetry signal to the RFS to modulate the downlink rf carrier.

The Antenna Subsystem receives and radiates rf energy in a prescribed manner.

The Data Acquisition Subsystem (DAS) acquires data from the science instruments and engineering sensors, generates timing signals, and formats the data for modulation by the FTS.

An Antenna Pointing Subsystem (APS) is used to control steerable antennas.

There may be a Data Storage Subsystem for storage and playback of data.

Associated with all of these hardware systems is a system analysis activity which is responsible for seeing that the subsystem parameters, interfaces, and the link between spacecraft and Earth are designed to achieve a level of performance required by the flight project, and necessary for the proper operation of the DSN ground systems. Each flight project is responsible for providing this activity.

2.3 THE TRACKING FUNCTION

The tracking function is the process by which the DSS measures the angular position, range, and radial velocity of the spacecraft through radio frequency contact and provides this metric data to the project. Radio frequency contact is achieved in one of three ways:

1) By transmitting an rf carrier from the DSS to the spacecraft, and tracking the phase of that carrier in the spacecraft transponder. This mode is referred to as uplink lock.
2) By transmitting an rf carrier internally derived in the spacecraft to a deep space station of the Deep Space Network, and tracking the phase of that carrier in the ground station receiver. This mode is referred to as downlink, or one-way tracking.
3) By transmitting an uplink rf carrier, phase-locking the spacecraft receiver to that carrier, and transmitting back to Earth a signal which is translated in frequency and phase coherent with the uplink signal. The frequency and phase of the signal received on Earth is tracked by a phase-lock loop receiver. This mode is referred to as two-way tracking.

The theory of operation of a phase-locked loop receiver is discussed in section IV.

Coherent phase tracking is used by DSN compatible telecommunication systems for two reasons. First, the telemetry and command digital detection systems using the free space channel make more efficient use of transmitted power than do noncoherent systems. Second, by using a phase-coherent tracking system, it is possible to accurately measure the Doppler shift of the carrier observed between the spacecraft and the ground station.

Tracking data is obtained through the following four measurement methods:

1) Angle tracking
2) Doppler
3) Ranging
4) Differenced range versus integrated Doppler (DRVID)

2.3.1 Angle Tracking

In angle tracking, the ground antenna is aimed at the spacecraft rf source to as small an angular resolution as possible. The angular coordinates are read out as the antenna is moved to follow the signal source, thus, by coordinate transformation, locating the spacecraft position on the celestial sphere. Local accuracy depends on the mechanical pointing accuracy of the antenna, the resolution of angular readout, and the beam shape of the antenna. Celestial accuracy includes the extent of knowledge of station location and time.

2.3.2 The Doppler System

The Doppler system is designed to measure the frequency shift of a spacecraft signal to high accuracy. This information is a direct measure of the spacecraft radial velocity, and a relative measure of its range. Doppler measurements can be taken during one or two-way tracking. The latter may be two or more orders of magnitude more accurate due to the greater stability of the DSIF master oscillator. Doppler data is the primary observable used to determine the trajectory of a spacecraft in flight. It will be discussed more fully in section IV.

2.3.3 The Ranging System

The ranging system consists of those elements necessary to generate a ranging code on the ground, modulate it onto an uplink rf carrier, track the carrier and modulation received by the spacecraft, translate the frequency of the received carrier, retransmit the carrier and ranging modulation to Earth (two-way tracking mode), receive the downlink signal on Earth, extract the ranging modulation, and compare the received ranging signal with the transmitted modulation to obtain a measurement of the round trip propagation delay. This measurement permits an estimate of the range of the spacecraft, and the properties of the transmission media. The ranging codes of the DSN are discussed in section VIII.

2.3.4 DRVID

DRVID is a method which is used to calibrate Doppler and ranging measurements for the differential effects of electron content in the

transmission medium. If DRVID (t) is the difference in meters between the ranging measured spacecraft range and the range measured by integrating the Doppler measurement of velocity at a time t (DRVID (t) = R(t) - $\int_o^t$ v(t) dt), then

$$\frac{d}{dt} \text{DRVID (t)} = \frac{40.3}{f^2} \left(\dot{I}_u + \frac{1}{G} \dot{I}_d\right) \qquad (2.3\text{-}1)$$

where

f = Uplink carrier frequency, Hz

G = Turnaround ratio of the spacecraft transponder

$\dot{I}_u$ = Time derivative of uplink electron content on the ray path, electrons/m^2sec

and

$\dot{I}_d$ = Time derivative of downlink electron content on the ray path, electrons/m^2sec.

When electron content is constant for the round-trip signal time (generally true for round-trip light times of less than 15 minutes),

$\dot{I} = \dot{I}_u = \dot{I}_d$ and

$$\dot{I}(t) = \frac{G^2}{1+G^2} \frac{f^2}{40.3} \frac{d}{dt} \text{DRVID (t)} \qquad (2.3\text{-}2)$$

Since ranging errors are a function of I (t) and doppler errors are a function of $\dot{I}$ (t), DRVID can be used to correct for this perturbation.

A detailed discussion of the DRVID theory is contained in reference 2-6. Reference 2-7 discusses its mechanization.

2.3.5 The Tracking System

Two-way tracking is preferred for Doppler and range measurements to obtain more precise data than can be obtained from a single downlink signal. A detailed analysis of the tracking function is presented in section IV. Figure 2-1 is a functional block diagram of the tracking system.

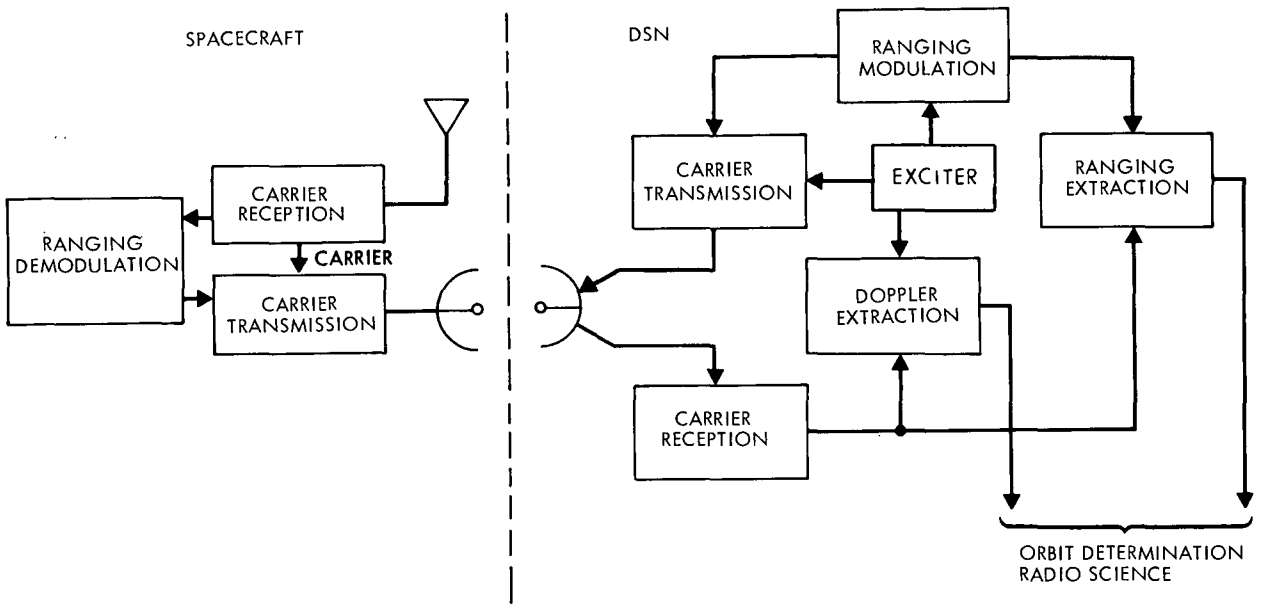

Fig. 2-1. Tracking and ranging system functional block diagram

2.4 THE TELEMETRY FUNCTION

The telemetry function is performed by those elements necessary to accept sensor data in analog and digital form, process the data for transmission, transmit the signal to Earth, receive the signal, extract the telemetry data from the received signal, and return the data to the project user. Figure 2-2 is a block diagram of the telemetry system.

The Deep Space Network provides a telemetry system which acquires telemetry data from the spacecraft and provides data to the project. The DSN uses the Multi-Mission Telemetry System (MMTS) of the DSIF which is sufficiently flexible to demodulate a wide class of digital spacecraft telemetry signals. The MMTS consists of receivers, subcarrier demodulators, symbol synchronizers, block decoders and convolutionally-encoded data decoders, and telemetry and command processors. These subsystems receive telemetry data from one or more spacecraft and process the data for transmission via

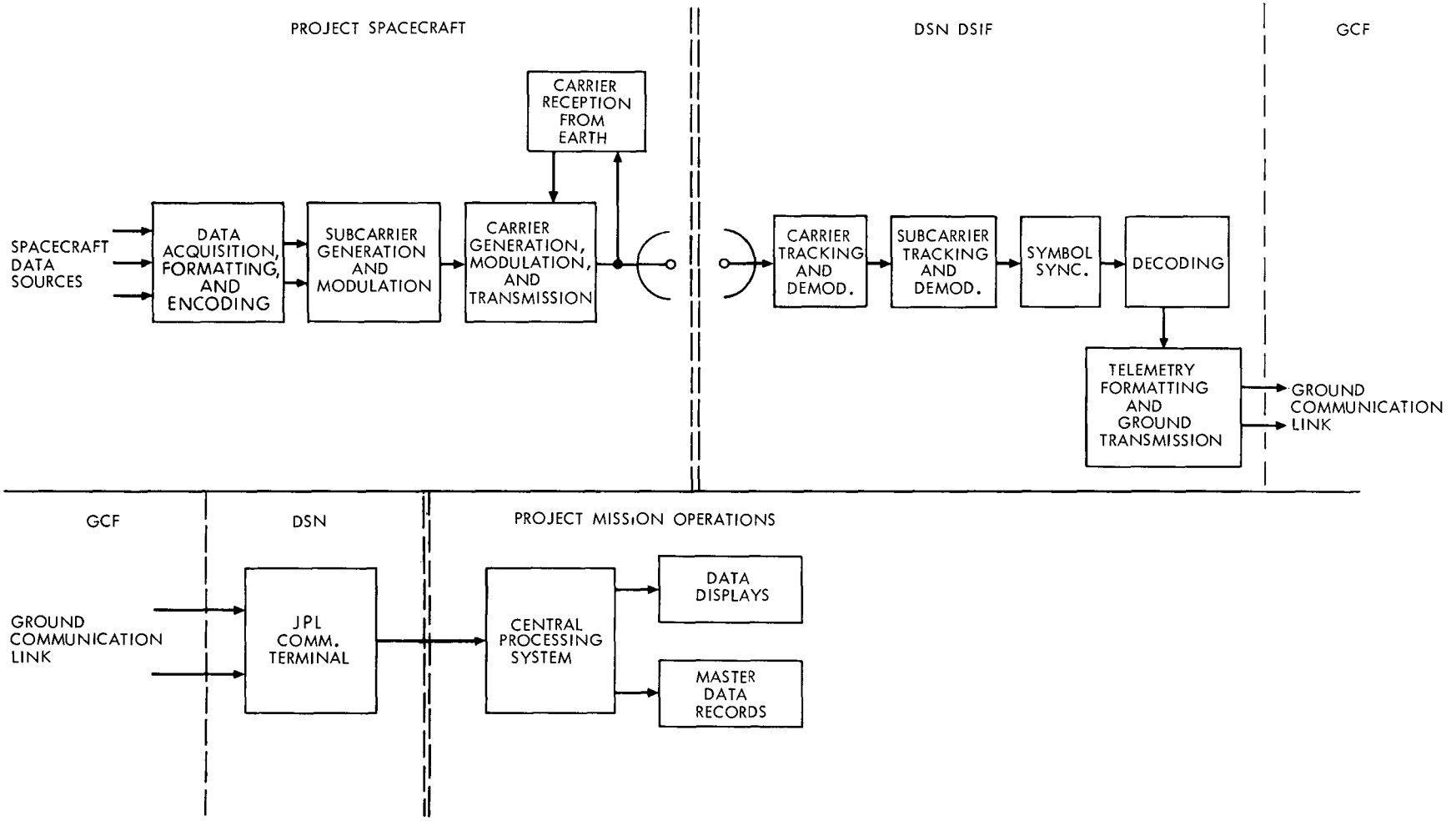

Fig. 2-2. Telemetry system block diagram

high speed data lines (HSDL) or wideband data lines (WDL) of the GCF, to the Network Control Center, located at the Jet Propulsion Laboratory in Pasadena, California. The quality of telemetry data obtained by the DSN is dependent on the proper design and specification of a large number of parameters which include the spacecraft subsystems, the telecommunications channel, and the facilities of the DSN.

The characterization of those parameters affecting the performance of the system which are independent of the modulation techniques employed, will be discussed in this section. The design and performance of specific telemetry modulation systems will be discussed in section V.

2.5 THE COMMAND FUNCTION

The command function is performed by those elements on the ground necessary to transmit project-initiated decisions to the DSS's, format, encode and time the commands to be sent to the spacecraft, modulate the uplink carrier with the command bits, verify that the correct commands were sent, and abort a command if errors in transmission are detected. It also is performed by those elements on board the spacecraft necessary to receive the command signal, demodulate and detect the command bits, and decode and execute the commands.

The Deep Space Network provides a Multi-Mission Command System (MMCS) which is sufficiently flexible to handle a range of command data rates and command word formats for one or more spacecraft. The system consists of a telemetry command processor (TCP), a command modulator, an rf exciter, and a transmitter. These elements work together to accommodate commands sent from the flight project, prepare them for transmission to the spacecraft, verify and send them. The spacecraft command system consists of subsystems capable of demodulating, detecting, and decoding the commands. The system designer must specify command rates and the parameters which determine the probability that a transmitted command will be correctly received, detected, and decoded.

The characterization of the parameters independent of the modulation techniques will be discussed in section II, while the parameters associated with the modulation techniques and word format will be discussed in section VI. A block diagram of the Command System is shown in Figure 2-3.

2.6 THE TELECOMMUNICATION LINK

The performance of the telecommunication system is determined by a set of parameters which can be separated into a group belonging to the telecommunication link, and groups belonging to the choice of command, telemetry, and ranging modulation techniques. The telecommunication link consists of those elements of the telecommunication system which are independent of modulation. It usually includes the rf exciter, transmitter, antennas, propagation medium, and receiver. There may be an uplink and a downlink. The configuration of the spacecraft transmitter, receiver, and antennas, the range between the spacecraft and Earth, the configuration of the ground system transmitter, receivers, and antennas, and the propagation medium of the rf signal will quantify the link. The link may be characterized by the ratio of total received power to system noise spectral density, P_T/N_o. This parameter includes the power-gain product, range of the spacecraft, system noise temperature, circuit losses associated with the equipment, errors in antenna pointing, and propagation medium. The power-gain product is a measure of the potential capability of a particular spacecraft configuration. P_T/N_o is a measure of the potential performance of the entire link.

The effectiveness with which the total received power can be used depends on the modulation and demodulation methods employed and the propagation environment, and is the subject of the sections dealing with tracking, telemetry and command.

2.6.1 Types of Links

The telecommunication channel can be classified in several ways. First, it can be divided into uplink and downlinks. Second, it can be classified in terms of rf frequency bands, e.g., S-band or X-band, and within these

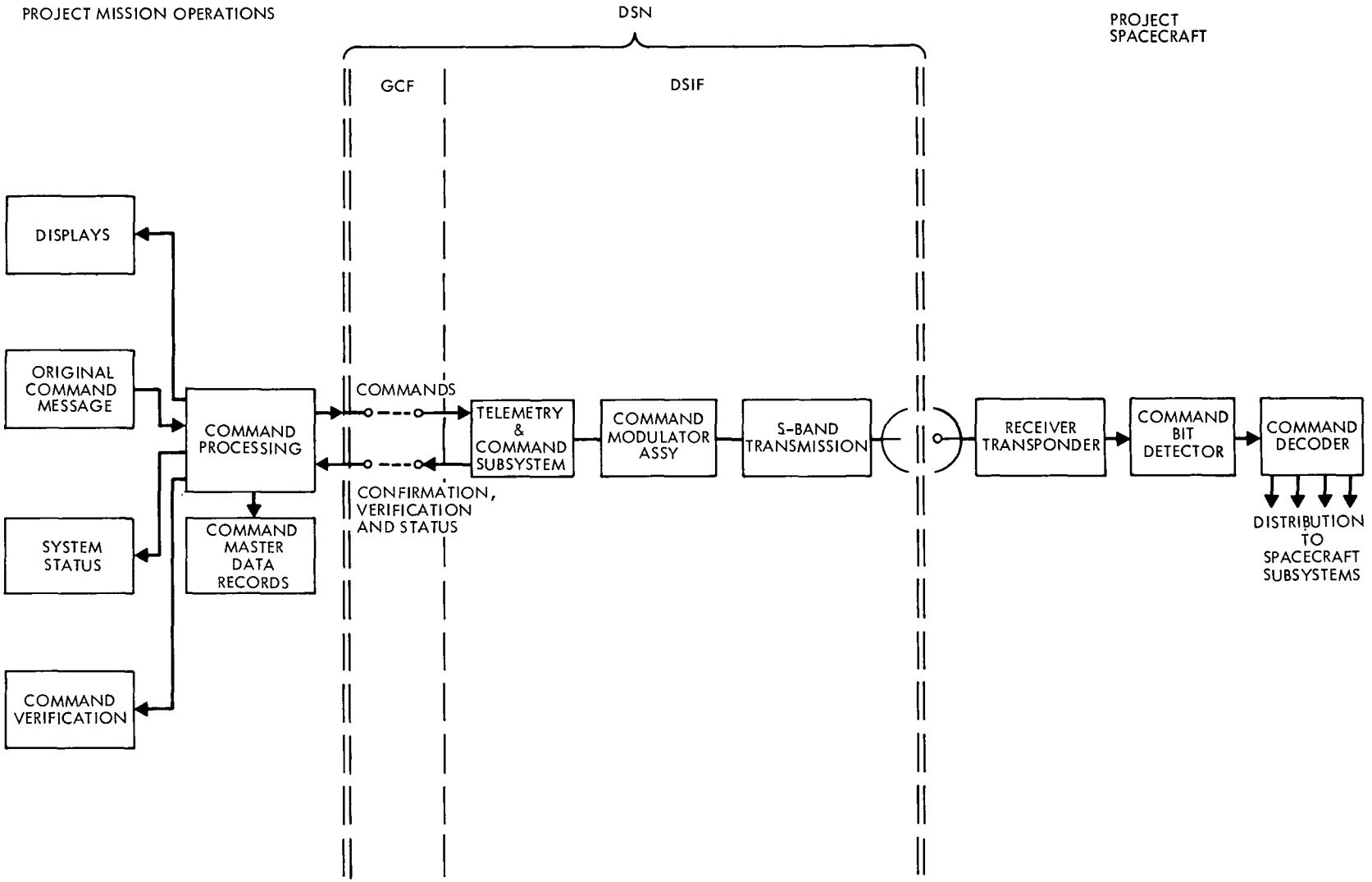

Fig. 2-3. Command system block diagram

bands, can be subdivided into frequency assignments. Third, it can be classified in terms of its propagation medium. Fourth, it can be classified in terms of its usage. For example, the link could be used for ranging, or telemetry, or both.

Each of these classifications of the link will result in a different characterization. For instance, P_T/N_o will obviously be different for an uplink and a downlink. The use of different frequencies and different propagation mediums will also affect P_T/N_o. Different trajectories or different mission times will affect P_T/N_o. Subsequently, it will be shown that the specification of P_T/N_o will determine the performance of a given telemetry, command or ranging system. Consequently, the careful determination of P_T/N_o is essential for the proper design of a telecommunication system.

2.6.2 Link Performance

There are three important types of performance for a telecommunication link. These are:

1) The performance when all parameters are at their design values
2) The performance when all parameters are at their worst case values
3) The performance when all parameters are at their best case values

The difference between the design parameter values and worst-case values are called adverse tolerances. The difference between design values and best case values are called favorable tolerances.

It should be recognized that these numbers are not hardware parameters. The design value is a theoretical number which is useful for planning, but is only one point in a range of performance that a component will exhibit, depending on age and environment. The tolerances are generally not statistical parameters but rather an engineering judgment that should include the range of unknowns in performance. They include estimates of subcontractor

performance as well as of environmental extremes. Therefore, the tolerances are also convenient numbers on which to base performance analysis, specification and test evaluation. Section III discusses the use of design values and tolerances and the types of parameters. Appendix A.3.1 discusses tolerance evaluation and definition for physical components.

2.6.3 Link Parameters

The general equations used for the computation of performance are derived from the basic equations for communications in the medium between spacecraft and ground station. The received power is computed using the following equation (2.6-1):

$$P(T) = P_{tr} L_{C_2} G_t G_r L_s L_A L_p L_c \qquad (2.6\text{-}1)$$

where

$P(T)$ = Total received power at input to spacecraft receiver case (uplink) or input to ground receiver or preamplifier (usually a maser amplifier)

P_{tr} = Total transmitter power at antenna terminals (uplink) or radio case (downlink)

L_{c_2} = 1 (uplink) or loss between radio case and antenna terminals, including impedance mismatch losses (downlink)

G_t = Transmitting antenna gain in the direction of the receiving antenna

G_r = Receiving antenna gain in the direction of the transmitting antenna

L_A = Loss (fractional gain) due to absorption in transmission medium

L_p = Polarization loss (fractional gain) between transmitting and receiving antennas due to mismatch in polarization patterns.

L_c = Circuit loss (fractional gain) between receiving antenna terminals and receiver case due to cabling loss.

and L_s = Loss (fractional gain) that would be experienced through a free space medium due to signal divergence with range and frequency dependence of receiving antenna capture area (space loss).

$$L_s = \left(\frac{\lambda}{4\pi R}\right)^2 \qquad (2.6\text{-}2)$$

where

R = Slant range of spacecraft with respect to ground station

and λ = Wavelength of radio signal

2.6.3.1 Transmitter Power. For the ground system, the total transmitter power, P_{tr}, is defined as the power input to the antenna feed connector. The values of DSIF transmitter power to be used in the project's performance calculations are published in reference 2-1.

For the spacecraft, the total transmitter power is the final amplifier output power reduced by the insertion losses due to filters, switches, and cables. The power, P_{tr}, is referenced to the radio case, where it is specified and measured. This number is reduced by the circuit loss to the antenna, before being radiated, as shown in Figure 2-4.

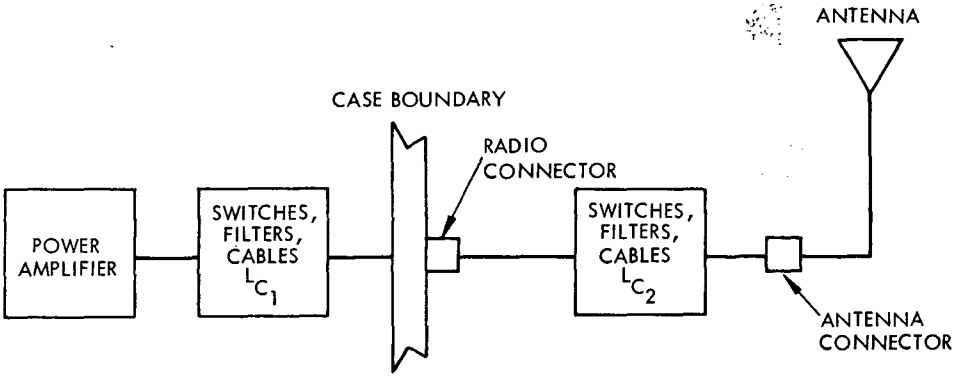

Fig. 2-4. Spacecraft transmitter power specification

Data necessary to calculate P_{tr} for the spacecraft are:

1) Power amplifier output power

2) Circuit loss to the rf case, L_{C_1}

Items 1) and 2) are measurable quantities which allow traceability between P_{tr} and the initial specification of the individual components which are used in the hardware procurement. This information is pertinent to the development of initial specifications of P_{tr} during the mission design and development phases. After actual spacecraft power measurements (at the subsystem case output) are made, they are substituted in the formula for P_{tr} and the individual elements are no longer appropriate data.

The circuit loss L_{C_2} must be measured to find the radiated power. Included in L_{C_2}, are the mismatch losses between the power amplifier and the cables, switches and filter. Mismatch loss, L_{MM}, in dB, is equal to:

$$L_{MM} = 10 \log \left(1 - |\rho|^2\right) \text{ where } |\rho| = \left|\frac{\text{reflected voltage}}{\text{incident voltage}}\right| \qquad (2.6\text{-}3)$$

ρ is developed from voltage-standing-wave-ratio (VSWR) specifications or measurements. Figure 2-5 plots L_{MM} versus VSWR.

$$\text{VSWR} \triangleq \frac{1 + |\rho|}{1 - |\rho|} = \frac{\text{maximum peak voltage}}{\text{minimum peak voltage}} \qquad (2.6\text{-}4)$$

2.6.3.2 Transmitting and Receiving Antenna Gains, G_t and G_r, and Space Loss, L_S. The transmitting and receiving antenna gains define the ability of the antennas to radiate or capture electromagnetic energy in the direction of the receiver and transmitter, respectively. The gain of an antenna in a direction Ω, is equal to the enhancement that is given to a signal of radiation intensity $U(\Omega)$ watts/m^2 when the antenna is compared with an ideal isotropic radiator.

That is,

$$G(\Omega) = \frac{U(\Omega)}{U_o} \qquad (2.6\text{-}5)$$

where $U_o = W/4\pi$, and W is the total radiated power.

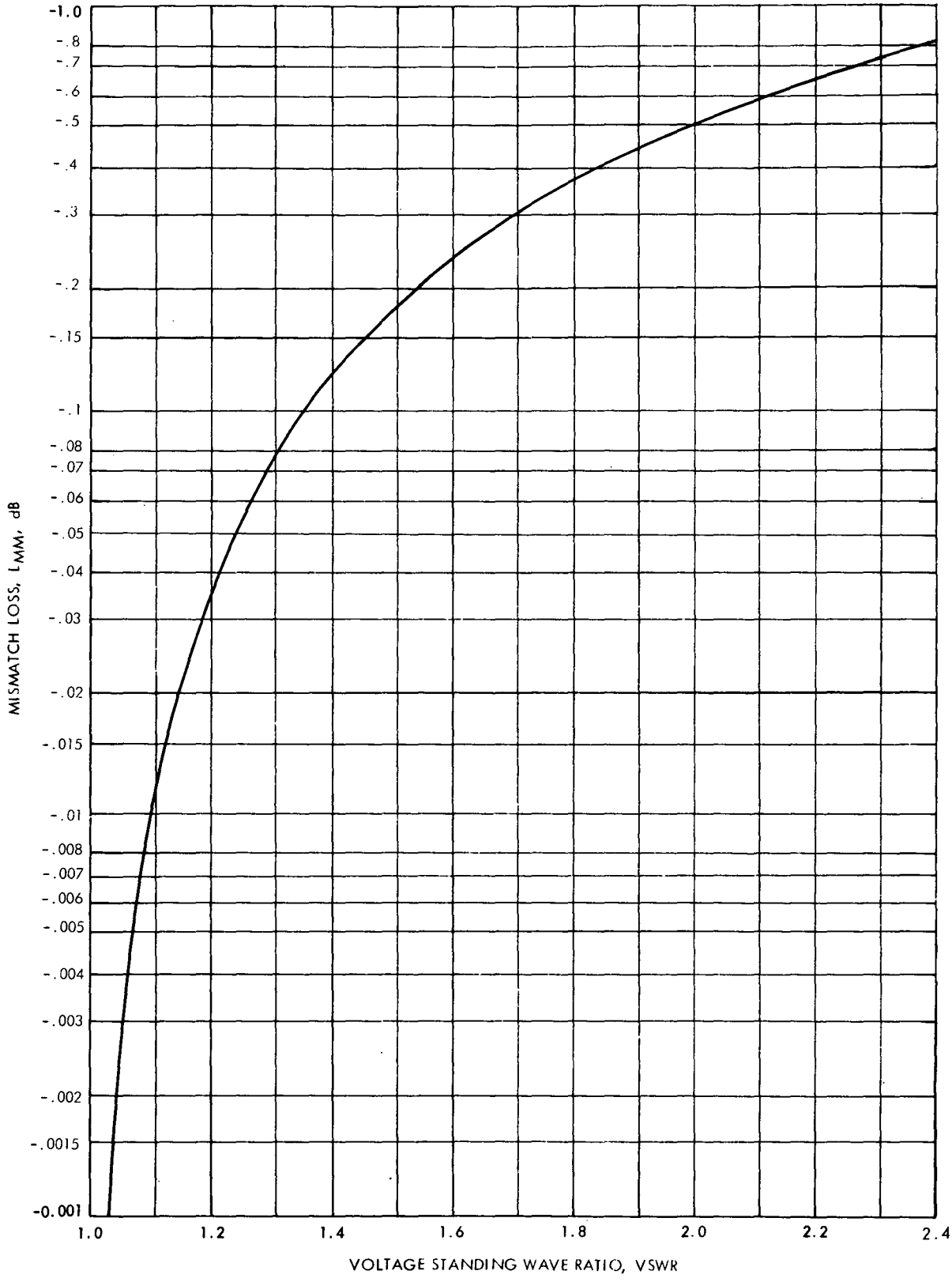

Fig. 2-5. Mismatch loss versus voltage standing wave ratio

It can be shown (ref. 2-2) that the transmit and receive patterns of a given antenna are identical at a given frequency.

For receiving antennas, the concept of capture area is useful. The capture area, A_c, of an antenna in a direction Ω is defined by:

$$A_c(\Omega) \triangleq \frac{P_r}{U(\Omega)} \tag{2.6-6}$$

where P_r is the power delivered by the feed system to a matched load when an infinite plane wave of intensity $U(\Omega)$ is incident on the antenna aperture.

The capture area is related to the antenna gain by (ref. 2-2):

$$G(\Omega) = \frac{4\pi}{\lambda^2} A_c(\Omega) \tag{2.6-7}$$

Now, if a transmitting antenna radiates a power $P_{tr}L_{C_2}$, the radiation intensity at a distance, R, from the antenna is

$$U(\Omega) = \frac{P_{tr}L_{C_2}G_t}{4\pi R^2} \tag{2.6-8}$$

if a free space transmission path is assumed. Thus, the power, P_r, at the receiving antenna terminals (neglecting antenna losses and assuming matched polarization) is:

$$P_r = A_c(\Omega)U(\Omega) = P_{tr}L_{C_2}G_tG_r\left(\frac{\lambda}{4\pi R}\right)^2 \tag{2.6-9}$$

where $(\lambda/4\pi R)^2$ is known as space loss, L_S, which relates the power transmitted to the power received for ideal isotropic antennas.

Although wind and gravity do not appreciably affect an electromagnetic wave, they do affect the received signal by distorting the antenna structure, thereby changing the gain. The effects of wind and gravity distortion on a 64-meter (DSS-14) peak antenna gain at X-band are given in ref. 2-1.

2.6.3.2.1 Spacecraft and Spacecraft Antenna Coordinates, and Pointing Error.

In order to assure system integrity and prevent misunderstanding, a uniform system of coordinates has been established for antenna positioning and pointing which is generally applicable to 3-axis stabilized vehicles that use the Sun and the star Canopus, as references.

The Mariner-type spacecraft coordinates are defined by Figure 2-6.

The spacecraft antenna coordinate system is defined analogously, where the boresight axis is at spacecraft coordinates ($Cone_B$, $Clock_B$). If the cone angle in the antenna coordinate system is denoted by γ, then the angle between the boresight axis and the Earth for a given spacecraft trajectory can be found from:

$$\cos\gamma = \sin(Cone_E)\sin(Cone_B)\cos(Clock_B - Clock_E) - \cos(Cone_E)\cos(Cone_B) \qquad (2.6\text{-}10)$$

where $Cone_E$ and $Clock_E$ are the angular coordinates of the Earth in the spacecraft system. For antenna patterns close to symmetrical, only γ is needed to specify the antenna gain. γ is called the pointing error for the antenna.

Section VII expands upon these parameters and gives further details.

2.6.3.3 Polarization Loss, L_p. Polarization is a property of electromagnetic radiation describing the spatial orientation of the field vectors. The transfer of power between two antennas is dependent on the polarization of the radiated wave and the characteristics and orientation of the receiving antenna. An electromagnetic wave is linearly polarized when the electric field lies in a plane normal to the direction of propagation. An electromagnetic wave is elliptically polarized when the electric vector describes an ellipse in a plane normal to the direction of propagation, making one complete revolution during one period of the wave. When the polarization properties of the transmitting and receiving antennas are not perfectly matched, the transfer of energy

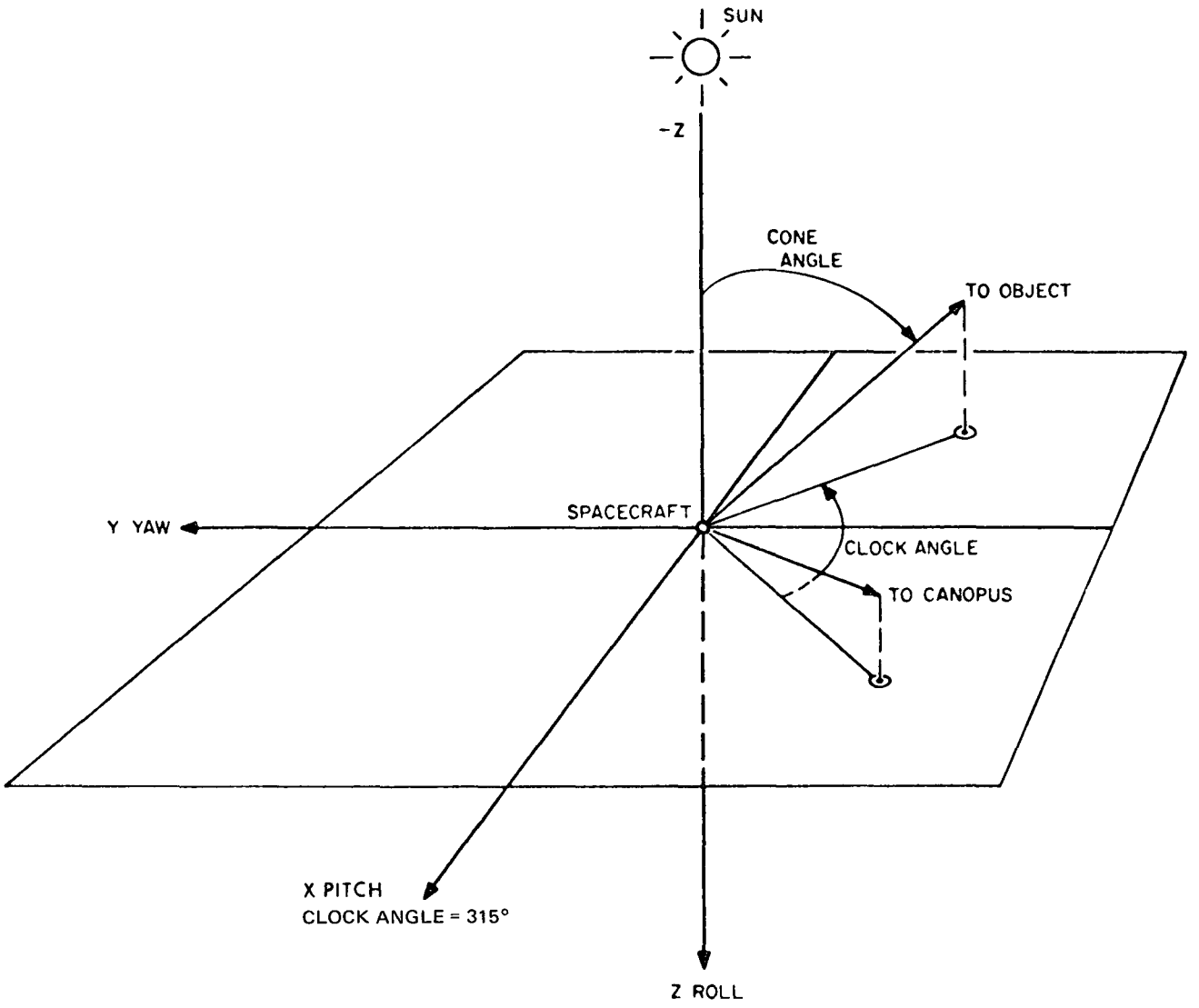

CONE ANGLE OF OBJECT: THE ANGLE FROM THE SPACECRAFT–SUN VECTOR TO THE SPACECRAFT–OBJECT VECTOR

CLOCK ANGLE OF OBJECT: THE ANGLE MEASURED CLOCKWISE (WHEN LOOKING TOWARDS THE SUN) FROM THE SUN–SPACECRAFT–CANOPUS PLANE TO THE SUN–SPACECRAFT–OBJECT PLANE. THE CLOCK ANGLE OF THE SPACECRAFT X AXIS IS TYPICALLY 315 deg

Fig. 2-6. Definition of Mariner-type spacecraft coordinates

between antennas is less efficient than would be expected by merely multiplying the space loss by the antenna gains. Thus, a loss, L_p, must be included in the range equation (2.6-1). Expressions for calculating L_p are provided in section VII.

2.6.3.4 Noise Temperature and Noise Spectral Density: N_o. Every antenna receives noise power from its environment, and every electronic component generates noise power in its operation. A signal detection device is valued by its ability to discriminate between that element of its input power that is signal and that which is noise. Thus, the detector's figure of merit is the minimum signal-power to noise-power ratio (SNR) at which it can generate a prescribed output signal quality.

In the systems considered here, the noise contribution to the signal can be approximated by an additive white, Gaussian process.* Thus, the noise power into the detector is equal to the system noise spectral density, N_o, times the system noise bandwidth, B_n.

The two-sided noise bandwidth, B_{n_j}, of an element, j, is defined by the equation:

$$B_{n_j} \triangleq \frac{\frac{1}{2\pi}\int_{-\infty}^{\infty} G_j(\omega)\, d\omega}{\left[G_j(\omega)\right]_{max}} \qquad (2.6\text{-}11)$$

where $G_j(\omega) = |H_j(i\omega)|^2$ is the gain function of the element, j, and $H_j(i\omega)$ is its frequency characteristic and $i = \sqrt{-1}$.

B_{n_j} can be viewed as the bandwidth of an ideal band-pass filter whose maximum response is the same as that of $H_j(i\omega)$ and whose output power in the presence of white noise is equal to that of $H_j(i\omega)$.

*For certain mission situations, this approximation is invalid. For example, noise components due to the solar corona, electric propulsion, Jupiter's atmosphere, high-speed atmospheric entry (ionization), and low uplink SNR for 2-way tracking do not follow this theory.

The system noise bandwidth is then:

$$B_n = \frac{\int_{-\infty}^{\infty} G_s(f)\, df}{[G_s(f)]_{max}} \tag{2.6-12}$$

where $$G_s(f) = \prod_{j=1}^{M} G_j(f) \tag{2.6-13}$$

is the system gain function of a system of M elements.

The contribution to the noise spectral density of a system element j, N_{oj} can be represented by (ref. 2-3):

$$N_{oj} = kT_jG_j \tag{2.6-14}$$

where

$$k = 1.38 \times 10^{-23}\ J/°K = 1.38 \times 10^{-20}\ m\ W\text{-}sec/°K$$

$$G_j = \text{Gain of element } j \triangleq [G_j(f)]_{max} \tag{2.6-15}$$

and

$T_j \triangleq$ The effective noise temperature of element j.

T_j = is that temperature at the input to a noiseless element which would result in a noise spectral density N_{oj} at its output.

The effective system noise temperature can be found by considering each element separately and combining them as shown in the following paragraphs.

2.6.3.4.1 System Noise Temperature, T_{es}. A receiving system is a cascade of electronic elements, each of which contributes noise power to the system. The total noise power depends on the gains and bandwidths of the various components. Since the ratio of signal-power to noise-power into the detector determines the system performance, it is vital to know the noise-power contribution of the system.

It is convenient to replace the receiver by an equivalent noise source and define the effective noise temperature, T_n, of the receiver by: (see 2.6.3.4.1.2)

$$N_o = \frac{N}{B_n} = k(T_n + T_i)G_s \triangleq kT_{es}G_s \qquad (2.6\text{-}16)$$

where

N_o = System noise spectral density

N = Total noise power

B_n = Receiver noise bandwidth

$k = 1.38 \times 10^{-20}$ mW - sec/°K

$T_i \triangleq \frac{N_{o_i}}{k}$, where N_{o_i} is the input noise spectral density.

G_s is the total system gain from the antenna terminals to the measurement point. $kT_iG_sB_n$ is the input noise power in the receiver bandwidth, multiplied by the system gain. T_i is equal to T_{ae}, the antenna noise temperature described in section 7.5.

Note that Gaussian white noise over the bandwidth B_n, is assumed for this expression.

$T_n + T_i$ is called the system temperature, T_{es}, referenced to the antenna terminals. Note that T_{es} differs from T_n in that different systems are involved. The theory is identical for both but it is convenient to use T_n since T_i is an exogenous variable.

2.6.3.4.1.1 Noise Temperature of an Element. The effective noise temperature referenced to the input of an element can be determined from the ratio of input to output signal-to-noise ratio. For a physical temperature T_{ij} at the input to element j, we define the noise factor or noise figure of element j by:

$$F_j(T_{ij}) \triangleq \frac{S_{inj}/N_{inj}}{S_{outj}/N_{outj}} \tag{2.6-17}$$

where S_{inj} = Input signal power

N_{inj} = Input noise power $\triangleq kT_{ij} B_{n_j}$

S_{outj} = Output signal power

N_{outj} = Output noise power

Remembering that the output noise power is the sum of input noise power and the noise power generated by an element, it can be shown that (see reference 2-3):

$$F_j(T_{ij}) = 1 + \frac{T_j}{T_{ij}} \tag{2.6-18}$$

where T_j, the effective noise temperature of element j is that temperature at the input of a noiseless element which would result in N_{outj} at the output.

For convenience in comparing different elements, the noise figure is usually measured at an input noise temperature

$$T_{ij} = T_o = 290°K$$

giving

$$F_j = 1 + \frac{T_j}{T_o} \tag{2.6-19}$$

or

$$T_j = (F_j - 1)T_o \tag{2.6-20}$$

The unmodified term "noise figure" in the literature refers to this $F_j = F_j(T_o)$.

Note that

$$F_j(T_{ij}) = (F_j - 1)\frac{T_o}{T_{ij}} + 1 \tag{2.6-21}$$

so that the effective noise temperature measured at T_{ij},

$$T_j = (F_j(T_{ij}) - 1)T_{ij} \equiv (F_j - 1)T_o \tag{2.6-22}$$

For an active element, such as an amplifier, F_j determines T_j independent of the input noise temperature and the physical temperature of the input. However, for a passive element (such as a cable) of gain G_j (loss $L_j = 1/G_j$), in thermal equilibrium with its environment.

$$T_{ij} = T_{outj} = \text{Ambient temperature} \triangleq T$$

and

$$F_j(T_{ij}) = \frac{1}{G_j} = L_j$$

so that the effective noise temperature of a loss is

$$T_{Lj} = (L_j - 1)T \tag{2.6-23}$$

where T is the ambient temperature. Note that for a loss, the effective noise temperature is dependent on the physical temperature of the component. The noise factor F_j could be defined as

$$F_j = 1 + (L_j - 1)\ \frac{T}{T_o}$$

Since F_j for a loss depends on the physical temperature of the component, it is not an especially useful concept, and when speaking of the noise temperature of a passive element, equation 2.6-23 is used instead.

2.6.3.4.1.2 Receiver System Temperature. For a cascaded system of M elements, passive or active, it can be shown (ref. 2-4) that the system effective noise temperature can be written as:

$$T_n = T_1 \frac{B_{n_1}}{B_n} + \frac{T_2}{G_1} \frac{B_{n_2}}{B_n} + \cdots + \frac{T_M}{G_1 G_2 \cdots G_{M-1}} \frac{B_{n_M}}{B_n} \tag{2.6-24}$$

where

$$T_n \triangleq \frac{N_s}{k B_n G_s}$$

N_s = The noise power contributed by the system

$$N_s = N_{out} - N_i G_s$$

N_{out} = The total output noise power of the system due to N_s and the input noise power N_i. The temperatures, T_j, are referenced as shown in Figure 2-7.

For $B_{n_j} = B_n$, we have the more common form of the system effective noise temperature,

$$T_n = T_1 + \frac{T_2}{G_1} + \cdots + \frac{T_M}{G_1 G_2 \cdots G_{M-1}} \tag{2.6-25}$$

We shall make this assumption in what follows.

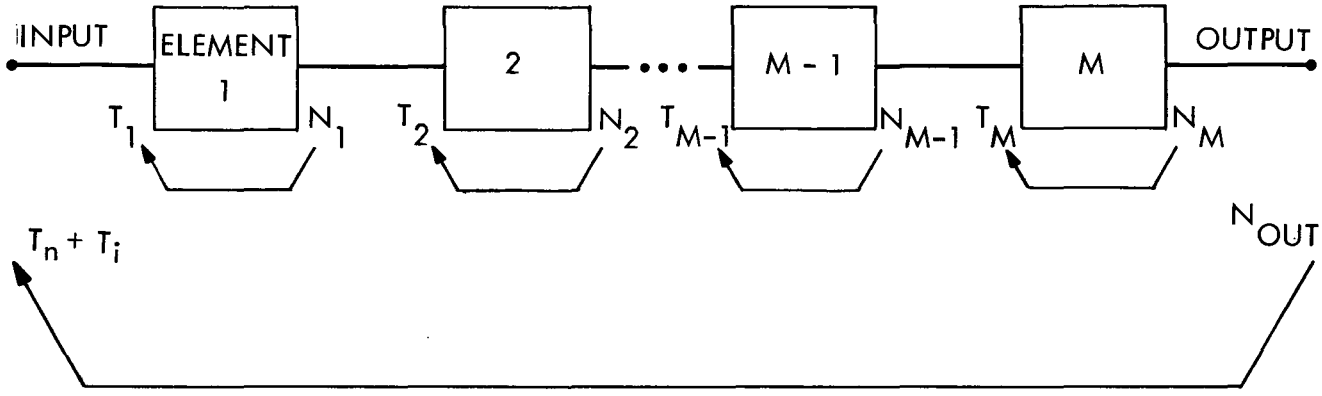

Fig. 2-7. Noise powers and their associated noise temperature reference points

Note that if the gain of one element in the cascade is very high and the noise figures of succeeding elements are not large, the expression for effective noise temperature may be truncated after the noise temperature term for that element. For example, if $G_3 >> 1$,

$$T_n \approx T_1 + \frac{T_2}{G_1} + \frac{T_3}{G_1 G_2}$$

and

$N_s \approx kT_n B_n G_s$, since the noise power contributions from elements 4 to M are small.

The effective system noise temperature as we have defined it, is the temperature at the input to the system which would result in a noise spectral

density, $N_o = kT_{es}G_s$ at the system output. It is also called the system noise temperature referenced to the system input.

Frequently, the system noise temperature is noted as referenced to a convenient point within the system. Thus, one may speak of the system noise temperature referenced to the receiver input. This noise temperature is defined as that temperature at the reference point which would result in the system noise spectral density at the system output. What this change of reference point amounts to, is a lumping of the appropriate subsystem gains into the definition of noise temperature.

The system noise temperature referenced to the input of element j would be:

$$T_{ej} = G_1 G_2 \cdots G_{j-1} T_{es}$$

and

$$N_o = kT_{ej}(G_j G_{j+1} \cdots G_M) \equiv kT_{es}G_s$$

The term in parentheses is called G_s' and is the system gain which follows the reference point.

2.6.3.4.1.3 Example. Consider the system of Figure 2-8. We have an antenna with incident noise power $N_i = k(T_g + T_a)B_n$. From the antenna to the receiver we have a loss, L_C^* db. The receiver has a noise figure F^* db, and gain G_R^* db. Then,

$$T_{es} = T_g + T_a + T_n = T_g + T_a + T(L_C - 1) + T_o(F - 1)L_C \quad (2.6\text{-}26)^{**}$$

where

$$L_c = 10^{L_c^*/10}, \quad F = 10^{F^*/10}$$

** Note that this equation typically is valid for a spacecraft receiver under low signal input, where $G_R >> 1$. Under high signal level operation G_R drops, and noise temperature contributions beyond the receiver become significant.

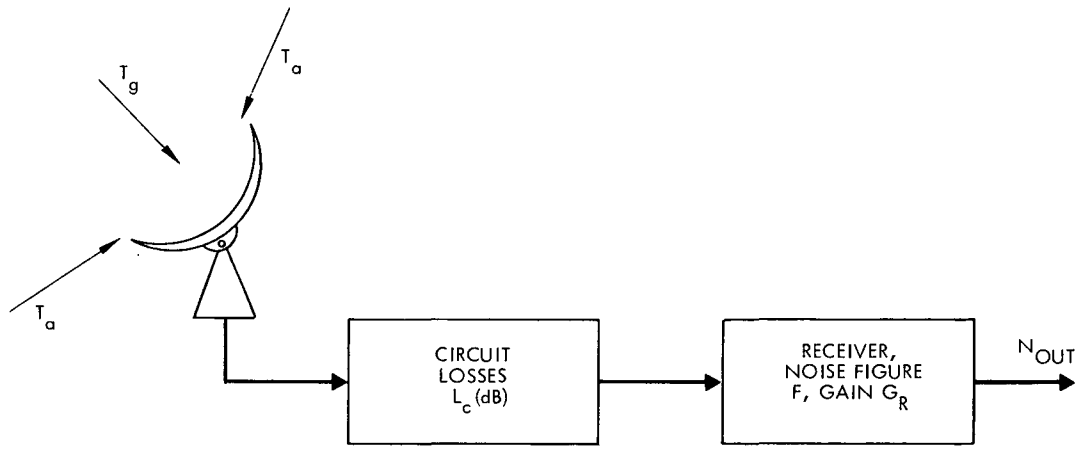

Fig. 2-8. Example for system temperature calculation

So that the total noise spectral density at the output of the receiver is:

$$N_o = k(T_g + T_a + T_n)G_R/L_c \tag{2.6-27}$$

where

$$G_R = 10^{G_R^*/10}$$

Out of the receiver, a received signal of power P(T) at the receiver case will have power

$$P_{out} = P(T)G_R \tag{2.6-28}$$

So that the signal power-to-noise spectral density ratio will be:

$$\frac{P_{out}}{N_o} = \frac{P(T)}{k(T_g + T_a + T_n)/L_c} = \frac{P(T)}{(kT_{es}/L_c)} \tag{2.6-29}$$

and it is not necessary to know G_R.

Note that we can choose to use the system noise temperature referenced to the receiver input, that is:

$$T_{er} = \frac{T_{es}}{L_c}$$

So that,

$$\frac{P_{out}}{N_o} = \frac{P(T)}{kT_{er}}$$

2.6.3.4.1.4 DSS Noise Spectral Density. The noise spectral density associated with the ground receiving system varies with the ground antenna pointing position. The minimum N_o exists when the antenna is pointing at zenith. It varies mainly with antenna elevation angle but is also sensitive to antenna azimuth angle.

Curves of the ground system noise temperature increase (ΔT) relative to zenith versus elevation angle are given in reference 2-1. Using these curves,

$$N_o/G_{SM} = \left[10 \log k\, T_{sys\ zenith} + \Delta T(\text{elev}) + \Delta T(\text{extraterrestrial})\right] \quad (2.6\text{-}30)$$

where G_{SM} is the gain of the system from the maser input flange to the detector.

Extraterrestrial noise can occur from celestial sources such as the Sun, Jupiter, and radio stars, as well as from such phenomena as atmospheric radiative transfer and scattering at X-band frequencies or from transmission through the solar corona during a superior conjunction phase of a mission at S- and X-bands. However, other sources may be identified for each flight project.

2.6.3.5 Absorption Loss, L_A, and Propagation Effects. The basic telecommunication channel for deep space missions consists of a propagation medium which is a vacuum, i.e., free space. However, significant effects may be observed when the rf signal passes through a perturbing medium. Such a medium may include the Earth and planetary atmospheres, the solar corona, multipath reflections from a planetary surface, or plasmas which may be generated by the spacecraft itself. A general medium may alter signal power, frequency spectrum, signal phase relationships, polarization, ray path and noise characteristics. The severity of these alterations depends on the nature of the medium and the frequency of the signal. This section examines several media which may be encountered in a typical spacecraft mission.

2.6.3.5.1 Atmospheric Phenomena. Earth-based communication with a deep space vehicle requires the transmission and reception of an rf signal through the Earth's atmosphere. For a spacecraft in proximity to another planet, propagation may occur through the planet's atmosphere, if any, as well.

When it passes through an atmosphere, an electromagnetic wave is altered in a manner generally inimical to a telemetry system's performance. However, the nature of signal degradation may reveal properties of the transmission medium valuable to experimenters. The telecommunications system designer must be aware of atmospheric effects since they can have a large effect on signal power, system noise temperature, system frequency choice, and even antenna aiming. The major effects on signals at S- or X-band frequencies are:

1) Attenuation of the signal caused by weather conditions such as rain, clouds, wind, snow, etc.
2) Increase in the DSIF system noise temperature due to weather.
3) Bending and defocusing of the signal due to the differential index of refraction of the atmosphere.

4) Attenuation caused by the presence of atmospheric plasmas in the transmission path.

5) Phase and amplitude modulation due to fluctuations of the medium in the ray path.

Other effects, such as scintillation and scattering, are generally small, and are omitted from this discussion.

2.6.3.5.1.1 Weather Effects. Weather conditions at the ground station can cause severe attenuation of the electromagnetic signal. The effect is frequency-dependent so that while an X-band signal is severely attenuated, the effect on an S-band signal may be negligible. The atmosphere contains oxygen, water vapor, and water droplets which absorb and reradiate electromagnetic waves. Since the oxygen content is fairly constant in time, it produces a constant background noise. However, the water vapor and water droplet content of the atmosphere fluctuate radically in time and in geographical location as the weather changes.

The atmospheric water content causes two major effects; attenuation, and increase in noise temperature of the ground system. At centimeter wavelengths, attenuation is caused primarily by droplets of sizes characteristic of rain and fog, with rain the major offender. For rain, the attenuation depends on such parameters as drop size, geometry and distribution, rain rate, distance the signal must travel through the rain, and the signal frequency. For clouds, the attenuation depends on the water content and cloud thickness.

The effective sky temperature due to the water vapor can be calculated if the distribution of water along the antenna beam is known. Reference 2-1 gives information on the increase in X-band system noise temperature which can be expected at DSS-14. The loss in dB caused by the change in system noise temperature is calculated by adding these noise temperature increases to the extraterrestrial noise temperature as in equation 2.6-30.

Figure 2-9 shows the total system degradation versus rain rate for an X-band signal. The degradation includes the signal attenuation, $L_{A\,rain}$, and the increase in system noise spectral density due to rain (ref. 2-5).

Weather conditions can be predicted on a probabilistic basis if the proper weather data is available for a sufficiently long period of time. Weather data for the Goldstone area is now being accumulated. From this data it may become possible to predict the probable loss as a function of the month of the year and the antenna elevation angle.

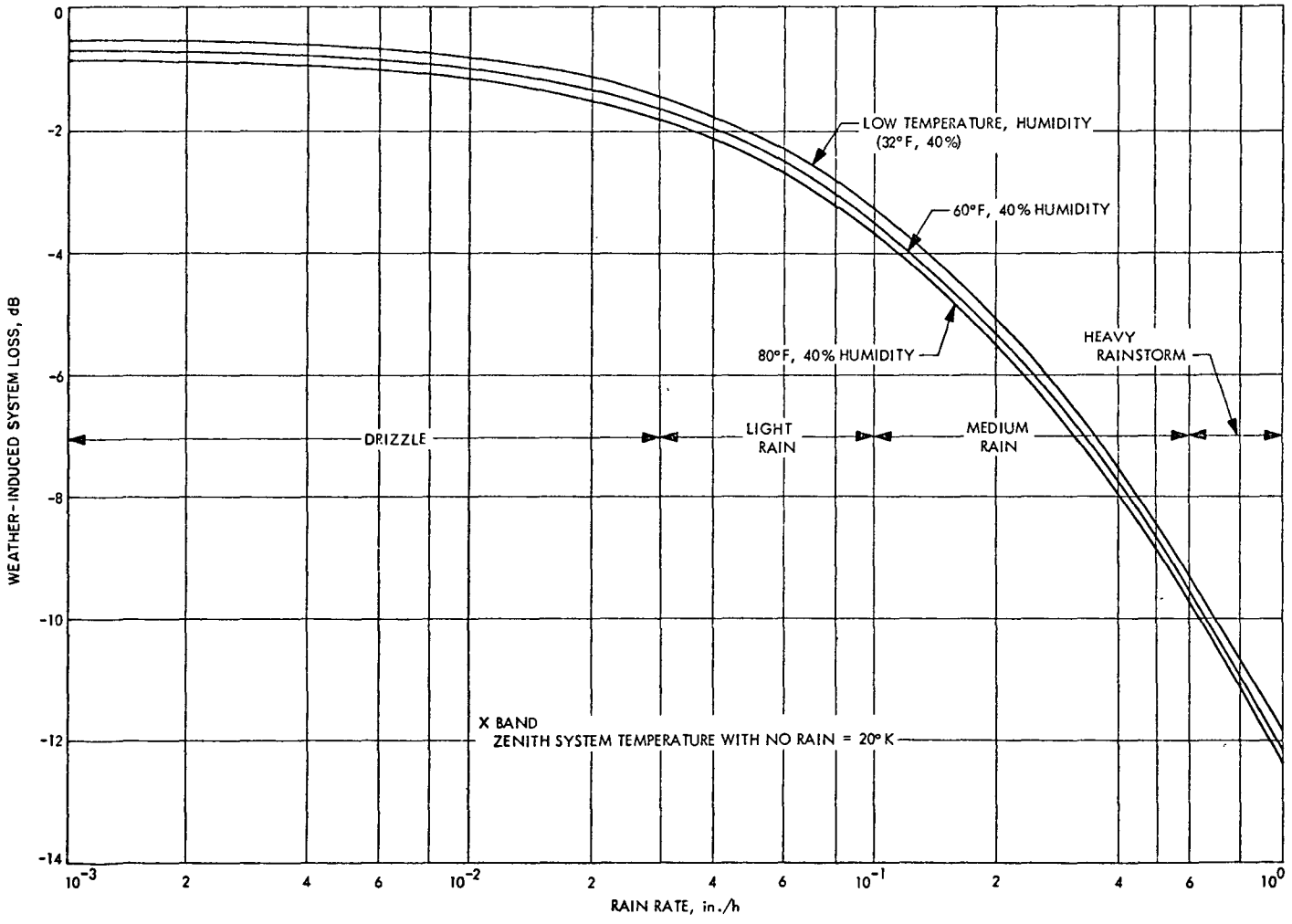

Fig. 2-9. X-band system degradation vs rain rate, elevation averaged

2.6.3.5.1.2 Index of Refraction Effects. When an electromagnetic wave passes from free space to a medium with an index of refraction greater than 1, the wave velocity decreases and the wave is bent. Planetary atmospheres have an index of refraction which varies with the height above the planet's surface. The atmosphere thus causes two effects. First, the index of refraction gradient generally causes beam divergence, since rays passing through the less dense upper portions of the atmosphere are not bent as much as those close to the surface. (Note that the opposite effect, namely beam focusing, can take place in the presence of an index of refraction gradient inversion. Such occurences are responsible for "ducting" in the Earth's troposphere. These effects are important for reception at very low elevation angles (less than 3 degrees) but are negligible for viewing signals through other planetary atmospheres since such observations must average the effect over large atmospheric areas.) Beam divergence results in less signal energy per unit area at the receiving antenna, corresponding to signal attenuation. Second, the wave is bent so that a source of radio energy has an apparent position shift.

The value of the index of refraction of a planetary atmosphere is determined by three observables, as follows:

1) The atmospheric composition
2) The change in atmospheric density with altitude
3) The plasma composition of an ionosphere

The change in index of refraction caused by the ionosphere can be readily calculated and the equation is included in the discussion of plasma propagation which follows. First, we shall consider neutral atmospheric effects only; the results may be easily modified for charged particle effects by changing the functional form of the index of refraction in the following discussion.

The effect of atmospheric density changes is more important than ionospheric effects for a generally neutral atmosphere, and is independent of frequency for 300 to 30,000 MHz. If we define refractivity as

$$N(r) = 10^6 (n(r) - 1) \tag{2.6-31}$$

where n(r) is the index of refraction and r is the radial distance from the center of the planet, then one model for the refractivity of a planetary atmosphere is an exponential function of the altitude $r - r_o$ (ref. 2-8).

$$N(r) = N_o e^{-\beta(r-r_o)} \tag{2.6-32}$$

where

N_o = Surface refractivity

r_o = Radius of the planet's surface

β = Inverse scale height

and β is assumed to be constant for the significant atmosphere.

Then

$$n(r) = (n_o - 1)e^{-\beta(r-r_o)} + 1 \tag{2.6-33}$$

where

n_o = Surface index of refraction

When a spacecraft transmits a signal through the atmosphere of an encountered planet, the signal will be bent and attenuated due to refractive effects.

The bending of a signal is (ref. 2-8)

$$E(h) = -2n(R)R\int_R^\infty \frac{n'(r)\,dr}{n(r)\left[n^2r^2 - n^2(R)R^2\right]^{1/2}} \qquad (2.6\text{-}34)$$

where

$E(h)$ = Angle the signal is bent by the atmosphere

h = Height of the closest approach of the ray path to the planet

$n'(r) = dn/dr$

and

$$R = r_o + h$$

The attenuation due to beam divergence is (ref. 2-8)

$$L_{An}(h) = 10 \log_{10}\left[1 + \frac{R_A R_E}{R_A + R_E}E'(h)\right] \quad \text{dB} \qquad (2.6\text{-}35)$$

where

R_A = Probe-planet distance

R_E = Earth-planet distance

and

$E'(h) = dE/dh$

For the model of equation (2.6-32), assuming no significant ionospheric effects

$$E(h) = 2 \times 10^{-6} N_o e^{-\beta h} \beta \left(\frac{\pi R}{2\beta}\right)^{1/2} \tag{2.6-36}$$

$$L_{An}(h) = 10 \log_{10} \left[1 + \frac{R_A R_E}{R_A + R_E} \left(\beta - \frac{1}{2R}\right) E(h)\right] \tag{2.6-37}$$

The extremely narrow beam of a DSN antenna intercepts a very small altitude differential in transmitting or receiving through the Earth's atmosphere, even at low elevation angles. Thus, attenuation due to beam spreading through the Earth's atmosphere is negligible. Bending can amount to as much as 1.5 mr at low (15 degree) elevation angles. This bending must be considered in pointing the antenna, since it is a significant fraction of the antenna beamwidth. At X-band, for example, the 64-m antenna, 3 dB beamwidth is only 0.67 mr. Thus, it becomes vital to aim the antenna at the apparent position of the source.

2.6.3.5.2 Propagation Through a Plasma. A plasma may be defined as a configuration of positively and negatively charged mobile particles which are electrically neutral. It may also contain neutral particles and electromagnetic radiation (photons). Communication with a spacecraft through a plasma becomes important when communicating through the solar corona, a planetary ionosphere, or a plasma sheath formed about a capsule during entry into a planetary atmosphere.

The plasma frequency, ω_p, the natural frequency of oscillation of the plasma ions and electrons, is:

$$\omega_p^2 = \frac{4\pi n_e e^2}{m_e} + \frac{4\pi n_i e^2}{m_i} \tag{2.6-38}$$

where

n_i = Number of ions/cm^3

n_e = Number of electrons/cm^3

e = Charge of an electron, statcoulombs

m_i = Mass of an ion, gm

m_e = Mass of an electron, gm

and unit ionization is assumed for the ions.

Generally, the ion motion is ignored because the ion mass is many times that of the electron mass. Thus,

$$\omega_p^2 \simeq \frac{4\pi n_e e^2}{m_e} \tag{2.6-39}$$

If plasma contains a magnetic field, the electrons will tend to rotate about the magnetic field lines at the cyclotron frequency.

$$\omega_c = \frac{eB}{m_e c} \tag{2.6-40}$$

where

B = Magnetic induction, gauss

and

c = Speed of light, cm/sec

(The cyclotron frequency of the ions is only one one-thousandth or so that of the electrons, and therefore is usually much too small to significantly affect an rf signal.)

If an rf signal encounters a plasma whose plasma or cyclotron frequencies are close to the frequency of the wave, a resonance is observed, and a large amount of energy may be transferred from the wave to the plasma, resulting in severe attenuation. For S-band, this requires an electron density of approximately 1.6×10^9 electrons/cm^3.

The attenuation caused by a plasma depends on the orientation of the propagation direction of the wave with respect to the magnetic field direction. If the plasma is tenuous and the direction of propagation is parallel to a uniform magnetic field which is strong compared to the field induced by the wave, then the power attenuation can be found from (ref. 2-9):

$$L_{Ap\pm} = \exp\left\{-\frac{4\pi}{\lambda} Z_p \, I_m\left\{\left[1 - \frac{\omega_p^2}{\omega^2}\left(\frac{\omega}{\omega \pm \omega_c}\right)\right]^{1/2}\right\}\right\} \tag{2.6-41}$$

$$L_{Ap\pm}(\mathrm{dB}) = \left\{-\frac{54.6}{\lambda} Z_p \, I_m\left\{\left[1 - \frac{\omega_p^2}{\omega^2}\left(\frac{\omega}{\omega \pm \omega_c}\right)\right]^{1/2}\right\}\right\} \tag{2.6-42}$$

where

Z_p = Plasma thickness

λ = Wavelength = $c/2\pi\omega$

$I_m(.)$ = Imaginary part

The + sign corresponds to a right circularly polarized (RCP) wave and the - sign to a left circularly polarized (LCP) wave.

In a similar fashion, the index of refraction is found to be (ref. 2-10):

$$n_{\pm} = \left[1 - \frac{\omega_p^2}{\omega(\omega \mp \omega_c)}\right]^{1/2} \qquad (2.6\text{-}43)$$

The following consequences are observable from these equations:

1) For a real index of refraction there is no attenuation
2) For an imaginary index of refraction there is attenuation, but no bending
3) Attenuation and refraction differ for LCP and RCP, if a magnetic field exists
4) The results will be different for different propagation directions.

Thus, the plasma is anisotropic and birefringent.

The general analysis, for arbitrary direction and with collisions, can be found in reference 2-11. For a "thick" plasma ($Z_p >> \lambda$), the collisionless attenuation results can be summarized by:

B = 0	$\Rightarrow$	Blackout for $\omega \leq \omega_p$
RCP wave parallel to B	$\Rightarrow$	Blackout for $\omega_c \leq \omega \leq \omega_+$
LCP wave parallel to B	$\Rightarrow$	Blackout for $\omega \leq \omega_-$
Wave direction perpendicular to B	$\Rightarrow$	Blackout for $\omega \leq \omega_-$ and $(\omega_p^2 - \omega_c^2)^{1/2} \leq \omega \leq \omega_+$

where

$$\omega_- = -\frac{\omega_c}{2} + \sqrt{\left(\frac{\omega_c}{2}\right)^2 + \omega_p^2}$$

and

$$\omega_+ = \frac{\omega_c}{2} + \sqrt{\left(\frac{\omega_c}{2}\right)^2 + \omega_p^2}$$

The above results are for a collisionless plasma. The effect of only a few collisions is to slightly broaden and round off the band gaps. In nature, the magnetic fields are not homogeneous but in many cases they can be approximated in small regions by homogeneous fields.

REFERENCES

2-1 Deep Space Network/Flight Project Interface Design Handbook Jet Propulsion Laboratory, 810-5, DSN Standard Practice (JPL internal document).

2-2 Silvers, S., ed., Microwave Antenna Theory and Design, Boston Technical Lithographers, Inc. (Lexington, Mass.: 1963).

2-3 Skolnik, M. I., Introduction to Radar Systems, McGraw-Hill (New York: 1962).

2-4 Mumford, W. W., and Schelbe, E. H., Noise Performance Factors in Communications Systems, Horizon House-Microwave, Inc. (Dedham, Mass.: 1968).

2-5 Potter, P. D., Shumate, M. S., Stelzried, C. T., and Wells, W. H. A Study of Weather Dependent Data Links for Deep Space Applications, Jet Propulsion Laboratory Technical Report No. 32-1392, October 15, 1969.

2-6 MacDoran, P. F., "A First Principles Derivation of the Differenced Range Versus Integrated Doppler (DRVID) Charged Particle Calibration Method," Jet Propulsion Laboratory Space Programs Summary 37-62, Vol. II, The Deep Space Network, March 31, 1970, pp. 28-34.

2-7 MacDoran, P. F., and Martin, W. L., "DRVID Charged Particle Measurement With a Binary-Coded Sequential Ranging System," Jet Propulsion Laboratory Space Programs Summary 37-62, Vol. II, The Deep Space Network, March 31, 1970, pp. 34-41.

2-8 Kliore, A., Cain, D. L., and Hamilton, T. W., Determination of Some Physical Properties of the Atmosphere of Mars from Changes in the Doppler Signal of a Spacecraft on an Earth-Occultation Trajectory, Jet Propulsion Laboratory Technical Report No. 32-674, October 15, 1964.

2-9 Spitzer, L., Physics of Fully Ionized Gases, Interscience Publishers, Inc. (New York: 1956).

2-10 Jackson, J. D., Classical Electrodynamics, John Wiley & Sons, Inc. (New York: 1962).

2-11 Mitra, S. K., The Upper Atmosphere, Royal Asiatic Society of Bengal, 1947.

SECTION III

TELECOMMUNICATIONS DESIGN CONTROL

3.1 MOTIVATION FOR DESIGN CONTROL

In Section II, the overall telecommunication system was described, showing that a large number of independent parameters determine the available total received P_T/N_o for the uplink and downlink. In Sections IV, V and VI it will be shown that a number of additional independent parameters determine how effectively the available P_T/N_o is used to provide the tracking, telemetry, and command capabilities of the telecommunication system.

Telecommunications design control at the Jet Propulsion Laboratory is achieved through the use of the Telecommunications Design Control Document which is required for each project. This document is designed to accomplish the following objectives:

1) To provide a single authoritative and respected document for each project;

2) To provide a compendium of information on which management control can be based;

3) To define and clarify the telecommunications system interface;

4) To assign responsibility for the system's elements to the proper organizations and individuals;

5) To provide a description and commitment for telecommunications performance;

6) To provide for a controlled update and traceable record of information; and

7) To provide information by which decisions as to effort allocation can be made.

The Telecommunications Design Control Document used by JPL is prepared in a format which is in accordance with the procedures explained in this section.

3.2 POLICY FOR THE DESIGN OF DEEP SPACE TELECOMMUNICATION SYSTEMS

As with any design process, it is important to have criteria against which the design can be measured to show when the iterative process is complete. In the design of its telecommunication systems, the JPL has used a deterministic worst case criterion for selecting the SNR margins. Although the criterion is not perfect, experience over many lunar and planetary flight projects has demonstrated that it is practical from the point of view of engineering and management. Its use for future JPL projects is Laboratory policy and is highly recommended for other telecommunication systems. The policy statement and criterion are as follows:

Policy for Telecommunication System Design and Design Control

I. The Division 33 [the Telecommunications Division of the JPL] policy regarding the criterion for an acceptable telecommunication system design and system design control are as follows:

II. The criterion for an acceptable telecommunication system design is that the system provide the required functional performance under prescribed conditions with the minimum safety margin necessary to cover design uncertainties. The criterion is met when the design received signal level under the prescribed conditions exceeds the signal level required for the specified functional performance by the sum of the adverse tolerances of these two parameters. The individual tolerances in the tolerance summation shall reflect the uncertainty over the largest practical collections of system elements.

III. There shall be a single document for each JPL flight project that serves as a management tool for design control, a description of system performance and a commitment by Division 33 to provide a given communication performance. The content of the document shall govern the telecommunication system design for each JPL flight project. It shall include design control tables, associated graphs, charts and explanatory material that demonstrate the extent to which the design meets the criterion for an acceptable design.

IV. The document for each JPL flight project shall be designated the (project name) Telecommunications Design Control. The development and maintenance of the document shall be the responsibility of Division 33 and shall be assigned to the Telecommunication System Cognizant Engineer for each project. The document shall be prepared according to established procedures and updated during the life of the project at established times commensurate with the project needs.

V. Division 33 will continue to recommend that non-JPL flight projects supported by the DSIF use the identical criterion for an acceptable telecommunications system design and identical techniques for telecommunication system design control.

VI. Division 33 will work continuously toward:

(1) Reducing to a reasonable minimum the number of elements in the link to which tolerances are separately assigned,

(2) Improving the accuracy of the performance predictions made during the design phase of a JPL flight project,

(3) The separate specification of the spacecraft and the DSIF portions of the link.

3.3 DESIGN CONTROL POLICY IMPLEMENTATION

It should be noted that there are three main parts to the design control policy statement: a design criterion; a management tool (the document); and an assignment of responsibility for implementation. The criterion and assignment of responsibility are self explanatory. The development and application of the design control requires further explanation and is discussed in the sections which follow.

3.3.1 The Telecommunications Design Control Document

Each flight project usually establishes a technical group which is responsible for the analysis of telecommunication requirements and the design of the telecommunication system. The resulting design is specified and controlled by a single authoritative document called the Telecommunication Design Control. This document contains:

1) Telecommunication link functional requirements;

2) Specifications of all spacecraft subsystem parameters affecting link performance;

3) Specifications of all spacecraft and DSIF interface parameters for the link;

4) Specifications of all DSN hardware parameters affecting link performance;

5) Design control tables for uplink carrier tracking, downlink carrier tracking, ranging, telemetry and command (see paragraph 3.3.2);

6) Predictions of telecommunication system performance versus time for the mission lifetime (see section IX).

The Telecommunication System cognizant engineer for each flight project has overall responsibility for the telecommunication design control. This responsibility includes preparation and publication of the design control document, assignment of responsibility for individual spacecraft design parameters, coordination with the flight project to assure that subsystem specification

documents are consistent with the Telecommunication Design Control and periodic updating of the document to reflect the current status of link performance.

The technical cognizant engineer for each spacecraft subsystem is responsible for providing the telecommunication system cognizant engineer with current values of those subsystem parameters affecting telecommunication link performance. He may be required to sign off his subsystem parameters on the approved design control tables.

The DSN manager for each flight project is responsible for identifying to the Telecommunications System cognizant engineer those individuals having responsibility for providing current and accurate values of each DSN parameter affecting link performance. These individuals may be asked to sign off their parameter values on the approved design control tables.

No functional requirements or parameter specifications may be changed without the consent of the Telecommunications System cognizant engineer.

3.3.2 Design Control Tables

In order to handle the problems of complex spacecraft and ground systems, and maintain a reliable estimate of the overall system performance, a simple but effective accounting technique called "Design Control Table" (DCT) was devised.

As shown in Tables 3-1 through 3-5, all of the factors that contribute to system performance are listed in the approximate order that one would find in tracing a signal through the system. Each parameter is listed in terms of design value and tolerance band.

The advantages of the design control table technique are that, first, it formalizes the accounting of system performance in a uniform manner that facilitates the comparison of competing systems. Second, it minimizes hidden pads or safety factors and the resulting over-design. Third, it readily indicates the least controlled parameters of the system (those with the largest tolerances) hence the areas where more knowledge and hardware improvement might be most profitable.

Table 3-1. Uplink carrier design control table

Table:_____ Mission:_____

Mode: _____

Launch Date _____ Arrival Date _____

Time in Mission:_____ By:_____ Date:_____

No.	Parameter	Design value	Tolerance Fav.	Tolerance Adv.	Source	Notes
	Total Channel					
1	Total transmitting power at antenna (dBm)					
2	Transmitting antenna gain (dB)					
3	Space loss (dB)					
4	Polarization loss (dB)					
5	Receiving antenna gain (dB)					
6	Cir loss antenna to rcvr (dB)					
7	Total rcvd pwr at rcvr case (dB) (1+2+3+4+5+6)					
8	Sys noise spec den/sys gain (dBm/Hz)					
9	Pwr/Noise spec den ratio (dB-Hz) (7-8)					
	Carrier Channel					
10	Carrier power/total power (dB)					
11	Limiter loss (dB)					
12	Carrier threshold trkg bandwidth ($2B_{LO}$)(dB)					
13	$SNR_{2B_{LO}}$ (dB) (9+10+11-12)					
14	Threshold $SNR_{2B_{LO}}$ (dB) 1σ phase jitter___° rms					
15	Carrier margin (13-14) (dB)					

Supporting Data

3a	F=_____MHz, R=_____KM	8a	Noise figure= _____dB+___dB- ___dB
3b	Includes: Absorption loss_____dB	8b	Sys noise Temp= _____°K+___°K- ____°K
4a	Ellipticity: Flt. Ant._____dB Grd. Ant._____dB	8c	Ant Temp = _____°K+___°K- ____°K
5a	Peak gain = _____dB+___dB- ___dB	10a	θ_{CMD}= _____° K = _____°/V +_____°/V - _____°/V T_{CMD} = _____V +_____V - _____V P_{CMD}/P_T=_____dB +____dB - _____dB θ_R= _____° T_R = _____ V +_____ V - _____V Rang Suppr _____dB+___dB-____dB (Carrier and data ch)
5b	Antenna _____		
5c	Pointing error: Cone | Clock Tracking ____° | ____° Limit cycle ____° | ____° Uncertainty ____° | ____°		
5d	Pointing loss = _____ dB+___dB-___dB (Includes worst case limit cycle)		
5e	Loss = _____ dB+___dB-___dB (No limit cycle)		
5f	Loss = _____ dB+___dB-___dB (Best limit cycle)		

Table 3-2. Downlink carrier design control table

Table:_____ Mission: _____

Mode: _____

Launch Date _____ Arrival Date _____

Time in Mission:_____ By: _____ Date: _____

No.	Parameter	Design value	Tolerance		Source	Notes
			Fav.	Adv.		
	Total Channel					
1	Total transmitting power at radio case (dBm)					
2	Cir loss to antenna (dB)					
3	Transmitting antenna gain (dB)					
4	Space loss (dB)					
5	Polarization loss (dB)					
6	Receiving antenna gain (dB)					
7	Tot rcvd pwr, MSR inp flange (dBm) (1+2+3+4+5+6)					
8	Sys noise spec den/sys gain (dBm/Hz)					
9	Pwr/noise spec den ratio (dB-Hz)(7-8)					
	Carrier Channel					
10	Carrier power/total power (dB)					
11	Limiter loss (dB)					
12a	Uplink VCO jitter loss in 2-way (dB)					
12b	Aux Osc jitter loss in 1-way (dB)					
13	Carrier threshold trkg bandwidth ($2B_{LO}$) (dB)					
14	$SNR_{2B_{LO}}$ (dB)(9+10+11+12-13)					
15	Threshold $SNR_{2B_{LO}}$ (dB) 1σ phase jitter ___° rms					
16	Carrier margin (14-15) (dB)					

Supporting Data

1a TWTA _____dBm+____dB- _____dB
1b Cir loss to case ____dB+___dB- _____dB

2a Incl mismatch loss__dB+___dB- _____dB
2b VSWR _____ + _____%- _____%

3a Peak gain = _____dB+____dB- _____dB
3b Antenna _____
3c Pointing error:

	Cone	Clock
Tracking	____°	____°
Limit cycle	____°	____°
Uncertainty	____°	____°

3d Pointing loss = _____dB+____dB- _____dB (Includes worst case limit cycle)
3e Loss = _____dB+____dB- _____dB (No limit cycle)
3f Loss = _____dB+____dB- _____dB (Best limit cycle)

4a F=_____ MHz, R= _____KM
4b Includes: Absorption loss_____ dB

5a Ellipticity: Flt. Ant. _____ dB
Grd. Ant._____ dB

6a Includes pointing and circuit loss.
Pointing loss_____ dB+ _____dB- _____dB
6b Includes surface deformation loss:
Wind loss_____dB
Low Elev. loss _____dB

8a Elev:_____°, Azimuth _____°
8b System noise temp:___°K+ _____°K- _____°K
8c Zenith noise temp:___°K+ _____°K- _____°K

10a
θ_1= _____°
K = _____°/V + _____°/V - _____°/V
T_1 = _____ V + _____ V - _____ V
θ_2 = _____°
T_2 = _____ V + _____ V - _____ V
P_{D1}/P_T= _____ dB+ _____dB- _____dB
P_{D2}/P_T= _____ dB+ _____dB- _____dB
θ_R= _____°
T_R = _____ V + _____V - _____ V

Rang Suppr (all ch):_____dB+ _____dB- _____dB

Table 3-3. Two-channel telemetry design control table

Table: _____ Mission: _____

Mode: _____

Launch Date _____ Arrival Date _____

Time in Mission: _____ By: _____ Date: _____

	No.	Parameter	Design value	Tolerance Fav.	Tolerance Adv.	Source	Notes
Total Channel	1	Total transmitting power at radio case (dBm)					
	2	Cir loss to antenna (dB)					
	3	Transmitting antenna gain (dB)					
	4	Space loss (dB)					
	5	Polarization loss (dB)					
	6	Receiving antenna gain (dB)					
	7	Tot rcvd pwr MSR inp flange (dBm) (1+2+3+4+5+6)					
	8	Sys noise spec den/sys gain (dBm/Hz)					
	9	Pwr/noise spec den ratio (dB-Hz) (7-8)					
Data One Channel	10	Data power/total power (dB)					
	11	Waveform distortion loss (dB)					
	12	Radio loss (dB)					
	13	Subcarrier demod loss (dB)					
	14	Bit sync/detection loss (dB)					
	15	Rate (dB. bps) bps					
	16	Rcvd ST/N_0(dB) (9+10+11+12+13-14-15)					
	17	Threshold ST/N_0(dB) ER=					
	18	Performance margin (dB) (16-17)					
Data Two Channel	19	Data power/total power (dB)					
	20	Waveform distortion loss (dB)					
	21	Radio loss (dB)					
	22	Subcarrier demod loss (dB)					
	23	Bit Sync/detection loss (dB)					
	24	Bit rate (dB. bps) bps					
	25	Rcvd ST/N_0(dB) (9 +19+20+21+22+23-24)					
	26	Threshold ST/N_0(dB) ER=					
	27	Performance margin (dB) (25-26)					

Supporting Data

1a TWTA _____ dBm+ _____dB- _____dB

1b Cir loss to case ___dB+ ___dB- _____dB

2a Incl mismatch loss___dB+ ___dB- _____dB

2b VSWR _____+ _____%- _____%

3a Peak gain = _____dB+ _____dB- _____dB

3b Antenna _____

3c Pointing error:

	Cone	Clock
Tracking	____°	____°
Limit cycle	____°	____°
Uncertainty	____°	____°

3d Pointing loss _____dB+ _____dB- _____dB
(Includes worst case limit cycle)

3e Loss _____dB+ _____dB- _____dB
(No limit cycle)

3f Loss _____dB+ _____dB- _____dB
(Best limit cycle)

4a F= _____ MHz, R= _____KM

4b Includes absorption loss _____ dB

5a Ellipticity: Flt. Ant. _____ dB
Grd. Ant. _____dB

6a Includes pointing and circuit loss.
Pointing loss ___ dB+ _____dB- _____ dB

6b Includes surface deformation loss:
Wind loss _____dB
Low elev. loss _____dB

8a Elev: _____°, Azimuth _____°

8b System noise temp: __°K+ _____°K- _____°K

8c Zenith noise temp: __°K+ _____°K- _____°K

10a θ_1 = _____°

& K = _____°/V + _____°/V - _____°/V

T_1 = _____ V + _____V - _____V

θ_2 = _____°

19a T_2 = _____ V + _____ V - _____ V

P_C/P_T = _____ dB+ _____ dB- _____dB

θ_R = _____°

T_R = _____V + _____V - _____ V

Rang Suppr (all ch): _____ dB+ _____ dB- _____ dB

12a Downlink: $2B_{LO}$ = ___ Hz. $(SNR)_{2B_{LO}}$ = _____ dB

&

21a Uplink: $2B_{LO}$ = ___Hz. $(SNR)_{2B_{LO}}$ = _____ dB

Table 3-4. Single-channel command design control table

Table:_____ Mission:_____

Mode:_____

Launch Date_____ Arrival Date_____

Time in Mission:_____ By:_____ Date:_____

No.	Parameter	Design value	Tolerance		Source	Notes
			Fav.	Adv.		
	Total Channel					
1	Total transmitting power at antenna (dBm)					
2	Transmitting antenna gain (dB)					
3	Space loss (dB)					
4	Polarization loss (dB)					
5	Receiving antenna gain					
6	Cir loss antenna to rcvr (dB)					
7	Total rcvd pwr at rcvr case (dB) (1+2+3+4+5+6)					
8	Sys noise spec den/sys gain (dBm/Hz)					
9	Pwr/noise spec den ratio (dB-Hz) (7-8)					
	Command Channel					
10	Data power/total power (dB)					
11	Waveform distortion loss (dB)					
12	Radio loss (dB)					
13	Subcarrier demod loss (dB)					
14	Bit sync/detection loss (dB)					
15	Circuit loss (dB)					
16	Bit rate (dB. bps)_____ bps					
17	Received ST/N_0(dB) (9+10+11+12+13+14+15-16)					
18	Threshold ST/N_0(dB) ER =_____					
19	Performance margin (dB) (17-18)					

Supporting Data

3a	F=_____ MHz, R=_____ KM	8a	Noise figure =_____ dB
3b	Includes: Absorption loss_____ dB	8b	Sys noise temp =_____ °K+_____ °K-_____ °K
4a	Ellipticity: Flt. Ant._____ dB Grd. Ant._____ dB	8c	Ant temp =_____ °K+_____ °K-_____ °K
5a	Peak gain =_____ dB+_____ dB-_____ dB	10a	θ_{CMD}= _____ ° K = _____ °/V +_____ °/V -_____ °V T_{CMD}= _____ V +_____ V -_____ V P_C/P_T= _____ dB +_____ dB -_____ dB θ_R= _____ ° T_R = _____ V +_____ V -_____ V
5b	Antenna _____		
5c	Pointing error: Cone | Clock Tracking ___ ° | ___ ° Limit cycle ___ ° | ___ ° Uncertainty ___ ° | ___ °		
5d	Pointing loss=_____ dB+_____ dB-_____ dB (Includes worst case limit cycle)		Rang Suppr _____ dB+_____ dB-_____ dB (Carrier and data channel)
5e	Loss = _____ dB+_____ dB-_____ dB (No limit cycle)	12a	Uplink carrier $2B_{LO}$= _____ Hz SNR IN $2B_{LO}$= _____ dB
5f	Loss = _____ dB+_____ dB-_____ dB (Best limit cycle)		

Table 3-5. Ranging design control table

Table: _____ Mission: _____

Mode: _____

Launch Date: _____ Arrival Date _____

Time in Mission: _____ By: _____ Date: _____

No.	Parameter	Design value	Tolerance		Source	Notes
			Fav.	Adv.		
	Uplink Total Channel					
1	Total transmitting power at antenna (dBm)					
2	Transmitting antenna gain (dB)					
3	Space loss (dB)					
4	Polarization loss (dB)					
5	Receiving antenna gain (dB)					
6	Cir loss antenna to rcvr (dB)					
7	Total rcvd pwr at rcvr case (dB) (1+2+3+4+5+6)					
8	Sys noise spec den/sys gain (dBm/Hz)					
9	Pwr/noise spec den ratio (dB-Hz) (7-8)					
	Spacecraft Turnaround Channel					
10	Ranging power/total power (dB)					
11	Uplink radio loss (dB)					
12	Ranging noise bandwidth (dB. Hz)					
13	SNR in rang. noise bandwidth (dB) (9+10+11-12)					
14	Limiter suppression (dB)					
	Downlink Total Channel					
15	Total transmitter power at radio case (dBm)					
16	Cir loss to antenna (dB)					
17	Transmitting antenna gain (dB)					
18	Space loss (dB)					
19	Polarization loss (dB)					
20	Receiving antenna gain (dB)					
21	Tot rcvd pwr, MSR inp flange (dBm) (15+16+17+18+19+20)					
22	Sys noise spec den/sys gain (dBm/Hz)					
23	Pwr/noise spec den ratio (dB-Hz) (21-22)					
	Ranging Channel					
24	Ranging power/total power (dB)					
25	Limiter suppression (dB) (parameter 14)					
26	Two-way radio loss (dB)					
27	Received ranging P_R/N_0 (dB-Hz) (23+24+25+26)					
28	Threshold ranging P_R/N_0 (dB-Hz)					
29	Performance margin (dB) (27-28)					

Table 3-5. Ranging design control table (contd)

No.	Supporting Data
	Uplink Total Channel
3a	F=_____ MHz, R=_____ KM
3b	Includes: Absorption loss_____ dB
4a	Ellipticity: Flt. Ant._____ dB Grd. Ant._____ dB
5a	Peak gain=_____dB+____dB-_____ dB
5b	Antenna_____
5c	Pointing error: Cone | Clock Tracking ____° | ____° Limit cycle ____° | ____° Uncertainty ____° | ____°
5d	Pointing loss _____ dB+____dB-_____dB (Includes worst case limit cycle)
5e	Loss _____ dB+____dB-_____dB (No limit cycle)
5f	Loss _____ dB+____dB-_____dB (Best limit cycle)
8a	Noise figure=_____dB+_____dB-_____dB
8b	Sys noise temp=_____°K+_____°K-_____°K
8c	Ant temp=_____°K+_____°K-_____°K
10a	θ_R= _____° K =_____°/V +____°/V -_____°/V T_R =_____ V +____ V -_____ V P_C/P_T= _____ dB+_____dB-_____dB θ_{CMD}= _____ °+ _____°- T_{CMD}= _____V + _____V - _____ V Command suppr _____dB+ _____dB-_____dB (Carrier and ranging ch)
	Spacecraft Turnaround Channel
11a	Uplink SNR in $2B_{LO}$=_____Hz _____dB
	Downlink Total Channel
15a	TWTA _____dBm+____dB-_____dB
15b	Cir loss to case ___dB+____dB-_____dB
16a	Incl mismatch loss___dB+____ dB-_____dB
16b	VSWR _____+ _____%-_____%
17a	Peak gain =_____dB+____dB-_____dB
17b	Antenna_____
17c	Pointing error: Cone | Clock Tracking ____° | ____° Limit cycle ____° | ____° Uncertainty ____° | ____°
17d	Pointing loss _____ dB+____dB-_____dB (Includes worst case limit cycle)
17e	Loss _____ dB+____dB-_____dB (No limit cycle)
17f	Loss _____ dB+____dB-_____dB (Best limit cycle)
18a	F=_____ MHz, R=_____ KM
18b	Includes: Absorption loss_____ dB
19a	Ellipticity: Flt. Ant._____ dB Grd. Ant._____ dB
20a	Includes pointing and circuit loss. Pointing loss=_____dB+_____dB-_____dB
20b	Includes surface deformation loss: Wind loss _____dB Low elev. loss_____dB
22a	Elev:_____°, Azimuth _____°
22b	System noise temp:___°K+_____°K-_____°K
22c	Zenith noise temp:___°K+_____°K-_____°K
	Ranging Channel
24a	θ_1= _____° θ_2= _____° K =_____°/V +___°/V -_____°/V T_1=_____ V +____ V -_____ V T_2=_____ V +____V -_____ V P_C/P_T= _____ dB+____dB-_____dB Telemetry suppr (carrier and ranging): _____ dB+ ____dB-_____dB
26a	Downlink: $2B_{LO}$=_____Hz. $(SNR)_{2B_{LO}}$=_____dB Uplink: $2B_{LO}$=_____Hz. $(SNR)_{2B_{LO}}$=_____dB
28a	_____Ranging System
28b	T_{acq}=_____ sec

3.4 INSTRUCTIONS FOR DCT PREPARATION

Design Control Tables are prepared by using three distinct values for each system parameter. These are:

1) Design value

2) Favorable tolerance

3) Adverse tolerance.

Design values are the best estimate of parameter values for:

1) Prescribed operating conditions under which the system must meet the specified performance

   Examples of prescribed operating conditions are:

   a) Ground station antenna elevation angle at 15 degrees

   b) Spacecraft antenna pointing error of 1 degree, due to combined tracking and limit cycling errors

   c) Ground antenna wind load of 30 mph

   d) Rain at 0.1 inches per hour.

2) Prescribed ambient spacecraft environment. The ambient environment is generally taken to be hard vacuum at 25°C.

3) A fixed mission time. The mission time is some given day in the mission, i.e., Launch + 5 days, encounter, etc.

The design value must not include any arbitrary pads or safety factors.

The choice of operating conditions, environment, and time for which to develop a DCT is based on inputs from the mission analysis and engineering personnel, and on the performance thresholds discovered from analyzing these inputs.

Tolerances are assigned for each parameter by the responsible parties, and are based on subjective as well as objective considerations. The major factors affecting tolerance specification and examples of them are as follows:

1) Uncertainty in the knowledge of the spacecraft environment through the mission (e.g., interplanetary electron density, spacecraft temperatures).

2) Uncertainties in the relation between theoretical models used for design and actual hardware performance (e.g., phase-locked-loop design).

3) Random variations in component properties (e.g., one percent resistors).

4) Systematic, but unpredictable variations in component properties (e.g., the effects of aging).

5) Skepticism over subcontractor performance (e.g., previous experience shows a bias toward the low end of the specification range for performance; see reference 3-1).

6) Measurement and estimation errors in testing (e.g., confidence factors in estimation of performance by bit error statistics).

Tolerances should be specified at low, but realistic values without arbitrary pads or safety factors. Large tolerances indicate areas that would profit from further investigation. Maintaining low tolerances and living within them is a mark of the capability and experience of the engineer.

Appendix A3.1 briefly discusses the pragmatic specification of a hardware tolerance value from measurement of a small number of samples.

3.4.1 Types of Parameters

There are five basic parameter types listed in the design control tables. They are:

1) Those that are verified and adjusted periodically to within a certain measurement tolerance.

   Example: Ground station transmitter power

2) Those that vary systematically throughout the mission within well-defined limits

   Examples:

   a) Communication range

   b) Station noise-temperature with ground antenna elevation angle

3) Those that vary randomly throughout the mission within well-defined limits

Example: Antenna pointing due to attitude limit cycling

4) Those that are relatively constant in flight

Examples:

a) Spacecraft circuit loss

b) Spacecraft antenna gain

5) Those that vary with spacecraft environment

Examples:

a) Spacecraft transmitter power with temperature and spacecraft voltage

b) Spacecraft modulation level with temperature and spacecraft voltage

Parameter type 5) can be either parameter type 2) or 3), depending on whether the relationship between the parameter value and spacecraft environment is a known function.

The general rules for developing the design values for the five types of parameters are listed in Table 3-6.

3.4.2 Performance Margins

The performance of a system function can usually be characterized by a single parameter. At some value of this parameter, the performance of the function is at the minimum acceptable level defined by the Project. This is known as the threshold level. The fraction by which the actual parameter value, V_A, differs from the threshold value, V_{TH}, is called the performance margin, PM. Thus,

$$PM = \frac{V_A}{V_{TH}} \quad \begin{cases} \geq 1 \text{ for acceptable performance} \\ < 1 \text{ for unacceptable performance} \end{cases}$$

Table 3-6. General rules for developing parameter design values

Type No.	Parameter type description	Design value development rule
1	Verified and adjusted periodically to within a certain measurement tolerance. e.g.: Ground parameter	Design value is the expected operational value.
2	Vary systematically in well-defined limits. e.g.: Ground station noise temperature	Design value is the lower bound of the parameter value within the operating limits.
3	Vary randomly in well-defined limits. e.g.: Attitude control limit cycle	
4	Constant in flight. e.g.: Antenna pattern	Design value is the expected flight value in the spacecraft ambient environment.
5	Vary with spacecraft environment. e.g.: Spacecraft transmitter power	

3.4.2.1 Carrier Performance Margin. The parameter used to characterize carrier phase tracking performance is the signal-to-noise power ratio in the carrier tracking loop bandwidth (SNR_B). At this value, SNR_{BTH}, the phase jitter in the loop, is at its maximum acceptable value.

The received SNR_B is:

$$SNR_B = \left(\frac{P_T}{N_o B_n}\right)\left(\frac{P_c}{P_T}\right)\Gamma \qquad (3.4\text{-}1)$$

where,

$\frac{P_T}{N_o}$ = Total signal power-to-noise spectral density ratio into the tracking loop

$\frac{P_c}{P_T}$ = Ratio of carrier signal power (power at the carrier frequency) to total signal power into the receiver

B_n = Effective noise bandwidth of the receiver at threshold (= $2B_{LO}$ for a PLL receiver). B_n is rigorously defined in section VIII, below

and

Γ = Limiter loss (fractional gain) due to any limiters which precede the carrier tracking loop. See section IV.

The design carrier performance margin is expressed by:

$$PM = \frac{SNR_B}{SNR_{BTH}} \tag{3.4-2}$$

3.4.2.2 Data Performance Margin. The parameter used to characterize data channel performance is usually the signal-to-noise spectral density ratio (ST/N_o) into the data detector. At a value $(ST/N_o)_{TH}$, the (bit or word) error rate of the data is at the maximum acceptable value defined by the Project.

The actual received ST/N_o is:

$$ST/N_o = \frac{P_T}{N_o}\left(\frac{P_D}{P_T}\right)\eta_{WDL}\eta_{RL}\eta_{SDL}\eta_{BSDL}{}^T \tag{3.4-3}$$

where

$\frac{P_D}{P_T}$ = Ratio of data signal power to total signal power

η_{WDL} = Loss (fractional gain) due to non-ideal subcarrier waveforms. See section V.

η_{RL} = Loss (fractional gain) due to phase jitter in the carrier tracking loop (radio loss). See section V.

η_{SDL} = Loss (fractional gain) due to phase jitter in the subcarrier tracking loop (subcarrier demodulator loss). See section V.

η_{BSDL} = Loss (fractional gain) due to symbol (bit) synchronization errors (bit sync and detection loss). See section V.

and

T = Symbol time (T_S) or bit time (T_B) depending on whether the data is coded or uncoded. T is equal to the reciprocal of the symbol (bit) rate.

The design data performance margin, PM is:

$$PM = \frac{ST/N_o}{(ST/N_o)_{TH}} \qquad (3.4\text{-}4)$$

Similar performance margins are developed for the ranging link. Tables 3-1 through 3-5 are explicit in defining the various performance margins.

Details of the distribution of received power and demodulation losses for the telemetry, command and ranging links are covered in the other sections.

3.4.3 DCT Formats

The formats used for DCT's have been standardized in order to be applicable to all flight projects and yet be flexible enough to reflect accurately the telecommunication performance for each flight project. A recommended set of DCT formats is presented as Tables 3-1 through 3-5 and should be used

G

as a standard starting point for each mission. Separate one page formats are provided for carrier tracking, ranging, telemetry, and command. Each table lists the parameters for these link functions, and contains instructions for computing the appropriate performance measures. Each table is designed to have enough information in it to stand alone, even though the link functions may be interdependent. Room is provided for data which clarify or support certain parameter design values and their tolerances.

The Spacecraft Telecommunications Systems Section has mechanized the preparation of the DCT's with a computer program known as TPAP (Telecommunications Performance and Analysis Program). This program provides a method of quickly updating the tables for changing capabilities and mission profiles and enables preparation of tables for many time points in an efficient manner. The output of TPAP has been formatted for direct use in the Telecommunications Design Control document. Samples of the output and a program description will be found in section IX.

3.4.4 DCT Description, Index, and Calculation Summary

Tables 3-7 through 3-11 present a line-by-line description of the DCT parameters and supplementary data of Tables 3-1 through 3-5, together with the method of calculation (where simple enough) and a guide to locating the parameter descriptions in this handbook.

Table 3-12 is a glossary of the abbreviations used in Tables 3-1 through 3-5 and 3-7 through 3-11.

DESIGN CONTROL TABLE
DESCRIPTION, INDEX AND CALCULATION SUMMARY
TABLE 3-7 THROUGH TABLE 3-11

Table 3-7. Uplink Carrier

a. Total Channel

Number	Parameter	Description	Summary of calculation: Design Value	Summary of calculation: Tolerances: Favorable	Summary of calculation: Tolerances: Adverse	Handbook discussion locations
1	Total Transmitting Power at Antenna (dBm)	Total Power into DSS Antenna in dB relative to 1 mW.	$P_{tr} = 10 \log_{10} P_{tr}(KW.) + 60.$, $P_{tr}(KW.)$ = transmitting power in kilowatts for DSN antenna to be used.	$10 \log P_{trmax} - 10 \log P_{tr}$	$10 \log P_{trmin} - 10 \log P_{tr}$	2.6.3, 2.6.3.1
2	Transmitting Antenna Gain (dB.)	Peak Gain of DSS Antenna. Includes Pointing and Circuit Loss, Wind and Gravity Deformation Loss.	G_t, see DSN documents for Antenna Peak Gain for Azimuth, Elevation, and Wind Loading considered. Includes Circuit Loss and Pointing Loss.	$G_{tmax} - G_t$	$G_{tmin} - G_t$	2.6.3, 2.6.3.2, 7.1.1
3	Space Loss (dB.)	Loss due to transmission medium.	$L_S + L_A = -(32.45 + 20 \log f + 20 \log R) + L_A$ f in MHz, R in km., L_A (<0) is Absorption Loss in dB and depends on frequency.	Tolerances due to uncertainty in L_A. R and f uncertainties are usually negligible $L_{Amin} - L_A$	$L_{Amax} - L_A$	2.6.3, 2.6.3.2
3a	f (MHz.) R (km.)	Frequency of Carrier Spacecraft - Earth Range				8.2.1, 8.2.1.1, 8.2.1.2, 8.2.1.3, 8.2.2
3b	Absorption Loss (dB.)	Space Loss includes factor for losses due to Atmospheric and Plasma Effects	L_A			2.6.3, 2.6.3.5, ff.
4	Polarization Loss (dB.)	Loss due to mismatch between Transmitting and Receiving Antennas' Polarization	DAP Tape: $L_p = 10 \log_{10}\left[\frac{1}{2} + \frac{2R_R R_T}{(1+R_R^2)(1+R_T^2)}\right]$ RCP Relative Patterns: $L'_p = L_p + 10 \log\left[\frac{4(1+R_R^2)(1+R_T^2)}{(1+R_R)^2(1+R_T)^2}\right]$ where, $R_R = 10^{E_R/20}$ is the axial ratio of the receiving antenna in the direction of the transmitting antenna, $R_T = 10^{E_T/20}$ is the axial ratio of the transmitting antenna in the direction of the receiving antenna, and E_R and E_T are the receiving and transmitting antenna ellipticities in those directions.	$-10 \log\left[\frac{1}{2} + \frac{2R_R R_T}{(1+R_R^2)(1+R_T^2)} + \frac{(1-R_R^2)(1-R_T^2)}{2(1+R_R^2)(1+R_T^2)}\right] + L_p$	$-10 \log\left[\frac{1}{2} + \frac{2R_R R_T}{(1+R_R^2)(1+R_T^2)} - \frac{(1-R_R^2)(1-R_T^2)}{2(1+R_R^2)(1+R_T^2)}\right] + L_p$	2.6.3, 2.6.3.3, 7.4, 7.4.1

Table 3-7. Uplink carrier (contd)

Number	Parameter	Description	Summary of calculation			Handbook discussion locations
			Design value	Tolerances		
				Favorable	Adverse	
4a	Ellipticity, Flt. Ant., Grd. Ant. (dB)	A measure of elliptical polarization used to find polarization loss.	$E_{T,R} = 20 \log R_{T,R}$, $R_{T,R}$ = Axial Ratio = maximum electric field/ minimum electric field.			7.4
5	Receiving Antenna Gain (dB)	Gain of the Spacecraft antenna in the direction of the incoming signal.	$G_r = G_{rs} + P_{Lr}$, G_{rs} = Antenna gain on the antenna pattern axis of symmetry (usually the electrical boresight axis). P_{Lr} = pointing loss from that axis.	Tolerances calculated for possible extremes of contributing error sources by varying S/C-Earth Vector over antenna pattern.		2.6.3, 2.6.3.2, 7.1.1, 7.7.1, 7.7.2
5a	Boresight Gain (dB)	Gain of the Spacecraft Antenna in the direction of the antenna pattern axis of symmetry.	G_{rs}			7.1, 7.1.1, 7.1.2, 7.1.2.1
5b	Antenna	Specifies which antenna is considered for the DCT, e.g. High Gain.				
5c	Pointing Error	Angular errors from axis of symmetry and off design S/C-Earth Vector.	Sum of angular errors from design antenna pointing referenced to clock, cone antenna coordinates. Used to calculate pointing loss and tolerances.			2.6.3.2.1, 7.2
	Tracking (cone°, clock°)	Angular position of S/C-Earth Vector measured from antenna axis of symmetry.	Calculated by transformation of Trajectory Data into antenna coordinates. Used to find design pointing loss.			7.2.1
	Limit Cycle (cone°, clock°)	Angular excursion due to worst case limit cycle, measured in antenna coordinates.	Given by Attitude Control and Transformed into antenna coordinates.			7.2.2
	Uncertainty (cone°, clock°)	Angular tolerances due to mechanical and electrical misalignments.	Sum of angular errors contributing to error in antenna pointing which is a function of temperature and S/C attitude			7.2.3
5d	Pointing Loss (dB) (Includes worst case limit cycle)	Deviation of antenna gain from Boresight Gain due to pointing errors evaluated for worst case limit cycle excursion.	$P_{Lr} = G_r$(clock, cone) - G_{rs} where G_r(clock, cone) is the antenna gain at the design S/C-Earth Vector coordinates.			7.3, 7.3.1, 7.3.2
5e	Loss (dB) (no limit cycle)	Pointing Loss calculated for zero limit cycle excursion.				

Table 3-7. Uplink carrier (contd)

Number	Parameter	Description	Summary of calculation			Handbook discussion locations
			Design value	Tolerances		
				Favorable	Adverse	
5f	Loss (dB) (Best limit cycle)	Pointing Loss calculated for minimum possible limit cycle excursion.				
6	Circuit Loss, Antenna to Receiver (dB)	Circuit Loss from the S/C antenna terminals to the receiver case.	L_c, measured or predicted on manufacturer's specification dB. Loss/ft. at f (MHz).	Tolerance on measurement or manufacturing.		2.6.3
7	Total Received Power at Receiver Case (dB.)	Total power into the receiver	$P(T) = P_{tr} + G_t + L_S + L_A + L_p + G_r + L_c = 1 + 2 + 3 + 4 + 5 + 6$	Sum of favorable tolerances $1 + 2 + 3 + 4 + 5 + 6$	Sum of adverse tolerances $1 + 2 + 3 + 4 + 5 + 6$	2.6.3
8	System Noise Spectral Density/ System Gain (dBm/Hz)	Gaussian white noise power per Hz introduced by the environment, cabling, switches, antenna, and receiver divided by the system gain prior to the detector, and following the receiver case.	$N_o/G_S = 10 \log k T_{es} L_c$, where $k = 1.38 \times 10^{-20}$ mW - sec/°K, T_{es} = effective system noise temperature.	$10 \log k T_{emin} - N_o/G_S$	$10 \log k T_{emax} - N_o/G_S$	2.6.3.4, 2.6.3.4.1, 2.6.3.4.1.2
8a	Noise Figure (dB.)	Ratio of input SNR to output SNR for receiver with input terminals at T_o	Noise Figure = $10 \log F$.	Measurement error or mfr. tolerances, temperature of receiver, supply voltage, age	Measurement error or mfr. tolerances, temperature of receiver, supply voltage, age	2.6.3.4.1.1
8b	System Noise Temperature °K	Temperature at antenna input which would result in N_o at detector input (i.e., system noise temp. referenced to antenna input)	$T_{es} = T_a + T_c(\frac{1}{L_c} - 1) + \frac{T_o(F-1)}{L_c}$ where T_a = antenna noise temperature, T_c = cable physical temperature, T_o = 290°K, and F = receiver noise figure measured at T_o			2.6.3.4.1, 2.6.3.4.1.2, 2.6.3.4.1.3
8c	Antenna Temperature (°K)	Noise Spectral Density measured at antenna terminals divided by Boltzman's Constant.	$T_a = \frac{\int_{4\pi} T(\Omega)\, G(\Omega)\, d\Omega}{\int_{4\pi} G(\Omega)\, d\Omega} + T_M$			7.5

Table 3-7. Uplink carrier (contd)

Number	Parameter	Description	Summary of calculation			Handbook discussion locations
			Design value	Tolerances		
				Favorable	Adverse	
			where Ω is solid angle, $T(\Omega)$ is the blackbody temperature of the environment, $G(\Omega)$ is the antenna pattern, and T_M includes noise power due to connectors, seams, etc. in the antenna.			
9	Power to Noise Spectral Density Ratio (dB Hz)	Ratio of Total power to Noise Spectral Density at the input of the detector.	$\frac{P(T)G_S}{N_o} = \frac{P_T}{N_o}$ = 7-8	Sum of favorable tolerances 7-8	Sum of adverse tolerances 7-8	2.6, 2.6.1, 2.6.3.4.1.3, 5.4.1, 5.6.3.2, 5.6.4.1
			b. Carrier Channel			
10	Carrier Power/ Total Power (dB.)	The allocation of power to the carrier as a fraction of total power (in dB.) (Carrier tracking loop BW $\ll$ modulation frequencies)	$P_C/P_T = 10 \log f(\theta_{CMD})$ where $f(\cdot)$ depends on the modulation scheme and the waveform of the subcarrier	Tolerances calculated for possible extremes of modulation index values.		5.4.2
10a	$\theta_{CMD}(^\circ)$, K, T_{CMD}	Command channel modulation index, modulator sensitivity, peak modulator drive voltage	$\theta_{CMD} = T_{CMD}K$ where K = modulator sensitivity ($^\circ$/VOLT) and T_{CMD} = voltage of modulator driving command signal	$\pm\Delta\theta_{CMD} = \pm\Delta T_{CMD}K \pm T_{CMD}\Delta K \pm\Delta T_{CMD}\Delta K$ where ΔT_{CMD} and ΔK are uncertainties in T_{CMD} and K due to temperature and other effects.		5.2.1.1, 5.4.2, 5.6.3, 5.6.4.2
	P_{CMD}/P_T (dB)	The allocation of power to the command channel as a fraction of total power (in dB)	$P_{CMD}/P_T = 10 \log g(\theta_{CMD})$ where $g(\cdot)$ depends on the modulation scheme and the waveform of the subcarrier $f(\theta_{CMD}) + g(\theta_{CMD}) = 1$	Tolerances calculated for possible extremes of modulation index values		6.3.2.1.1, 6.3.2.2.1, 6.3.2.3.3
	$\theta_R(^\circ)$, T_R	Ranging channel modulation index, peak modulator drive voltage	$\theta_R = T_R K$, T_R = voltage of modulator-driving ranging signal.	$\pm\Delta\theta_R = \pm\Delta T_R K \pm T_R\Delta K \pm\Delta T_R\Delta K$		5.2.1.1, 5.4.2, 5.6.3
	Ranging Suppression (dB) (Carrier and data channel)	Factor which is added to parameter 10 and to P_{CMD}/P_T to reflect the decreased carrier and data power available when ranging is "on".	$10 \log \cos^2\theta_R$	Parameter for reference only, as tolerances are changed by adding ranging modulation to uplink signal		A5.2.5, A5.2.7
11	Limiter Loss (dB)	Loss due to limiter on input to S/C carrier tracking PLL.	Limiter Loss, Γ, is a function of signal-to-noise ratio at the limiter input, 9 + 10	Tolerances calculated using tolerances on 9 + 10		4.3.3.3

Table 3-7. Uplink carrier (contd)

Number	Parameter	Description	Summary of calculation			Handbook discussion locations
			Design value	Tolerances		
				Favorable	Adverse	
12	Carrier Threshold Tracking Bandwidth ($2B_{Lo}$) (dB Hz)	Noise bandwidth of carrier tracking loop for design point (threshold) P_T/N_o.	Specified and measured 2 B_{Lo} (dB Hz) = 10 log 2 B_{Lo}(Hz)	Specified and measurement error	Specified and measurement error	4.3.1, 4.3.3.4
13	$SNR_{2B_{Lo}}$ (dB)	Signal-to-noise power ratio into the S/C carrier tracking PLL for a bandwidth of $2B_{Lo}$.	$SNR_{2B_{Lo}} = \frac{P_T}{N_o} + \frac{P_c}{P_T} + \Gamma - 2\ B_{Lo}$ $= 9 + 10 + 11 - 12$	Sum of favorable tolerances 9 + 10 + 11 + 12	Sum of adverse tolerances 9 + 10 + 11 - 12	3.4.2, 4.3.3
14	Threshold $SNR_{2B_{Lo}}$ (dB)	Minimum SNR in $2B_{Lo}$ (minimum parameter 13) acceptable for the required accuracy of carrier tracking.	$SNR_{2B_{Lo}}$ corresponding to the maximum acceptable phase jitter $\sigma = f(SNR_{2B_{Lo}})$	Theoretical value, no tolerances		3.4.2, 4.3.3.4
	1σ phase jitter (°rms)	Maximum acceptable phase error standard deviation				4.3.3.1, 4.3.3.3, 4.3.3.5, 4.3.3.6
15	Carrier margin (dB)	Power margin above minimum acceptable value for proper carrier tracking.	Margin = $SNR_{2B_{Lo}} - (SNR_{2B_{Lo}})_{TH}$	Sum of favorable tolerances 13 - 14	Sum of adverse tolerances 13 - 14	3.4.2

Table 3-8. Downlink carrier

a. Total Channel

Number	Parameter	Description	Summary of calculation			Handbook discussion locations
			Design value	Tolerances		
				Favorable	Adverse	
1	Total Transmitting Power at radio case (dBm)	Total power out of S/C transmitter terminals measured relative to 1 mw.	$P_{tr} = P_{TWTA} + L_{C1}$	$P_{trmax} - P_{tr}$	$P_{trmin} - P_{tr}$	2.6.3, 2.6.3.1
1a	TWTA (dBm)	Output power measured at Traveling Wave Tube Amplifier	$P_{TWTA} = 10 \log P_{TWTA}(w) + 30$ measured	$P_{TWTAmax} - P_{TWTA}$	$P_{TWTAmin} - P_{TWTA}$	2.6.3.1
1b	Circuit loss to case (dB).	Loss between TWTA terminals and transmitter case	L_{C1}, measured	Specification or statistics	Specification or statistics	2.6.3.1
2	Circuit loss to antenna (dB)	Loss between receiver case and antenna terminals, including impedance mismatch losses.	$L_{C2} = L_{C3} + L_{MM}$, L_{C3} = measured circuit loss, L_{MM} = mismatch loss, predicted from VSWR	Specification or statistics	Specification or statistics	2.6.3.1
2a	Mismatch loss (dB)	Loss between receiver and antenna due to impedance mismatching. Represents a reflection of usable power.	$L_{MM} = 10 \log (1 - \lvert\rho\rvert^2)$ where $\lvert\rho\rvert = \left\lvert \frac{\text{Reflected Voltage}}{\text{Incident Voltage}} \right\rvert = \frac{VSWR - 1}{VSWR + 1}$	Specification or statistics	Specification or statistics	2.6.3.1
2b	VSWR (%)	Voltage standing wave ratio	$VSWR = \frac{1}{100} VSWR(\%) = \frac{1 + \lvert\rho\rvert}{1 - \lvert\rho\rvert}$	Specification or statistics	Specification or statistics	2.6.3.1
3	Transmitting Antenna Gain (dB)	Gain of S/C antenna in the direction of the receiving antenna	$G_t = G_{ts} + P_{Lt}$	—	—	2.6.3, 2.6.3.2, 7.1.1
3a-3f	See Table 3-7, Uplink Carrier DCT, parameters 5a-5f					
4, 4a, 4b	Space Loss. See Table 3-7, Uplink Carrier DCT, parameters 3, 3a, 3b	—	—	—	—	—
5, 5a	Polarization Loss See Table 3-7, Uplink Carrier DCT, parameters 4, 4a	—	—	—	—	—

Table 3-8. Downlink carrier (contd)

Number	Parameter	Description	Summary of calculation			Handbook discussion locations
			Design value	Tolerances		
				Favorable	Adverse	
6	Receiving Antenna Gain (dB)	Peak gain of DSS Antenna Includes Pointing and Circuit Loss, Wind and Gravity Deformation Loss.	$G_r = G_{rz} + L_c + L_D + L_{pt}$ G_{rz} = Antenna gain at Zenith with no circuit loss	$G_{rmax} - G_r$	$G_{rmin} - G_r$	2.6.3, 2.6.3.2, 7.1.1 7.1, 7.1.1, 7.1.2
6a	Pointing and Circuit Loss (dB)	Loss due to mispointing of DSS Antenna and circuit loss between antenna terminals and MASER input flange	L_c, circuit loss L_{pt}, pointing loss			2.6.3
6b	Surface Deformation Loss		$L_D = L_W + L_G$			2.6.3.2
	Wind Loss (dB)	Loss due to wind loading on antenna surface, varies with wind speed and elevation angle	L_W			
	Low Elevation Loss (dB)	Loss due to gravity loading on antenna surface	L_G, since the antenna has a 45° Elevation angle design point, L_G is a gain near an elevation angle of 45°			
7	Total received power at MASER input flange	Total power into the MASER	$P(T) = P_{tr} + G_t + L_s + L_A + L_p + G_r = 1 + 2 + 3 + 4 + 5 + 6$	Sum of favorable tolerances 1 + 2 + 3 + 4 + 5 + 6	Sum of adverse tolerances 1 + 2 + 3 + 4 + 5 + 6	2.6.3
8	System Noise Spectral Density/ System Gain (dbm/Hz)	Gaussian white noise power per Hz introduced by the environment, cabling, switches, antenna, and MASER, divided by the System Gain prior to the detector and after the MASER input flange	$N_o/G_{SM} = 10 \log k T_{es}$, where $k = 1.38 \times 10^{-20}$ mW-sec./°K where G_{SM} = system gain prior to the detector and after the MASER input flange	$10 \log k T_{emax} - N_o/G_{SM}$	$10 \log k T_{emin} - N_o/G_{SM}$	2.6.3.4, 2.6.3.4.1, 2.6.3.4.1.2, 2.6.3.4.1.3, 2.6.3.4.1.4
8a	Elevation (°), Azimuth (°)	Elevation and Azimuth angles of the DSS antenna (determines the ground interception by the antenna side lobes).	Given in trajectory data.			

Table 3-8. Downlink carrier (contd)

Number	Parameter	Description	Summary of calculation			Handbook discussion locations
			Design value	Tolerances		
				Favorable	Adverse	
8b	System Noise Temperature (°K)	Temperature, referenced to MASER input, which would result in N_o at detector input	T_{es} = effective system noise temperature referenced to antenna input multiplied by the circuit loss between the antenna terminals and the MASER input flange. $T_{es} \triangleq T_{ez} + \Delta T_e(az, el)$	Measurement error and weather	Measurement error and weather	2.6.3.4.ff, 7.5
8c	Zenith Noise Temperature (°K)	Noise Temperature of DSS System with the antenna pointed at the vertical and looking at "cold sky", referenced to maser input.	T_{ez}	Measurement error and weather	Measurement error and weather	2.6.3.4.1.4
9	Power to Noise Spectral Density Ratio (dBHz)	Ratio of Total power to Noise Spectral Density at the input to the detector	$\frac{P(T)G_{SM}}{N_o} = \frac{P_T}{N_o}$ = 7 - 8	Sum of favorable tolerances 7 - 8	Sum of adverse tolerances 7 - 8	2.6, 2.6.1, 2.6.3.4, 3.4.2, 5.4.1, 5.6.3.2, 5.6.4.1, A5.3.2
			b. Carrier Channel			
10	Carrier Power/ Total Power (dB)	The allocation of power to the carrier as a fraction of total power (in dB)	P_c/P_T = 10 log $f(\theta_1, \theta_2)$ where $f(\cdot,\cdot)$ depends on the modulation scheme and the waveforms of the subcarriers.	Tolerances calculated for possible extremes of modulation index values.		5.4.2, 5.4.3
10a	$\theta_1(°)$, $\theta_2(°)$, K, T_1, T_2	Data channels 1 and 2 modulation indices, modulator sensitivity. Channels 1 and 2 peak modulator drive voltage.	θ_1, = T_1K, θ_2 = T_2K, where K = modulator sensitivity (°/volt) and $T_{1,2}$ = voltage of modulator-driving data signal (1 or 2).	$\pm\Delta\theta_{1,2} = \pm\Delta T_{1,2}K \pm T_{1,2}\Delta K \pm \Delta T_{1,2}\Delta K$ where $\Delta T_{1,2}$ and ΔK are uncertainties in $T_{1,2}$ and K due to temperature and other effects.		5.2.1.1, 5.4.2, 5.6.3, 5.6.4.2, A5.3
	P_{D1}/P_T(dB), P_{D2}/P_T(dB)	The allocation of power to data channels 1 and 2 as fractions of total power (in dB)	$P_{D1,D2}/P_T$ = 10 log $g_{1,2}(\theta_1, \theta_2)$ where $g_{1,2}(\cdot,\cdot)$ depend on the modulation scheme and the waveforms of the subcarriers.	Tolerances calculated for possible extremes of modulation index values.		5.4.2, 5.4.3
	$\theta_R(°)$, T_R	Ranging channel modulation index, peak modulator drive voltage	θ_R = T_RK, T_R = voltage of modulator-driving ranging signal	$\pm\Delta\theta_R = \pm\Delta T_R K \pm T_R\Delta K \pm \Delta T_R\Delta K$		5.4.2, 5.6.3, 5.6.4.2

Table 3-8. Downlink carrier (contd)

Number	Parameter	Description	Summary of calculation			Handbook discussion locations
			Design value	Tolerances		
				Favorable	Adverse	
11	Limiter Loss (dB) See Table 3-7, Uplink Carrier DCT, parameter 11		Limiter Loss, Γ, is a function of 9 + 10	Tolerances calculated using tolerances on 8 + 9.		4.3.3.3
12a	Uplink VCO Jitter Loss in 2-way (dB).	Loss in SNR for DSS carrier tracking loop due to uplink jitter in S/C PLL when in 2-way tracking mode (2-way radio loss)	Carrier Suppression is a function of phase jitter in S/C received carrier and depends on uplink carrier power received at the S/C and ratio of S/C and ground $2B_L$'s.	Tolerances calculated using uplink parameters.		5.4.5.1
12b	Auxiliary Oscillator Jitter Loss in 1-way (dB)	Loss in SNR for DSS carrier tracking loop due to jitter in auxiliary S/C oscillator frequency source. Applicable to 1-way tracking (1-way radio loss).	Carrier Suppression is a function of phase jitter in aux. osc. on S/C and ground $2B_L$.	Tolerances calculated using aux. osc. performance.		4.3.3.6, 5.4.5.1
13	Carrier Threshold Tracking Bandwidth ($2B_{LO}$) (dBHz). See Table 3-7. Uplink Carrier DCT parameter 12 for DSS.	—	—	—	—	—
14	$SNR_{2B_{LO}}$ (dB)	Signal-to-noise power ratio into the DSS carrier tracking loop for a bandwidth of $2B_{LO}$.	$SNR_{2B_{LO}} = \frac{P_T}{N_o} + \frac{P_c}{P_T} + \Gamma + \text{Jitter}$ Loss - $2B_{LO}$ = 9 + 10 + 11 + 12 - 13 where 12a or b is chosen according to the mode of interest	Sum of favorable tolerances 9 + 10 + 11 + 12 - 13	Sum of adverse tolerances 9 + 10 + 11 + 12 - 13	3.4.2, 4.3.3
15	Threshold SNR $SNR_{2B_{LO}}$ (dB). See Table 3-7, Uplink Carrier DCT, parameter 14	—	—	—	—	—
16	Carrier margin (dB). See Table 3-7, Uplink Carrier DCT, parameter 15	—	—	—	—	—

Table 3-9. Telemetry

a. Total Channel

Number	Parameter	Description	Summary of calculation			Handbook discussion locations
			Design value	Tolerances		
				Favorable	Adverse	
1-9	See Table 3-8, Downlink Carrier DCT, parameters 1-9.	—	—	—	—	—
	b. Data One Channel					
10	Data Power/Total Power. See Table 3-8, Downlink Carrier DCT, parameter 10a	—	—	—	—	—
11	Waveform Distortion Loss (dB)	Loss due to a non-ideal subcarrier waveform resulting in a mismatched SDA filter.	η_{WDL}, waveform distortion loss is a function of actual subcarrier waveform and the SDA demodulation process.	Specification on waveform asymmetry rise time, fall time, etc.		5.3.1, 5.3.4, 5.3.4.2 5.4.6, 5.4.6.1
12	Radio Loss (dB)	Loss due to jitter in DSS carrier tracking loop	η_{RL}, depends on mode (1-way or 2-way), DSS carrier tracking loop bandwidth, data rate, and SNR in receiver loop bandwidth	Tolerances calculated from Downlink Carrier DCT tolerances and Uplink Carrier DCT tolerances		5.4.5, 5.4.5.1, 5.6.4.3, A5.1
12a	Downlink: $2B_{LO}$, $SNR_{2B_{LO}}$. See Table 3-8, Downlink Carrier DCT, parameters 13, 14					
12b	Uplink: $2B_{LO}$, $SNR_{2B_{LO}}$. See Table 3-7, Uplink Carrier DCT, parameters 12, 13					
13	Subcarrier Demodulator Loss (dB)	Loss due to jitter in SDA subcarrier tracking loop	Analogous to Radio Loss $= \eta_{SDL}$			5.4.5, 5.4.5.2, 5.6.4.3, A5.1
14	Bit Sync/Detection Loss (dB)	Loss due to symbol synchronization errors	Depends on timing error and signal energy to-noise spectral density ratio into the symbol sync loop. $= \eta_{BSDL}$	Tolerances calculated from specifications and tolerances on signal energy-to-noise spectral density ratio.		5.4.5, 5.4.5.3, 5.6.4.3, A5.1

Table 3-9. Telemetry (contd)

Number	Parameter	Description	Summary of calculation			Handbook discussion locations
			Design value	Tolerances		
				Favorable	Adverse	
15	Bit Rate (dB bps) _____bps	Bit rate (in dB) for Data Channel 1. Bit rate (in bits/sec) for Data Channel 1.	10 log (bit rate), bit rate in bits per second. Bit rate = $1/T_{B1}$ where T_{B1} = bit time	Tolerances are negligible		5.3.2, 5.4.1, 5.5, 5.6.3, 5.6.3.1, 5.6.3.2, 5.6.5, A5.2, 8.3.4.2
16	Received ST_B/N_o (dB)	Received signal energy-to-noise spectral density ratio out of bit sync loop	$ST_B/N_o = \frac{P_T}{N_o} + \frac{P_D}{P_T} + \eta_{WDL} + \eta_{RL} + \eta_{SDL} + \eta_{BSDL} + T_{B1}$ = 9 + 10 + 11 + 12 + 13 + 14 - 15	Sum of favorable tolerances 9 + 10 + 11 + 12 + 13 + 14 - 15	Sum of favorable tolerances 9 + 10 + 11 + 12 + 13 + 14 - 15	5.4.1, 5.4.4
17	Threshold ST_B/N_o (dB)	Minimum acceptable ST_B/N_o, at this value the error rate (word or bit) is its maximum permissible value	$(ST_B/N_o)_{TH} = f(ER)$	Theoretical Value, no tolerances		3.4.2, 5.3.2 5.3.3.1, 5.3.5.1, 5.4.4, 5.5
	ER	Error Rate which results in the given threshold.	ER = P_E, the probability of bit or word error	Project Determined, no tolerances		3.4.2, 5.3.1, 5.3.2, 5.3.3.1, 5.3.3.2.1.1, 5.3.3.2.1.2, 5.3.3.2.1.3, 5.3.5, 5.3.5.1, 5.4.4, 5.5
18	Performance Margin (dB)	Data Channel 1 margin of ST_B/N_o for acceptable data return	Margin = $ST_B/N_o - (ST_B/N_o)_{TH}$ = 16 - 17	Sum of favorable tolerances 16-17	Sum of adverse tolerances 16-17	3.4.2
c. Data Two Channel						
19-27	See above, Data One Channel Parameters 10-18 for Data Two Channel	—	—	—	—	—

Table 3-10. Single-channel command

a. Total Channel

Number	Parameter	Description	Summary of calculation			Handbook discussion locations
			Design value	Tolerances		
				Favorable	Adverse	
1-9	See Table 3-7, Uplink Carrier DCT, parameters 1-9	–	–	–	–	–
b. Command Channel						
10	Data Power/Total Power See Table 3-7. Uplink Carrier DCT, parameter 10a	–	–	–	–	–
11	Waveform Distortion Loss. See Table 3-9, Parameter 11 for Command Uplink	–	–	–	–	–
12	Radio Loss. See Table 3-9, Parameter 12 for Command Uplink	–	–	–	–	–
13	Subcarrier Demod Loss (dB)	Loss due to jitter in subcarrier tracking loop	Analogous to radio loss = η_{SDL}			6.3.2.2.2.1, 6.3.2.3.4.3
14	Bit Sync/Detection Loss (dB)	Loss due to symbol synchronization errors	Depends on timing error and signal energy-to-noise spectral density ratio into the symbol sync loop = η_{BSDL}	Tolerances calculated from specifications and tolerances on signal energy-to-noise spectral density ratio		6.3.2.2.2.2
15	Circuit Loss (dB)	Losses due to other circuit elements such as filters, cables, A/D converters (digital system)	Measured and calculated for particular elements = η_c	Measured, specified and calculated for specific elements		6.3.2.3.4.1, 6.3.2.3.4.2
16-19	See Table 3-9, Telemetry DCT Parameters 15-18 for Command Uplink	–	–	–	–	-

Table 3-11 Ranging

a. Uplink Total Channel

Number	Parameter	Description	Summary of calculation: Design value	Summary of calculation: Tolerances: Favorable	Summary of calculation: Tolerances: Adverse	Handbook discussion locations
1-9	See Table 3-7, Uplink Carrier DCT, parameters 1-9	–	–	–	–	–
	b. Spacecraft Turnaround Channel					
10	Ranging Power/ Total Power (dB.)	The allocation of power to the ranging channel as a fraction of total power (in dB.)	$P_R/P_T = 10 \log \sin^2\theta_R$ for square wave ranging signals	Tolerances calculated for possible extremes of modulation index values.		5.4.2
10a	$\theta_R, K, T_R, P_C/P_T, \theta_{CMD}, T_{CMD}$ see Table 3-7, Uplink Carrier DCT, parameters 10, 10a		$P_C/P_T = 10 \log \cos^2\theta_R$			
	Command Suppression (dB.) (Carrier and ranging channels)	Factor which is added to parameter 10 and P_C/P_T to reflect the decreased carrier and ranging power available when command modulation is applied.	$10 \log f(\theta_{CMD})$, where $f(\cdot)$ depends on the modulation scheme and the waveform of the subcarrier	Parameter for reference only, as tolerances are changed by command modulation addition.		As in A5.2.5 for command
11	Uplink radio loss. See Table 3-9, Telemetry DCT, parameter 12 for uplink.	–	η_{RL} –	–	–	–
12	Ranging Noise Bandwidth (dBHz)	S/C Transponder noise bandwidth.	$10 \log B_{nR}$(Hz), B_{nR} is typically 1.5×10^6 Hz for Mariner Type S/C	$10 \log B_{nRmin} - 10 \log B_{nR}$ Assumes that B_{nRmin} does not cut off ranging signal power	$10 \log B_{nRmax} - 10 \log B_{nR}$ Assumes that B_{nRmax} does not gain ranging signal power	2.6.3.4, 8.3.3
13	SNR in Ranging Noise Bandwidth (dB.)	Signal-to-Noise Power Ratio in S/C Ranging Transponder, prior to limiter.	$SNR_{B_{nR}} = \frac{P_T}{N_o} + \frac{P_R}{P_T} + \eta_{RL} - B_{nR}$ $= 9 + 10 + 11 - 12.$	Sum of favorable tolerances 9 + 10 + 11 - 12	Sum of adverse tolerances 9 + 10 + 11 - 12.	As in 3.4.2 for ranging, 8.3.3

Table 3-11 Ranging (contd)

Number	Parameter	Description	Summary of calculation			Handbook discussion locations
			Design value	Tolerances		
				Favorable	Adverse	
14	Limiter Suppression (dB.)	Ranging Power/Ranging Power + Noise Power at Limiter Output.	$\Gamma = 10 \log \left(\frac{P_R}{P_R + N_o B_{nR}} \right)$ where ( ) is a function of SNR in B_{nR}.	$\Gamma\ (SNR_{max}) - \Gamma$	$\Gamma\ (SNR_{min}) - \Gamma$	4.3.3.3
	c. Downlink Total Channel					
15-23	See Table 3-8, Downlink Carrier DCT, parameters 1-9	–	–	–	–	–
	d. Ranging Channel					
24	Ranging Power/ Total Power (dB.)	Since Telemetry is usually not turned off, it is included in the ranging DCT expression for P_R/P_T	$P_R/P_T = 10 \log \sin^2\theta_R + 10 \log f(\theta_1, \theta_2)$	Tolerances include Telemetry mod. index variations.		5.4.2
24a	$\theta_1(°)$, $\theta_2(°)$, K, T_1, T_2, P_C/P_T(dB) See Table 3-8. Downlink Carrier DCT, parameters 9, 9a		$P_C/P_T = 10 \log \cos^2\theta_R + 10 \log f(\theta_1, \theta_2)$			
	Telemetry Suppression (dB.) (Carrier and ranging)	Factor which is added to parameter 23 and P_C/P_T to reflect the decreased carrier and ranging power available for the particular telemetry mode being used.	$10 \log f(\theta_1, \theta_2)$, where $f(\cdot, \cdot)$ depends on the modulation scheme and the waveforms of the subcarriers.			As in A5.2.5 for telemetry
25	Limiter Suppression (dB.) See above, parameter 14	–	–	–	–	–
26-26a	Two-Way Radio Loss (dB.) See Table 3-9, Telemetry DCT, parameters 12, 12a	–	η_{RL} –	–	–	–

Table 3-11. Ranging (contd)

Number	Parameter	Description	Summary of calculation			Handbook discussion locations
			Design value	Tolerances		
				Favorable	Adverse	
27	Received Ranging P_R/N_o (dB.)	Ranging Signal Power-to-Noise Spectral Density Ratio on the ground	$P_R/N_o = \frac{P_T}{N_o} + \frac{P_R}{P_T} + \Gamma + \eta_{RL}$ $= 23 + 24 + 25 + 26$	Sum of favorable tolerances 23 + 24 + 25 + 26	Sum of adverse tolerances 23 + 24 + 25 + 26	As in 3.4.2
28	Threshold Ranging P_R/N_o (dB.)	P_R/N_o required for an acquisition time T_{acq} with 0.95 probability	$(P_R/N_o)_{TH} = 36.58 - 10 \log T_{acq}$ for composite coded ranging system (Tau) $(P_r/N_o)_{TH} = 18.69 - 10 \log T_{acq}$ for sequentially coded ranging system (Mu) where T_{acq} is in seconds, and minimum T_{acq} is 80 seconds.	No tolerances, theoretical value.		8.3.3
28a	____Ranging System	Mu, Tau, or Mk I				
28b	T_{acq} =____(sec)	Time to acquire with 0.95 probability	Specified by project			8.3.3 8.3.3
29	Performance Margin (dB.)	Margin in P_R/N_o for 95% probability of correct acquisition of the ranging code in T_{acq} or less.	Margin = $P_R/N_o - (P_R/N_o)_{TH}$ $= 27 - 28$	Tolerances equal to tolerances on P_R/N_o, parameter 27, above		3.4.2

Table 3-12. Glossary of Abbreviations

Abbreviation	Complete Word(s)
ant.	antenna
aux. osc.	auxiliary oscillator
bps	bits per second
BW	bandwidth
ch	channel
cir	circuit
CMD	command
den	density
elev.	elevation
ER	error rate
flt.	flight
grd.	ground
incl	includes
inp	input
MSR	MASER
pwr	power
R	refers to ranging
rang	ranging
rcvd	received

Abbreviation	Complete Word(s)
rcvr	receiver
rms	root mean square
S/C	spacecraft
SNR	signal-to-noise power ratio
spec	spectral
suppr	suppression
sys	system
T	refers to total
temp	temperature
tot	total
trkg	tracking
TWTA	traveling-wave tube amplifier
VCO	voltage-controlled oscillator
VSWR	voltage standing wave ratio
Θ	a modulation index
σ	standard deviation
1-way	one-way tracking
2-way	two-way tracking
subscripts 1, 2	refers to data channel 1 or 2

REFERENCES

3-1. Gilchriest, C. E., and M. K. Tam, The Probability Density Function of a Hardware Performance Parameter, Jet Propulsion Laboratory Technical Memorandum 33-439, September 1, 1970.

APPENDIX A3.1

TOLERANCE SPECIFICATION OF A HARDWARE PARAMETER

A3.1.1 TOLERANCE SPECIFICATION

The procurement specification of an element must be consistant with the specification of the design value for its performance. That is, the expected value of the performance measure for specified environmental conditions (temperature, pressure, voltage, etc.). Prior to procurement the probability distribution of performance may be estimated by the methods of Reference 3-1. Design value and tolerances may be derived from these estimated distributions. When hardware is completed and delivered the design value and tolerances are initially developed in the following manner.

Usually the procurement specification consists of specifications of a performance measure at expected and at worst-case environmental conditions. The element qualification is based on its performance at the worst-case conditions.

A batch of N elements that have passed qualification would typically have the performance distributions shown in Figures A.3.1-1, A3.1-2, and A3.1-3.

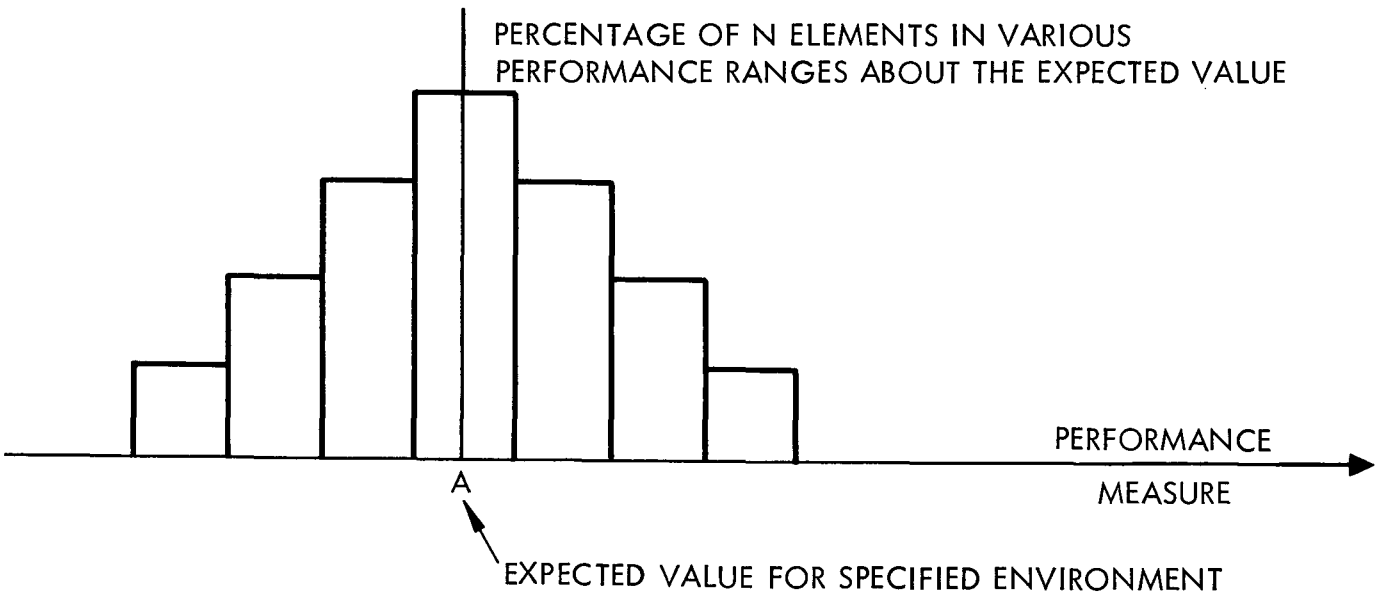

Fig. A3.1-1. Element performance distribution for specified environmental conditions

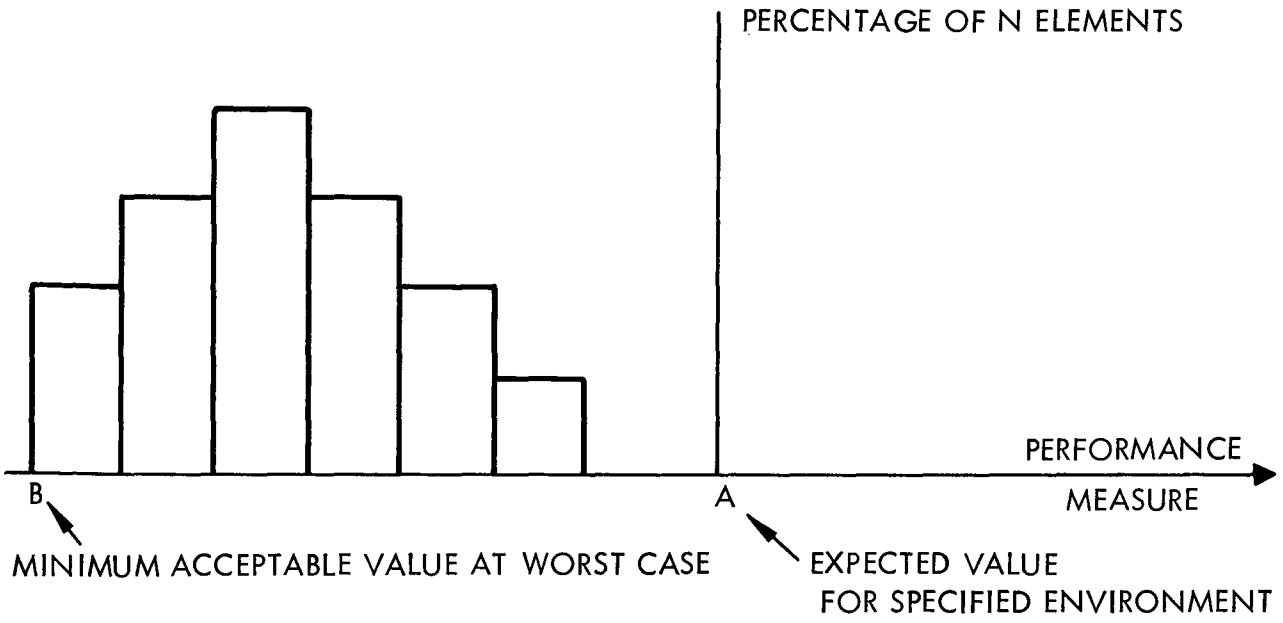

Fig. A3.1-2. Element performance distribution for worst-case environmental conditions

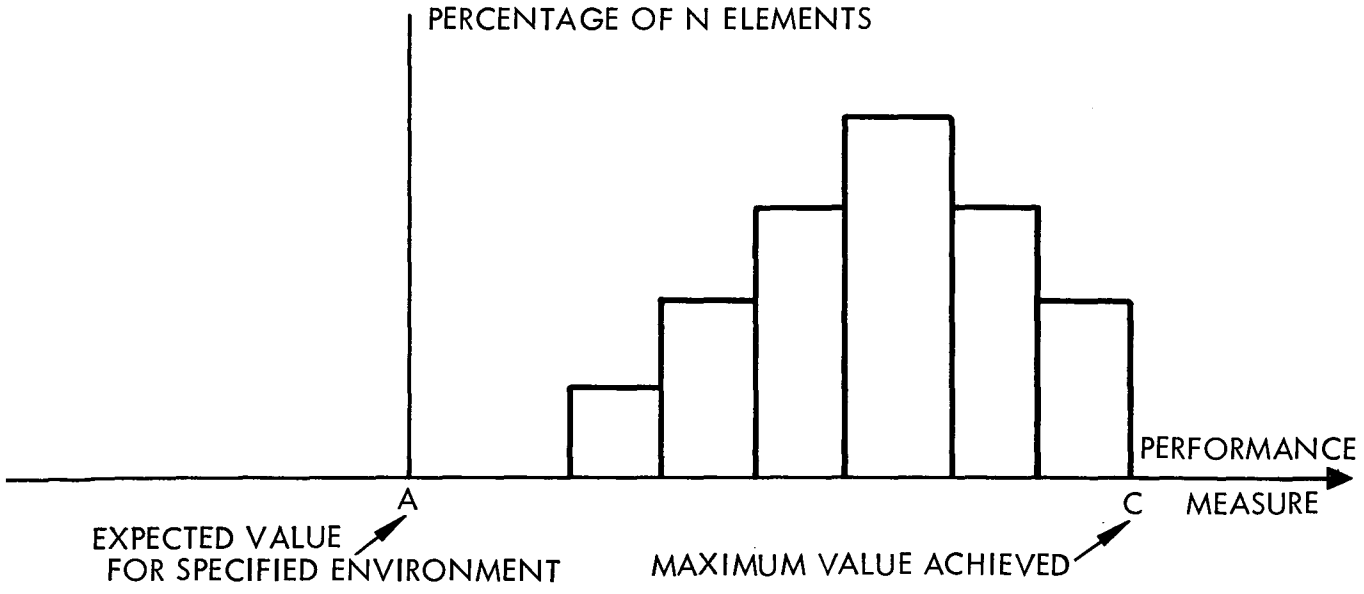

Fig. A3.1-3. Element performance distribution for best-case environmental conditions

The design value is point A in Figures A3.1-2 and A3.1-3. The adverse tolerance is B/A. The favorable tolerance is C/A. Notice that during the system design phase, the tolerances cover extreme environmental conditions, measurement uncertainty and manufacturer variability.

In some instances, the procurement specification may include an incentive clause associated with achievement of better than minimum performance at worst-case conditions. This type of specification normally would tend to move all the distributions shown to the right. Any additional knowledge of procurement history along these lines that may bias the expected value should be factored in the initial specification of the performance design value, if possible. Reference 3-1 gives information on predicting the performance of future hardware procurements.

The same specification techniques are used for each element. The combined design values of power gains, and losses make up the design performance prior to measurement. The independent tolerances of power, gain, and losses are added linearly to form tolerances on design performance. However, any correlation or cancelling effect of one tolerance with another is to be taken into consideration.

SECTION IV

RADIO TRACKING

4.1 INTRODUCTION

The purpose of a radio tracking system is to obtain and maintain radio contact with a spacecraft in order to command, receive data from, and discern the trajectory of the vehicle. The technique used by the DSN for tracking deep space vehicles is to employ, both in the spacecraft and on the ground, phase-lock loop (PLL) receivers which track the phase of the carrier component of the received signal. The PLL generates a reference signal which is phase coherent with the received carrier. This reference is then used in the spacecraft receiver to demodulate the command and ranging signals, and provide a reference for generating a downlink carrier which is phase coherent with the uplink carrier but shifted in frequency by the spacecraft transponder. On the ground, the PLL generates a reference signal which is phase coherent with the downlink signal. This reference is used to demodulate the telemetry subcarriers, obtain Doppler shift data, and demodulate the ranging signal which was transmitted to the spacecraft.

The project typically will use radio tracking data for determining the spacecraft trajectory [Orbit Determination (OD) process] and for making radio science measurements during such times as planetary occultation and superior conjunction.

The purpose of this section is threefold, as follows:

1) To describe the tracking system
2) To characterize the process of obtaining the phase reference of a received carrier signal
3) To characterize the quality of Doppler and range measurements made by the DSN

This information should be used by the telecommunication system designer to establish and achieve a prescribed quality of tracking data for his flight project.

4.2 TRACKING SYSTEM DESCRIPTION

Figure 4-1 is a functional diagram of the tracking system, including elements of both the spacecraft and the DSN. As shown, the DSN utilizes antennas, receivers, a frequency timing standard, and other assemblies in deep space stations of the Deep Space Instrumentation Facility (DSIF) to receive and track the signal transmitted by the spacecraft. Two modes of tracking are typical. One-way tracking occurs when the spacecraft carrier is generated by an auxiliary crystal oscillator (aux. osc.). The carrier may be modulated with telemetry data, and is amplified prior to transmission to Earth. Two-way tracking occurs when a deep space station generates an uplink carrier signal using a stable frequency standard, the spacecraft tracks the uplink signal and derives a signal which is an estimate of the received carrier phase and frequency, and this signal is used to drive the spacecraft exciter. The carrier thus generated may be modulated with telemetry or ranging signals, amplified, and retransmitted to Earth. The deep space station then receives and tracks the downlink signal, derives a signal which is an estimate of the phase of the received downlink carrier, and compares this signal with the transmitted signal to obtain a measure of the Doppler shift in frequency due to the spacecraft radial velocity. The deep space stations may also modulate the uplink signal with a ranging code. This code is retransmitted by the spacecraft to Earth where it is detected and compared with the phase of the transmitted code to obtain a measure of the range of the spacecraft.

Figures 4-2 and 4-3 are more detailed diagrams of the tracking system configurations used in the 26-m and 64-m deep space stations.

4.3 PHASE-LOCK LOOP RECEIVER CHARACTERISTICS

Phase-lock loop receivers of the double-conversion heterodyne type, are employed by the DSIF and compatible spacecraft. The DSIF receiver configuration is shown in Figure 4-4, and a typical spacecraft receiver in Figure 4-5. These receivers operate at S- and/or X-band and utilize automatic gain control (AGC) and a phase-lock loop (PLL) preceded by a bandpass limiter.

The noise temperature of a receiver is predominantly determined by the design of the first receiver stage because of its very high gain. For the

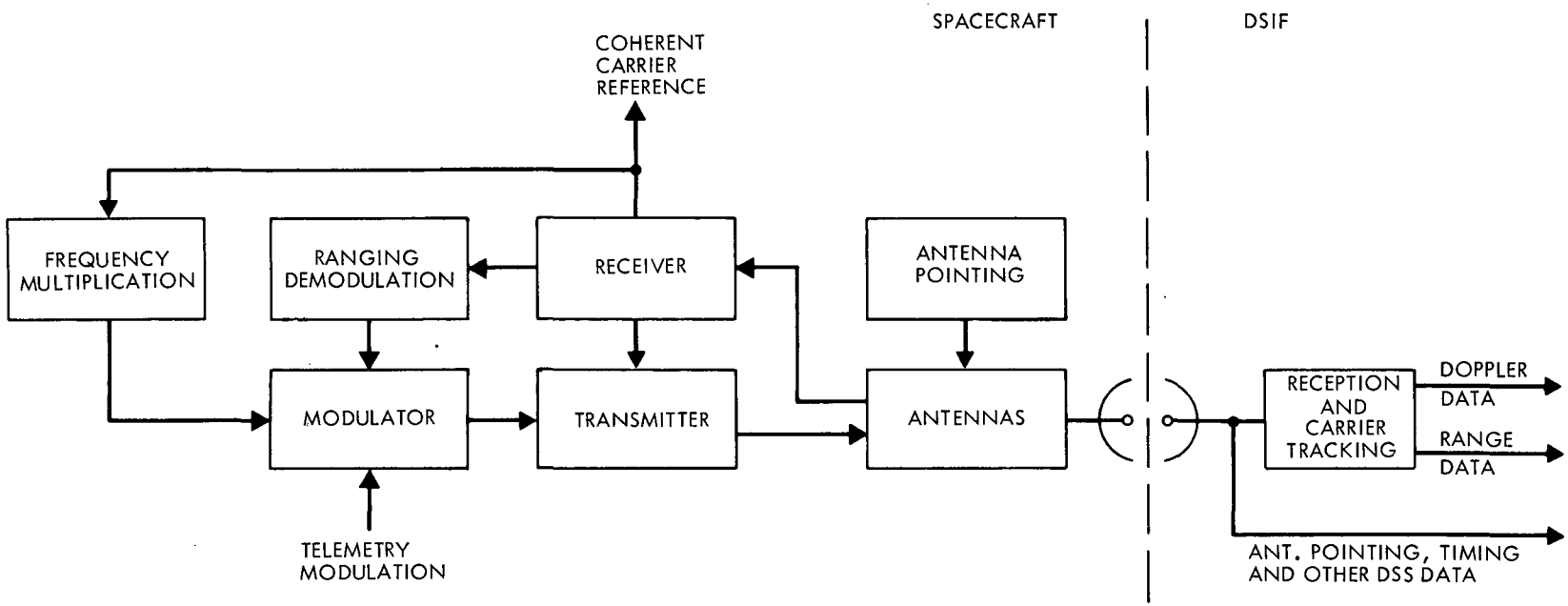

Fig. 4-1. Radio tracking system

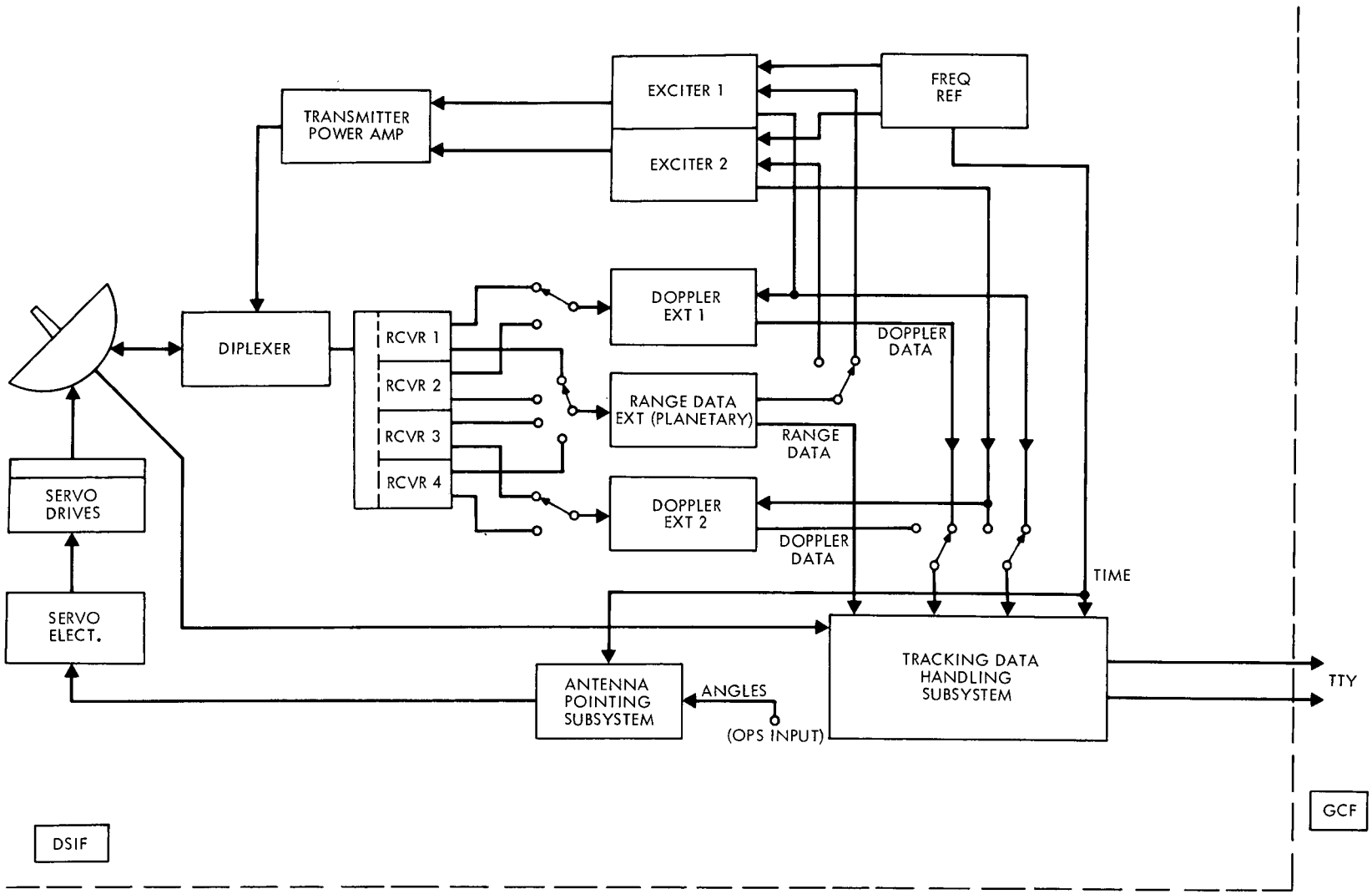

Fig. 4-2. DSS 14 (64 meter) DSIF tracking system functional diagram

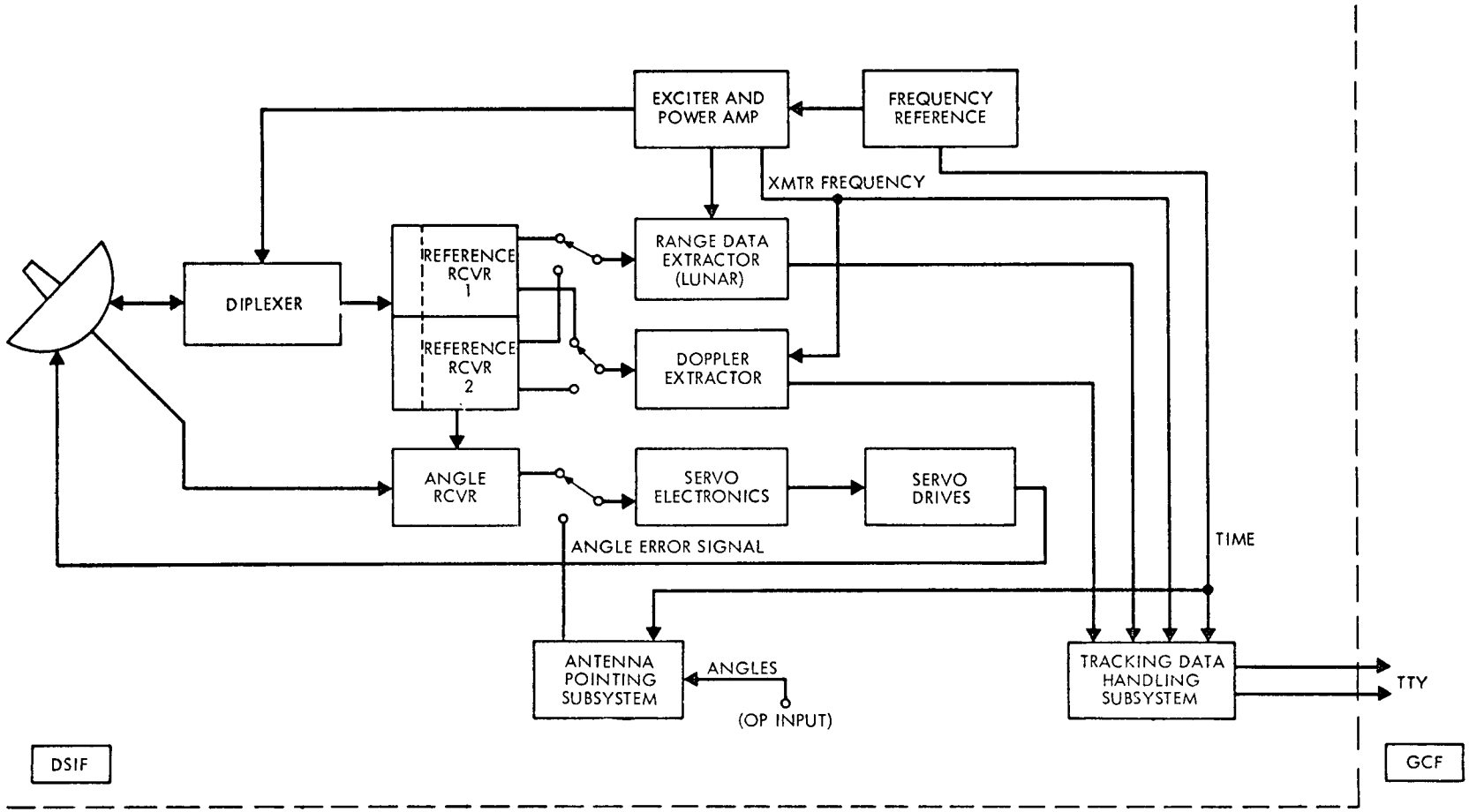

Fig. 4-3. 26 meter DSIF tracking system functional diagram

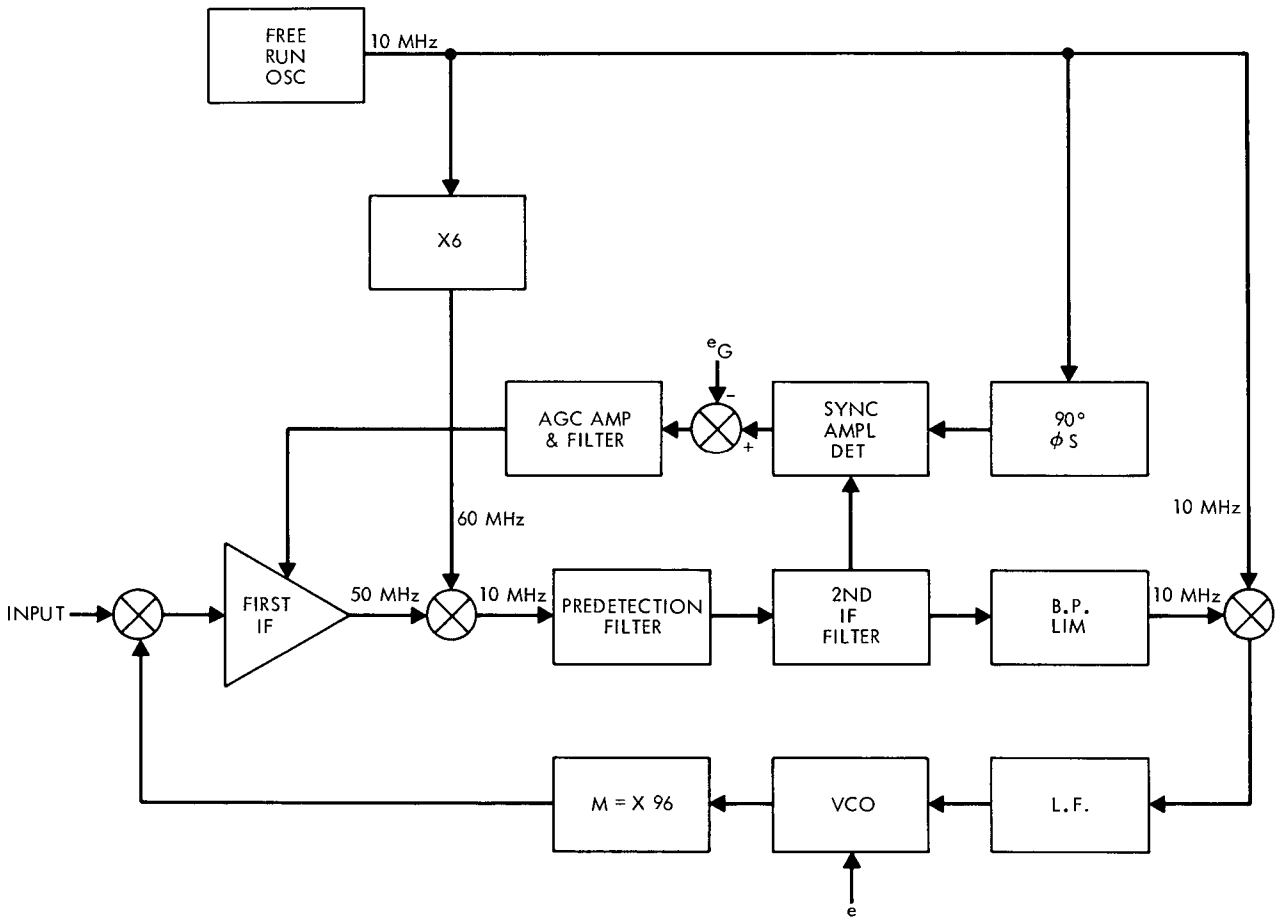

Fig. 4-4. DSIF receiver configuration

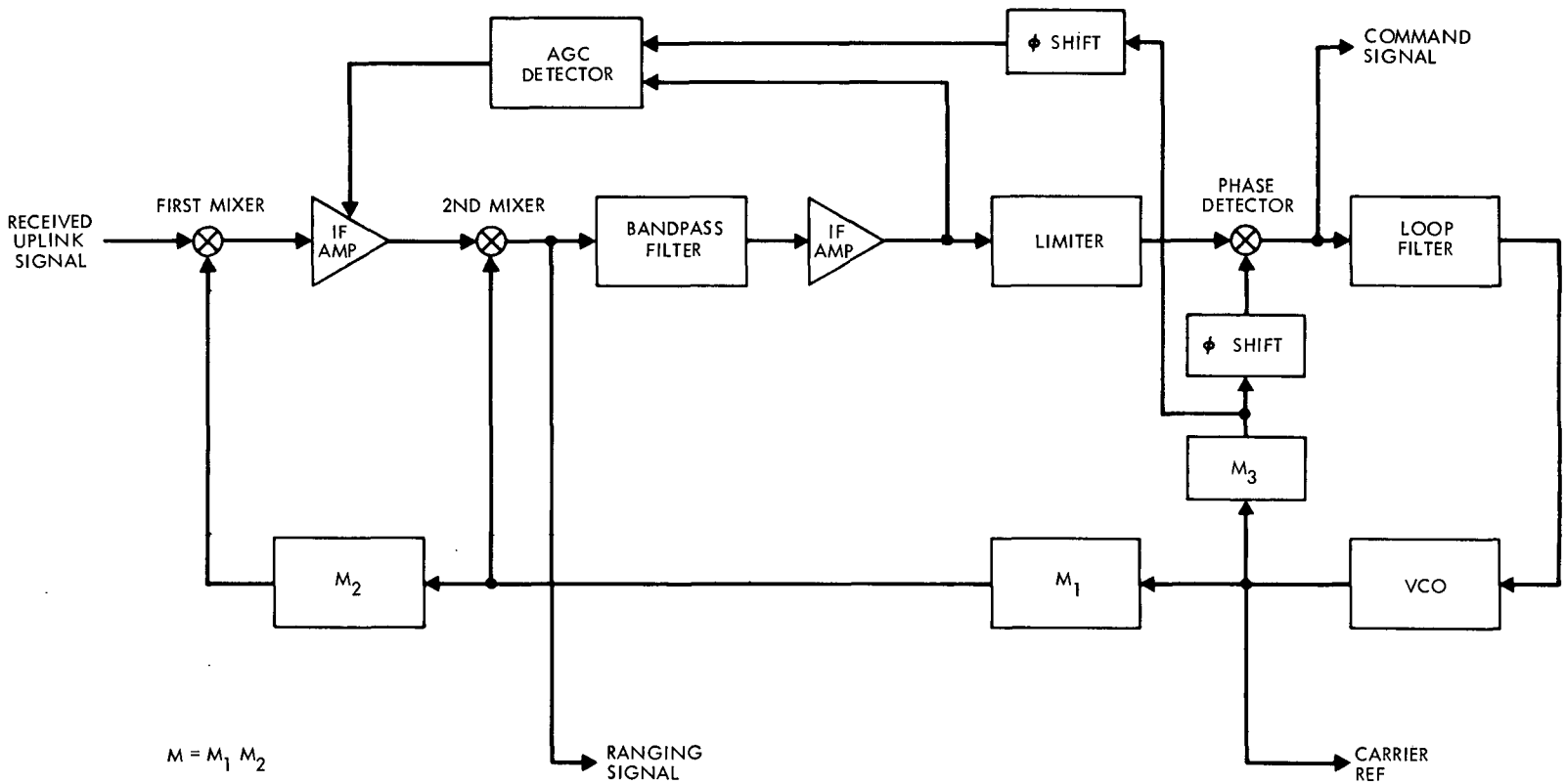

Fig. 4-5. Typical spacecraft receiver

DSIF, the first receiver stage is the maser amplifier at the antenna. For spacecraft receivers, it is usually the first mixer. The heterodyne design is employed to translate the rf signal down to a frequency for which stable phase detectors can be built. Automatic gain control is required to provide a signal whose amplitude is within the dynamic range of the amplifier stages. The band-pass limiter minimizes the total mean square error of the loop over a wide range of input signal-to-noise ratios. This configuration has been shown in reference 4-1 to provide near optimum PLL performance.

The design, performance, and characteristics of phase-lock loop receivers have been extensively studied. (See references 4-1 to 4-5.) Some of the characteristic PLL phenomena related to tracking functions are summarized in this section.

4.3.1 Noise-Free PLL Characteristics

The essential elements of a phase-lock loop which govern the noise-free behavior of a PLL receiver are shown in Figure 4-6. The input signal X(t) is multiplied with the output signal of the VCO, in the phase detector. An error signal is generated, which is filtered to remove the high-frequency terms of the multiplication process. The filtered error signal drives the VCO frequency in such a manner that the VCO frequency and phase approximate the frequency and phase of the input signal. The characteristic equation which describes the dynamic behavior of the loop is:

$$\theta(t) = \phi(t) + AK \frac{F(p)}{p} \sin \phi(t)$$

or

$$\hat{\theta}(t) = \left[\frac{AKF(p)}{p}\right] \sin \phi(t) \qquad (4.3\text{-}1)$$

where:

$\theta(t)$ = Input signal phase
$\phi(t)$ = $\theta(t) - \hat{\theta}(t)$, error signal
$\hat{\theta}(t)$ = Phase estimate generated by the VCO
A = Input signal amplitude
K = Loop gain
F(p) = Transfer function of the loop filter

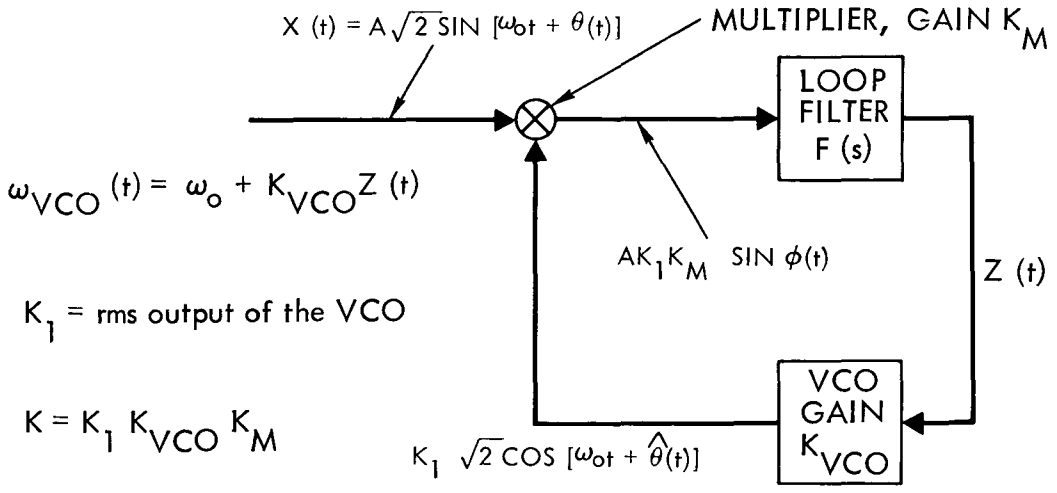

Fig. 4-6. Simple model of a phase-lock loop

p = Differential operator, $\frac{d}{dt}$

The loop order, L, is:

$$L = n + 1$$

where

n = Number of poles in the loop filter transfer function

Typically, the input phase consists of modulation, and of Doppler due to the radial motion of the spacecraft relative to the DSS tracking station. Thus,

$$\theta(t) = x(t) + d(t) \qquad (4.3\text{-}2)$$

where

$x(t)$ = Modulation

$d(t)$ = Doppler shift

The Doppler shift can be expanded in a Taylor series to obtain

$$d(t) = \phi_o + \Omega_o t + \frac{\Lambda_o}{2} t^2 + \ldots + \frac{x_n t^n}{n!} \qquad (4.3\text{-}3)$$

Here,

ϕ_o = Initial phase offset of the incoming signal from the free-running VCO phase.

Ω_o = Frequency offset of the incoming signal from the free-running VCO frequency.

Λ_o = Rate of change of the incoming signal frequency

x_n = nth time derivative of the incoming carrier phase.

The first three terms of equation 4.3-3 are the most important for typical spacecraft trajectories.

A steady-state phase error ϕ_{ss} will occur when d(t) has a finite number of Taylor series coefficients such that

$$n \doteq \ell + 1 \qquad (4.3\text{-}4)$$

where

ℓ = Number of poles at the origin of F(s)

n = As defined in equation 4.3-3.

If $n > \ell + 1$, $\phi(t)$ is unbounded and the loop will eventually lose lock.

The DSIF receivers and most typical spacecraft receivers use passive second-order loop filters of the form:

$$F(s) = \frac{1 + \tau_2 s}{1 + \tau_1 s} \qquad (4.3\text{-}5)$$

The time constants are usually chosen with $\tau_1 >> \tau_2$, so that F(s) approaches the perfect integrator:

$$F(s) \simeq \frac{1 + \tau_2 s}{\tau_1 s} \quad \text{for } \tau_1 s >> 1 \tag{4.3-6}$$

For the filter of equation (4.3-5), the PLL can track the Doppler signal.

$$d(t) = \phi_o + \Omega_o t \tag{4.3-7}$$

with a steady-state phase error (reference 4-2)

$$\phi_{ss} \triangleq \sin^{-1}\left(\frac{\dot{d}(t)}{AK} + \frac{\ddot{d}(t)\tau_1}{AK}\right) = \sin^{-1}\left(\frac{\Omega_o}{AK}\right) \tag{4.3-8}$$

given that the loop is initially in lock, and that no noise is present in the loop. The phase error is commonly referred to as static phase error (SPE) and Ω_o is referred to as the Doppler frequency shift.

Given that the loop is out-of-lock, the PLL will be able to acquire lock in a finite period of time if $d(t) = \phi_o + \Omega_o t$ and Ω_o is less than a certain magnitude called the loop pull-in range. The loop pull-in range must be determined experimentally, since current models are of insufficient accuracy.

If the initial frequency offset, Ω_o, is within the loop pull-in range, the time required to achieve lock is given by (reference 4-6):

$$t_{\text{freq. acq}} = \sqrt{2\pi^2 \frac{\tau_2}{\tau_1}}\left(\frac{r+1}{r}\right)\frac{\Omega_o^2}{\omega_L} \tag{4.3-9}$$

where

ω_L = PLL loop bandwidth (discussed below), $r = AK\tau_2^2/\tau_1$, and the signal-to-noise power ratio in the loop is greater than 10 dB. For SNR's less than 10 dB, the equation consistently gives too small a time.

If a small rate ($\wedge_o$) is present in d(t), then the SPE will vary slowly according to

$$\phi_{ss} = \sin^{-1}\left(\frac{\Omega_o}{AK} + \frac{\wedge_o t}{AK} + \frac{\wedge_o \tau_1}{AK}\right) \qquad (4.3\text{-}10)$$

Eventually, the loop will reach a maximum value of ϕ for which it will drop lock. The frequency offset corresponding to this condition is called the hold-in range of the loop.

Also of interest is the maximum Doppler rate for which the loop can acquire phase lock. This is termed the maximum sweep rate, and is of interest because the DSIF will sweep the uplink transmitter frequency over some range in order to acquire initial phase lock in the spacecraft receiver. The maximum sweep rate must be determined experimentally, but a good approximation may be found from (ref. 4-10):

$$\dot{f}_{acq} = \frac{\left[1 - (\eta)^{-1/2}\right]\left(\frac{\alpha_\ell}{\alpha_{\ell o}}\right)}{\pi \tau_2^{\,2}} \qquad (4.3\text{-}11)$$

where

α_ℓ = Limiter signal amplitude suppression factor, discussed in paragraph 4.3.3.3 below

$\alpha_{\ell o}$ = Limiter signal amplitude suppression factor, at loop threshold

η = Signal-to-noise power ratio in the loop bandwidth and

$\dot{f}_{acq}$ = The sweep rate that provides 90% probability of acquisition

According to Gardner (ref. 4-4, p. 49), $\dot{f}_{acq}$ predicted by equation 4.3-11 should be reduced by $\sqrt{2}$ to compensate for an error in the value of loop gain used in reference 4-10.

Two additional characteristics of PLL receivers are their transfer function, H(s), and their two-sided loop bandwidth ω_L (= $2B_L$).* The transfer function is defined by:

$$\hat{\theta}(s) = H(s) \quad \theta(s) \tag{4.3-12}$$

where $\hat{\theta}(s)$ and $\theta(s)$ are the Laplace transforms of $\hat{\theta}(t)$ and $\theta(t)$, respectively.

When the phase error ϕ is small, $\phi \simeq \sin \phi$ and H(s) is approximately:

$$H(s) = \frac{F(s)\ AK}{s + AKF(s)} \tag{4.3-13}$$

When the loop filter is of the form:

$$F(s) = \frac{1 + \tau_2 s}{1 + \tau_1 s},$$

Then,

$$H(s) = \frac{1 + \tau_2 s}{1 + (\tau_2 + \frac{1}{AK})\ s + (\frac{\tau_1}{AK})\ s^2} \tag{4.3-14}$$

The loop bandwidth, ω_L, is defined to be

$$\omega_L \triangleq \frac{1}{2\pi j} \int_{-j\infty}^{j\infty} |H(s)|^2 ds \tag{4.3-15}$$

Using the linearized loop,

$$\omega_L \simeq \frac{r + 1}{2\tau_2} \tag{4.3-16}$$

where the assumption $r\tau_1 >> \tau_2$ has been used.

*ω_L is the two-sided bandwidth of the PLL. B_L is the single-sided loop bandwidth. Both notations are conventionally used in the literature.

4.3.2 Practical Receiver PLL's

Receivers used by the DSIF and most spacecraft are of the double conversion superheterodyne type preceded by a bandpass limiter, as shown in Figures 4-4 and 4-5.

The noise-free characteristics described in the preceding section apply to these receivers, with the exception that the amplitude gain product, AK, is computed using the relation:

$$AK = \alpha_\ell K_D K_{VCO} M K_{DC} 360 \text{ sec}^{-1} \qquad (4.3\text{-}17)$$

where

α_ℓ = Limiter suppression factor (to be discussed)

K_D = Phase detector gain (volts/deg)

K_{VCO} = VCO gain (Hz/volt)

M = VCO multiplication factor

K_{DC} = Gain of the loop filter.

4.3.3 Receiver PLL Characteristics in The Presence of Noise

In its first stage, the spacecraft receiver will generate white gaussian noise which is added to the received signal. This noise prevents the receiver from making a perfect phase reference estimate even in the absence of Doppler shift or phase modulation.

When tracking in the one-way mode, the DSIF receivers experience the same characteristics. When tracking in the two-way mode, noise generated in the spacecraft receiver is transmitted on the downlink signal so that the signal received by the DSIF contains phase noise to which its receiver noise is added.

The signal may also acquire noise from celestial sources. The discussion to follow considers only receiver noise. The behavior of PLL's in the presence of noise is important to the system designer because the prescribed quality of tracking, command, and telemetry data must be achieved when the PLL's are operating in a noisy environment.

4.3.3.1 Phase Error Distribution in a PLL. The probability density function of the PLL phase error for a first order loop when the signal is corrupted by white gaussian noise was shown by Viterbi (reference 4-3) to be

$$p(\phi) = \frac{\exp(\eta \cos\phi)}{2\pi I_o(\eta)}, \quad |\phi| \leq \pi \tag{4.3-18}$$

where $p(\phi)$ = Probability density function of the loop phase error at the phase detector output,

$\eta = \frac{2P}{N_o \omega_L}$ = Signal-to-noise ratio in the bandwidth of the the linearized loop, i.e., SNR in B_L (see below)

P = Input signal power, A^2, in the loop bandwidth

ω_L = PLL two-sided loop bandwidth

$I_o(.)$ = Zeroth order imaginary Bessel function

and N_o = Input noise spectral density, watts/Hz.

For many applications, the density function (equation 4.3-18) is a good approximation for second order loops. For precise work, Lindsey has developed a better solution (reference 4-5) which, however, is quite complex to evaluate. The adequacy of equation (4.3-18) can be judged from Figure 4-7 (taken from ref. 4-5), where the distribution derived (solid curve) from (4.3-18) is superimposed on the experimental distribution for values of η in the range 0 dB < η < 6.5 dB. Figure 4-8 shows the cumulative distributions

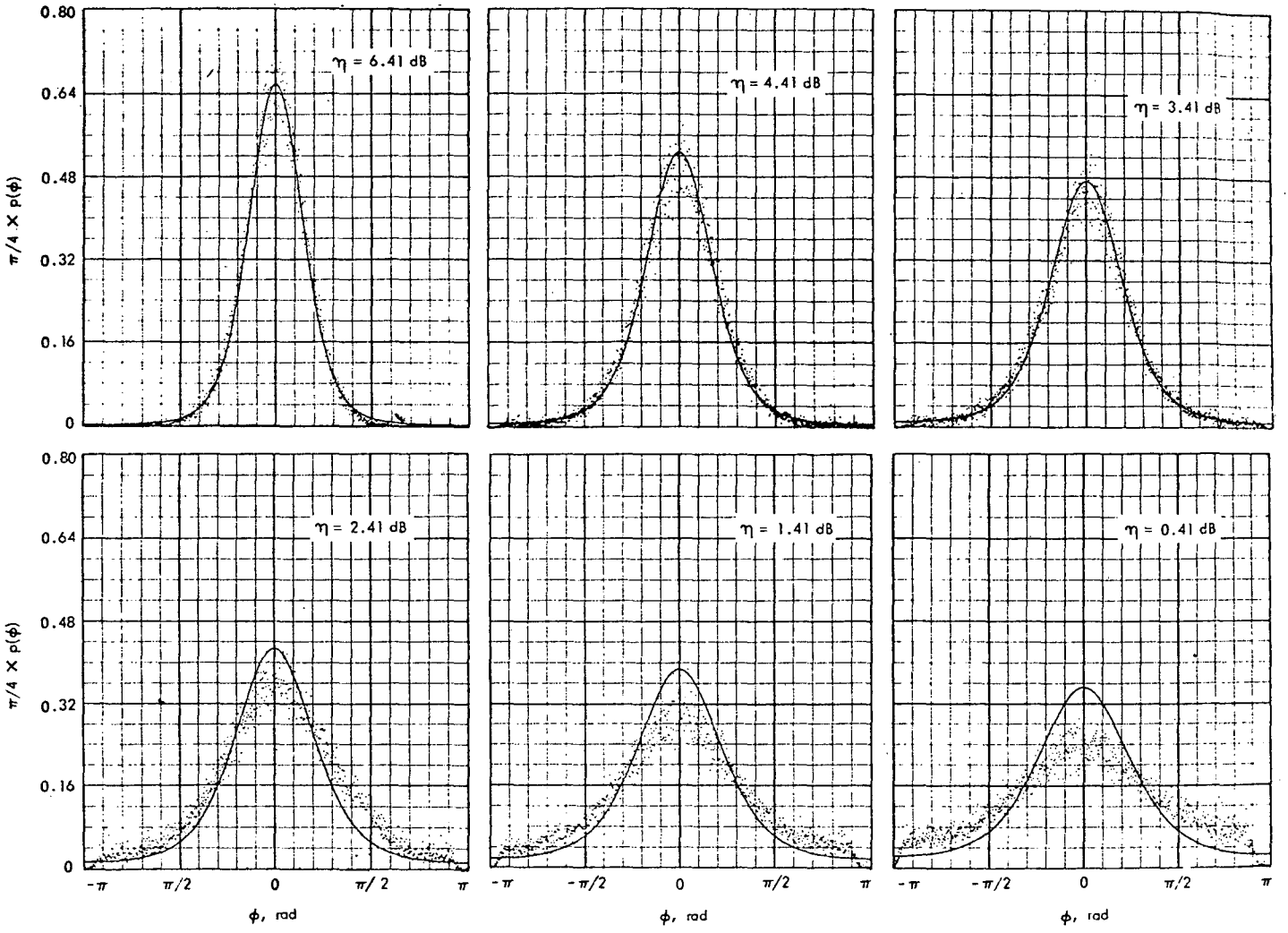

Fig. 4-7. Phase-error distributions for various values of η

of the measured phase error for the same values of η. This figure demonstrates that the probability of losing lock is very small for $\eta > 6.41$ dB. Figure 4-9 plots the variance of phase error, as derived for a linear loop approximation ($\sin \phi \approx \phi$), for equation (4.3-18), and experimentally.

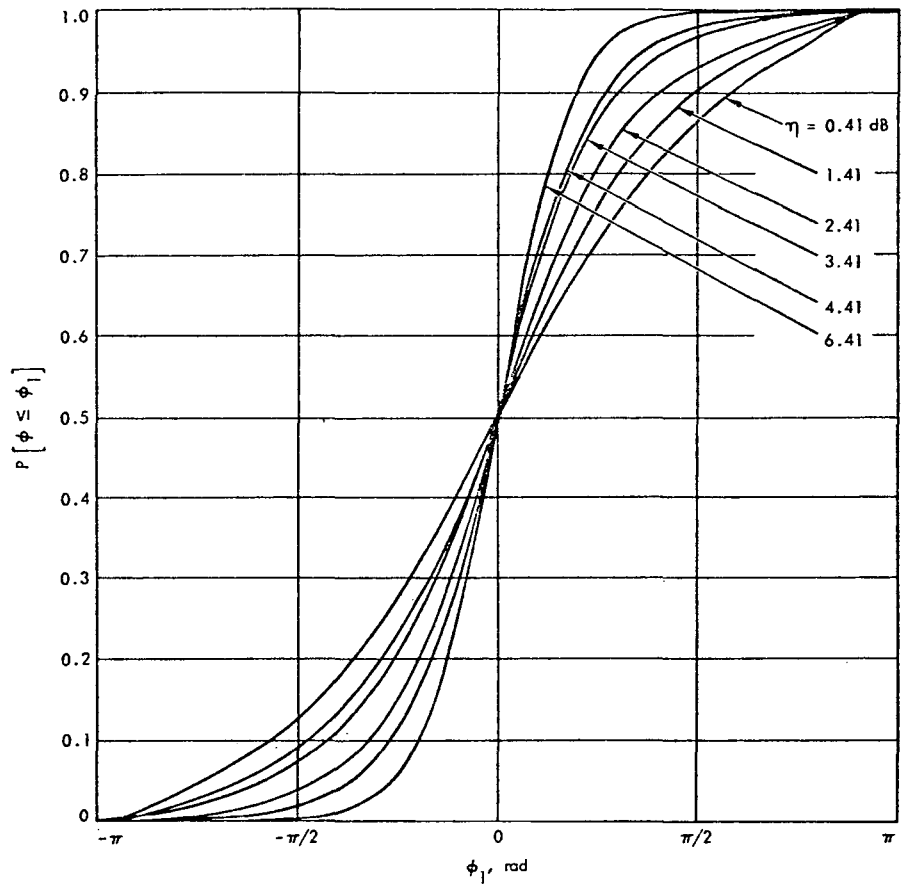

Fig. 4-8. Cumulative distribution of the measured phase error

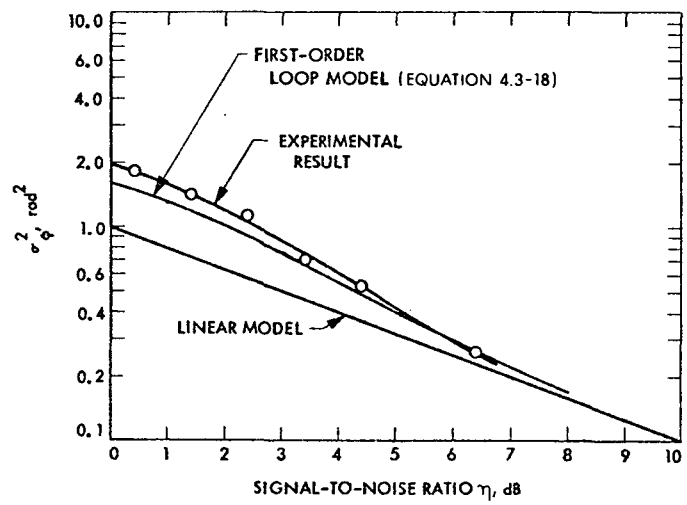

Fig. 4-9. Experimental and analytical results relative to the variance of the phase error

4.3.3.2 Cycle Slipping. A PLL receiver "slips a cycle" when the magnitude of its phase error process exceeds 2π radians. The occurrence of a cycle slip is a random event depending on the noise in the PLL and the deterministic phase error, and introduces errors in Doppler tracking. There are two different parameters describing this event: the mean time to first cycle slip and the average number of cycle slips per second.

The mean time to first cycle slip is defined as the average time the phase error takes to go from 0 to $\pm 2\pi$ radians. Lindsey (Ref. 4-6) has shown that

$$\tau\omega_L = \left(\frac{r+1}{r}\right)^2 \frac{\eta}{2} \int_{-2\pi}^{2\pi} \int_{-2\pi}^{\phi} \left[C - u(\chi)\right] \exp\left[U(\chi) - U(\phi)\right] d\chi d\phi \qquad (4.3\text{-}19)$$

where

$$C = \frac{\int_{0}^{2\pi} \exp\left[U(\chi)\right] d\chi}{\int_{-2\pi}^{2\pi} \exp\left[U(\chi)\right] d\chi} \qquad (4.3.20)$$

and

$$U(\chi) = -\left(\frac{r+1}{r}\right)\eta\cos\chi - \frac{\eta}{2r}\chi^2 - \eta\frac{\Omega_o}{AK}\chi \qquad (4.3.21)$$

In (4.3-19) and (4.3-20), τ is the mean time to first cycle slip and $u(\chi)$ is the unit step function.

Another way of looking at cycle slipping is to assume that the PLL runs continuously [i.e., $\phi(t)$ ranges over $(-\infty,\infty)$ reduced modulo 2π] and to compute the average number of slips, both plus and minus, per second. Theoretical results in this case have not been accurate when compared with simulations. However, a reasonable engineering approximation is:

$$\overline{S} \approx \frac{1}{\tau} \qquad (4.3\text{-}22)$$

where $\overline{S}$ is the average number of slips per second. Figure 4-10 shows a plot of τ^{-1} and a simulation $\overline{S}$ versus SNR in the threshold loop bandwidth ($2B_{LO}$) for a Mariner-type receiver.

The parameter $\overline{S}$ may be used to compute the probability of loss of lock. Assume that the event {k slips in t seconds} is Poisson. Then its probability is

$$P\{\text{k slips in t sec.}\} = \frac{(\overline{S}t)^k \exp(-\overline{S}t)}{k!} \tag{4.3-23}$$

Now define the event {loss of lock in t seconds} as the event {k slips in t sec., $k \geq 1$}. Then from (4.3-23) its probability is:

$$P\{\text{loss of lock in t sec.}\} = 1 - \exp(-\overline{S}t) \tag{4.3-24}$$

Experimental justification of the Poisson assumption is given in references 4-7 and 4-8.

4.3.3.3 Bandpass Limiting. Bandpass limiters (a bandpass filter followed by an amplitude hard limiter) are used in phase-lock loop receivers to maintain a constant total power at the input to the loop. This minimizes the total mean square error of the loop over a wide range of input signal-to-noise ratios.

The bandpass limiter may be characterized by the filter bandwidth, ω_ℓ. If η_ℓ is the SNR in the filter bandwidth, then the power in the signal component of the limiter output spectrum, α_ℓ^2, is determined from:

$$\alpha_\ell = \sqrt{\frac{\pi}{2}}\left(\frac{\eta_\ell}{2}\right)^{1/2} \exp\left(-\frac{\eta_\ell}{2}\right)\left[I_o\left(\frac{\eta_\ell}{2}\right) + I_1\left(\frac{\eta_\ell}{2}\right)\right] \tag{4.3-25}$$

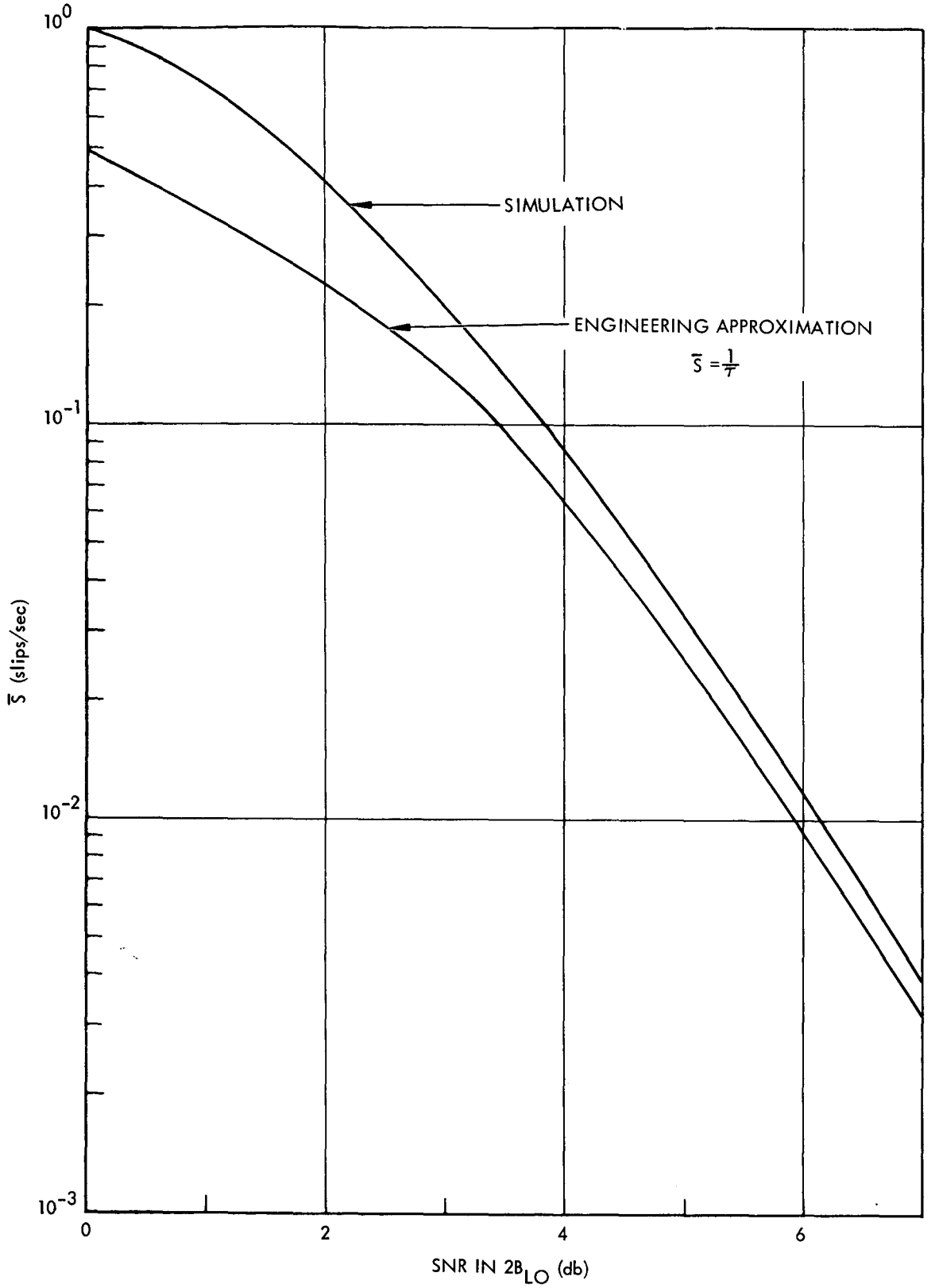

Fig. 4-10. Mean number of cycle slips per second versus SNR in a $2B_{LO}$ of 18 Hz

where

$$\eta_\ell = \frac{2P}{N_o \omega_\ell} = 2\eta_o \left(\frac{\omega_{Lo}}{\omega_\ell} \right) = \eta_o \frac{2B_{LO}}{B_\ell} \tag{4.3-26}$$

and η_o, defined as $P/(N_o \omega_{LO})$, or SNR in $2B_{LO}$, is not the SNR in $2B_L$ at threshold in the bandpass limiter case (see paragraph 4.3.3.4).

The quantity α_ℓ is commonly referred to as the limiter signal amplitude suppression.

Equation 4.3-25 may be approximated by the rational polynominal (reference 4-2):

$$\alpha_\ell^2 \simeq \frac{0.7854\eta_\ell + 0.4768\eta_\ell^2}{1 + 1.024\eta_\ell + 0.4768\eta_\ell^2} \tag{4.3-27}$$

which is plotted in Figure 4-11. For the linear model of a PLL, the variance of the phase error is given by

$$\sigma_\phi^2 = \frac{N_o \omega_L}{2P} \tag{4.3-28}$$

For the linear model of a PLL preceded by a bandpass limiter,

$$\sigma_\phi^2 = \left(\frac{N_o \omega_L}{2P} \right) \Gamma = \frac{1}{\eta} \tag{4.3-29}$$

Where Γ is the limiter performance factor, or limiter loss (reference 4-2), and η is the SNR in B_L. Γ can be approximated by (Ref. 4-9):

$$\Gamma \simeq \frac{1 + \eta_\ell}{0.862 + \eta_\ell}, \text{ for } \omega_\ell > 10\omega_L \tag{4.3-30}$$

(Refer to Figure 4-12). The loop bandwidth is now

$$\omega_L = \frac{1 + r}{2\tau_2 \left(1 + \frac{\tau_2}{r\tau_1} \right)} \tag{4.3-31}$$

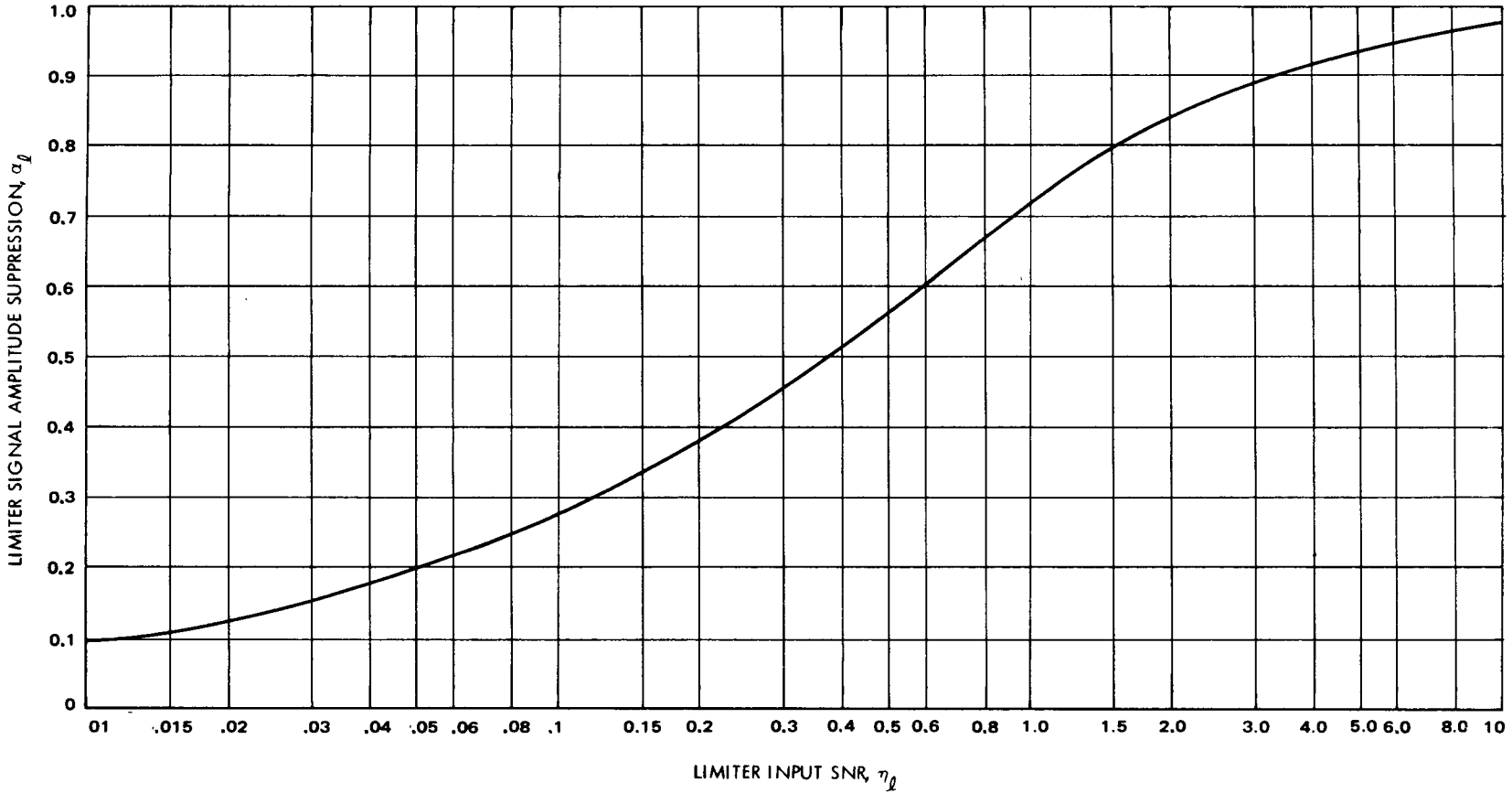

Fig. 4-11. Variation of α_ℓ with limiter input SNR, η_ℓ

Where r becomes

$$r = \alpha_\ell K_D K_{VCO} M K_{DC} 360 \tau_2^2/\tau_1$$

4.3.3.4 Receiver Threshold. It is useful in the design, specification, and performance analysis of PLL receivers to define a receiver threshold, or design point condition. By convention, the design point condition occurs when the variance of the loop phase error is unity, and the variance is represented by a linearized PLL. In actual fact, the variance of a linearized loop is different from that of an actual nonlinear loop when its variance is one. The fiction that the loop is linear in the definition of threshold is used so that the mathematically tractable expression:

$$P_o \triangleq N_o \omega_{Lo} \tag{4.3-32}$$

at threshold* can be used to define the threshold condition.

In practice, PLL receivers are designed by specifying the threshold loop bandwidth, ω_{Lo}, and the receiver noise spectral density, N_o. The receiver sensitivity, P_o, is then determined by definition from 4.3-32. The limiter suppression factor at threshold may be calculated by substituting $\eta_{\ell o} = \dfrac{2B_{LO}}{B_\ell}$ into equation 4.3-25 or 4.3-27 to obtain $\alpha_{\ell o}$.

Now the PLL receiver characteristics may be determined as a function of signal level referenced to the threshold loop bandwidth. For instance, the actual loop bandwidth is

$$\omega_L = \omega_{Lo}\left(\frac{1 + \frac{r}{\mu}o}{1 + r_o}\right)\left(\frac{1 + \frac{\tau_2}{r_o \tau_1}}{1 + \frac{\mu\tau_2}{r_o\tau_1}}\right) \tag{4.3-33}$$

*The subscript ($_o$) by convention represents a threshold condition.

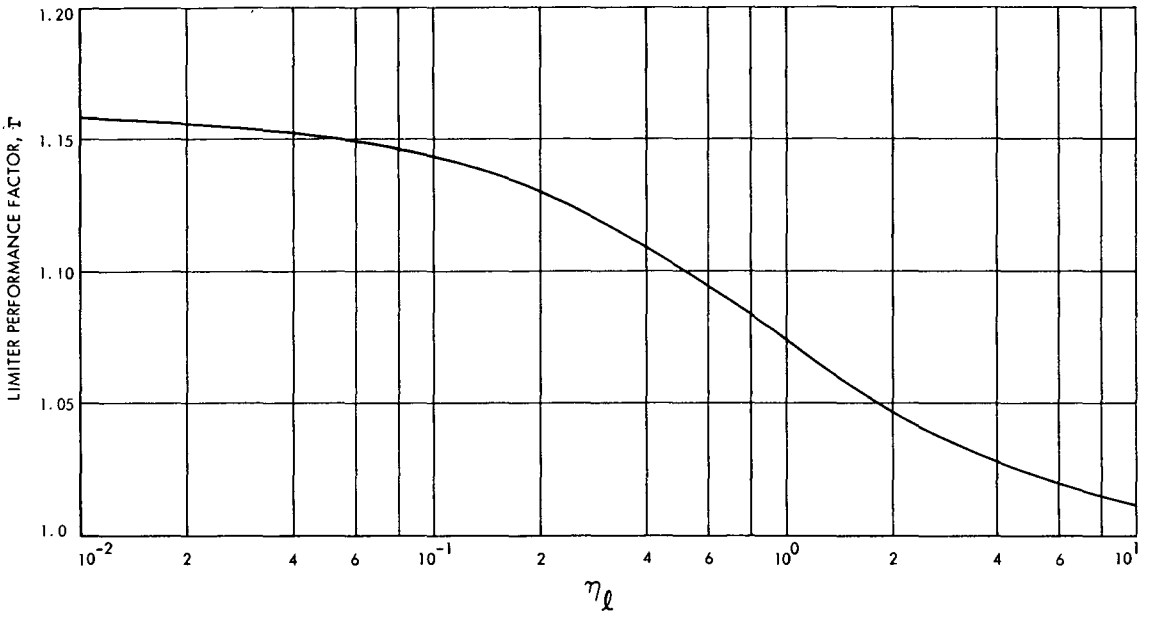

Fig. 4-12. Variation of the parameter Γ with limiter input SNR, η_ℓ

where

$$\mu = \frac{\alpha_{\ell o}}{\alpha_\ell}$$

$$r_o = \frac{\alpha_{\ell o} K_D K_{VCO} M K_{DC} 360 \tau_2^2}{\tau_1} = \mu r \qquad (4.3\text{-}34)$$

Typically $r_o \tau_1 >> \tau_2$ so that

$$\omega_L \approx \omega_{Lo} \left(\frac{1 + \frac{r_o}{\mu}}{1 + r_o} \right) \qquad (4.3\text{-}35)$$

With no limiter in the system, $B_L/B_{LO} \equiv 1$. However, with a bandpass limiter, B_L/B_{LO} is a function of η_o, r_o, and $2B_{LO}/B_\ell$. For $2B_{LO}/B_\ell$ very small (<.002), there is no significant dependence on this parameter. For this case, and $r_o\tau_1 >> \tau_2$, Figure 4-13 plots B_L/B_{LO} versus η_o, Figure 4-14 plots B_L/B_{LO} versus η, and Figure 4-15 plots η versus η_o for various values of r_o. Note that η is SNR in B_L, whereas η_o is defined as SNR in $2B_{LO}$ and that B_L/B_{LO} evaluated at η = 3 dB is not equal to one. This is because η_o is a definition and does not include the limiter performance factor, Γ, thus the SNR in $2B_{LO}$ is not the actual SNR in the phase-locked loop bandwidth. These curves were derived through equations 4.3-26, 4.3-27, 4.3-29, 4.3-30, and 4.3-35, and the definition

$$\eta = \eta_o \left(\frac{2B_{LO}}{B_L}\right) \frac{0.862 + \eta_o \dfrac{2B_{LO}}{B_\ell}}{1 + \eta_o \dfrac{2B_{LO}}{B_\ell}}$$

They are also useful for determining radio loss for a given SNR in $2B_{LO}$ as described in section V.

4.3.3.5 Receiver Phase Error Variance. When the signal level at the input to a PLL preceded by a bandpass limiter is so low that the loop is in its non-linear region of operation, phase error variance σ^2 is (ref. 4-5):

$$\sigma^2 = \frac{\pi^2}{3} + \frac{4}{I_o(\eta)} \sum_{k=1}^{\infty} \frac{(-1)^k I_k(\eta)}{k^2} \qquad (4.3\text{-}36)$$

where

$$\eta = \left(\frac{2P}{N_o \omega_{Lo}}\right)\left(\frac{1}{\Gamma}\right)\left(\frac{1 + r_o}{1 + \dfrac{r_o}{\mu}}\right) \qquad (4.3\text{-}37)$$

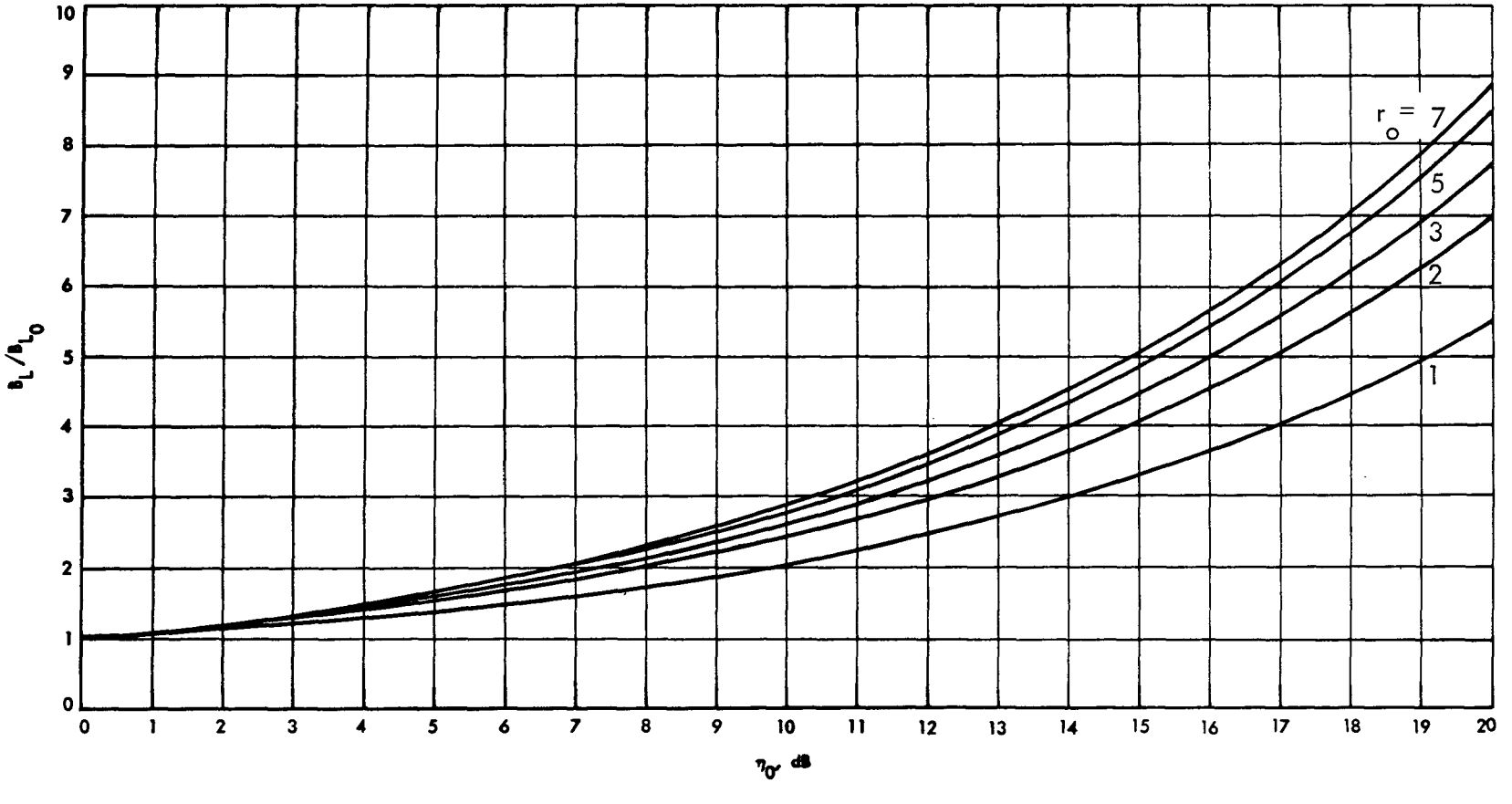

Fig. 4-13. B_L/B_{LO} versus SNR in $2B_{LO}$ with r_o as a parameter ($2B_{LO}/B_\ell \ll 1$)

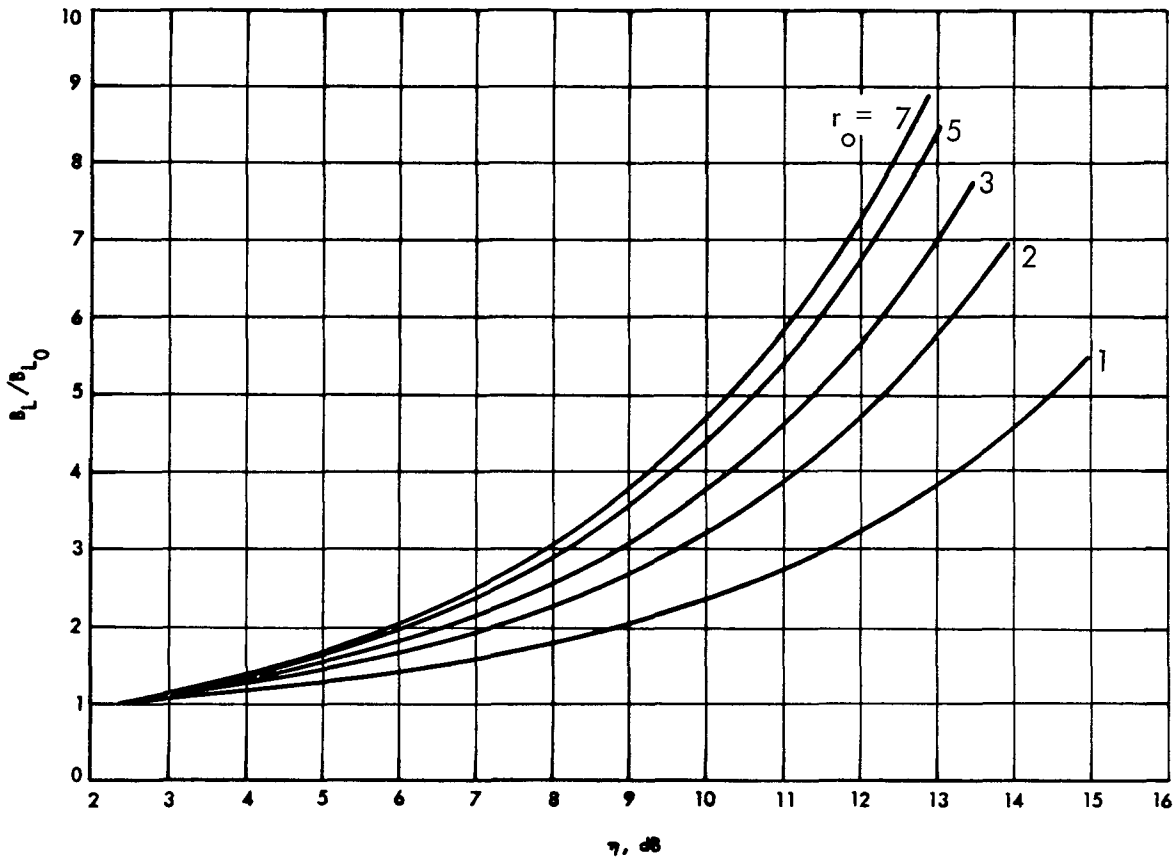

Fig. 4-14. B_L/B_{LO} versus SNR in B_L with r_o as a parameter ($2B_{LO}/B_\ell \ll 1$)

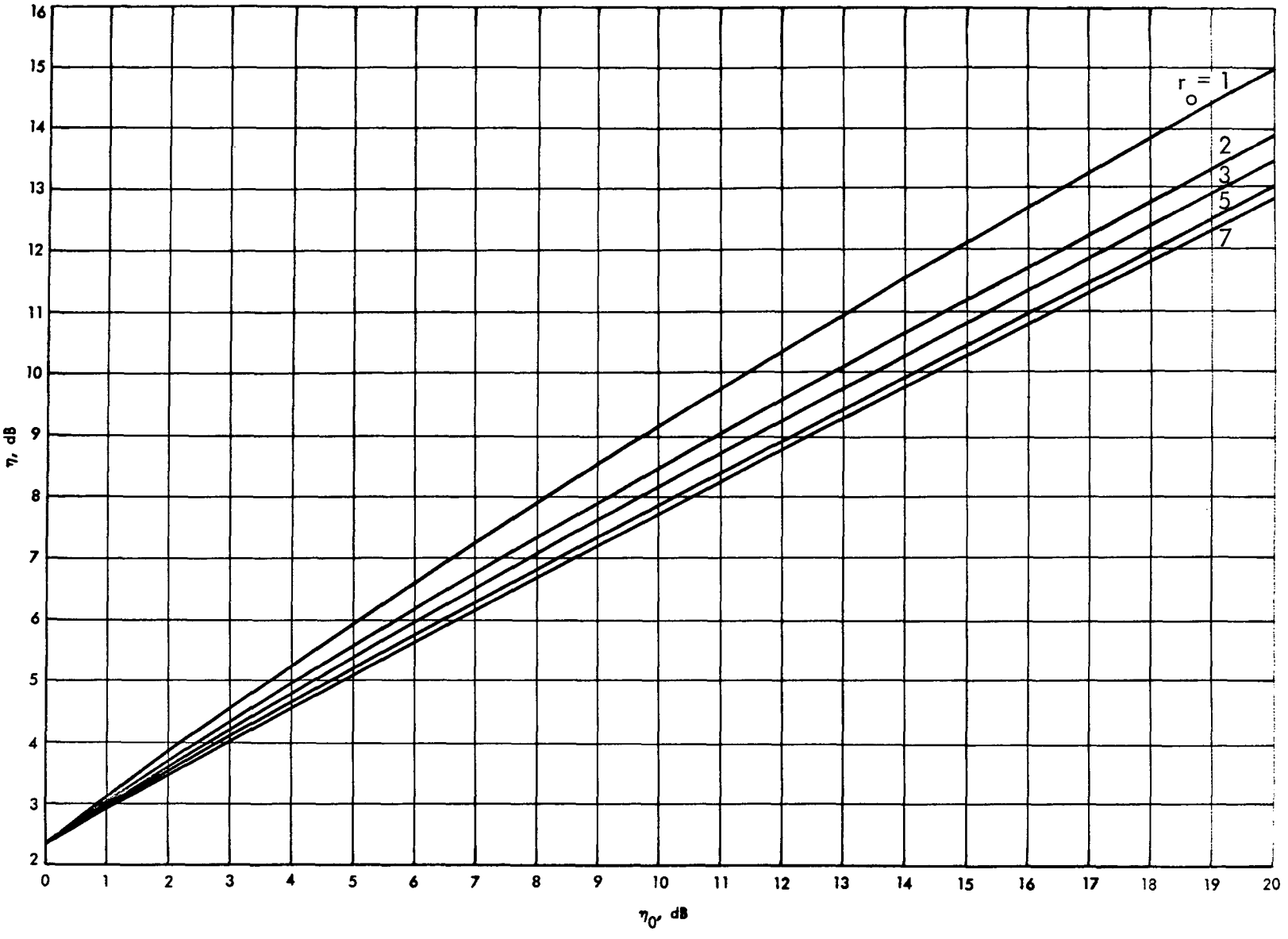

Fig. 4-15. SNR in B_L versus SNR in $2B_{LO}$ with r_o as a parameter ($2B_{LO}/B_\ell \ll 1$)

Above a value of η of 7 or 8 dB, the linear theory results of equation (4.3-29) hold quite accurately (see Figure 4-9).

In order to accurately demodulate the data, the signal-to-noise ratio in the loop, η, must be large enough so that the probability of slipping a cycle is very low. The loop will lose lock momentarily if the instantaneous phase angle, ϕ, exceeds the range $\pm \pi/2$ radians. We can choose the probability of this occurrence to lie at some multiple of σ. Then equation 4.3-28 gives the corresponding η, and use of equations 4.3-33 and 4.3-29 with the proper parameters gives the minimum SNR in $2B_{LO}$ to provide for low probability of loss of lock. Figure 4-15 also plots the relation between η and η_o for $2B_{LO}/B_\ell \ll 1$.

Empirical results which include limiter suppression and system efficiency, suggest a minimum recommended operating SNR in $2B_{LO}$ of 10 dB for the ground receivers. The effect of system efficiency will be discussed in section V.

4.3.3.6 PLL Receiver Tracking Errors. Two types of tracking errors are important in deep space communications. These are errors in one-way tracking and errors in two-way tracking. One-way tracking occurs when the DSIF is transmitting, and the S/C is receiving, or when the S/C is transmitting from its internal auxiliary oscillator and the DSIF is receiving. Two-way tracking errors occur in the DSIF receiver when the DSIF is transmitting to the spacecraft, and the spacecraft transponder transmits a carrier derived from the received uplink signal.

In this section, the subscripts used, apply as follows:

1 = One-way parameter

2 = Two-way parameter

When tracking in the one-way mode, the receiver phase error is

$$\phi_{r_1} = \theta_1 - \hat{\theta}_1 \qquad (4.3\text{-}38)$$

where

θ_1 = Receiver carrier phase

$\hat{\theta}_1$ = Carrier phase estimate

When tracking in the two-way mode, the receiver phase error in the downlink receiver is

$$\phi_{r_2} = \theta_2 + \hat{\theta}_1 - \hat{\theta}_2 \tag{4.3-39}$$

where

θ_2 = Doppler shift in phase between the spacecraft and the DSIF receiver

$\hat{\theta}_2$ = Estimate of the received downlink carrier phase.

The two-way phase error variance under strong signal conditions is (ref. 4-5):

$$\sigma^2_{\phi_{r_2}} = \frac{1}{\eta_1} + \frac{1}{\eta_2} \tag{4.3-40}$$

where

$$\eta_1 = \left(\frac{2P_{c_1}}{\omega_{1o}N_{1o}}\right)\left(\frac{1}{G^2\Gamma_1 K_R(k_1, k_2, \beta)}\right)$$

$$\eta_2 = \frac{2P_{c_2}}{\omega_{2o}N_{2o}}\left(\frac{1 + r_{2o}}{1 + \frac{r_{2o}}{\mu_2}}\right)\frac{1}{\Gamma_2}$$

$$K_R = \frac{k_2}{k_1}\left[\frac{2k_1\beta + 4\beta^2(1+\beta) + \beta^3(1+\beta)k_1k_2 + 2k_2\beta^4}{k_1^2 + 2k_1\beta + 2\beta(k_1+k_2-k_1k_2)+2\beta^3k_2+k_2^2\beta^4}\right]\left(\frac{1}{r_{1o}+1}\right)$$

$$k_i = \frac{2}{r_i} = \frac{2\mu_i}{r_{i_o}}, \quad i = 1, 2$$

$$\beta = \frac{\omega_{10}(r_{20} + 1)}{\omega_{20}(r_{10} + 1)}$$

G = Transponder turnaround ratio

For equation 4.3-40 to be valid, G should be approximately unity.

Using nonlinear two-way tracking theory (ref. 4-5), the probability density function for the phase error in the downlink receiver is approximated by:

$$p(\phi_{r_2}) = \frac{I_o\left(|\eta_1 + \eta_2 \exp(j\phi_{r_2})|\right)}{2\pi I_o(\eta_1) I_o(\eta_2)} \qquad |\phi_{r_2}| \leq \pi \qquad (4.3\text{-}41)$$

which is shown in Figure 4-16 for $\eta_1 = \eta_2$.

The phase error variance is no longer given by equation 4.3-39. It is now:

$$\sigma_{\phi_{r_2}}^2 = \frac{\pi^2}{3} + 4\sum_{k=1}^{\infty} \frac{(-1)^k I_k(\eta_1) I_k(\eta_2)}{k^2 I_o(\eta_1) I_o(\eta_2)} \qquad (4.3\text{-}42)$$

4.3.3.7 Two-Way Doppler Errors Due to Receiver Noise. There are many sources of error in making a Doppler measurement. One of these is the error due to receiver noise.

The estimated Doppler shift, or, in Lindsey's terminology (ref. 4-5), the Doppler error, ϕ_{d_2}, is given by

$$\phi_{d_2} = \hat{\theta}_2 - \theta_o \qquad (4.3\text{-}43)$$

where

θ_o = Transmitted uplink carrier phase

$\hat{\theta}_2$ = DSIF receiver estimate of the received carrier phase

When both uplink and downlink received signals are strong, the variance in Doppler error is (ref. 4-5):

$$\sigma^2_{\phi_{d_2}} = \frac{1}{d_1} + \frac{1}{d_2} \tag{4.3-44}$$

where

$$d_1 = \left(\frac{2P_{C_1}}{\omega_{1o}N_{1o}}\right)\left(\frac{1}{G^2\Gamma_1 K_D(k_1 k_2, \beta)}\right)$$

$$d_2 = \left(\frac{2P_{C_2}}{N_{2o}\omega_{2o}}\right)\left(\frac{1 + r_{2o}}{1+r_{2o}/\mu_2}\right)\frac{1}{\Gamma_2}$$

$$K_D(k_1, k_2, \beta) = \left(\frac{1}{r_{1o} + 1}\right)\left(\frac{k_1(2+k_1)+2(k_1+k_2+2)(\beta+\beta^2)+k_2(2+k_2)\beta^3}{k_1{}^2+2k_1\beta + 2(k_1+k_2-k_1k_2)\beta^2+2k_2\beta^3+k_2{}^2\beta^4}\right)$$

$$k_i = \frac{2\mu_i}{r_{io}}, \; i=1, 2$$

If either the uplink or downlink received signal power is not very much greater than its threshold design value, nonlinear theory applies, then:

$$p(\phi_d) = \frac{I_o\left(|d_1 + d_2 \exp(j\phi_d)|\right)}{2\pi \quad I_o(d_1)I_o(d_2)} \qquad |\phi_d| \leq \pi \tag{4.3-45}$$

which is shown in Figure 4-16 for $d_1 = d_2$, with ϕ_d replacing ϕ_{r_2}, and $d_1 = d_2$ replacing η and the variance of ϕ_d is

$$\sigma^2_{\phi_d} = \frac{\pi^2}{3} + 4\sum_{k=1}^{\infty}\frac{(-1)^k I_k(d_1)I_k(d_2)}{k^2 I_o(d_1)I_o(d_2)} \tag{4.3-46}$$

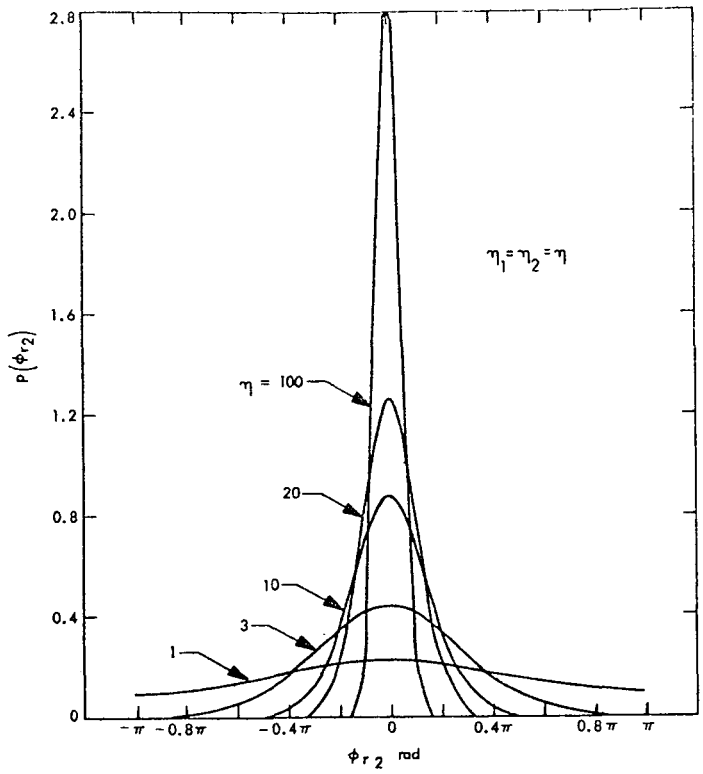

Fig. 4-16. Probability distribution of the two-way phase error, $p(\phi_{r_2})$ vs two-way phase error, ϕ_{r_2}

4.4 DOPPLER TRACKING

Doppler tracking is a technique whereby the radial velocity of the spacecraft away from the tracking station is determined by measuring the Doppler frequency shift of the rf signal received from the spacecraft. For accurate Doppler tracking, the DSIF transmitter must operate at a precisely known frequency. In the majority of spacecraft tracking, the range rates are small enough so that the transmitter can be tuned to a constant frequency (called track synfreq) just after two-way acquisition, which will permit tracking by the spacecraft transponder throughout the pass with acceptable tracking loop phase errors.

Occasionally it is necessary to retune to a second track synfreq during a pass, due to higher range rates than can be accommodated with one setting. During this mid-pass tuning ranging modulation must be removed, and, if the subcarrier frequencies are not sufficiently high, command modulation must be removed. Since the tuning rate is imprecisely controlled, Doppler data is not accurate when it returns one round-trip light time later. Thus, some minutes of tracking data and perhaps command capability are lost. Often these losses are acceptable. However, in the case of very high range rates, the above procedures may not be adequate. The problems of high range-rate tracking are described in paragraph 4.4.3 below.

The DSIF can acquire tracking data by the use of two types of Doppler measurement. One-way Doppler is obtained by observing the received frequency and comparing it with the assumed frequency of the spacecraft auxiliary oscillator. Two-way Doppler is obtained by tracking the spacecraft in a two-way mode and comparing the uplink transmitted frequency with the received downlink frequency. Because of its much greater accuracy, two-way Doppler tracking data is the principal observable used in determining spacecraft trajectories.

4.4.1 Doppler Tracking Observables

Figure 4-17 is a functional diagram of the Doppler tracking system employed by the DSN. A very stable frequency reference is employed in the ground stations as a master oscillator. The master oscillator provides a frequency reference for a frequency synthesizer which is used to establish the ground transmitter frequency, ω_{GT}. The ground station transmits an rf carrier signal which is received by the PLL receiver in the spacecraft. The received frequency at the input to the spacecraft receiver's first mixer is ω_{SR}. This frequency differs from ω_{GT} by the uplink Doppler shift, due to the spacecraft's velocity away from the tracking station, and is

$$\omega_{SR} = \sqrt{\frac{c - \dot{R}}{c + \dot{R}}} \, (\omega_{GT} + \dot{\phi}_{UD}) \qquad (4.4\text{-}1)$$

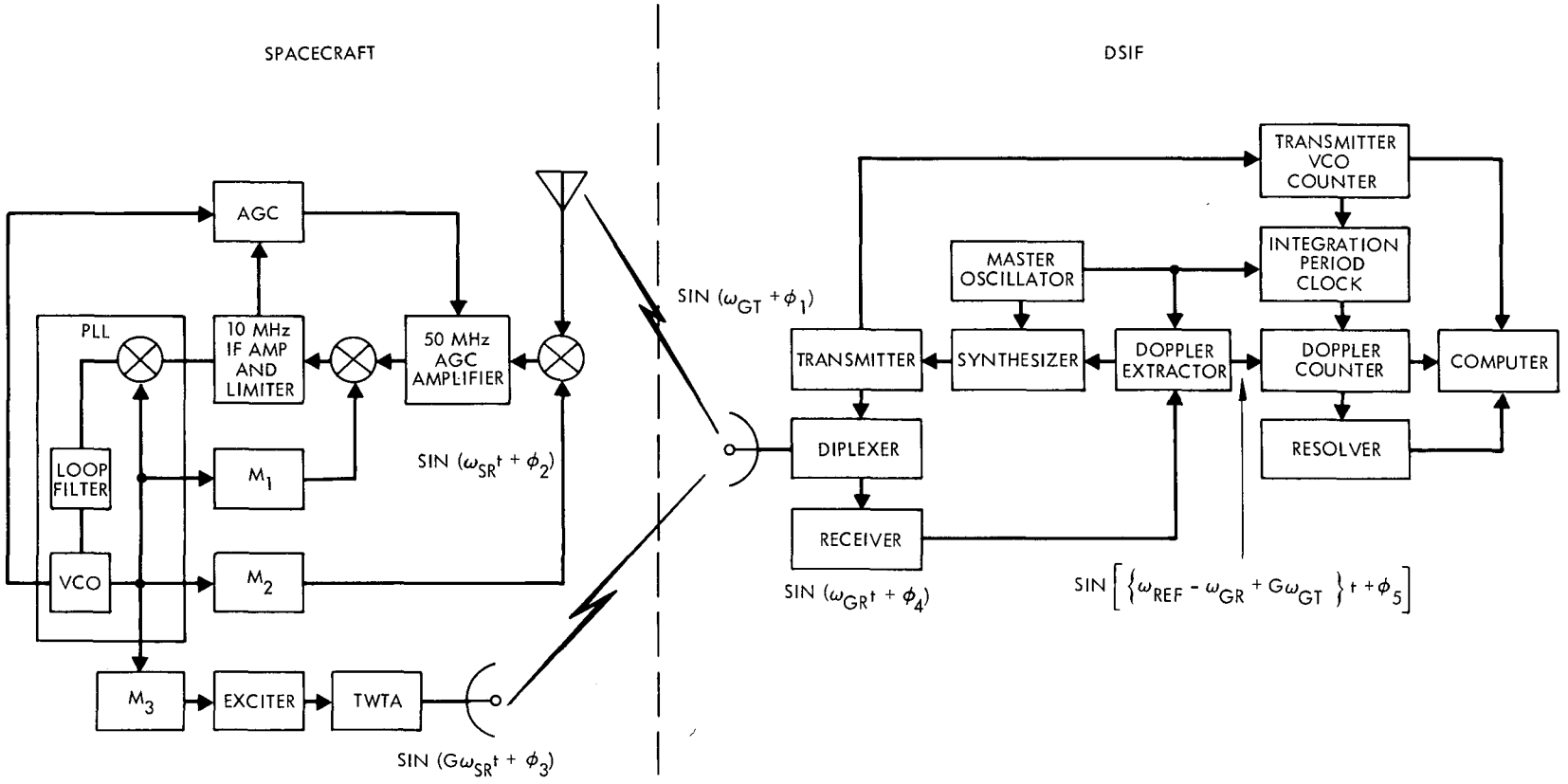

Fig. 4-17. Doppler tracking system functional block diagram

where

c = Free space propagation speed of the radio wave

$\dot{R}$ = Spacecraft range rate

$\dot{\phi}_{UD}$ = Rate-of-change of uplink phase delays

$\dot{\phi}_{UD}$ is the rate-of-change of any phase delays not due to the radial motion of the spacecraft, originating between the transmitter frequency reference and the spacecraft receiver input, as observed at the receiver input. The primary source of this delay variation is the charged particles along the propagation path of the uplink signal. This effect will be discussed below for up and downlinks.

The spacecraft receiver forms an estimate of the phase and frequency of the received signal, coherently multiplies the signal frequency by the transponder turnaround ratio, G, and transmits a downlink rf carrier at a frequency ω_{ST}, which is

$$\omega_{ST} = G\ \hat{\omega}_{SR} \tag{4.4-2}$$

$\hat{\omega}_{SR}$ = S/C receiver estimate of the received frequency.

The transponder ratio, G, for DSIF-compatible spacecraft is 240/221 for S-band or 880/221 for S-band uplink and X-band downlink.

The ground receiver observes a received frequency, ω_{GR}, which differs from the transmitted downlink frequency by the downlink Doppler shift.

$$\omega_{GR} = \sqrt{\frac{c - \dot{R}}{c + \dot{R}}}\ (\omega_{ST} + \dot{\phi}_{DD}) \tag{4.4-3}$$

where $\dot{\phi}_{DD}$ is the rate of change of downlink phase delays from the spacecraft receiver input to the ground receiver output not caused by the radial motion of the spacecraft. $\dot{\phi}_{DD}$ includes phase delays due to both charged particles and spacecraft receiver delays. Normally, charged particles are the major source of this phase delay variation.

The ground station PLL receiver forms an estimate of the phase and frequency of the received signal. This estimate is compared with the frequency of the transmitted signal by the Doppler extractor to obtain an estimate of the two-way Doppler frequency shift.

Combining equations 4.4-1 through 4.4-3, the estimated received frequency is

$$\hat{\omega}_{GR} \simeq \sqrt{\frac{c - \dot{R}}{c + \dot{R}}} \left\{ G \sqrt{\frac{c - \dot{R}}{c + \dot{R}}} \left(\omega_{GT} + \dot{\phi}_{UD}\right) + \dot{\phi}_{DD} \right\} \tag{4.4-4}$$

if $\hat{\omega}_{SR} \simeq \omega_{SR}$.

When $c >> \dot{R}$, which is usually the case, the estimate of the frequency received on the ground is

$$\hat{\omega}_{GR} = G\omega_{GT} \left(1 - \frac{2\dot{R}}{c}\right) + E_1 + E_2 \tag{4.4-5}$$

Where E_1 is the error in $\hat{\omega}_{GR}$ due to uplink phase shifts and E_2 is the error in $\hat{\omega}_{GR}$ due to downlink phase shifts.

$$E_1 = G\left(1 - \frac{2\dot{R}}{c}\right)\dot{\phi}_{UD} \tag{4.4-6}$$

$$E_2 = \left(1 - \frac{\dot{R}}{c}\right)\dot{\phi}_{UD} \tag{4.4-7}$$

The two-way doppler shift, D_2, is defined as

$$D_2 \triangleq \hat{\omega}_{GR} - G\omega_{GT} \tag{4.4-8}$$

So

$$D_2 \simeq G\omega_{GT} \left(-\frac{2\dot{R}}{c}\right) + E_1 + E_2 \tag{4.4-9}$$

However, the actual quantity observed in the station at the output of the Doppler extractor is D_2 shifted by a 1-MHz reference, ω_{ref}, derived from the station master oscillator. This is done so that one may distinguish

between positive and negative Doppler shifts. The observed signal frequency at the output of the Doppler extractor, ω_D, is:

$$\omega_D = \omega_{ref} - D_2 \tag{4.4-10}$$

The measurement of spacecraft slant range rate is therefore:

$$\dot{R} = \frac{c}{2G\omega_{GT}} \left(\omega_D - \omega_{ref} + E_1 + E_2 \right) \tag{4.4-11}$$

The range rate, $\dot{R}$, is used for determining the spacecraft trajectory during flight.

As noted above, the Doppler shifts in the uplink and downlink signals are important parameters in the design of the spacecraft telecommunication system. They are also important in the assignment of rf channels to the flight project by the DSN, as discussed in section VIII.

The downlink two-way Doppler, D_2, is given by equation 4.4-9.

The uplink one-way Doppler shift is defined by

$$D_1 \triangleq \omega_{SR} - \omega_{GT} \tag{4.4-12}$$

$$D_1 \simeq \omega_{GT} \left(- \frac{\dot{R}}{c} \right) \tag{4.4-13}$$

Equally important are the Doppler rates, $\dot{D}_1$ and $\dot{D}_2$. These are given by

$$\dot{D}_1 \simeq - \left(\frac{\omega_{GT}}{c} \right) \ddot{R} \tag{4.4-14}$$

$$\dot{D}_2 \simeq - \left(\frac{2G\omega_{GT}}{c} \right) \ddot{R} \tag{4.4-15}$$

4.4.2 Doppler Errors due to Charged Particles

When an electromagnetic wave propagates through a tenuous plasma, the phase velocity, v_p, differs from the speed of light in vacuum, c, by the formula

$$v_p = \frac{c}{\left(1 - \frac{\omega_p^2}{\omega^2}\right)^{1/2}} \qquad (4.4\text{-}16)$$

where ω_p = The plasma frequency.

For $\omega_p << \omega$, the interplanetary condition for S-band transmission,

$$v_p \approx c\left(1 + \frac{1}{2}\frac{\omega_p^2}{\omega^2}\right) \qquad (4.4\text{-}17)$$

Conceptually, the Doppler measurement of range considers the elapsed time between transmission and reception of a phase point. Thus, the derived range is

$$R = \frac{c}{2}\int_{path} \frac{ds}{v_p} \qquad (4.4\text{-}18)$$

where the integration is over the round-trip ray path.

ω_p depends on local electron density, so that it can be shown (reference 4-11) that the range measured by Doppler means, R_D, is given by:

$$R_D(t) = \frac{1}{2}\int_{path} ds - \frac{A}{f^2} I(t) \qquad (4.4\text{-}19)$$

where

$$A = \frac{1}{4}\left(\frac{e^2}{4\pi^2 \epsilon_o m_e}\right) = 20.15 \text{ (rationalized mks units)}$$

I = Combined uplink and downlink electron columnar content, electrons/m^2

e = Electron charge

m_e = Electron mass

ϵ_o = Permittivity of free space

The Doppler observable is then

$$\dot{R}_D(t) = \frac{1}{2} \frac{d}{dt} \int_{path} ds - \frac{A}{f^2} \dot{I}(t) \qquad (4.4\text{-}20)$$

The first term is equal to the actual range rate, $\dot{R}(t)$, plus other Doppler error terms $R_E(t)$, so that

$$\dot{R}(t) = R_D(t) - \dot{R}_E(t) + \frac{A}{f^2} \dot{I}(t) \qquad (4.4\text{-}21)$$

4.4.3 S/X Differential Doppler

The frequency dependence of the plasma effect on the Doppler observables can be used to correct the range-rate error and measure the total electron content.

The differential phase delay between a high frequency downlink carrier and a low-frequency downlink carrier, both of which are coherent with the uplink carrier, can be measured periodically through the mission to give (reference 4-12):

$$I(t) = -\Delta t_p(t) \frac{1}{\frac{2A}{c}\left(\frac{1}{f_1^2} - \frac{1}{f_2^2}\right)} \qquad (4.4\text{-}22)$$

where

f_2 = Frequency of high-frequency carrier

f_1 = Frequency of low-frequency carrier

and

Δt_p = Differential phase delay between carriers

$\Delta t_p = \frac{n}{f_1}$

where

n = Number of cycles slipped between the low-frequency carrier and the harmonic of the high-frequency carrier which has the frequency f_1

For the DSIF, the choice f_1 = S-band, f_2 = X-band, and $f_2/f_1 = 11/3$ can be made.

4.4.4 Very-High Range Rate Tracking

For phases of some missions (e.g., a close Jupiter flyby) range rates may become so high as to make special procedures necessary for maintaining two-way lock. Since such range rates are likely to occur for the most critical times in the mission (e.g., encounter or motor burn), it becomes vital to maintain command, ranging, and Doppler measurement capability. Difficulty in maintaining lock arises from several sources:

1) The Doppler frequency shift, even in cruise, may be so large as to exceed the dynamic range of the ground transmitter and/or receiver. That is, the ground referenced frequencies may depart from the design frequency channel in which the spacecraft operates.

2) With the standard DSIF exciter/receiver fixed-frequency configuration, the tuning required to maintain an acceptable spacecraft tracking-loop phase error may become so frequent and require so much time, as to result in unacceptable losses in the available amount of command, ranging, and Doppler measurement capability.

3) The Doppler rate may become so high as to exceed the tuning rate capability of the ground equipment.

4) Telemetry performance margins during encounter range rates are likely to be quite small, since the spacecraft is designed for peak data return at this time and a large performance margin indicates overdesign.

5) Subcarrier and data frequency shifts may seriously degrade data detection performance.

Several stratagems are available to lessen the impact of these conditions, while still using the standard DSIF equipment.

1) Additional exciter and receiver VCO's can be installed to handle communication in the shifted channels. Similar modifications can be made available for subcarrier and symbol loops.

2) Wide tracking subcarrier, and symbol detection bandwidths can be used to accommodate high range-rates and accelerations.

3) Tuning times can be chosen to make the least impact on mission capabilities.

Strategies can be devised by using the data available on tuning ranges, tuning rates, bandwidths, and recommended signal levels found in reference 4-13, however, each requires some degradation in performance. This degradation can be eliminated by the use of another device now being developed by the DSIF: the programmed local oscillator (PLO). This device outputs a precisely known frequency which varies with time according to predictions of spacecraft range and range rates. Thus, the exciter output is set at the frequency which, altered by Doppler, will be the best-lock frequency when the signal arrives one-way light time later at the spacecraft. The receiver frequency is tuned to where it will remain in-lock with this frequency, altered by Doppler, when it returns after the round-trip light time. By this means, command, ranging, and Doppler measurement can be maintained throughout a pass.

REFERENCES

4-1 Jaffe, R. M, and Rechtin, E., "Design and Performance of Phase-Lock Circuits Capable of Near Optimum Performance Over a Wide Range of Input Signals and Noise Levels," IRE Transactions on Information Theory, Vol. IT-1, March 1955, pp. 66-76.

4-2 Tausworthe, R. C., Theory and Practical Design of Phase-Locked Receivers, Volume 1, Jet Propulsion Laboratory, Technical Report No. 32-819, February 15, 1966.

4-3 Viterbi, A. J., Principles of Coherent Communications, McGraw-Hill (New York: 1966).

4-4 Gardner, F. M., Phaselock Techniques, John Wiley & Sons (New York: 1966).

4-5 Lindsey, W. C., A Theory for the Design of One-Way and Two-Way Phase-Coherent Communication Systems, Phase-Coherent Tracking Systems, Jet Propulsion Laboratory Technical Report No. 32-986, July 15, 1969.

4-6 Lindsey, W. C., "Coding and Synchronization Studies: Moments of the First Passage Time in Generalized Tracking Systems," Jet Propulsion Lab, Space Programs Summary 37-58, Vol. III, pp 63-66.

4-7 Charles, F. J., and Lindsey, W. C., "Some Analytical and Experimental Phase-Locked Loop Results for Low Signal-to-Noise Ratios, IEEE Proc., Vol. 54, No. 9, September 1966, pp. 1152-1166.

4-8 Sanger, D., and Tausworthe, R., "Digital Communication and Tracking: Experimental Study of the First Slip Statistics of the Second Order Phase Locked Loop, "Jet Propulsion Lab, Space Programs Summary 37-43, Vol. III, pp. 76-80.

4-9 Tausworthe, R. C., "Information Processing: Limiters in Phase-Locked Loops: A Correction to Previous Theory," Jet Propulsion Lab, Space Programs Summary 37-54, Vol. III, December 31, 1968, pp. 201-204.

4-10 Frazier, J. P., and Page, J., "Phase-Lock Loop Frequency Acquisition Study," Trans. IRE, SET-8, September, 1962.

4-11 MacDoran, P. F., "A First-Principles Derivation of the Differential Range Versus Integrated Doppler (DRVID) Charged-Particle Calibration Method," Jet Propulsion Laboratory Space Programs Summary 37-62, Vol. II, The Deep Space Network, March 31 1970, pp.28-34.

4-12 Koehler, R. L., "Radio Propagation Measurements of Pulsed Plasma Streams from the Sun, Using Pioneer Spacecraft," J. of Geophys. Res., Vol. 73, No. 15, August 1, 1968, pp 4883-4894.

4-13 Deep Space Network/Flight Project Interface Design Handbook, Jet Propulsion Laboratory, 810-5, DSN Standard Practice (JPL internal document).

SECTION V

TELEMETRY SYSTEM DESIGN

5.1 INTRODUCTION

The purpose of a telemetry system for interplanetary spacecraft is to transmit to Earth information of scientific and engineering value, and of the physical condition of the spacecraft. It is the goal of the telemetry system designer to produce a spacecraft system design which will provide the required amount of information of a specified quality in the most efficient and cost-effective manner possible. The design must be consistent with the resources of the project and the capabilities and resources of the Deep Space Network for the time period in which the spacecraft will operate. Finally, the design must be based on predictable performance, and the parameters governing the final quality of the data must be carefully analyzed, tested, and controlled.

This section describes the elements of telemetry system design techniques, compatible with the DSN, currently available to the system designer; factors which determine the efficiency of the telemetry system; factors which determine data quality; the type of data required for producing a good telemetry system design; and tradeoff considerations for selection between single and dual subcarrier design.

5.2 DESCRIPTION OF THE TELEMETRY SYSTEM

A telemetry system for interplanetary spacecraft performs the functions described below. It obtains data in the spacecraft from the data handling system in a form ready to be coded and modulated. Data may originally be in analog form from sensors and instruments, or it may be inherently discrete or digital data, such as counter readings, status information, or synchronization codes. This data is usually processed into binary digits whose period and clock rate are accurately known. The digital telemetry system may code any or all of this data into code symbols. Figure 5-1 is a functional block diagram representation of a telemetry system for interplanetary spacecraft.

The telemetry system also performs a modulation function. Under certain circumstances, a project may choose an analog modulation scheme for

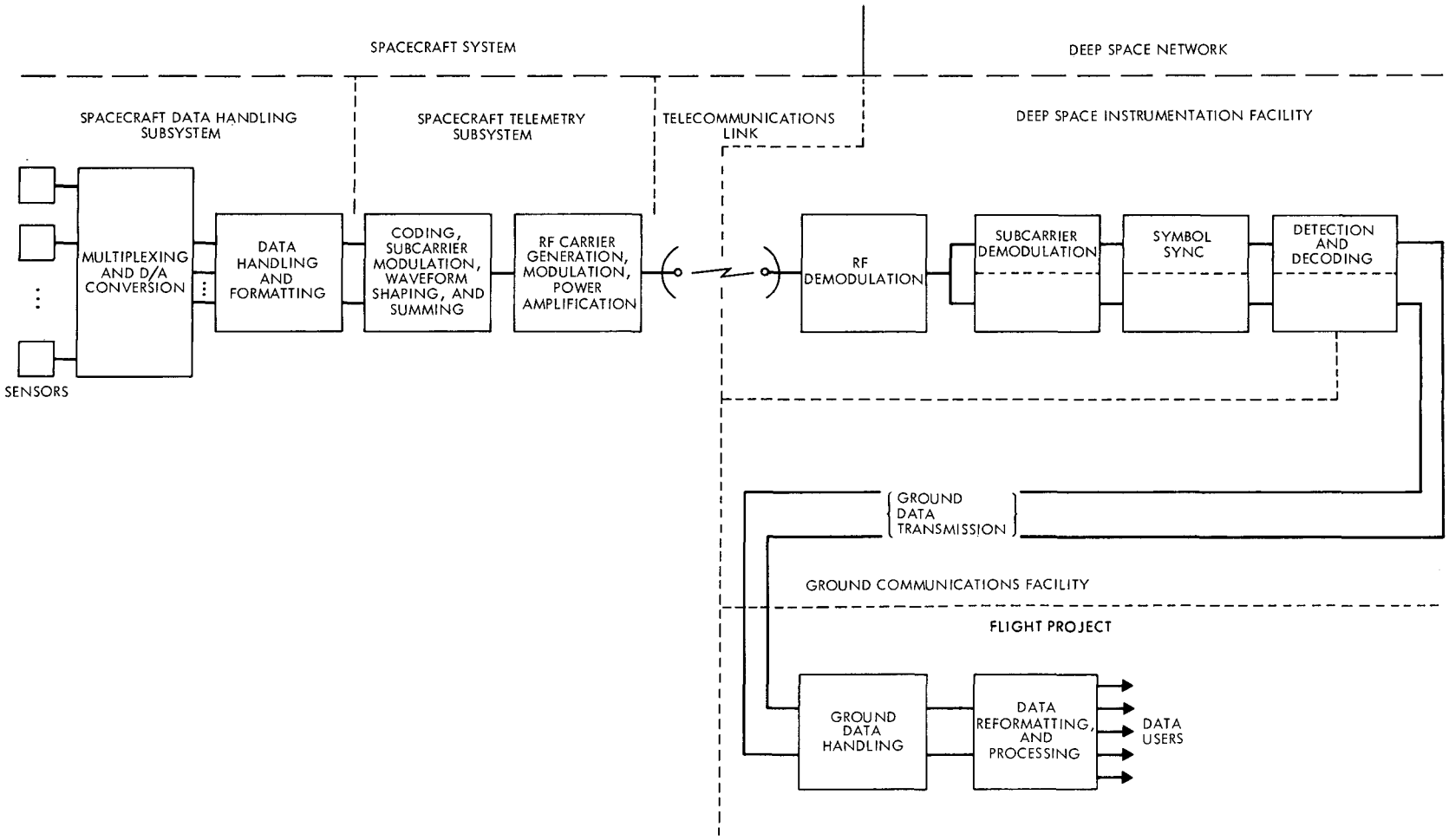

Fig. 5-1. Generalized telemetry system

some of its data. However, the Multi-Mission Telemetry System (MMTS) of the DSN is not equipped to demodulate and process analog data, so the project must supply mission-dependent analog demodulation equipment. The DSN is set up to handle digital telemetry systems, and some choice as to modulation technique is available to the system designer. Digitized data is normally modulated onto one or more subcarriers. Each subcarrier constitutes a data channel. The data-bearing subcarriers are processed to obtain a desired waveform, and are combined into a composite telemetry signal. Since transmission of electromagnetic radiation to Earth is more efficient at microwave frequencies, an rf carrier is generated and the composite telemetry signal modulates the carrier.

The DSN is equipped to receive at S- and X-band (64-meter stations) frequencies, so that the spacecraft may transmit data on two carriers, one in each band. The rf signal is amplified and radiated by an antenna whose gain pattern is designed with the unique requirements of the mission in mind.

On the ground, antennas of the DSN intercept the radiated rf power and amplify the signal, using low-noise masers. Each subcarrier is demodulated by a Subcarrier Demodulator Assembly (SDA). If analog modulation is used by the spacecraft, the project-supplied mission-dependent demodulator obtains its data at this point. If a DSN-compatible modulation technique is used, the SDA will recover data from the signal, and produce a waveform which consists of demodulated data bits, plus noise.

The output from the SDA is fed to the Symbol Synchronizer Assembly (SSA) which integrates the data over a bit time using a matched filter, and detects transitions in the integrated data, to establish symbol sync and to make an estimate of the transmitted symbols.

If no coding was used, the estimated data bits are sent to the Telemetry and Command Data Handling System (TCD) for recording data at the station, and for formatting and subsequent transmission from the tracking station to the Project where the data is decommutated and presented to the data users.

If the data was coded on board the spacecraft, the detected symbols from the SSA are fed to a decoder before processing in the TCD. At present there exists a Block Decoder Assembly (BDA) for decoding (32, 6) and (16, 5)

Biorthogonal Block Codes, and a Data Decoder Assembly (DDA) which decodes convolutionally encoded data. The decoded data is then presented to the TCD for recording and transmitting to the project.

5.2.1 Modulation Techniques for Digital Communications

Demodulation capability is presently available at the DSS for signals whose rf carrier and subcarriers are phase modulated. A phase-lock-loop receiver is employed by the MMTS to obtain a phase reference so that the carrier is coherently demodulated.

The MMTS can accommodate signals utilizing either square- or sine-wave subcarriers. Normally one or two simultaneous subcarriers are used. The number is limited by the number of SDA's and SSA's available in the stations.

5.2.1.1 Phase Shift Keyed Modulation. Figure 5-2 shows a schematic representation of a spacecraft telemetry system using multiple subcarriers which phase modulate an rf carrier. In other words, the signal transmitted by the spacecraft is of the form

$$y(t) = \sqrt{2P_t}\ \sin\left\{\omega_c t + \phi_o + \theta_1 (D_1 \oplus SC_1) + \theta_2 (D_2 \oplus SC_2) + \ldots\right\} \quad (5.2\text{-}1)$$

where

$y(t)$ = Transmitted waveform

P_t = Transmitted power at the transmitting antenna terminals

ω_c = Carrier frequency

ϕ_o = Phase reference, a random variable, uniformly distributed between 0 and 2π

θ_i = Modulation index (degrees) for the i^{th} subcarrier channel

D_i = Binary data symbols in the i^{th} channel

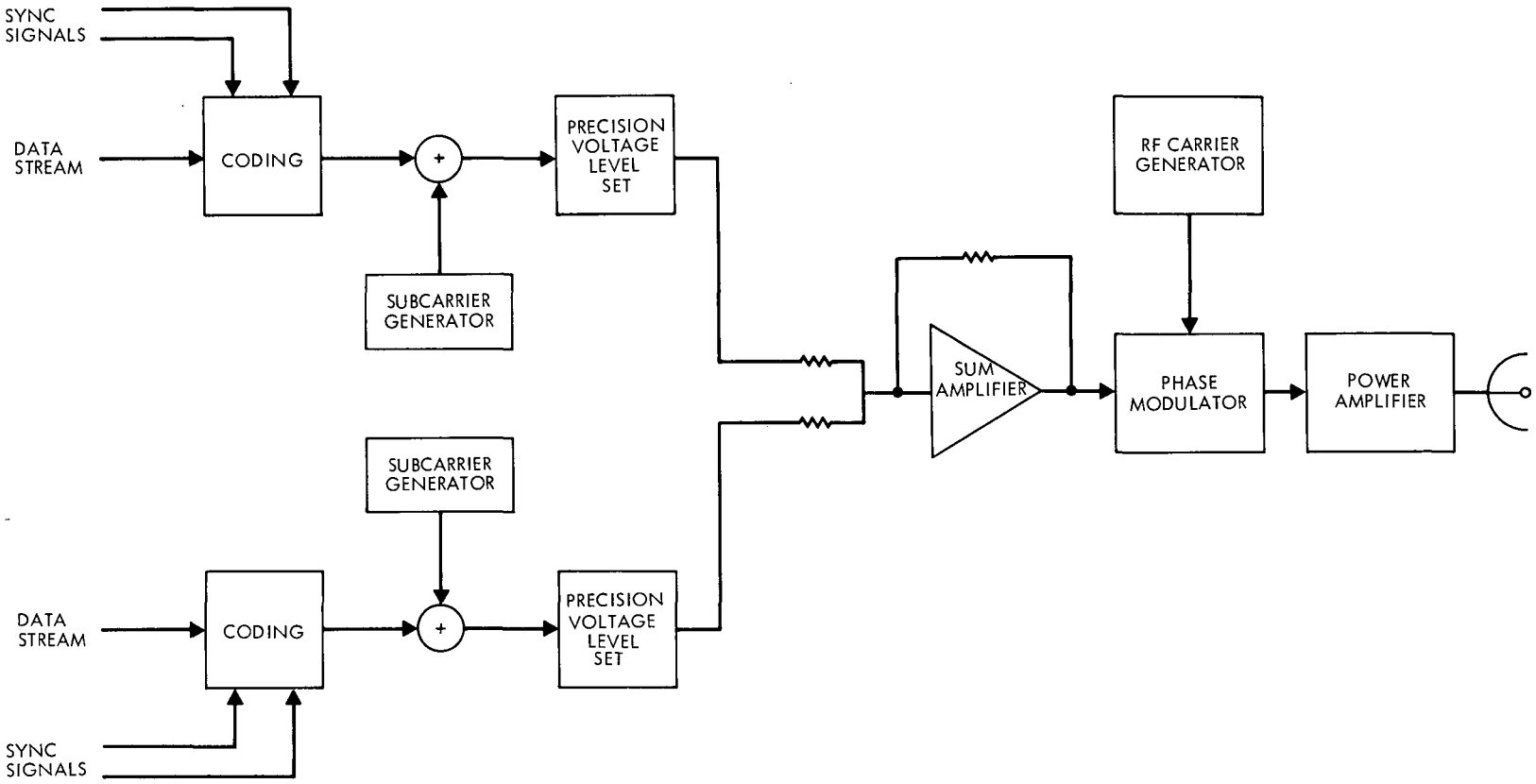

Fig. 5-2. Spacecraft telemetry subsystem

SC_i = Subcarrier waveform in the i^{th} channel

$\oplus$ = Modulo 2 addition for square-wave subcarriers and multiplication for sine waves.

The phase modulator is a device which shifts the phase of the rf carrier in linear proportion to the voltage applied by the composite telemetry waveform. The modulation indices, θ_i, are defined by

$$\theta_i \triangleq T_i K \tag{5.2-2}$$

where

θ_i = Modulation index (degrees)

T_i = Peak voltage level of the i^{th} telemetry channel (volts)

K = Phase modulator sensitivity (degrees per volt)

Figure 5-3 shows how the phase-lock receiver derives a carrier reference by which the subcarrier and data may be demodulated from the received waveform. The received signal, x(t), is mixed with a monochromatic signal of the estimated frequency of x(t). The output of the mixer consists of a waveform having components of the form $\cos(\phi - \hat{\phi})$ and $\cos(2\omega_c t + \phi + \hat{\phi})$. The loop filter is a low-pass filter which removes the double frequency terms to produce a slowly varying error signal which changes the output of a voltage controlled oscillator (VCO) in such a way that the phase of the VCO output $\hat{\phi}$ tries to match the average phase ϕ of x(t). In the absence of noise, if the free-running frequency of the VCO is identical to x(t) and if the changes in $\phi(t)$ due to modulation are of a frequency very much greater than the loop bandwidth of the receiver, $\hat{\phi}$ will equal ϕ, and the carrier reference from the VCO will be coherent with the phase of the received carrier.

Practical receivers will introduce some white gaussian noise in the first amplifier before the receiver, so that the phase of x(t) is corrupted by additive noise of one-sided spectral density N_o (watts/Hz). The phase estimate $\hat{\phi}$ generated by the receiver will be an imperfect replica of the phase of the received rf carrier. The receiver in this case is said to be partially coherent.

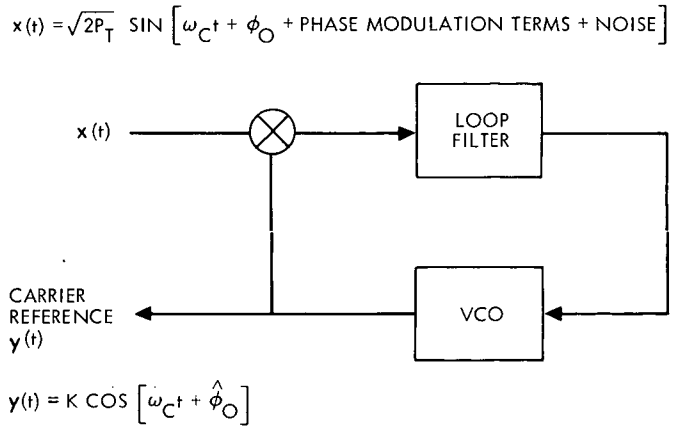

Fig. 5-3. Carrier tracking phase lock loop

More details on the operation of the phase locked loop receiver may be found in references 5-1 and 5-2 and in section IV.

The received signal, x(t), is demodulated as follows: The signal x(t) is multiplied by the carrier reference derived by the phase lock loop (PLL) to obtain the waveform

$$x(t) \cos (\omega_c t + \hat{\phi})$$

where

$\hat{\phi}$ = Estimate of the phase reference ϕ_o.

The components about $2\omega_c$ are filtered out, leaving

$$\sin \left\{\phi + \theta_1 (D_1 \Theta SC_1) + \theta_2 (D_2 \Theta SC_2) + \ldots\right\} \qquad (5.2\text{-}3)$$

where

$$\phi = \phi_o - \hat{\phi}$$

The frequencies of the subcarrier SC_1, SC_2, etc. must be sufficiently far apart so that the terms $D_i \Theta SC_i$ each occupy different portions of the frequency spectrums. The data-bearing subcarriers can each be isolated by an SDA, and each subcarrier removed from its data. For convenience in circuit

design, the process of removing the carrier reference is performed in the SDA after removal of the subcarriers. Conceptually, the procedure for removal of the subcarriers is the same as that described above. Figure 5-4 gives a schematic representation of the entire demodulation process.

5.3 CHANNEL QUALITY

Of prime concern in the design of any telemetry system is the quality of the data which is returned to the user. It is the responsibility of the telemetry system designer to obtain the requirements for data quality from each user in his project, and thus determine design point values of the appropriate parameters of his system.

The quality of analog signals can usually be expressed in terms of the mean square error of the signal immersed in noise. The quality of digital data is usually expressed in terms of either the data bit error rate or the data word error rate. The choice of bit or word error rate as a criterion will depend primarily on the type and use of the data.

The parameters appropriate for specifying the quality of data depend on the type of communication channel and the modulation techniques applied. For the free-space channel usually encountered by deep space vehicles, the channel is characterized as Gaussian, and the noise (which is almost entirely generated in the front end of the receiver) is white, additive noise characterized by some constant noise spectral density, N_o watts/Hz.

For other types of channels occasionally encountered by deep space vehicles, such as a multipath channel, the characterization is other than Gaussian. It may be Rician, or in the extreme, a non-parametric characterization may be necessary.

We will primarily be concerned here with Gaussian white additive noise.

5.3.1 Data Error Rate Requirements

It is the responsibility of the telemetry system designer to collaborate with Project personnel to establish meaningful specifications of data error rate requirements. These specifications must be established early in the planning phase of the mission so that appropriate design decisions can be made.

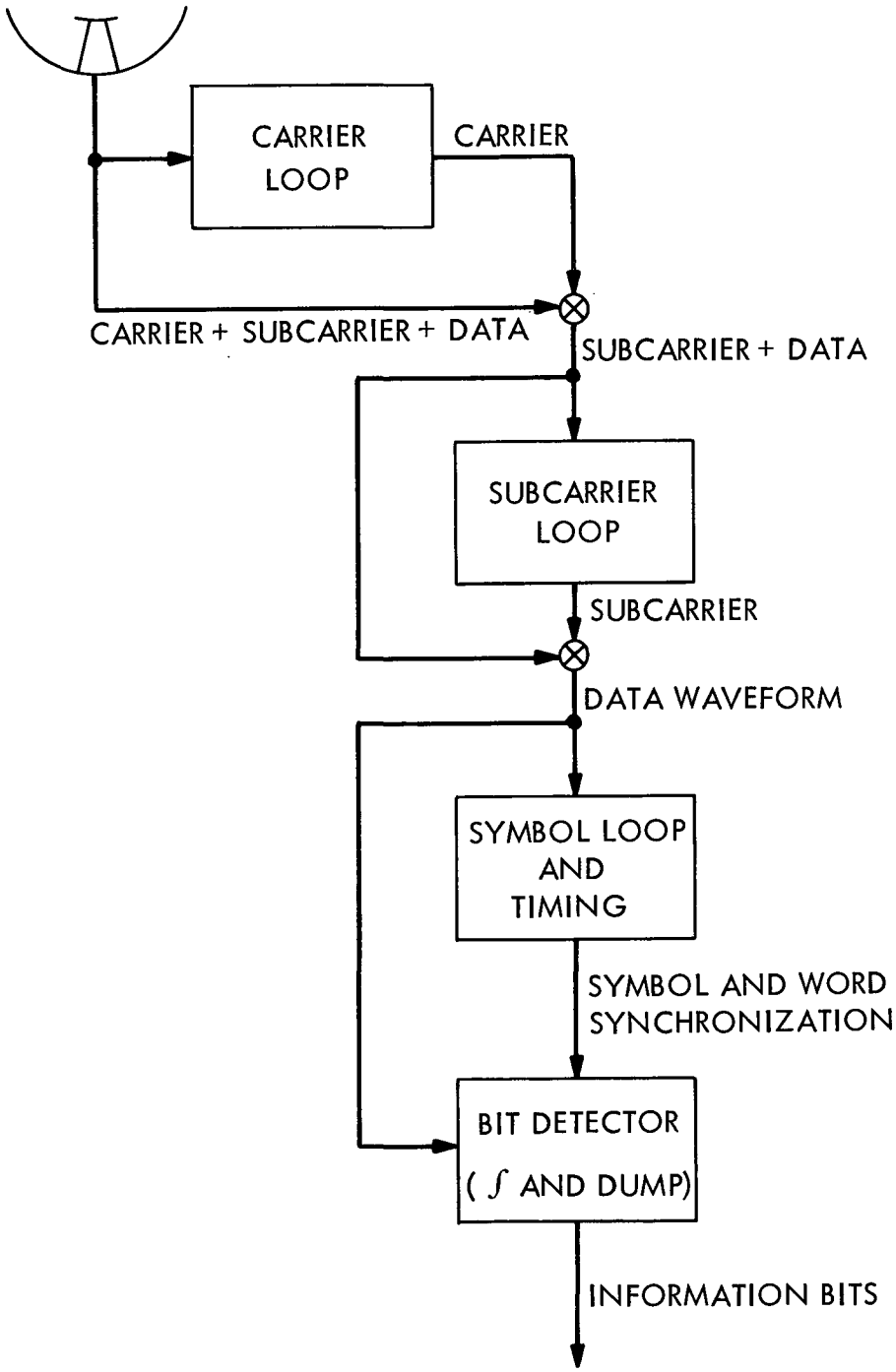

Fig. 5-4. Schematic representation of the demodulation process

There are generally two types of data generated by a deep space vehicle for telemetering to Earth. First, there is data which is inherently digital in nature. Examples of this data are pseudo-noise (PN) sequences used for synchronization of data, status bits, and counting. The quality of this kind of data is described in terms of an average bit error rate.

The second type of data is obtained from instruments or sensors, and is inherently analog. This data may have some noise associated with it generated by the measurement process (cf. ref. 5-3), or it may be essentially clean data. In any event, analog data must be converted to binary digits by some sort of analog-to-digital (A/D) converter and processed for transmission by the telemetry system. The bit stream accepted by the telemetry modulation subsystem will contain bits which stand by themselves, and groups of bits which are data words representing some quantization of analog information.

Data word quality may be specified by their user in terms of either average word error rate, or an average bit error rate, depending upon the use of the data and the convenience of the Project.

The quality of the communication channel is not always identical to the quality of the data provided to the user. The measure of the quality of the received bits depends on the type of channel (whether Gaussian or otherwise) on the type of coding used, and on the method of detection used. Typically, the performance of the telemetry system is measured by the bit error rate at the output of the symbol synchronizer if the data bits are uncoded, or by the word error rate of block coded words at the output of the BDA, or by bit error rates and erasure rates at the output of the DDA for convolutionally encoded, sequentially decoded data. For a purely Gaussian channel, the symbol errors out of the SSA will be independent of each other. If the channel is not Gaussian (for example, if it contains multipath effects), the symbol errors may come in bursts.

Since symbol synchronization is obtained by estimating transitions from the output of the SDA, a low transition density of the transmitted symbols will cause symbol errors to be produced in bursts.

Although the symbol errors may be independent of each other, the detection of block coded words is made on a word basis, hence word errors rather than bit errors are independent.

When the channel is convolutionally encoded and sequentially decoded, two types of errors are made: bit errors and buffer overflows, or erasures. Erasures may be stored on tape so that the received symbols are not lost. However, the time required to decode some erasures may be prohibitively expensive, so that some amount of data will not be provided to the user. When using sequential decoding, the erasure rate must be specified by the project and ground rules for post-mission decoding of the erasures should be established.

Viterbi decoding of data does not produce erasures, since a decision as to the state of every bit is made. Bit errors occur, but they are grouped in bursts of one to two constraint lengths of the code. Also, the performance of the Viterbi algorithm is known to be sensitive to bursts of errors in the incoming symbol stream so that Viterbi decoding would not be appropriate for slow fading multipath channels (fading over many bits).

The elements of block and convolutional encoding and of block, sequential, and Viterbi decoding will be discussed below.

The average error rate measured at the DSN station is not always the same as the error rate specified by the data users. In addition to errors measured at the stations, the ground handling of the data (e.g., transmitting data from the station to the project, deformatting, and processing of the data for presentation to the user) will introduce errors due to occasional loss of frame sync, and occasional data outages.

Typically, errors introduced by the ground system will be of the burst error variety. Thus, specification of an average bit or word error rate to be delivered to the users will insufficiently characterize the ground link. For example, data delivered through the GCF may be essentially error-free for long periods of time and then degrade to unusable error rates for periods (see reference 5-28).

The prime mode of correcting errors made in the GCF portion of the ground link is post-pass playback of the magnetic tape records made at the station. If sufficient playback time is not available to fulfill data quality and quantity requirements, the records can be transported to the Project for post processing. In the case of GCF data outages, near real-time correction may be possible if two DSS's are tracking the vehicle, by bringing up the second station. Thus, it is desirable to plan the mission trajectory to obtain tracking

redundancy at critical periods, if sufficient DSS schedule flexibility is available.

Errors made in Project data processing can be corrected in near-real-time by recalling the affected data from the GCF computer storage devices, located at the JPL terminal of the GCF. The effect of ground or space link errors in the frame sync PN code can be reduced by software adjustment of the allowable number of errors in the code. However, the designer must investigate the likelihood of PN-like sequences in the data and minimize the possibility of false frame sync by proper design of telemetry word time sequence.

While the telemetry system designer is not responsible for ground data handling, he must be aware of the problems so that he can accurately relate the error rates measured at the station to the error rates in the data returned to the user.

5.3.2 Uncoded Channel Performance

In this section, the performance of the uncoded Gaussian channel with white additive noise, will be discussed. The performance of a receiver for a binary digital signal depends on the phase coherence of the receiver and the type of modulation employed at the transmitter. Following Viterbi (Rev. 5-2), a transmitted signal may be written as

$$s_j(t) = C_j(t) \sin\left\{\omega_o t + \theta_j(t) + \phi\right\} \quad \begin{matrix} 0 < t < T_s \\ j = 0, 1 \end{matrix} \qquad (5.3\text{-}1)$$

where

T_s = Symbol period

The modulation scheme determines the form of $\theta_j(t)$ and $C_j(t)$ whereas the ability of the receiver to track ϕ is a measure of its coherence.

The receiver which operates on a signal with additive noise sees the waveform.

$$y(t) = s_j(t) + n(t)$$

For a receiver of this type, the optimum detector is a matched filter, or correlation detector. It is this type of detector which is employed by the MMTS to detect transmitted symbols. (For a brief discussion of matched

filter detection, see ref. 5-29; a more general tutorial is contained in ref. 5-30.) The correlation detector can be modeled as in Figure 5-5. The detector model is predicated on the assumption that each transmitted symbol is equally likely, and that each symbol has equal energy.

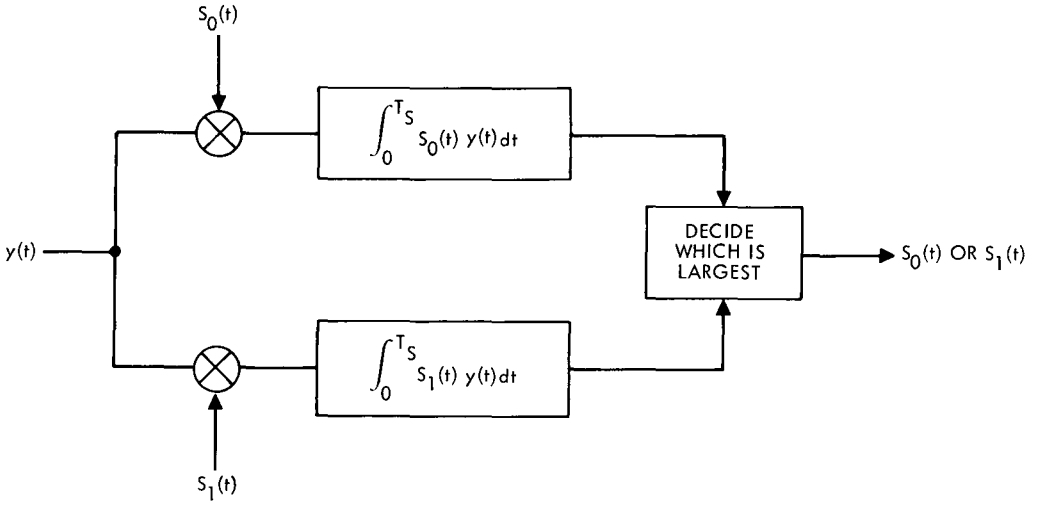

Fig. 5-5. Correlation detector

The energy of each symbol out of the detector is

$$\mathcal{E} = \int_0^{T_s} S_o^2(t)dt = \int_0^{T_s} S_1^2(t)dt \qquad (5.3\text{-}2)$$

where

$\mathcal{E}$ = Energy per symbol

A measure of the distinguishability of the two signals is the normalized integral inner product, ρ.

$$\rho \triangleq \frac{1}{\mathcal{E}} \int_0^{T_s} S_o(t)S_1(t)dt \qquad (5.3\text{-}3)$$

What follows assumes that the receiver obtains perfect knowledge of the transmitted phase reference, ϕ, and of the transmitted symbol transition time. Then, as shown in reference 5-2, the probability of symbol error, P_E, is

$$P_E = 1 - \int_{-\infty}^{\sqrt{\frac{\mathcal{E}(1-\rho)}{N_o}}} \frac{\exp(-y^2/2)}{\sqrt{2\pi}}\, dy = \frac{1}{2}\,\mathrm{erfc}\,\sqrt{\frac{\mathcal{E}(1-\rho)}{2N_o}} \qquad (5.3\text{-}4)$$

where

$$\mathrm{erfc}(x) = 1 - \frac{2}{\sqrt{\pi}} \int_o^x e^{-t^2} dt$$

If the transmitted symbols S_o and S_1 are 0 and 1, respectively, they are orthogonal ($\rho = 0$).

If they are 1 and -1, they are antipodal ($\rho = -1$). Antipodal signals are ordinarily transmitted by deep space vehicles to prevent difficulties in zero detection in the presence of noise.

If the binary symbols have a signal power of S watts and last for T_B seconds, $\mathcal{E} = ST_B$. Thus, the error probability for uncoded symbols transmitted over a Gaussian channel and detected in white additive noise is

$$P_E = \frac{1}{2}\,\mathrm{erfc}\,\sqrt{\frac{ST_B}{N_o}} \qquad (5.3\text{-}5)$$

It is this characterization of the error rate of the uncoded channel which is used to specify a design point value of ST_B/N_o for the uncoded telemetry system. Figure 5-6, for k = 1, is the bit error performance curve of an uncoded channel with perfect carrier reference and perfect symbol sync.

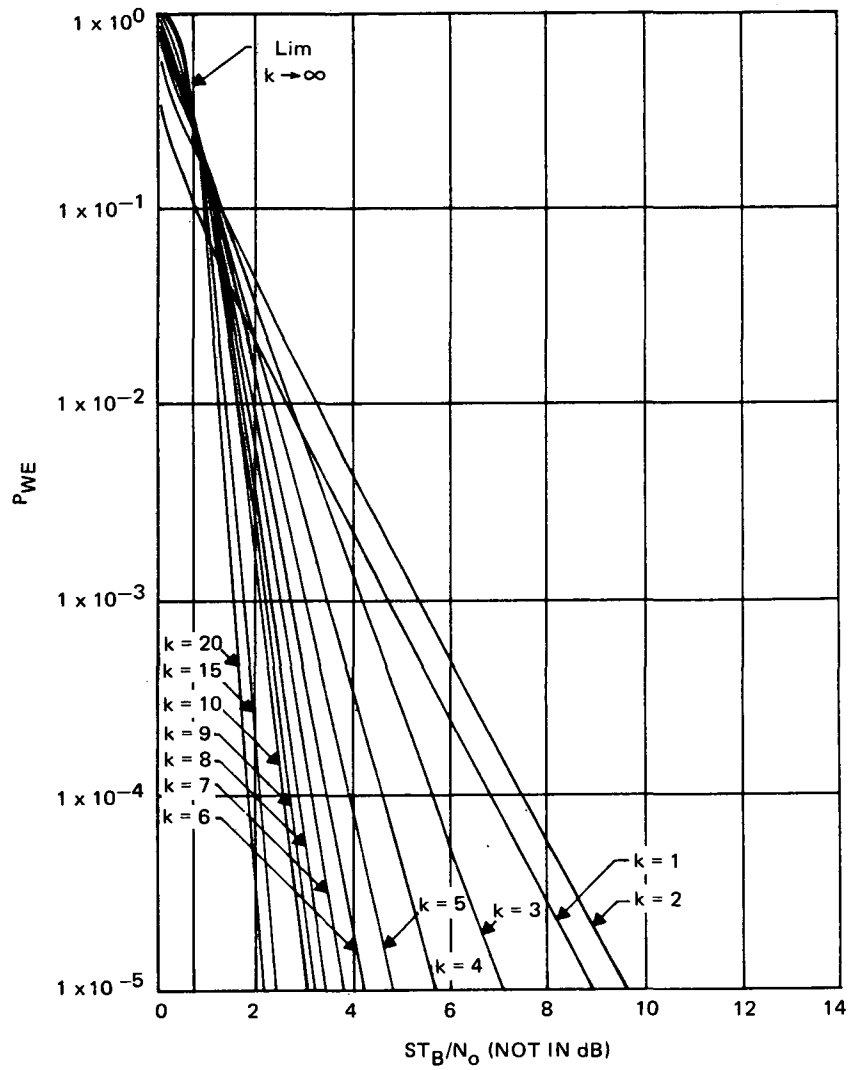

Fig. 5-6. Word error probability versus ST_B/N_o for a $(2^{k-1}, k)$ biorthogonal block code

(Ref. 5-4, A. J. Viterbi, 'Phase-Coherent Communication over the Continuous Gaussian Channel' in S. W. Golomb, Ed., DIGITAL COMMUNICATIONS WITH SPACE APPLICATIONS, Copyright 1964. Reprinted by permission of Prentice-Hall, Inc., Englewood Cliffs, New Jersey.)

In the Gaussian channel we are discussing, symbol errors are independent thus, for an uncoded channel, the probability of word error in a word length of k bits is:

$$P_{WE} = 1 - (1 - P_E)^k \tag{5.3-6}$$

Table 5-1 tabulates bit error probability versus ST_B/N_o for an uncoded channel (from ref. 5-4).

5.3.3 Channel Coding

A classic result in information theory is that the error probability can be reduced if the information bandwidth is increased. Coding is the process of mapping k data bits into n code symbols to expand the transmission bandwidth in a particular way. Decoding is the inverse process performed by mapping the detected n symbol estimates into k data bits. If an efficient code is selected and a good decoding scheme used, the k data bits will have a lower average bit error probability for the same ST_B/N_o than if they were transmitted uncoded.

The MMTS is equipped to decode both biorthogonal block code and convolutional codes. The Block Decoder Assembly (BDA) accepts code symbols from the SSA and decodes either (16, 5) or (32, 6) biorthogonal code words. The Data Decoder Assembly (DDA) is a small computer which is programmed to decode a rate 1/2, constraint length 32, convolutional code using a sequential decoding algorithm. There are plans to develop a Viterbi decoding algorithm for the DDA which would decode short constraint length convolutional codes.

5.3.3.1 Block Codes. When a block of data bits taken k at a time are mapped into a sequence of n symbols taken from a finite set of possible symbol sequences, the process is known as block coding and the code is called an (n, k) block code. Each of the 2^k possible data words is uniquely mapped into one of 2^n possible code words. If each bit in the data word is independent of the other bits, and is equally likely to be a "1" or "0", then the possible code

Table 5-1. Bit error probability versus ST_B/N_o for an uncoded channel*

ST_B/N_o		P_E	ST_B/N_o		P_E
Ratio	dB		Ratio	dB	
.080	-10.969	.34458	3.125	4.948	.00621
.125	- 9.031	.30854	3.380	5.289	.00466
.180	- 7.447	.27425	3.645	5.617	.00347
.245	- 6.108	.24196	3.920	5.933	.00256
.320	- 4.948	.21185	4.205	6.238	.00187
.405	- 3.925	.18406	4.500	6.532	.00135
.500	- 3.010	.15865	4.805	6.817	.0009689
.605	- 2.182	.13566	5.120	7.093	.0006882
.720	- 1.427	.11507	5.445	7.360	.0004843
.845	- .731	.09680	5.780	7.619	.0003377
.980	- .088	.08056	6.125	7.871	.0002333
1.125	0.512	.06681	6.480	8.116	.0001597
1.280	1.072	.05480	6.845	8.354	.0001082
1.445	1.599	.04457	7.220	8.585	.0000727
1.620	2.095	.03593	7.605	8.811	.0000484
1.805	2.565	.02872	8.405	9.245	.0000209
2.000	3.010	.02275	7.245	9.659	.0000087
2.205	3.434	.01787	10.125	10.054	.0000036
2.420	3.838	.01391	11.045	10.432	.0000015
2.645	4.224	.01073	12.005	10.794	.0000006
2.880	4.594	.00820			

*Source: Ref. 5-4, A. J. Viterbi, 'Phase-Coherent Communication over the Continuous Gaussian Channel' in S. W. Golomb, Ed., DIGITAL COMMUNICATIONS WITH SPACE APPLICATIONS, Copyright 1964. Reprinted by permission of Prentice-Hall, Inc., Englewood Cliffs, New Jersey.

word signals $s_n(t)$ which are generated are all equally probable and therefore contain the same energy $\mathcal{E}$.

The detector for block-coded words for coherent reception in white noise can be modeled as a device consisting of 2^k correlators whose outputs are sampled at the word time, T_w. The correlator outputs are compared, and the data word corresponding to the largest correlator output is chosen as the detected word. (The physical mechanization of the block decoder (BDA) is slightly different than this model.)

The performance of the block code generated depends on the distinguishability of the code words. A measure of this distinguishability is the set of normalized inner products.

$$\rho_{rn} = \rho_{nr} = \frac{\int_o^{T_w} S_n(t)S_r(t)dt}{\mathcal{E}} \tag{5.3-7}$$

Orthogonal codes are a class of block codes for which $n = 2^k$, $\rho_{nr} = 0$ when $n \neq r$, and $\rho_{nr} = 1$ when $n = r$.

For this class of codes, the quantity ρ_{nr} may be expressed as the identity matrix,

$$\rho_{nr} = \begin{bmatrix} 1 & 0 & \cdots & 0 \\ 0 & 1 & & \\ \vdots & & \ddots & \\ 0 & & & 1 \end{bmatrix} \tag{5.3-8}$$

Such a code can be represented by a Hadamard matrix. For example, if $k = 1$, and $n = 2$,

$$H_1 = \begin{bmatrix} 0 & 0 \\ 0 & 1 \end{bmatrix} \text{ is the code dictionary for the data words } \begin{bmatrix} 0 \\ 1 \end{bmatrix}, \text{ that is, a "0" data bit becomes the symbol sequence 00, and a "1" data bit becomes 01.} \tag{5.3-9}$$

For k = 2, n = 4,

$$H_2 = \begin{bmatrix} H_1 & H_1 \\ H_1 & \overline{H}_1 \end{bmatrix} = \left[\begin{array}{cc|cc} 0 & 0 & 0 & 0 \\ \underline{0} & \underline{1} & \underline{0} & \underline{1} \\ 0 & 0 & 1 & 1 \\ 0 & 1 & 1 & 0 \end{array}\right] \text{ is the dictionary for } \begin{bmatrix} 0 & 0 \\ 0 & 1 \\ 1 & 0 \\ 1 & 1 \end{bmatrix} \qquad (5.3\text{-}10)$$

In general

$$H_{k+1} = \begin{bmatrix} H_k & H_k \\ H_k & \overline{H}_k \end{bmatrix} \qquad (5.3\text{-}11)$$

The effective bandwidth required by the block code symbols may be reduced by one-half, if instead of an orthogonal code, a biorthogonal code is used. This code results from combining an orthogonal code with its complement. The biorthogonal code is represented as

$$H_{k+1} = \begin{bmatrix} H_k \\ \hline \overline{H}_k \end{bmatrix} \qquad (5.3\text{-}12)$$

and $n = 2^{k-1}$.

The performance of biorthogonal codes has been derived in reference 5-4. The probability of a k-bit word error is shown to be

$$P_{WE} = 1 - \int_{-\sqrt{2ST_W/N_o}}^{\infty} \frac{\exp(-V_1^2/2)}{\sqrt{2\pi}} \left[\int_{-V_1 - \sqrt{\frac{2ST_W}{N_o}}}^{V_1 + \sqrt{\frac{2ST_W}{N_o}}} \frac{\exp(-V^2/2)}{\sqrt{2\pi}} dV \right]^{2^{k-1}-1} dV_1 \qquad (5.3\text{-}13)$$

where

$$T_W = kT_B$$

assuming that the channel is Gaussian with white additive noise, and that a perfect carrier phase reference and a perfect word timing reference are available at the receiver.

Equation (5.3-13) is used to establish the design point ST_B/N_o necessary to achieve a required P_{WE}. Figure 5-6 (from ref. 5-4) compares P_{WE} versus ST_B/N_o for biorthogonal codes with various choices of k. Figures 5-7 and 5-8 compare uncoded and biorthogonal coded word error rates for the same number of information bits, k, per word.

The information bit error rate of a biorthogonal code is found to be

$$P_{BE} = \frac{1}{2} P_{WE} + \frac{1}{2} P_1 \qquad (5.3\text{-}14)$$

where

$$P_1 = \int_{-\infty}^{-\sqrt{2ST_W/N_o}} \frac{\exp(-V^2/2)}{\sqrt{2\pi}} \left[\operatorname{erf}\left(\frac{V}{\sqrt{2}} + \sqrt{\frac{ST_w}{N_o}} \right) \right]^{2^{k-1}-1} dV$$

for $k \geq 5$, the bit and word error rates can be approximately related by

$$P_{BE} = \left(\frac{2^{k-1}-1}{2^k-1} \right) P_{WE} \qquad (5.3\text{-}15)$$

Figure 5-9 plots P_{BE} versus ST_B/N_o for biorthogonal block codes. Tables 5-2 and 5-3 give bit and word error rates versus ST_B/N_o for (16, 5) and 32, 6) biorthogonal codes.

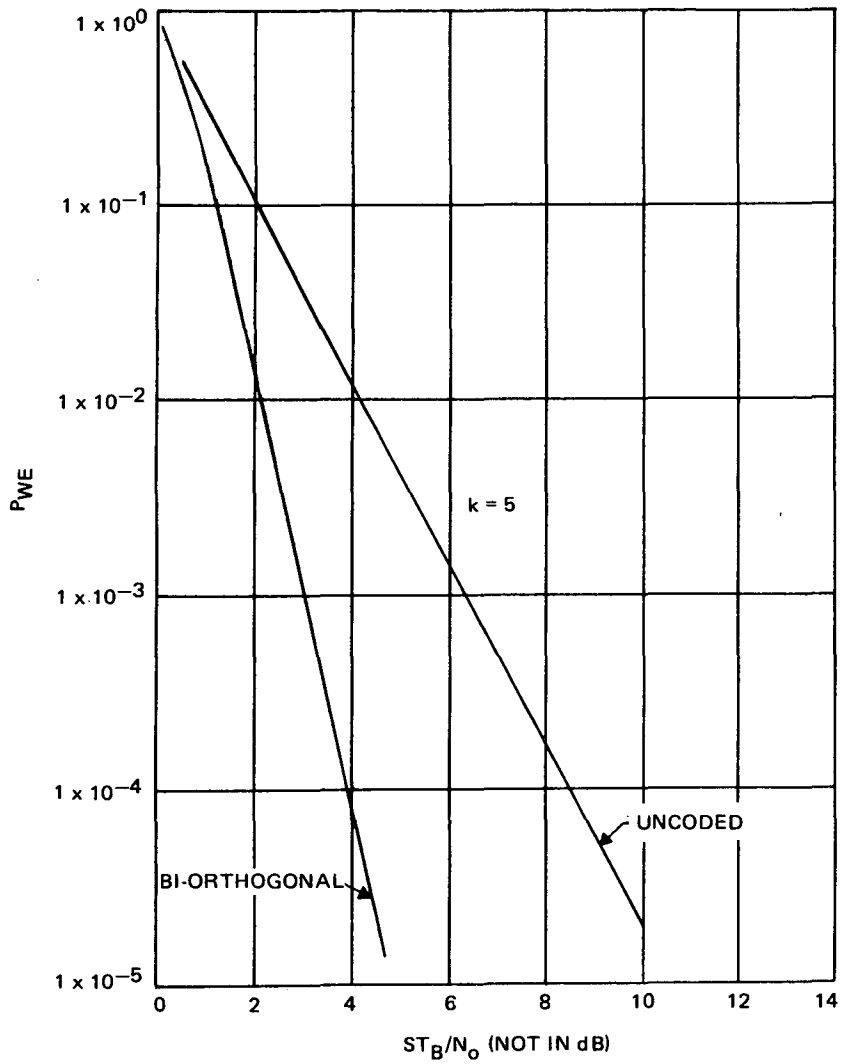

Fig. 5-7. Word error probability versus ST_B/N_o for uncoded and biorthogonally block coded words of information bit length 5

(Ref. 5-4, A. J. Viterbi, 'Phase-Coherent Communication over the Continuous Gaussian Channel' in S. W. Golomb, Ed., DIGITAL COMMUNICATIONS WITH SPACE APPLICATIONS, Copyright 1964. Reprinted by permission of Prentice-Hall, Inc., Englewood Cliffs, New Jersey.)

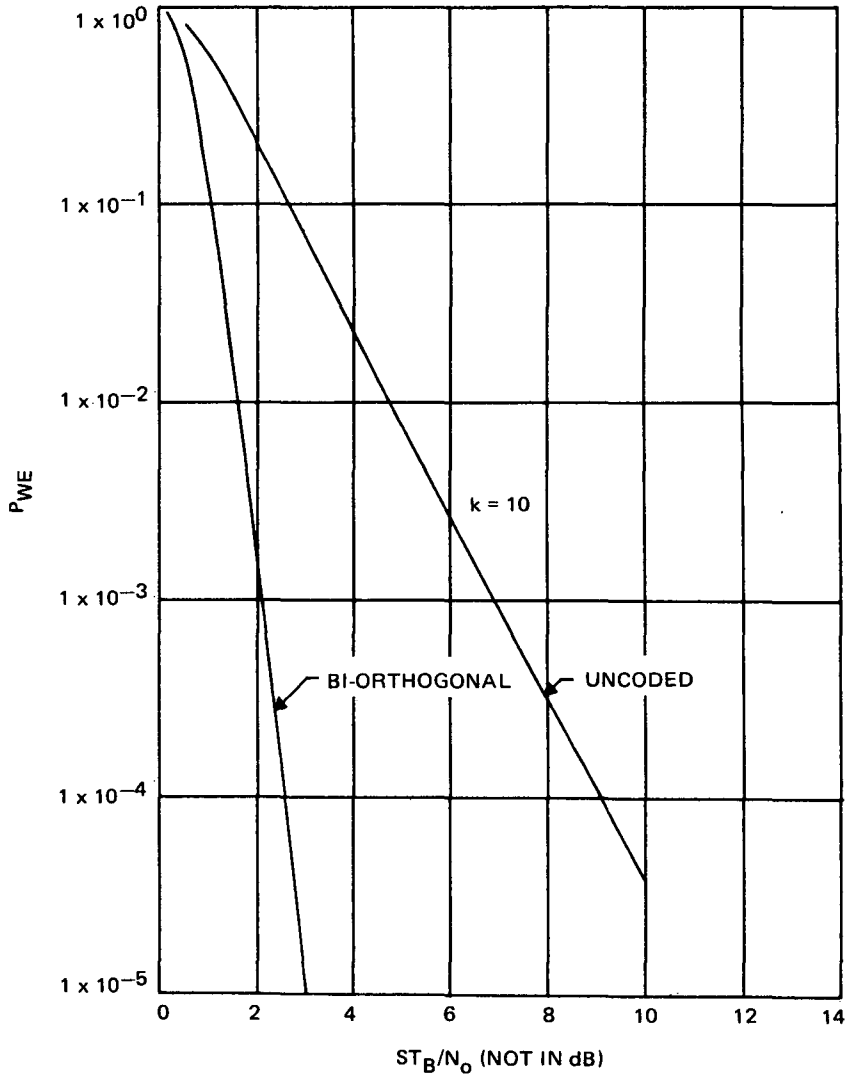

Fig. 5-8. Word error probability versus ST_B/N_0 for uncoded and biorthogonal block coded words of information bit length 10

(Ref. 5-4, A. J. Viterbi, 'Phase-Coherent Communication over the Continuous Gaussian Channel' in S. W. Golomb, Ed., DIGITAL COMMUNICATIONS WITH SPACE APPLICATIONS, Copyright 1964. Reprinted by permission of Prentice-Hall, Inc., Englewood Cliffs, New Jersey.)

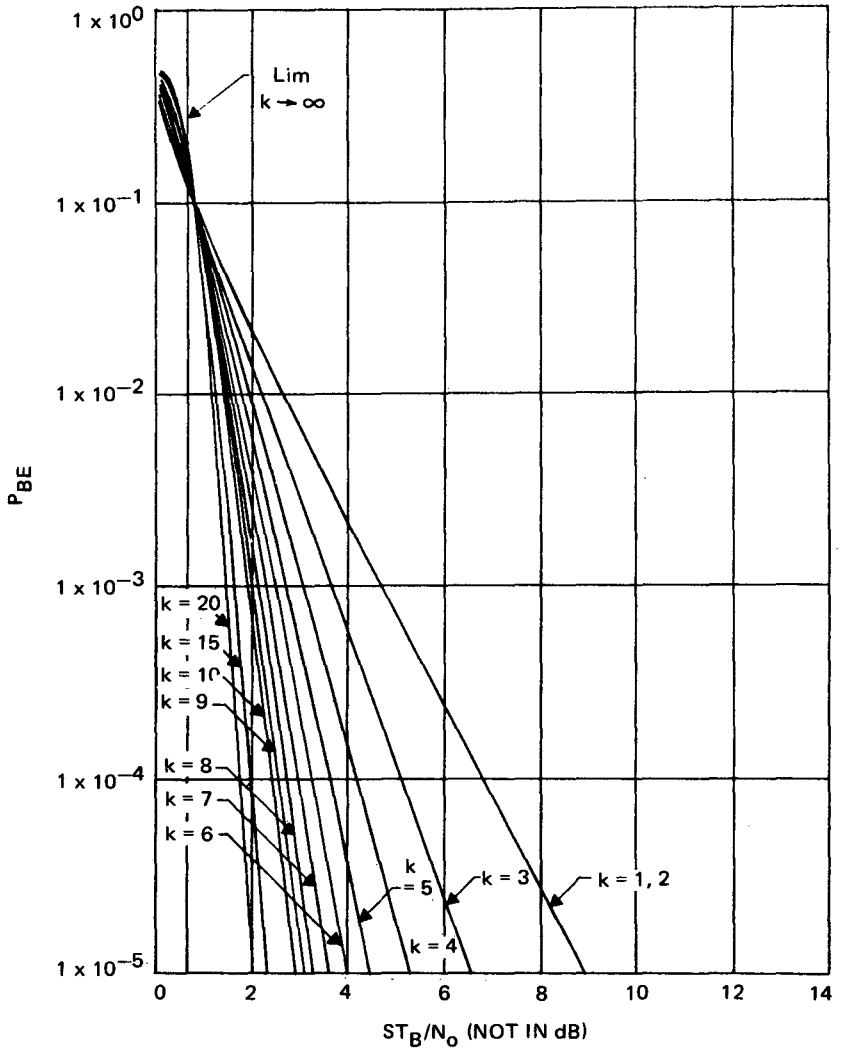

Fig. 5-9. Information bit error versus ST_B/N_o for $(2^{k-1}, k)$ biorthogonal block codes

(Ref. 5-4, A. J. Viterbi, 'Phase-Coherent Communication over the Continuous Gaussian Channel' in S. W. Golomb, Ed., DIGITAL COMMUNICATIONS WITH SPACE APPLICATIONS, Copyright 1964. Reprinted by permission of Prentice-Hall, Inc., Englewood Cliffs, New Jersey.)

Table 5-2. Word and information bit error probabilities for a (16, 5) biorthogonal block code versus ST_B/N_o*

ST_B/N_o		P_{WE}	P_{BE}	ST_B/N_o		P_{WE}	P_{BE}
Ratio	dB			Ratio	dB		
.080	-10.969	.85116	.42736	1.445	1.599	.05913	.02957
.125	- 9.031	.79879	.40033	1.620	2.095	.03947	.01973
.180	- 7.447	.73687	.36891	1.805	2.565	.02554	.01277
.245	- 6.108	.66666	.33356	2.205	3.434	.00976	.00488
.320	- 4.948	.59029	.29525	2.645	4.224	.00330	.0016516
.405	- 3.925	.43065	.25532	3.125	4.948	.0009940	.0004970
.500	- 3.010	.43065	.21535	3.645	5.617	.0002666	.0001333
.605	- 2.182	.35375	.17688	4.205	6.238	.0000640	.0000320
.720	- 1.427	.28265	.14133	4.805	6.817	.0000139	.0000069
.845	- .731	.21945	.10972	5.445	7.360	.0000028	.0000014
.980	- .088	.16545	.08272	6.125	7.871	.0000006	.0000003
1.125	0.512	.12105	.06053	6.845	8.354	.0000002	.0000001
1.280	1.072	.08591	.04295	7.605	8.811	.0000001	.0000000

*Source: Ref. 5-4, A. J. Viterbi, 'Phase-Coherent Communication over the Continuous Gaussian Channel' in S. W. Golomb, Ed., DIGITAL COMMUNICATIONS WITH SPACE APPLICATIONS, Copyright 1964. Reprinted by permission of Prentice-Hall, Inc., Englewood Cliffs, New Jersey.

Table 5-3. Word and information bit error probabilities for a (32, 6) biorthogonal block code versus ST_B/N_o*

ST_B/N_o		P_{WE}	P_{BE}	ST_B/N_o		P_{WE}	P_{BE}
Ratio	dB			Ratio	dB		
.080	-10.969	.89275	.44690	1.280	1.072	.07518	.03759
.125	- 9.031	.84480	.42284	1.620	2.095	.03054	.01527
.180	- 7.447	.78465	.39243	2.000	3.010	.01063	.00531
.245	- 6.108	.71300	.35654	2.420	3.838	.00318	.00159
.320	- 4.948	.63192	.31597	2.880	4.594	.0008199	.0004100
.405	- 3.925	.54474	.27237	3.380	5.289	.0001831	.0000916
.500	- 3.010	.45560	.22780	3.920	5.933	.0000357	.0000179
.605	- 2.182	.36893	.18447	4.500	6.532	.0000062	.0000031
.720	- 1.427	.28873	.14436	5.120	7.093	.0000010	.0000005
.845	- .731	.21807	.10903	5.780	7.619	.0000002	.0000001
.980	- .088	.15878	.07939	6.480	8.116	.0000001	.0000000
1.125	0.512	.11136	.05568				

*Source: Ref. 5-4, A. J. Viterbi, 'Phase-Coherent Communication over the Continuous Gaussian Channel' in S. W. Golomb, Ed., DIGITAL COMMUNICATIONS WITH SPACE APPLICATIONS, Copyright 1964. Reprinted by permission of Prentice-Hall, Inc., Englewood Cliffs, New Jersey.

5.3.3.1.1 Mechanization of the Block Encoder. On board the spacecraft, a unit known as a block coder is provided to accept data bits in blocks and convert them into code symbols. An n-symbol block coded word, $\underline{S}_i$, is generated from a k-bit data word $\underline{D}_i$ in accordance with the matrix operation.

$$\underline{S}_i = \underline{G} \oplus \underline{M} \oplus \underline{D}_i \qquad (5.3\text{-}16)$$

Where $\underline{G}$ and $\underline{M}$ are matrices which determine the code, and $\oplus$ indicates matrix multiplication followed by modulo 2 reduction of the resulting matrix elements.

The BDA is designed to decode the (n, k) biorthogonal codes (16, 5) and (32, 6). The matrices $\underline{G}$ and $\underline{M}$ are shown in Figures 5-10 and 5-11. Synchronization of the code words in the decoder is facilitated by half-adding to the $\underline{S}_i$ code symbols a PN sequence called a Comma Free Vector, $\underline{C}$. The sequence is 2^k symbols long, so that no transmitted sequence of n symbols overlapping two successive code words can be a member of the dictionary of possible code words. The transmitted symbols are thus $\underline{S}_i \oplus \underline{C}$.

$$\underline{M} = \underbrace{\begin{bmatrix} 1 & 0 & 0 & 0 & 0 \\ 1 & 1 & 0 & 0 & 0 \\ 1 & 0 & 1 & 0 & 0 \\ 1 & 0 & 0 & 1 & 0 \\ 1 & 0 & 0 & 0 & 1 \end{bmatrix}}_{5} \Big\} 5$$

$$\underline{G} = \underbrace{\begin{bmatrix} 1 & 0 & 0 & 0 & 0 \\ 1 & 0 & 0 & 0 & 1 \\ 1 & 0 & 0 & 1 & 0 \\ 1 & 0 & 0 & 1 & 1 \\ 1 & 0 & 1 & 0 & 0 \\ 1 & 0 & 1 & 0 & 1 \\ 1 & 0 & 1 & 1 & 0 \\ 1 & 0 & 1 & 1 & 1 \\ 1 & 1 & 0 & 0 & 0 \\ 1 & 1 & 0 & 0 & 1 \\ 1 & 1 & 0 & 1 & 0 \\ 1 & 1 & 0 & 1 & 1 \\ 1 & 1 & 1 & 0 & 0 \\ 1 & 1 & 1 & 0 & 1 \\ 1 & 1 & 1 & 1 & 0 \\ 1 & 1 & 1 & 1 & 1 \end{bmatrix}}_{5} \Big\} 16$$

Fig. 5-10. $\underline{G}$ and $\underline{M}$ matrices for a (16, 5) biorthogonal block encoder

$$\underline{M} = \underbrace{\begin{bmatrix} 1 & 0 & 0 & 0 & 0 & 0 \\ 1 & 1 & 0 & 0 & 0 & 0 \\ 1 & 0 & 1 & 0 & 0 & 0 \\ 1 & 0 & 0 & 1 & 0 & 0 \\ 1 & 0 & 0 & 0 & 1 & 0 \\ 1 & 0 & 0 & 0 & 0 & 1 \end{bmatrix}}_{6} \Bigg\} 6$$

$$\underline{G} = \begin{bmatrix} 1 & 0 & 0 & 0 & 0 & 0 \\ 1 & 0 & 0 & 0 & 0 & 1 \\ 1 & 0 & 0 & 0 & 1 & 0 \\ 1 & 0 & 0 & 0 & 1 & 1 \\ 1 & 0 & 0 & 1 & 0 & 0 \\ 1 & 0 & 0 & 1 & 0 & 1 \\ 1 & 0 & 0 & 1 & 1 & 0 \\ 1 & 0 & 0 & 1 & 1 & 1 \\ 1 & 0 & 1 & 0 & 0 & 0 \\ 1 & 0 & 1 & 0 & 0 & 1 \\ 1 & 0 & 1 & 0 & 1 & 0 \\ 1 & 0 & 1 & 0 & 1 & 1 \\ 1 & 0 & 1 & 1 & 0 & 0 \\ 1 & 0 & 1 & 1 & 0 & 1 \\ 1 & 0 & 1 & 1 & 1 & 0 \\ 1 & 0 & 1 & 1 & 1 & 1 \\ 1 & 1 & 0 & 0 & 0 & 0 \\ 1 & 1 & 0 & 0 & 0 & 1 \\ 1 & 1 & 0 & 0 & 1 & 0 \\ 1 & 1 & 0 & 0 & 1 & 1 \\ 1 & 1 & 0 & 1 & 0 & 0 \\ 1 & 1 & 0 & 1 & 0 & 1 \\ 1 & 1 & 0 & 1 & 1 & 0 \\ 1 & 1 & 0 & 1 & 1 & 1 \\ 1 & 1 & 1 & 0 & 0 & 0 \\ 1 & 1 & 1 & 0 & 0 & 1 \\ 1 & 1 & 1 & 0 & 1 & 0 \\ 1 & 1 & 1 & 0 & 1 & 1 \\ 1 & 1 & 1 & 1 & 0 & 0 \\ 1 & 1 & 1 & 1 & 0 & 1 \\ 1 & 1 & 1 & 1 & 1 & 0 \\ 1 & 1 & 1 & 1 & 1 & 1 \end{bmatrix}$$

Fig. 5-11. $\underline{G}$ and $\underline{M}$ matrices for a (32, 6) biorthogonal block encoder

The implementation of the block coder is shown schematically in Figure 5-12a.

5.3.3.1.2 Decoding Received Symbols. The ground received symbols are demodulated and output through an RC filter in the subcarrier demodulation assembly (SDA), as described above. The partially integrated symbol stream is digitized by an ADC in the symbol synchronizer assembly (SSA). The SSA then applies a correction to the digitized, RC filtered signal, to approximate the output which would be observed from a matched filter (perfect integrator).

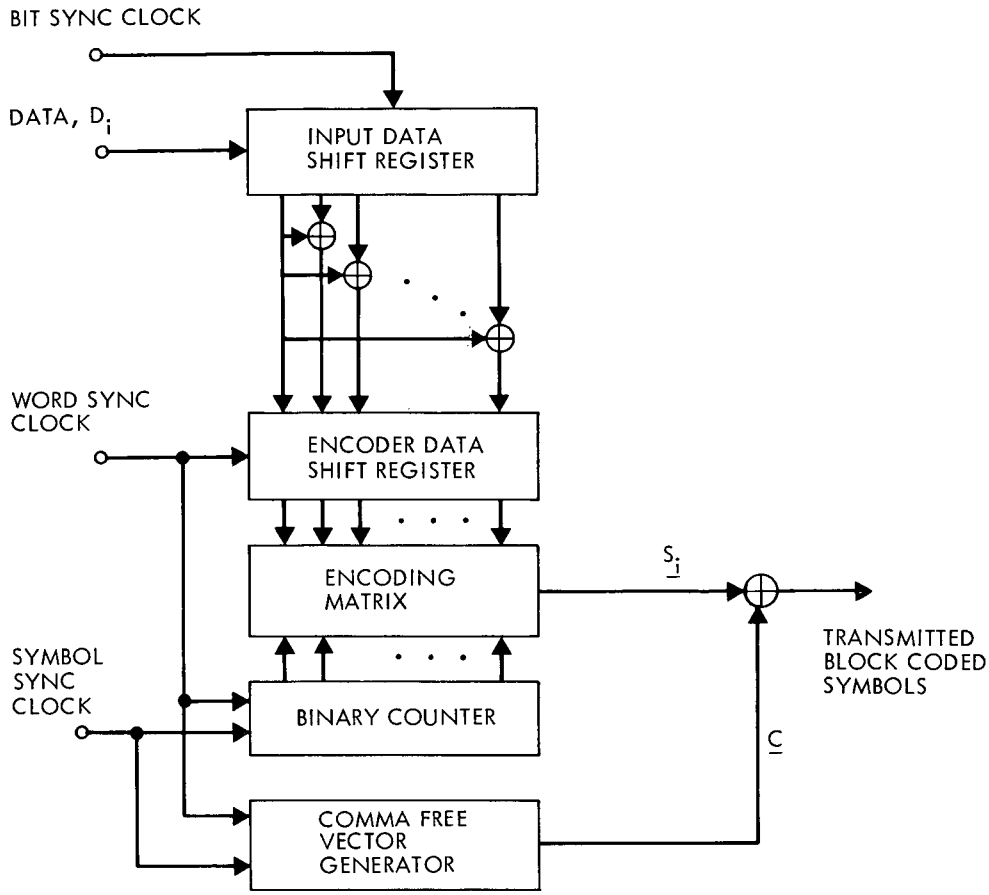

Fig. 5-12a. Encoder block diagram

In order to obtain and maintain symbol sync the SSA calculates the integral from midsymbol to midsymbol across a transition. If this integral is zero, symbol sync has been obtained. Non-zero values generate an error signal which drives the symbol sync loop to the correct lock point. This symbol sync loop is a phase-locked loop with a digital loop filter.

Word sync is derived in the block decoder assembly (BDA). A correlation is performed between an input word length of symbols and each word of the code dictionary, and the ratio of the largest correlation value to the typical correlation value is computed and stored. The BDA then shifts the candidate word sample by one symbol and repeats the process until the number

of shifts equals the number of symbols in a code word. Because of the comma free nature of the input, the above ratio is much higher for in-sync words than for out-of-sync position choices, therefore the BDA shifts the data to that word sample with the highest ratio and announces word sync.

Following word sync acquisition, the BDA decodes the symbol stream to data bits by selecting that bit pattern in its dictionary which corresponds to the highest correlation between the symbols and the stored symbol possibilities. Thus, if k-bit words are used, 2^k correlations must be performed per 2^{k-1} word synchronized symbols. This maximum likelihood detection is performed by 2^k parallel correlators, which, because of the ±1 waveform, perform correlation by simple addition. The most likely words are then formatted and output for transmission to the users.

This process is depicted in Figure 5-12b. A comprehensive description of the block decoding principles is available in reference 5-5.

5.3.3.2 Convolutional Coding. Another code class coming into favor for deep space communication is convolutional codes. At present, the theory for convolutional coding must be supplemented by trail-and-error code choice and computer simulated code performance investigations, in constrast to the closed-form solutions for block codes (cf. references 5-9, 5-10, 5-11). These methods, however, have produced performance uniformly better than that of block coding for a given symbol-rate to data-rate ratio. In addition, the encoder implementation is simpler and thus less costly and more reliable for spacecraft operation than that of a block encoder.

Binary convolutional codes may be generated in the manner shown in Figure 5-13. The binary input data is shifted bit by bit into a K-stage shift register. With every shift, the commutator samples v output lines from adder 1 through adder v and forms a binary symbol output of the serial samplings called a code branch. Thus, if the input bit rate is $1/T_B$, the output symbol rate, $1/T_s$, is equal to $1/bT_B$. Such an encoder generates a "constraint length K, rate 1/v (bits/symbol) convolutional code." K is called the constraint length because each input bit affects, or constrains, the subsequent Kv output symbols derived from K input bit shifts. This results in a code which is sensitive to burst errors.

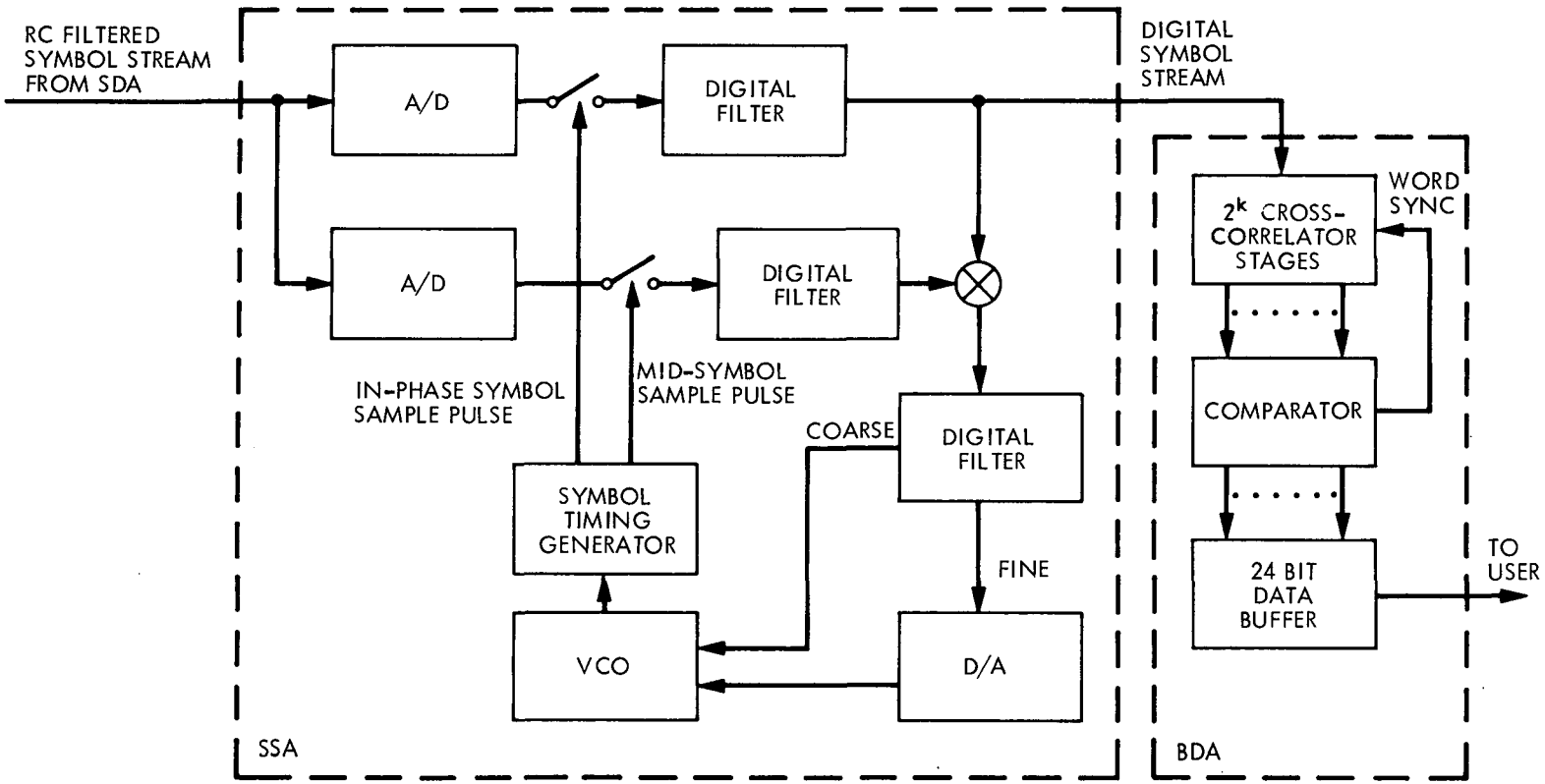

Fig. 5-12b. Conceptual model of block decoding

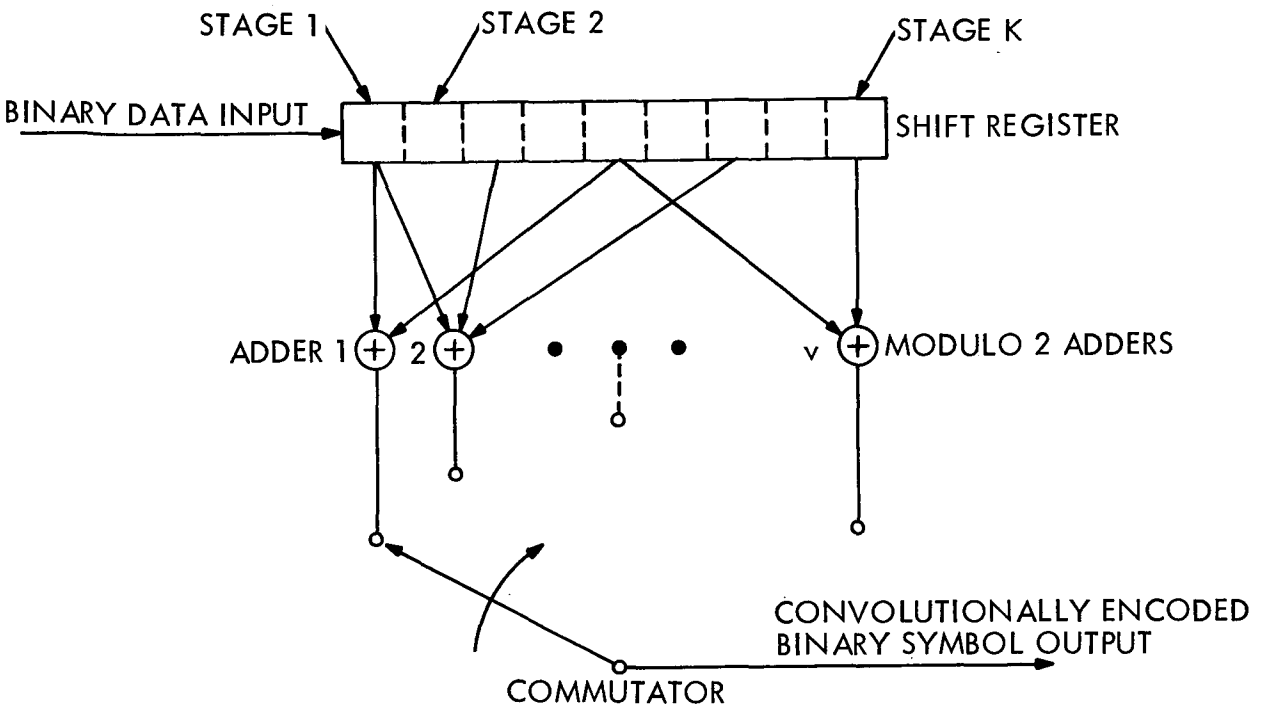

Figure 5-13. Length K, rate 1/v convolutional encoder
(Source: Reference 5-12 with permission)

In general, the binary input data is entered b bits per commutator cycle into a bK-stage shift register. Thus, if the input bit rate is $1/T_B$, the shift register accepts a new input every bT_B seconds, and the output symbol rate is equal to v/bT_B. This encoder generates a "constraint length K, rate b/v (bits/symbol), convolutional code."

The particular code sent depends on the manner in which the adders are connected to the shift register. These connections are denoted by a set of vectors

$$\bar{g}_\ell = (g_{\ell 1}, g_{\ell 2}, \ldots, g_{\ell v}) \quad \ell = 1, 2 \ldots K \qquad (5.3\text{-}17)$$

where $g_{\ell j} = 1$ denotes a connection between the ℓth stage of the shift register and the jth adder, and $g_{\ell j} = 0$ denotes the absence of a connection. The complete set of $\bar{g}_\ell$ and the parameter b define the code. Figure 5-14 demonstrates the meaning of $\bar{g}_\ell$.

If the data bits are sent as part of the output, the code is termed "systematic," otherwise, it is "nonsystematic." Thus, a systematic code is one for which

$$g_{\ell j} = \delta_{\ell j}; \ell = 1, 2, \ldots, K, \ j = 1, 2, \ldots, b \text{ where}$$

$\delta_{\ell j}$ is the Kronecker delta

$$\delta_{\ell j} = \begin{cases} 1, \ell = j \\ 0, \ell \neq j \end{cases}$$

A code is also termed systematic if the data appears in other than the 1 through bth stages, however, restricting the data to these stages is merely a relabeling process for stage numbers in the general case.

It can be shown (reference 5-15) that for K large the performance of a systematic code of constraint length K is approximately equal to the performance of a nonsystematic code of constraint length $K(1 - b/v)$. Thus, systematic codes have significantly poorer performance than nonsystematic for equal encoder and decoder complexity.

However, systematic codes have the advantage of the quick-look property. That is, since the data is present explicitly in the symbol stream, it can be examined without decoding (with the symbol error rate). Massey and Costello (reference 5-16) have demonstrated that for b = 1, nonsystematic codes can be developed for which the data can be recovered explicitly by adding the symbols produced by each modulo 2 adder of the encoder. This gives a nonsystematic code with the quick-look property for which the data error rate is approximately v times the symbol error rate. Such a code will give a data bit error only if there is an odd number of errors in the length v symbol branch. Thus, if P_s is the probability of symbol error, the probability of error in the quick-look data bit is,

The K = 4, v = 3, b = 1, encoder shown

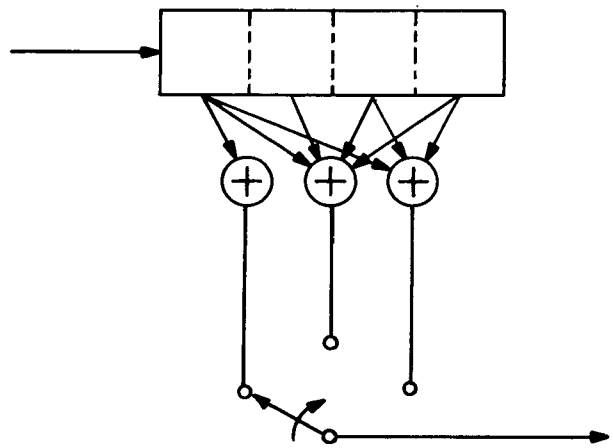

has the connection vector description

$$\bar{g}_1 = (1, 1, 1)$$
$$\bar{g}_2 = (0, 1, 0)$$
$$\bar{g}_3 = (0, 1, 1)$$
$$\bar{g}_4 = (0, 1, 1)$$

or, in matrix form

$$\{g_{\ell j}\} = \begin{pmatrix} 1 & 1 & 1 \\ 0 & 1 & 0 \\ 0 & 1 & 1 \\ 0 & 1 & 1 \end{pmatrix}$$

Figure 5-14. Example for connection vector notation.
(Source: Reference 5-12, with permission)

$$P_{QL} = \sum_{k=0}^{B} \frac{v!\, P_s^{2k+1} (1-P_s)^{v-(2k+1)}}{[v-(2k+1)]!\,(2k+1)!} \qquad (5.3\text{-}18)$$

where

$$B = \left\lfloor \frac{v-1}{2} \right\rfloor$$

$\lfloor x \rfloor$ indicates $\lfloor x \rfloor$ = the greatest integer $\leq x$.

and we have assumed branch synchronization, that is, the decoder knows which adder generated each symbol.

In order to send a block of L data bits, the shift register is initialized to the all-zeros state. The bits are then shifted in, b by b until all L have been shifted out of the register and it is again filled with zeros. Thus, L input bits give (L + bK) v/b output symbols including v initial output zeros, where Kv is the minimum "tail" for a data symbol block. The data rate then is

$$R_N = \frac{b}{v}\left(1 + \frac{bK}{L}\right)^{-1} \text{ bits per symbol} \qquad (5.3\text{-}19)$$

or

$$R_N = \frac{b}{v} \text{ for } L \gg bK, \text{ the typical case.}$$

This section has defined the terms referred to in specifying a convolutional code. Next, we shall discuss the problem of decoding convolutionally encoded data.

5.3.3.2.1 Decoding Convolutional Codes. It can be shown (reference 5-12), that the probability of error for optimum decoding is bounded by a function times 2^{-K}. However, a brute force maximum likelihood optimum decoder requires 2^L computations to decode each block of length L bits and tail K bits. Such a decoder would severely limit bit rates with even extremely fast computation capability. Thus, methods have been found which permit decoding at reasonable bit rates with excellent, though less than optimum performance.

Two of the most widely known and analyzed schemes for non-optimum decoding are sequential decoding by the Fano algorithm and a modified maximum likelihood (Viterbi) decoding algorithm. The Fano algorithm has been demonstrated operationally with a software system for Pioneer IX. Very fast Fano and Viterbi machines now exist and may soon provide a DSIF operational system. Reference 5-8 tabulates the available parameters for DSN-compatible coding schemes using these decoding methods. The following sections give brief descriptions of these methods and the parameters necessary for performance prediction. References are cited for detailed investigation.

5.3.3.2.1.1 Sequential Decoding - The Fano Algorithm. In any decoding scheme, for any type of code, a measure must be found for determining how much better one data hypothesis is than another. This measure is known as the "metric" and depends on the type of code, the method of decoding and the type of transmission channel. The general methods of metric determination are discussed in reference 5-12. This reference also presents a good discussion of sequential decoding and the Fano algorithm.

The brute force optimum decoding process for convolutional codes determines the metric for each of the 2^L possible code paths influenced by each L bits (Lv symbols) and picks the best of these metric values as that connected with the correct data hypothesis for that path. (Note that henceforth we shall assume b = 1.)

The approach of sequential decoding is to search the code bit-by-bit (v symbols per bit) and select an initial data hypothesis for the first v symbols encountered whose metric lies above a preset threshold value. This threshold is chosen to lie between the known values of the error-free metric and the nearest incorrect-hypothesis metric. Since each data hypothesis affects Kv symbols, an incorrect assumption will generate a metric which increasingly diverges from the error-free value. When the calculated metric crosses threshold, the previous data bit assumption is ruled invalid and the computer backs up v symbols to attempt another hypothesis. If this change of assumption does not work, the computer retreats another v symbols. The process continues until an acceptable path is found.

For very noisy data, all 2^K branches may be examined; if this occurs without success, the threshold criterion is loosened, and the attempt is repeated. In general, however, many paths need not be scrutinized, and thus a computational saving results. For example, if the first assumption is within threshold, 2^{K-1} other trials may be eliminated, with an exponential saving in number of computations. If an error is not detected within Kv symbols, the error is undetectable by the algorithm, and is passed by the system.

As indicated above, as the signal-to-noise ratio decreases, the required number of computations per v symbols increases. If the decoding device has a storage capacity, ΓQ computer bits, assigned to store the received data, where

Q = Receiver output per v symbols (metric) quantization in bits

and

Γ = Number of Q-length storage words

and if

$\lambda = vT_s/T_c$

where

T_s = Symbol time

vT_s = Time to receive one data bit

and

T_c = Computational time required to search through one data hypothesis (one code branch), then if B, the number of computations on a branch exceeds $\lambda\Gamma$, the storage capacity of the decoder will be exceeded. This occurrence is known as overflow or erasure.

An overflow can occur for $B < \lambda\Gamma$ if the previous computations have filled storage. For a low error-rate system, however, the probability of this situation must be small and thus the probability of overflow is approximately $P(B > \lambda\Gamma)$. (When high error rates are acceptable, other expressions

are valid, cf. reference 5-14). When an overflow occurs, the decoder must resynchronize on the data. This is the reason for finite block size on the transmitted sequence. The decoder discards the remainder of the block and resynchronizes on the tail of K or more zero bits. The probability that all or part of a data block will be lost is approximately $LP(B > \lambda\Gamma)$.

For $P(B > \lambda\Gamma)$ to be small, a value of $\Gamma >> K$ is required, so that Q, Γ, and λ determine the storage requirements. Each decoded hypothesis requires 1 bit, so that the required storage is approximately $\Gamma(Q + 1)$ bits.

For any sequential decoding scheme, there is a data rate R_o' bits per symbol (also referred to as R_{comp} in the literature) above which $\overline{B}$, the average number of branches searched per bit decoded, is unbounded. Thus, we require that $R_N < R_o'$. R_o' depends on Q, the metric quantization, and the type of transmission channel. In general,

$$R_o' = -\log_2 \sum_{h=1}^{Q} \left[\sum_{\ell=1}^{A} p_\ell \sqrt{q_{\ell h}} \right]^2 \qquad (5.3\text{-}20)$$

where

A = Number of signal levels transmitted

p_ℓ = The probability of transmitted signal level ℓ

and

$q_{\ell h}$ = Probability of receiving metric h given that signal ℓ was sent.

For an additive white gaussian noise (AWGN) channel with $Q = \infty$, and antipodal signals,

$$R_o \triangleq \lim_{Q \to \infty} R_o' = 1 - \log_2 (1 + \exp(-ST_B R_N/N_o)) \qquad (5.3\text{-}21)$$

In the limit of infinite bandwidth expansion, ST_B/N_o approaches 2 ln 2 = 1.42 dB or 3 dB above Shannon's limit. For a quantization Q = 8, this value increases by about 0.2 dB, while for Q = 2 (i.e., hard decision) about 2 dB is lost (see ref. 5-13). Figure 5-15 plots $R_{N_{max}}$ versus ST_B/N_o for $Q = \infty$.

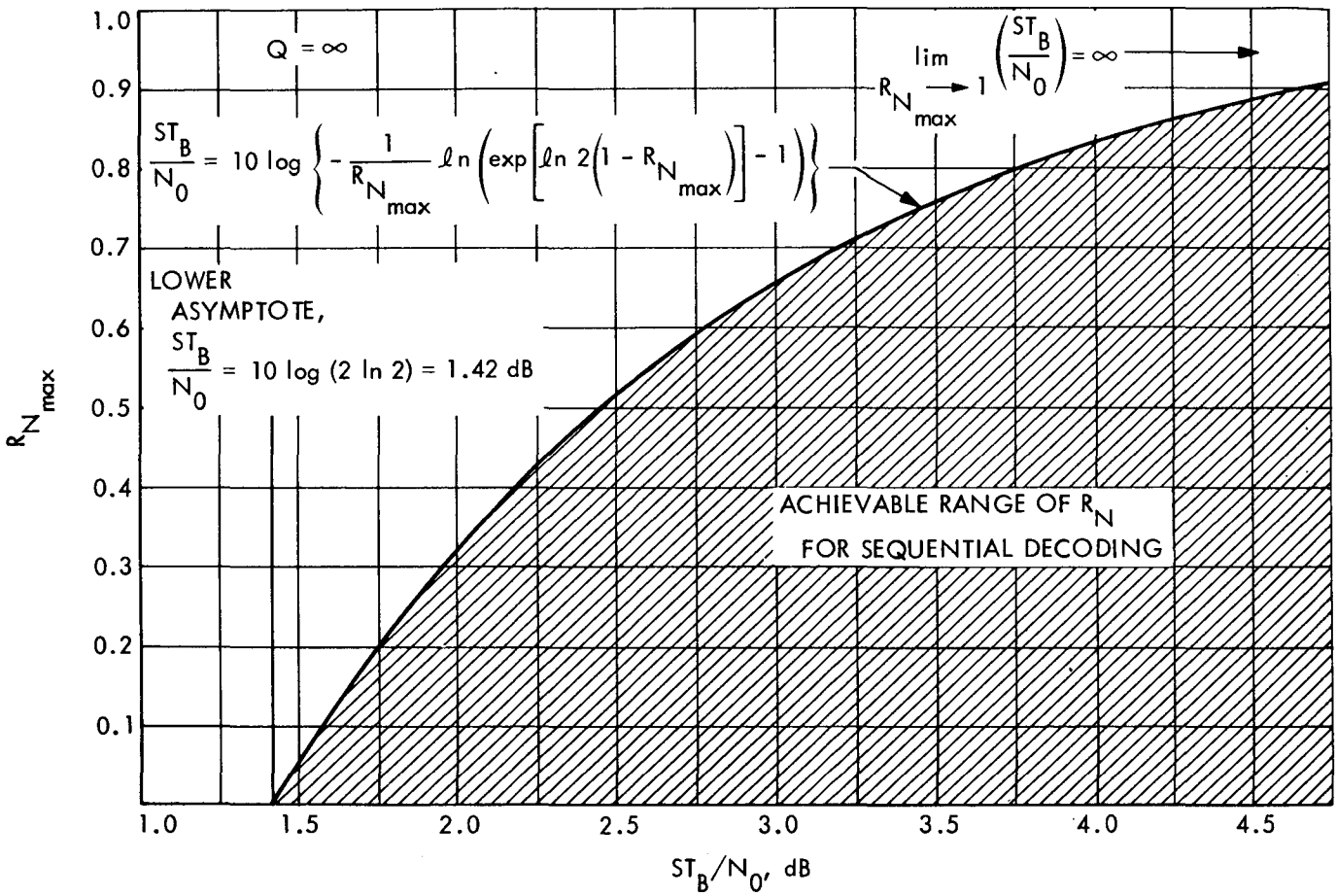

Fig. 5-15. Maximum achievable code rate for sequential decoding with infinite metric quantization versus ST_B/N_o

The Fano sequential decoding algorithm is distinguished by its use of a running threshold. As long as the metric is growing, this algorithm searches a single path and tightens the threshold value. When forced to retreat, the algorithm loosens the threshold until a renewed forward search becomes possible. Reference 5-12 discusses the algorithm in detail.

Simulations by Bluestein and Jordan (as quoted in reference 5-12) have demonstrated some fundamental properties of the Fano algorithm:

1) The mean number of branches searched, per branch received, $\overline{B}$ depends primarily on the ratio R_N/R_o' and grows very rapidly for $R_N/R_o' > 0.9$.

2) The probability of undetectable error decreases as 2^{-K} and can easily be made negligible with respect to errors caused by overflow for K's which are orders of nagnitude less than Γ.

3) $$P(B > \lambda\Gamma) \approx 3^{-(1 - R_N/R_o')} \quad (\lambda\Gamma)^{-(2.9 - 2 R_N/R_o')} \tag{5.3-22}$$

for $\lambda\Gamma \gg 1$, $R_N < R_o'$, and $\lambda > \overline{B}$

Thus, for a system with $2^{-K} \ll LP(B > \lambda\Gamma)$ and $Kv \ll L$, the probability of bit error is negligible when compared to the rate of bit discards due to overflow. This rate P_D, is just equal to one-half the probability of block error, since overflow will happen on the average when one-half of the block is decoded.

Thus,

$$P_D = \frac{L}{2} P(B > \lambda\Gamma) \tag{5.3-23}$$

Using Bluestein's and Jordan's empirical formula (5.3-22) for an AWGN channel with $Q \to \infty$, a little algebra demonstrates that for a probability of bit discard P_D,

$$ST_B/N_o \approx -\frac{v}{\log e} \log \left\{ \exp \left[\frac{\log 2}{\log e} \left(1 - \frac{1}{v} \frac{\log 3 + 2 \log \lambda\Gamma}{\log P_D + \log 6 + 2.9 \log \lambda\Gamma - \log L} \right) \right] - 1 \right\} \tag{5.3-24}$$

where ST_B/N_o is expressed as a fraction, not in dB, $\lambda\Gamma >> 1$, $R_N < R_o$ over the range of ST_B/N_o considered. These bit discards will occur in bursts of average length L/2.

Equation 5.3-24 assumes a "good" code, and does not take the place of simulation runs with the actual code design.

It should be noted that overflows can be processed to yield good data by playing back erased blocks into the decoder at a slower rate. The breakpoint for such additional processing will occur where the additional data gained does not justify the additional processing cost.

Figure 5-16 from reference 5-10 shows some simulation results for Fano sequential decoding with K = 32 and $R_N = 1/2$. The letters represent

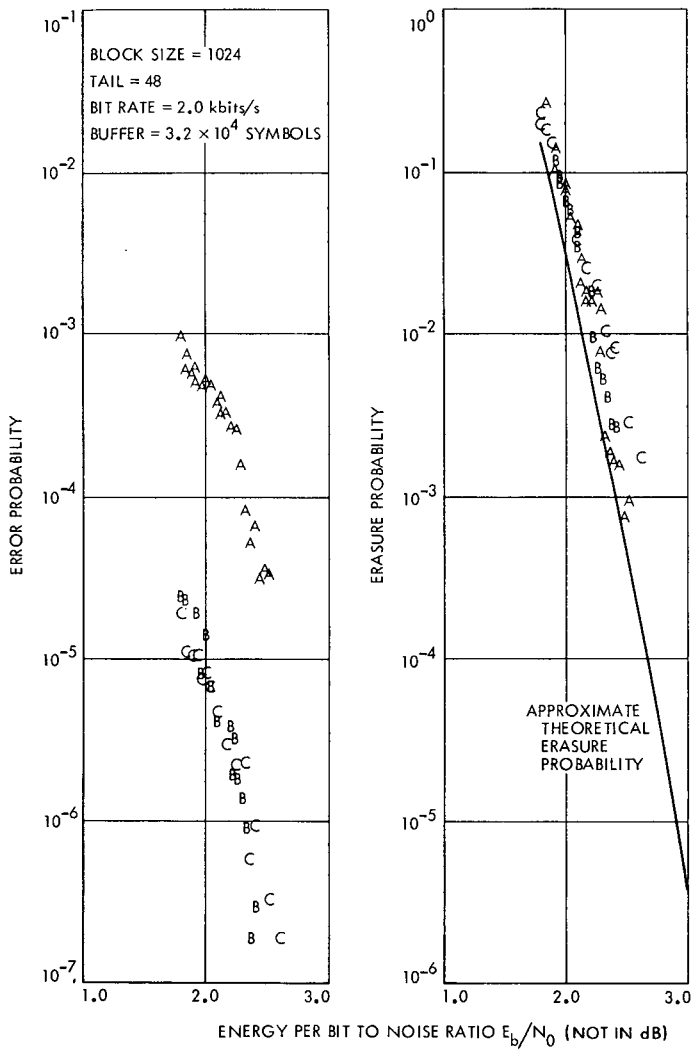

Fig. 5-16. Bit error and block erasure probabilities for a JPL experimental Fano sequential decoder.

three different codes. Code A is a systematic code, code B is a nonsystematic quick-look code and code C is nonsystematic. The curve "Approximate Theoretical Erasure Probability" was obtained from the results of reference 5-14, rather than equation (5.3-24).

Reference 5-32 presents a method by which erasure probabilities can be reduced at the sacrifice of chronologically ordered data. The method is based on the theories of computer time-sharing and can achieve marked improvement at low erasure rates (10^{-2} or less) and slight-to-moderate improvement above that level.

5.3.3.2.1.2 Maximum Likelihood (Viterbi) Decoding. Maximum likelihood, or Viterbi, decoding is a nonsequential decoding method which takes advantage of the fact that a single information bit can affect only Kv symbols (K branches) in the received code. Thus, it proceeds through the received symbols by choosing the most likely path out of the entire ensemble of possible transmitted paths for each group of K branches. For binary data, the algorithm proceeds in the following manner:

1) Each branch can only be reached by two paths. Compute the metric for both paths entering each branch and discard the paths with the smaller pairwise metric. Thus for 2^K paths, eliminate one half, leaving 2^{K-1} survivors.

2) At the next branch, we again have 2^K paths since each can go two ways. Repeat step 1, multiplying the branch metrics by the stored value of each path metric, and again eliminate one half of the possible paths leaving 2^{K-1} survivors.

3) Continue this process indefinitely.

This procedure is the optimum decoding method for convolutional codes if continued through a block into the tail of K-1 known data bits. These bits eliminate all but one of the stored 2^{K-1} paths to give the best possible estimate of the data sequence. However, without this tail, the Viterbi decoder in the above form will never make a decision as to the correct path. Therefore, the algorithm is modified to make a data choice after proceeding several constraint lengths past a data bit.

An additional error probability is introduced by this procedure. For a very noisy channel ($E_S/N_O \ll 1$, $E_S = ST_S$) the error due to this truncation is less than the probability of bit error if (reference 5-18)

$$\frac{M}{K} > \begin{cases} \dfrac{1}{1 - 2R_N/C} & 0 \le R_N \le C/4 \\ \dfrac{1}{2\left(1 - \sqrt{R_N/C}\right)^2} & C/R \le R_N \le C/2 \\ \dfrac{1 - R_N/C}{\left(1 - \sqrt{R_N/C}\right)^2} & C/2 \le R_N \le C \end{cases} \qquad (5.3\text{-}25)$$

where

M/K = Number of constraint lengths to a decision

and

$C = E_S/(N_O \ln 2)$ = channel capacity

For example, for a rate $R_N = C/2$, $M > (5.8)\,K$; thus we require 2^{K-1} shift registers of (5.8) K length for parallel computation. Figure 5-17 plots this relationship versus ST_B/N_o.

With this modification, Viterbi decoding has certain desirable properties:

1) The number of computations is proportional to 2^K, independent of rate.

2) Decoding can proceed at the data rate if the comparisons are done in parallel; therefore, the decoder does not have to be 10 to 20 times faster than the data rate, as in sequential decoding.

3) No block-tail structure is necessary; data may be continuous.

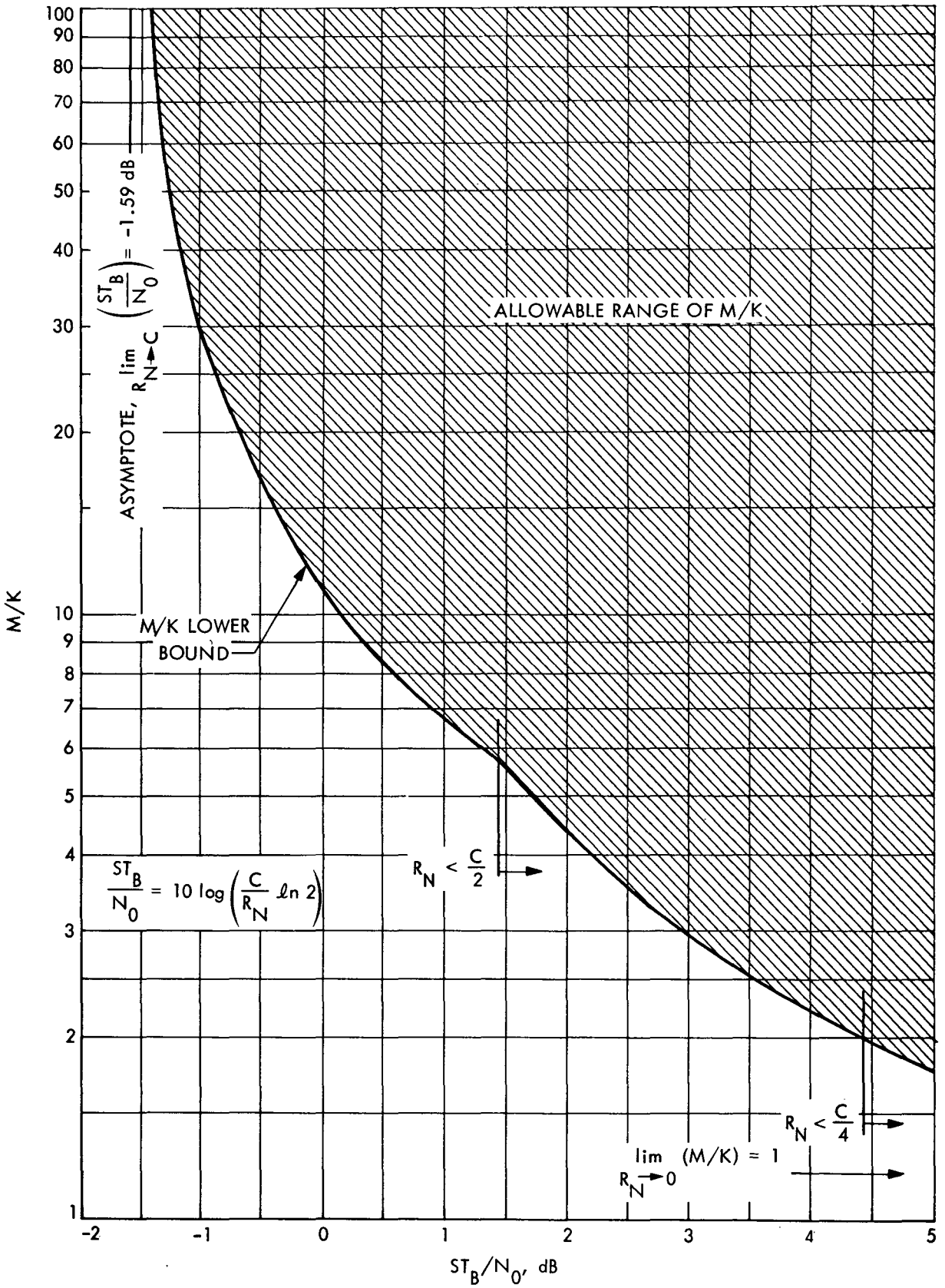

Fig. 5-17. Range of the number of constraint lengths for truncation in a Viterbi decoder which gives an additional probability of error less than P_{BE}.

4) Time to decode is fixed; therefore buffering is unnecessary.

5) Performance is typically 1 dB better than for biorthogonal codes of the same complexity.

Since decoder size grows as 2^K, Viterbi decoding is limited to short constraint length codes; hence, it becomes vital to select a "good" code. With the long constraint lengths typical of sequential decoding, less care can be taken in code selection, and better error rates can be obtained. Ironically, Viterbi decoding is most useful at high data rates. Sequential decoding, although less than optimal, is more useful at low data rates where machine speed can be 10 to 20 times faster than the bit rate, and advantages can be gained by the choice of large K.

Viterbi (reference 5-18) has derived very tight bounds on the probability of error for Viterbi decoding. These bounds must be evaluated numerically. This has been done in reference 5-19 and the results are shown in Figures 5-18 and 5-19. The difference between simulations and the error bounds is primarily due to a finite quantization loss of about 0.2 dB.

Heller and Jacobs (reference 5-19) have shown that, for a fixed constraint length, channel efficiency is increased by roughly the increase in channel capacity when the rate is decreased. Thus, performance improvement may be gained by increasing the bandwidth expansion if the effects on carrier tracking performance are small. The improvement, however, is not in proportion to the bandwidth expansion ratio. Thus, for a change from rate 1/2 to rate 1/3, the gain is between 0.3 to 0.5 dB, considerably less than 10 log 3/2 = 1.76 dB. If K is allowed to vary as well, Heller and Jacobs' results indicate that performance is approximately equal for encoders of equal complexity. Thus, the number of distinguishable states of an encoder is $2^{b(K-1)}$, so that the encoders K = 3, $R_N = 2/3$, and K = 5, $R_N = 1/2$ each have 16 states. The performance of these encoders differs by only 0.2 dB for equally good codes. Because of the steepness of the probability of error versus E_b / N_O curves for a coded system ($E_b = ST_B$), small losses due to phase jitter in the carrier tracking loop cause large adverse changes in the received bit error rate. For a data rate $1/T_B >> 2B_{LO}$, errors generated during Viterbi decoding will occur over a small enough time that the phase error in the carrier loop, ϕ,

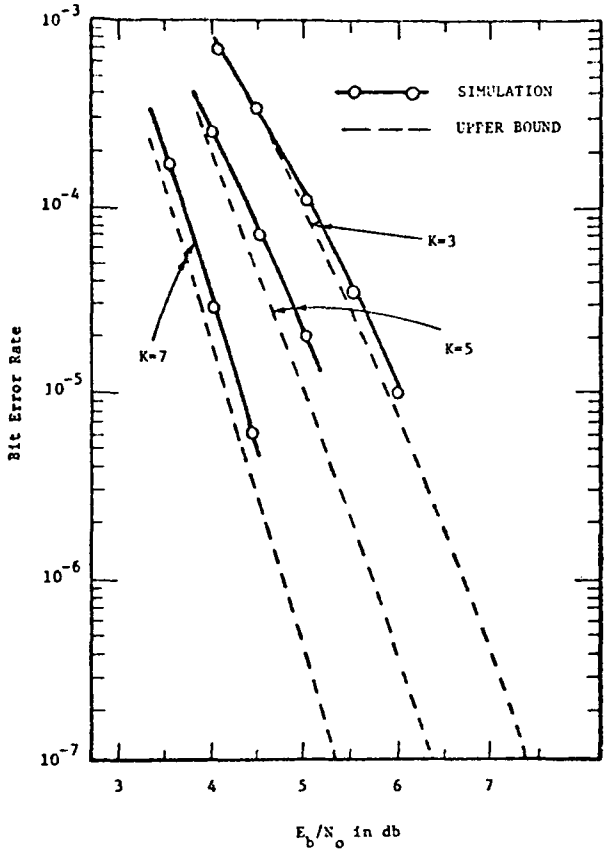

Fig. 5-18. Bit error rate versus E_b/N_o for rate 1/2 Viterbi decoding. 8-level quantized simulations with 32-bit paths, and infinitely finely quantized transfer function bound, K = 3, 5, 7.
(Source: Reference 5-19, with permission)

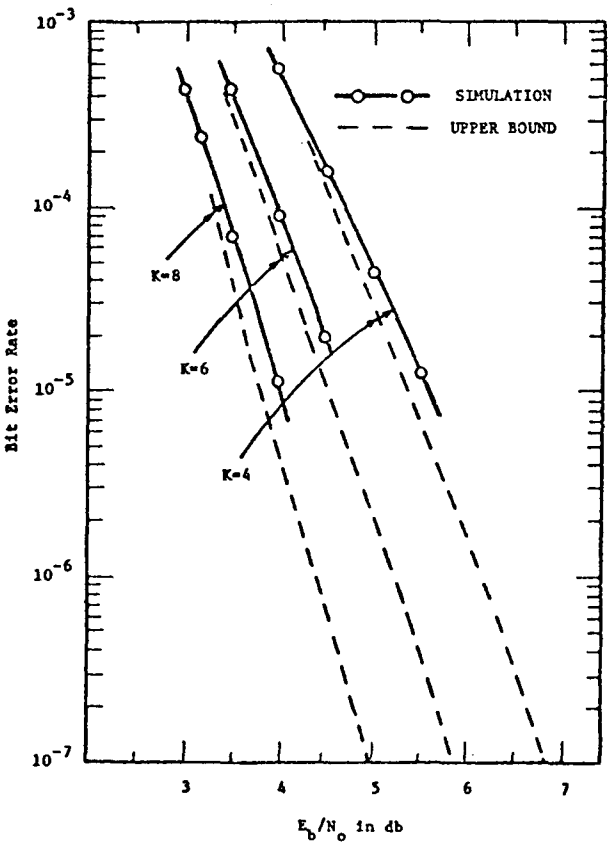

Fig. 5-19. Bit error rate versus E_b/N_o for rate 1/2 Viterbi decoding. 8-level quantized simulations with 32-bit paths, and infinitely finely quantized transfer function bound, K = 4, 6, 8.
(Source: Reference 5-19, with permission)

will remain constant and errors will be independent. Following reference 5-19, if the probability of bit error is written as

$$P_B = f(E_b/N_O) \tag{5.3-26}$$

then

$$P_B(\phi) = f(E_b \cos^2\phi/N_O) \tag{5.3-27}$$

For a distribution $p(\phi)$, the system bit error probability is

$$P_B' = \int_{-\pi}^{\pi} p(\phi)\ P_B(\phi)\ d\phi \qquad (5.3\text{-}28)$$

Figure 5-20, taken from reference 5-19, plots P_B' versus E_b/N_O for a K = 7, R_N = 1/2 code and a second-order tracking loop,

where

$$p(\phi) \simeq \frac{\exp(\eta \cos \phi)}{2\pi I_O(\eta)} \qquad \eta >> 1$$

where η = loop SNR. We see that P_B' is a very strong function of η. The difference at a constant error rate between the curves for finite η and $\eta = \infty$ is the one-way radio loss for Viterbi decoding of the convolutional code. Radio loss, η_{RL}, will be discussed in paragraph 5.4.5.

5.3.3.2.1.3 Comparison of Sequential and Viterbi Decoding. In Table 5-4, we consider some of the tradeoff considerations in selecting sequential or Viterbi decoding methods (see reference 5-19).

Heller and Jacobs have further shown that since sequential decoding is very sensitive to receiver AGC variations, it may only be practical to have hard decision capability (Q = 2). Under these circumstances, at $P_B \sim 10^{-5}$, a K = 5 to 7, R_N = 1/2, Q = 8 Viterbi decoder has performance equivalent to a K = 41, R_N = 1/2, Q = 2 sequential decoder, although for $P_B < 10^{-8}$, the sequential machine is superior.

5.3.3.3 Concatenated Coding. The acceptable ST_B/N_o threshold for a telemetry channel is controlled by the transmitted data with the lowest allowable error rate. If it happens that the required error rate for this data is significantly lower than the requirements for the bulk of the telemetry, transmission of the entire data stream at the lowest error rate may prove very costly in terms of power or data rate. Examples for which this situation may obtain include:

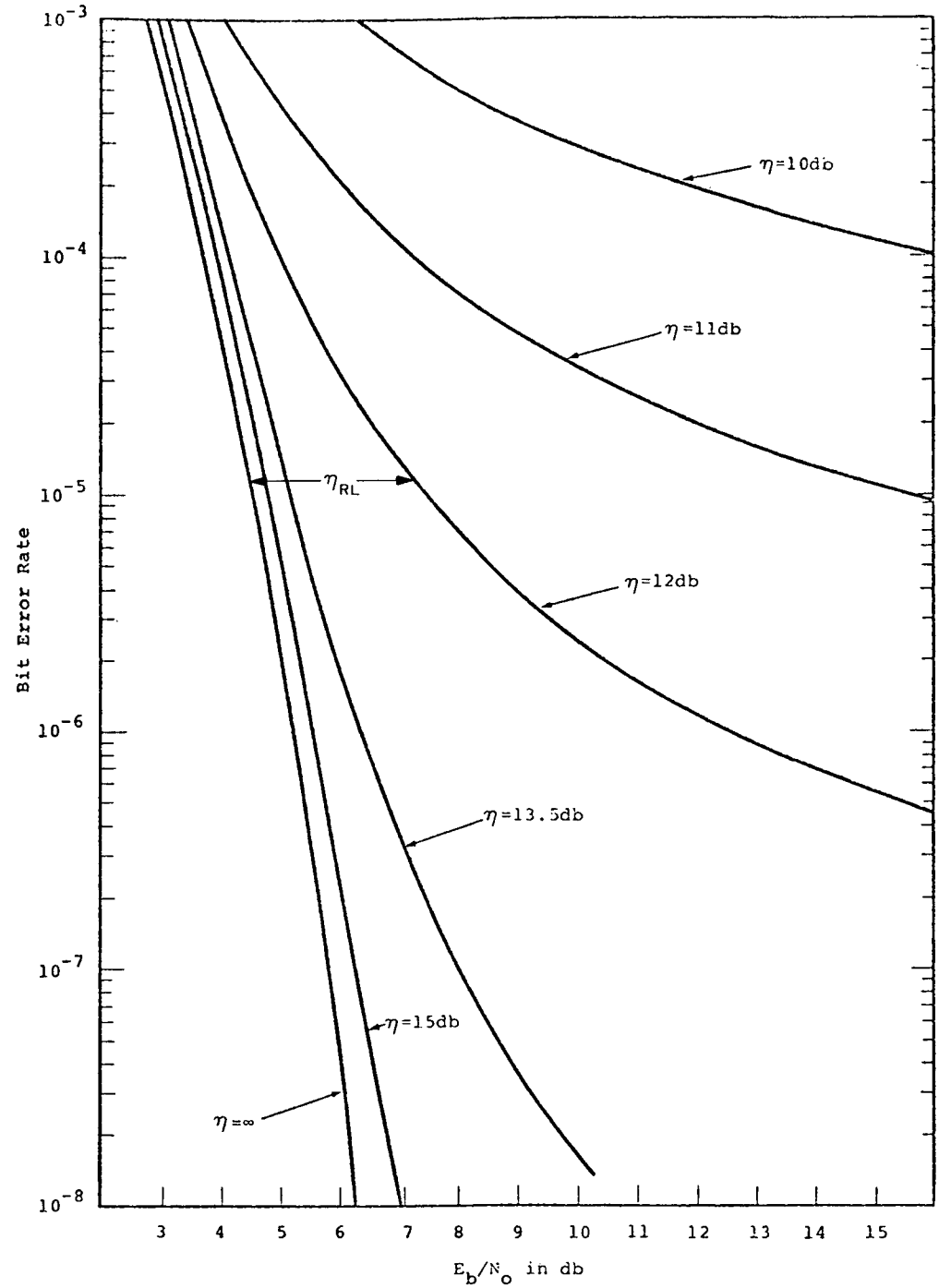

Fig. 5-20. Performance curves for rate 1/2; K = 7 Viterbi decoder with 8-level quantization as a function of carrier phase tracking loop signal-to-noise ratio η
(Source: Reference 5-19, with permission)

Table 5-4. Tradeoff considerations for Viterbi and sequential decoding methods

System Variables	Viterbi	Sequential
Bit Errors in Output	Short bursts of 10 to 20 bit errors	Bit error probability can be made extremely low, but errors come in bursts of up to L bits at a time
Decoder Delay	Short, less than 100 T_B delay	Output may be delayed many thousands of bit times
Transmitted Data Format	Continuous	In blocks with tail of no data added
Choice of Rate and Quantization	Decoder completely insensitive to these variables	Storage requirements strongly dependent on Q and R_N
Sensitivity to AGC of Receiver	Insensitive	Very sensitive for large Q
Sensitivity to Carrier Loop Phase Error	Shown in Figure 5-20	Much more sensitive due to steeper curve; also, phase varies over long error bursts, implying errors are not independent.

1) TV transmission may require error rates of 1 in 10^3, while other experiments occupying a fraction of the channel may require 1 in 10^5.

2) Only long and completely error-free data frames may be useful for certain experiments.

3) Certain key data may require extremely high confidence.

To alleviate this problem, at least three methods are available:

a) Adding another telemetry channel for the low error rate data;
b) Interplex modulation; and
c) Concatenated coding.

The method of concatenated coding is illustrated in Figure 5-21. Concatenated coding allows the use of additional coding for part of the data without loading the remaining data by that additional redundancy. In its use of a combination of two separate coding schemes, concatenated coding requires little new theory, but much analysis must be performed to determine the proper inner and outer codes and decoding methods. The following are some of the considerations important in the use of concatenated coding:

1) Additional coding means additional redundancy or check bits at the cost of less transmitted information. Therefore, only few data which really need higher confidence should be protected by additional coding.

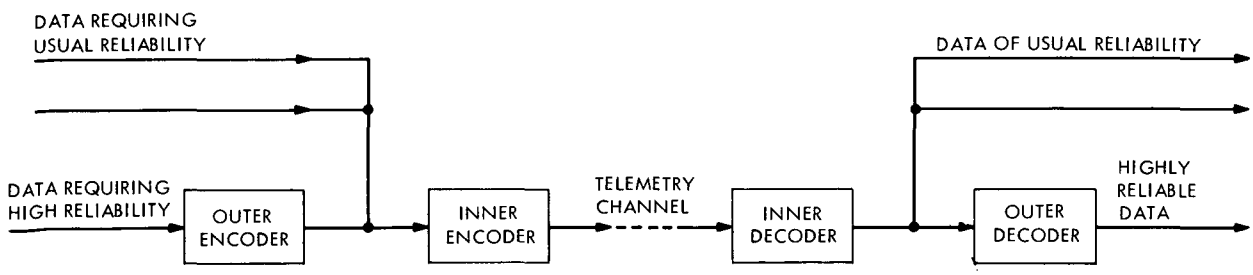

Fig. 5-21. Concatenated coding scheme

2) Increased data reliability can be gained as a trade-off between additional redundancy, encoding/decoding complexity and data deletion. If, for example, the deletion of a small amount of unreliable data can be permitted, the required redundancy and/or complexity decreases remarkably.

3) Simple algebraic coding/decoding can be used effectively for outer coding.

4) The outer code has to be of a burst-error correcting type because the errors of the inner decoder are bursts of wrong codewords or codeframes of the inner code.

5) For effective outer coding, it is of advantage if the codewords of the inner code have fixed locations in the data format, i.e., if inner coding and data frames are synchronous. The parameters of the outer code depend strongly on the inner coding scheme. For example, for convolutional/sequential decoding in the inner decoding scheme, the error probability of decoded frames, in principle, can be made as small as desired by making the constraint length of the convolutional code long enough. The problem is that some frames might not be decoded due to time limitations of the sequential decoder. For the outer decoder, this has the advantage that the location of the erroneous elements are known. In this case, the erroneous elements are called erasures rather than errors. Erasures can be corrected with much less redundancy and/or decoding complexity than errors.

If maximum likelihood decoding (block decoding or convolutional/Viterbi decoding) is chosen for inner decoding, all data are decoded and errors are undetected. In this case, a more complicated error correcting procedure and/or error detection (with deletion of erroneous data) has to be used in the outer decoding.

The application of concatenated coding is discussed in references 5-20 through 5-27.

A concatenated coding scheme has been used for the Mariner Mars 1971 Infrared Interferometer Spectrometer (IRIS) experiment, where an improvement of two orders of magnitude in probability of bit error was achieved. Reference 5-27 discusses the coding scheme used.

A basic block diagram of the outer decoder with detector-corrector processing is given in Figure 5-22, taken from the reference. Typical input/

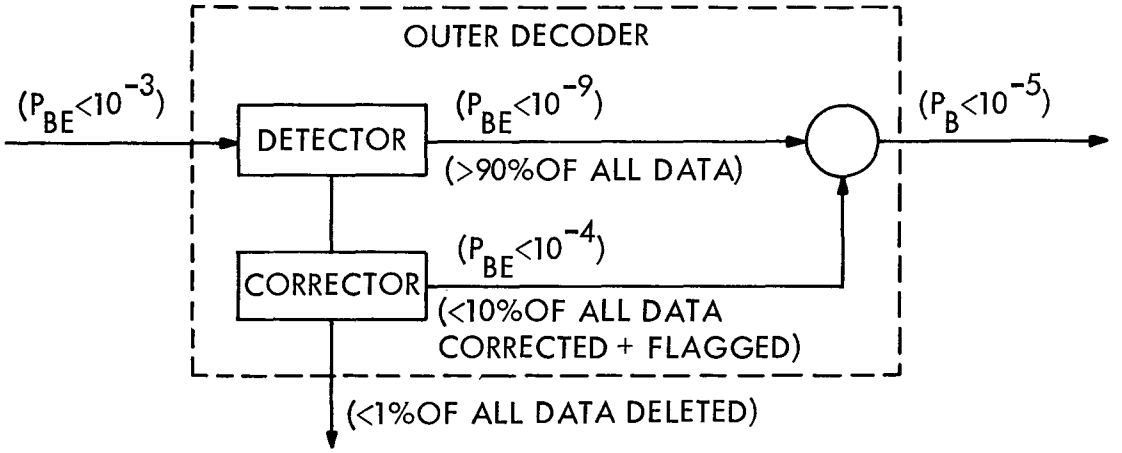

Fig. 5-22. Outer decoder with detector-corrector processing (MM'71 IRIS) (P_{BE} = bit error probability)

output values are included in parentheses. Figure 5-23 shows the bit error probability vs signal-to-noise ratio for the (n = 6, M = 2, k = 6) generalized Hamming outer code and a biorthogonal (n = 32, k = 6) inner code used, where n is the number of symbols formed from k information bits and M is the number of check elements in the outer code.

5.3.4 Data Synchronization

The accuracy of data symbol synchronization is vital to the quality of telemetry data finally presented to the users. There are two aspects to synchronization accuracy. The first involves the method by which data is formatted and synchronized on the spacecraft before transmission to Earth. The second aspect is the quality of data synchronization obtained on the ground and how the data is deformatted.

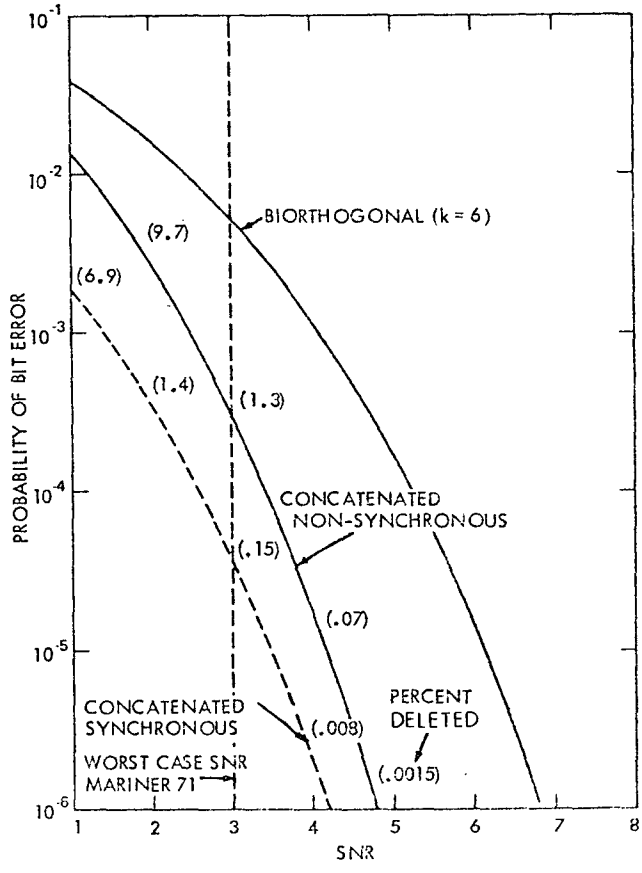

Fig. 5-23. Probability of bit error after outer decoding vs signal-to-noise ratio, SNR, for concatenated synchronous and nonsynchronous systems as referenced to a biorthogonal (k = 6) code. (MM'71 IRIS)

5.3.4.1 Types of Synchronization. In the spacecraft, data is obtained from sensors, digitized, formatted into frames and outputted in a serial bit stream for transmission to Earth. To deformat the data properly, some form of frame sync is needed. This is usually a PN code word which is added to the beginning of the frame. In some cases, subformatting is provided, and PN sync codes may occur more than one time per frame.

Once the data is formatted and processed into a serial data stream, the data bits are modulated onto subcarriers, or they are mapped into code symbols and then modulated onto subcarriers. If data is to be sent uncoded, no special synchronization code is required, but it is subject to one condition;

there must be a minimum rate of transitions between "1's" and "0's" in the data to assure acquisition of symbol sync and good efficiency in the SAA at the DSS. A minimum transition density of 10 to 20 percent is recommended. If long sequences of all "1's" or all "0's" are anticipated, such as an all black or all white TV picture or a computer memory readout where some of the memory is blank, some sort of transition generator should be added to the flight data system to aid in the symbol synchronization at the DSS. However, care must be taken to prevent a loss in transition density in more typical data.

If data is block coded, the flight data system must provide, in addition to the data bits, a bit sync clock pulse, a word sync clock pulse, and code symbol sync clock pulse.

If the block code chosen uses data words k bits long, the word sync rate R_{WS} must be 1/k of the bit sync rate, R_B.

$$R_{WS} = \frac{1}{k} R_B \tag{5.3-29}$$

A symbol sync pulse must be provided which is exactly $M = 2^k - 1$ times the word sync rate.

$$R_{SS} = \left(2^k - 1\right) \quad R_{WS} = \left(\frac{2^k - 1}{k}\right) R_B \tag{5.3-30}$$

If a convolutional encoder of rate 1/v and constraint length K is used, the spacecraft data system must supply a symbol sync pulse to the coder which is exactly v times the bit rate. Then,

$$R_{SS} = vR_B \tag{5.3-31}$$

5.3.4.2 Use of Synchronization in Ground Processing. When the transmitted symbols are received on Earth, the various synchronizations that were put into the data must be recovered and used.

After the carrier and subcarrier have been demodulated, the received data symbols plus noise are outputted from the SDA. The SSA accepts this output, integrates the data-plus-noise, and attempts to estimate the original synchronization from the integrated data. The noise in the SDA output tends to mask the data transitions so that an imperfect symbol sync reference will be derived. Thus, the efficiency of symbol synchronization is a function of the signal energy per bit, ST_B/N_o. Furthermore, during the times when there are no transitions in the symbol stream, the reference oscillator may drift out of sync with the symbols. Thus, the efficiency of symbol sync is also a function of the data transition density.

The symbol synchronization reference is used in the correlation detection of data bits or code words. If symbol sync is imperfect, the error probabilities will be worse than that predicted in equations (5. 3-5) and (5. 3-13).

If data is uncoded, the SSA will produce estimates of the data bits. These bits are formatted by the TCP for transmission from the stations to the Project. If the data is block coded, the data symbols are passed on to the BDA. The BDA must obtain word synchronization by looking for high correlation with words in the block code dictionary. Again, imprecise knowledge of word sync will degrade the error probability of equation (5. 2-13).

If data is convolutionally encoded, the code symbols from the SSA are presented to the DDA for detection. If the symbols are not perfectly synchronized, the error rate of the convolutional decoder is increased. The DDA must generate branch synchronization and block synchronization from the incoming symbols. Block synchronization is generated from the tail appended to the data. Branch synchronization is generated automatically if the code is properly chosen. Sometimes advantage may be gained by the addition of a sync sequence to the encoder output on the spacecraft. Reference 5-31 discusses the conditions required for branch synchronization.

For a Viterbi decoder, no block sync is necessary. Branch sync considerations are discussed in reference 5-31.

After the data bits have been detected or decoded they are formatted and prepared for transmission to the Project over one of the communications lines used by the DSN. These lines are the Ground Communications Facility

(GCF), the High Speed Data Link (HSDL), the Wide-Band Data Link (WDL), and the Microwave Link. In some cases, the data is put into a buffer so that the Project's computers may accept the data bits at the proper time in the computation cycle. The computer must first obtain frame sync from the data bits, and then deformat the data. To do this, the computer algebraically compares the received data sequence with the known frame sync code. Since the data bits will have some error probability associated with them, the frame sync algorithm in the computer should declare the data in sync even though there are a few disagreements between the received bits and the sync code word.

Though the data may be in sync, it is necessary for the computer to look at each sync code word to ensure that the data remains in sync. Momentary interruptions in the data occur. For example, the data during spacecraft tape recorder playback will be momentarily interrupted when tape drive direction is changed. A threshold number of acceptable discrepancies in the sync word to maintain frame sync should be based on a knowledge of the expected bit error probability of the incoming data bits, and the probability that frame sync may be lost due to data interruptions.

The probability of frame sync loss strongly affects the quality of data returned to the user.

5.3.5 Relating Channel Error Rates to User Error Rates

To predict the quality of data ultimately handed the user, it is necessary to construct a model of error sources, such as shown in Figure 5-24. Physical sensors of analog data can be thought of as having some information bandwidth, and as introducing some kind of noise into its output.

In digitizing, the analog data is quantized into one of 2^k discrete levels. This quantization represents a bandwidth upper limit on the information obtained from the sensors. Each sensor is sampled at some rate which depends on the number of sensors to be sampled and the channel transmission rate. This sampling also limits the information bandwidth.

Data handling errors on the spacecraft occur primarily in the storage of digital or analog data on a tape recorder. Good design practice indicates that if recording errors are to contribute a negligible amount to the

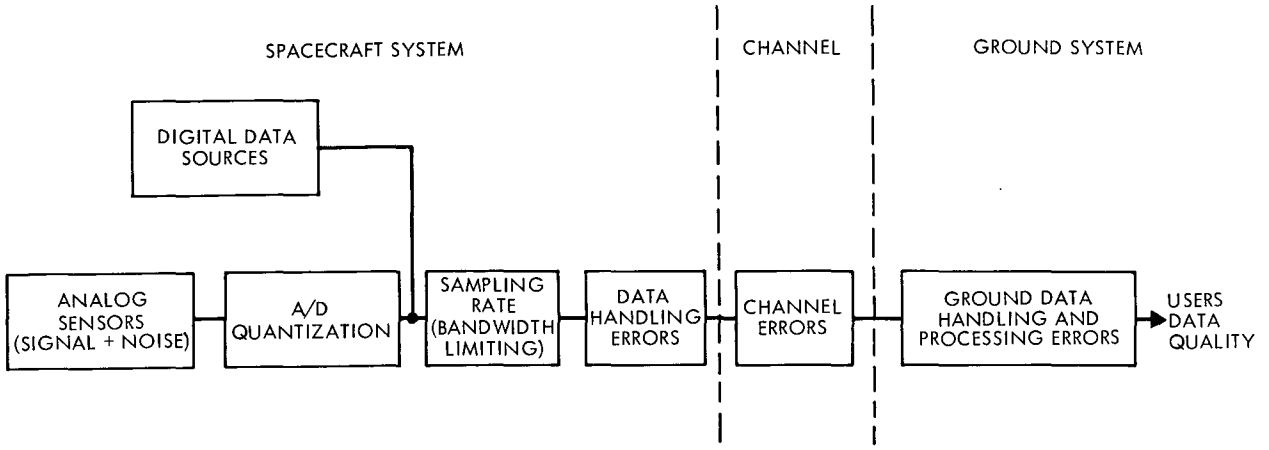

Fig. 5-24. Data quality model

user's error rate, they should be at least an order of magnitude less than the channel's error rate.

Channel errors are introduced in the process of detecting the transmitted signal imbedded in noise. The error probabilities which have been discussed parametrically in the preceding sections depend on the received signal-to-noise ratio, and the ability of the ground system to recover data synchronization.

Ground data handling errors are of the following two types:

1) Bit errors are introduced in the transmission of data between the tracking station and Network Control Center

2) Synchronization errors and loss of data occur due to computer limitations.

To be negligible, bit errors introduced in the ground communications process should be at least an order of magnitude lower than the channel error rate.

Loss of data due to buffer overflows should be minimized by matching the data rates and data processing required to the capabilities of the computer. Ideally, the ability to deliver a prescribed quantity of data should be a specification on the ground system performance.

Loss of data due to synchronization errors can occur when bit errors in the data going into the computer cause the computer to:

1) Think it has frame sync when in fact it does not;

2) Think it has lost frame sync when in fact the data is still synchronized;

3) Or lose frame sync entirely.

These errors are a function of the type of channel coding used and the bit or word error rates associated with the coding.

5.3.5.1 User Error Rates as a Function of Channel Error Rates. One important aspect of the problem of modeling the user's data quality is to relate the bit or word error probability of the channel to the bit or word error probability of the user. What follows, assumes that all errors other than channel errors are negligible.

The user may wish to specify his data quality in terms of an average bit error rate. If the channel is uncoded, then the channel bit error rate is identical to the user bit error rate, and the bit errors will be independent of each other.

$$P_{B\ USER} = P_{B\ CHANNEL} \tag{5.3-32}$$

The user may wish to specify his data quality in terms of an average word error rate for data of some length, M. If the channel is uncoded, then the probability that the word will be in error is one minus the product of the probability that each bit is correct.

$$P_{W\ USER}(M) = 1 - (1 - P_{B_{CH}})^{M} \approx MP_{B_{CH}} \tag{5.3-33}$$

assuming

$$P_{B_{CH}} \ll 1$$

For the uncoded channel, these word errors will be independent of each other.

If the channel is block encoded, the detection of 5- or 6-bit words is performed. Thus, an entire block of 5 or 6 bits is correct, or the word is in error and one or more bits are in error. The coded word errors are independent of each other, but the bit errors come in bursts. A user may be interested in data words whose length is different than that of the block coded word transmitted as a block of code symbols. Consequently, the user's data word error rate, ϵ_D, will be different from the block coded word error rate, ϵ_C. The ratio of ϵ_D/ϵ_C depends on the length of the data word, the block coded word, the probability of coded word errors, and the relative synchronization of data words with code words. In general, the lowest user data word error rate occurs when the number of code words which overlap a data word is minimized.

If the data channel is block coded and the user is interested in the average bit error rate, the bit error rate is given by equation (5.3-14).

5.4 TELEMETRY SYSTEM EFFICIENCY

Telemetry channels for deep space vehicles have typically been power limited rather than bandwidth limited. For this reason, the efficiency of a telemetry system design is measured by how much power is required to achieve a given data rate with a given maximum bit error rate. The design and performance of a telemetry system can be conveniently referenced to the ratio of total received power to system noise spectral density, P_T/N_o. This parameter was discussed in detail in section 2. There it was shown that P_T/N_o is completely determined by the spacecraft transmitter power, the spacecraft and ground station antenna gain patterns, ground system noise temperature, and the orientation of the spacecraft as a function of its mission trajectory.

In this section, it will be shown how to relate the performance of a particular telemetry system to the independent variable P_T/N_o, and how a telemetry system may be optimized as a function of P_T/N_o.

5.4.1 Relationship Between P_T/N_o and ST_B/N_o

In any modulation system, the signal energy per bit (which determines the bit error probability of a telemetry channel) may be related to the total received power by a relationship of the form

$$\frac{ST_B}{N_o} = \left(\frac{P_T}{N_o}\right)\left(\frac{P_D}{P_T}\right) T_B \eta_{WDL} \eta_S \qquad (5.4\text{-}1)$$

where

P_D = Sideband power available for use as signal energy

T_B = Bit time

η_{WDL} = Subcarrier waveform distortion loss

η_S = Efficiency of the demodulation process.

The quantity P_D/P_T depends on the type of modulation scheme used. The quantity η_s is an efficiency factor which relates the ideal error rates (e.g., as expressed in equations (5.3-5) and 5.3-13)), to the actual error rates. η_s is less than one because of the inability of the receiver and demodulators to obtain perfectly coherent phase references and synchronization timing references. η_{WDL} represents the loss due to an imperfect subcarrier waveform in the received signal and is less than one.

5.4.2 PSK Modulation

Deep space projects which utilize the DSN are required to keep the spectrums of their telemetry data outside the tracking loop bandwidth of the DSIF receivers. This is conveniently done by modulating data onto a subcarrier prior to modulating the carrier. The SDA's will remove the subcarrier from the data prior to carrier and data detection. Each SDA is designed to accommodate a sine wave or a square wave phase-modulated subcarrier.

Square-wave subcarriers provide the more efficient use of available sideband power. The sideband power depends strictly on the phase modulation indices, and is summarized in Table 5-5 for perfect subcarrier waveforms.

Table 5-5. Sideband power/total power allocations for phase modulation using square-wave subcarriers

Type of Channel	Channel Power Ratios	Power Allocation For Each Component
Single Data Channel	P_C/P_T	$\cos^2\theta$
	P_D/P_T	$\sin^2\theta$
Two Data Channels	P_C/P_T	$\cos^2\theta_1 \cos^2\theta_2$
	P_{D_1}/P_T	$\sin^2\theta_1 \cos^2\theta_2$
	P_{D_2}/P_T	$\sin^2\theta_2 \cos^2\theta_1$
Single Data Channel With Ranging	P_C/P_T	$\cos^2\theta \cos^2\theta_R$
	P_D/P_T	$\sin^2\theta \cos^2\theta_R$
	P_R/P_T	$\sin^2\theta_R \cos^2\theta$
Two Data Channels With Ranging	P_C/P_T	$\cos^2\theta_1 \cos^2\theta_2 \cos^2\theta_R$
	P_{D_1}/P_T	$\sin^2\theta_1 \cos^2\theta_2 \cos^2\theta_R$
	P_{D_2}/P_T	$\sin^2\theta_2 \cos^2\theta_1 \cos^2\theta_R$
	P_R/P_T	$\cos^2\theta_1 \cos^2\theta_2 \sin^2\theta_R$

P_T = Total signal power
P_C = Carrier power
P_D = Data power
P_R = Ranging power
θ = Modulation index

5.4.3 Interplex Modulation

When more than one subcarrier is used to phase modulate data onto the carrier, power appears in intermodulation sidebands. This power is unrecoverable and represents a loss. Interplex is a method whereby data from a high-power subcarrier is modulated onto a low-power subcarrier. In the demodulation process, the data power in the low-power subcarrier occurs in what used to be the intermodulation sideband, so that more efficient use is made of the total received power when a high modulation index (>45°) is required for the high-rate channel.

5.4.3.1 Type I Interplex. Figure 5-25 shows the modulation scheme for Type I interplex.

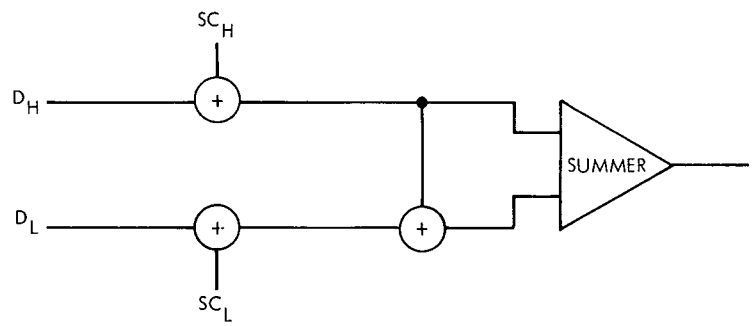

Fig. 5-25. Type I interplex modulator

The high power data, D_H, is modulated onto its subcarrier, and then modulated again with the low power data $\oplus$ subcarrier. The received waveform becomes

$$X(t) = \sqrt{2P_T}\ \sin\left[\omega_c t + \phi_o + \theta_H(D_H \oplus SC_H) + \theta_L(D_H \oplus SC_H \oplus D_L \oplus SC_L)\right] \quad (5.4\text{-}2)$$

The waveform is demodulated in the receiver, using the carrier reference and the reference shifted 90 degrees.

Thus, the quadrature channel contains

$$X(t)\ \cos(\omega_c t + \hat{\phi}) \tag{5.4-3}$$

and the in-phase channel contains

$$X(t)\ \sin(\omega_c t + \hat{\phi}) \tag{5.4-4}$$

Low-rate data is obtained from the quadrature channel, and high-rate data from the in-phase channel.

The power obtained is

$$\frac{P_{D_H}}{P_T} = \left(\sin\theta_H \cos\theta_L\right)^2 \tag{5.4-5}$$

and

$$\frac{P_{D_L}}{P_T} = \left(\sin\theta_H \sin\theta_L\right)^2 \tag{5.4-6}$$

An improvement of $\tan^2\theta_H$ is obtained in the low-rate channel over the non-interplexed PSK system for perfect square-wave subcarriers and constant modulation indices. Table 5-6 presents the ratios of data power to total power when interplex is used. Actually, the optimum modulation indices for interplex will differ from those for non-interplexed. In general, interplex gives a gain of at least 2 dB in P_T/N_o over the non-interplexed mode (see reference 5-43).

5.4.3.2 Type II Interplex. Type II interplex combines the channels slightly differently, as shown in Figure 5-26.

High-rate data is combined with its subcarrier and sent to the summer. The high-rate data is mod-2 added to the low-rate data, half-added with the low-rate subcarrier, and also sent to the summer. The received waveform is

$$X(t) = \sqrt{2P_T}\ \sin\left[\omega_c t + \phi_o + \theta_H(D_H \oplus SC_H) + \theta_L(D_H \oplus D_L \oplus SC_L)\right] \tag{5.4-7}$$

Table 5-6. Sideband power/total power allocations for interplexed phase modulation using square-wave subcarriers

Type of Channel	Channel Power Ratios	Power Allocations For Each Component
Two Data Channels	P_C/P_T	$\cos^2\theta_H \cos^2\theta_L$
	P_{D_H}/P_T	$\sin^2\theta_H \cos^2\theta_L$
	P_{D_L}/P_T	$\sin^2\theta_H \sin^2\theta_L$
Two Data Channels With Ranging	P_C/P_T	$\cos^2\theta_H \cos^2\theta_L \cos^2\theta_R$
	P_{D_H}/P_T	$\sin^2\theta_H \cos^2\theta_L \cos^2\theta_R$
	P_{D_L}/P_T	$\sin^2\theta_H \sin^2\theta_L \cos^2\theta_R$
	P_R/P_T	$\sin^2\theta_R \cos^2\theta_H \cos^2\theta_L$

P_T = Total signal power

P_C = Carrier power

P_{D_H} = High-rate data power

P_{D_L} = Low-rate data power

P_R = Ranging power

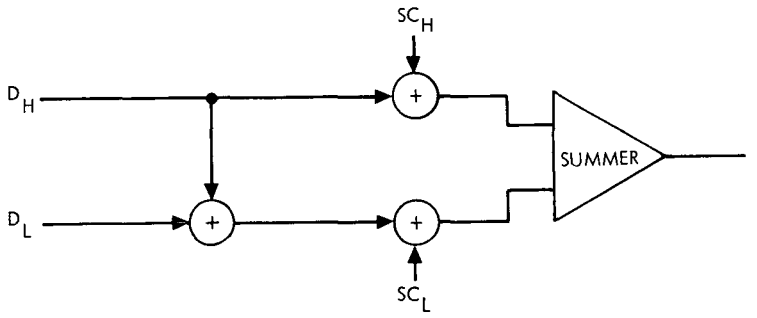

Fig. 5-26. Type II interplex modulator

The waveform is detected by the receiver as in Type I, but now the in-phase channel produces $D_L \oplus SC_H$.

The subcarrier reference derived from subcarrier demodulation of the high-rate channel must now be used to detect D_L. From an operational standpoint, this means that both channels must be properly operating to obtain the low-rate data. However, the bandwidth requirements on the spacecraft are simpler for Type II interplex.

The power allocation for each data channel remains the same as for Type I interplex.

5.4.4 Probability of Error Versus ST_B/N_o

Figure 5-27 directly compares the probability of bit error for channels that are uncoded and (32,6) block coded, have perfect carrier, subcarrier and sync references, and perfect subcarrier waveforms.

5.4.5 System Losses

Equations (5.3-5) and (5.3-13) give analytic expressions relating the probability of error to ST_B/N_o. These expressions are used to establish a design point value of ST_B/N_o corresponding to a required error rate. Similarly, simulations are used for convolutional coding schemes.

These results assume that the carrier phase reference is derived perfectly by the receiver, that the subcarrier phase reference is derived

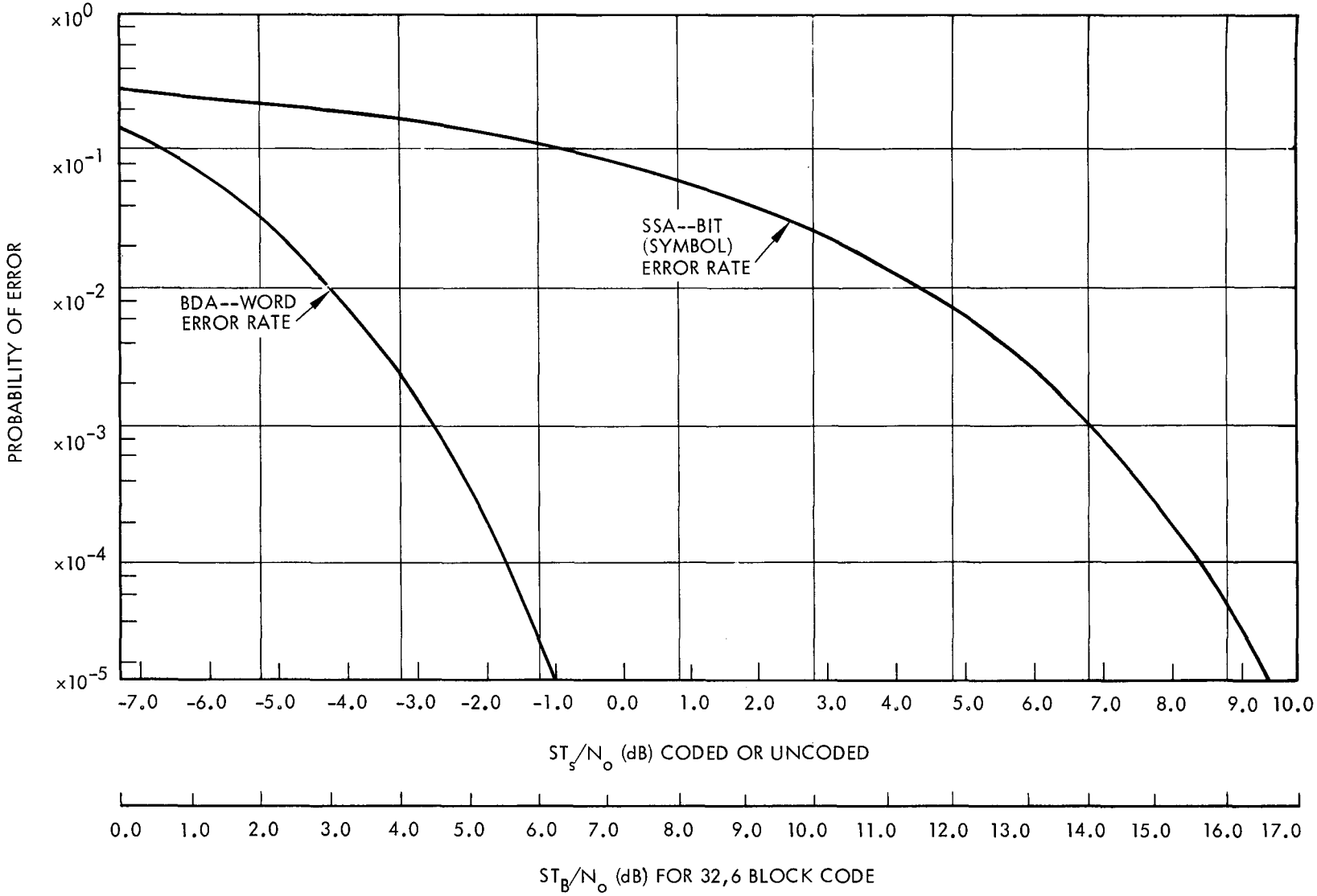

Fig. 5-27. Bit error rate for uncoded and (32,6) block coded channels

perfectly, and that the symbol and word timing references are also derived perfectly. However, for a finite available P_T/N_o, these references are imperfectly known, and the uncertainty appears as phase jitter on the carrier, subcarrier, and symbol timing references. Consequently, the measured probability of bit error will be worse than predicted by equations (5.3-5) and (5.3-13) and convolutional coding simulations which neglect these effects. In particular, as Heller and Jacobs have noted (Reference 5-19), the effect of carrier phase jitter on performance is always more severe for coded than for uncoded systems. This effect arises from two sources. First, for a coded system the curve of probability of error versus ST_B/N_o is much steeper than for an uncoded system. The effective loss in ST_B/N_o due to phase jitter thus causes relatively more degradation for coded systems than uncoded. Second, unless care is taken in phase-locked loop design, the phase error may depend on ST_S/N_o, which is much smaller for coded systems than for uncoded.

A convenient way of accounting for the reference uncertainties is to define a quantity η_S, known as the system efficiency or system loss.

$$\eta_S \triangleq \frac{\text{Theoretically required data power, } P_D}{\text{Actual required data power, } P_D} \tag{5.4-8}$$

The system loss is usually understood to be the linear sum, in decibels, of the individual losses assigned to the subcarrier demodulator, and the bit or symbol synchronizer. Thus,

$$\eta_S = \eta_{RL} + \eta_{SDL} + \eta_{BSDL}\,(\text{dB}) \tag{5.4-9}$$

where η_{RL} = Radio loss (dB)

η_{SDL} = Subcarrier demodulation loss (dB)

η_{BSDL} = Bit sync and detection loss (dB)

In reality, each of these systems contributes simultaneously to the total loss, and only under restricted circumstances can the total be approximated by the sum of the three. Appendix A5.1 shows that, when valid, this approximation is generally optimistic and is an upper bound on η_S.

The following sections give expressions for radio loss (RL), subcarrier demodulator loss (SDL), and bit sync and detection loss (BSDL). Further explication may be found in appendix A5.1.

5.4.5.1 Radio Loss. Radio loss is defined as the loss attributed to the radio system when the subcarrier demodulator and the bit synchronizer are operating perfectly. Radio loss is caused by imperfect tracking of the downlink carrier phase and depends on the method of data detection through the probability of information errors. Associated with the two modes of tracking, as described in section 4.3.3.6, are two modes of radio loss, one-way and two-way. In what follows, we shall assume that the ground receiver and spacecraft receiver have zero static phase error.

When the telecommunications link is operating in a one-way mode, the telemetry data is modulated on a carrier generated by the auxiliary oscillator in the spacecraft. For the uncoded case, there are two limiting forms of (one-way) radio loss, depending on the data rate.

For uncoded data, if the bit time, T_B, is much smaller than the response time of the ground receiver's PLL ($T_B \ll 1/B_L$), then the radio system efficiency is (see appendix A5.1):

$$\eta_{HI} = \frac{\left[\text{erfc}^{-1}(2\overline{P}_{BE})\right]^2}{\left(\frac{ST_B}{N_o}\right)_{in}} \tag{5.4-10}$$

where $\overline{P}_{BE}$ is the probability of bit error as a function of $(ST_B/N_o)_{in}$ weighted by the probability density function of ϕ, the phase error, and averaged over $-\pi \le \phi \le \pi$, and if $\text{erfc}^{-1}(x) = y$, then $x = \text{erfc}(y)$.

$(ST_B/N_o)_{in}$ is the actual signal energy to noise spectral density ratio into the detector.

If T_B is much larger than the loop response time ($T_B \gg 1/B_L$), then the efficiency is:

$$\eta_{LOW} = \left[\frac{I_1(\eta)}{I_o(\eta)}\right]^2 \tag{5.4-11}$$

where $\eta = 2P/N_o\omega_L$ is the SNR in the PLL.

If T_B does not satisfy either extreme then the true efficiency can be approximated by:

$$\eta_{RL} = (1 - a_c)\eta_{LOW} + a_c\eta_{HI} \tag{5.4-12}$$

where

$$a_c = \frac{\delta_c}{4}\left[1 - \frac{\delta_c}{8}\left(1 - \exp\left(-8 / \delta_c\right)\right)\right] \tag{5.4-13}$$

and

$$\delta_c = \frac{2}{\omega_L T_B} = \frac{1}{B_L T_B} \tag{5.4-14}$$

Figure 5-28 plots a_c versus δ_c. Figure 5-29 plots η_{HI} and η_{LOW} versus η with $(ST_B/N_o)_{in}$ as a parameter for η_{HI}. By using these figures in conjunction with Figures 4-14, 4-15, and 4-16, the one-way radio loss for uncoded telemetry can be determined for various parameter choices.

Radio loss can also be regarded as,

$$\eta_{RL} = \frac{\left(\frac{ST_B}{N_o}\right)_{eq}}{\left(\frac{ST_B}{N_o}\right)_{in}} \tag{5.4-15}$$

That is, $(ST_B/N_o)_{eq.}$ is the signal energy-to-noise spectral density ratio which would give the same average probability of error in a perfectly coherent system ($\omega_L \longrightarrow 0$) as $(ST_B/N_o)_{in}$ gives in the actual system.

The one-way radio loss curves of Figure 5-29 are general, and do not assume particular spacecraft or ground parameters.

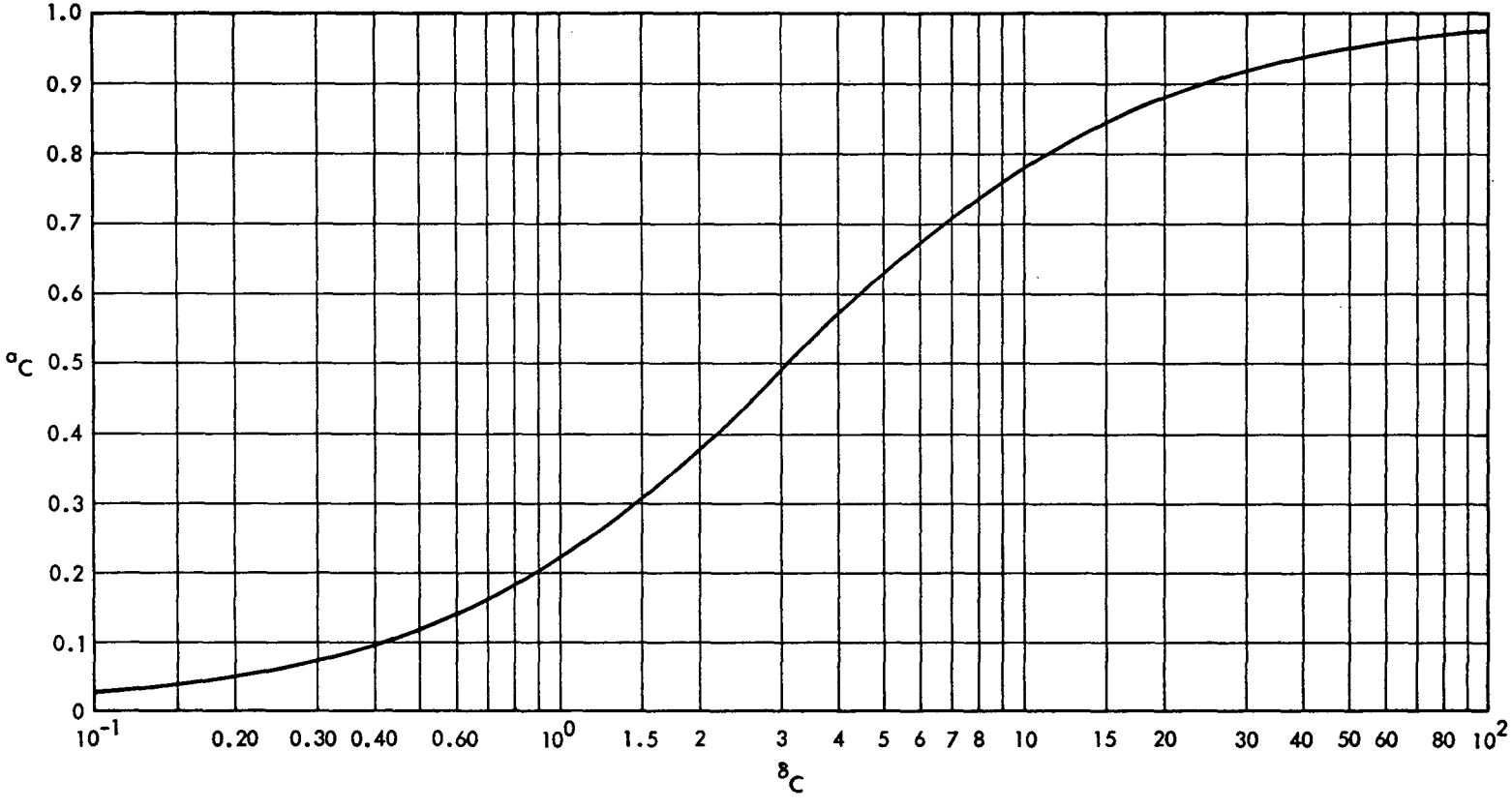

Fig. 5-28. Radio loss interpolation parameter versus $\delta_c = 1/B_L T_B$

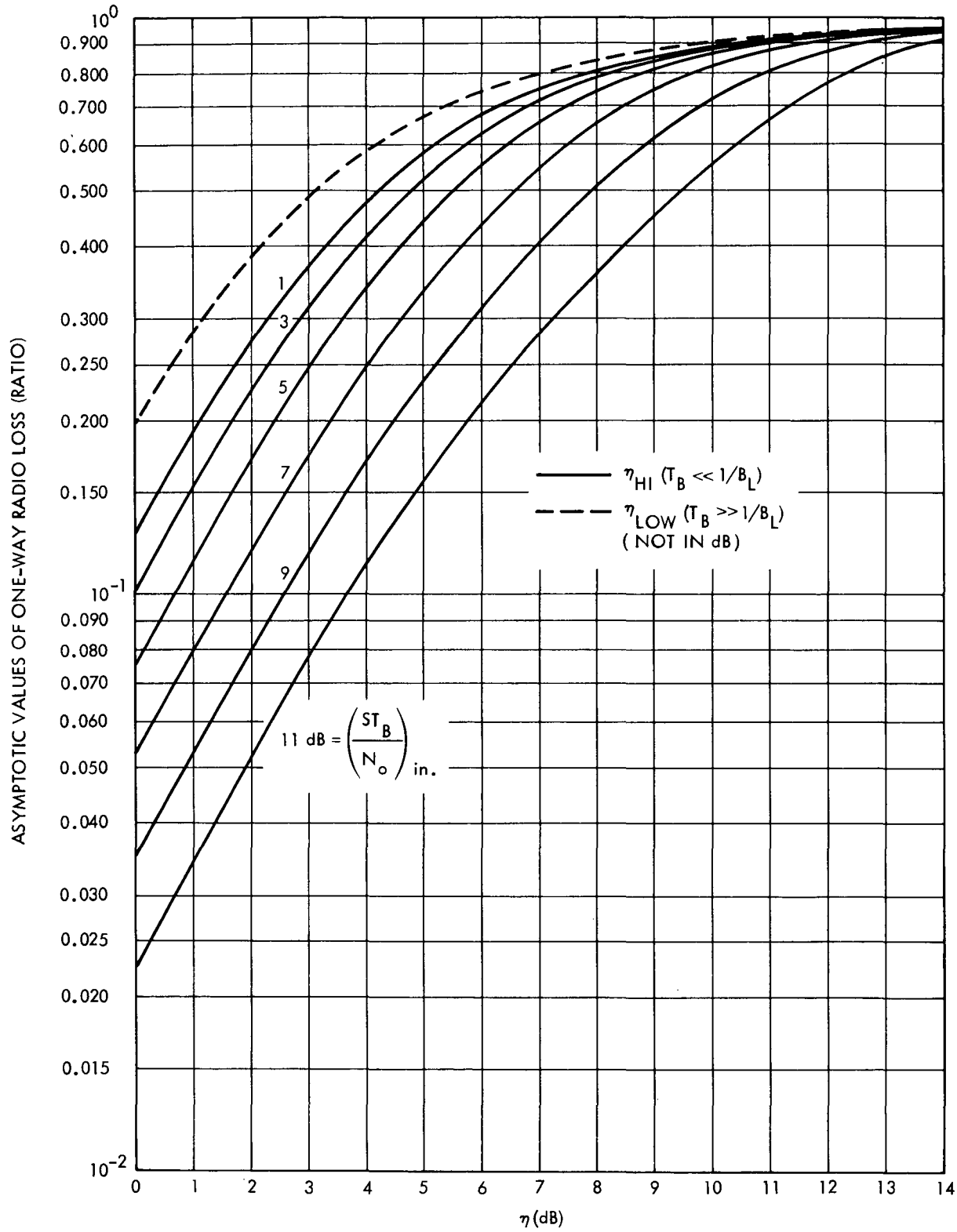

Fig. 5-29. Asymptotic values of one-way radio loss versus SNR in B_L for uncoded telemetry

The equations 5.4-10 through 5.4-15 apply for uncoded two-way radio loss as well if the one-way probability density function for ϕ is replaced by the two-way function. Figures 5-30 through 5-34 plot the asymptotic values (η_{HI} and η_{LOW}) of two-way radio loss versus ground SNR in $2B_{LO}$ for uncoded telemetry with spacecraft SNR in $2B_{LO}$ as a parameter and ground $2B_{LO}$ = 12 Hz. Figures 5-35 through 5-39 assume ground $2B_{LO}$ = 3 Hz. Both sets of figures use the DSIF parameters $r_o = 2$, B_ℓ = 2200 Hz, and the spacecraft parameters $r_o = 2$, B_ℓ = 5000 Hz, and $2B_{LO}$ = 18 Hz. The turnaround ratio G = 240/221.

For the coded case, no closed form solution such as (5.4-10) exists. Hence, the efficiency must be computed numerically and is represented by equation (5.4-15), where, for block codes,

$$\overline{P}_{WE}\left[\left(\frac{ST_B}{N_o}\right)_{in}\right] = \lim_{\omega_L \to 0} \overline{P}_{WE}\left[\left(\frac{ST_B}{N_o}\right)_{eq.}\right] \qquad (5.4\text{-}16)$$

Figure 5-40 plots one-way radio loss versus SNR in B_L with $(ST_B/N_o)_{in}$ as a parameter for (32, 6) block coded telemetry. Figures 5-41 through 5-45 plot two-way radio loss versus ground SNR in $2B_{LO}$ for (32, 6) block-coded telemetry with spacecraft SNR in $2B_{LO}$ as a parameter and ground $2B_{LO}$ = 12 Hz. Figures 5-46 through 5-50 assume ground $2B_{LO}$ = 3 Hz. Both sets of figures use the parameters r_o, B_ℓ, spacecraft $2B_{LO}$ and G as quoted above for uncoded telemetry. Note that because of the different form of detection, the parameter δ_c does not appear in the solution. The values plotted for these cases are actual radio loss and require no interpolation.

Figure 5-51 plots a sample curve of one-way radio loss, taken from Figure 5-20, for convolutionally encoded/Viterbi decoded data with rate 1/2, constraint length 7, and 8-level quantization (see paragraph 5.3.3.2.1.2).

5.4.5.2 Subcarrier Demodulator Loss. Subcarrier demodulator loss is defined as the loss attributed to the SDA system when the radio and the symbol synchronizer are operating perfectly. The theory is analogous to that for radio loss and, for uncoded telemetry, also has two limiting cases. In what follows, we assume that ones and zeros are equally likely in the data stream and that bits are independent.

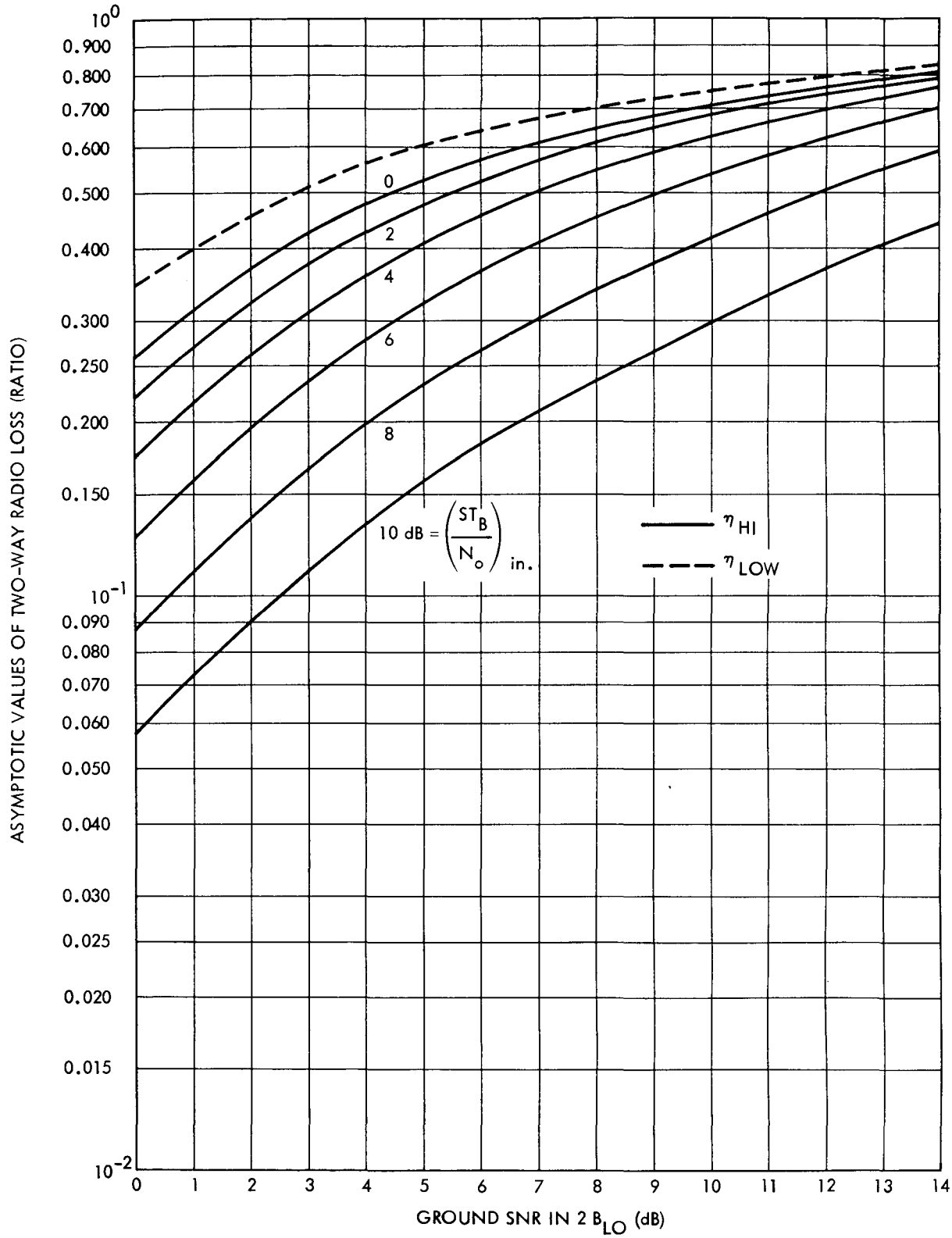

Fig. 5-30. Asymptotic values of two-way radio loss versus ground SNR in $2B_{LO}$ for uncoded telemetry, spacecraft SNR in $2B_{LO}$ = 7 dB, ground $2B_{LO}$ = 12 Hz

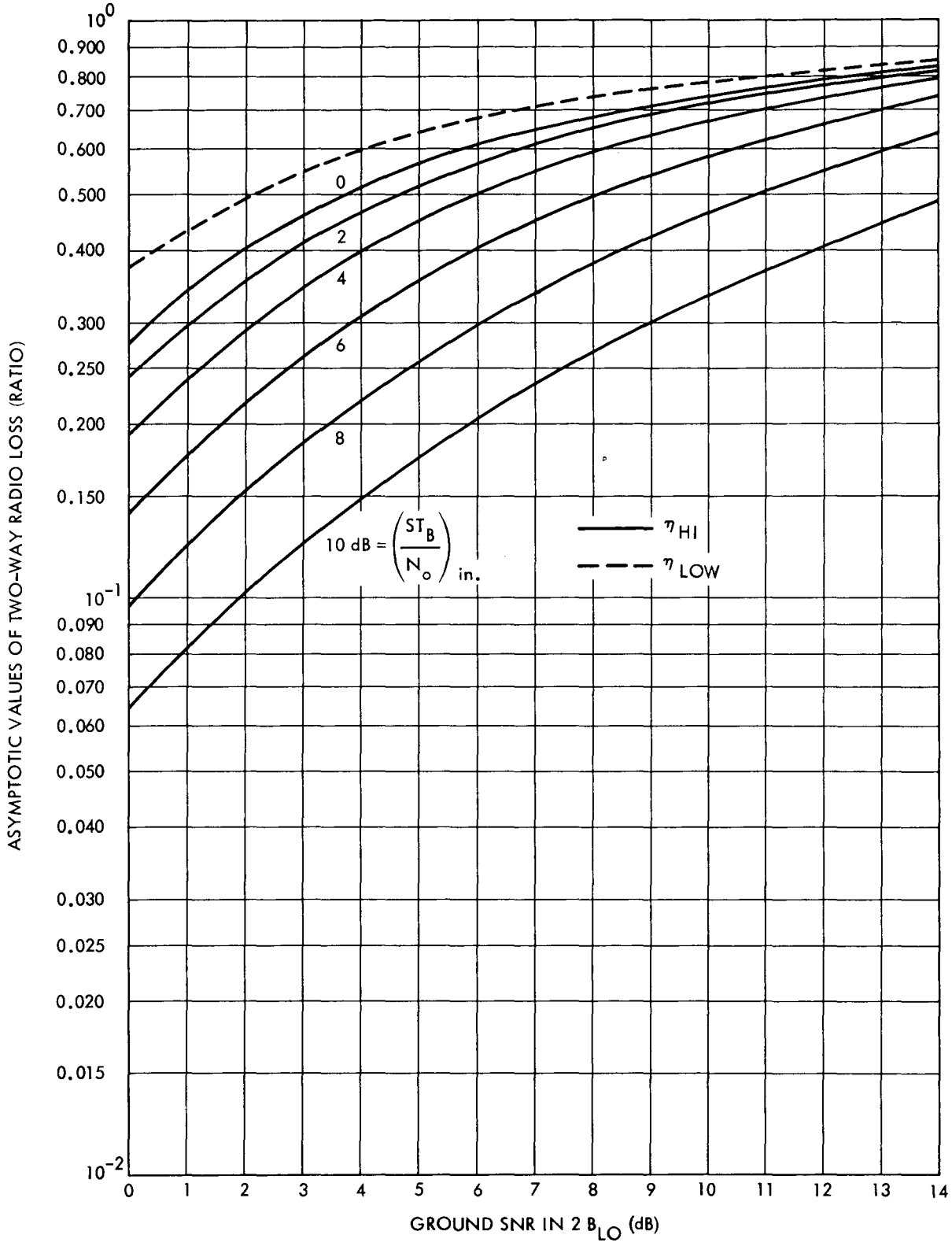

Fig. 5-31. Asymptotic values of two-way radio loss versus ground SNR in $2B_{LO}$ for uncoded telemetry, spacecraft SNR in $2B_{LO}$ = 10 dB, ground $2B_{LO}$ = 12 Hz

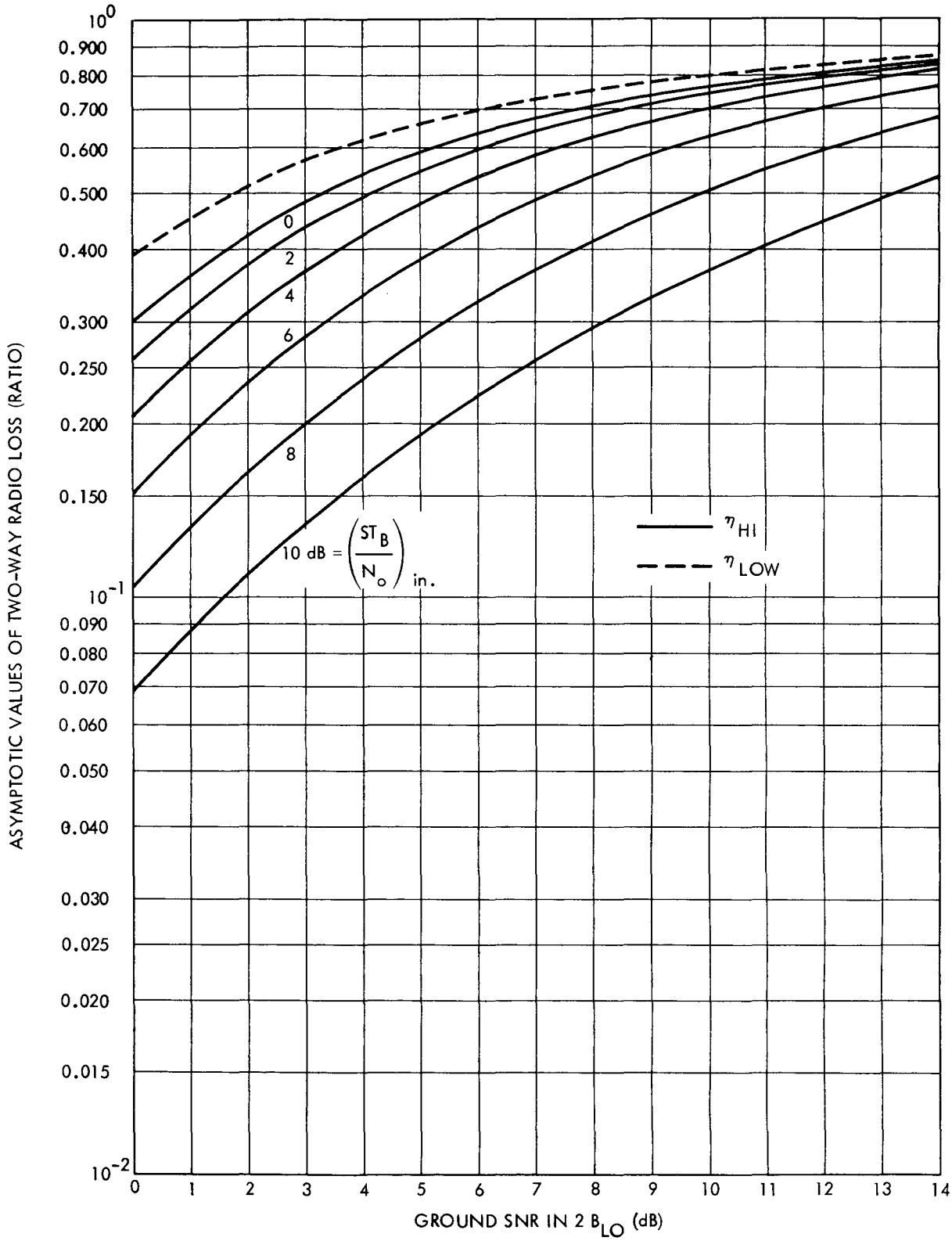

Fig. 5-32. Asymptotic values of two-way radio loss versus ground SNR in $2B_{LO}$ for uncoded telemetry, spacecraft SNR in $2B_{LO}$ = 13 dB, ground $2B_{LO}$ = 12 Hz

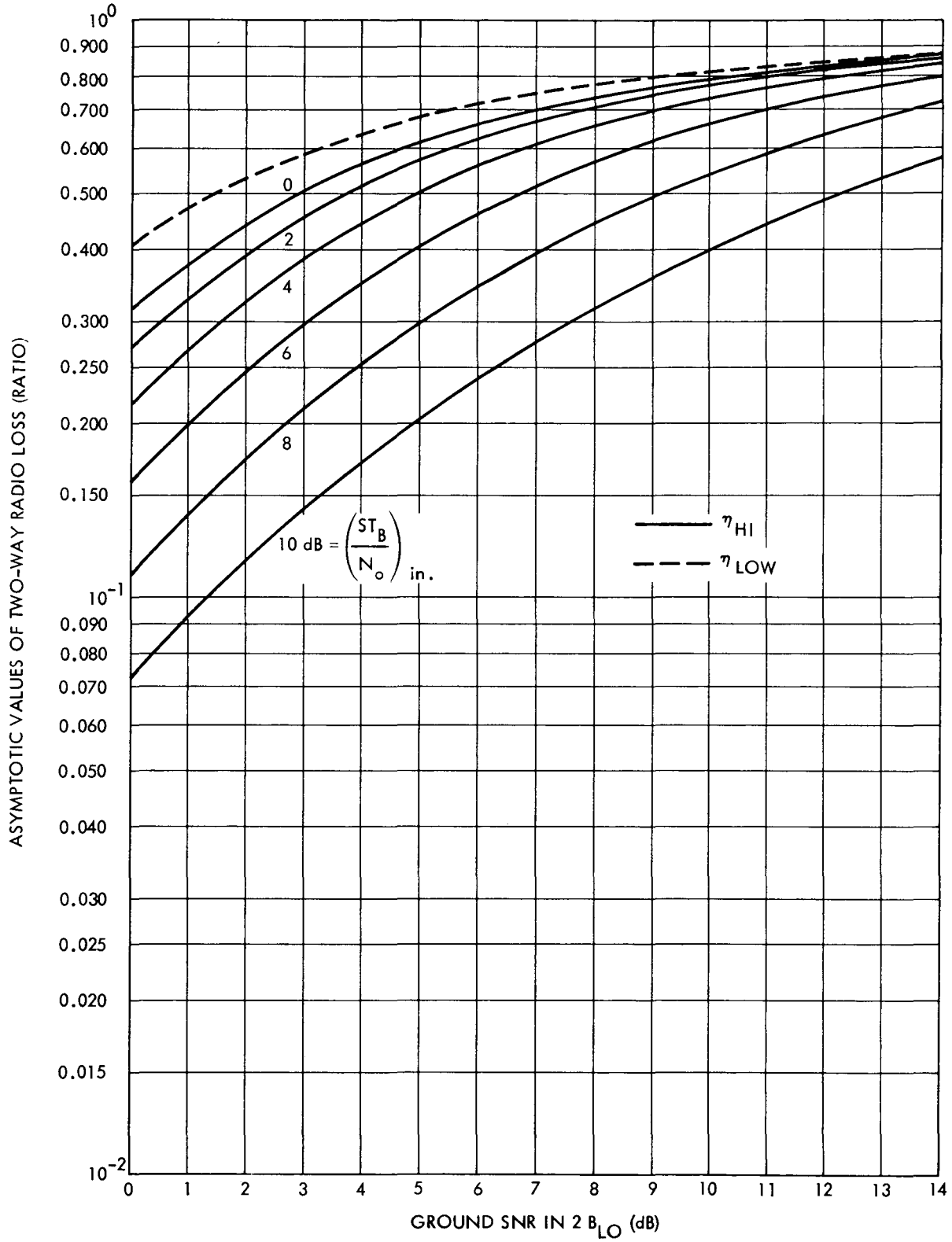

Fig. 5-33. Asymptotic values of two-way radio loss versus ground SNR in $2B_{LO}$ for uncoded telemetry, spacecraft SNR in $2B_{LO}$ = 16 dB, ground $2B_{LO}$ = 12 Hz

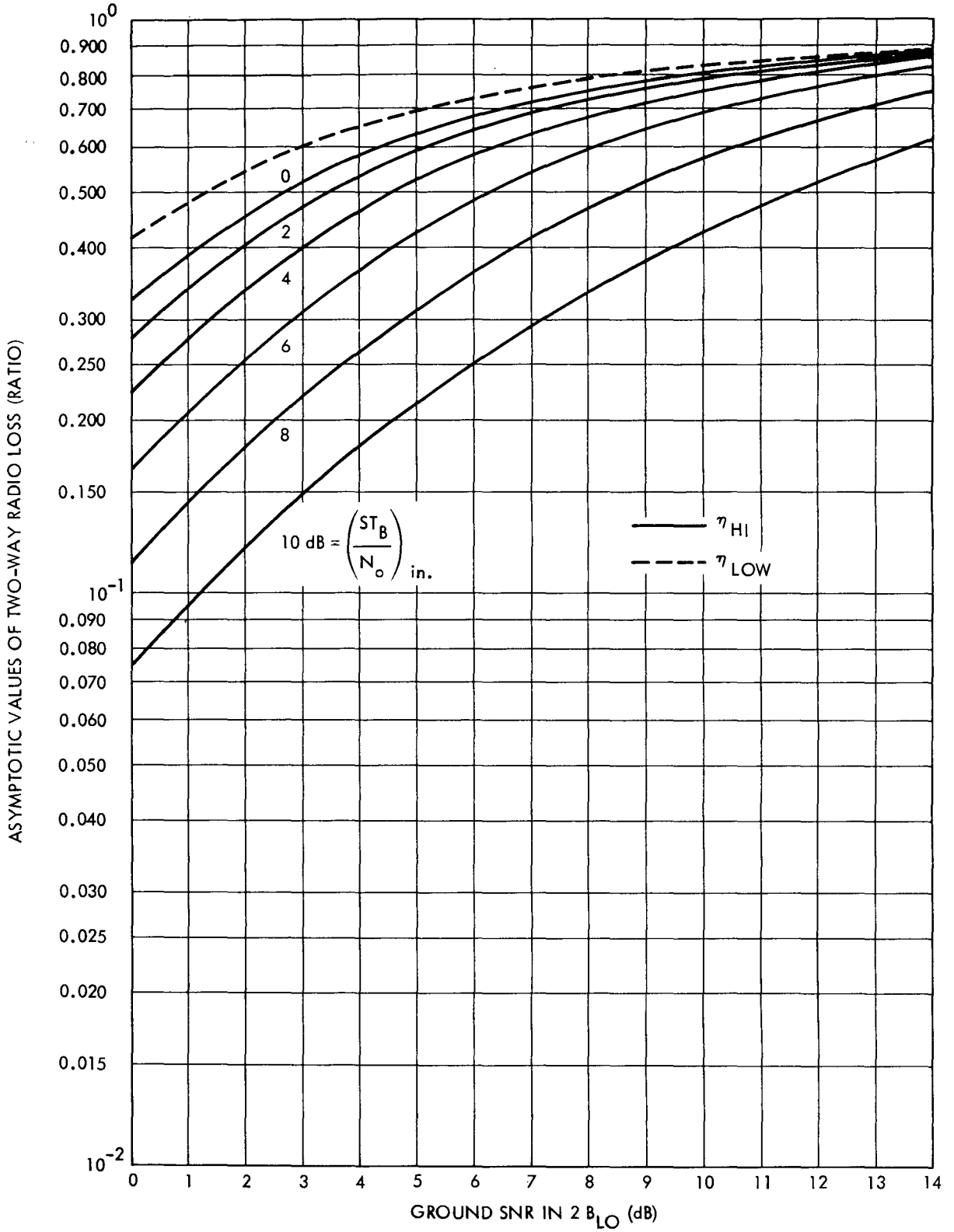

Fig. 5-34. Asymptotic values of two-way radio loss versus ground SNR in $2B_{LO}$ for uncoded telemetry, spacecraft SNR in $2B_{LO}$ = 19 dB, ground $2B_{LO}$ = 12 Hz

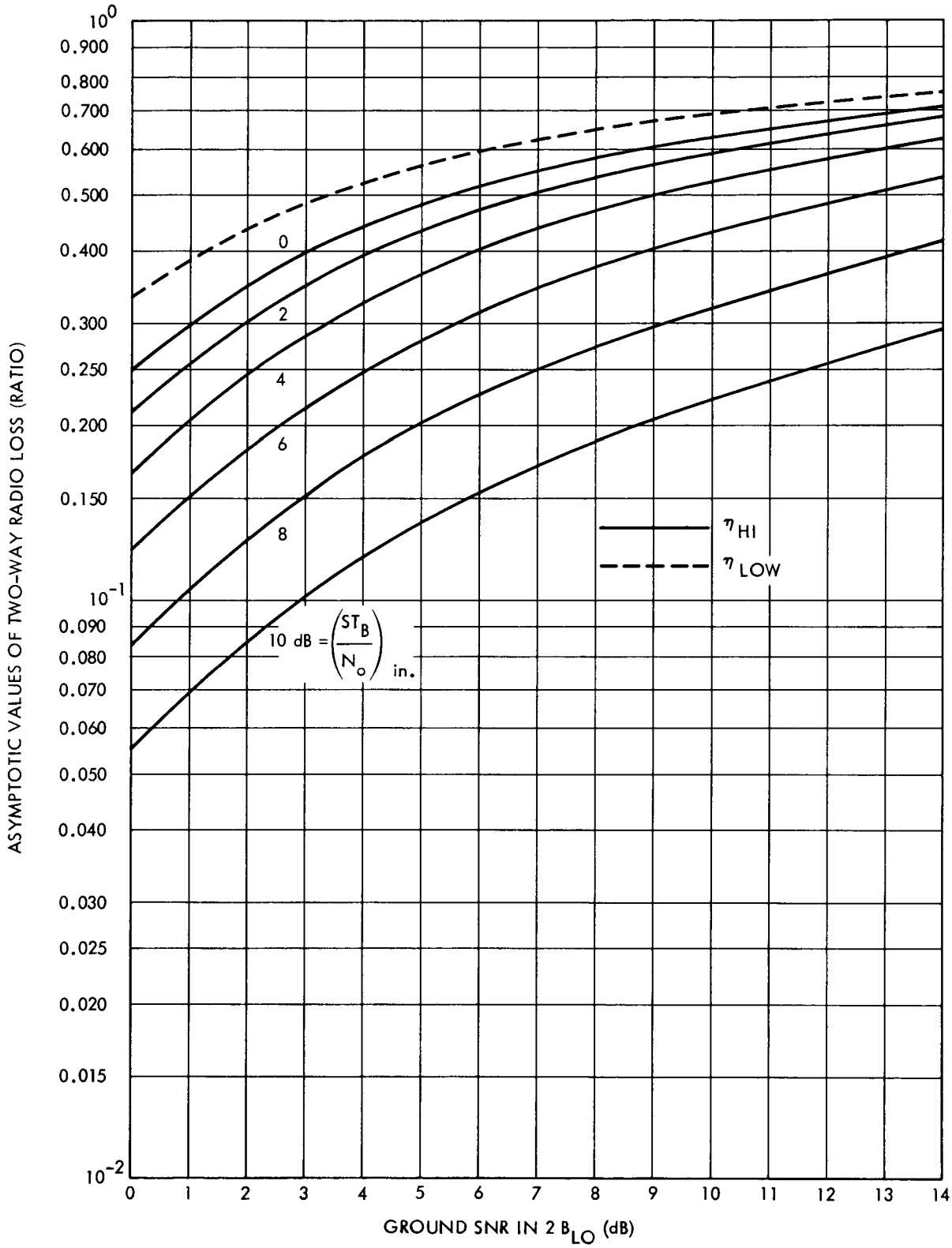

Fig. 5-35. Asymptotic values of two-way radio loss versus ground SNR in $2B_{LO}$ for uncoded telemetry, spacecraft SNR in $2B_{LO}$ = 7 dB, ground $2B_{LO}$ = 3 Hz

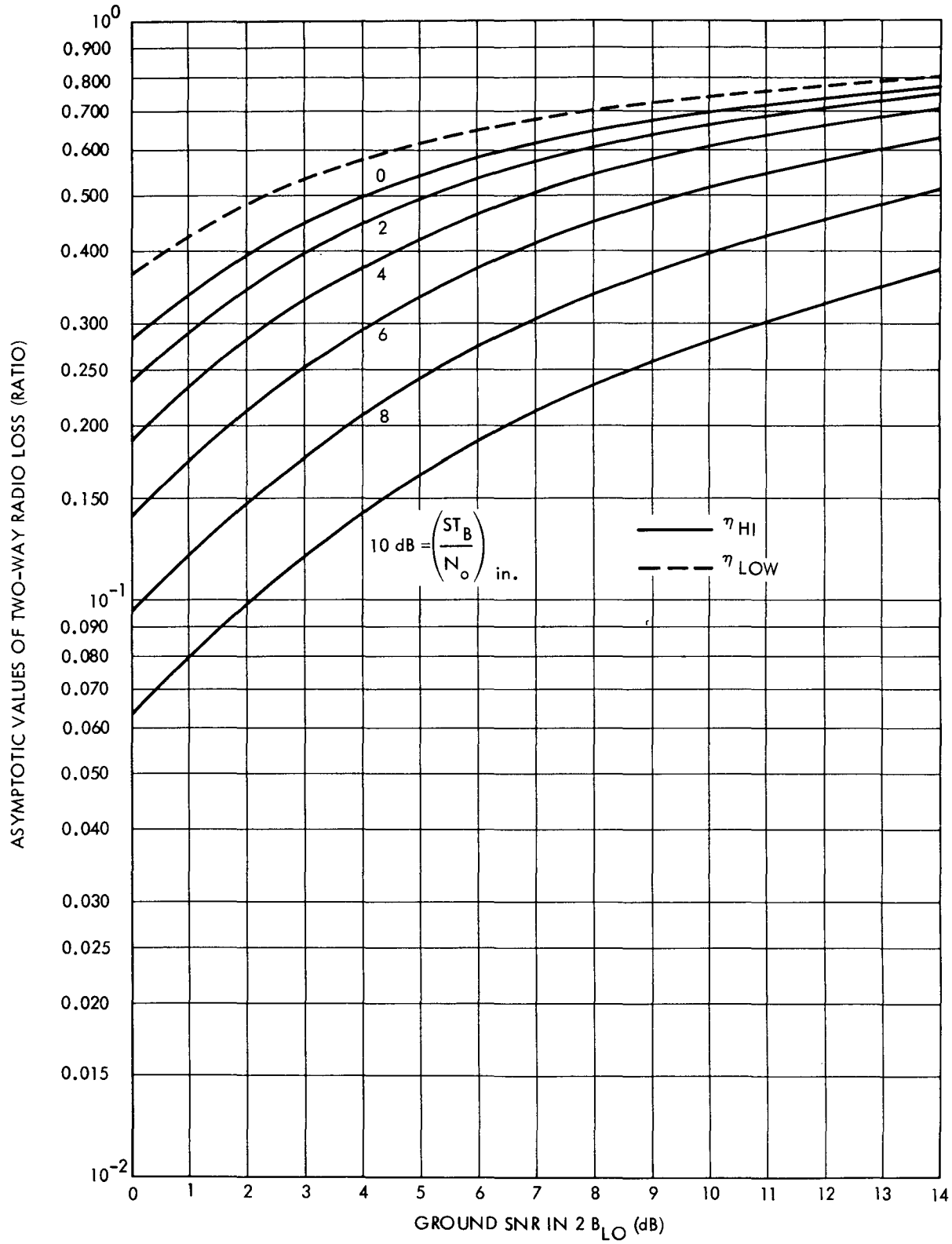

Fig. 5-36. Asymptotic values of two-way radio loss versus ground SNR in $2B_{LO}$ for uncoded telemetry, spacecraft SNR in $2B_{LO}$ = 10 dB, ground $2B_{LO}$ = 3 Hz

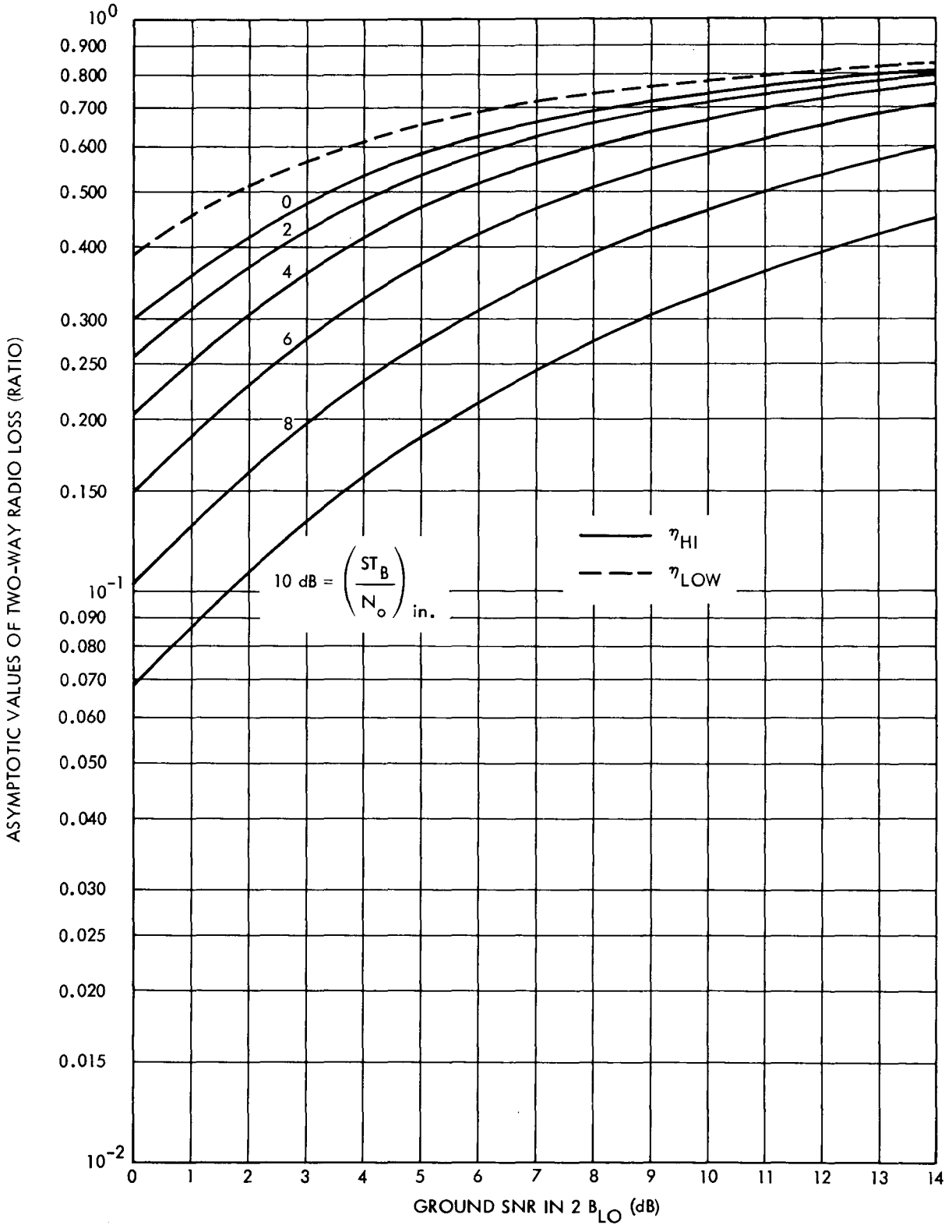

Fig. 5-37. Asymptotic values of two-way radio loss versus ground SNR in $2B_{LO}$ for uncoded telemetry, spacecraft SNR in $2B_{LO}$ = 13 dB, ground $2B_{LO}$ = 3 Hz

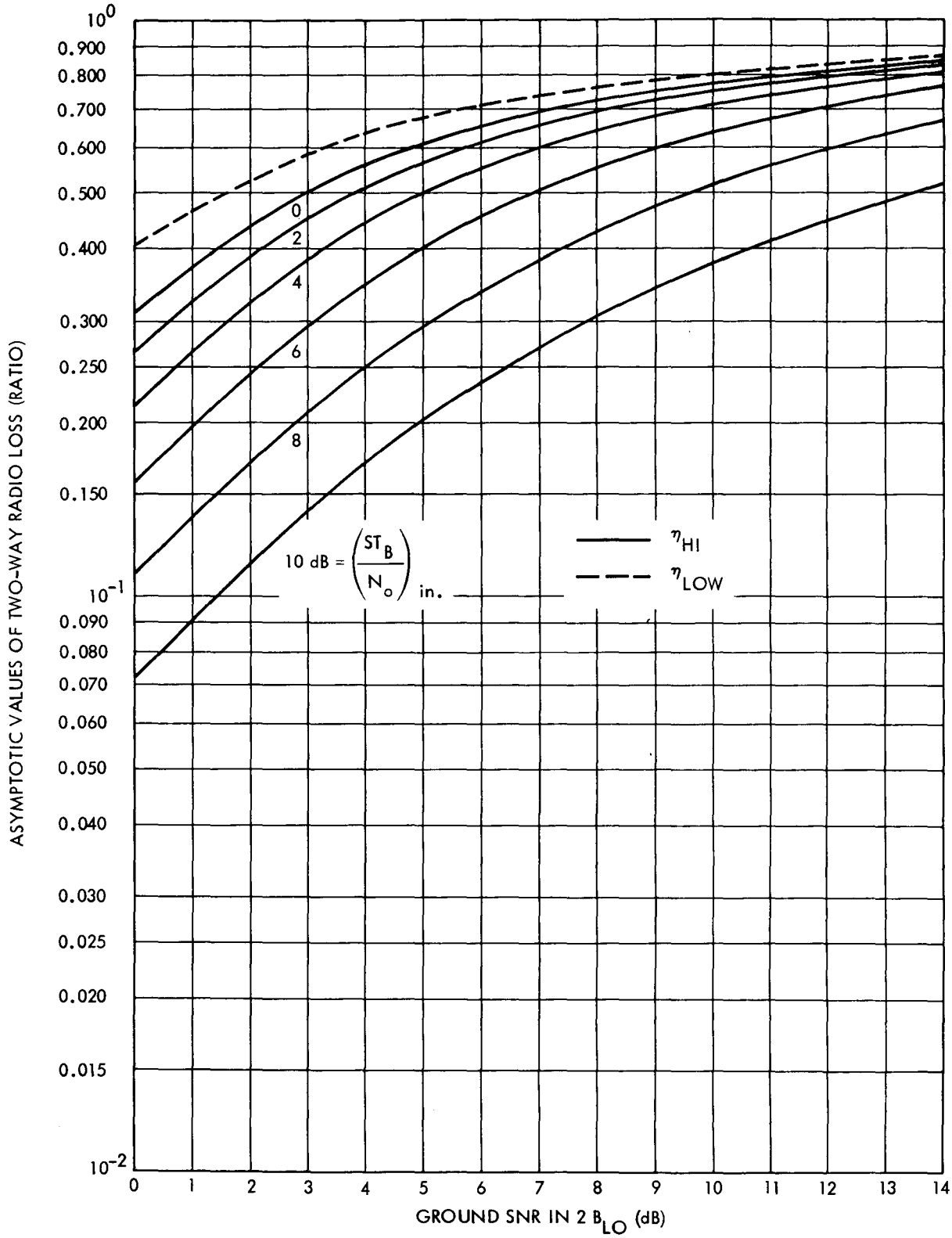

Fig. 5-38. Asymptotic values of two-way radio loss versus ground SNR in $2B_{LO}$ for uncoded telemetry, spacecraft SNR in $2B_{LO}$ = 16 dB, ground $2B_{LO}$ = 3 Hz

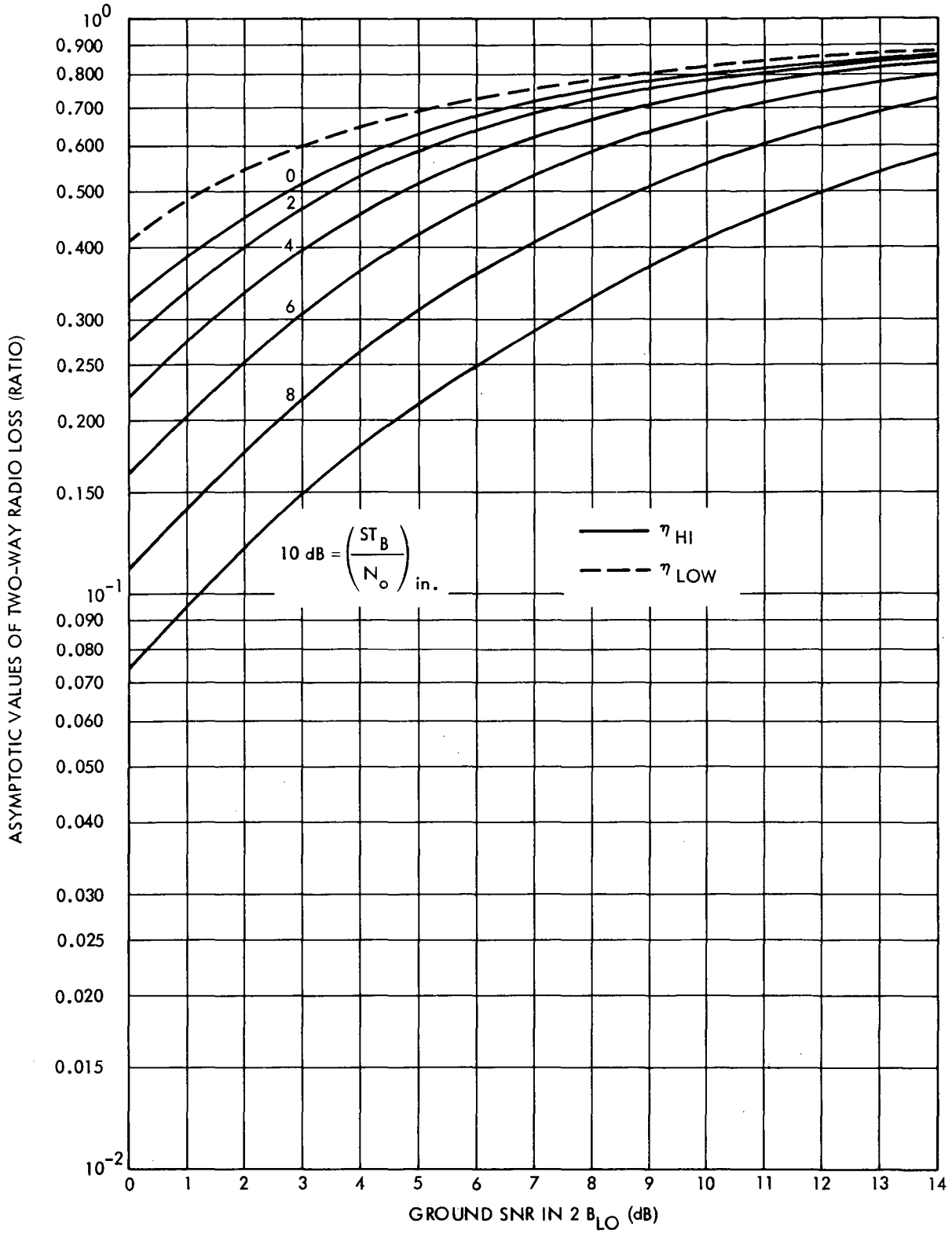

Fig. 5-39. Asymptotic values of two-way radio loss versus ground SNR in $2B_{LO}$ for uncoded telemetry, spacecraft SNR in $2B_{LO}$ = 19 dB, ground $2B_{LO}$ = 3 Hz

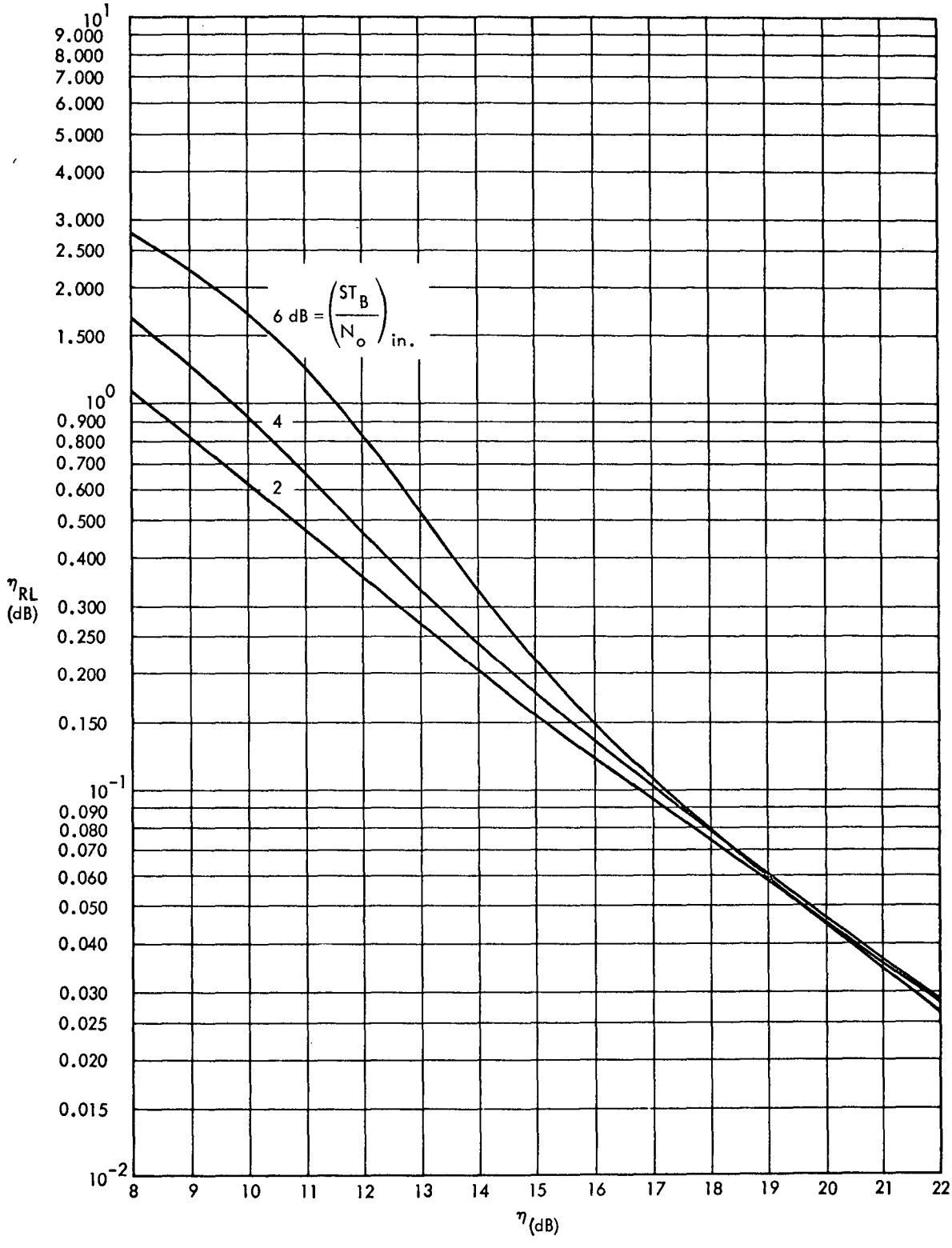

Fig. 5-40. One-way radio loss versus SNR in B_L for (32, 6) block coded telemetry.

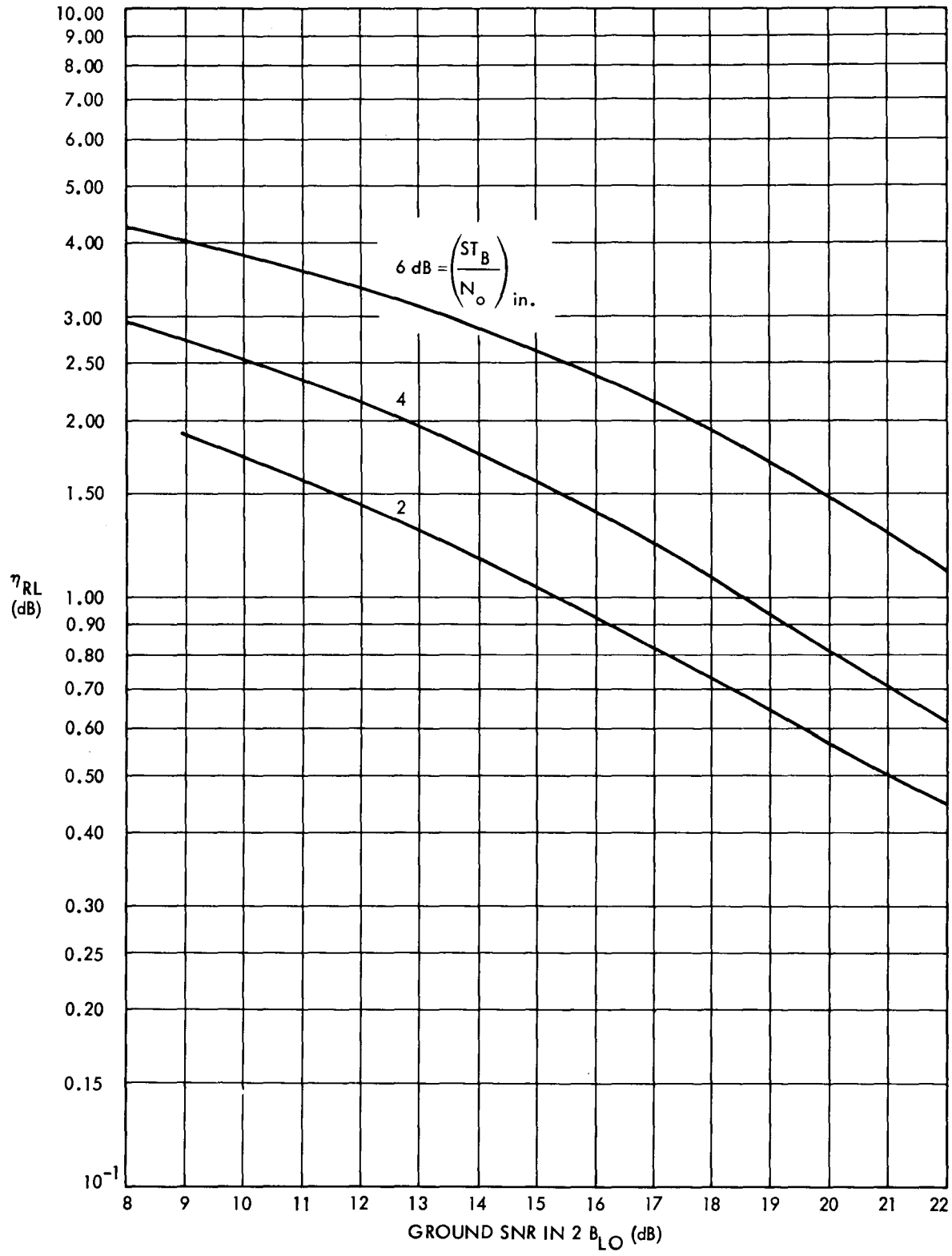

Fig. 5-41. Two-way radio loss versus ground SNR in $2B_{LO}$ for (32, 6) block-coded telemetry, spacecraft SNR in $2B_{LO}$ = 7 dB, ground $2B_{LO}$ = 12 Hz.

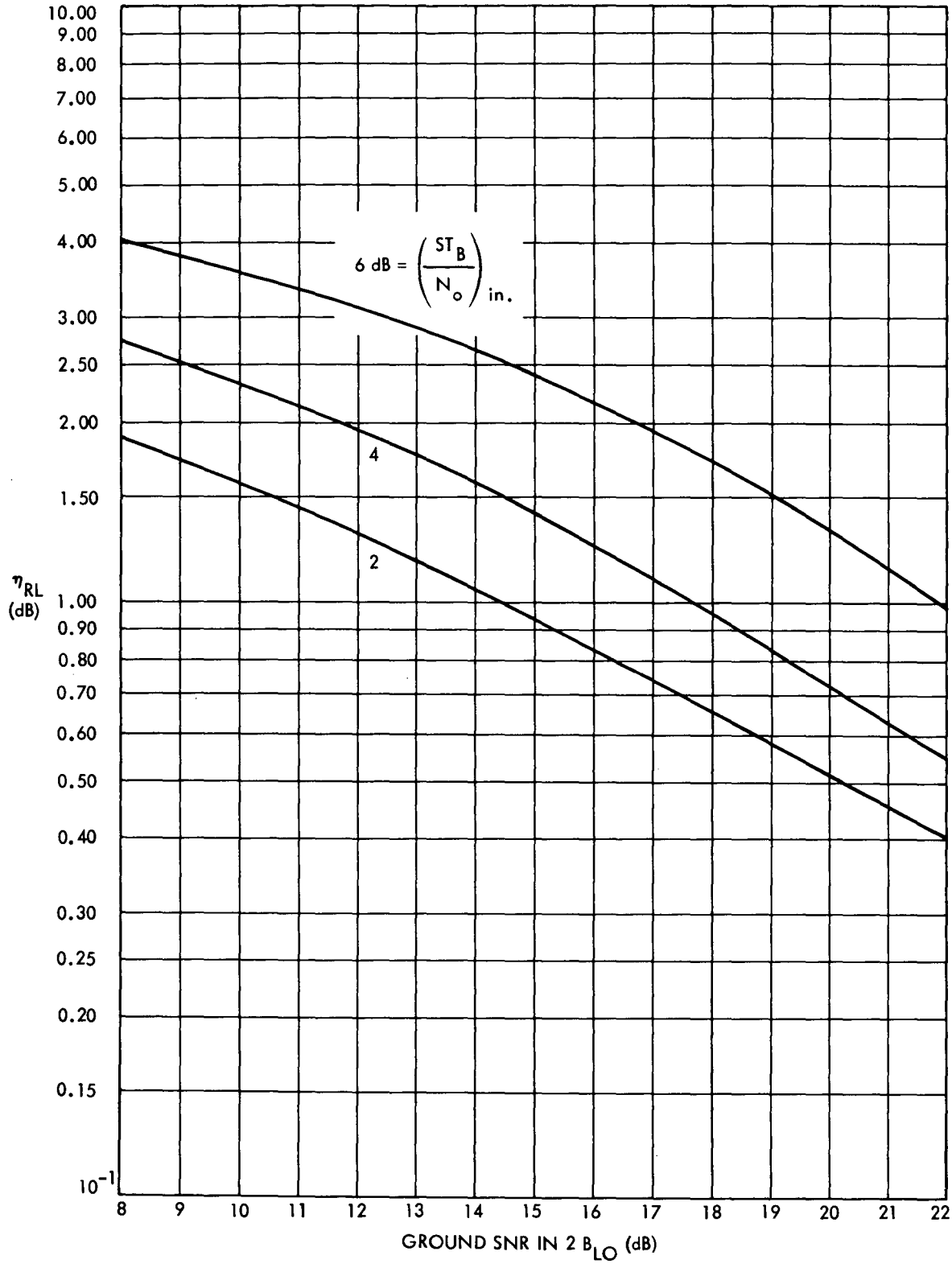

Fig. 5-42. Two-way radio loss versus ground SNR in $2B_{LO}$ for (32,6) block-coded telemetry, spacecraft SNR in $2B_{LO}$ = 10 dB, ground $2B_{LO}$ = 12 Hz.

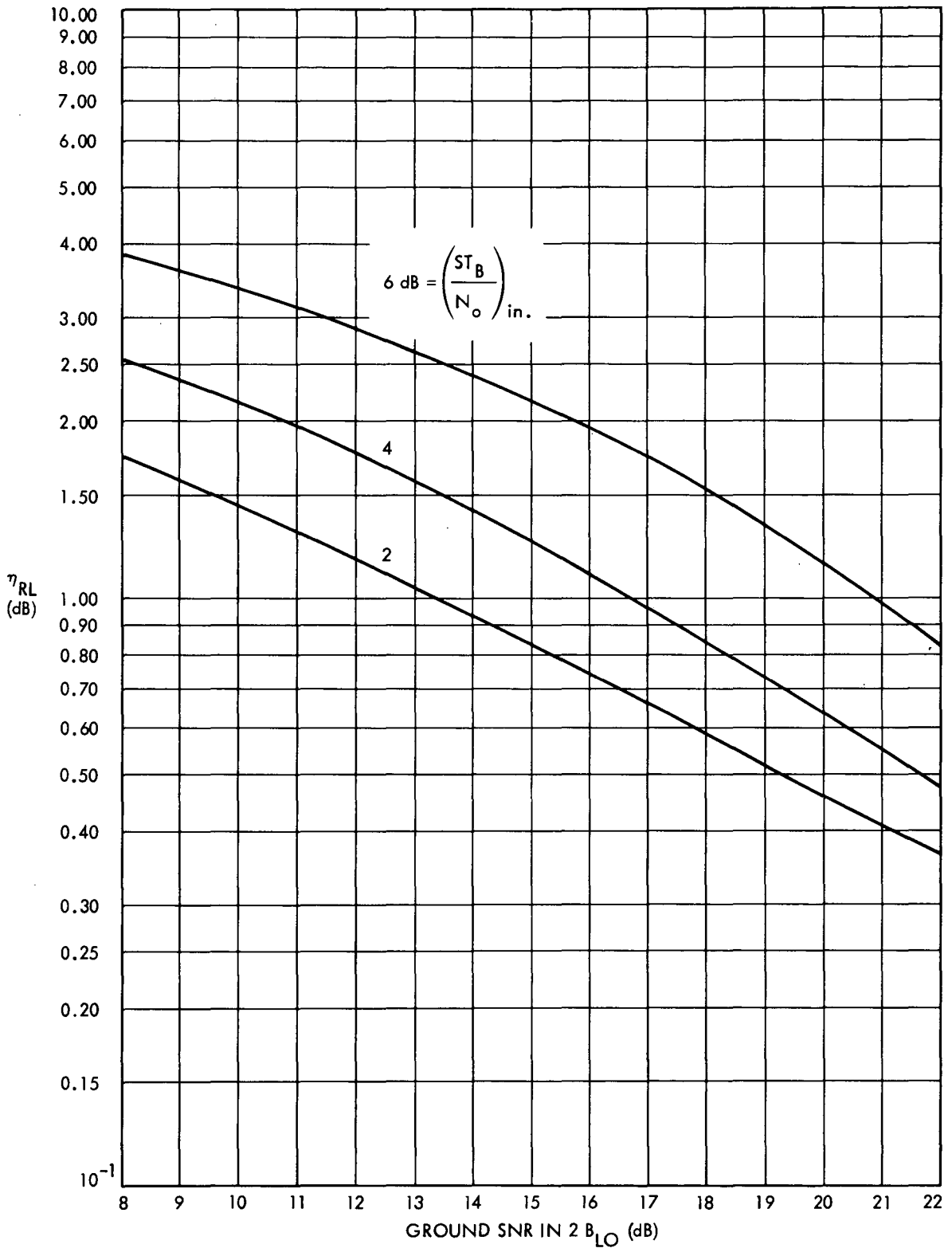

Fig. 5-43. Two-way radio loss versus ground SNR in $2B_{LO}$ for (32, 6) block-coded telemetry, spacecraft SNR in $2B_{LO}$ = 13 dB, ground $2B_{LO}$ = 12 Hz.

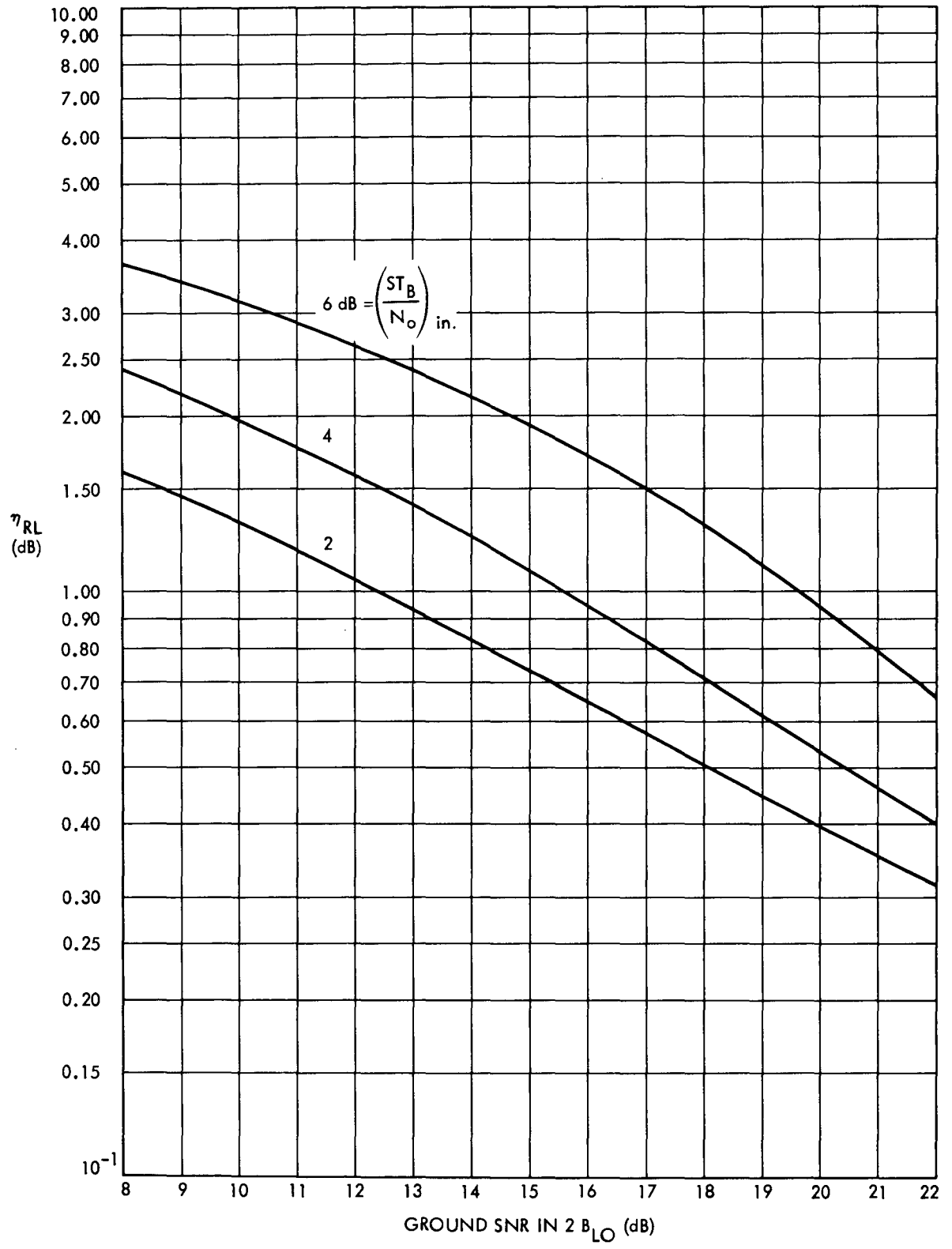

Fig. 5-44. Two-way radio loss versus ground SNR in $2B_{LO}$ for (32, 6) block-coded telemetry, spacecraft SNR in $2B_{LO}$ = 16 dB, ground $2B_{LO}$ = 12 Hz.

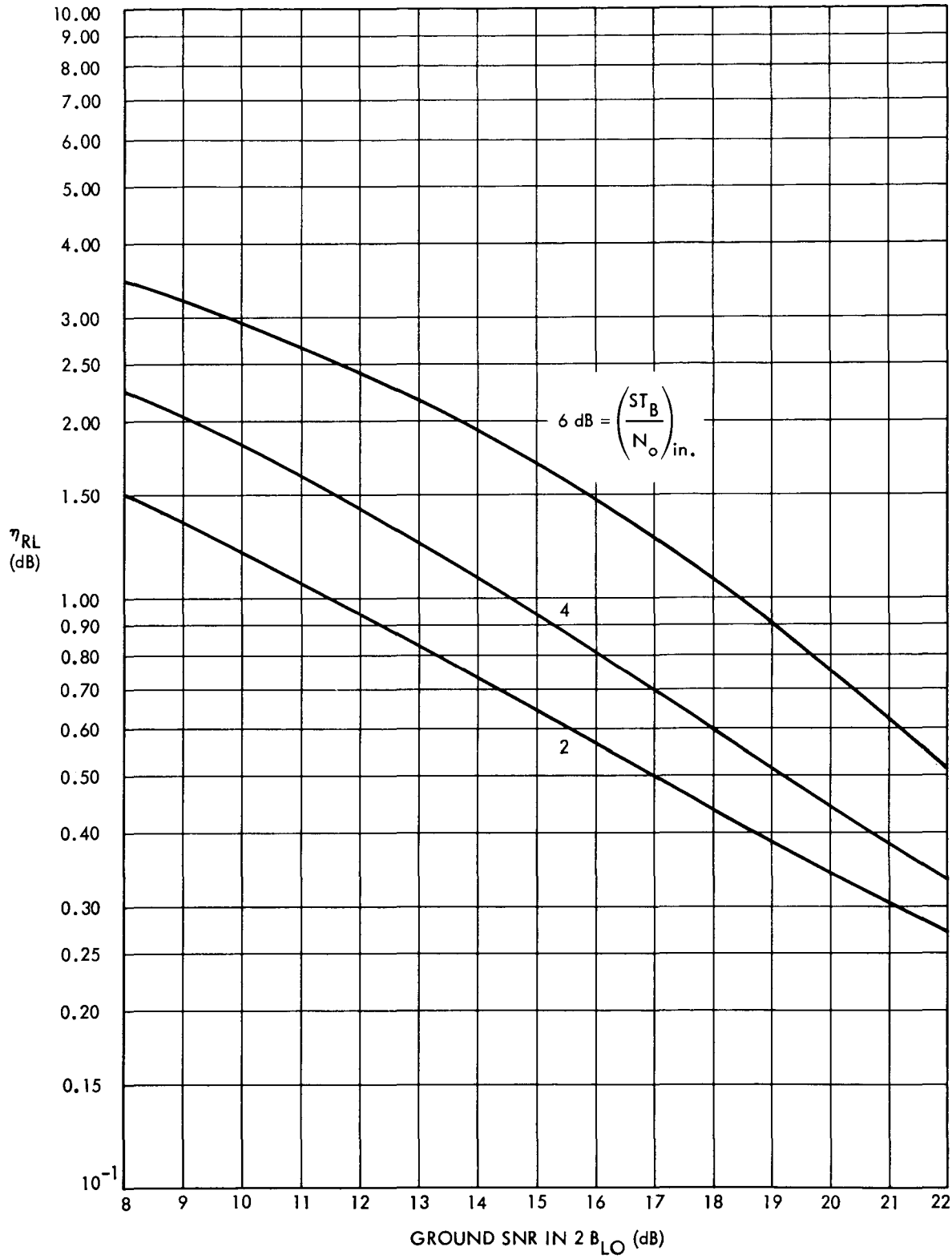

Fig. 5-45. Two-way radio loss versus ground SNR in $2B_{LO}$ for (32, 6) block-coded telemetry, spacecraft SNR in $2B_{LO}$ = 19 dB, ground $2B_{LO}$ = 12 Hz.

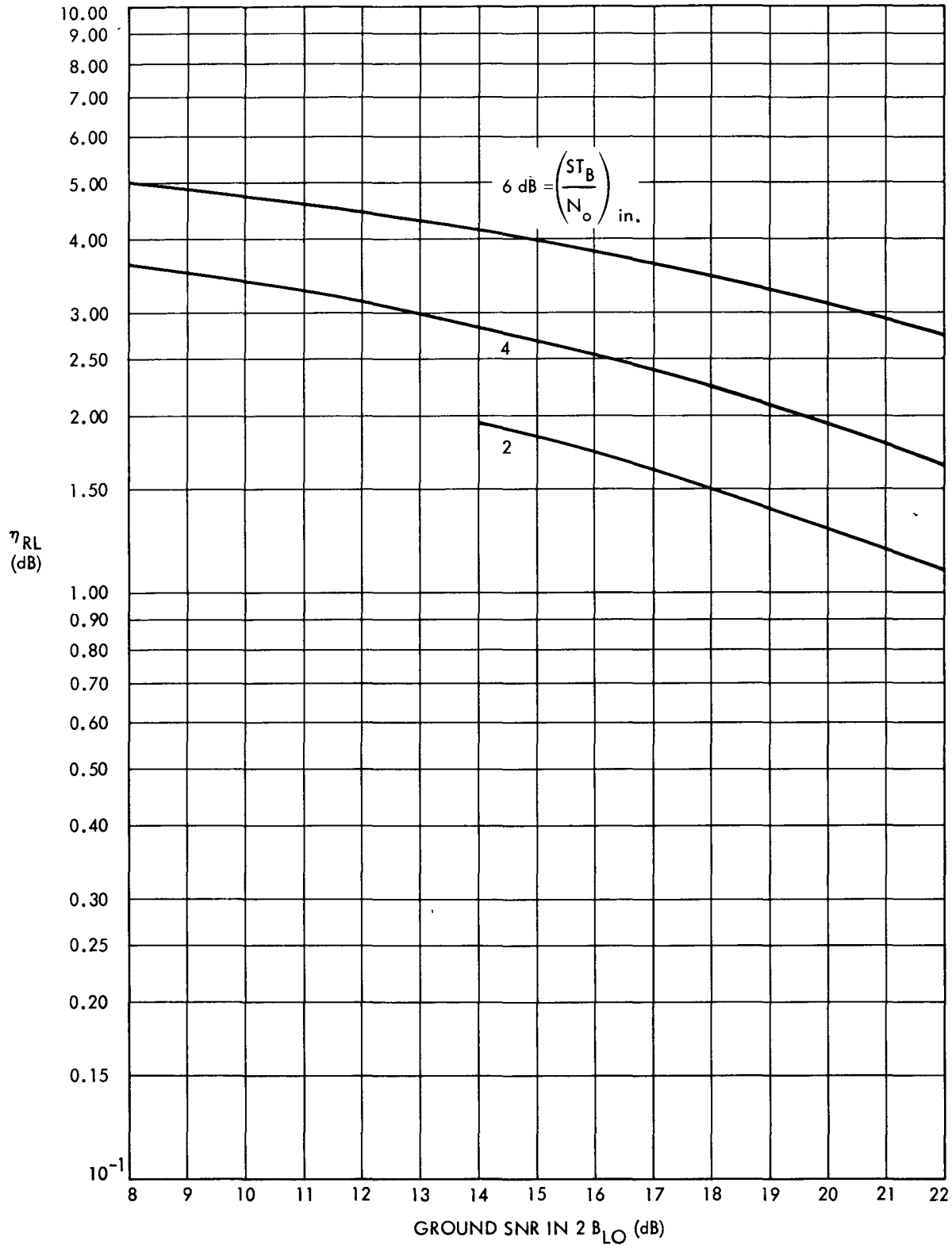

Fig. 5-46. Two-way radio loss versus ground SNR in $2B_{LO}$ for (32,6) block-coded telemetry, spacecraft SNR in $2B_{LO}$ = 7 dB, ground $2B_{LO}$ = 3 Hz.

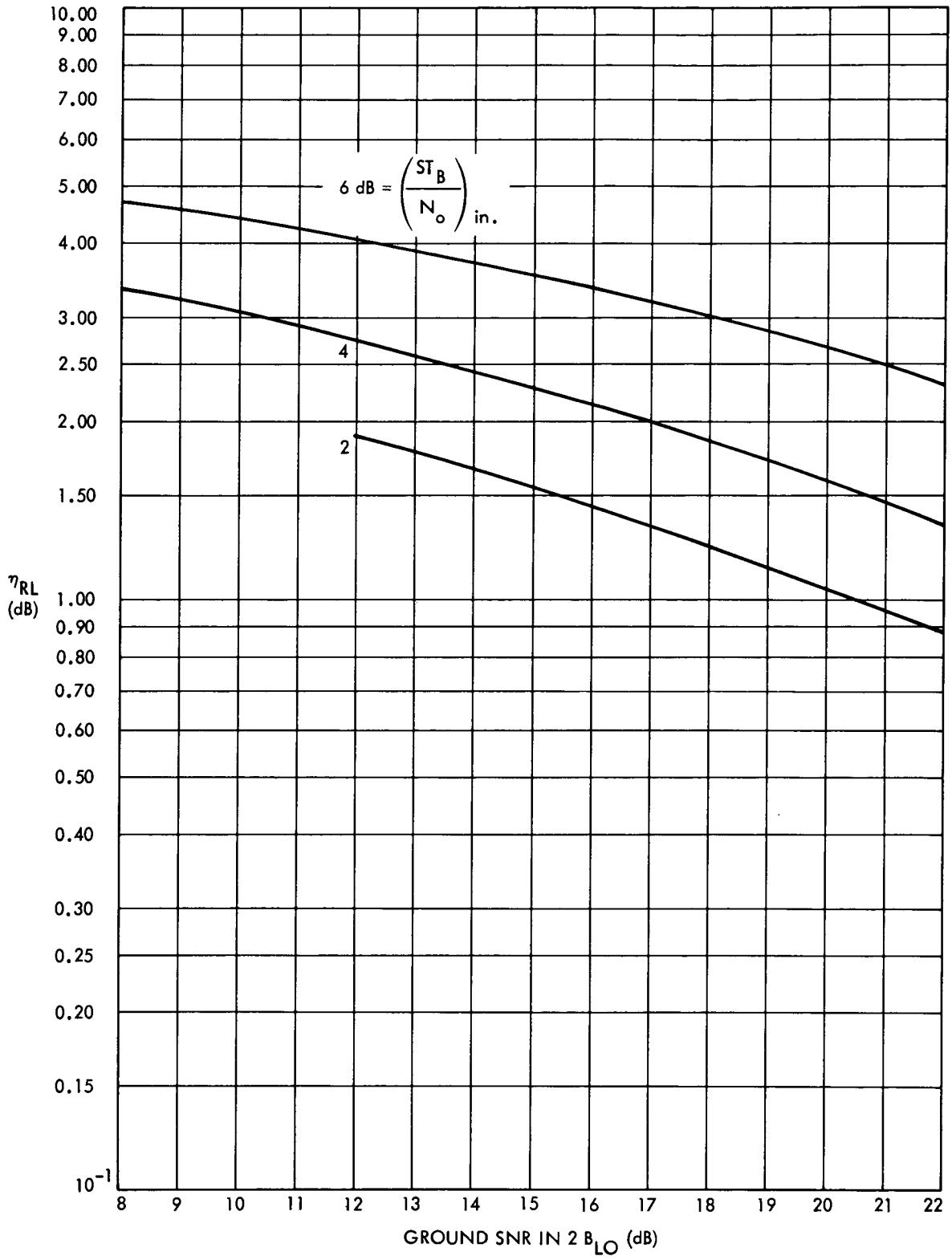

Fig. 5-47. Two-way radio loss versus ground SNR in $2B_{LO}$ for (32,6) block-coded telemetry, spacecraft SNR in $2B_{LO}$ = 10 dB, ground $2B_{LO}$ = 3 Hz.

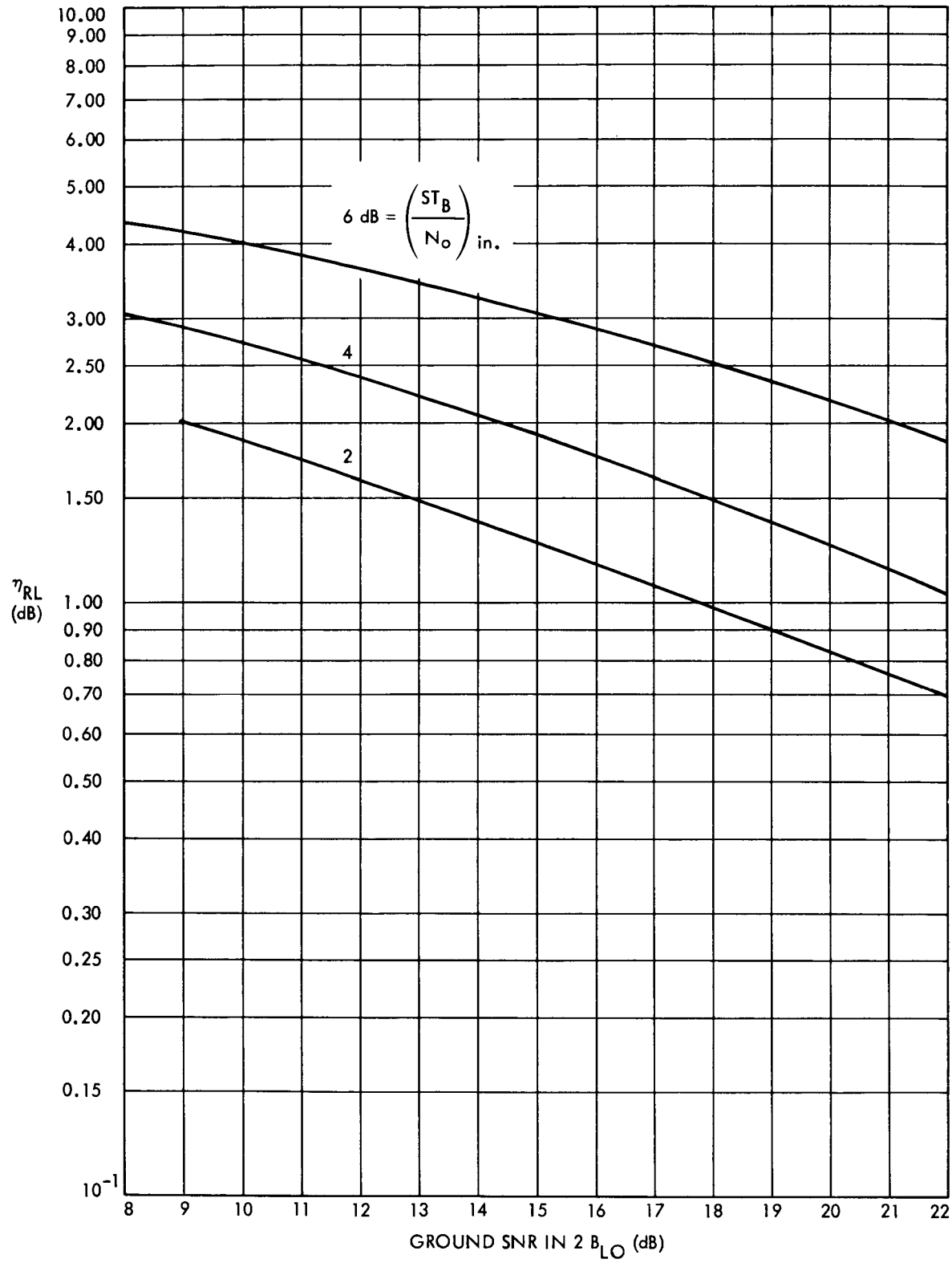

Fig. 5-48. Two-way radio loss versus ground SNR in $2B_{LO}$ for (32,6) block-coded telemetry, spacecraft SNR in $2B_{LO}$ = 13 dB, ground $2B_{LO}$ = 3 Hz.

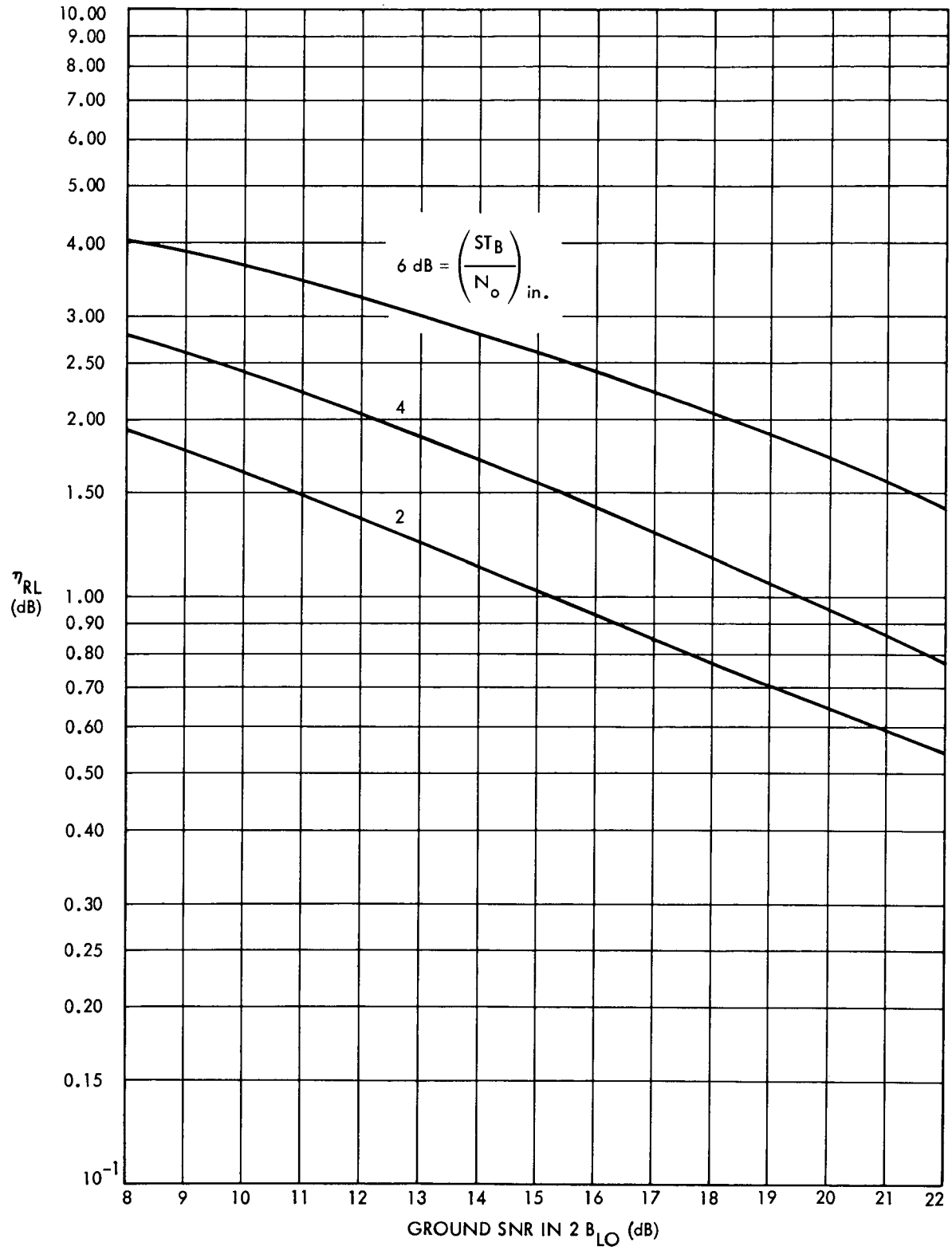

Fig. 5-49. Two-way radio loss versus ground SNR in $2B_{LO}$ for (32, 6) block-coded telemetry, spacecraft SNR in $2B_{LO}$ = 16 dB, ground $2B_{LO}$ = 3 Hz.

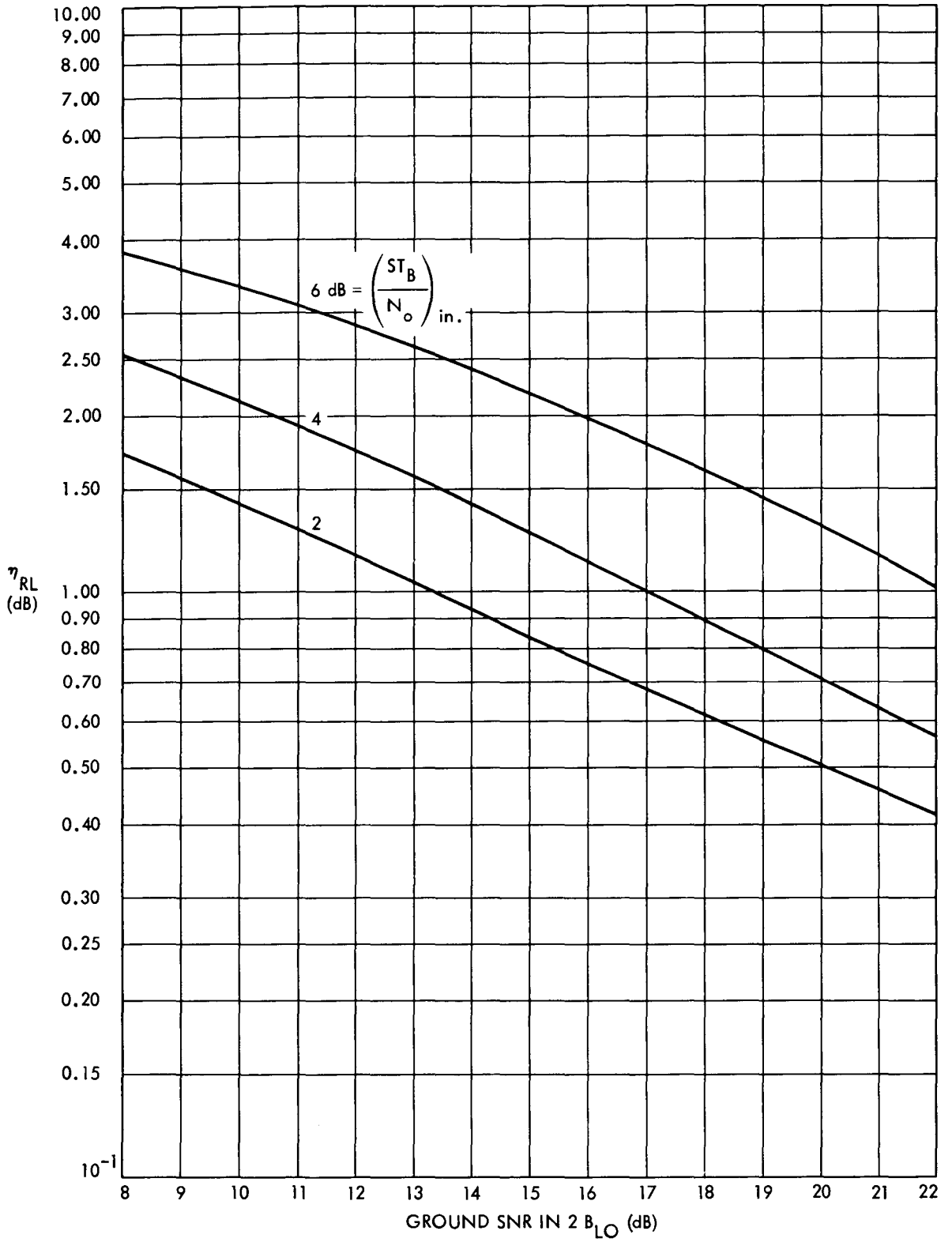

Fig. 5-50. Two-way radio loss versus ground SNR in $2B_{LO}$ for (32, 6) block-coded telemetry, spacecraft SNR in $2B_{LO}$ = 19 dB, ground $2B_{LO}$ = 3 Hz.

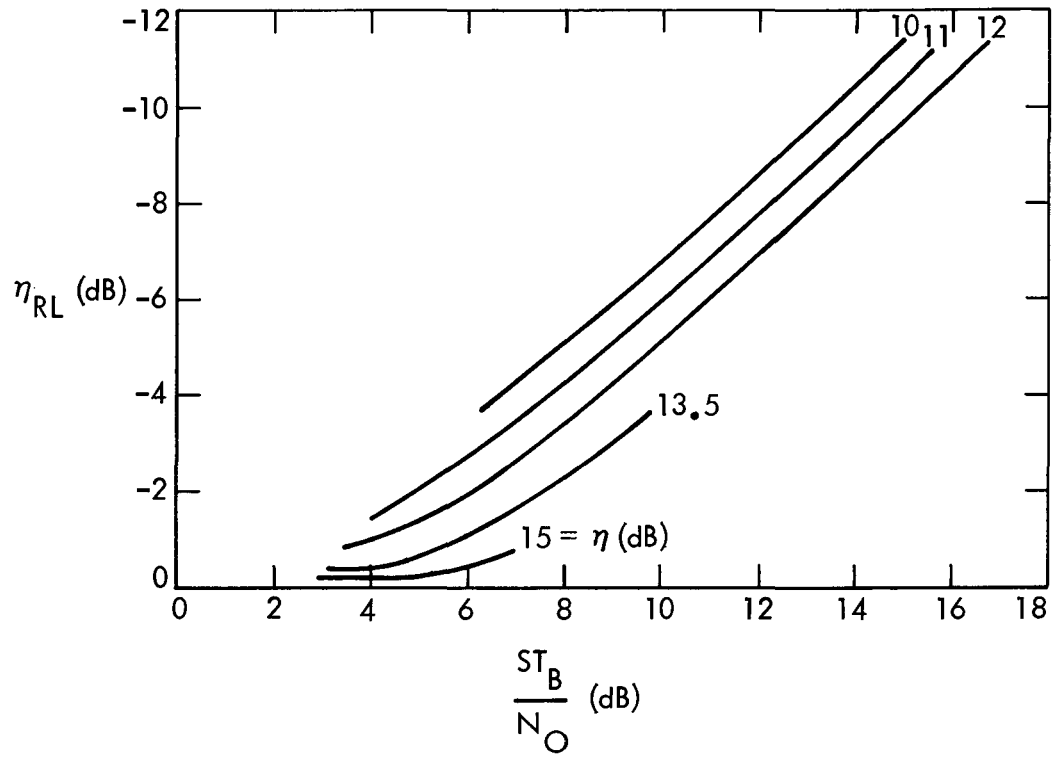

Fig. 5-51. One-way radio loss versus ST_B/N_o with SNR in B_L as a parameter for rate 1/2, k = 7, Q = 8 convolutional coded/Viterbi decoded telemetry (see Figure 5-20)

If T_B is much smaller than the response time of the SDA's PLL ($T_B \ll 2/\omega_{LSC}$),

$$\eta_{HI} = \left[\text{erfc}^{-1}\left(2\overline{P}_{BE}\right)\right]^2 \Big/ \left(\frac{ST_B}{N_o}\right)_{in} \tag{5.4-17}$$

where

$$\overline{P}_{BE} = \frac{1}{2}\int_{-\infty}^{\infty} \exp\frac{\left[-(\phi - \overline{\phi})^2/2\sigma_\phi{}^2\right]}{\sqrt{2\pi\sigma_\phi{}^2}} \text{erfc}\left[\sqrt{\left(\frac{ST_B}{N_o}\right)_{in}}\left(1 - \frac{2}{\pi}|\phi|\right)\right] d\phi \tag{5.4-18}$$

and

$$\bar{\phi} = \frac{\Delta f_{\text{subcarrier}}}{G_{SCL}} \tag{5.4-19}$$

represents a subcarrier frequency offset.

G_{SCL} is the open-loop gain of the SDA and is equal to (reference 5-40):

$$G_{SCL} = G_{SCL_o} \left(\frac{\alpha_{SL}}{\alpha_{SL_o}}\right)\left(\frac{\alpha'}{\alpha'_o}\right) \tag{5.4-20}$$

where

$$\alpha' = 0.769 \left(\frac{0.877 + 0.2\left(\frac{ST_B}{N_o}\right)_{in}^{1.2}}{1.0 + 0.2\left(\frac{ST_B}{N_o}\right)_{in}^{1.2}} \right) \text{erf}\left(\sqrt{\frac{2}{3}\left(\frac{ST_B}{N_o}\right)_{in}}\right) \tag{5.4-21}$$

$$\alpha_{SL} = \text{erf}\left(\sqrt{\frac{2\eta_{SC\ell}}{\pi}}\right) \tag{5.4-22}$$

$\eta_{SC\ell}$ = SNR in the bandwidth of filter F_{A_2} as shown in Figure 5-52, and the subscript "o" indicates the design point value.

Figure 5-53 plots Δf subcarrier versus $(\alpha')^2$ S/N_o with $\bar{\phi}$ as a parameter for the three loop bandwidth settings of the SDA.

Also,

$$\sigma_\phi^2 = \frac{\Gamma_{SL}\left(\frac{\pi}{2\alpha'}\right)^2}{\eta_{SC}} \tag{5.4-23}$$

where

$\eta_{SC} = \frac{2P}{N_o \omega_{LSC}}$ = SNR in the subcarrier loop bandwidth ω_{LSC}, and

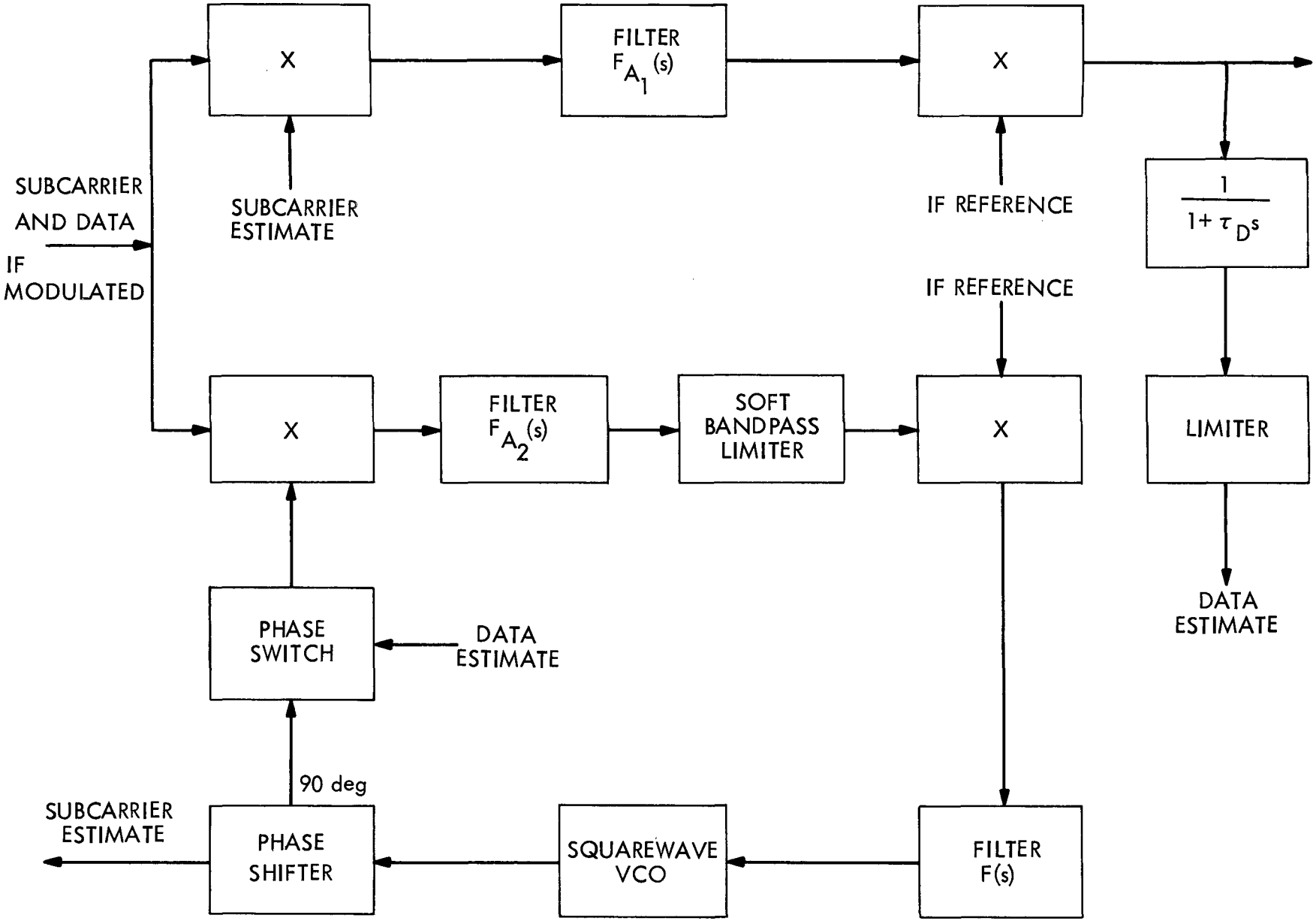

Fig. 5-52. Telemetry subcarrier demodulator functional block diagram

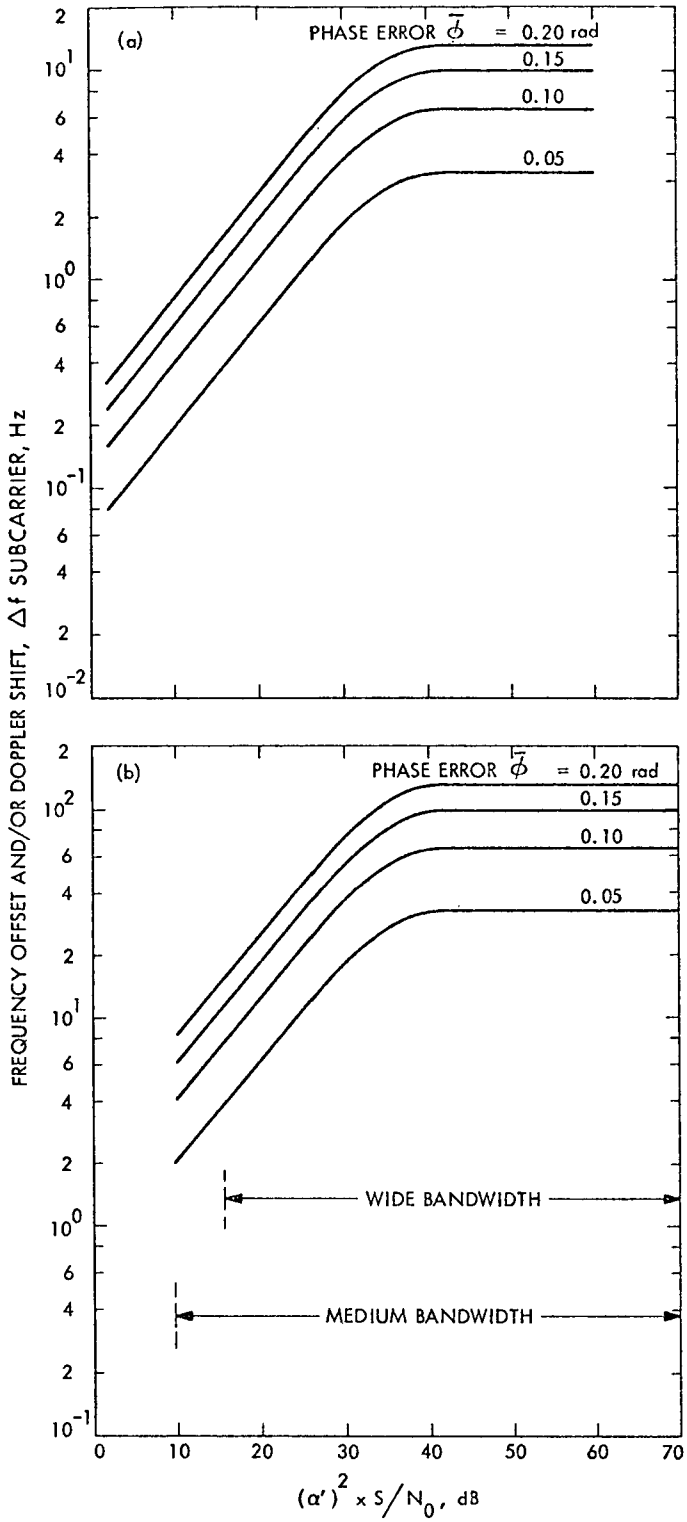

Fig. 5-53. Subcarrier frequency offset vs signal-to-noise spectral density ratio parameter, subcarrier loop noise bandwidth: (a) narrow, (b) medium or wide.

$$\Gamma_{SL} \approx \frac{1 + 0.345\,\eta_{SC\ell} + 50\,\eta_{SC\ell}^{5}}{0.862 + 0.690\,\eta_{SC\ell} + 50\,\eta_{SC\ell}^{5}} \tag{5.4-24}$$

is a soft limiter suppression factor and is presented in Figure 5-54.

For the low data rate case ($T_B >> 2/\omega_{LSC}$),

$$\eta_{LOW} = \left[1 - \frac{2}{\pi}\bar{\phi}\,\mathrm{erf}\left(\frac{\bar{\phi}}{\sqrt{2\sigma_\phi^2}}\right) - \left(\frac{8\sigma_\phi^2}{\pi^3}\right)^{1/2} \exp\left(-\frac{\phi^2}{2\sigma_\phi^2}\right)\right]^2 \tag{5.4-25}$$

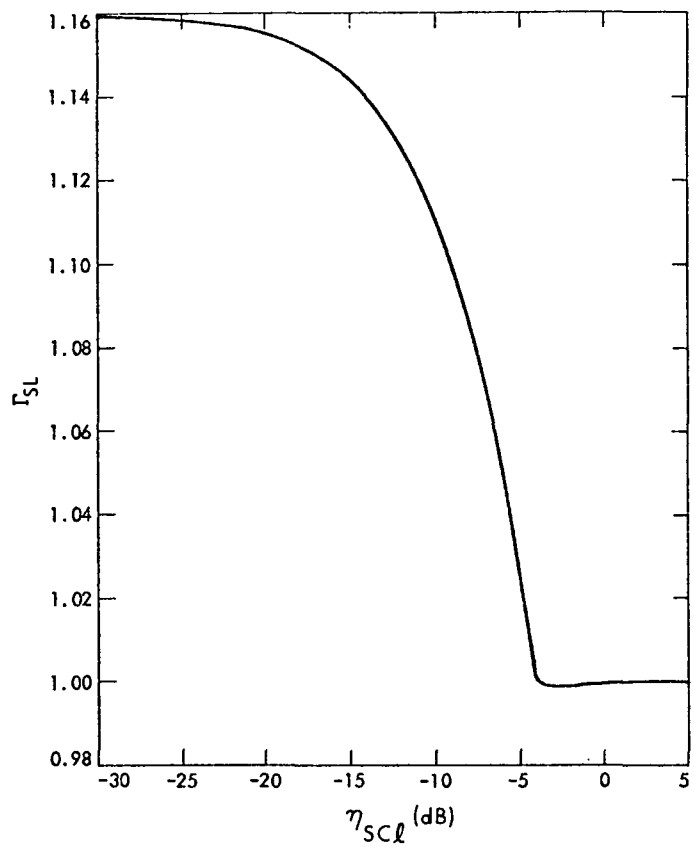

Fig. 5-54. Ratio of input signal-to-noise spectral density to output signal-to-noise spectral density vs soft bandpass limiter input signal-to-noise ratio.

The interpolation scheme for SDA efficiencies for the uncoded case is

$$\eta_{SDL} = (1 - a_{SC})\eta_{LOW} + a_{SC}\eta_{HI} \tag{5.4-26}$$

where

$$a_{SC} = \frac{0.09135\delta_{SC} + \delta^2_{SC}}{1 + 3.3718\delta_{SC} + \delta^2_{SC}} \tag{5.4-27}$$

and

$$\delta_{SC} = \frac{2}{\omega_{LSC} T_B} \tag{5.4-28}$$

Figure 5-55 plots the relationship of equation (5.4-27).

The block coded case treatment is similar to the treatment for radio loss. Representative curves are given in Figures 5-56 and 5-57.

5.4.5.3 Bit Sync and Detection Loss. Bit sync and detection loss, or synchronization loss, is the loss attributed to the bit or symbol synchronizer when the radio and the SDA are operating perfectly. The loss is due to a symbol timing error, τ, which causes the detector to be sampled at $T' = T(1 + 2|\tau|)$. The efficiency for uncoded data is

$$\eta_{BSDL} = \frac{\left[\text{erfc}^{-1}(2\overline{P}_{BE})\right]^2}{\left(\frac{ST_B}{N_o}\right)_{in}} \tag{5.4-29}$$

where

$$\overline{P}_{BE} = \int_{-1/2}^{1/2} \frac{1}{2}\,\text{erfc}\left[\sqrt{\left(\frac{ST_B}{N_o}\right)_{in}}\,(1 - 2|\tau|)\right] p(\tau)d\tau \tag{5.4-30}$$

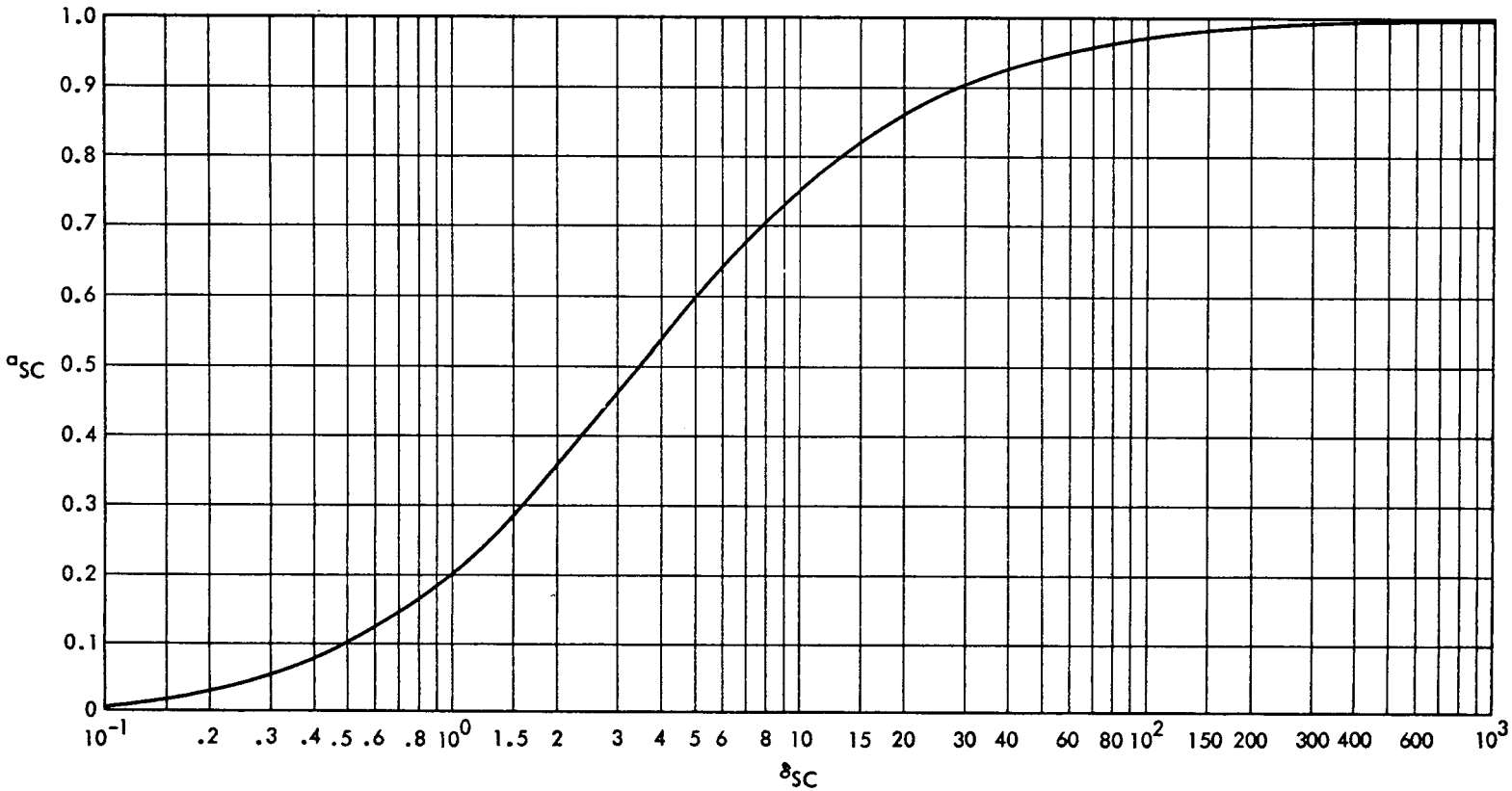

Fig. 5-55. Subcarrier demodulator loss interpolation parameter versus $\delta_{SC} = 1/B_{LSC}\ T_B$.

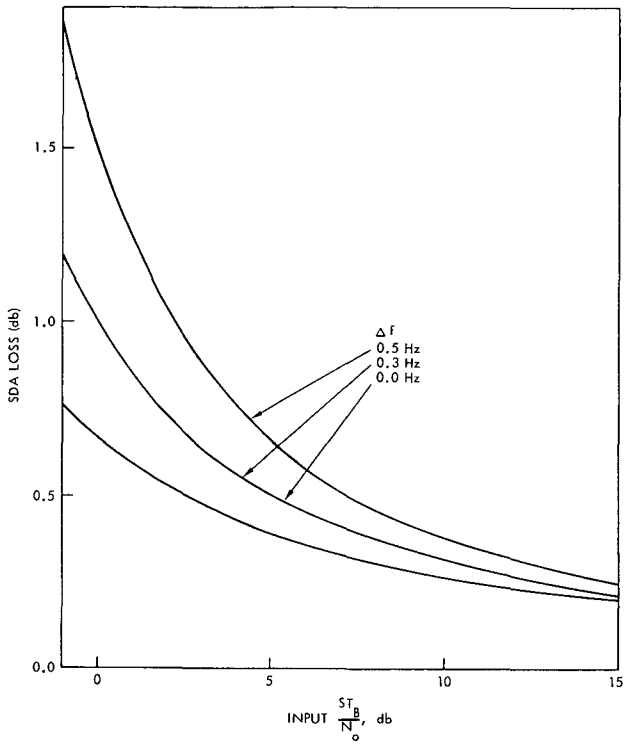

Fig. 5-56. SDA loss vs input ST_B/N_o for uncoded telemetry with subcarrier offset, bit rate = 8 1/3 bps, SDA loop BW-narrow

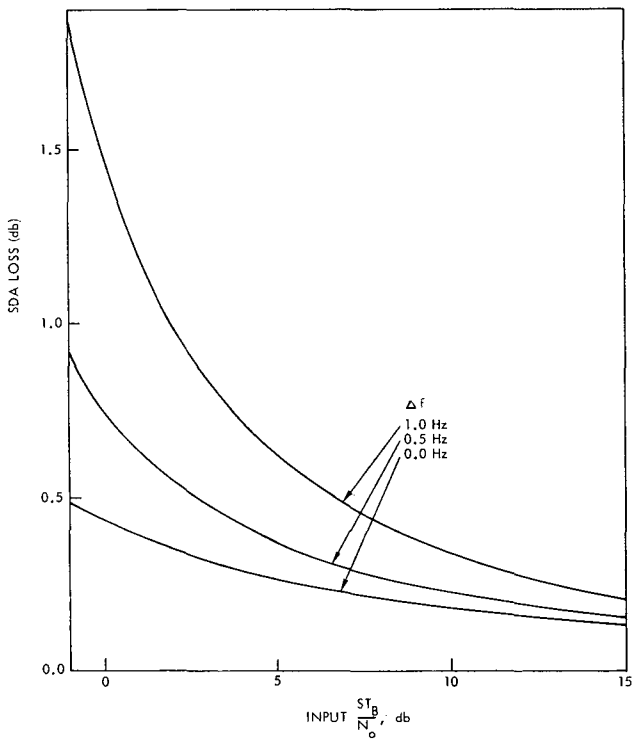

Fig. 5-57. SDA loss vs input ST_B/N_o for uncoded telemetry with subcarrier offset, bit rate = 33 1/3 bps, SDA loop BW-narrow

and

$$p(\tau) = \frac{1}{2}\,\delta(\tau) + \frac{1}{2}\,p'(\tau), \qquad -\frac{1}{2} \le \tau \le \frac{1}{2} \tag{5.4-31}$$

where $\delta(\cdot)$ is the Dirac delta function and $p'(\tau)$ is approximately zero mean Gaussian for the SNR >>1 in the bit loop bandwidth, B_{BSL}, and $2B_{BSL}T_B$ <<1. Reference 5-41 gives standard deviations for some types of analog bit sync loops. Note that we have assumed 50 percent transition density in the data stream. η_{BSDL} for coded data depends on the detection process.

5.4.6 Subcarrier Waveform Distortion Loss

The SDA is designed to optimize performance for a perfect sine or square wave subcarrier input. If the actual input differs from the ideal form, a degradation in performance will be observed. This degradation is called waveform distortion loss, η_{WDL}; it is the effective loss in ST_B/N_o caused by an imperfect subcarrier waveform which is coherently received. As is the case with η_{RL}, η_{SDA} and η_{BSDL}, the consideration of η_{WDL} as a separate loss depends on high total system efficiency. In addition, it assumes that the data pulses are perfectly square. η_{WDL} is defined by the following equations:

Single-channel telemetry:

$$\eta_{WDL} = -20 \log \left\{ \frac{1}{T_S} \int_{t'}^{t'+T_S} \frac{\sin\left[\theta \hat{s}(t)\right]}{\sin\theta}\, dt \right\} \quad \text{in dB} \tag{5.4-32}$$

where T_S = Subcarrier period

t' = Arbitrary time offset

$s(t)$ = Received subcarrier waveform

and

$\hat{s}(t)$ = Reference waveform in the SDA, assumed perfect, with period T_S

This equation assumes that T_B/T_S >> 1 or an integer, where T_B is bit time.

Dual channel telemetry:

$$\eta_{WDL_1} = -20 \log_{10} \left\{ \frac{1}{T} \int_{t'_1}^{t'_1 + T} \hat{s}_1(t) \; \frac{\sin\left[\theta_1 \, s_1(t)\right] \cos\left[\theta_2 \, s_2(t)\right]}{\sin \theta_1 \cos \theta_2} dt \right\} \quad \text{in dB} \tag{5.4-33}$$

where the subscripts denote the channel and T is the least common multiple (LCM) of T_{S_1} and T_{S_2}. η_{WDL_2} is found by simply exchanging subscripts. Here, the assumption is made that $T_{B_1}/T >> 1$ or an integer.

Interplex type I telemetry:

$$\eta_{WDL_H} = -20 \log \left\{ \frac{1}{T} \int_{t'_H}^{t'_H + T} \hat{s}_H(t) \; \frac{\sin\left[\theta_H \, s_H(t)\right] \cos\left[\theta_L \, s_H(t) \, s_L(t)\right]}{\sin \theta_H \cos \theta_L} dt \right\} \quad \text{in dB} \tag{5.4-34}$$

and

$$\eta_{WDL_L} = -20 \log \left\{ \frac{1}{T} \int_{t'_L}^{t'_L + T} \hat{s}_L(t) \; \frac{\sin\left[\theta_H \, s_H(t)\right] \sin\left[\theta_L \, s_H(t) \, s_L(t)\right]}{\sin \theta_H \sin \theta_L} dt \right\} \quad \text{in dB} \tag{5.4-35}$$

where L = Low rate channel

H = High rate channel

$T = \text{LCM}\,(T_{S_L}, T_{S_H})$

and $T_{B_H}/T >> 1$ or an integer for equation (5.4-34)

$T_{B_L}/T >> 1$ or an integer for equation (5.4-35).

Interplex type II telemetry:

For type II interplex, equation (5.4-33) applies.

Because the SDA is designed to be synchronous with a perfect input, an imperfect wave will cause some shift of phase between the reference and the input even when perfectly locked. For η_{WDL} on the order of tenths of a dB, however, the assumption of synchronous transition starts (that is the time of switching from -1 to > -1 is identical) between $\hat{s}(t)$ and s(t) at multiples of T_S causes no significant change of results.

In general, these equations must be numerically integrated. When spacecraft hardware is available, they can be evaluated by use of numerical data on s(t) obtained by actual measurement.

During the design phase, it is useful to have an analytical model for s(t) which can be used to find the losses resulting from various specifications on the hardware. The next section describes such a model for square-wave subcarriers.

5.4.6.1 Square-wave Subcarrier Waveform Model

Typically, a square wave is specified in terms of four parameters: asymmetry, droop, overshoot, and rise time.

If the wave begins to flip from -1 to +1 at time t, from +1 to -1 at time $t + \frac{T_S}{2} + \Delta T_S$, and again from -1 to +1 at $t + T_S$ (see Figure 5-58), the asymmetry is defined as:

$$\text{Asymmetry} = 100 \frac{\Delta T_S}{T_S} \% \qquad (5.4\text{-}36)$$

Droop is defined as the percentage deviation of the end of each subcarrier pulse relative to its midpulse height (which is normalized to have unit amplitude because, in practice, the modulation subcarrier amplitude is adjusted to have its specified value at approximately the middle of each subcarrier pulse):

$$\text{Droop} = 100\ d\ \% \qquad (5.4\text{-}37)$$

where the deviation is denoted by d.

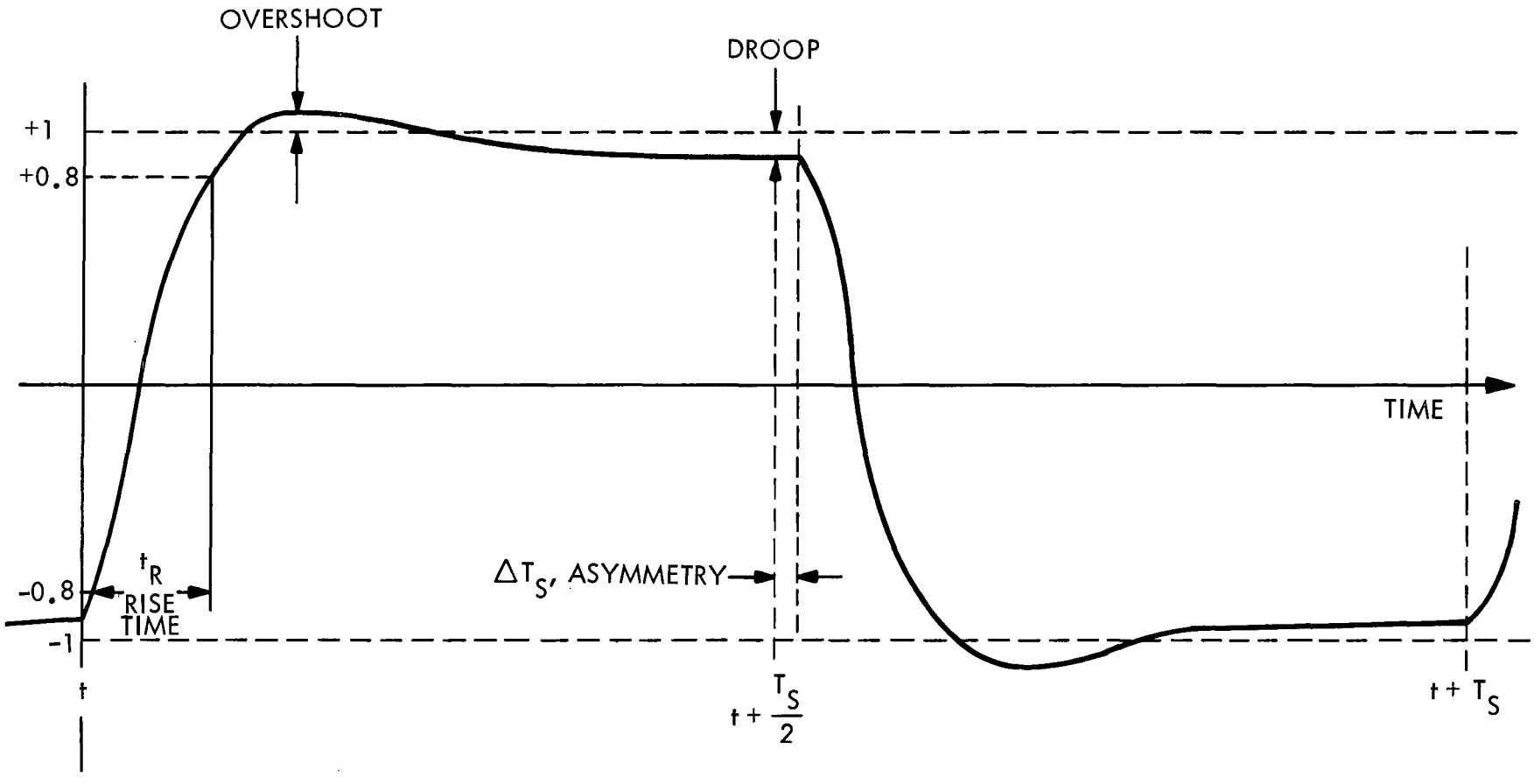

Fig. 5-58. Subcarrier waveform specification parameters

By convention, the rise time, t_R is defined as the interval during which a rising edge of the subcarrier goes from -0.8 to +0.8 (10% to 90% of the full transition). The fall time, t_F is similarly defined for the falling edge, and η_{WDL} is minimized when $t_R = t_F$, which we shall assume here.

Overshoot is defined as the maximum height of the rising wave minus its midpoint value and divided by the total signal changes. With the normalization described,

$$\text{Overshoot} = \frac{s_{max} - 1}{2} \; 100\% \tag{5.4-38}$$

If we assume that s(t) has a rising edge starting at t = 0, and that the positive subcarrier pulses are asymmetrically longer than the negative pulses: then over the range $0 \leq t \leq T_S$, we can describe s(t) by:

$$s(t) = \begin{cases} 1 - 2\exp(-\zeta\omega_n t)\left[\cos\left(\sqrt{1-\zeta^2}\,\omega_n t\right) + \dfrac{\zeta}{\sqrt{1-\zeta^2}}\sin\left(\sqrt{1-\zeta^2}\,\omega_n t\right)\right] \\ \quad + d\left[1 - \dfrac{4t}{(T_S + 2\Delta T_S)}\right]; \; 0 \leq t \leq \dfrac{T_S}{2} + \Delta T_S, \\ -1 + 2\exp\left[-\zeta\omega_n\left(t - \dfrac{T_S}{2} - \Delta T_S\right)\right]\left[\cos\left(\sqrt{1-\zeta^2}\,\omega_n\left(t - \dfrac{T_S}{2} - \Delta T_S\right)\right)\right. \\ \quad \left. + \dfrac{\zeta}{\sqrt{1-\zeta^2}}\sin\left(\sqrt{1-\zeta^2}\,\omega_n\left(t - \dfrac{T_S}{2} - \Delta T_S\right)\right)\right] \\ \quad - d\left[1 - \dfrac{4\left(t - \frac{T_S}{2} - \Delta T_S\right)}{(T_S - 2\Delta T_S)}\right]; \; \dfrac{T_S}{2} + \Delta T_S \leq t \leq T_S \end{cases} \tag{5.4-39}$$

where T_S, ΔT_S, and d have been defined, and ζ and ω_n are related to the damping factor and natural frequency of the second order system from which this equation was derived (ref. 5-42).

ω_n and ζ must be varied iteratively to give the proper rise time and overshoot desired for the specifications to be investigated. As a starting point for the iteration, overshoot depends primarily on ζ for the case d = 0,

$$\text{Overshoot} = 100 \exp\left(\frac{-\zeta\pi}{\sqrt{1-\zeta^2}}\right)\%$$

or

$$\zeta = \frac{-\frac{1}{\pi}\ln\left(\frac{\text{overshoot}}{100}\right)}{\left[1+\frac{1}{\pi^2}\ln^2\left(\frac{\text{overshoot}}{100}\right)\right]^{1/2}} \qquad d = 0$$

Figure 5-59 plots overshoot as a function of ζ for d = 0. Rise time t_R must be found by iteration after setting a trial value of ζ. As a beginning,

$$t_R \sim \frac{2\zeta}{\omega_n}$$

Typically, component development is such that the primary factor in waveform distortion loss is asymmetry. Considering the complexity of the equations given above, it is often desirable to sacrifice accuracy for calculation facility. If only asymmetry is considered,

$$\sin\left[\theta\, s_1(t)\, s_2(t)\right] = s_1(t)\, s_2(t) \sin\theta, \text{ and } \cos\left[\theta\, s_1(t)\, s_2(t)\right] = \cos\theta,$$

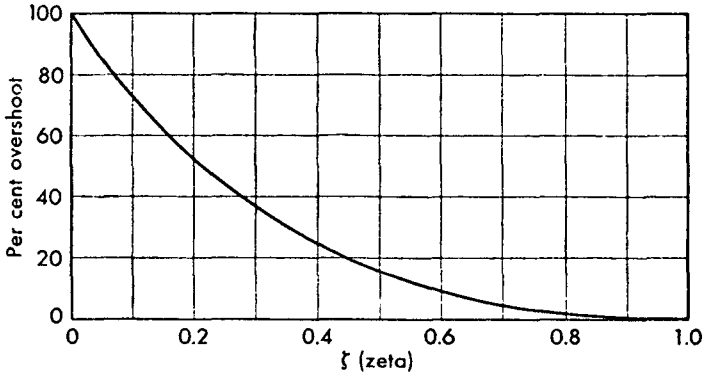

Fig. 5-59. Overshoot as a function of ζ for d = 0

(Ref. 5-42, from Control Systems Design by C. J. Savant, Jr. Copyright 1964 by McGraw-Hill Book Company. Used with permission of McGraw-Hill Book Company.)

thus,

$$\eta_{WDL} = -20 \log \left(1 - \frac{2\,\Delta T_S}{T_S}\right) \text{dB}$$

for all telemetry modes.

5.5 DATA RATE CAPACITY OF THE TELEMETRY CHANNEL

Shannon (ref. 5-6) defined channel capacity as the data rate below which one could code and achieve a probability of zero bit errors for a given SNR. In designing telemetry systems for deep space vehicles, it is more practical to define the available data rate channel capacity as the maximum data rate one may transmit to achieve a prescribed probability of error for a given P_T/N_o and a given telemetry system configuration. This section is concerned with calculating the available channel capacity for some commonly used telemetry systems.

5.5.1 The Data Rate Equation

It was shown in section 5.4, that the signal energy per bit could be related to the total received power by

$$\frac{ST_B}{N_o} = \left(\frac{P_T}{N_o}\right)\left(\frac{P_D}{P_T}\right) T_B \eta_S \qquad (5.5\text{-}1)$$

The data rate, $D_R = 1/T_B$.

Thus, the data rate equation for a single channel system is

$$D_R = \frac{(P_T/N_o)(P_D/P_T)\eta_S}{(ST_B/N_o)} \qquad (5.5\text{-}2)$$

The maximum allowable probability of error determines a design point value of ST_B/N_o, and this value depends on the coding used. Thus, a threshold SNR, $(ST_B/N_o)_{TH}$, will be established. The maximum data rate will be

$$D_{R\,max} = \frac{(P_T/N_o)(P_D/P_T)\eta_S}{(ST_B/N_o)_{TH}} \qquad (5.5\text{-}3)$$

If more than one data channel is used, simultaneous equations must be satisfied.

$$D_{R_{1\,max}} = \frac{(P_T/N_o)\left(P_{D_1}/P_T\right)\eta_{S_1}}{(ST_B/N_o)_{TH_1}} \tag{5.5-4}$$

and

$$D_{R_{2\,max}} = \frac{(P_T/N_o)\left(P_{D_2}/P_T\right)\eta_{S_2}}{(ST_B/N_o)_{TH_2}} \tag{5.5-5}$$

and so forth:

$D_{R_{1\,max}}$ and $D_{R_{2\,max}}$ are coupled in the sense that P_{D_1}/P_T and P_{D_2}/P_T are coupled through their functional relations to modulation indices.

Appendix A5.2 presents the maximum data rates evaluated for various Pulse Code Modulation/Phase Modulation (PCM/PM) channel schemes with square-wave subcarriers.

5.6 TELEMETRY SYSTEM OPTIMIZATION

The process of optimizing the telemetry system is one of selecting those values of certain parameters which produce the most efficient telemetry system. A good measure of efficiency is the amount of total received power required for a particular configuration to achieve the necessary bit error rates.

5.6.1 Criteria for Optimization

In general, the performance of a particular deep space telemetry system can be characterized by the bit or word error rates required, the data rates, and the total received signal power to noise spectral density ratio, P_T/N_o. There are a number of ways one can go about optimizing a system.

First, one can specify fixed bit error rates and fixed data rates, then optimize to minimize the required P_T/N_o.

One can specify a fixed P_T/N_o and fixed data rates, then minimize a resulting bit error rate.

Finally, one may hold P_T/N_o and the error rates fixed, and maximize a data rate.

The choice of which method to use is really one of convenience, since the optimized parameters will be the same in any event.

The optimization procedure will reveal two constraints which are not immediately obvious. First, the inherent phase noise of the radio frequency oscillators prevents the choice of an arbitrarily small carrier tracking bandwidth. Thus, the telemetry bit error rate will be inordinately high for bit rates much less than the receiver loop bandwidth because of instabilities in the phase reference for demodulating the telemetry sidebands. Second, the use of high telemetry data rates requires that most of the transmitted power be in the sidebands. However, because of modulation index stability factors in practical designs (see Section 5.6.4.2), at least 10 percent of the available power must be left in the carrier (ref. 5-7).

It is convenient to begin by considering P_T/N_o and the bit error rates as fixed independent parameters, and to optimize the system to maximize a data rate. This method has the advantage that a curve of available channel capacity versus P_T/N_o can be readily constructed. Such curves are very useful in the planning stages of a mission, when data rates are selected. Once the data rates have been selected by the project, the criteria of minimizing the required P_T/N_o becomes more useful. This criterion has the effect of maximizing the performance margins in each of the telemetry channels.

A final consideration in the criteria for optimization is whether the system is to be optimized for best performance when all of the system parameters are at their design values, or whether to optimize performance assuming the parameters are at their adverse values. It is the policy of the Jet Propulsion Laboratory to design the telemetry system so that an acceptable

mission will be achieved when all of the parameters are at their adverse values. By this criterion, it is logical to optimize the system assuming the adverse parameter values. However, the policy also requires implementation of data rates to take advantage of design values of performance, where possible. If the project wishes to implement separate modes of operation for design telemetry performance, the system for these modes should be optimized using design values.

5.6.2 Optimizable Parameters

There are two types of parameters which affect the performance of the telemetry system. They are:

1) Those parameters affecting the total received P_T/N_o.

2) Those parameters affecting the use and allocation of P_T/N_o.

The first type of parameters was considered in section II. In general, the available P_T/N_o is strongly trajectory dependent.

The second type will be considered in this section. In a single-channel system, the use and allocation of P_T/N_o can be represented by the equation

$$P_T/N_o = \frac{(ST_B/N_o)D_R}{(P_D/P_T)\eta_S} \qquad (5.6\text{-}1)$$

where

ST_B/N_o = The SNR per bit required to achieve some probability of error

D_R = Data rate

η_S = System efficiency

P_D/P_T = Allocation of power to the data sideband

For more than one channel, the allocation of power is represented by the simultaneous set of equations

$$P_T/N_o = \frac{(ST_B/N_o)_1 D_{R_1}}{(P_D/P_T)_1 \eta_{S_1}}$$

$$P_T/N_o = \frac{(ST_B/N_o)_2 D_{R_2}}{(P_D/P_T)_2 \eta_{S_2}} \qquad (5.6\text{-}2)$$

$$\vdots$$

$$P_T/N_o = \frac{(ST_B/N_o)_n D_{R_n}}{(P_D/P_T)_n \eta_{S_n}}$$

For each of the n channels, there will be an ST_B/N_o, a data rate, a system loss parameter, and an allocation of total power to the data sideband. Each of these parameters has been described earlier in this chapter.

For our purposes, the process of optimization consists of selecting one of the n data channels as the channel whose data rate is to be maximized. The rest of the data channels, the ST_B/N_o values, and P_T/N_o must be specified. Then, the parameters for the channel k chosen, $(P_D/P_T)_k$, and η_{S_k}, are adjusted to maximize the desired data rate.

Alternatively, one may specify all of the data rates and ST_B/N_o values, and adjust the $(P_D/P_T)_k$, and η_{S_k}, to minimize the required P_T/N_o.

As discussed earlier, $(P_D/P_T)_k$ depends on the modulation indices selected for each channel, and whether square- or sine-wave subcarriers are used. The system losses depend in a nonlinear fashion on several parameters.

They depend on the modulation indices, P_T/N_o, data rate, bit-error rate, receiver loop bandwidth, transition density of data, spacecraft mixer amplifier bandwidth, spacecraft rf phase modulator bandwidth, and type of coding employed for each channel.

It is this myriad of parameters affecting η_S in a nonlinear fashion which makes optimizing the telemetry system a complex task.

5.6.3 Optimization of the Modulation Index

The most easily adjusted parameter in the telemetry system is the modulation index. This parameter determines the allocation of power in the various sidebands, and strongly affects the magnitude of the system losses. In this analysis, the other parameters affecting the performance are assumed to be held constant.

5.6.3.1 Optimization of the Single-Channel Telemetry System With a Square-Wave Subcarrier. The single-channel system can be described by

$$D_R = \frac{\left(\frac{P_T}{N_o}\right)\left(\frac{P_D}{P_T}\right)\eta_S}{\left(\frac{ST_B}{N_o}\right)} \tag{5.6-3}$$

For a square-wave subcarrier,

$$\frac{P_D}{P_T} = \sin^2\theta$$

Thus, the maximum data rate, $D_{R\,max}$, can be computed by setting the derivative of D_R with respect to θ equal to zero, giving:

$$\theta_{opt} = \tan^{-1}\left\{\frac{-2\eta_S}{\left(\frac{d\eta_S}{d\theta}\right)}\right\} \tag{5.6-4}$$

It can be seen that the optimum modulation index for a single-channel system depends entirely on the proper characterization of the system losses. These losses have been modeled in section 5.4.5 and θ_{opt} can be found numerically by varying θ while choosing values of P_T/N_o, receiver loop bandwidth, $2B_{LO}$, receiver IF bandwidth (B_ℓ), threshold ST_B/N_o, and coding scheme.

5.6.3.2 Optimization of the Two-Channel Telemetry System With Square-Wave Subcarriers. The optimization process of the two-channel system is similar to the single-channel system, except that two new independent variables exist. The two channel system may be described by the following two equations

$$D_{R_1} = \frac{\left(\frac{P_T}{N_o}\right)\left(\frac{P_{D_1}}{P_T}\right)\eta S_1}{\left(\frac{ST_B}{N_o}\right)_1} \tag{5.6-5}$$

$$D_{R_2} = \frac{\left(\frac{P_T}{N_o}\right)\left(\frac{P_{D_2}}{P_T}\right)\eta S_2}{\left(\frac{ST_B}{N_o}\right)_2} \tag{5.6-6}$$

For square-wave subcarriers,

$$\frac{P_{D_1}}{P_T} = \sin^2\theta_1 \cos^2\theta_2$$

$$\frac{P_{D_2}}{P_T} = \sin^2\theta_2 \cos^2\theta_1$$

If the telemetry channels are interplexed, and it is assumed that $(S/N_o)_2 > (S/N_o)_1$, the power ratios to be used are

$$\frac{P_{D_1}}{P_T} = \sin^2\theta_1 \sin^2\theta_2$$

$$\frac{P_{D_2}}{P_T} = \sin^2\theta_2 \cos^2\theta_1$$

The procedure now is to select one of the data rates as the one to be maximized. The other data rate, P_T/N_o, $(ST_B/N_o)_1$, $(ST_B/N_o)_2$, $2B_{LO}$, B_ℓ, and the coding for each channel are held constant. Then the two modulation indices may be optimized and D_{R_2} may be maximized by setting

$$\frac{\partial D_{R_2}}{\partial \theta_1} = 0 \tag{5.6-7}$$

$$\frac{\partial D_{R_2}}{\partial \theta_2} = 0 \tag{5.6-8}$$

subject to the constraint

$$D_{R_1} = \frac{\left(\frac{P_T}{N_o}\right)\left(\frac{P_{D_1}}{P_T}\right)\eta_{S_1}}{\left(\frac{ST_B}{N_o}\right)_1} \tag{5.6-9}$$

Also, other constraints may be imposed on the optimization process, if required. For instance, a minimum carrier power constraint may be added to obtain the required quality of doppler data.

In general, η_{S_1} and η_{S_2} are nonlinear functions of variables θ_1 and θ_2. Thus, it is necessary to construct a computer algorithm to compute optimum modulation indices, as in the single-channel case. However, the optimization problem may be simplified when P_T/N_o is very large and η_{S_1} and η_{S_2} are

correspondingly close to unity. In appendix A5.3, it is shown that for non-interplexed telemetry, the optimum θ_1 and θ_2 are given by:

$$\theta_{1_{opt}} = \sin^{-1}\left\{\left(\frac{D_{R_1}\left(\frac{ST_B}{N_o}\right)_1}{\frac{P_T}{N_o}}\right)^{1/4}\right\} \tag{5.6-10}$$

$$\theta_{2_{opt}} = \cos^{-1}\left\{\left(\frac{D_{R_1}\left(\frac{ST_B}{N_o}\right)_1}{\frac{P_T}{N_o}}\right)^{1/4}\right\} \tag{5.6-11}$$

$$D_{R_{2_{max}}} = \frac{\frac{P_T}{N_o}}{\left(\frac{ST_B}{N_o}\right)_2} \sin^2 \theta_{2\ opt} \cos^2 \theta_{1\ opt} \tag{5.6-12}$$

Equation (5.6-12) can also be written as:

$$\frac{D_{R_{2\ max}}}{D_{R_1}} = \frac{\left(\frac{ST_B}{N_o}\right)_1}{\left(\frac{ST_B}{N_o}\right)_2}\left[\frac{\frac{P_T}{N_o D_{R1}}}{\left(\frac{ST_B}{N_o}\right)_1} - 2\left(\frac{\frac{P_T}{N_o D_{R1}}}{\left(\frac{ST_B}{N_o}\right)_1}\right)^{\frac{1}{2}} + 1\right] \tag{5.6-13}$$

which approaches $(P_T/N_o D_{R_1})/(ST_B/N_o)_2$ as $(P_T/N_o D_{R_1})/(ST_B/N_o)_1$, becomes large. Figure 5-60 plots $D_{R_{2\ max}}/D_{R_1}$ as a function of $(P_T/N_o D_{R_1})/(ST_B/N_o)_1$ for representative values of the ratio $(ST_B/N_o)_1/(ST_B/N_o)_2$, and shows the asymptotic behavior.

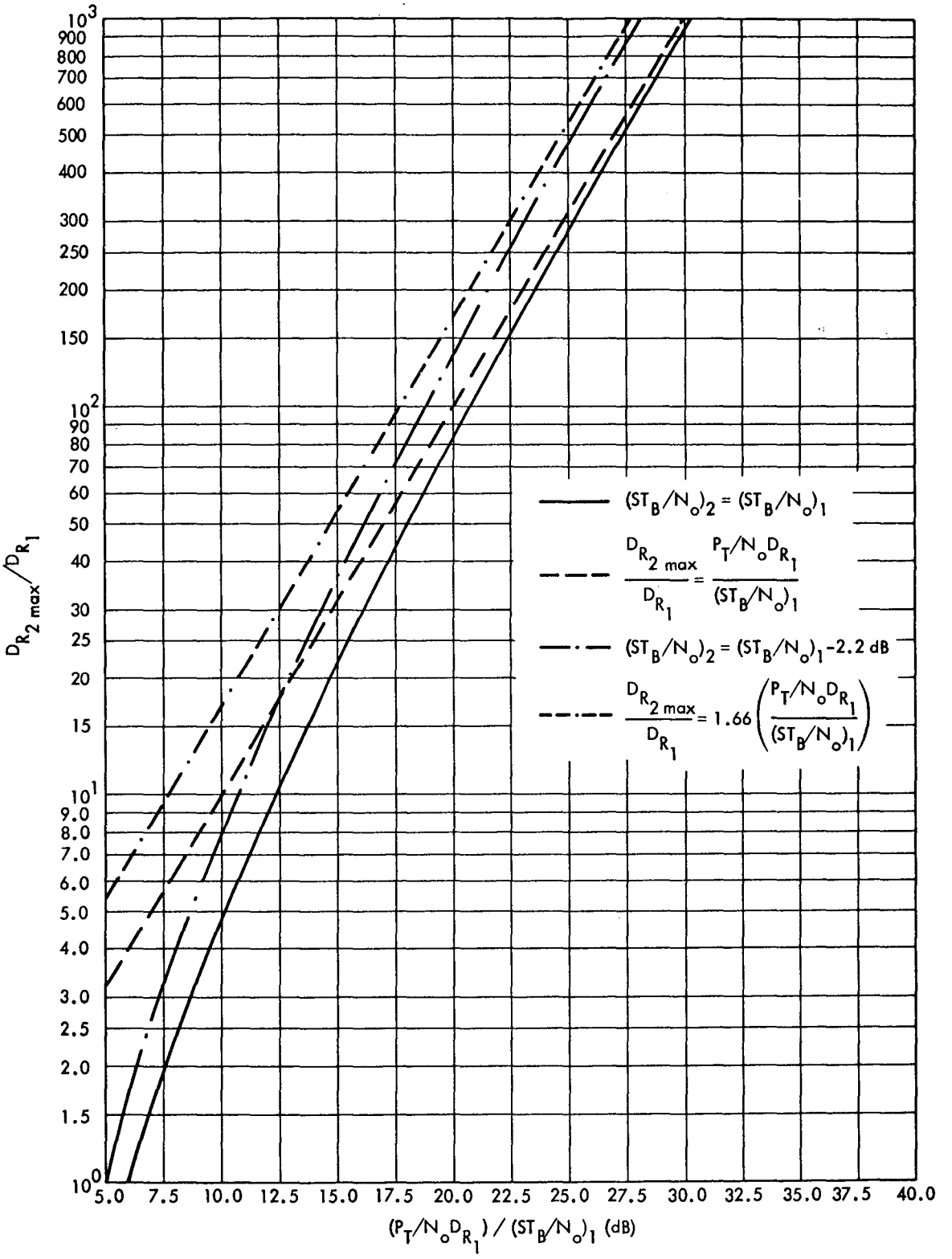

Fig. 5-60. Maximized data channel 2 data rate versus $(P_T/N_oD_{R_1})/(ST_B/N_o)_1$ for high system efficiency and non-interplexed telemetry

If both data rates are known and it is desired to optimize θ_1 and θ_2 by minimizing the required P_T/N_o, then the optimum modulation indices are given by

$$\theta_{1_{opt}} = \tan^{-1}\left\{\left(\frac{D_{R_1}\left(\frac{ST_B}{N_o}\right)_1}{D_{R_2}\left(\frac{ST_B}{N_o}\right)_2}\right)^{1/4}\right\} \tag{5.6-14}$$

$$\theta_{2_{opt}} = \tan^{-1}\left\{\left(\frac{D_{R_2}\left(\frac{ST_B}{N_o}\right)_2}{D_{R_1}\left(\frac{ST_B}{N_o}\right)_1}\right)^{1/4}\right\} \tag{5.6-15}$$

and

$$\left(\frac{P_T}{N_o}\right)_{min} = \frac{D_{R_1}\left(\frac{ST_B}{N_o}\right)_1}{\sin^2\theta_{1_{opt}}\cos^2\theta_{2_{opt}}} = \frac{D_{R_2}\left(\frac{ST_B}{N_o}\right)_2}{\sin^2\theta_{2_{opt}}\cos^2\theta_{1_{opt}}} \tag{5.6-16}$$

or,

$$\left(\frac{P_T}{N_o}\right)_{min} = \left[\sqrt{D_{R_1}\left(\frac{ST_B}{N_o}\right)_1} + \sqrt{D_{R_2}\left(\frac{ST_B}{N_o}\right)_2}\right]^2 \tag{5.6-17}$$

Figure 5-61 plots $(P_T/N_o)_{min}$ versus $D_{R_2}\,(ST_B/N_o)_2$ for various values of $D_{R_1}\,(ST_B/N_o)_1$.

If the available P_T/N_o is too low for the relations $\eta_{S_1} \simeq 1$ and $\eta_{S_2} \simeq 1$ to hold, then a computer evaluation of optimum mod indices is necessary. Values of P_T/N_o, D_{R_1}, ST_B/N_o required for each channel, receiver loop and

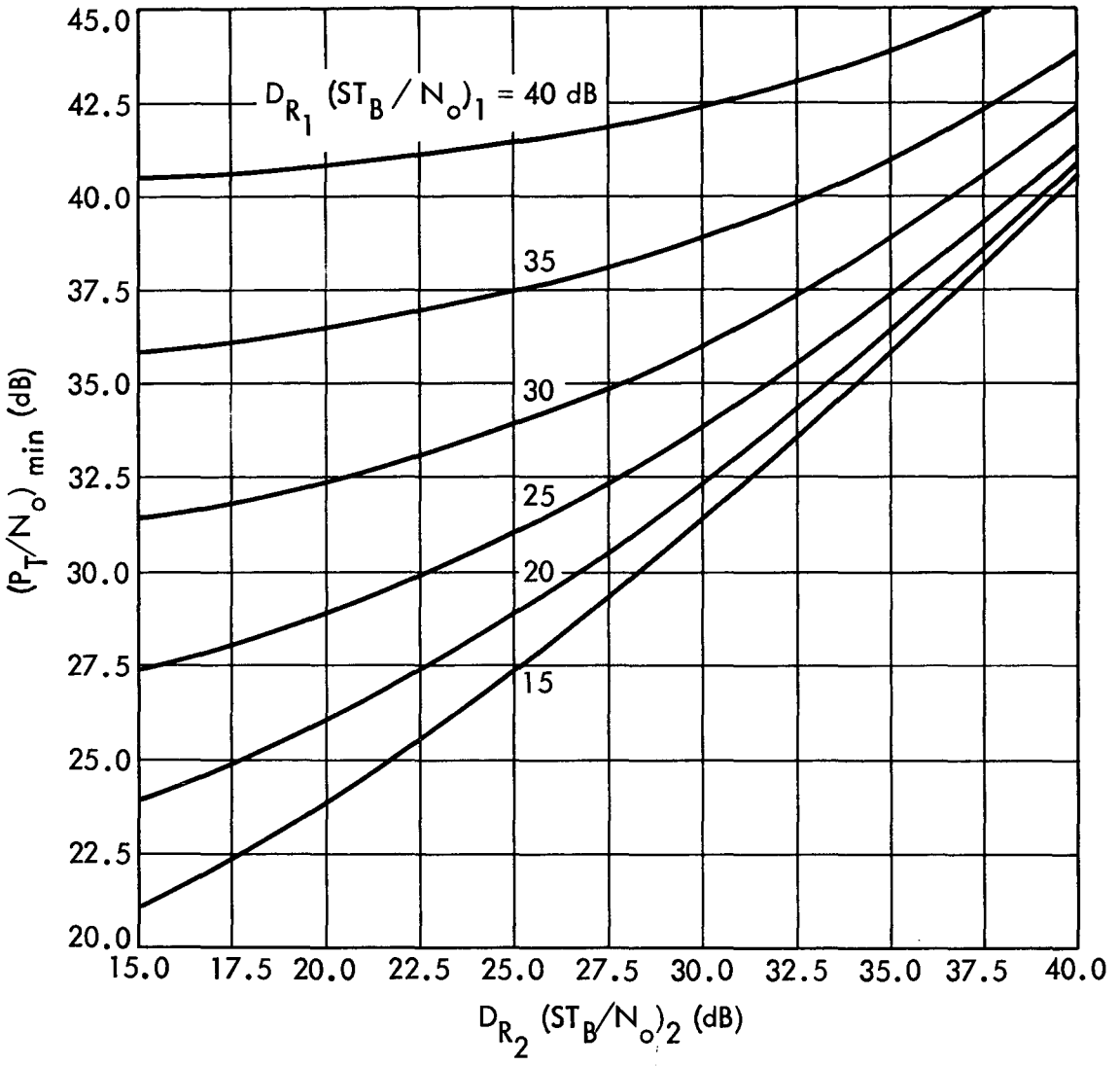

Figure 5-61. Minimum P_T/N_o versus $D_{R_2}(ST_B/N_o)_2$ and $D_{R_1}(ST_B/N_o)_1$ for high system efficiency and non-interplexed telemetry

IF bandwidths, and the coding types for each channel are held constant and θ_1 and θ_2 are varied subject to constraints on ST_B/N_o.

5.6.4 Effects of Parameter Tolerances on Optimization of Mod Indices

Since the optimized values of mod index depend on P_T/N_o, ST_B/N_o, and system losses, the tolerances associated with P_T/N_o, ST_B/N_o, system losses, and modulation indices, will affect the value of optimum mod index.

Two types of optimum modulation index (OMI) may be computed. The OMI's associated with design parameters, and the OMI's associated with adverse parameters. The use of design OMI's or adverse OMI's should depend on whether a mode is for design performance or adverse performance.

5.6.4.1 Tolerances on P_T/N_o. As shown in section II, P_T/N_o is calculated by using the spacecraft transmitter output power, spacecraft and ground circuit losses, spacecraft and ground antenna gains, space loss, pointing losses, polarization losses, and system noise spectral density. Each of these parameters has a tolerance associated with it which when added linearly, produces for the link the sum of the adverse tolerances, (ΣAT). One can calculate, therefore, a design available P_T/N_o and an adverse available P_T/N_o.

5.6.4.2 Modulation Index Tolerances. Two hardware parameters determine the value of the modulation index. These are the modulator sensitivity, K degrees per volt, and the voltage of the signal driving the modulator, T volts. Each independent modulation index requires a separate driving signal, T_i, while the modulator sensitivity, K, is common for all modulation indices. Thus,

$$\theta_i = T_i K, \qquad i = 1, 2, \ldots \tag{5.6-18}$$

The values of K and T_i will vary with temperature, so that the mod indices will vary with temperature. Thus, we model the variation in modulation index, $\Delta\theta_i$, as

$$\theta_i \pm \Delta\theta_i = (T_i \pm \Delta T_i)\ (K \pm \Delta K) \tag{5.6-19}$$

where θ_i, T_i and K are design values. Then

$$\pm\Delta\theta_i = \pm\Delta T_i K \pm T_i \Delta K \pm \Delta T_i \Delta K \qquad (5.6\text{-}20)$$

A convenient way of visualizing the modulation tolerances is to construct a vector space of all possible modulation index values about the design values. The modulation indices can be at any point within the space. For example, a single-channel system using a single mod index has a vector space consisting of a line (see Figure 5-62).

For a two-channel system, the mod indices can vary over the space shown in Figure 5-63.

Three or more channels can be similarly viewed, using a mod index vector space.

The effect of tolerances on modulation indices is that the power allocations P_{D_i}/P_T vary as the mod indices vary. The favorable and adverse values of P_{D_i}/P_T will correspond to mod indices which lie somewhere on the boundary of the vector space. For example, in a two-channel square-wave subcarrier system,

$$\frac{P_C}{P_T} = \cos^2\theta_1 \cos^2\theta_2.$$

The point on Figure 5-63 corresponding to the adverse P_C/P_T occurs where θ_1 and θ_2 are greatest. This point is labeled point 1.

Table 5-7 summarizes the adverse and favorable tolerance points of Figure 5-63 associated with a two-channel square-wave subcarrier system.

When selecting the optimum mod indices, the use of equations (5.6-10) through (5.6-17) will result in some initial optimum mod index values to begin numerical analysis. To optimize for adverse performance, the initial mod indices must be modified so that their adverse points (refer to Table 5-7) are equal to the initial mod index values. The design mod indices will then be suboptimum, but the adverse indices will be optimum.

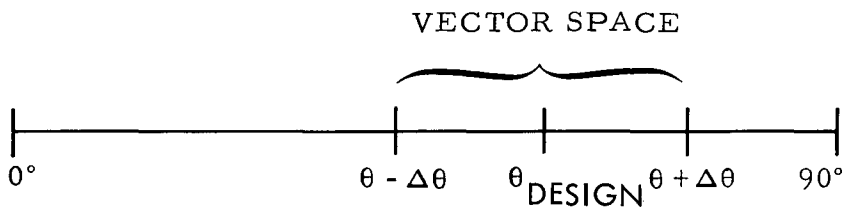

Fig. 5-62. Single-channel modulation index tolerance

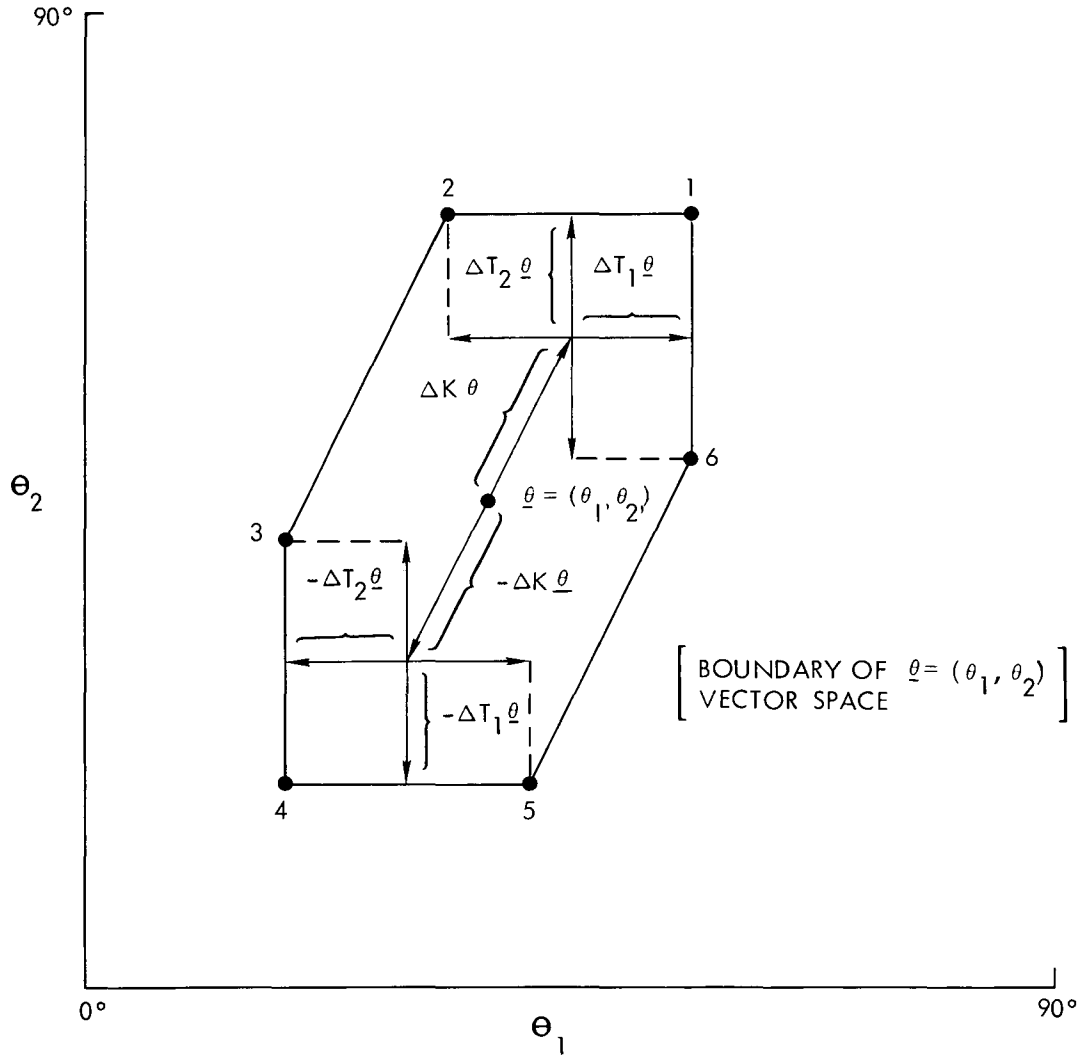

Fig. 5-63. Two-channel modulation index tolerances

Table 5-7. Favorable and adverse tolerance points for a two-channel square-wave subcarrier subsystem

Parameter	Corresponding point numbers	
	Adverse	Favorable
P_C/P_T	1	4
P_{D_1}/P_T	2	5
P_{D_2}/P_T	5	2

5.6.4.3 System Loss Tolerances. There are two reasons why tolerances exist on the system losses. First, changes in P_T/N_o and modulation indices will change the system losses in a manner prescribed by the mathematical model of system losses. Second, there is a tolerance assessed which reflects the level of confidence that the model accurately describes the observed losses.

Tolerances of the first kind can be calculated by the system designer using his knowledge of P_T/N_o and modulation index tolerances. Tolerances of the second kind will be somewhat subjective in nature. The best measure of confidence in the model will come from comparing predictions of the model with test data taken from past flight projects, and from tests designed to specifically measure the losses.

The easiest way to incorporate these losses into the optimization of adverse modulation indices when using equations (5.6-10) through (5.6-17) is to increase the required ST_B/N_o by the tolerances on η_S for each channel.

5.6.5 Information Capacity of the Optimized Telemetry System

The capacity of the optimized telemetry system is presented in this section for several cases of practical interest.

For a single-channel square-wave subcarrier system using uncoded data, the maximum data rates versus P_T/N_o and the corresponding optimum modulation index (OMI) versus P_T/N_o are shown in Figures 5-64 and 5-65 for various bit error rates.

For a two-channel square-wave subcarrier system using two uncoded channels, the maximum high-rate data rates versus P_T/N_o and the corresponding OMI's versus P_T/N_o are shown in Figures 5-66 and 5-67 for various low-rate data rates.

For a two-channel square-wave subcarrier system using an uncoded low data rate channel and a block coded high data rate channel, the maximum high-rate data rates versus P_T/N_o and corresponding OMI's versus P_T/N_o are shown in Figures 5-68 and 5-69 for various low-rate data rates.

The data rates and modulation indices presented in Figures 5-64 through 5-69 assume nominal performance parameters only. When using these curves to size a telemetry system, allowances must be made for tolerances on modulation indices and system losses.

5.7 COMPARISON OF SINGLE VS MULTIPLE SUBCARRIER TELEMETRY CHANNELS

The design and performance of both one- and two-channel telemetry systems has been considered above. This part of section V presents a comparison of the performance and complexity of the two types of systems so that the system designer may choose whichever is more appropriate for his project.

5.7.1 Performance Measures

In order to compare different telemetry systems, it is necessary to agree on a meaningful measure of system performance. Three measures of performance are proposed. First, the P_T/N_o required by the system provides an absolute measure of the system efficiency and performance. Second, a relative measure of efficiency is the ratio of P_T/N_o required by a perfectly coherent single-channel system with ideal coding at the Shannon limit to the P_T/N_o required by the actual system. This measure gives a percent efficiency evaluation of the actual system compared to the ideal system. The third measure is the percent loss in data by using a two-channel system rather than

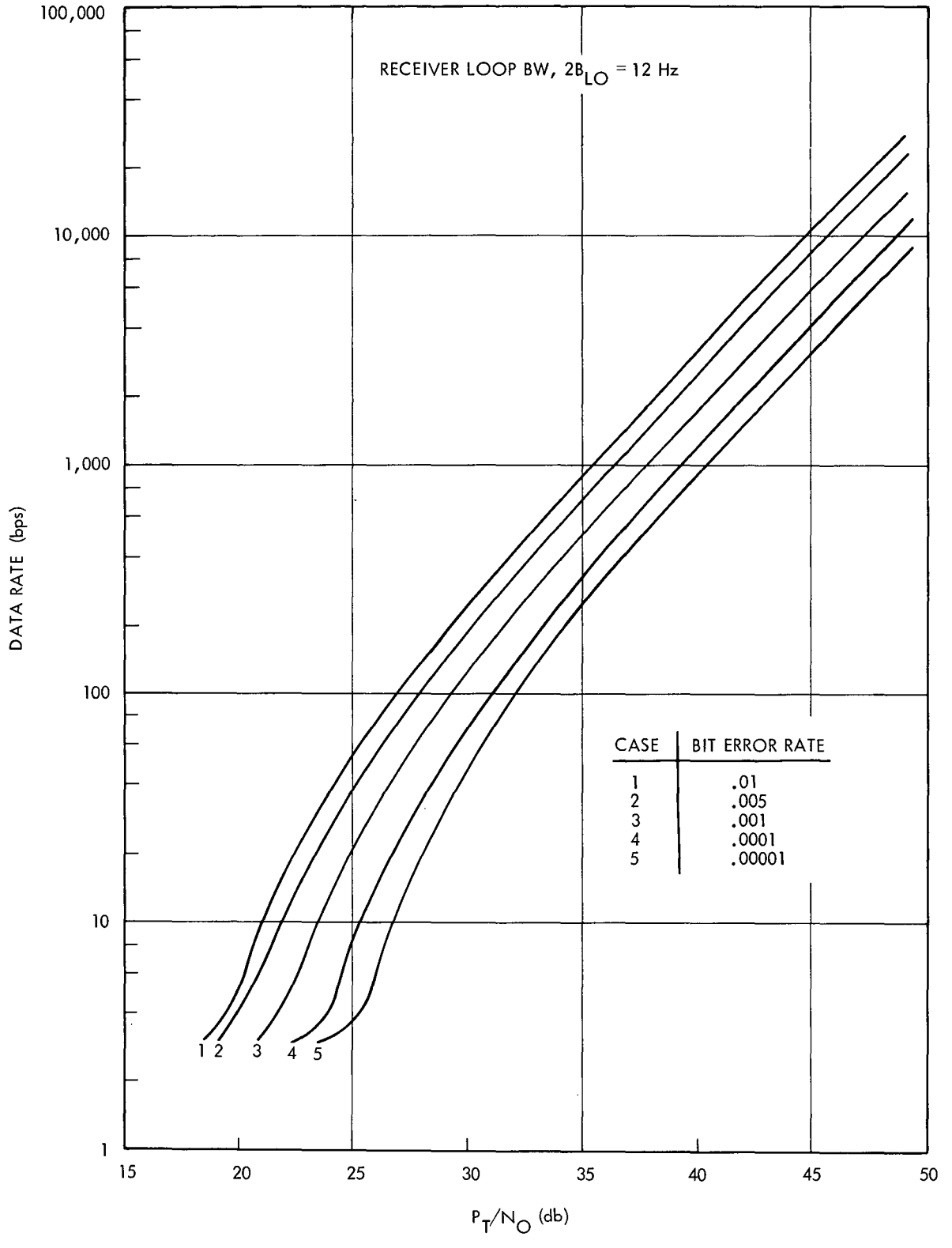

Fig. 5-64. Maximum available data rates, single-channel telemetry, data uncoded

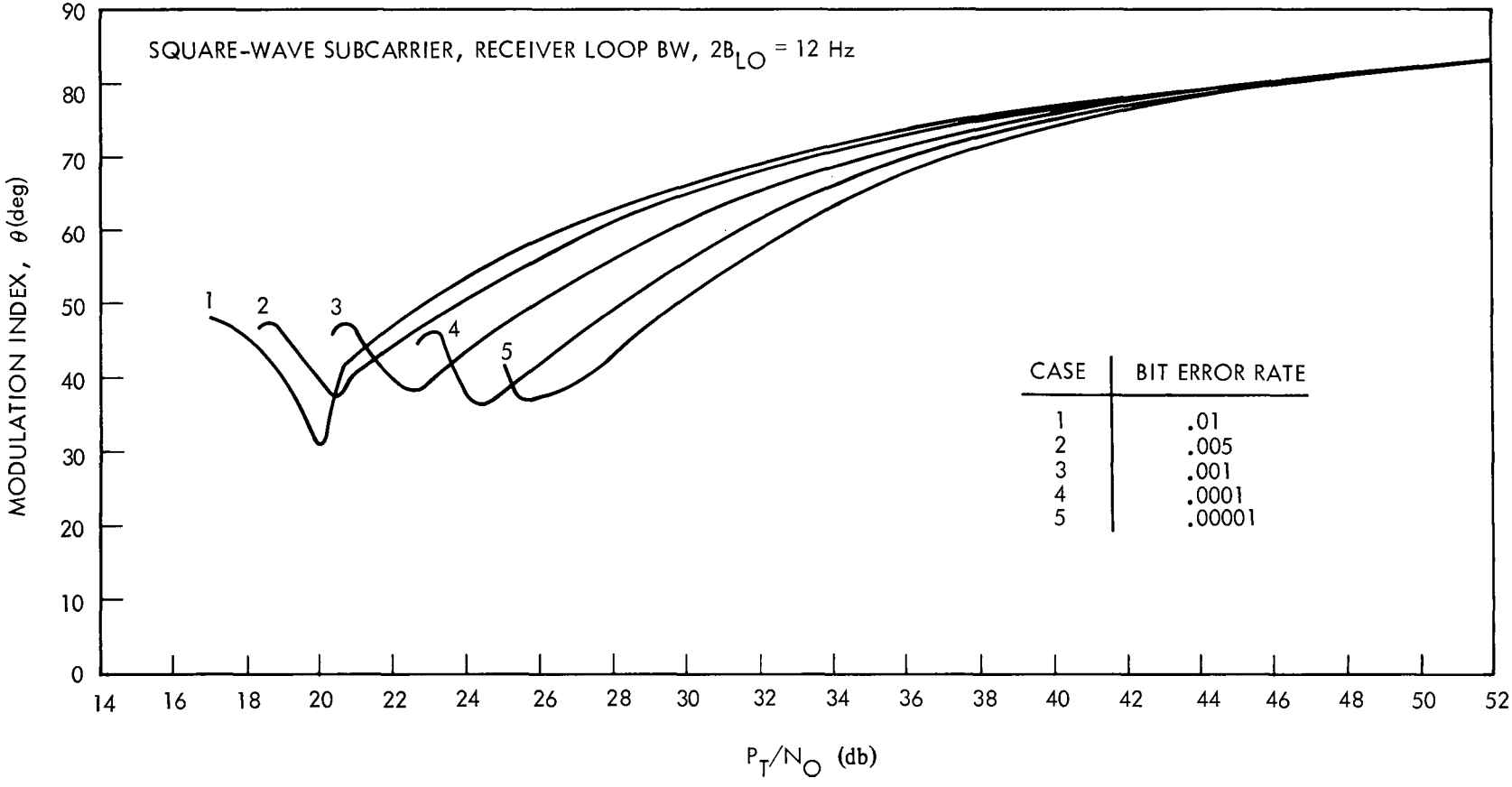

Fig. 5-65. Optimum modulation indices, single-channel telemetry, data uncoded

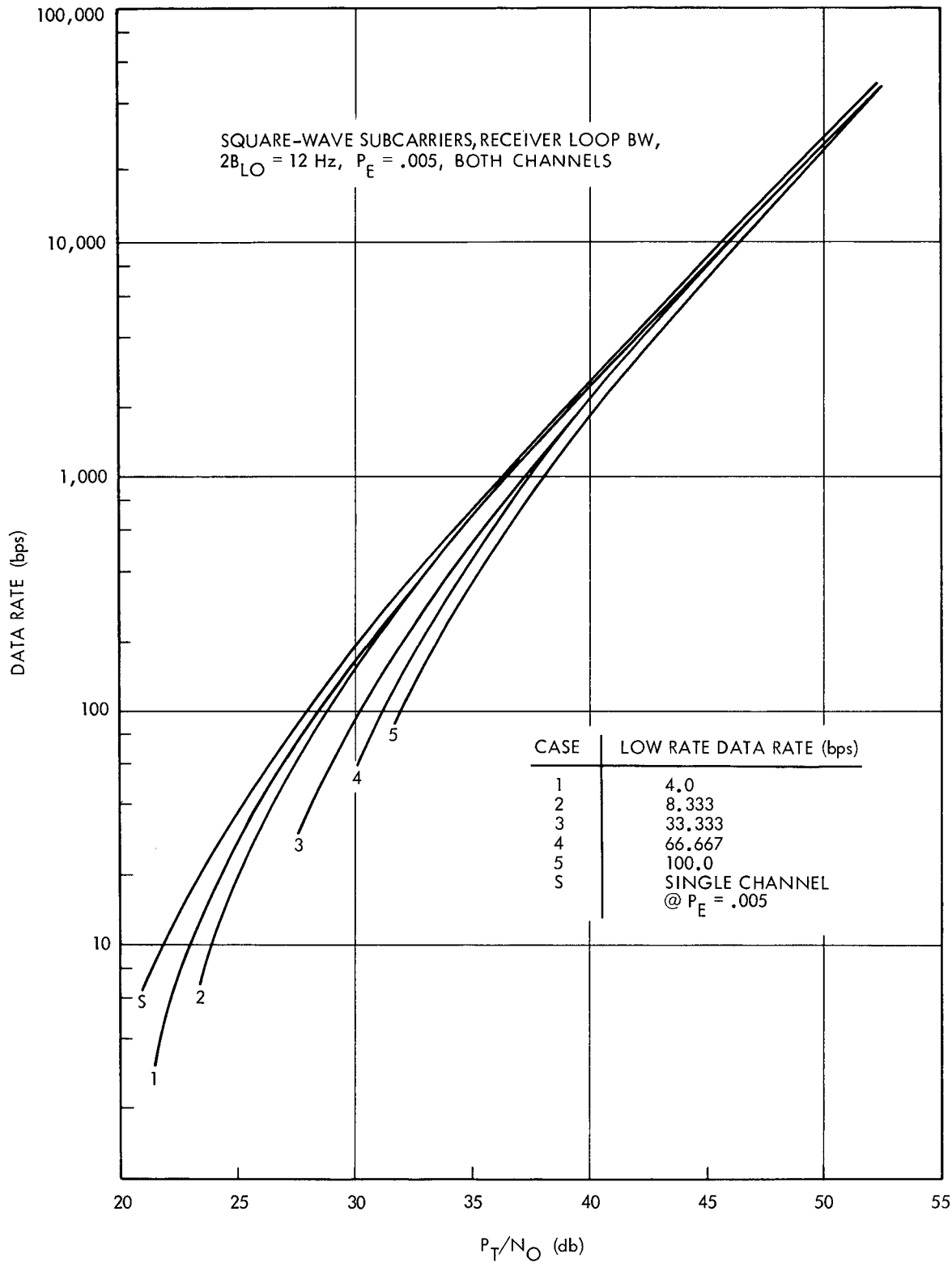

Fig. 5-66. Maximum available data rate, two-channel telemetry, both channels uncoded

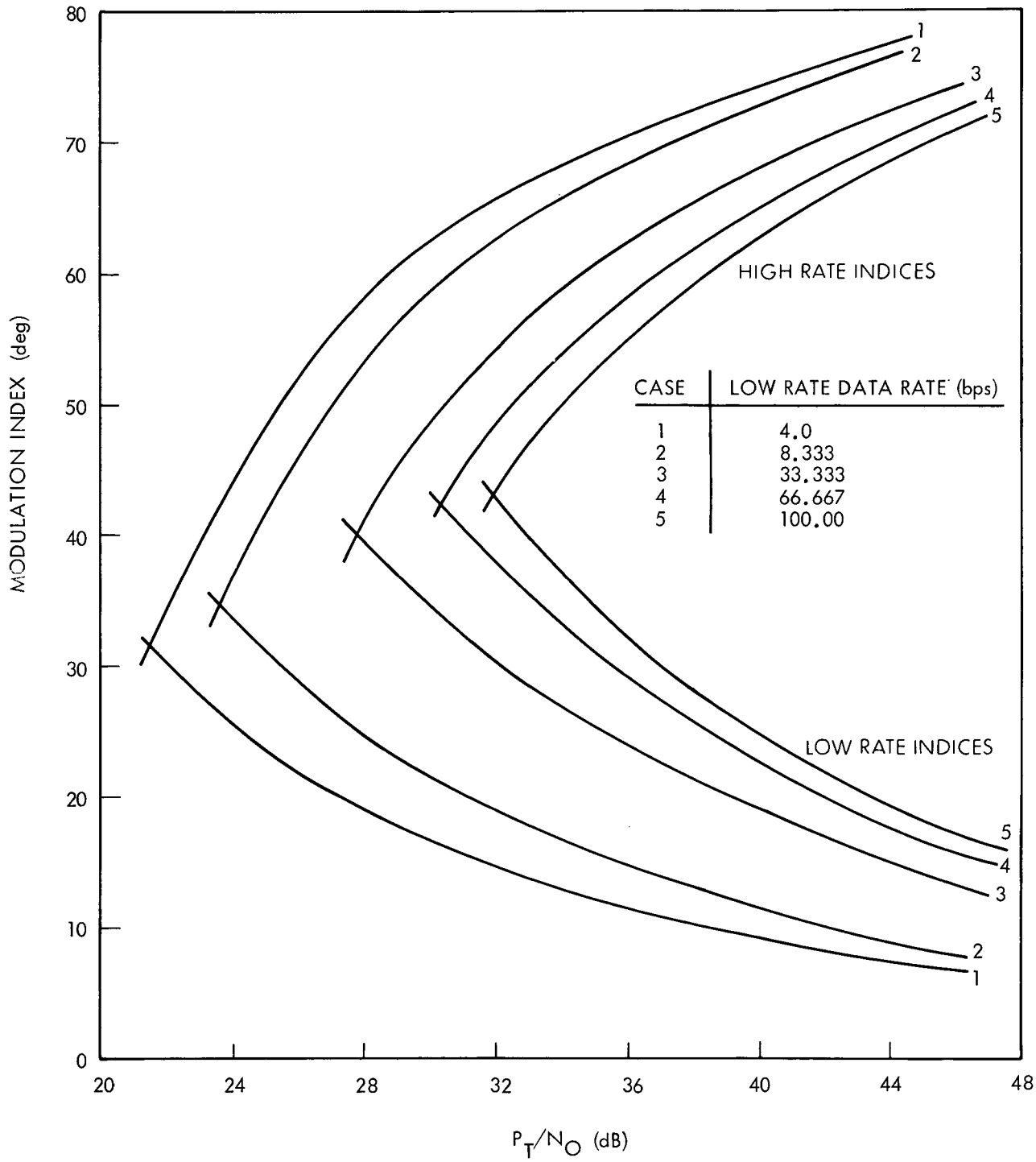

Fig. 5-67. Optimum modulation indices, two-channel telemetry, uncoded data

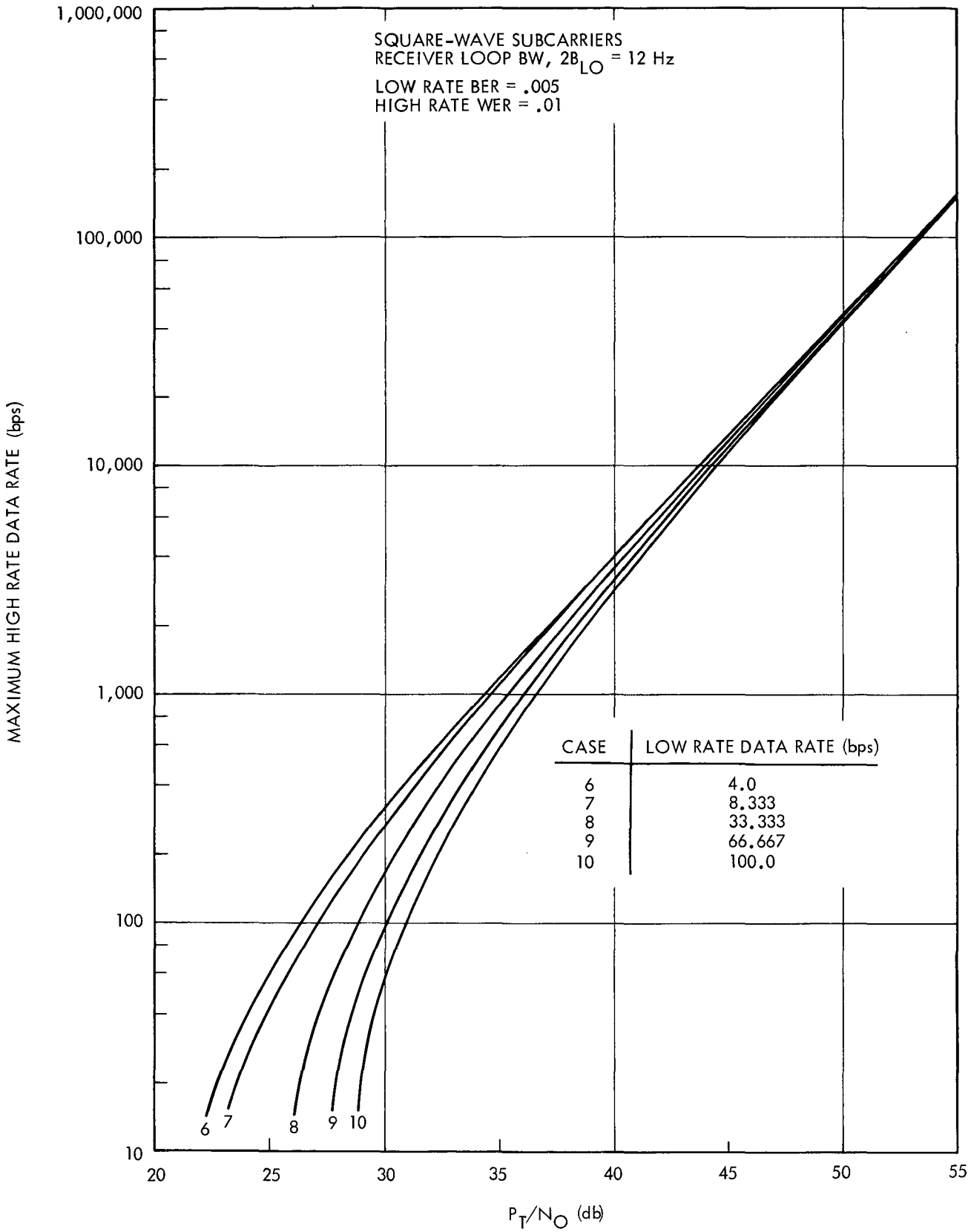

Fig. 5-68. Maximum data rates, two-channel telemetry, coded high-rate data

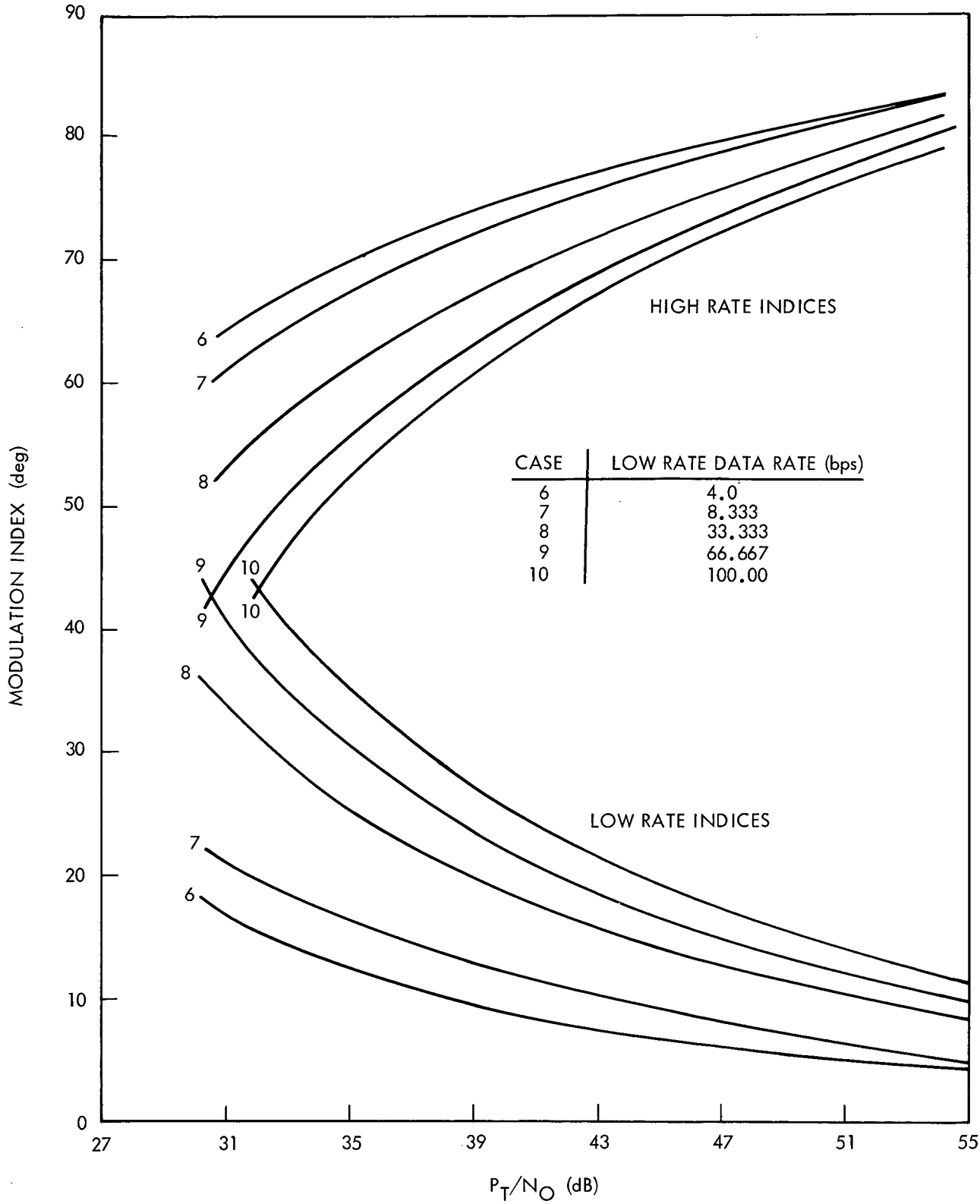

Fig. 5-69. Optimum modulation indices, two-channel telemetry, coded high-rate data

a single-channel system. Alternatively, the measure can compare the percent improvement in total data rate by using a single-channel system instead of a two-channel system.

5.7.2 Performance Criteria

Criterion #1: The data necessary to compare telemetry systems by the criteria of absolute value of P_T/N_o required has already been presented.

Criterion #2: Shannon's formula for channel capacity, C, of a channel of bandwidth W, perturbed by additive Gaussian white noise of one-sided spectral density N_o is

$$C = W \log_2 \left(1 + \frac{S}{N_o W}\right) \tag{5.7-1}$$

In the limit as coding expands W toward infinity,

$$\lim_{W \to \infty} \quad C = \frac{S}{N_o \ln 2} \tag{5.7-2}$$

To use this as a measure of system efficiency, we define D_T to be the sum of all data rates required by the telemetry system. An equivalent ideal single-channel system would operate at data rate D_T, and due to perfect coherence, could allocate all received power to the data spectrum, with a zero bit error rate. Thus,

$$D_T = \frac{S}{N_o \ln 2} = \frac{P_T}{N_o \ln 2}$$

or

$$\left(\frac{P_T}{N_o}\right)_{req'd} = D_T \ln 2 \tag{5.7-3}$$

The relative system efficiency is defined as

$$\eta_{TS} \triangleq \frac{\left(\frac{P_T}{N_o}\right)_{\text{req'd ideal}}}{\left(\frac{P_T}{N_o}\right)_{\text{req'd actual}}} \tag{5.7-4}$$

$$\eta_{TS} = \frac{D_T \ln 2}{\left(\frac{P_T}{N_o}\right)_{\text{req'd actual}}} \tag{5.7-5}$$

and

$$D_T \triangleq \sum_{i=1}^{N} D_i \quad i = 1, 2, \cdots N \text{ channels} \tag{5.7-6}$$

Criterion #3: The third criterion compares one- and two-channel systems based on the difference in available data rates for a given P_T/N_o. The percent loss in data rate in using the two-channel system rather than the single-channel (SC) system is defined as

$$\text{Percent Data Rate Loss} = \frac{Dr_{SC} - (Dr_1 + Dr_2)}{Dr_{SC}} \times 100 \tag{5.7-7}$$

Figure 5-70 presents this loss for various practical two-channel uncoded square-wave subcarrier systems.

Alternately, one may consider the percent gain in data rate in using a single-channel system rather than a two-channel system. Here, the percent data rate gain may be defined by

$$\text{Percent Data Rate Gain} = \frac{Dr_{SC} - (Dr_1 + Dr_2)}{(Dr_1 + Dr_2)} \times 100 \tag{5.7-8}$$

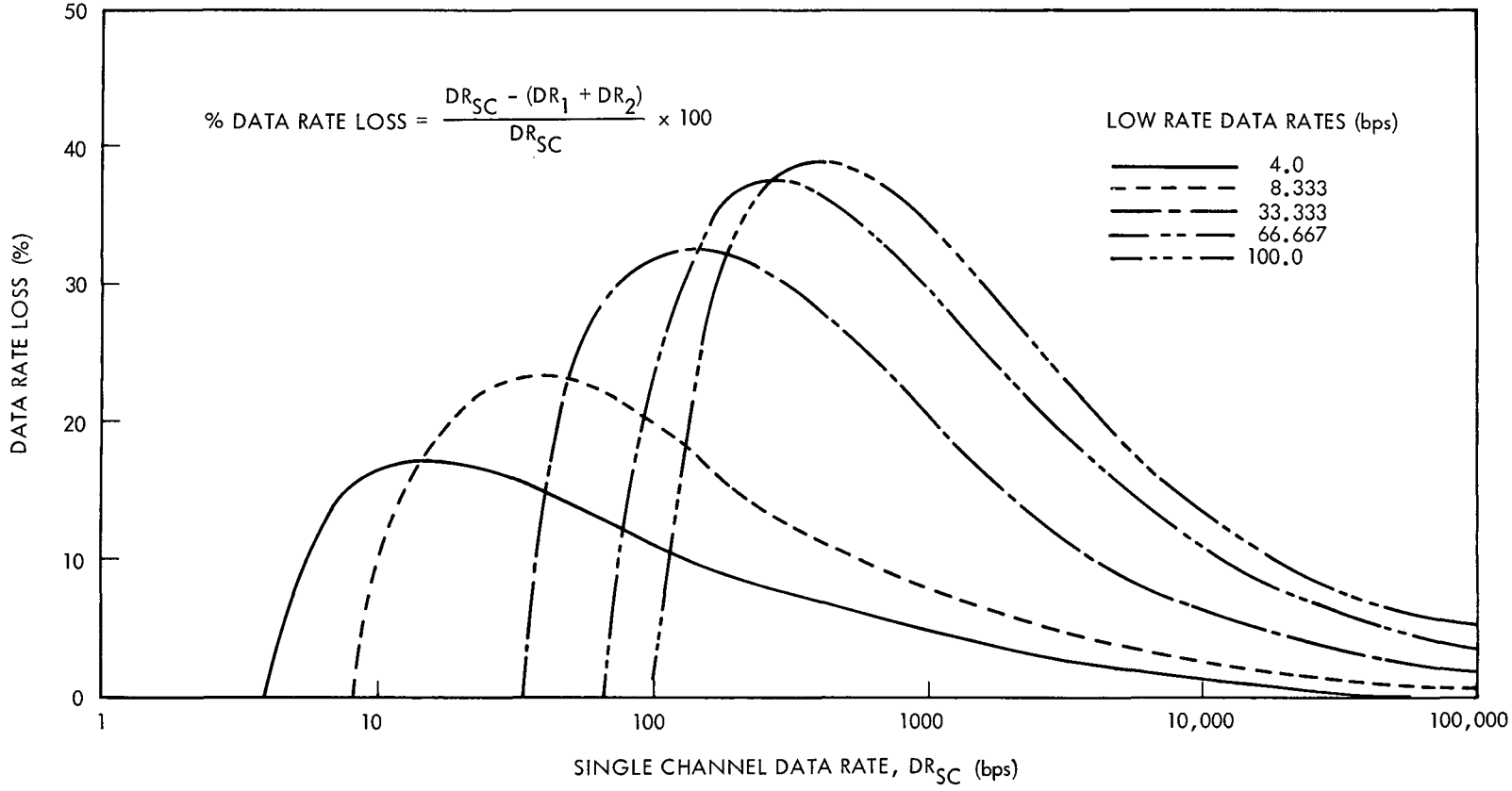

Fig. 5-70. Relative telemetry system performance, two-channel, uncoded, square-wave telemetry

5.7.3 Spacecraft Configurations for One or Two Telemetry Channels

Figure 5-71 is a block diagram of the spacecraft configuration for a single-channel telemetry system. The Flight Data System (FDS) obtains, samples, conditions, and formats both engineering and science data. It generates the clock signals which set the data rates, provides sync signals to the Telemetry Modulation Unit (TMU) for coding, and provides control signals to the TMU for selecting the different mod indices for the different telemetry modes.

The TMU accepts the data stream, codes the data if requested by the FDS, generates a single subcarrier, biphase modulates the symbol stream onto the subcarrier, selects the appropriate mod index level set circuit, and presents an accurately controlled waveform to the Radio Frequency Subsystem (RFS) phase modulator for carrier modulation and transmission to Earth.

Figure 5-72 is a block diagram of the spacecraft configuration for a two-channel telemetry system. It is similar to the single-channel system in that all of the functions of the single-channel TMU and FDS are performed in the two-channel system. The two-channel system must perform the additional functions of generating a second subcarrier, biphase modulating the data onto it, accurately controlling the waveform to be modulated, and linearly summing the two channels to provide a composite telemetry output signal with which to drive the RFS phase modulator.

5.7.4 Ground Configurations for One or Two Telemetry Channels

Figure 5-73 is a block diagram of the ground configuration used to support a two-channel telemetry system. In this configuration, the receiver provides a carrier tracking reference and presents the received waveform to each of two SDA's. The SDA's each remove a subcarrier, and then the rf carrier. Each SDA passes its waveform to an SSA which performs matched filter detection of the symbol stream and obtains symbol sync for the BDA or DDA. The TCP for the science data stream takes the decoded data bits, and formats them for transmission over the GCF lines to the Project.

If interplex modulation is employed on the spacecraft, the SDA handling the low-rate subcarrier must be aligned so that its carrier phase reference is in-phase with the incoming carrier. The other SDA remains aligned so that its carrier phase reference is in quadrature to the incoming carrier.

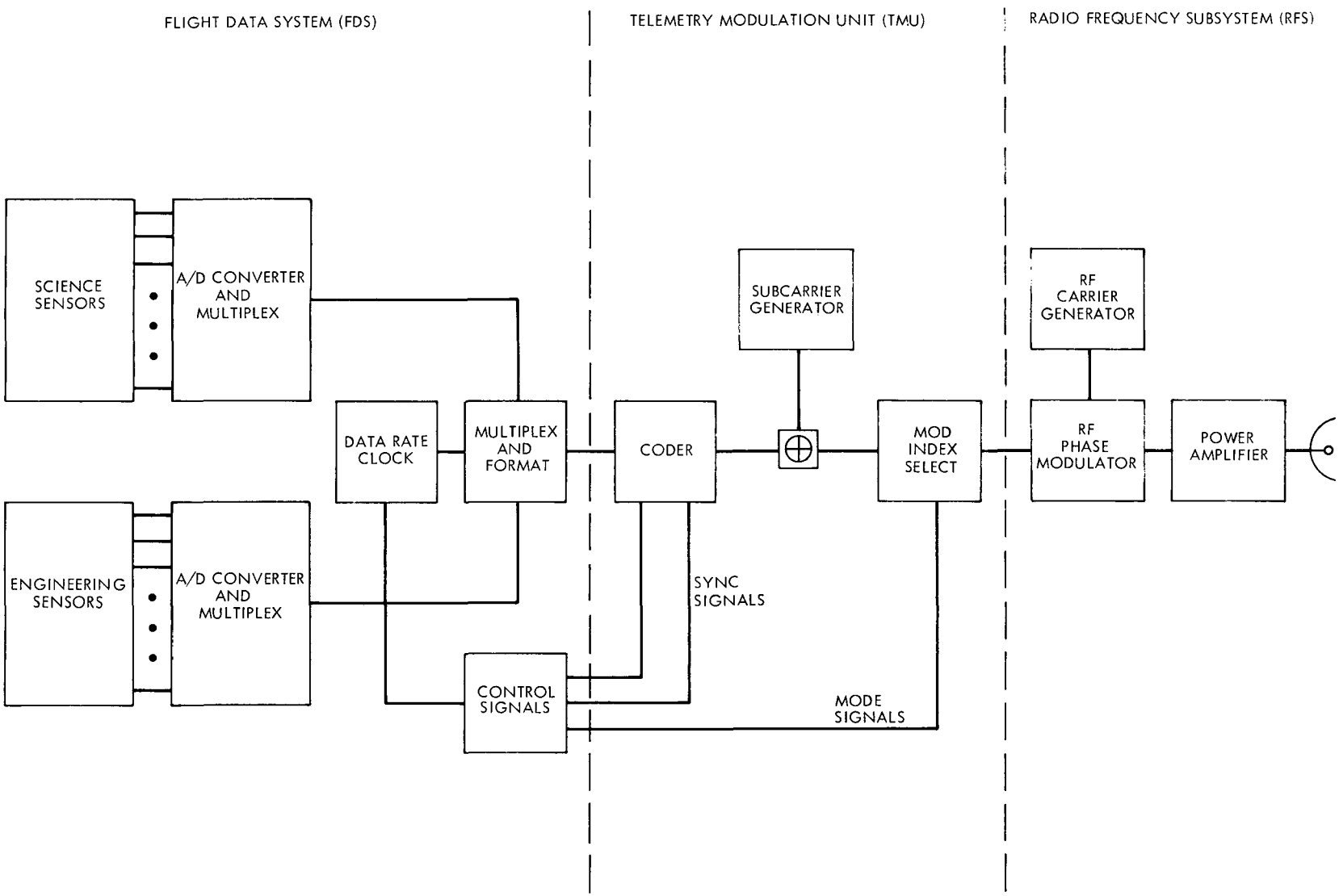

Fig. 5-71. Spacecraft configuration for single-channel telemetry

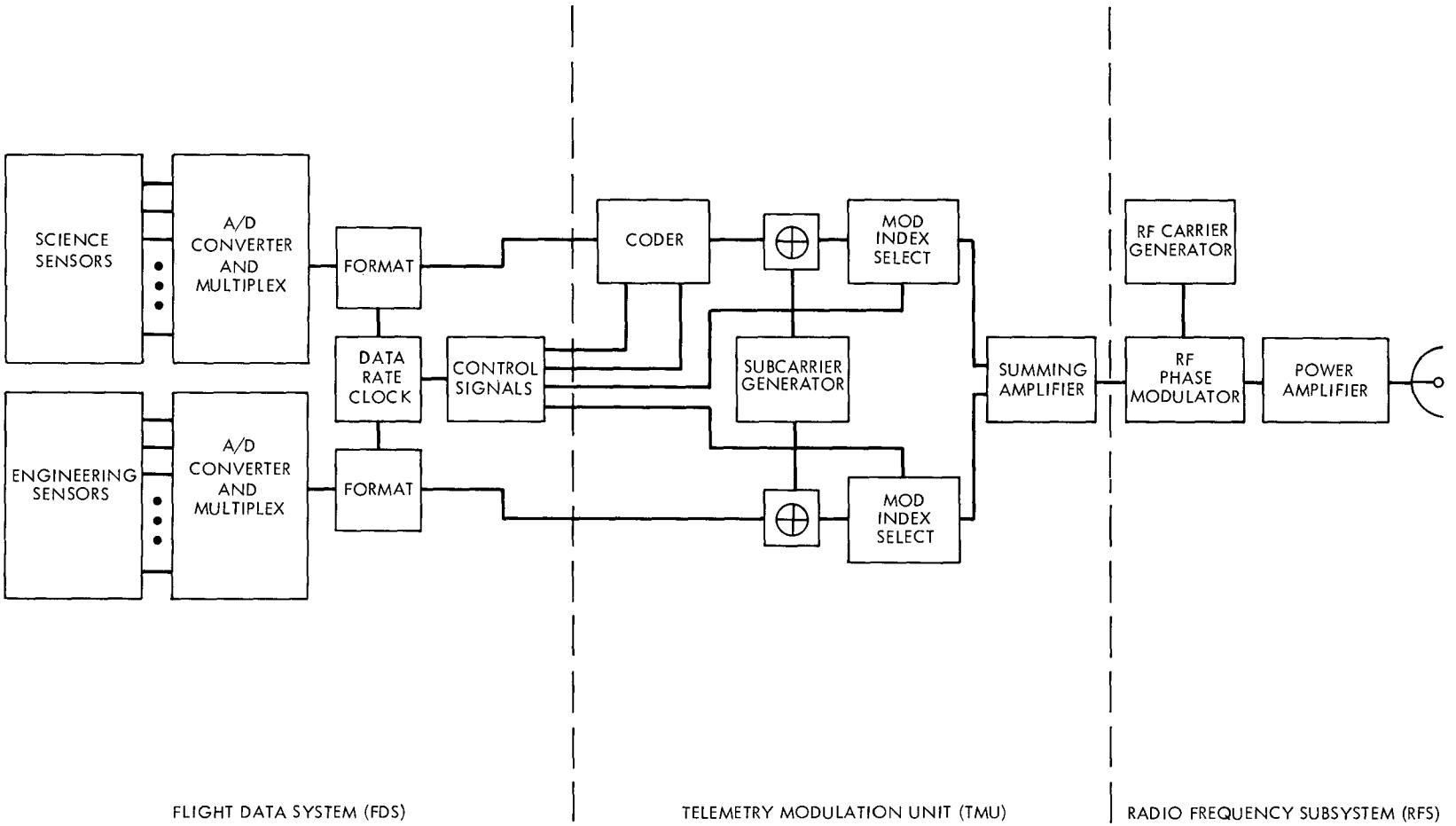

Fig. 5-72. Spacecraft configuration for two-channel telemetry

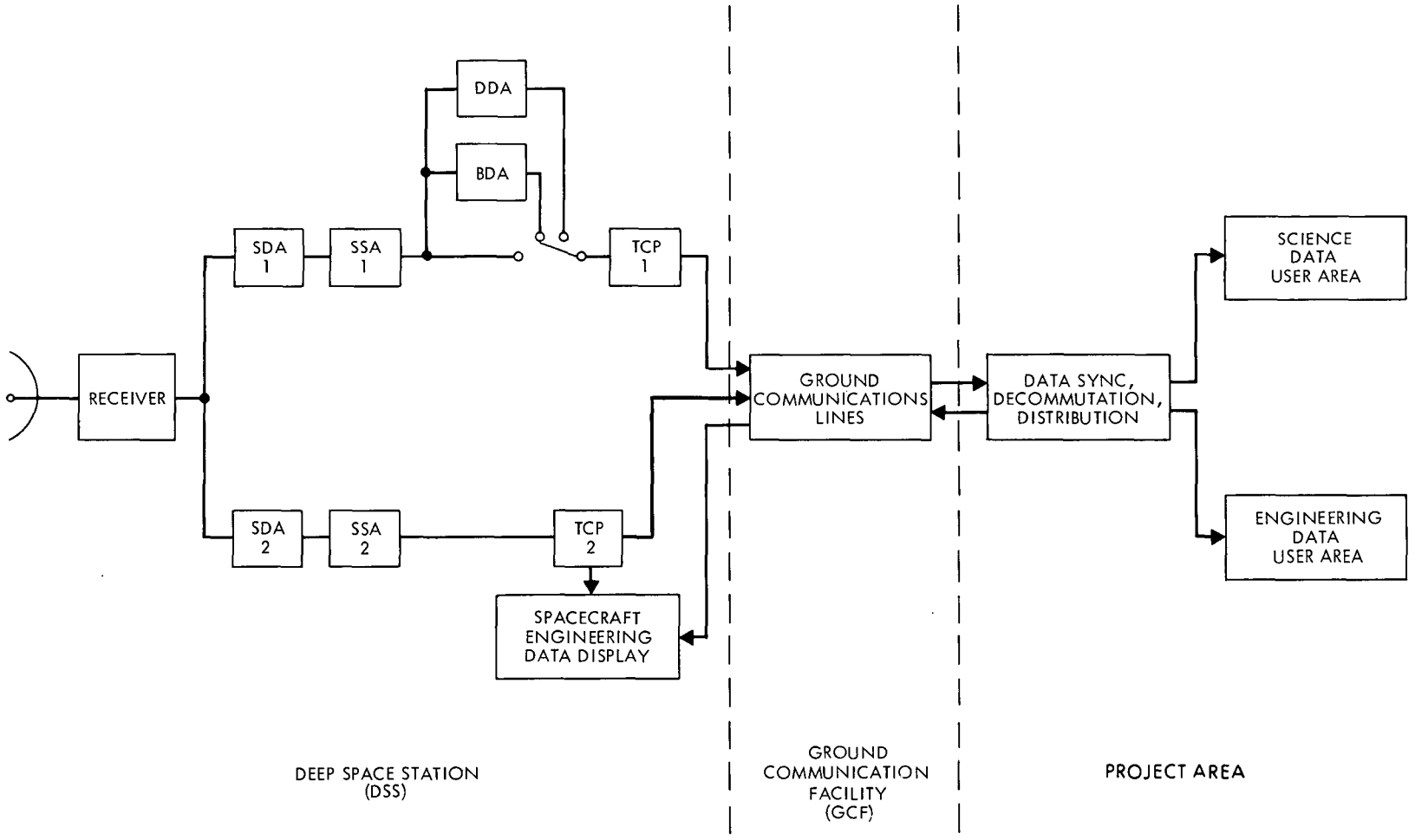

Fig. 5-73. Ground configuration for two-channel telemetry

The stations require spacecraft receiver static phase error (SPE) and uplink SNR to be available at the operations console of the DSS. This data is decommutated by the Project from the incoming telemetry stream and sent back over the GCF lines to the stations for display.

Figure 5-74 is a block diagram of the ground configuration necessary to support a one-channel telemetry system, in which only a single SDA, SSA, BDA, DDA, and TCP string is used.

5.7.5 Tradeoff Summary

To aid in comparing the one- versus two-channel system for any particular project, this section summarizes the advantages and disadvantages of each.

5.7.5.1 One-Channel System.

Advantages:

1) More efficient use of received total power (P_T/N_o).
2) Adverse tolerance due to modulator sensitivity changes is reduced.
3) Only one spacecraft subcarrier frequency required.
4) Only one spacecraft biphase modulator required.
5) No mixer-amplifier required. This reduces waveform distortion loss and improves the reliability of the TMU.
6) Only one SDA, SSA, BDA or DDA, and TCP is required in each DSS.
7) May reduce the number of operational modes and thereby reduce project testing.

Disadvantages:

1) Channel symbol-error rate for all types of data will be identical. Therefore, the lowest required symbol-error rate must be obtained for all data.

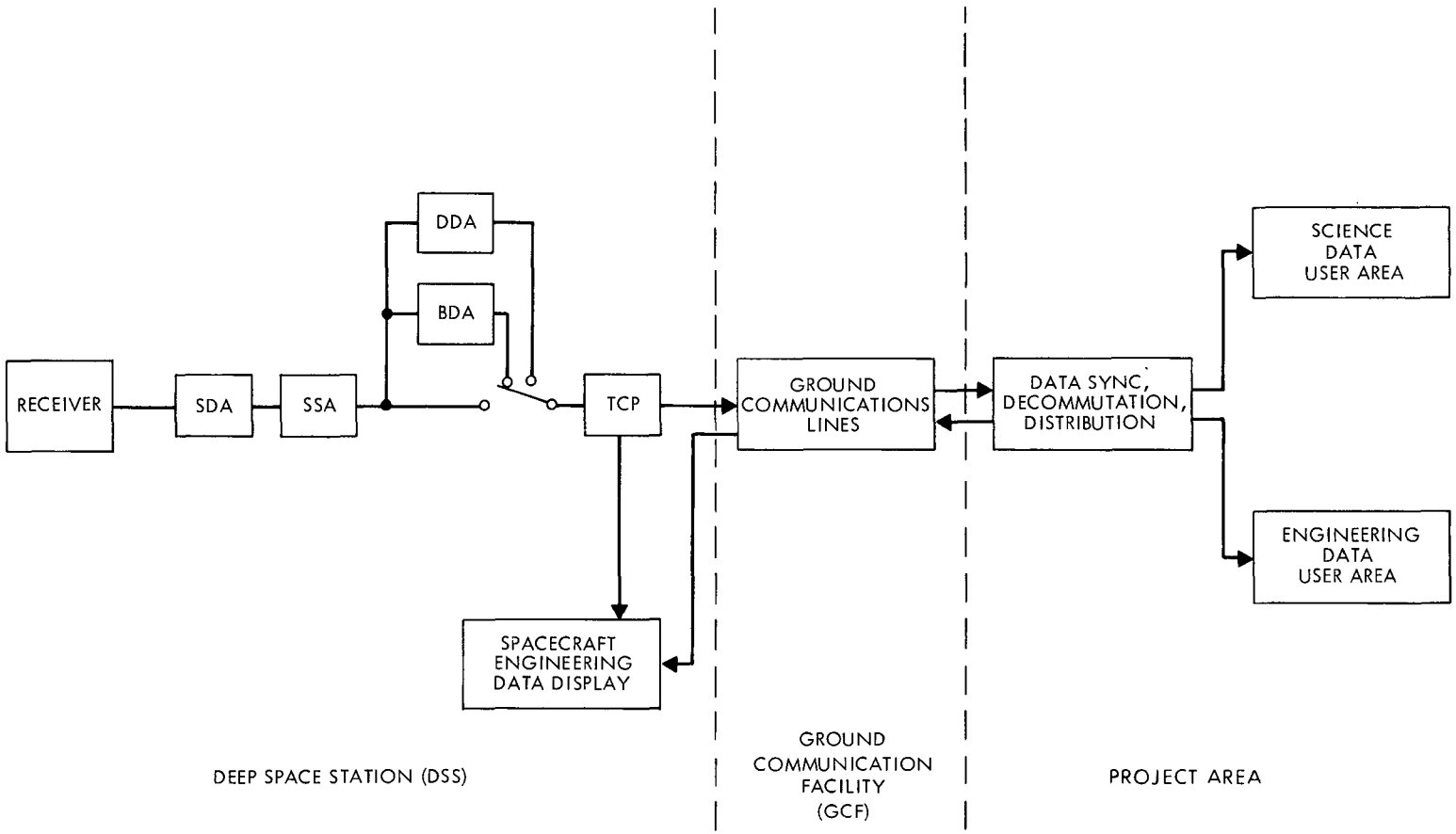

Fig. 5-74. Ground configuration for single-channel telemetry

2) When all science data is on one channel the data rates and bit error rates will be coupled. Some data will be of much better quality than necessary at the possible expense of data rate.

3) Concatenated coding may be required for some data, e.g., non-imaging data.

4) Specification of optimum mod index is more dependent on system loss model.

5.7.5.2 Two-Channel System.

Advantages:

1) Engineering data may be allocated its own subcarrier channel, thereby improving the reliability of the engineering data return.

2) Independent data rate control and independent data quality specifications are available to the users for each channel.

Disadvantages:

1) Mixer amplifier required on spacecraft.

2) More modulation indices required (i.e., more level set circuits).

3) More spacecraft operating modes to be tested.

4) Intermodulation losses and an extra channel's system losses make less efficient use of total received power (P_T/N_o).

5) Adverse tolerance in each channel is greater than in a one channel system due to the cross coupling of the modulation indices.

6) Requires two strings of SDA's, SSA's, BDA's or DDA's, TCP's and GCF lines in each DSS station. Twice as many racks of equipment must be maintained, checked out, calibrated, and operated than for one-channel telemetry.

REFERENCES

5-1. Tausworthe, R. C.; Theory and Practical Design of Phase-Locked Receivers, Volume I, Jet Propulsion Laboratory, Technical Report No. 32-819, February 15, 1966.

5-2. Viterbi, A. J.; Principles of Coherent Communications, McGraw-Hill (New York: 1966).

5-3. Murray, B. C., and Davies, M. E.: "Space Photography and the Exploration of Mars," Applied Optics, Vol. 9, No. 6, June 1970, pp. 1270-1281.

5-4. Golomb, Solomon W., ed; Digital Communications with Space Applications, Prentice Hall (Englewood Cliffs, N. J.: 1964).

Note: The bit error probabilities for biorthogonal codes of Appendix Four of reference 5-4 are incorrect in the first and second printings. Correct values may be found in the third and subsequent printings. Values presented in the tables here are correct.

5-5. Tausworthe, R. C., Easterling, M. F., and Spear, A. J.; A High-Rate Telemetry System for the Mariner Mars 1969 Mission, Jet Propulsion Laboratory Technical Report No. 32-1354, April 1969.

5-6. Shannon, C. E., and Weaver, W.; The Mathematical Theory of Communication, University of Illinois Press (Urbana, Ill.: 1949).

5-7. Hall, J. R., and Easterling, M.; "The Technology of Ground Stations in the Deep Space Network from 1958 to 1968," IEEE, Proc. of International Conference on Communications, Conference Record, Vol. 4, L. Winner, ed., Philadephia, Pa., June 12-14, 1968, pp. 576-585.

5-8. Deep Space Network/Flight Project Interface Design Handbook, Jet Propulsion Laboratory, 810-5, DSN Standard Practice.

5-9. Layland, J. W., "Information Systems: Performance of Short Constraint Length Convolutional Codes and a Heuristic Code-Construction Algorithm," Jet Propulsion Laboratory Space Program Summary 37-64, Vol. II, August 31, 1970, pp. 41-44.

5-10. Layland, J. W., "Information Systems: Multiple-Mission Sequential Decoder — Comparing Performance Among Three Rate 1/2, K = 32 Codes," Jet Propulsion Laboratory Space Programs Summary 37-64, Vol. II., August 31, 1970, pp. 50-52.

5-11. Heller, J. A., "Sequential Decoding: Short Constraint Length Convolutional Codes," Jet Propulsion Laboratory Space Programs Summary 37-54, Vol. III, December 31, 1968, pp. 171-177, and correction "Sequential Decoding: Improved Performance of Short Constraint Length Convolutional Codes," Jet Propulsion Laboratory Space Programs Summary 37-56, Vol. III, April 30, 1969, p. 83.

5-12. Wozencraft, J.M., and Jacobs, I.M., Principles of Communication Engineering, John Wiley & Sons (New York: 1965).

5-13. Forney, G.D., Jr., "Coding and Its Application in Space Communications," IEEE Spectrum, June 1970, pp. 47-58.

5-14. Heller, J.A., "Sequential Decoding: A Model for Buffer Overflow in Sequential Decoding," Jet Propulsion Laboratory Space Programs Summary 37-56, Vol. III, April 30, 1969, pp. 78-83.

5-15. Bucher, E.A., and Heller, J.A., "Error Probability Bounds for Systematic Convolutional Codes," IEEE Trans. Inform. Theory, Vol. IT-16, Mar. 1970, pp. 219-224.

5-16. Massey, J.L., and Costello, D.J., Jr., "Nonsystematic Convolutional Codes for Sequential Decoding in Space Applications," IEEE Trans. on Commun. Technology, Vol. COM-19, No. 5, Oct. 1971, pp. 806-813.

5-17. Layland, J.W., and Lushbaugh, W.A., "A Flexible High-Speed Sequential Decoder for Deep Space Channels," IEEE Trans. on Commun. Technology, Vol. COM-19, No. 5, Oct. 1971, pp. 813-820.

5-18. Viterbi, A.J., "Convolutional Codes and Their Performance in Communication Systems," IEEE Trans. on Commun. Technology, Vol. COM-19, No. 5, Oct. 1971, pp. 751-772.

5-19. Heller, J.A., and Jacobs, I.M., "Viterbi Decoding for Satellite and Space Communication," IEEE Trans. on Commun. Technology., Vol. COM-19, No. 5, Oct. 1971, pp. 835-848.

5-20. Forney, G.D., Concatenated Codes, M.I.T. Press (Cambridge, Mass.: 1966).

5-21. Codex Corporation, Final Report: A Study of Hybrid Sequential and Algebraic Decoding Techniques, Contract NAS2-4877, Jan. 1969.

5-22. Jelinek, F., and Cocke, J., "Bootstrap Hybrid Decoding for Symmetrical Binary Input Channels," Information and Control, March 1971.

5-23. Codex Corporation, Phase II Report: Coding for Deep Space Telemetry, Contract NAS2-2874, March 1966.

5-24. Falconer, D.D., "A Hybrid Coding Scheme for Discrete Memoryless Channels," Bell System Techn. J., Vol. 48, March 1969.

5-25. Odenwalter, J.P. "Concatenation of Convolutional and Block Codes," First NASA Coded Communications Conference, Jet Propulsion Laboratory, Pasadena, California, February 1970.

5-26. Hofmann, L.B., "Performance Results for a Hybrid Coding System," International Telem. Conf., Washington, D.C., September 1971.

5-27. Dorsch, B., and Miller, W., Error Control Using a Concatenanted Code, NASA TND-5775, June 1970.

5-28. McClure, J.P., "Ground Communications Facility 50-kbps Wideband Data Error Rate Test," Jet Propulsion Laboratory Technical Report 32-1526, Vol. VI, December 15, 1971, pp. 149-157.

5-29. Schwartz, M., Bennett, W.R., and Stein, S., Communication Systems and Techniques, McGraw-Hill (New York: 1966), pp. 63-68, 310-313.

5-30. Turin, G.L., "An Introduction to Matched Filters," IRE Trans. on Information Theory, June 1960.

5-31. Layland, J.W., "Information Systems: Synchronizability of Convolutional Codes;" Jet Propulsion Laboratory Space Programs Summary 37-64, Vol. II, August 31, 1970, pp. 44-50.

5-32. Layland, J.W., "An Optimum Buffer Management Strategy for Sequential Decoding," Jet Propulsion Laboratory Technical Report 32-1526, Vol. VI, December 15, 1971, pp. 106-111.

5-33. Helstrom, C.W., Statistical Theory of Signal Detection, 2nd Edition, Pergamon Press (Oxford: 1968).

5-34. Lindsey, W.C., A Theory for the Design of One-Way and Two-Way Phase-Coherent Communication Systems, Phase-Coherent Tracking Systems, Jet Propulsion Laboratory Technical Report No. 32-986, July 15, 1969.

5-35. Lindsey, W.C., Performance of Phase Coherent Receivers Preceded by Bandpass Limiters, Jet Propulsion Laboratory Technical Report No. 32-1162, 1967.

5-36. Papoulis, A., Probability, Random Variables and Stochastic Processes, McGraw-Hill (New York: 1965).

5-37. Layland, J.W., "Telemetry Bit Synchronization Loop," Jet Propulsion Laboratory Space Programs Summary 37-56, Vol. III, pp. 204-215.

5-38. Tausworthe, R.C., "Communications Systems Development: Efficiency of Noisy Reference Detection," Jet Propulsion Laboratory Space Programs Summary 37-54, Vol. III, pp. 195-201.

5-39. Rudin, W., Real and Complex Analysis, McGraw-Hill (New York: 1966).

5-40. Brockman, M.H., "MMTS: Performance of Subcarrier Demodulator," Jet Propulsion Laboratory Space Programs Summary 37-52, Vol. II. July 31, 1968, pp. 127-141.

5-41. Simon, M. K., "Nonlinear Analysis of an Absolute Value Type of an Early-Late Gate Bit Synchronizer," IEEE Trans. on Commun. Technol., Vol. COM-18, No. 5, October 1970, pp. 589-596.

5-42. Savant, C. J. Jr., Control Systems Design, McGraw-Hill (New York: 1964).

5-43. Levitt, B. K., "Interplex: An Analysis of Optimized Power Allocation for Two and Three Channel PSK/PM Telecommunications Systems," Jet Propulsion Laboratory Quarterly Technical Review, Vol. 2, No. 1, April 1972, pp. 143-151.

APPENDIX A5. 1

TELEMETRY SYSTEM LOSS ANALYSIS

A5. 1. 1 INTRODUCTION

As explained in section 5.4.5, "System Losses," the total loss is not necessarily the (dB) sum of the losses due to the radio, subcarrier demodulator, and symbol synchronizer. This appendix describes how the total system loss is computed, in general, and discusses the circumstances for which the total system loss can be approximated by the sum of the three subsystem losses.

A5. 1. 2 SYSTEM LOSS MODEL

In the following description, the symbol synchronizer is assumed to operate perfectly, since its effects can be added at the end. Thus, the model for detecting telemetry data is shown in Figure A5. 1-1. The signal received from space has coded or uncoded binary data, biphase modulated on a square-wave subcarrier which is phase modulated on a sinusoidal carrier. The radio tracks this input by means of a carrier phase locked loop (PLL) and sends an IF frequency version to the demodulator. The demodulator, usually called the Subcarrier Demodulator Assembly (SDA), extracts the baseband signal, consisting of data plus a Gaussian noise process, and sends it to the matched filter detector. In doing so, the SDA uses partially coherent carrier and subcarrier references, the latter being derived by a subcarrier PLL within the SDA. The detector then filters the SDA output and decides what was originally sent.

Because of this partially coherent demodulation, the signal level at the SDA output is lower than at the input. This signal level reduction increases the probability of detection error. The next section predicts these effects.

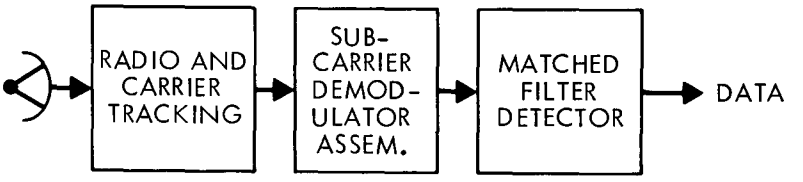

Fig. A5. 1-1. Telemetry system loss model

A5.1.3 PROBABILITY OF DETECTION ERROR

Consider the functional diagram of the demodulator shown in Figure A5.1-2. Single-channel telemetry adequately models the system losses so that the input signal is

$$S_i(t) = \sqrt{2}\,A \cos\left[\omega_c t + \theta_m m(t)\,sq(\omega_{sc}t)\right] + n_i(t) = \sqrt{2}\,A \cos\,\omega_c t \cos\theta_m + \sqrt{2}\,A\,m(t)\,\sin\omega_c t \sin\theta_m\,sq(\omega_{sc}t) + n_i(t),\ t\epsilon\,[0,\ T_s] \quad \text{(A5.1-1)}$$

where

ω_c, ω_{sc} = Carrier and subcarrier frequencies respectively

$m(t)$ = Binary data

θ_m = Data modulation angle

$sq(\omega_{sc}t)$ = Square wave subcarrier

$n_i(t)$ = Channel-added white Gaussian noise process with one-sided noise spectral density N_o (watts/Hz)

T_s = Symbol time (inverse of the symbol rate)

and ϵ indicates "is within the interval ..."

The carrier and subcarrier references are $\cos(\omega_c t + \phi_c(t))$ and $sq(\omega_{sc}t + \phi_{sc}(t))$, respectively, where $\phi_c(t)$, $\phi_{sc}(t)\epsilon[-\pi, \pi]$.

Carrying out the operations indicated in Figure A5.1-2 yields the baseband output signal

$$S_o(t) = A(\phi_c(t),\ \phi_{sc}(t))m(t) + n_o(t),\ t\epsilon\,[0,\ T_s] \quad \text{(A5.1-2)}$$

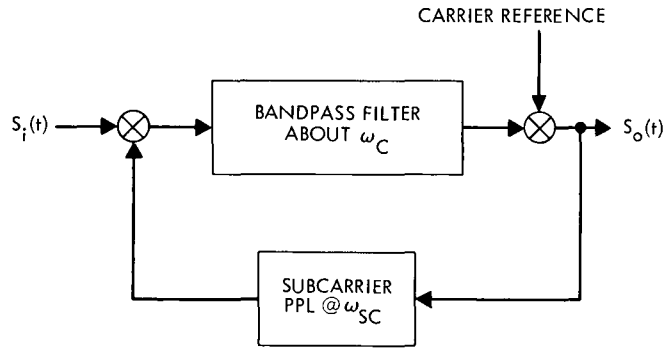

Fig. A5.1-2. Demodulator model

where

$$A(\phi_c(t), \phi_{sc}(t)) = A \cos \phi_c(t)\left(1 - \frac{2}{\pi} \mid \phi_{sc}(t) \mid\right), \; t\epsilon\left[0, T_s\right] \qquad \text{(A5.1-3)}$$

and $n_o(t)$ is the output band-limited noise process, assumed to be Gaussian and white with one-sided spectral density N_o.

Note that the true amplitude of $S_o(t)$, (A5.1-3), is less than or equal to the amplitude with no phase errors, A. It is this term that causes additional detection errors to be made.

For uncoded binary antipodal data*, and the detector of Figure A5.1-3, the probability of bit error is:

$$P_{BE} = \frac{1}{2} \operatorname{erfc}\left(\frac{\bar{g}}{4}\sqrt{\frac{N_o}{T_B}}\right) \qquad \text{(A5.1-4)}$$

where

$$\bar{g} = \frac{4}{N_o}\int_0^{T_B} A\left(\phi_c(t), \phi_{sc}(t)\right) dt \qquad \text{(A5.1-5)}$$

is the mean of the input to the decision device (see references 5-33 and 5-34), and T_B = bit time.

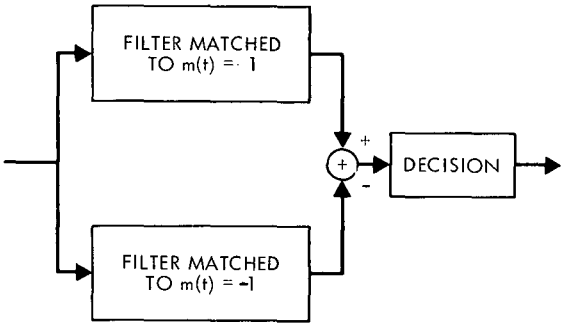

Fig. A5.1-3. Detector model

*The results for coded data are easily extended by using the appropriate error probabilities and symbol or word time in place of bit time.

Note that if there are no phase errors, then (A5.1-4) reduces to the familiar form

$$P_{BE} = \frac{1}{2}\,\mathrm{erfc}\left(\sqrt{\frac{A^2 T_B}{N_o}}\right) \qquad \text{(A5.1-6)}$$

The problem of evaluating (A5.1-4) and (A5.1-5) is discussed next.

A5.1.4 LIMITING CASES

There are three limiting cases in which (A5.1-4) and (A5.1-5) can be written explicitly. These cases depend on whether T_B is greater or less than the response times of the two PLL's, where loop response time is given by

$$T_R = \frac{1}{B_L} \qquad \text{(A5.1-7)}$$

and where B_L is the one-sided loop bandwidth (see reference 5-36).

A5.1.4.1 Case I: Bit Time Much Greater Than Carrier and Subcarrier PLL Response Times.

If the bit rate is very small so that $T_B >> T_{R_C}$ and $T_B >> T_{R_{sc}}$, then the two phase errors will vary rapidly over the interval $[0,\ T_B]$. Hence, assuming $\phi_c(t)$ and $\phi_{sc}(t)$ to be ergodic processes (reference 5-36), (A5.1-5) becomes:

$$\bar{g} = \frac{4}{N_o} E\left[A\left(\phi_c(t),\ \phi_{sc}(t)\right)\right] T_B \qquad \text{(A5.1-8)}$$

where E denotes mathematical expectation. Then (A5.1-4) becomes:

$$\bar{P}_{BE} = \frac{1}{2}\,\mathrm{erfc}\left(E\left[A\left(\phi_c(t),\ \phi_{sc}(t)\right)\right]\sqrt{\frac{T_B}{N_o}}\right) \qquad \text{(A5.1-9)}$$

A5.1.4.2 Case II: Bit Time Much Less Than Carrier and Subcarrier PLL Response Times.

If the bit rate is so large as to make $T_B \ll T_{R_C}$ and $T_B \ll T_{R_{sc}}$, then the phase errors will be nearly constant over $[0, T_B]$. Thus, (A5.1.5) will be

$$\bar{g} = \frac{4}{N_o} A(\phi_c, \phi_{sc}) T_B \tag{A5.1-10}$$

where ϕ_c and ϕ_{sc} are the constant realizations of the stochastic processes $\{\phi_c(t),\ 0 \le t \le T_B\}$ and $\{\phi_{sc}(t),\ 0 \le t \le T_B\}$, respectively. In this case, then (A5.1-4) is a random variable which depends on the random variables ϕ_c and ϕ_{sc}, hence,

$$\bar{P}_{BE} = E\left[\frac{1}{2}\,\mathrm{erfc}\left(A(\phi_c, \phi_{sc})\sqrt{\frac{T_B}{N_o}}\right)\right] \tag{A5.1-11}$$

A5.1.4.3 Case III: Bit Time Much Greater Than Carrier and Much Less Than Subcarrier PLL Response Times.

Since the bandwidth of the subcarrier loop is one to three orders of magnitude smaller than the carrier loop bandwidth, some low bit rate might make $T_B \gg T_{R_C}$ while $T_B \ll T_{R_{sc}}$. Then (A5.1-5) would be:

$$\bar{g} = \frac{4}{N_o} E_{\phi_c}\left[A(\phi_c(t), \phi_{sc})\right] T_B \tag{A5.1-12}$$

where E_{ϕ_c} stands for expectation with respect to $\phi_c(t)$. Thus, (A5.1-4) would be

$$P_{BE} = E_{\phi_{sc}}\left[\frac{1}{2}\,\mathrm{erfc}\left(E_{\phi}\left[A(\phi_c(t), \phi_{sc}(t))\right]\sqrt{\frac{T_B}{N_o}}\right)\right] \tag{A5.1-13}$$

A5.1.4.4 Bit Timing Error.

At this point, it is convenient to include the effects of a bit timing error (see reference 5-37). We assume data of 50% transition density so that such an error causes the integral in (A5.1-5) to be evaluated from 0 to $T_B' =$

$T_B(1 - 2|\tau|)$ where τ represents the timing error in fractions of the bit duration T_B and is a mixed random variable * with range $[-1/2, 1/2]$. Mathematically, this causes T_B to be replaced by T_B' in all equations following (A5.1-4). Furthermore, the error probabilities are now random variables and must be averaged over the distribution of τ. Defining

$$\left(\frac{ST_B}{N_o}\right)_{in} \triangleq \frac{A^2 T_B}{N_o} \tag{A5.1-14}$$

then the average error probabilities for the three limiting cases are:

Case I: $T_B \gg T_{R_C}$, $T_B \gg T_{R_{sc}}$

$$\overline{P}_{BE_I} = \frac{1}{2} E_\tau \left[\operatorname{erfc}\left(E_{\phi_c, \phi_{sc}} \left[\cos\phi_c \left(1 - \frac{2}{\pi}|\phi_{sc}|\right)\right] \sqrt{\left(\frac{ST_B}{N_o}\right)_{in} (1-2|\tau|)} \right) \right] \tag{A5.1-15}$$

Case II: $T_B \ll T_{R_C}$, $T_B \ll T_{R_{sc}}$

$$\overline{P}_{BE_{II}} = \frac{1}{2} E_{\tau, \phi_c, \phi_{sc}} \left[\operatorname{erfc}\left(\cos\phi_c \left(1 - \frac{2}{\pi}|\phi_{sc}|\right) \sqrt{\left(\frac{ST_B}{N_o}\right)_{in} (1-2|\tau|)} \right) \right] \tag{A5.1-16}$$

Case III: $T_B \gg T_{R_C}$, $T_B \ll T_{R_{sc}}$

$$\overline{P}_{BE_{III}} = \frac{1}{2} E_{\tau, \phi_{sc}} \left[\operatorname{erfc}\left(E_{\phi_c}\left[\cos\phi_c\right] \left(1 - \frac{2}{\pi}|\phi_{sc}|\right) \sqrt{\left(\frac{ST_B}{N_o}\right)_{in} (1-2|\tau|)} \right) \right] \tag{A5.1-17}$$

* τ is either zero over $[0, T_B]$ with probability 1/2 or it is some other value between -1/2 and +1/2 with density function $p'(\tau)/2$ (see references 5-37 and 5-41).

A5.1.5 SIGNAL ENERGY-TO-NOISE SPECTRAL DENSITY LOSS AND INTERPOLATION

ST_B/N_o loss is defined in the following way (see reference 5-38): Let the error probability of the telemetry system as a function of input ST_B/N_o be denoted by $P_e\left((ST_B/N_o)_{in}\right)$. Let $(ST_B/N_o)_{eq.}$ be the value of signal energy-to-noise spectral density ratio which, when inputted to a perfectly coherent system, yields an error probability equal to $\overline{P}_e\left((ST_B/N_o)_{in}\right)$. From (A5.1-6) then:

$$\frac{1}{2}\ \text{erfc}\left(\sqrt{(ST_B/N_o)_{eq.}}\right) = \overline{P}_{BE}\left((ST_B/N_o)_{in}\right) \qquad \text{(A5.1-18)}$$

Hence

$$(ST_B/N_o)_{eq.} = \left\{\text{erfc}^{-1}\left[2\,\overline{P}_{BE}\left((ST_B/N_o)_{in}\right)\right]\right\}^2 \qquad \text{(A5.1-19)}$$

Finally, the efficiency, or ST_B/N_o loss is defined by

$$\eta = \frac{(ST_B/N_o)_{eq.}}{(ST_B/N_o)_{in}} = \frac{1}{(ST_B/N_o)_{in}}\left\{\text{erfc}^{-1}\left[2\,\overline{P}_{BE}\left((ST_B/N_o)_{in}\right)\right]\right\}^2 \qquad \text{(A5.1-20)}$$

Now let η_I, η_{II}, η_{III} be the ST_B/N_o losses corresponding to the three limiting cases of error probability. For the operating SNR's required for the carrier and subcarrier tracking loops, the probability of $|\phi_c|$ and/or $|\phi_{sc}|$ exceeding $\pi/2$ is very small. If we neglect these probabilities, then the arguments of the bit error probabilities are always positive. Since erfc of a positive argument is a convex function, then by Jensen's inequality (see reference 5-39):

$$P_{BE_{II}} \geq P_{BE_{III}} \geq P_{BE_I} \qquad \text{(A5.1-21)}$$

hence, by (A5.1-20)

$$\eta_{II} \leq \eta_{III} \leq \eta_I \qquad \text{(A5.1-22)}$$

Since the three probabilities in (A5.1-21) are only limiting cases, $\overline{P}_{BE}\left((ST_B/N_o)_{in}\right)$ must be either in the range

$$P_{BE_I} \leq \overline{P}_{BE}\left((ST_B/N_o)_{in}\right) \leq P_{BE_{III}}$$

or in

$$P_{BE_{III}} \leq \overline{P}_{BE}\left((ST_B/N_o)_{in}\right) \leq P_{BE_{II}}$$

These ranges correspond to the following two ranges of η:

$$\eta_I \geq \eta \geq \eta_{III} \tag{A5.1-23}$$

or

$$\eta_{III} \geq \eta \geq \eta_{II} \tag{A5.1-24}$$

Whether η satisfies (A5.1-23) or (A5.1-24) depends on the relative values of T_B, T_{R_C}, and $T_{R_{sc}}$ (see section A5.1.4).

The limiting values of η can be computed if the joint probability density of ϕ_c, ϕ_{sc}, and τ is known, and the true value of η can be approximated by interpolation. Tausworthe (reference 5-38) has devised two interpolation schemes which apply here. For all bit rates such that T_B ranges from

$$T_B \ll T_{R_C} \ll T_{R_{sc}}$$

to

$$T_{R_C} \ll T_B \ll T_{R_{sc}}$$

η is given by

$$\eta = (1 - a_c)\eta_{II} + a_c\eta_{III} \tag{A5.1-25}$$

where

$$a_c = \frac{\delta_c}{4}\left[1 - \frac{\delta_c}{8}\left(1 - e^{-8/\delta_c}\right)\right] \tag{A5.1-26}$$

and

$$\delta_c = \frac{T_{R_C}}{T_B} \tag{A5.1-27}$$

For all bit rates such that T_B ranges from

$$T_{R_C} \ll T_B \ll T_{R_{sc}}$$

to

$$T_{R_C} \ll T_{R_{sc}} \ll T_B$$

η is given by

$$\eta = (1 - a_{sc})\eta_{III} + a_{sc}\eta_I \tag{A5.1-28}$$

where

$$a_{sc} = \frac{0.09135\,\delta_{sc} + \delta_{sc}^2}{1 + 3.3718\,\delta_{sc} + \delta_{sc}^2} \tag{A5.1-29}$$

and

$$\delta_{sc} = \frac{T_{R_{sc}}}{T_B} \tag{A5.1-30}$$

A5.1.6 VALIDITY OF SUMMING LOSS CONTRIBUTIONS

In general,

$$\eta = h\left(E_{\phi_c,\ \phi_{SC},\tau}\left[f(\phi_c,\ \phi_{SC},\ \tau)\right]\right)$$

where the functions $f(\cdot)$ and $h(\cdot)$ have been defined implicitly above. We compute total system loss by the equation

$$\eta_S = \eta_{RL}\,\eta_{SDL}\,\eta_{BSDL}$$

where

$$\eta_{RL} \triangleq h\left(E_{\phi_c,}\left[f(\phi_c,\ 0,\ 0)\right]\right)$$

$$\eta_{SDL} \triangleq h\left(E_{\phi_{SC}}\left[f(0,\ \phi_{SC},\ 0)\right]\right)$$

and

$$\eta_{BSDL} \triangleq h\left(E_{\tau}\left[f(0,\ 0,\ \tau)\right]\right)$$

It is clear that, in general, $\eta_S \neq \eta$. However, we can show that, in certain circumstances η_S is an upper bound on system efficiency (lower bound on radio loss). To show this, we make the assumption that reduction of the jitter of any system loop increases the system efficiency. Thus, we write

$$\eta \leq h\left(E_{\phi_c,\ \phi_{SC}}\left[f(\phi_c,\ \phi_{SC},\ 0)\right]\right) \leq \eta_{RL} \qquad \text{(A5.1-31)}$$

Then

$$\eta = h\left(E_{\phi_c,\ \phi_{SC}}\left[f(\phi_c,\ \phi_{SC},\ 0)\right]\right)\left(1 - \delta_1\right) \qquad \text{(A5.1-32)}$$

where $\delta_1 \geq 0$.

But, if $\eta_{BSDL} \geq (1 - \delta_1)$ (A5.1-33)

then

$$\eta \leq h\left(E_{\phi_c,\ \phi_{SC}}\left[f(\phi_c,\ \phi_{SC},\ 0)\right]\right)\ \eta_{BSDL} \tag{A5.1-34}$$

Similarly, from equation (A5.1-31)

$$h\left(E_{\phi_c,\ \phi_{SC}}\left[f(\phi_c,\ \phi_{SC},\ 0)\right]\right) = \eta_{RL}\ (1 - \delta_2) \tag{A5.1-35}$$

where $\delta_2 \geq 0$

So that, if $\eta_{SDL} \geq (1 - \delta_2)$ (A5.1-36)

and $$h\left(E_{\phi_c,\ \phi_{SC}}\left[f(\phi_c,\ \phi_{SC},\ 0)\right]\right) \leq \eta_{RL}\ \eta_{SDL} \tag{A5.1-37}$$

Thus, combining equations (A5.1-34) and (A5.1-37)

$$\eta \leq \eta_{RL}\ \eta_{SDL}\ \eta_{BSDL} = \eta_S \tag{A5.1-38}$$

for $\eta_{SDL} \geq (1 - \delta_2)$ and $\eta_{BSDL} \geq (1 - \delta_1)$.

So that as η_{SDL} and η_{BSDL} approach 1, we may expect that η_S will become a good approximation to η. However, since we do not know δ_1 and δ_2 at the present state of theory, it is vital to accurately measure system efficiency on actual hardware to provide realistic performance prediction and analysis. For design, however, we must approximate η, therefore we proceed to give the equations used to calculate η_{RL}, η_{SDL}, and η_{BSDL}.

A5.1.6.1 Radio Loss

η_{RL} is usually called radio loss. From sections A5.1.4 and A5.4.5, the error probabilities are

$$\overline{P}_{BE_{HI}}\left[\left(\frac{ST_B}{N_o}\right)_{in}\right] = \frac{1}{2} E\left[\operatorname{erfc}\left(\cos\phi_c\sqrt{\left(\frac{ST_B}{N_o}\right)_{in}}\right)\right]$$

$$= \frac{1}{2}\int_{-\pi}^{\pi} p(\phi_c)\operatorname{erfc}\left(\cos\phi_c\sqrt{(ST_B/N_o)_{in}}\right) d\phi_c$$

$$T_B \ll T_{R_C} \qquad \text{(A5.1-39)}$$

and

$$\overline{P}_{BE_{LOW}}\left[\left(\frac{ST_B}{N_o}\right)_{in}\right] = \frac{1}{2}\operatorname{erfc}\left(E(\cos\phi_c)\sqrt{\left(\frac{ST_B}{N_o}\right)_{in}}\right)$$

$$T_B \gg T_{R_C} \qquad \text{(A5.1-40)}$$

where

$$E\left[\cos\phi_c\right] = \int_{-\pi}^{\pi}\cos\phi_c p(\phi_c)\, d\phi_c$$

From section A5.1.5 the efficiencies are

$$\eta_{HI} = \frac{1}{(ST_B/N_o)_{in}}\left\{\operatorname{erfc}^{-1}\left[2\overline{P}_{BE_{HI}}\left((ST_B/N_o)_{in}\right)\right]\right\}^2 \qquad \text{(A5.1-41)}$$

and

$$\eta_{LOW} = E^2\left[\cos\phi_c\right] \tag{A5.1-42}$$

Finally,

$$\eta(\phi_c) = (1 - a_c)\,\eta_{LOW} + a_c\eta_{HI} \tag{A5.1-43}$$

where a_c is given in section A5.1.5.

A5.1.6.2 Subcarrier Demodulator Loss

SDA loss is defined as η_{SDL}. The error probabilities are

$$\overline{P}_{BE_{HI}}\left[\left(\frac{ST_B}{N_o}\right)_{in}\right] = \frac{1}{2}\int_{-\pi}^{\pi} p(\phi_{SC})\,\mathrm{erfc}\left(\left(1 - \frac{2}{\pi}\left|\phi_{SC}\right|\right)\sqrt{\left(\frac{ST_B}{N_o}\right)_{in}}\right)d\phi_{SC}$$

$$T_B \ll T_{R_{SC}} \tag{A5.1-44}$$

and

$$\overline{P}_{BE_{LOW}}\left[\left(\frac{ST_B}{N_o}\right)_{in}\right] = \frac{1}{2}\,\mathrm{erfc}\left(E\left[1 - \frac{2}{\pi}\left|\phi_{SC}\right|\right]\sqrt{\left(\frac{ST_B}{N_o}\right)_{in}}\right)$$

$$T_B \gg T_{R_{SC}} \tag{A5.1-45}$$

The efficiencies are given by

$$\eta_{HI} = \frac{1}{(ST_B/N_o)_{in}}\left\{\mathrm{erfc}^{-1}\left[2P_{BE_{HI}}\left((ST_B/N_o)_{in}\right)\right]\right\}^2 \tag{A5.1-46}$$

and

$$\eta_{LOW} = E^2 \left[1 - \frac{2}{\pi} \left| \phi_{SC} \right| \right] \qquad \text{(A5.1-47)}$$

Finally

$$\eta(\phi_{sc}) = (1 - a_{sc})\, \eta_{LOW} + a_{sc} \eta_{HI} \qquad \text{(A5.1-48)}$$

A5.1.6.3 Symbol Sync and Detection Loss

The loss in SNR due to a timing error is η_{BSDL}. In this case there is only one probability of error, namely

$$\begin{aligned} \overline{P}_{BE}\left((ST_B/N_o)_{in} \right) &= \frac{1}{2} E \left[\operatorname{erfc} \left(\sqrt{(ST_B/N_o)_{in} (1 - 2|\tau|)} \right) \right] \\ &= \frac{1}{4} \int_{-1/2}^{1/2} p(\tau) \operatorname{erfc} \left(\sqrt{(ST_B/N_o)_{in} (1 - 2|\tau|)} \right) d\tau \\ &\quad + \frac{1}{4} \operatorname{erfc} \left(\sqrt{(ST_B/N_o)_{in}} \right) \end{aligned} \qquad \text{(A5.1-49)}$$

and one efficiency

$$\eta(\tau) = \frac{1}{(ST_B/N_o)_{in}} \left\{ \operatorname{erfc}^{-1} \left[2\overline{P}_{BE}\left((ST_B/N_o)_{in} \right) \right] \right\}^2 \qquad \text{(A5.1-50)}$$

APPENDIX A5.2

MAXIMUM DATA RATES FOR PCM/PM TELEMETRY SYSTEMS WITH SQUARE-WAVE SUBCARRIERS

A5.2.1 INTRODUCTION

This appendix evaluates the maximum data rates given in section 5.5.1 for several examples of PCM/PM telemetry systems with square-wave subcarriers as they are used on Mariner-type spacecraft, and presents parametric graphs of these maximum data rates.

A5.2.2 SINGLE-CHANNEL PCM/PM WITH SQUARE-WAVE SUBCARRIER

The ratio of data power to total power for data, biphase modulated onto a square-wave subcarrier and phase-modulated onto an rf carrier is

$$\frac{P_D}{P_T} = \sin^2\theta$$

Thus,

$$D_{Rmax} = \frac{(P_T/N_o)\,(\sin^2\theta)\eta_S}{(ST_B/N_o)_{TH}} \qquad \text{(A5.2-1)}$$

Figure A5.2-1 presents D_{Rmax} versus θ in the one-way mode for various P_T/N_o values for uncoded data. $(ST_B/N_o)_{TH}$ is chosen as 5.2 dB, representing an error rate of 0.005.

Figure A5.2-2 presents D_{Rmax} versus θ in the one-way mode for various P_T/N_o values for block coded data. The word error rate is fixed at 0.01.

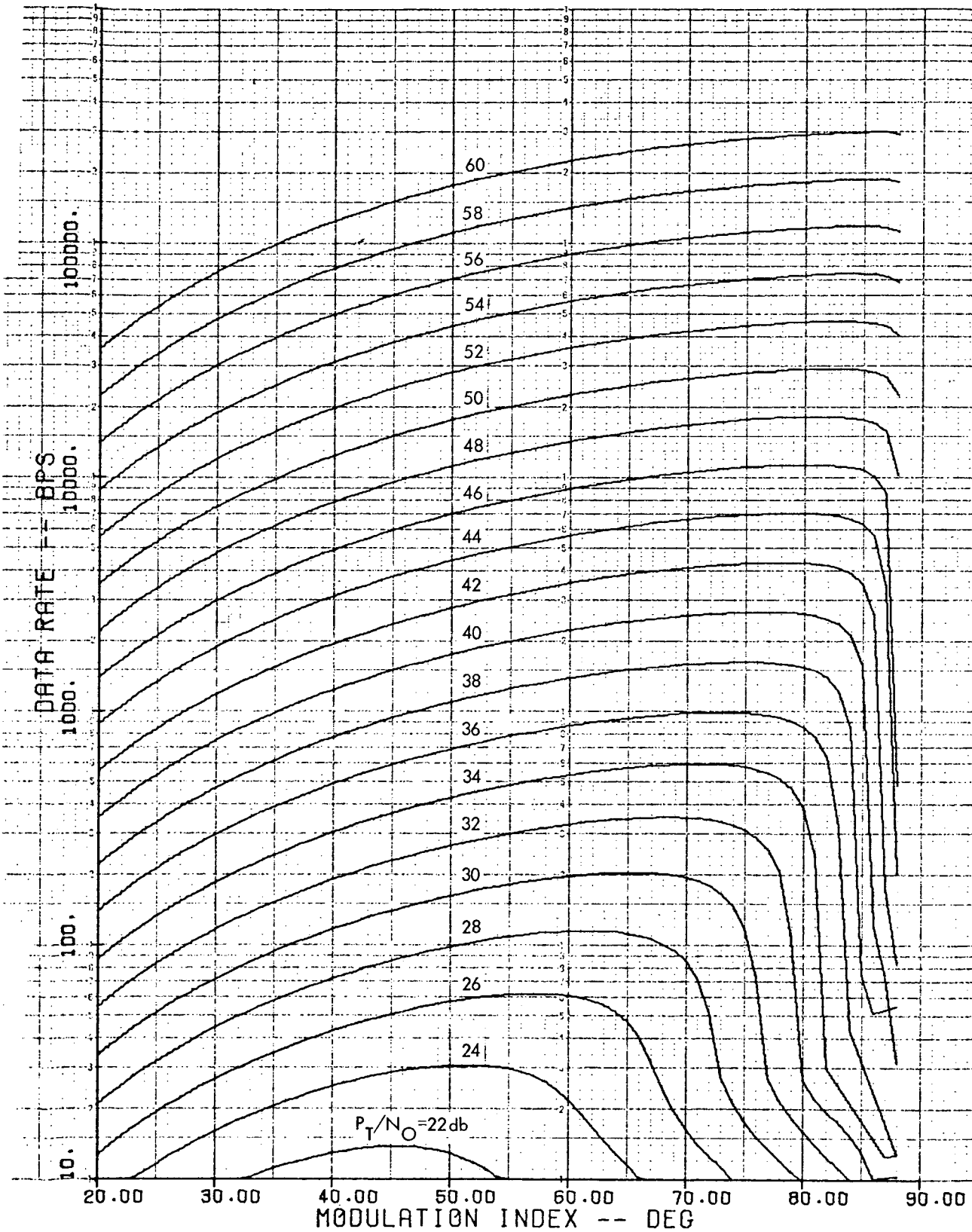

Fig. A5.2-1. Single-channel available data rate vs modulation index, uncoded data, BER = .005

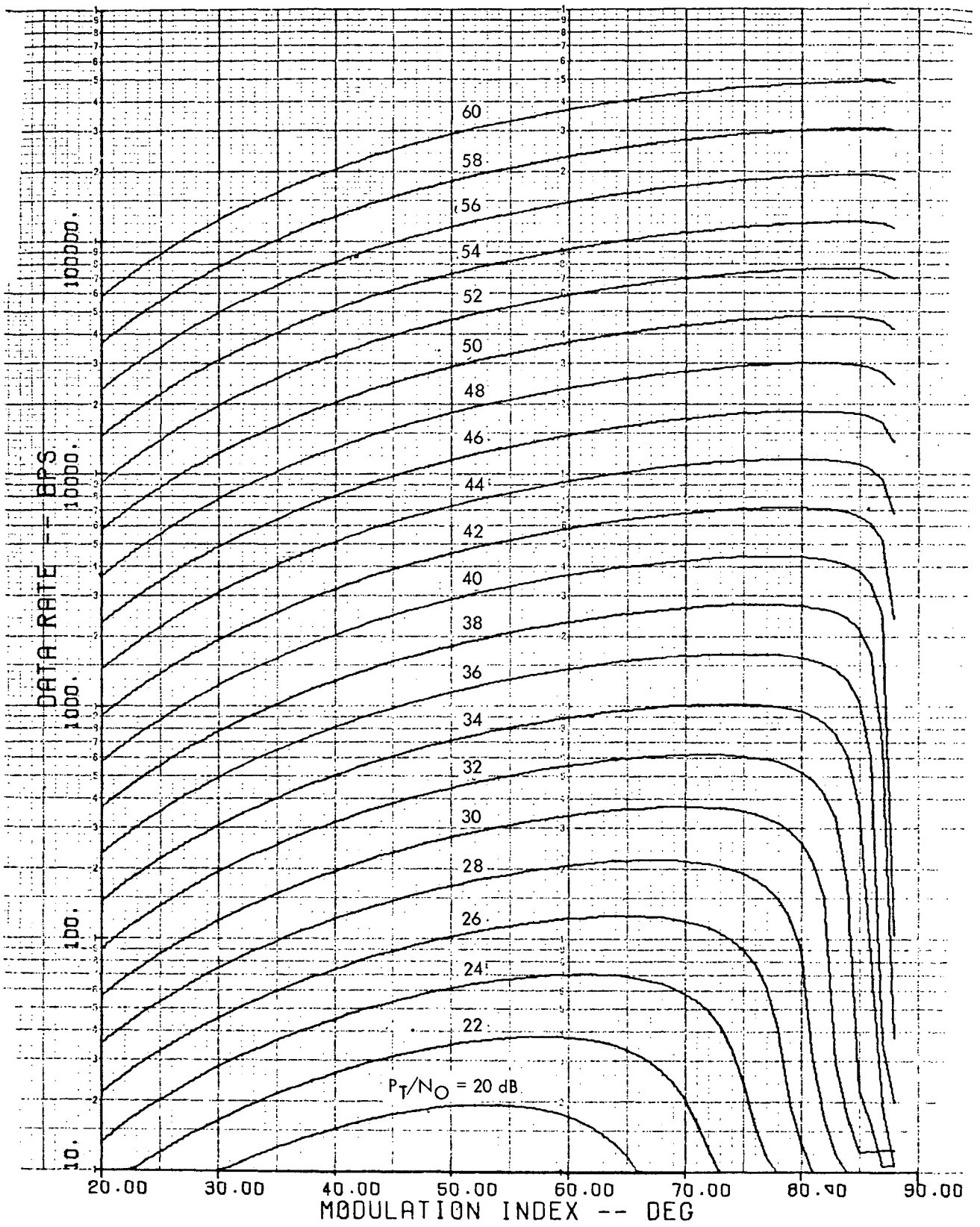

Fig. A5.2-2. Single-channel available data rate vs modulation index, (32, 6) block coded data, WER= .01

A5.2.3 TWO-CHANNEL PCM/PM MODULATION WITH SQUARE-WAVE SUBCARRIERS

The ratios of data power to total power for two channels of data, biphase modulated onto two square-wave subcarriers and phase-modulated onto an rf carrier are:

$$\frac{P_{D_1}}{P_T} = \sin^2\theta_1 \cos^2\theta_2$$

$$\frac{P_{D_2}}{P_T} = \sin^2\theta_2 \cos^2\theta_1$$

Thus,

$$D_{R_{1max}} = \frac{(P_T/N_o)\left(\sin^2\theta_1 \cos^2\theta_2\right)\eta_{S_1}}{(ST_B/N_o)_{TH_1}} \qquad \text{(A5.2-2)}$$

and

$$D_{R_{2max}} = \frac{(P_T/N_o)\left(\sin^2\theta_2 \cos^2\theta_1\right)\eta_{S_2}}{(ST_B/N_o)_{TH_2}} \qquad \text{(A5.2-3)}$$

A5.2.4 SINGLE-CHANNEL PCM/PM MODULATION WITH SQUARE-WAVE SUBCARRIER AND RANGING

The ratio of data power to total power for a single data-channel, biphase modulated on a square-wave subcarrier and phase-modulating an rf carrier simultaneously with ranging is

$$\frac{P_D}{P_T} = \sin^2\theta \cos^2\theta_R$$

where θ_R = Ranging modulation index.

The maximum data rate is

$$D_{Rmax} = \frac{(P_T/N_o)\left(\sin^2\theta \cos^2\theta_R\right)\eta_S}{(ST_B/N_o)_{TH}} \qquad \text{(A5.2-4)}$$

where $(ST_B/N_o)_{TH}$ is the required value for the data channel.

If the uplink SNR is very high, η_S can be modeled using one-way radio loss. Then, the results are identical to those of section A5.2.3 if θ is substituted for θ_1 and θ_R is substituted for θ_2.

A5.2.5 TWO-CHANNEL PCM/PM MODULATION WITH SQUARE-WAVE SUBCARRIERS AND RANGING

The ratios of data power to total power for two data channels, biphase modulated onto square-wave subcarriers and then phase-modulating an rf carrier simultaneously with ranging is

$$\frac{P_{D_1}}{P_T} = \sin^2\theta_1 \cos^2\theta_2 \cos^2\theta_R$$

$$\frac{P_{D_2}}{P_T} = \sin^2\theta_2 \cos^2\theta_1 \cos^2\theta_R$$

The maximum data rates are

$$D_{R_{1max}} = \frac{(P_T/N_o)\left(\sin^2\theta_1 \cos^2\theta_2 \cos^2\theta_R\right)\eta_{S_1}}{(ST_B/N_o)_{TH_1}} \qquad \text{(A5.2-5)}$$

$$D_{R_{2max}} = \frac{(P_T/N_o)\left(\sin^2\theta_2 \cos^2\theta_1 \cos^2\theta_R\right)\eta_{S_2}}{(ST_B/N_o)_{TH_2}} \qquad \text{(A5.2-6)}$$

If the uplink SNR is very high, $\eta_{S_{1,2}}$ can be modeled using one-way radio loss. Then the data rates of section A5.2.3 for two-channel telemetry will be degraded by the ranging suppression, $\cos^2\theta_R$.

A5.2.6 TWO-CHANNEL PCM/PM INTERPLEX MODULATION WITH SQUARE-WAVE SUBCARRIERS

The ratios of data power to total power for two channels of data, biphase modulated onto two square-wave subcarriers, interplexed, and phase-modulated onto an rf carrier are:

$$\frac{P_{D_L}}{P_T} = \sin^2\theta_L \sin^2\theta_H$$

$$\frac{P_{D_H}}{P_T} = \sin^2\theta_H \cos^2\theta_L$$

where $\theta_H > \theta_L$, and $\theta_H > 45°$.

Thus,

$$D_{R_{Hmax}} = \frac{(P_T/N_o)\left(\sin^2\theta_H \cos^2\theta_L\right)\eta_{S_H}}{(ST_B/N_o)_{TH_H}} \qquad \text{(A5.2-7)}$$

$$D_{R_{Lmax}} = \frac{(P_T/N_o)\left(\sin^2\theta_L \sin^2\theta_H\right)\eta_{S_L}}{(ST_B/N_o)_{TH_L}} \qquad \text{(A5.2-8)}$$

A5.2.7 TWO-CHANNEL PCM/PM DATA INTERPLEXED WITH SQUARE-WAVE SUBCARRIERS AND WITH RANGING

The ratios of data power to total power for two channels of data, biphase modulated onto two square-wave subcarriers, interplexed, and phase-modulated onto an rf carrier simultaneously with ranging are:

$$\frac{P_{D_L}}{P_T} = \sin^2\theta_L \sin^2\theta_H \cos^2\theta_R$$

$$\frac{P_{D_H}}{P_T} = \sin^2\theta_H \cos^2\theta_L \cos^2\theta_R$$

where $\theta_H > \theta_L$, and $\theta_H > 45°$.

Thus,

$$D_{R_{Hmax}} = \frac{(P_T/N_o)\left(\sin^2\theta_H \cos^2\theta_L \cos^2\theta_R\right)\eta_{S_H}}{(ST_B/N_o)_{TH_H}} \qquad \text{(A5.2-9)}$$

$$D_{R_{Lmax}} = \frac{(P_T/N_o)\left(\sin^2\theta_H \sin^2\theta_L \cos^2\theta_R\right)\eta_{S_L}}{(ST_B/N_o)_{TH_L}} \qquad \text{(A5.2-10)}$$

If the uplink SNR is very high, η_S can be modeled using one-way radio loss. Then the data rates of section A5.2.6 for two-channel interplexed telemetry will be degraded by the ranging suppression, $\cos^2\theta_R$.

APPENDIX A5.3

OPTIMUM MODULATION ANGLES FOR A TWO-CHANNEL TELEMETRY SYSTEM WITH SQUARE-WAVE SUBCARRIERS AT HIGH P_T/N_o

A5.3.1 MAXIMIZATION OF CHANNEL 2 DATA RATE FOR A GIVEN P_T/N_o

The problem is to maximize

$$D_{R_2} = \frac{(P_T/N_o)\left(\sin^2\theta_2 \cos^2\theta_1\right)\eta_{S_2}}{(ST_B/N_o)_2} \tag{A5.3-1}$$

with respect to θ_1 and θ_2

$$\left(\frac{\partial D_{R_2}}{\partial\theta_1} = \frac{\partial D_{R_2}}{\partial\theta_2} = 0\right)$$

subject to the constraint

$$D_{R_1} = \frac{(P_T/N_o\left(\cos^2\theta_2 \sin^2\theta_1\right)\eta_{S_1}}{(ST_B/N_o)_1} \tag{A5.3-2}$$

and with the condition that P_T/N_o is very large, so that $\eta_{S_1} = \eta_{S_2} = 1$.

We incorporate (A5.3-2) into (A5.3-1) to get the unconstrained relations:

$$D_{R_2} = \frac{(P_T/N_o)\left[1 - \dfrac{D_{R_1}(ST_B/N_o)_1}{(P_T/N_o)\sin^2\theta_1}\right]\cos^2\theta_1}{(ST_B/N_o)_2} \tag{A5.3-3}$$

or

$$D_{R_2} = \frac{(P_T/N_o)\left[1 - \frac{D_{R_1}(ST_B/N_o)_1}{(P_T/N_o)\cos^2\theta_2}\right]\sin^2\theta_2}{(ST_B/N_o)_2} \qquad \text{(A5.3-4)}$$

These relations are identical, merely involving substitution for θ_1 or θ_2 from A5.3-2 into A5.3-1.

Then, from (A5.3-3),

$$\frac{\partial D_{R_2}}{\partial \theta_1} = \frac{P_T/N_o}{(ST_B/N_o)_2}\left\{-2\cos\theta_1\sin\theta_1 + 2\frac{D_{R_1}(ST_B/N_o)_1}{P_T/N_o}\cot\theta_1\csc^2\theta_1\right\} \qquad \text{(A5.3-5)}$$

and, from (A5.3-4),

$$\frac{\partial D_{R_2}}{\partial \theta_2} = \frac{P_T/N_o}{(ST_B/N_o)_2}\left\{2\sin\theta_2\cos\theta_2 - 2\frac{D_{R_1}(ST_B/N_o)_1}{P_T/N_o}\tan\theta_2\sec^2\theta_2\right\} \qquad \text{(A5.3-6)}$$

Setting

$$\frac{\partial D_{R_2}}{\partial \theta_1} = \frac{\partial D_{R_2}}{\partial \theta_2} = 0$$

gives the results presented in Section 5.6.3.2, namely,

$$\theta_{1_{opt}} = \sin^{-1}\left\{\left(\frac{D_{R_1}(ST_B/N_o)_1}{P_T/N_o}\right)^{1/4}\right\} \tag{A5.3-7}$$

and

$$\theta_{2_{opt}} = \cos^{-1}\left\{\left(\frac{D_{R_1}(ST_B/N_o)_1}{P_T/N_o}\right)^{1/4}\right\} \tag{A5.3-8}$$

A5.3.2 MINIMIZATION OF P_T/N_o FOR GIVEN DATA RATES

From A5.3-1 and A5.3-2,

$$P_T/N_o = \frac{D_{R_1}(ST_B/N_o)_1}{\sin^2\theta_1 \cos^2\theta_2} \tag{A5.3-9}$$

and

$$P_T/N_o = \frac{D_{R_2}(ST_B/N_o)_2}{\sin^2\theta_2 \cos^2\theta_1} \tag{A5.3-10}$$

where the assumption is made that the minimum P_T/N_o will be large enough so that $\eta_{S_1} = \eta_{S_2} = 1$. This must be verified with the actual numbers of the particular case of interest.

Using A5.3-1 and A5.3-2 again, we find:

$$P_T/N_o = \frac{D_{R_1}(ST_B/N_o)_1}{\sin^2\theta_1\left[1 - \dfrac{D_{R_2}(ST_B/N_o)_2}{(P_T/N_o)\cos^2\theta_1}\right]} \tag{A5.3-11}$$

and

$$P_T/N_o = \frac{D_{R_2}(ST_B/N_o)_2}{\sin^2\theta_2\left[1 - \frac{D_{R_1}(ST_B/N_o)_1}{(P_T/N_o)\cos^2\theta_2}\right]} \tag{A5.3-12}$$

Solving, we get

$$P_T/N_o = \frac{D_{R_1}(ST_B/N_o)_1}{\sin^2\theta_1} + \frac{D_{R_2}(ST_B/N_o)_2}{\cos^2\theta_1} \tag{A5.3-13}$$

and

$$P_T/N_o = \frac{D_{R_1}(ST_B/N_o)_1}{\cos^2\theta_2} + \frac{D_{R_2}(ST_B/N_o)_2}{\sin^2\theta_2} \tag{A5.3-14}$$

Setting

$$\frac{\partial(P_T/N_o)}{\partial\theta_1} = \frac{\partial(P_T/N_o)}{\partial\theta_2} = 0$$

gives:

$$\theta_{1_{opt}} = \mathrm{Tan}^{-1}\left\{\left(\frac{D_{R_1}(ST_B/N_o)_1}{D_{R_2}(ST_B/N_o)_2}\right)^{1/4}\right\} \tag{A5.3-15}$$

and

$$\theta_{2_{opt}} = \mathrm{Tan}^{-1}\left\{\left(\frac{D_{R_2}(ST_B/N_o)_2}{D_{R_1}(ST_B/N_o)_1}\right)^{1/4}\right\} \tag{A5.3-16}$$

deriving the results shown in section 5.6.3.2.

SECTION VI

COMMAND SYSTEM

6.1 INTRODUCTION

From Earth, the Command System is the means by which a project controls the activities of its spacecraft. During mission operations, project personnel prepares a list of command instructions for the spacecraft and loads these commands into its Multimission Command System (MMC) and transmits them via an uplink telecommunications channel to the spacecraft. The project may elect to verify commands which have been received at the station prior to transmission enable. The spacecraft command system detects and decodes the commands, then provides an output to the appropriate spacecraft user subsystems. The effects of the commands may be monitored on Earth via telemetry data.

This section discusses the DSN Multimission Command System, typical spacecraft command subsystems which are compatible with the DSN, and the preparation of design control tables for the control of command link performance between the DSIF and the spacecraft.

6.2 DSN MULTIMISSION COMMAND SYSTEM (MMC)

6.2.1 MMC Description

The DSN Multimission Command System uses elements of the DSIF and GCF to function in the following manner: Commands are prepared and formatted by the project, and sent via the GCF to the deep space stations (DSSs) where the commands are accepted and reformated by the Telemetry and Command Data Subsystem (TCD) of the DSIF. Once received, the DSS transmits back to the project a verify message containing the command data received and the reconstructed command bit sequence. The verify message is processed by the project, and if acceptable, an enable message is transmitted to the DSS. The enable message causes the command to be transferred at the correct time from the TCD to the Command Modulation Assembly (CMA) where the command bits are modulated onto subcarriers which then modulate the DSS transmitter for transmission to the spacecraft. A command may be aborted at any time up to the transmission of the last bit in a command word.

A more complete description of the DSN MMC may be obtained from references 6-1 through 6-3.

6.2.2 DSIF MMC Capabilities

The key part of the DSN MMC which affects the spacecraft design and performance is the DSIF Multimission Command System, which is described in references 6-4 through 6-6. The MMC uses portions of the TCD for software functions, the CMA for generating the command waveforms, and the exciters, transmitters, and antennas for rf carrier modulation and transmission. The MMC can provide certain types of modulation. These are:

1) Single-channel FSK using sine wave subcarriers

2) Single-channel FSK using square wave subcarriers

3) Single-channel PSK using sine wave subcarriers

4) Single-channel PSK using square wave subcarriers

5) Dual-channel PSK using sine and square wave subcarriers

6) Direct-carrier phase modulation

Data rates are variable for types 1) through 4) from 1 bit/min to 10 bps.

Subcarrier frequencies for types 1) through 4) may be selected from 100 Hz to 1 MHz with 0.1 Hz resolution.

Modulation type 5) utilizes one channel to transmit a PN code modulating a square-wave subcarrier to establish bit sync in the spacecraft receiver. The second channel is a sine-wave subcarrier, phase modulated with command data. The two channels are combined linearly and modulated onto the rf carrier for transmission to the spacecraft. The bit rate for this system is fixed at 1 bps. This modulation scheme is known as the dual channel command system.

In modulation type 6), the command waveform is phase modulated directly onto the carrier. The data rates range from 200 bps to 1 kbps. Complete performance specification for the CMA is presented in reference 6-5.

6.3 SPACECRAFT COMMAND SYSTEMS

A spacecraft command system may be conveniently divided into two subsystems: the command detector, and the command decoder. The function of the detector is to detect and remove the binary command data from the received signal and present it in a serial bit stream to the decoder. The decoder then determines the validity of its input and if it is a valid command, passes it as a decision to the spacecraft. The decoder, therefore, depends only on command format and tends to be oriented toward a specific mission. The detector, on the other hand, is dependent on the uplink modulation scheme.

6.3.1 Detector Performance

The spacecraft command detector configuration and performance depend on the choice of uplink signal implementation as defined by one of the six DSN-compatible modulation methods described above. Mariner spacecraft have used the 2-channel PSK command system described below. In addition, two single channel command systems are described, references 6-11 through 6-28 give more detailed information on these systems which will be used on Helios and Viking Orbiter'75.

6.3.2.1 Detector Performance for the 2-Channel Command System. The 2-channel PSK command system has been described by Bryden (reference 6-17) and its theory of operation discussed by Springett (reference 6-18). The command detector accepts the command signal from the Radio Subsystem after the rf carrier has been demodulated, acquires subcarrier and bit sync, and detects the command data bits.

The command detector of the Mariner Mars 1969 (MM'69) System is shown in Figure 6-1. The DSIF transmits a signal of the form

$$\sqrt{2P_{tr}}\sin\left\{\omega_c t + \theta_s \mathrm{PN} \oplus \mathrm{Sq}\ (2\omega_s t) + \theta_D D \sin(\omega_s t)\right\} \qquad (6.3\text{-}1)$$

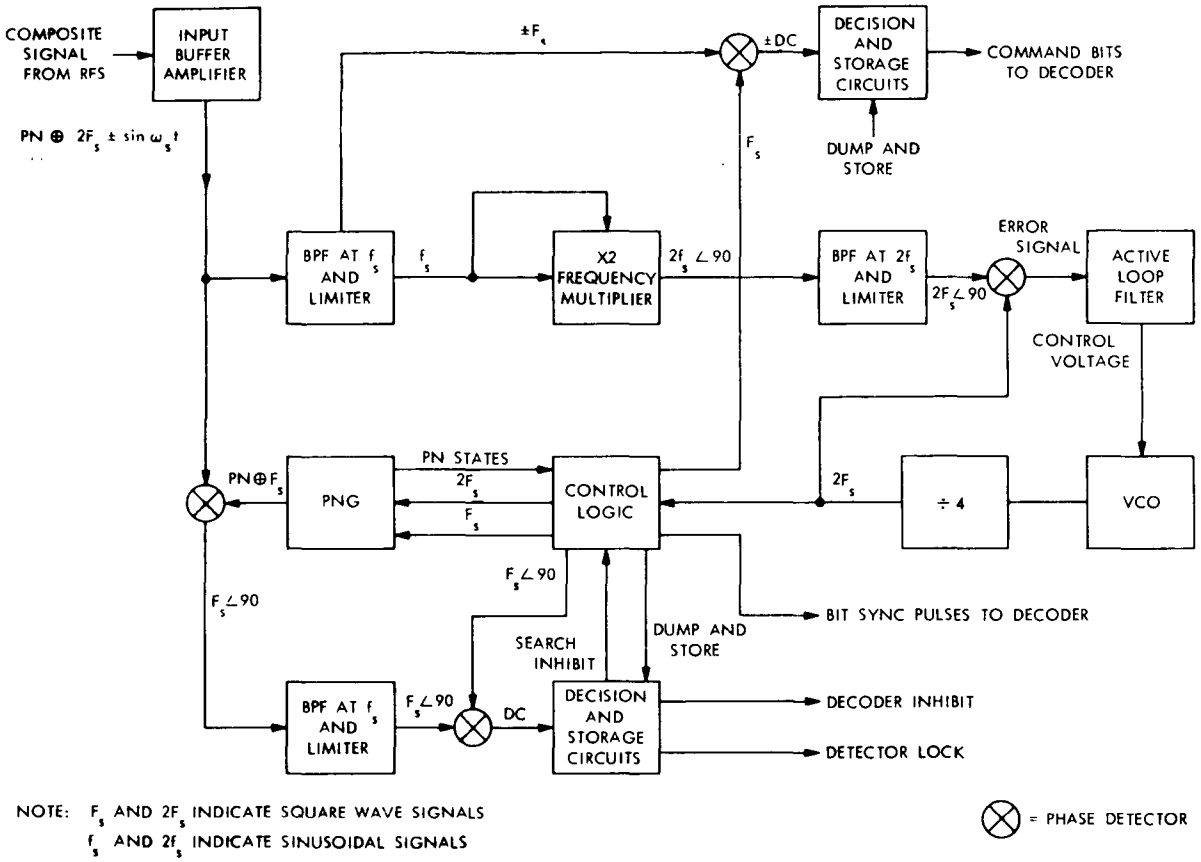

Fig. 6-i. Spacecraft command subsystem detector functional block diagram, two channel system (MM'69)

where

ω_c = Rf carrier frequency

ω_s = Subcarrier frequency

θ_s = Sync channel modulation index

θ_D = Data channel modulation index

PN = Digital PN sequence

$Sq(\omega_s t)$ = Square-wave subcarrier of frequency ω_s

D = Data bits (±1)

P_{tr} = Transmitted power

After reception and demodulation of the rf carrier by the receiver, the command detector obtains the subcarrier reference by passing the input signal through a bandpass filter centered at ω_s, and detecting a phase reference using a phase-lock loop. Bit sync is obtained by correlating an internally generated sequence of the form

$$PN \oplus Sq(\omega_s t)$$

with the incoming signal to form

$$PN \oplus Sq(\omega_s t) \oplus PN \oplus Sq(2\omega_s t) = Sq(\omega_s t) \ \underline{/90^\circ}$$

when the ground generated and spacecraft generated codes correlate. The $Sq(\omega_s t)$ $\underline{/90^\circ}$ signal is demodulated by the reference subcarrier signal derived from the detector phase lock loop, and an error signal is detected in the presence of noise by a matched filter. If three successive error signals are detected by the matched filter, then the local PN generator is advanced one bit each cycle until correlation is achieved. The matched filter is biased so that a single in-lock indication occurs with some specified low probability (1.5×10^{-2} for Mariner Mars '69) when noise only is present at the detector input.

The command data bits are detected after bit sync has been acquired. This is done by passing the input signal through a bandpass filter to remove the sync channel modulation, demodulating the subcarrier from the data signal $D \sin(\omega_s t)$ using the reference subcarrier, and detecting the data bits with a second matched filter sampled at the bit time, using bit sync derived by the sync channel.

The DSIF transmits to the spacecraft a signal of the form given by equation 6.3-1. The spacecraft receives the waveform having total signal power P_T, and demodulates the carrier, so that the input to the command

detector is

$$\sqrt{P_T}\left\{\left(\frac{P_S}{P_T}\right)^{1/2}\left[PN\Theta Sq\ (2\omega_s t)\right] + \left(\frac{P_D}{P_T}\right)^{1/2}\left[D\sin(\omega_s t)\right] + n(t)\right\} \qquad (6.3\text{-}2)$$

where

P_T = Total received power

$\frac{P_S}{P_T}$ = Ratio of sync channel power to total power

$\frac{P_D}{P_T}$ = Ratio of data channel power to total power

$n(t)$ = Additive noise generated by the receiver

6.3.1.1.1 Power Allocation. The ratios of sync power and data power are determined by their modulation indices as defined in equation 6.3-1. They are

$$\frac{P_D}{P_T} = 2J_1^2(\theta_D)\cos^2\theta_s \qquad (6.3\text{-}3)$$

$$\frac{P_S}{P_T} = J_o^2(\theta_D)\sin^2\theta_s \qquad (6.3\text{-}4)$$

The power remaining in the carrier with command modulation on is given by

$$\frac{P_C}{P_T} = J_o^2(\theta_D)\cos^2\theta_s \qquad (6.3\text{-}5)$$

where

$J_i(\cdot)$ are the i^{th} order Bessel functions of the first kind.

Power must be allocated to the carrier to allow the radio receiver PLL to acquire phase lock and track the carrier signal with some acceptable amount of phase jitter.

Power must be allocated to the sync channel to allow the PN code to be correlated, thus obtaining bit sync.

Finally, power must be allocated to the data channel to obtain subcarrier reference, and to enable the matched filter to perform bit detection with a minimum of bit errors.

Modulation indices are selected to minimize the bit error rate when the carrier tracking loop of the receiver and the command detector sync channel are performing in a prescribed way.

6.3.1.1.2 Sync Channel Performance. The sync channel performance is specified in terms of its acquisition properties, and its ability to remain in lock once lock is achieved. Performance is specified at the input SNR corresponding to the data channel's threshold design point. At this threshold, the project generally specifies

1) The probability of a single out-of-lock indication given an in-lock condition.

2) The probability of two consecutive out-of-lock indications

3) The probability of three consecutive out-of-lock indications

4) The probability that the command decoder does not respond to a transmitted command.

5) The probability of indicating two consecutive in-lock conditions given that no command signal is present.

6) The maximum time to PN acquisition with probability of 0.99.

The power required in the sync channel to achieve these probabilities is determined experimentally.

6.3.1.1.3 Data Channel Performance. The performance of the data channel typically is measured in terms of its bit error rate. For phase coherent, uncoded demodulation, the bit error probability P_{BE}, is given by

$$P_{BE} = \frac{1}{2}\text{erfc}(\sqrt{ST_B/N_o}) \tag{6.3-6}$$

where

$\text{erfc}(\cdot)$ = Complementary error function

ST_B/N_o = Signal energy-to-noise spectral density ratio in the data portion of the spectrum

However, due to the fact that the P_T/N_o received by the spacecraft is finite, the carrier PLL cannot produce a perfect carrier reference for demodulation, and the sync channel cannot produce a perfect sync reference for detection. Consequently, the error probability in equation (6.3-6) is increased. We say that the ST_B/N_o is degraded (reduced) by the system losses, η_s

Thus, P_{BE} is as given in 6.3-6 and

$$\frac{ST_B}{N_o} \triangleq \left(\frac{P_T}{N_o}\right)\left(\frac{P_D}{P_T}\right)T_B\eta_s, \quad 0 < \eta_s < 1 \tag{6.3-7}$$

where

T_B = Bit time

η_s = System efficiency, or system loss

The system loss is primarily composed of losses due to a noisy carrier reference η_{RL} (called radio loss), noisy sync reference, η_{BSDL} (called bit sync and detection loss), and any attenuation of the input signal to the matched filter caused by filtering, limiting and other associated circuit losses, η_c (called circuit losses).

Thus,

$$\eta_s \simeq \eta_{RL}\eta_{BSDL}\eta_c \tag{6.3-8}$$

An expression for radio loss has been derived by F. Reed (ref. 6-10) for the case where the bit rate is much less than the receiver loop bandwidth. It is

$$\eta_{RL} = \left[\frac{I_1\left(\frac{2P_c}{N_o 2B_L}\right)}{I_o\left(\frac{2P_c}{N_o 2B_L}\right)}\right]^2 \tag{6.3-9}$$

where

$I_k(\cdot)$ = k^{th} order imaginary Bessel function

Sync losses and circuit losses are determined experimentally.

6.3.1.2 Detector Operation for the Analog Single Channel Command System

The analog command detector block diagram is shown in Figure 6-2, and its manner of operation is described below. In the figure, F_s stands for the signal $\sin(2\pi f_s t)$ and the circumflex ($\wedge$) denotes "estimates".

The analog single channel command system accepts the bi-phase modulated sinusoidal signal from the Radio Frequency Subsystem after the RF carrier has been demodulated at (1). The subcarrier loop utilizes a PLL configuration to estimate the phase coherent subcarrier reference (2). This reference is used in the bit sync loop to derive the phase coherent bit synchronization reference signal (3) by an early-late difference of absolute values type PLL. Together the references provide timing signals for the required detector and decoder logic operations when the detector is receiving data.

The lock detector is needed to ensure the presence of the proper signal. Its operation is to sum the absolute magnitudes of four consecutive

data bits and compare this result with a pre-set threshold value. If this result exceeds the threshold value, "in-lock" is announced and the decoder is enabled.

6.3.1.2.1 Power Allocation

The DSIF transmits a signal of the form

$$\sqrt{2\,P_{tr}}\,\sin\left\{\omega_c t + \theta_D D(t)\,\sin(\omega_s t)\right\} \qquad (6.3\text{-}10)$$

where

ω_c = RF carrier frequency

ω_s = Subcarrier frequency = $2\pi f_s$

θ_D = Data modulation index

$D(t)$ = Data bits

P_{tr} = Transmitted power

The ratio of data power, P_D to total received power, P_T, is determined by its modulation index.

$$\frac{P_D}{P_T} = 2\,J_1^{\,2}(\theta_D) \qquad (6.3\text{-}11)$$

The ratio of carrier power, P_c, to total received power with command modulation on is given by,

$$\frac{P_c}{P_T} = J_0^{\,2}(\theta_D) \qquad (6.3\text{-}12)$$

where $J_i(\cdot)$ are the i^{th} order Bessel functions of the first kind.

Power must be allocated to the carrier to allow the radio receiver PLL to acquire lock and track the carrier signal with some acceptable amount of phase jitter. Power allocated to the data channel is used to obtain subcarrier and bit sync references, and to enable the matched filter to perform bit detection with a predictable bit error rate.

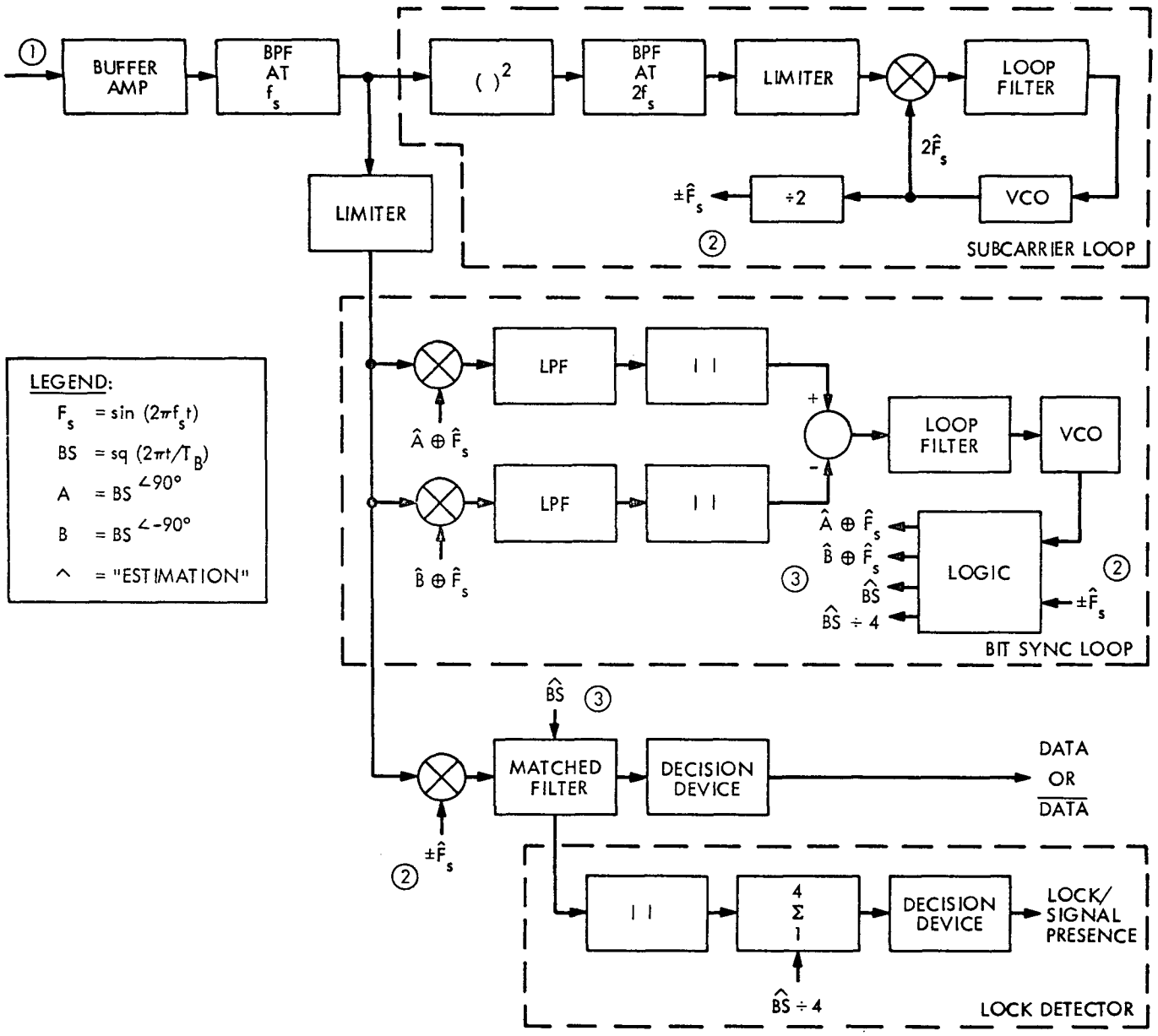

Fig. 6-2. Analog command detector block diagram

The modulation index is selected to minimize the bit error rate when the carrier tracking loop of the receiver and the command detector are performing in a prescribed way.

6.3.1.2.2 Channel Performance

Unlike the two-channel system, the single channel system does not require a separate sync channel to provide the necessary timing to the synchronous "matched filter" since the data channel alone generates and maintains the necessary subcarrier and bit sync signals. Thus the data channel performance is specified in terms of its ability to acquire these reference signals, its overall acquisition time, its bit error probability, and its ability to detect the presence of the proper signal. Performance is specified at the command detector threshold ST_B/N_o. At this threshold ST_B/N_o, the project generally specifies

1) The bit error probability
2) The worst case acquisition time with probability of .99
3) The probability of indicating in-lock with noise only
4) The probability of indicating out-of-lock when the signal is present
5) The minimum data transition density since the bit synchronizer performance is very sensitive to the data transition density.

For phase coherent, uncoded demodulation, the bit error probability P_{BE}, is given by

$$P_{BE} = \frac{1}{2} \operatorname{erfc} \left(\sqrt{ST_B/N_o}\right) \tag{6.3-13}$$

where

erfc (•) = Complementary error function

ST_B/N_o = Signal energy-to-noise spectral density ratio in the data portion of the spectrum

However, due to the fact that the P_T/N_o, received by the spacecraft is finite, the carrier PLL cannot produce a perfect carrier reference for demodulation, and the data channel cannot produce a perfect subcarrier and bit sync reference for detection. Consequently, the error probability in the equation above is increased over that of a perfectly coherent system. We say that the ST_B/N_o is degraded (reduced) by the system losses, η_s.

Thus, P_{BE} is as given above and

$$\frac{ST_B}{N_o} \triangleq \left(\frac{P_T}{N_o}\right)\left(\frac{P_D}{P_T}\right) T_B \eta_s, \quad 0 < \eta_s < 1 \tag{6.3-14}$$

where

T_B = Bit time

η_s = System efficiency

The system loss is primarily composed of losses due to a noisy carrier reference η_{RL} (called radio loss), noisy subcarrier reference, η_{SDL} (called subcarrier demodulation loss), noisy sync reference, η_{BSDL} (called bit sync and detection loss) and any attenuation of the input signal to the matched filter caused by filtering, limiting and other associated circuit losses, η_c (called circuit losses).

Thus,

$$\eta_s \approx \eta_{RL}\, \eta_{SDL}\, \eta_{BSDL}\, \eta_c \tag{6.3-15}$$

η_{RL} is discussed in paragraph 5.4.5.1, and circuit losses must be measured for the particular system. η_{SDL} and η_{BSDL} for the analog single channel command system are discussed below.

6.3.1.2.2.1 Command Subcarrier Demodulation Loss, η_{SDL}. The subcarrier loop of the analog single channel command system (Figure 6-2) is known as a "squaring" loop. Reference 6-11 derives the probability density function $p(\phi)$, for the phase of the output subcarrier reference. For a second-order subcarrier PLL the phase error density is approximated by:

$$p(\phi) = \frac{\exp\left[2\beta\,\phi + \alpha\cos 2\phi\right]}{4\pi^2 \exp(-\pi\beta)\,\left|I_{j\beta}(\alpha)\right|^2} \int_{2\phi}^{2(\phi+\pi)} \exp\left[-\beta x - \alpha\cos x\right]\,dx$$

$$|\phi| \leq \frac{\pi}{2} \tag{6.3-16}$$

where

$$\beta = \left(\frac{r+1}{r}\right)^2 \frac{\eta'_{sc}}{2\omega_{SCL}} \left[4\pi(f_{sc} - f_o) - \frac{(\tau_1 - \tau_2)r}{\tau_2^2}\left(1 + \frac{\tau_2}{(r+1)\,\tau_1\,\eta'_{sc}\,\sigma_G^2}\right)\overline{\sin 2\phi}\right] \tag{6.3-17}$$

$$\alpha = \left(\frac{r+1}{r}\right)\eta'_{sc} - \frac{(\tau_1 - \tau_2)}{\tau_1\, r\, \sigma_G^2} \tag{6.3-18}$$

$$\sigma_G^2 = \overline{\sin^2 2\phi} - (\overline{\sin 2\phi})^2 \tag{6.3-19}$$

$$\overline{\sin 2\phi} = \mathrm{Im}\left[\frac{I_{1-j\beta}(\alpha)}{I_{-j\beta}(\alpha)}\right] \tag{6.3-20}$$

$$\overline{\sin^2 2\phi} = \frac{1}{2} - \frac{1}{2}\,\mathrm{Re}\left[\frac{I_{2-j\beta}(\alpha)}{I_{-j\beta}(\alpha)}\right] \tag{6.3-21}$$

f_{sc} = Received subcarrier frequency

f_o = Quiescent frequency of the VCO

j = $\sqrt{-1}$

$I_v(x)$ = Modified Bessel function of complex order v and argument x

r = Loop damping coefficient

ω_{SCL} = Two sided subcarrier loop bandwidth

τ_1, τ_2 = Loop filter time constants

} see section IV

η'_{sc} = Effective SNR in the loop bandwidth = $(\eta_{sc}/4)\, S_L$

η_{sc} = Equivalent SNR in the loop bandwidth of a standard second order PLL = $2P/N_o\, \omega_{SCL}$

and S_L = "Squaring" loss

S_L is of the form

$$S_L = 1 + \left[\frac{K_L}{\eta_{sc}\gamma}\right]^{-1} \tag{6.3-22}$$

where γ = Ratio of the two-sided loop bandwidth to the bandwidth of the BPF preceding the squaring device = $2\omega_{SCL}/W_\ell$

and K_L depends on the type of BPF used as shown in Table 6-1.

Then if the conditional bit error probability is

$$P_{BE}(\phi) = \frac{1}{2}\ \text{erfc}\left[\sqrt{\left(\frac{ST_B}{N_o}\right)_{in}}\ \cos\phi\right] \tag{6.3-23}$$

the average probability of bit error is

$$\overline{P}_{BE} = \int_{-\frac{\pi}{2}}^{\frac{\pi}{2}} P_{BE}(\phi)\, p(\phi)\, d\phi \tag{6.3-24}$$

Table 6-1. Squaring loss constant, K_L, for various types of band pass filter*

Filter Type	Equivalent Low Pass Transfer Characteristics $H\|(j\omega_m)\|^2$	K_L
Ideal BPF	$1 \quad ; \quad \|\omega_m\| < \frac{\pi W_\ell}{4}$ $0 \quad ;$ otherwise	1
nth - order Butterworth (n = 1 is an RC filter)	$\frac{1}{1+\left(\frac{\omega_m}{\omega_\ell}\right)^{2n}}; \quad \omega_\ell = \frac{(2n-1)\pi W_\ell}{2\Gamma(\frac{1}{2n})\Gamma(2-\frac{1}{2n})}$	$\frac{2n-1}{2n}$
Gaussian	$\exp\left[-2\left(\frac{\omega_m}{\omega_\ell}\right)^2\right]; \quad \omega_\ell = \sqrt{2\pi}\, W_\ell$	$\frac{1}{\sqrt{2}}$
Sinusoidal Roll-off ($o \leq \zeta \leq 1$)	$\frac{1}{4}\left[1-\sin\frac{\pi}{2}\left(\frac{\omega_m-\omega_\ell}{\zeta\omega_\ell}\right)\right]^2 ; \quad \|\omega_m-\omega_\ell\| \leq \zeta\omega_\ell$ $0 \quad ; \quad \omega_m-\omega_\ell \geq \zeta\omega_\ell$ $1 \quad ; \quad -\omega_\ell \leq \omega_m-\omega_\ell \leq -\zeta\omega_\ell$ where $\omega_\ell = \frac{\pi W_\ell}{2(1-\frac{1}{4}\zeta)}$	$\frac{1-\frac{29}{64}\zeta}{1-\frac{1}{4}\zeta}$

where $|\omega_m| = 2\pi\,(f_{sc} - f_o)$

*Source: Reference 6-11, with permission

and

$$\eta_{SDL} = \left[\text{erfc}^{-1}\left(2\bar{P}_{BE}\right)\right]^2 \quad \left[\left(\frac{1}{\frac{ST_B}{N_o}}\right)_{in}\right] \tag{6.3-25}$$

This analysis can also be applied to the two-channel command system (see Figure 6-1).

6.3.1.2.2.2 Command Bit Sync and Detection Loss, η_{BSDL}. A command system will typically have a very low probability of bit error at the specified threshold, or, equivalently, $ST_B/N_o >> 1$, throughout the mission. Reference 6-12 shows that, for this condition, the distribution of bit sync jitter, $p'(\tau)$, for the absolute value type of early-late gate bit synchronizer can be represented by the zero mean Gaussian distribution

$$p'(\tau) = \frac{1}{\sqrt{2\pi\sigma}} \quad \exp\left(-\frac{\tau^2}{2\sigma^2}\right) \tag{6.3-26}$$

where

$$\sigma^2 = \left[8\left(\frac{ST_B}{N_o}\right)\left(\frac{1}{2B_{BSL}T_B}\right)\right]^{-1} \tag{6.3-27}$$

τ = Sync offset in units of bit time, $-\frac{1}{2} \leq \tau \leq \frac{1}{2}$

B_{BSL} = Single sided loop bandwidth of the equivalent bit sync PLL.

and we have assumed that $2 B_{BSL} T_B << 1$.

Using this relation in equations (5.4-28), (5.4-27) and (5.4-26) gives η_{BSDL} for the analog single channel command system described.

6.3.1.3 Detector Operation for the Digital Single Channel Command System.

The digital single channel command system accepts a square wave subcarrier modulated by data bits from the RF receiver output. As in the

analog command system, the digital command system establishes two levels of synchronization, viz. subcarrier sync and bit sync.

To accomplish this synchronization in the digital system, transmitted commands are prefixed by a length of unmodulated subcarrier, and then by a length of subcarrier modulated by bit sync only. The digital command system first establishes subcarrier sync by comparing the unmodulated subcarrier with a reference signal. Then a replica of the bit-sync modulated subcarrier is used as a reference to establish bit sync. Upon establishing these references, the system can detect data. All of the functions of synchronization and data detection are performed by the process of cross-correlation. One unique design feature of this system is a method of discrete-step phase-tracking which compensates for small frequency offsets due to doppler shifts and/or oscillator instabilities. This method of phase-tracking is performed by accumulating, for an interval of one data bit period, a sum of samples taken near the transitions of the signal. The polarity of the sum determines the direction of the adjustment made to the phase of the demodulation reference.

The block diagram for the Mark VI configuration of the digital command system is presented in Figure 6-3. As in the analog system, the digital system requires a lock detector to ensure the presence of the proper signal. The sum of five consecutive bits is used to check against a pre-set threshold value.

6.3.1.3.1 Digital Command System Algorithm

The digital command system is basically a correlation device. During subcarrier acquisition the correlator estimates the peak point on the correlation curve by cross-correlating the input signal with internally generated, phase-shifted estimates of this signal. The estimate whose phase most closely agrees with that of the input signal is chosen as the subcarrier demodulation reference. The command input waveform is sampled 16 times per subcarrier cycle and correlated with 16 reference waveforms which are offset with respect to each other by increments of one sample period, thus the digital correlation curve seen by the system is the staircase function shown in Figure 6-4b and differs from the continuous correlation curve of Figure 6-4a.

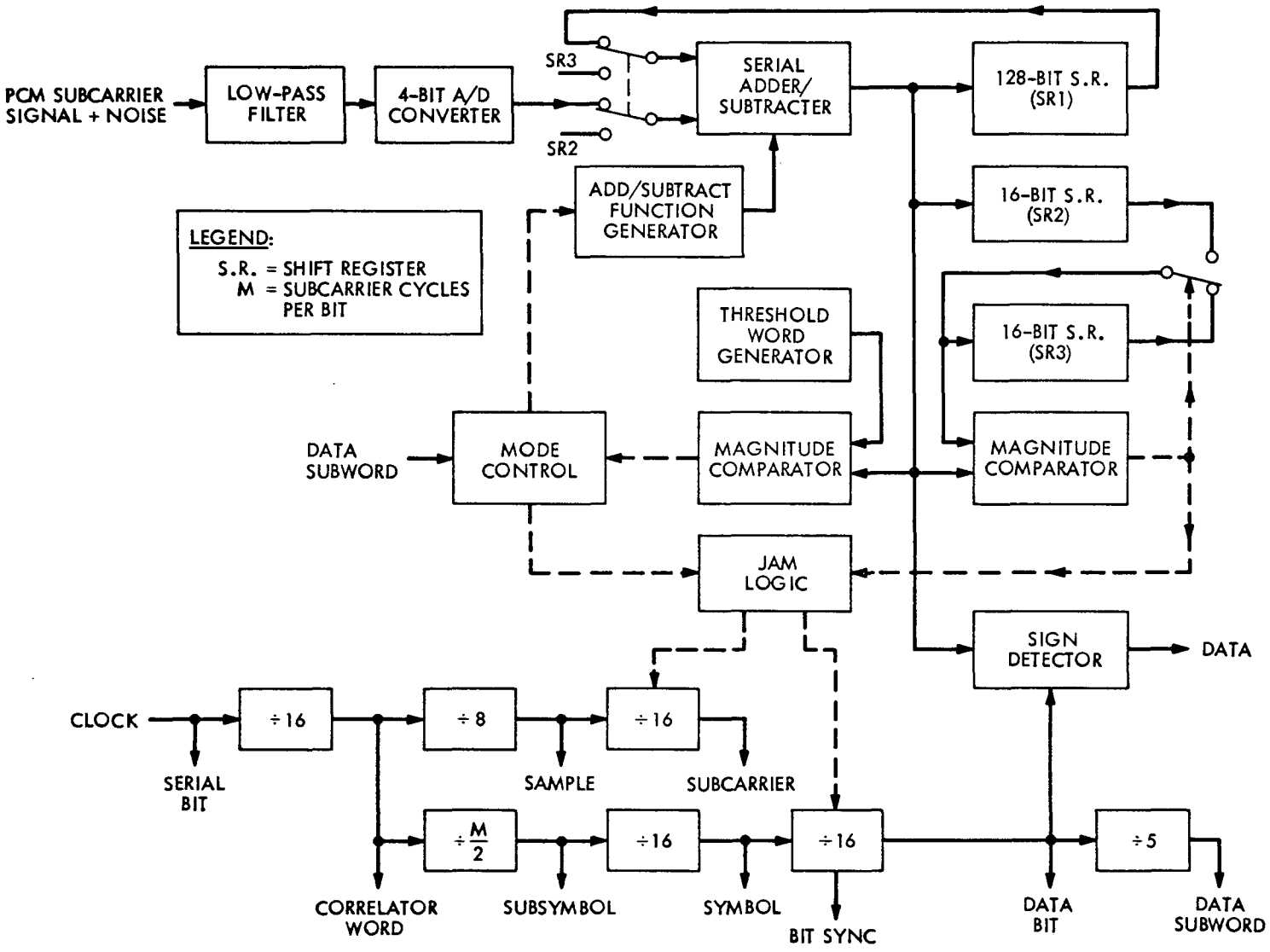

Fig. 6-3. Digital command detector MK VI block diagram

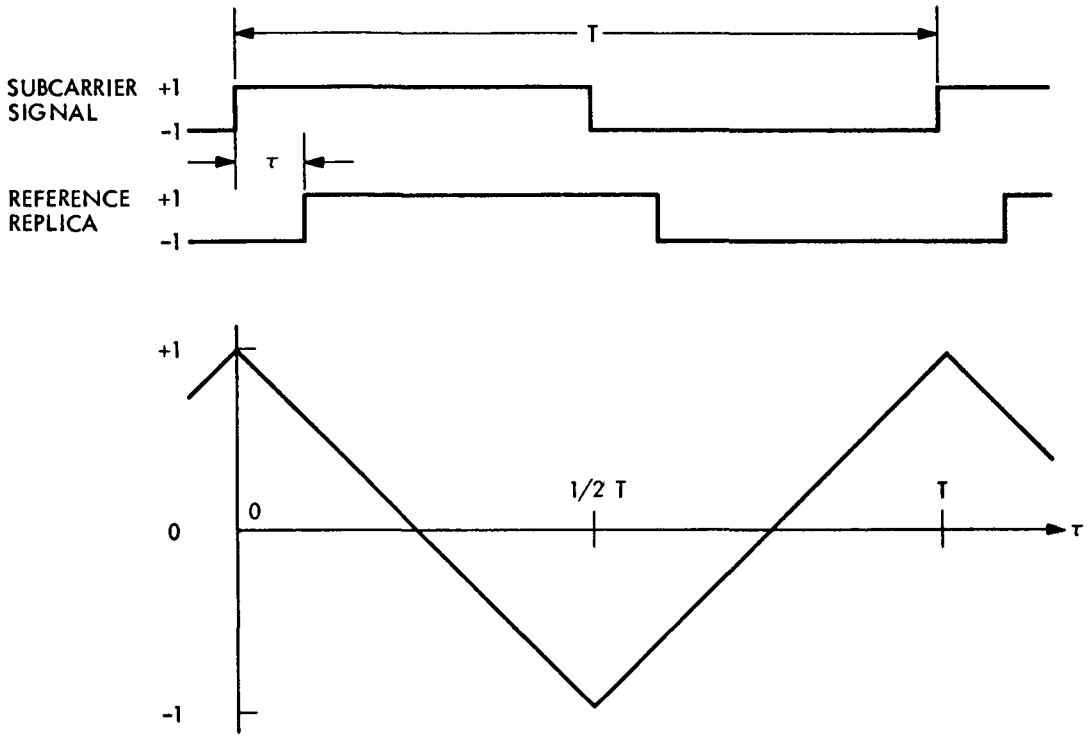

a. CONTINUOUS CORRELATION CURVE

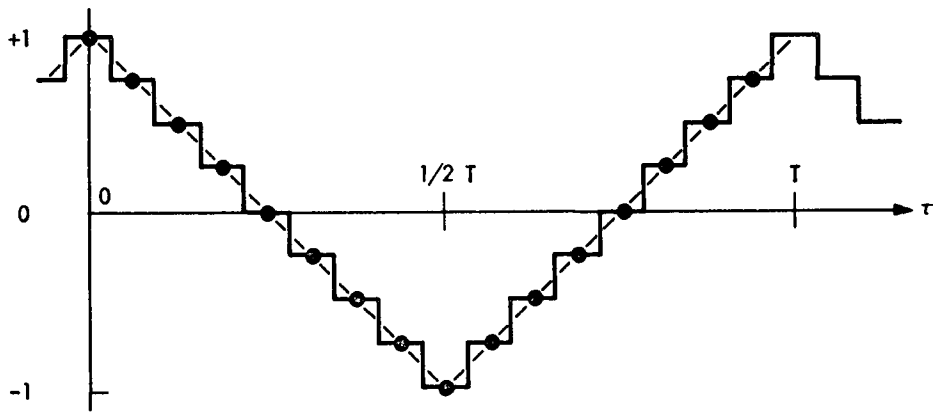

b. DISCRETE APPROXIMATION

Fig. 6-4. Correlation properties of the subcarrier signal

Subcarrier and bit sync acquisition are performed in sequence according to the basic system algorithm shown in Figure 6-5. In its initial state, the system simultaneously correlates 16 phase-shifted replicas of subcarrier with the incoming signal for 5 bit periods. A correlation time of 5 bit-times is required to make each of the threshold tests reliable. At the end of this 5 bit-times, if the largest correlation value exceeds a preset threshold value, the system advances to its second mode of operation. If threshold is not exceeded the system stays in its original state (mode 1) and repeats the subcarrier correlations.

In mode 2 the correlation against the subcarrier reference is repeated, and threshold is again checked. If threshold is exceeded the system enters mode 3, where it selects the replica having the largest correlation value as the best subcarrier estimate and "jams" the subcarrier clock to the indicated phase. The system then leaves mode 3 and automatically enters mode 4, which is a wait of 50 bit periods. During this mode 4 the system tracks the subcarrier phase offsets between the transmitted signal and its internally generated replica which are caused by doppler shifts and/or oscillator instabilities. The 50 bits are needed to accomplish this tracking with a small steady-state average phase error. Entry into mode 5 is automatic after the completion of the 50 bits.

In mode 5 the system attempts to find if bit sync is present. During this mode the system continues the subcarrier threshold tests as before and as long as threshold tests are successful, the system assumes that bit sync is not modulated on the incoming signal. If a test fails, the system assumes bit sync is on; then the system enters mode 6.

In mode 6 the system attempts to find bit sync. During this mode the incoming signal is correlated for 5 bit periods against the 16 phase-shifted sequences of the bit sync squarewave, which is synchronous in a preset way with the data bits. If threshold is not exceeded the system goes to mode 10, otherwise threshold is exceeded and the system acquires bit sync by locating that phase of the bit sync waveform which has the largest correlation value. This is done in mode 7, and the bit sync clock is jammed to its proper phase. The system then enters mode 8, where it waits for the start of the next data bit, and then proceeds to mode 9. In this mode, the system tracks both

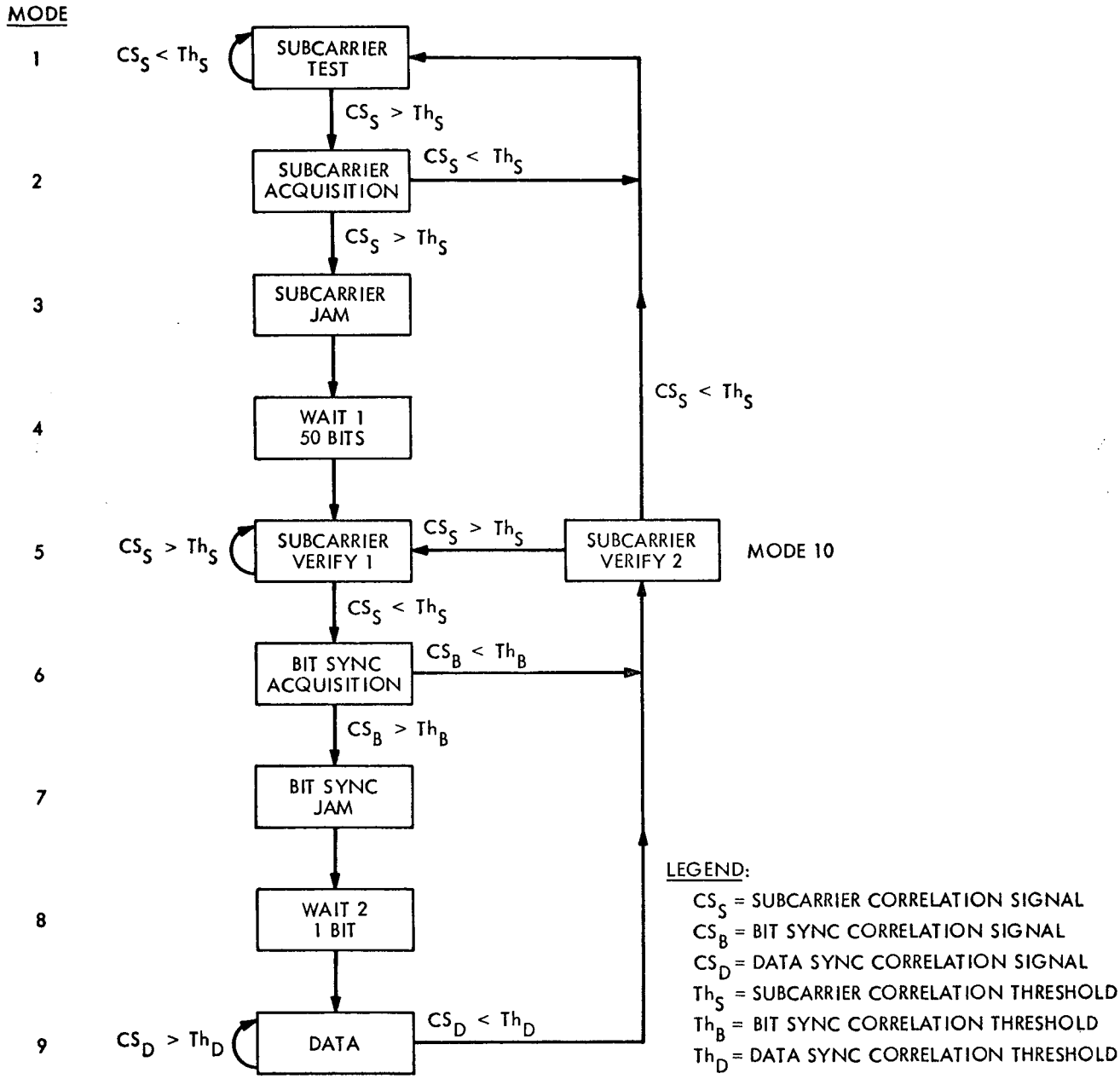

Fig. 6-5. Detector operation flow diagram

subcarrier and bit sync phase offsets for 10 bits. After 10 bit times, all synchronization is complete and the system begins to detect data bits. During this mode 9 the system tracks both subcarrier and bit sync phase offsets. Tracking is accomplished by forming a sum of samples taken near the known transitions of the signal. The sum is compared to zero at the end of 1 bit of accumulation time, and the sign of the sum determines the direction of the clock bump. The clock is bumped a fixed discrete amount in either direction (advance or retard).

Detection of data is accomplished simply by performing the correlation operations described earlier. With all phases now determined, however, only the in-phase correlation is of concern. This in-phase correlation is an approximation to the output of a matched filter, which is known to be the optimum detector.

In mode 9 the system also performs the monitoring of signal presence, or lock detection. The lock detector forms the sum of the magnitudes of 5 data bit correlations and compares this sum to a threshold. If threshold is not exceeded the system declares "out-of-lock" and goes to mode 10. In mode 10 a subcarrier threshold test is performed. If threshold is exceeded, then system enters mode 5; if not, it returns to mode 1.

6.3.1.3.2 Command Prefix

The acquisition procedures described in section 6.3.2.3.1 cannot succeed unless the proper signal component is present during each of the correlation modes. Specifically, during modes 1 and 2 unmodulated subcarrier must be present, and during mode 6 subcarrier modulated by the bit sync must be present. To meet these requirements, the prefix shown in Figure 6-6 is sent before each series of commands. The signal format is biphase modulation with a binary (square-wave) subcarrier.

In designing this prefix signal, worst-case conditions must be the prime consideration. When the system is initially in mode 1, it has no sync information and may begin to correlate at an arbitrary time with respect to the transmitted prefix. Consequently, there may exist a mode 1 correlation

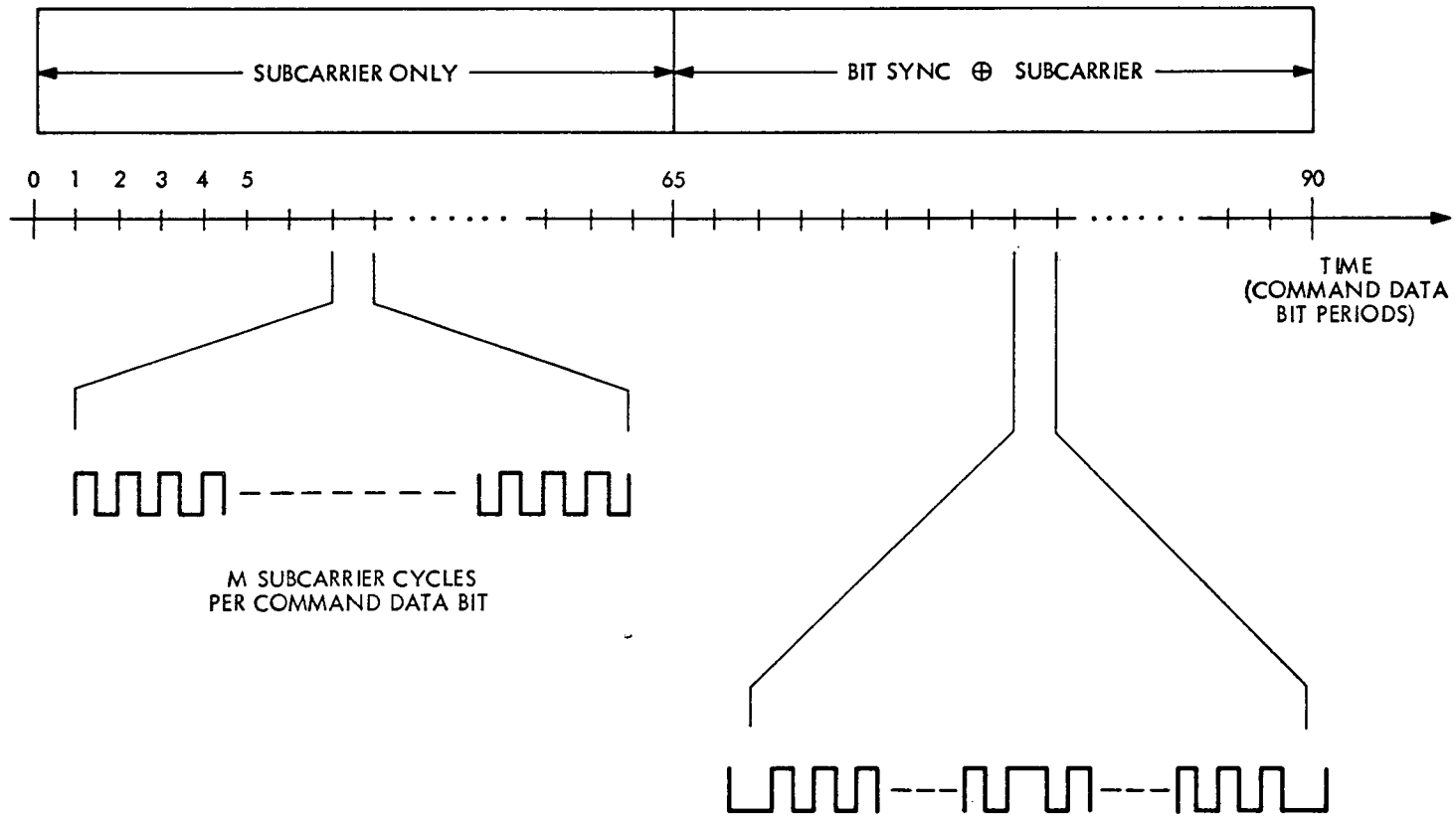

Fig. 6-6. Command acquisition signal

for which the prefix is only present for part of the correlation time. If this first correlation does not exceed threshold, mode 1 must be repeated and a situation such as that shown in Figure 6-7a will exist. To allow for successful completion of mode 1 and mode 2 in this case, 10 more command bit times (10M subcarrier cycles) of unmodulated subcarrier will be required after the unsuccessful mode 1 correlation is completed. As a conservative worst-case design, it may be assumed that the prefix is present during all of the unsuccessful correlation. This would require a total of 15 command bit times of unmodulated subcarrier if both mode 1 and mode 2 are to be completed. Thus, 15 command bit times of the prefix are allowed for unmodulated subcarrier.

A different situation occurs if the mode 1 correlation is successful even though the prefix is only partially present. This condition is shown in Figure 6-7b. (Note that the "jam" modes consume a negligible amount of time and therefore are not shown). In such a case, mode 1 and mode 2 have more than ample time for completion, but the timing of the mode 5 bit sync correlation becomes critical. If the mode 1 correlation were completed very early into the prefix, it might be possible for the system to enter mode 5 before the bit sync portion of the prefix arrives. This situation is prevented by the mode 4 waiting period. As a very conservative worst-case design, it may be assumed that the mode 1 correlation is completed at the very beginning of the prefix. In this case the required waiting period would have to be 50 bits, which is the time allotted to mode 4. Figure 6-7b also points up the reason for the existence of mode 2; if the mode 1 correlation is successful with only partial correlation with the prefix, the resultant correlation values are likely to be very bad estimates of the subcarrier phase. The existence of mode 2 guarantees that prefix will be present over the entire phase-determining correlation.

From Figure 6-7b, we see that if worst-case conditions prevail in that situation, the 5-bit mode 4 waiting period will consume 50 command bit times of unmodulated subcarrier. In this case 20 command bit times of bit sync-modulated subcarrier would be needed to successfully complete modes 5 and 6. To allow for this eventuality, 20 command bit times of the prefix are allotted to bit sync modulated subcarrier.

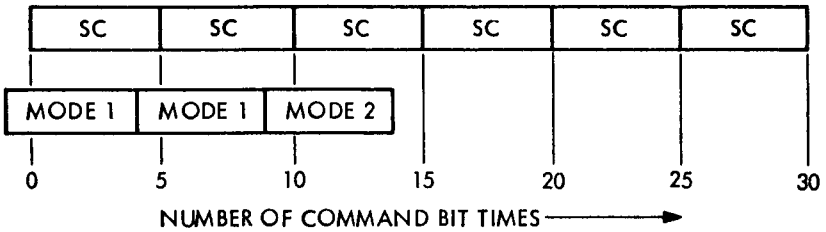

a. INITIAL MODE 1 UNSUCCESSFUL

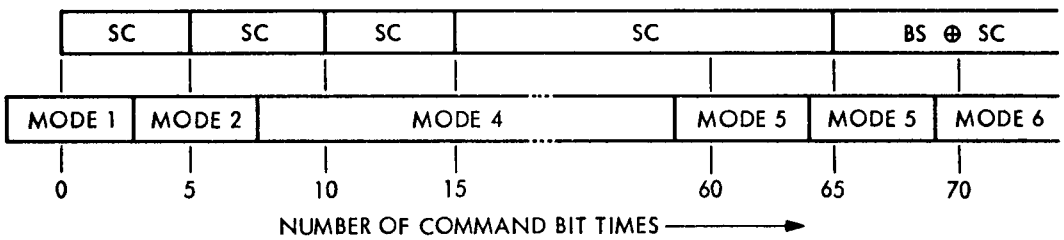

b. INITIAL MODE 1 SUCCESSFUL

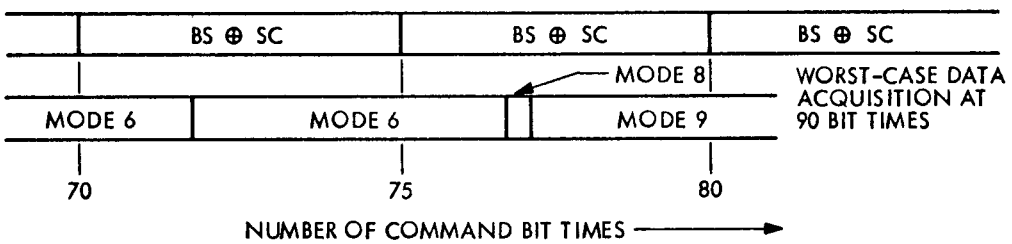

c. MODES 8 AND 9

Fig. 6-7. Prefix timing diagrams

Thus, with the prefix signal shown in figure 6-6, the system should be able to successfully acquire subcarrier sync and bit sync. However, it should be noted that modes 5 and 6 (including the small amount of time for mode 7) may be completed at any point during an actual transmitted data bit period since the initial phase offset is random. Even though sync has been established, it will be necessary for the system to wait until the start of the next bit before it begins to detect data. This is the purpose of mode 8, as shown in Figure 6-7c. After mode 8 the system tracks the phase offsets of subcarrier and bit sync for 10 command bit times. This 10 bits of tracking ensures that all synchronization is complete and that the system is ready to output data.

6.3.1.3.3 Power Allocation

The digital single channel command system must detect and acquire both subcarrier and bit sync references in sequence before detecting data. To accomplish this synchronization in sequence, commands transmitted from the DSIF are prefixed by a short burst of unmodulated subcarrier and of the subcarrier bi-phase modulated by bit sync. During the data detection mode the command information bits are bi-phase modulated by the subcarrier and the bit sync. The transmitted DSIF signal for each mode described above can be written as

$$\sqrt{2P_{tr}}\ \sin\left\{\omega_c t + \theta_D \mathrm{Sq}\,(\omega_s t)\right\} \quad \text{for subcarrier detection and acquisition modes,} \tag{6.3-28}$$

$$\sqrt{2P_{tr}}\ \sin\left\{\omega_c t + \theta_D \mathrm{BS}\oplus\mathrm{Sq}(\omega_s t)\right\} \quad \text{for bit sync detection and acquisition modes,} \tag{6.3-29}$$

and

$$\sqrt{2P_{tr}}\ \sin\left\{\omega_c t + \theta_D \mathrm{D(t)}\oplus\mathrm{BS}\oplus\mathrm{Sq}(\omega_s t)\right\} \quad \text{for data detection mode} \tag{6.3-30}$$

where

ω_c = RF carrier frequency

ω_s = Subcarrier frequency

θ_D = Data modulation index

D(t) = Data bits

BS = Bit sync square wave of frequency ω_s/M or $1/T_B$

P_{tr} = Transmitted power

$Sq(\omega_s t)$ = Square-wave subcarrier of frequency ω_s.

The ratio of data power, P_D to total receiver power, P_T, is determined by the modulation index as,

$$\frac{P_D}{P_T} = \sin^2 \theta_D \qquad (6.3\text{-}31)$$

The ratio of carrier power, P_c to total power with command modulation on is given by

$$\frac{P_c}{P_T} = \cos^2 \theta_D \qquad (6.3\text{-}32)$$

6.3.1.3.4 Channel Performance

The performance of the data channel is measured in terms of its overall acquisition time, its bit error rate, and its ability to detect the presence of the transmitted signal. Since subcarrier and bit sync acquisition are performed in sequence according to the basic system algorithm, the overall probability as well as the probability associated with each mode must be specified. For phase coherent, uncoded demodulation, the bit error probability P_{BE}, is given by

$$P_{BE} = \frac{1}{2} \operatorname{erfc} \left(\sqrt{ST_B/N_o}\right) \qquad (6.3\text{-}33)$$

Due to the system losses, the ST_B/N_o is degraded.

Thus, P_{BE} is given by equation (6.3-33)

where

$$\frac{ST_B}{N_o} \triangleq \left(\frac{P_T}{N_o}\right)\left(\frac{P_D}{P_T}\right) T_B \eta_s \qquad (6.3\text{-}34)$$

η_s = System efficiency

The system loss is primarily composed of losses due to a noisy carrier reference η_{RL}, low pass filtering loss η_{LPF}, analog to digital quantization loss $\eta_{A/D}$, subcarrier demodulation loss η_{SDL}, and bit synchronization and detection loss η_{BSDL}.

Thus,

$$\eta_s = \eta_{RL}\eta_{LPF}\eta_{A/D}\eta_{SDL}\eta_{BSDL} \qquad (6.3\text{-}35)$$

6.3.1.3.4.1 Low Pass Filtering Loss, η_{LPF}, and Choice of Sampling Time.

The subcarrier demodulation process of the digital system of Figure 6-3, can be modeled as a second-order, all-digital PLL, as shown in Figure 6-8. The low pass filtering loss can be estimated by assuming a square wave input to a flat, sharp cutoff low pass filter model. In the discussed design, W, the LPF bandwidth is chosen to be

$$W = 16/T_{sc} \qquad (6.3\text{-}36)$$

where T_{sc} $\left(= T_B/M\right)$ is the subcarrier period. With this choice the first seven harmonics of a squarewave input pass the filter, and $\eta_{LPF} \approx 0.2$ dB.

The choice of W also determines the optimum sampling time of the A/D converter. The mean and variance of the signal amplitude leaving the A/D are given by:

$$\mu = N\sqrt{S} \tag{6.3-37}$$

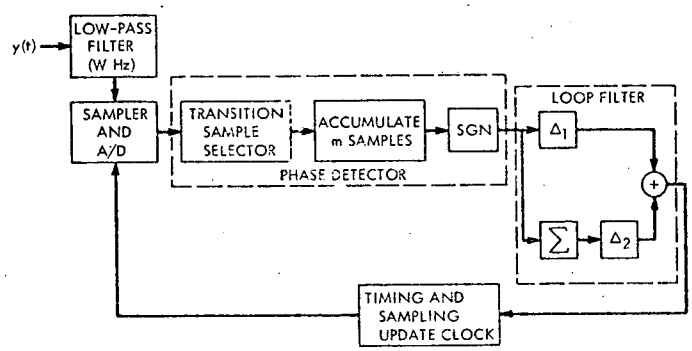

Fig. 6-8 Block diagram for all-digital, second-order phase-locked loop.

and
$$\sigma^2 = N\ W\ \frac{N_o}{2} \tag{6.3-38}$$

where $N = T_B/t_s$ = Number of samples per bit time

S = Signal power

$\frac{N_o}{2}$ = Two sided noise spectral density of the Gaussian noise process entering the A/D.

t_s = Sampling time and is an integer fraction of T_{sc} when the loop is in lock.

and we have assumed loop synchronization and independence of samples. The signal to noise ratio into the PLL is then given by μ^2/σ^2, or,

$$SNR = \frac{NS}{\frac{N_o}{2} W} = \left(\frac{2ST_B}{N_o}\right)\left(\frac{N}{T_B W}\right) = \left(\frac{2ST_B}{N_o}\right)\left(\frac{t_s}{W}\right) \qquad (6.3\text{-}39)$$

The autocorrelation function of the noise samples from an ideal low pass filter is

$$R_n(t) = \sigma^2 \frac{\sin(\pi W t)}{\pi W t} \qquad (6.3\text{-}40)$$

Sampling with period $\frac{1}{W}$, $\frac{2}{W}$, $\frac{3}{W}$, etc., ensures that the samples are uncorrelated, which is equivalent to independence for a Gaussian process. Clearly, the SNR is maximized if sampling is done at the fastest rate, or

$$t_s = \frac{1}{W} = \frac{T_{sc}}{16} \qquad (6.3\text{-}41)$$

This yields a SNR of $\frac{2ST_B}{N_o}$, which is the theoretical maximum.

6.3.1.3.4.2 Analog-to-Digital Quantization Loss, $\eta_{A/D}$

By converting an analog signal to a digital form some loss in effective signal energy to noise spectral density ratio occurs.

Reference 6-13 shows that, for a quantizer (A/D converter) of infinite range, the quantizer may be considered to add independent random noise with variance

$$\sigma^2_{A/D} = \frac{q^2}{12} \qquad (6.3\text{-}42)$$

when the width of a quantization level, q, is a small fraction of the dynamic

range of the quantized variable. If the quantized variable is Gaussian, this criterion is equivalent to requiring that $q \leq \sigma$, where σ is the standard deviation of the noise process into the A/D converter, $\sigma = \sqrt{\frac{N_o}{2} W}$.

When the range of the quantizer is adjusted so that saturation occurs only for noise of amplitude greater than 3σ, the quantizer may be modeled as an infinite quantizer with the results quoted above.

In the system described, a 4-bit A/D is used, with 16 quantization levels, and the gain of the A/D is adjusted to conform to the 3σ criterion. The loss, $\eta_{A/D} = 0.1$ dB.

6.3.1.3.4.3 Subcarrier Demodulation Loss, η_{SDL}

The digital subcarrier demodulator of Figure 6-8 can be modeled as an equivalent second-order PLL with phase variance (ref. 6-14),

$$\sigma_\phi^2 = \frac{\alpha^2 \Delta_2 \pi^3}{4 \eta_{SCL} \Delta_1} + \frac{\alpha \Delta_1 \pi^{5/2}}{\sqrt{2 \eta_{SCL}}} + \frac{41}{4} \Delta_2^2 + \left(\frac{\delta f_{sc} T_B}{12}\right)^2, \text{ rad.}^2 \tag{6.3-43}$$

where

$\alpha = \frac{\Delta T_{sc}}{T_{sc}}$

ΔT_{sc} = Duration of subcarrier transition of the lowpass filtered subcarrier

Δ_1 = "Bump" size 1, measured in fractions of T_{sc}

Δ_2 = "Bump" size 2, measured in fractions of T_{sc}

$\eta_{SCL} = \frac{mS}{N_o W}$ = signal-to-noise ratio of the sum of samples taken over a time MT_{sc}, excluding samples taken during the subcarrier transition

δ = Relative doppler offset, Hz/Hz

f_{sc} = Subcarrier frequency = $1/T_{sc}$

and, for the derivation if this formula, $\Delta_1 = 4\Delta_2$. The "bumps" correct the loop timing by $2\pi(\Delta_1 + \Delta_2)$ every M subcarrier cycles. The above theory is derived on the assumptions that loop SNR $\geq$ 10 dB, $\sigma_\phi > \Delta_1$, and $2\sigma_\phi < \Delta T_{sc}/2$.

η_{SDL} is found using conderations similar to those in paragraph 5.4.5.2, with σ_ϕ given by equation (6.3-43).

6.3.1.4 Performance Comparison of the Detectors for the Three Systems

The performance of the three detectors described above can be compared in terms of the total command power needed to establish the specified system bit error rate, the acquisition properties, the ability to track the subcarrier and bit sync offsets due to doppler shifts and/or oscillator instabilities, the total system losses, and the lock detector statistics.

Comparing these three systems on the basis of the same threshold bit error rate, the two-channel system requires more total command power because some power must be allocated to the sync channel. The analog single-channel system, which generates synchronization from the data alone has been developed in order to maximize the power allocated to the data. This single-channel system is about 5 db better on a subsystem basis than the corresponding two-channel system. Due to the much longer flight time for the future missions and the reliability advantage of digital elements over analog elements, the digital single-channel system is being developed. Its performance is in most respects superior to the analog system, in some respects by orders of magnitude.

Since all three detectors must acquire both subcarrier and bit sync references before data detection, the command acquisition time can be compared in terms of the total command bits needed to establish the system synchronization and to ensure valid data with the maximum frequency offsets specified for the system. Furthermore, since each acquisition process is a random event, we must consider the probability distribution of acquisition time.

To ensure that valid data is processed, both single channel command systems gate the matched filter output data with a logic signal. This logic signal is generated by summing the absolute magnitudes of matched filter output data and comparing this result with a pre-set threshold value. If it

exceeds the pre-set threshold value the lock detector announces that the system is "in-lock" or synchronized. For the 2-channel system, the matched filter output data is gated with a sync signal from the separate sync channel. The probabilility of being in-lock with no signal present, P (In/noise), and the probability of being out-of-lock with a signal present, P (Out/signal) are very important parameters in the system design.

Table 6-2 presents a performance comparison between the dual channel command system used on Mariners '69, '71, and '73, and two single channel command systems, one designed for Helios and the other for the Viking Orbiter.

Table 6-2. Performance comparison of three command detectors

Comparison Characteristics	2-channel PN detector (Mariner)	Single channel analog detector (Helios)	Single channel digital detector (Viking Orbiter)
Modulation format	PSK data PCM sync	PSK	PCM
Command data $\frac{P_D T_B}{N_o}$ required for $P_{BE} = 10^{-5}$	11.7 dB (Sync channel requires power, $P_S = 2P_D$)	10.9 dB	10.5 dB
Maximum acquisition time with probability of false acquisition	511 T_B 10^{-2}	360 T_B 10^{-2}	90 T_B 3×10^{-5}
Data rate (bps)	1	4	4
Multiple data rate capability	none	none	1 to 256 bps
Lock detector statistics: P (In/Noise) P (Out/Signal)	 $< 1.5 \times 10^{-2}$ $< 1.6 \times 10^{-3}$	 $< 10^{-3}$ $< 2 \times 10^{-6}$	 $< 10^{-5}$ $< 10^{-5}$
Dependence on data transition density	none	dependent	none
Subcarrier waveform	sinewave	sinewave	squarewave

6.3.2 Decoder Performance

The command decoder takes the detected data bits which were transmitted from the ground according to some fixed format scheme, deformats these bits, and provides switch closures to appropriate user subsystems. The performance of a particular decoder will depend on:

1) Detector performance
2) Information coding
3) Design of the decoder
4) Types of commands used by the project and their function
5) Formats of possible commands

Typically, each flight project will tailor its command types and formats to its unique needs. The decoder design and the detector design are uniquely structured. Consequently, an analysis must be performed for each project to assess the decoder performance. This analysis must take into account the project specified formats, the detector statistics, and the telecommunication link performance. Ideally, the project should specify those decoder characteristics which affect mission operations, and then the necessary detector statistics should be derived with which to establish telecommunications link performance thresholds.

The aim of this section is to provide some insight into the type of analysis required to assess decoder performance, and to indicate in a general way how this may be accomplished.

6.3.2.1 Command Word Formats, MM'69 Example. Typically, there will be several types of commands used by a project. The command decoder is required to distinguish between them. Mariner-type spacecraft have used three kinds of commands:

1) Direct commands (DC's)

2) Coded commands (CC's)

3) Quantitative commands (QC's)

The decoder distinguishes among these by recognizing the command word format. Figure 6-9 lists the Mariner Mars '69 command word formats.

DIRECT COMMAND WORD FORMAT

COMMAND BIT NUMBER	1	2	3	4	5	6	7	8	9	10	11	12	13	14	15	16	17	18	19	20	21	22	23	24	25	26
COMMAND BIT IDENTIFICATION	COMMAND DECODER START			DC SUBADDRESS																DC ADDRESS						
COMMAND BIT VALUE	1	1	0	0	0	0	0	1	1	ALL ZEROS										VARIABLE						

CODED COMMAND WORD FORMAT

COMMAND BIT NUMBER	1	2	3	4	5	6	7	8	9	10	11	12	13	14	15	16	17	18	19	20	21	22	23	24	25	26
CC&S BIT NUMBER									1	2	3	4	5	6	7	8	9	10	11	12	13	14	15	16	17	18
BIT VALUE — FIRST COMPUTER CC	1	1	0	0	1	1	1	1	0	1	0	PROGRAM														PARITY
BIT VALUE — SECOND COMPUTER CC	1	1	0	0	1	1	1	1	0	1	PROGRAM															
BIT VALUE — WORD INTERROGATE	1	1	0	0	1	1	1	1	0	0	1	MEMORY ADDRESS							ALL ZEROS							
BIT VALUE — FIXED SEQUENCER CC	1	1	0	0	1	1	1	1	0	0	0	REGISTER ADDRESS	PARITY	TIME DURATION												POLARITY
BIT VALUE — TOLERANCE DETECTOR DISABLE	1	1	0	0	1	1	1	1	0	1	1	ALL ZEROS													PARITY	1

QUANTITATIVE COMMAND FORMAT

COMMAND BIT NUMBER	1	2	3	4	5	6	7	8	9	10	11	12	13	14	15	16	17	18	19	20	21	22	23	24	25	26
COMMAND BIT IDENTIFICATION	COMMAND DECODER START			QC ADDRESS						SWITCH CLOSURE FOR EACH ONE															
COMMAND BIT VALUE	1	1	0	VARIABLE						VARIABLE NUMBER OF CONSECUTIVE ONES																

Fig. 6-9. Mariner Mars 1969 command word format

Every command word is 26 bits long. The first three bits are always 110, and indicate the beginning of a new command word. If bits 4 through 9 are 000011, the word is a direct command. This induces a single switch closure in a subsystem addressed by bits 20 through 26.

Coded commands are used to direct the Central Computer and Sequencer (CC&S). Coded command bits 4 through 9 determine which CC is being transmitted, and bits 10 through 26 are then sent to the CC&S. These bits are themselves formatted to be recognized by the CC&S and include parity checks for bit errors.

Quantitative commands are used to step the science instrument scan platform a prescribed number of incremental steps. The command decoder recognizes a QC address in bits 4 through 9. The corresponding switch is closed for each consecutive "1" transmitted in bits 10 through 26.

Figure 6-10 is a block diagram of the MM'69 command decoder. The command decoder functions by accepting an enable signal, command bits, and bit sync. The command bits are shifted into data registers, and the type of command and its location are determined by a decoding matrix. If the enable signal indicates that the detector is in lock, then the decoder closes a universal isolation switch (UIS) leading to the appropriate subsystem, as instructed by the decoded command word.

6.3.2.2 Decoder Performance Criteria. There are two important conditions which prevent perfect operation of the command decoder. These are:

1) Bit errors produced by the command detector

2) An out of lock indication of the command detector

Commands may be processed correctly, incorrectly, or not processed at all when a bit error occurs and the detector is in lock. If the detector gives an out-of-lock indication, no commands are processed.

The project-specified performance of the command decoder must be used to determine:

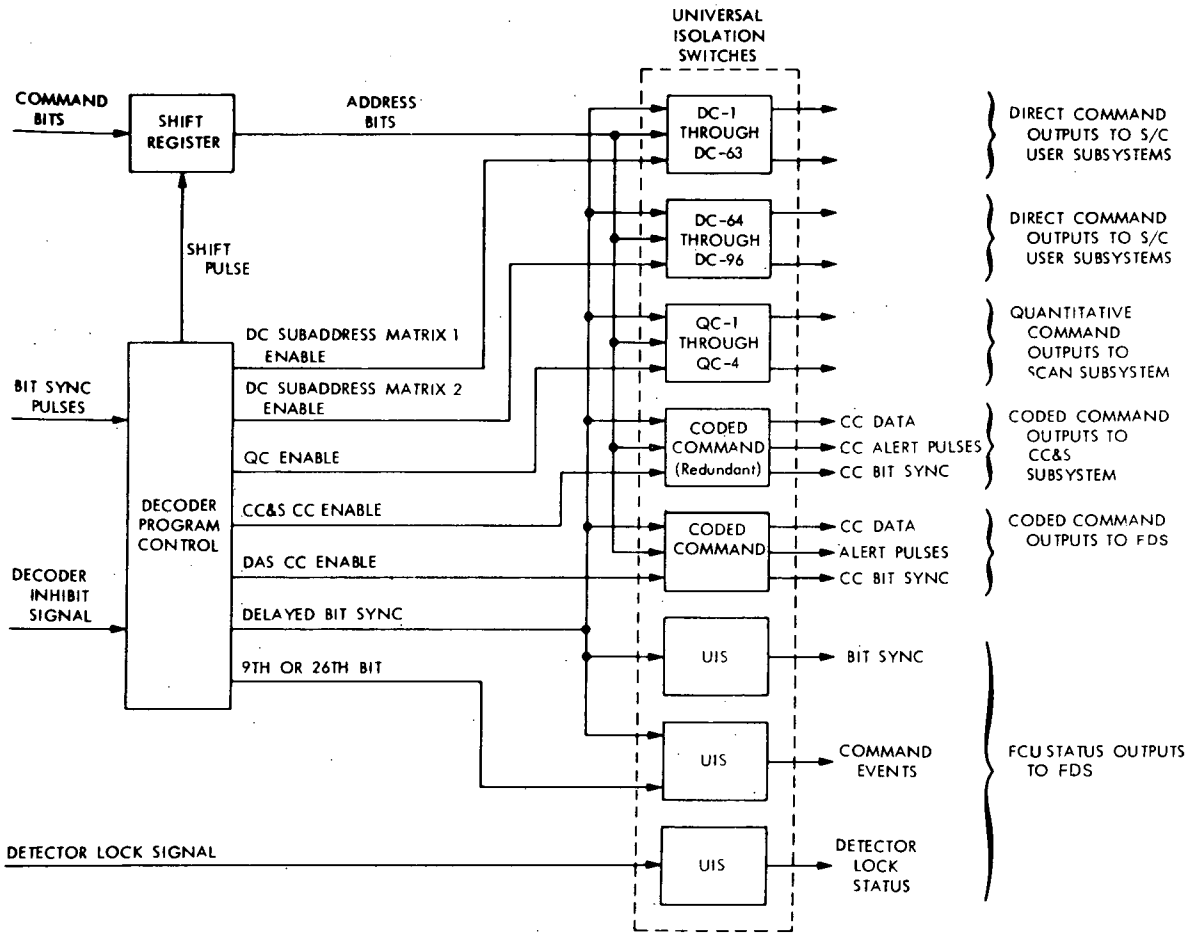

Fig. 6-10. Command decoder functional block diagram

1) The required maximum bit error probability of the detector when the detector is in lock; and

2) the probability that the detector yields an out-of-lock indication when commands are being transmitted.

To characterize the command decoder performance, the project should specify the following four probabilities:

1) P_{WE} = The probability of issuing a command other than the one transmitted (word error probability)

2) P_{NR} = The probability that the command system does not respond to a single transmitted command (no response probability)

3) P_{CW} = The probability that the command system properly responds to a transmitted command (correct word probability)

4) P_{FC} = The probability of issuing a command when none is sent.

Given that a command is transmitted,

$$P_{CW} + P_{NR} + P_{WE} = 1 \tag{6.3-44}$$

since for this condition these probabilities are all inclusive and mutually exclusive.

These probabilities are analyzed in terms of the command detector statistics for the Mariner'64 and Mariner'69 missions in Reference 6-7 and for Viking Orbiter'75 in Reference 6-28. The results are summarized below.

The detector performance is calculated using the following probabilities: If A is the event that a bit error occurs, and B is the event that the detector is out of lock, then

$\theta_1 \triangleq p(\bar{A} \cdot \bar{B})$ = The probability of a correct bit with the detector in-lock.

$\theta_2 \triangleq p(A \cdot \bar{B})$ = The probability of a bit error with the detector in-lock.

$\theta_3 \triangleq p(\bar{A} \cdot B)$ = The probability of a correct bit with the detector out-of-lock.

$\theta_4 \triangleq p(A \cdot B)$ = The probability of a bit error with the detector out-of-lock.

If the link performance and the detector design are such that A and B are independent, then

$$\theta_1 + \theta_2 + \theta_3 + \theta_4 = 1 \tag{6.3-45}$$

The θ_i probabilities are given in terms of bit error rate and out-of-lock statistics by:

p(A) = Bit error rate

p(B) = The probability of an out-of-lock indication

Thus,

$$\theta_1 = p(A)p(B)$$

$$\theta_2 = p(A)[1 - p(B)]$$

$$\theta_3 = p(B)[1 - p(A)] \qquad (6.3\text{-}46)$$

$$\theta_4 = 1 - [p(A) + p(B) - p(A)p(B)]$$

To calculate the appropriate word probabilities, it is necessary to define the multinominal distribution

$$f(X_1, X_2, X_3, X_4) = \frac{n!}{X_1! X_2! X_3! X_4!} \theta_1^{X_1} \theta_2^{X_2} \theta_3^{X_3} \theta_4^{X_4} \qquad (6.3\text{-}47)$$

where

X_i = the number of times the i^{th} combination of the events A, B, $\bar{A}$, and $\bar{B}$ occur in n bits.

For the Mariner-type command systems, a single command will not be processed unless the command detector is in-lock and the command word is preceded by 26 zeros (to ensure that a false word start pattern 110 is not recognized). Thus,

$$P_{CW} = f(35, 0, 0, 0) = \theta_1^{35} \qquad (6.3\text{-}48)$$

since

n = 26 zeroes + 3 word-start + 6 bit address

X_1 = 35 correct bits and detector in-lock

X_2 = 0 bit errors and detector in-lock

X_3 = 0 out-of-lock and some bit errors

X_4 = 0 correct bits and detector out-of-lock

The probability of a word error must be calculated from the particular command dictionary used by the project by means of the probabilities in equation (6.3-46) and the multinominal distribution of equation (6.3-47).

The probability of no response is calculated from

$$P_{NR} = 1 - P_{CW} - P_{WE} \tag{6.3-49}$$

REFERENCES

6-1 Kinder, W. J., and E. C. Gatz, "Description of DSN Systems: 1. Command System, "Jet Propulsion Laboratory Space Programs Summary 37-56, Vol. II, March 31, 1969, pp. 3-7.

6-2 Stinnet, W. G., "DSN Command System Analysis Group, "Jet Propulsion Laboratory Space Programs Summary 37-66, Vol. II, December 1970, pp. 146-150.

6-3 Rakunas, R. R., and A. Schulze, "DSN Multiple-Mission Command System, "Deep Space Network Progress Report for March-April 1971, Jet Propulsion Laboratory, Technical Report No. 32-1526, Vol. II pp. 4-6.

6-4 Wilcher, J. H., S. Friesema, J. Woo, and R. B. Crow, "DSIF MMCS," Jet Propulsion Laboratory Space Programs Summary 37-59, Vol. II, September 30, 1969, pp. 119-139.

6-5 Crow, R. B., S. Friesema, J. Wilcher, and J. Woo, "DSIF MMC System," Jet Propulsion Laboratory Space Programs Summary 37-63, Vol. II, May 31, 1970, pp. 77-94.

6-6 DSIF Command System, Document 810-5, Rev. A, pp. 2-78 through 2-84 (JPL internal document).

6-7 McBiles, C. D., "Final Report, Task 15, Command Performance Definition Study," Contract 951700 with the Jet Propulsion Laboratory and Motorola, Inc., 11/18/66.

6-8 Bryden, J. N., Mariner (Venus'62) Flight Telecommunications System, Jet Propulsion Laboratory Technical Report No. 32-377.

6-9 Springett, J., Telemetry and Command Techniques for Planetary Spacecraft, Jet Propulsion Laboratory Technical Report No. 32-495.

6-10 Reed, F., "Final Report, Task 17, Optimum Transponder Threshold Study," Contract 951700 with the Jet Propulsion Laboratory and Motorola, Inc., 1/11/67.

6-11 Lindsey, W. C., and M. K. Simon, "The Performance of Suppressed Carrier Tracking Loops in the Presence of Frequency Detuning," IEEE Proc., Vol. 58, No. 9, September 1970, pp. 1315-1321.

6-12 Simon, M. K., "Nonlinear Analysis of an Absolute Value Type of Early-Late Gate Bit Synchronizer," IEEE Trans. on Commun. Technol., Vol. COM-18, No. 5, October, 1970, pp. 589-596.

6-13 Widrow, B., "A Study of Rough Amplitude Quantization by Means of Nyquist Sampling Theory," IRE Trans. on Circuit Th., Vol. CT-3, December 1956, pp. 266-256.

F

6-14 Holmes, J. K., and C. R. Tegnelia, Digital Command System Second-Order Subcarrier Tracking Performance, Jet Propulsion Laboratory Technical Report 32-1540, October 1, 1971.

6-15 Hurd, W. J., "Digital Transition Tracking Symbol Synchronizer for SNR Coded Systems," IEEE Tran. Comm. Tech., April 1970.

6-16 Holmes, J., "Coding and Synchronization Research: Performance of and All-Digital Command System Timing Loop, "Jet Propulsion Laboratory Space Programs Summary 37-64, Vol. III, August 31, 1970, pp. 17-22.

6-17 Carl, C., "Approximate Analysis of Command Lock Detector Performance," Jet Propulsion Laboratory Space Programs Summary 37-63, Vol. III, pp. 51-58.

6-18 Simon, M. K., "The Effect of Limiter Suppression on Command Detection Performance," Jet Propulsion Laboratory Space Programs Summary 37-63, Vol. III, pp. 66-70.

6-19 Springett, J. C., and M. K. Simon, "An Analysis of the Phase Coherent-Incoherent Output of the Bandpass Limiter," Jet Propulsion Laboratory Space Programs Summary 37-63, Vol. III, pp. 70-80.

6-20 Couvillon, L. A., "Spacecraft Command Techniques," Jet Propulsion Laboratory Space Programs Summary 37-59, Vol. III, pp. 68-71.

6-21 Butman, S., L. A. Couvillon, R. Goldstein, R. Green, and J. K. Holmes, "Analysis of a Digital Single-Channel Command System," Jet Propulsion Laboratory Space Programs Summary 37-61, Vol. III, pp. 25-31.

6-22 Tegnelia, C. R., "Digital Command System Development," Jet Propulsion Laboratory Space Programs Summary 37-61, Vol. III, pp. 126-130.

6-23 Springett, J. C., and W. J. Weber "Preliminary System Testing of the Proposed TOPS All-Digital Command Detection," Jet Propulsion Laboratory Space Programs Summary 37-62, Vol. III, pp. 92-99.

6-24 Holmes, J. K., "Performance of a First-Order Digital Phase-Locked Loop," Jet Propulsion Laboratory Space Programs Summary 37-63, Vol. III, pp. 28-34.

6-25 Holmes, J. K., "Performance of an All-Digital Command System Timing Loop," Jet Propulsion Laboratory Space Programs Summary 37-64, Vol. III, pp. 17-23.

6-26 Holmes, J. K., "A Note on the Optimality of the All-Digital Command System Timing Loop," Jet Propulsion Laboratory Space Programs Summary 37-65, Vol. III, pp. 19-22.

6-27 Chadwick, H. D., "A Markov Chain Technique for Determining the Acquisition Behavior of a Digital Tracking Loop," Jet Propulsion Laboratory Quarterly Technical Review, Vol. I, No. 4, January 1972, pp. 49-58.

6-28 Tegnelia, C., and Meahl, M., Final Report: Digital Command Detector Development, Jet Propulsion Laboratory Report 900-547, April 28, 1972.

SECTION VII

SPACECRAFT ANTENNA PATTERNS

7.1 ANTENNA GAIN PATTERN

To permit the transfer of information between a spacecraft and Earth, the radio signal is radiated into space by an antenna. The simplest conceptual antenna is the isotropic radiator, which distributes the radiated power uniformly into space. Thus, for a total radiated power, W, we would see a radiation intensity $W/4\pi$ per unit solid angle, independent of our angular position with respect to the antenna.

With a known target direction or range of directions it becomes desirable to concentrate the radiated power in the useful areas. For this purpose, a directional antenna may be designed so that the radiation intensity is a function of the direction, Ω.

If we define $U(\Omega)$ as the radiation intensity for a total radiated power W and $U_o = W/4\pi$, then we can define an antenna gain function

$$G(\Omega) \triangleq \frac{U(\Omega)}{U_o} \tag{7.1-1}$$

Plots of $G(\Omega)$ = constant, are known as antenna patterns.

$G_m \triangleq \max[G(\Omega)]$ is called peak antenna gain, or, frequently, antenna gain.

In general

$$\int_{\text{all } \Omega} G(\Omega)d\Omega = 4\pi t \tag{7.1-2}$$

where t, the power transmission coefficent, is less than 1 for realizable antennas because of resistive losses in the antenna structure.

7.1.1 Antenna Gain Function

The antenna gain function $G(\Omega)$ is generally a complicated relationship which depends on the type of antenna, the type of feed, the structure on which the antenna and the feed are mounted, and the perturbations due to fabrication. It can be approximated closely by numerical techniques during design (see references 7-1 and 7-2).

It is important to note that the gain functions for receive and transmit are identical for a given frequency. However, when referring to a receiving antenna, the concept of capture area is useful. The antenna capture area is defined as the ratio of the power, W, delivered by the feed to a matched load, and the power density (P_I) watts per unit area normally incident on the antenna aperture by an infinite plane wave.

$$A_c \triangleq \frac{W}{P_I} \tag{7.1-3}$$

The aperture efficiency is defined as

$$\eta = A_c/A_p \tag{7.1-4}$$

where A_p is the physical aperture area. η generally ranges between 0 and 1 but theoretically may be greater than 1. The power transmission coefficient is absorbed into η. A_c may be found by the relationship

$$A_c = G_m \lambda^2/4\pi \tag{7.1-5}$$

Simple representations of the antenna gain function may be used to understand parametric variations, but are not useful for detailed analysis because of the invalidity of the simplifying assumptions.

For example, for a perfect circular paraboloidal antenna (no feed blockage, no deformation) with uniform illumination, the antenna gain function is given by

$$G(\theta) = \eta\left(\frac{2\pi a}{\lambda}\right)^2\left(\frac{2J_1(u)}{u}\right)^2 \qquad (7.1\text{-}6)$$

where

$$u = \frac{2\pi a}{\lambda}\sin\theta$$

a = antenna radius

η = antenna efficiency (between 0.5 and 0.7 for this type of antenna)

λ = wavelength

and θ is the polar angle measured from the antenna axis (the boresight) (references 7-1 and 7-2).

Figure 7-1 compares this equation, evaluated for Mariner Mars 1969 antenna parameters, with the measured pattern. The two differ considerably in beamwidth, gain and null location. Particularly striking is the difference in the secondary lobes. The magnitude of these undesired lobes is due to uniform illumination. If the feed pattern is tapered, they are greatly diminished; this is what is seen in the actual antenna pattern.

To find $G(\Omega)$ for a nonuniform feed is a considerable undertaking, and gets too deeply involved in antenna design rather than system design. Thus, the best course of action is to use measured patterns scaled appropriately for the new mission. Table 7-1 presents some scaling parameters.

For quick estimation of the antenna gain pattern of an axisymmetric antenna, a useful approximate formula is:

$$G(\theta) = k_1\left(\frac{\sin k_2\theta}{\theta}\right)^2 \qquad (7.1\text{-}7)$$

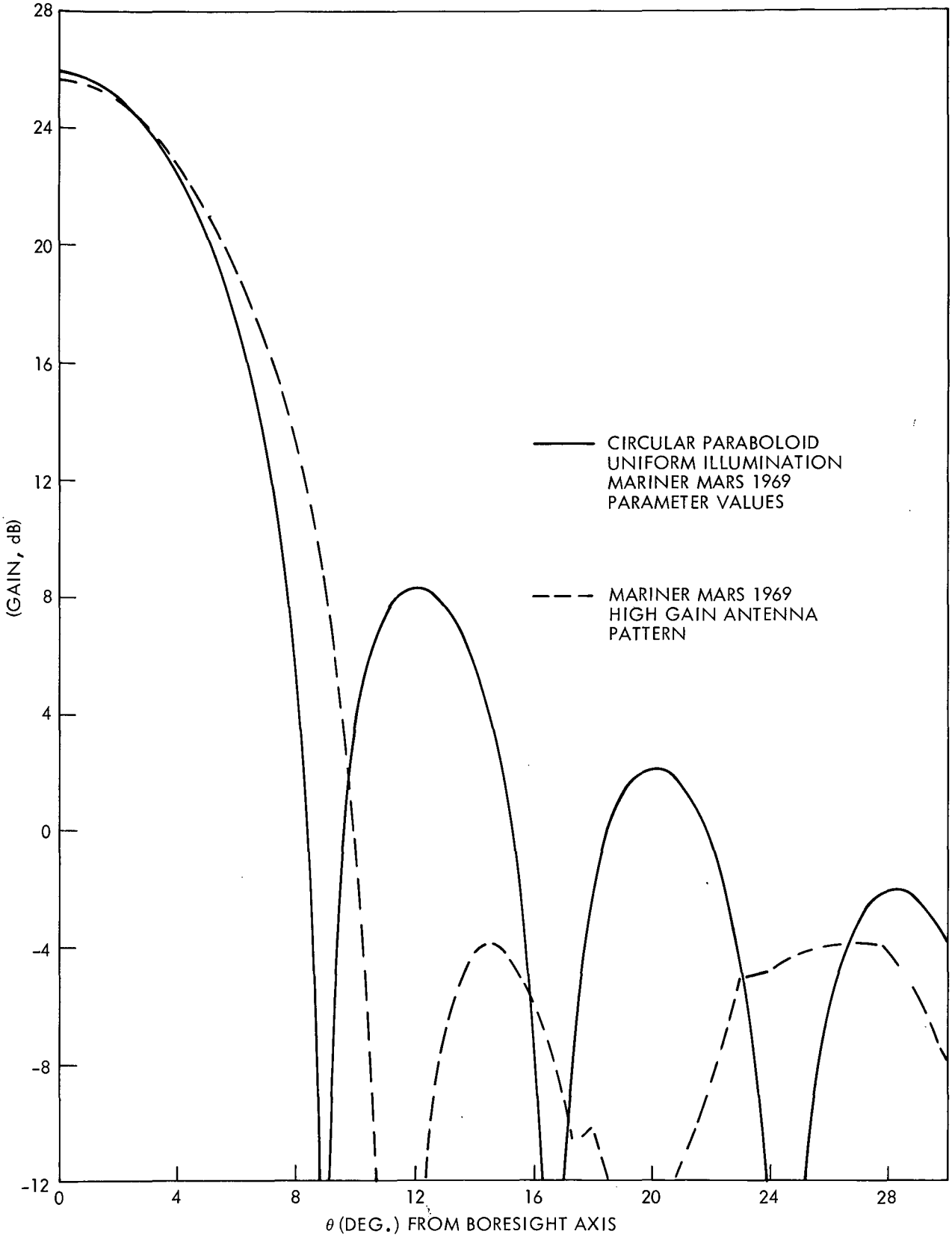

Fig. 7-1. Comparison of a simple theoretical model and actual pattern for the Mariner Mars 1969 high-gain antenna

Table 7-1 Properties of typical antennas

Configuration	Gain above isotropic radiator	3 dB beamwidth (deg)
Isotropic radiator	1	360
Infinitesimal dipole or loop	1.5	90 (toroidal pattern)
Half-wave dipole	1.64	78 (toroidal pattern)
Paraboloid (Area A, diameter D)	$(6.3 \text{ to } 8.8)A/\lambda^2$	$(60 \text{ to } 70)\frac{\lambda}{D}$
Open mouth waveguide (Area A, E-plane dimension d_E, H-plane d_H)	$10A/\lambda^2$	$\theta_E = 56\lambda/d_E$ $\theta_H = 67\lambda/d_H$
Optimum Horn (Mouth Area A, E-plane dimension d_E, H-plane d_H)	$7.5A/\lambda^2$	$\theta_E = 56\lambda/d_E$ $\theta_H = 67\lambda/d_H$
Optimum biconical horn (height h)		
Vertical Polarization	$1.2h/\lambda$	$56\lambda/h$ (toroidal pattern)
Horizontal Polarization	$1.6h/\lambda$	$67\lambda/h$ (toroidal pattern)

where

$$k_1 = G_m/k_2^2$$

$$k_2 = 2.78/\theta_o$$

$$G_m = 9.42\theta_o^{-1.96}$$

G_m is the on-axis gain (the antenna gain) expressed as a ratio, θ_o is the half-power beamwidth (3-db beamwidth, i.e., $G(\theta_o/2) = G_m/2$), and θ_o and θ are measured in radians.

Figures 7-2, 7-3, and 7-4 plot this approximation for several cases. It is clear that this formula is insufficiently accurate for low-gain antenna application.

7.1.2 Antenna Gain

Antenna gain is defined as the maximum gain and is typically the on-axis gain. However, for some antenna types, the antenna gain is not a maximum at a single point, and may be a maximum off the axis of symmetry. For example, a biconical antenna has a plane of maximum gain which is perpendicular to the axis of symmetry of the ideal toroidal pattern.

Table 7-1 tabulates some information for antennas of interest to the telecommunications system analyst.

For high-gain requirements, a paraboloidal reflector antenna is usually chosen for deep space applications. At DSN operating frequencies (S- and X-Band), reflectors are favored over arrays because of their narrow beam, low-noise characteristics. In addition, the reflector has a very high bandwidth of operation, whereas phased arrays do not. Reflectors are favored over lenses on the basis of weight and cost.

7.1.2.1 Antenna Gain Tolerances. In fabrication and during operation the antenna gain function may differ from the design function by several dB over the pattern. This can be due to differences in surface conductivity, impedance matching, reflector configuration, and other factors. The error can be represented closely by a function of the form

$$\text{Gain error} = \pm (k_1 + k_2 P_L + k_3)$$

where

k_1 is in dB

$P_L = G(\Omega) - G_m$, the pointing loss defined in Paragraph 7.3

k_2 is in dB/dB of pointing loss

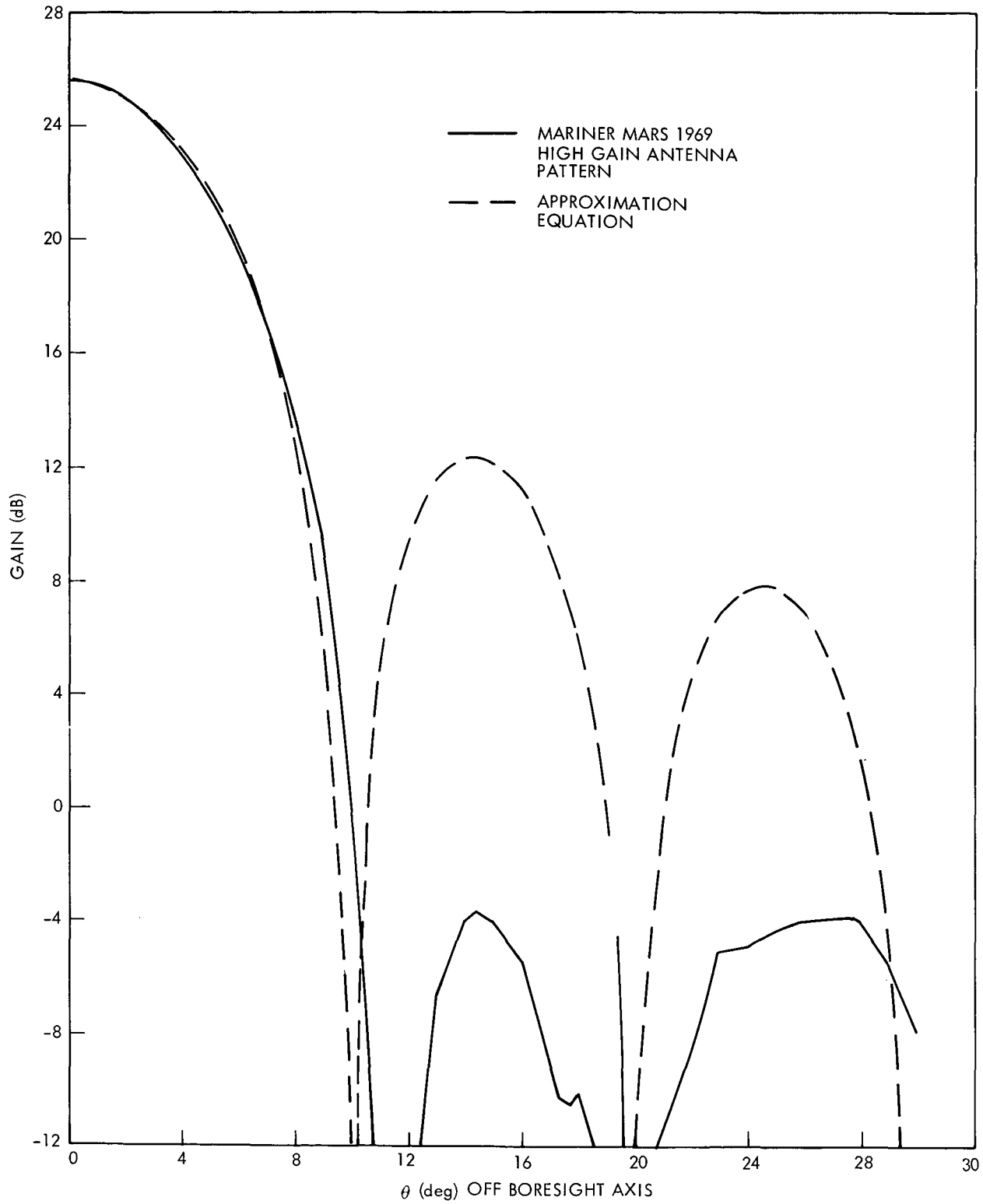

Fig. 7-2. General comparison of actual pattern and approximation equation for the Mariner Mars 1969 high-gain antenna

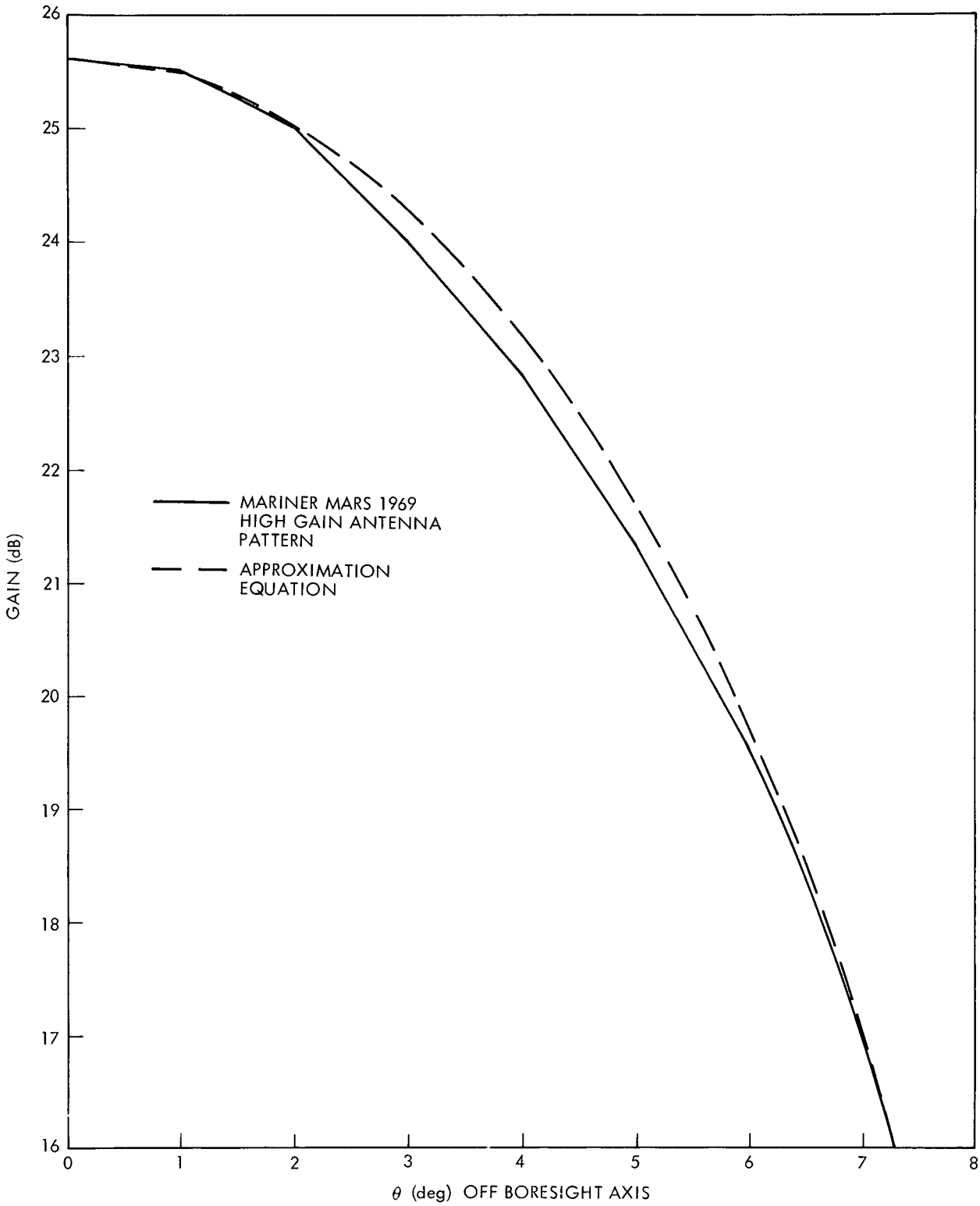

Fig. 7-3. Detailed comparison of actual pattern and approximation equation for the Mariner Mars 1969 high-gain antenna

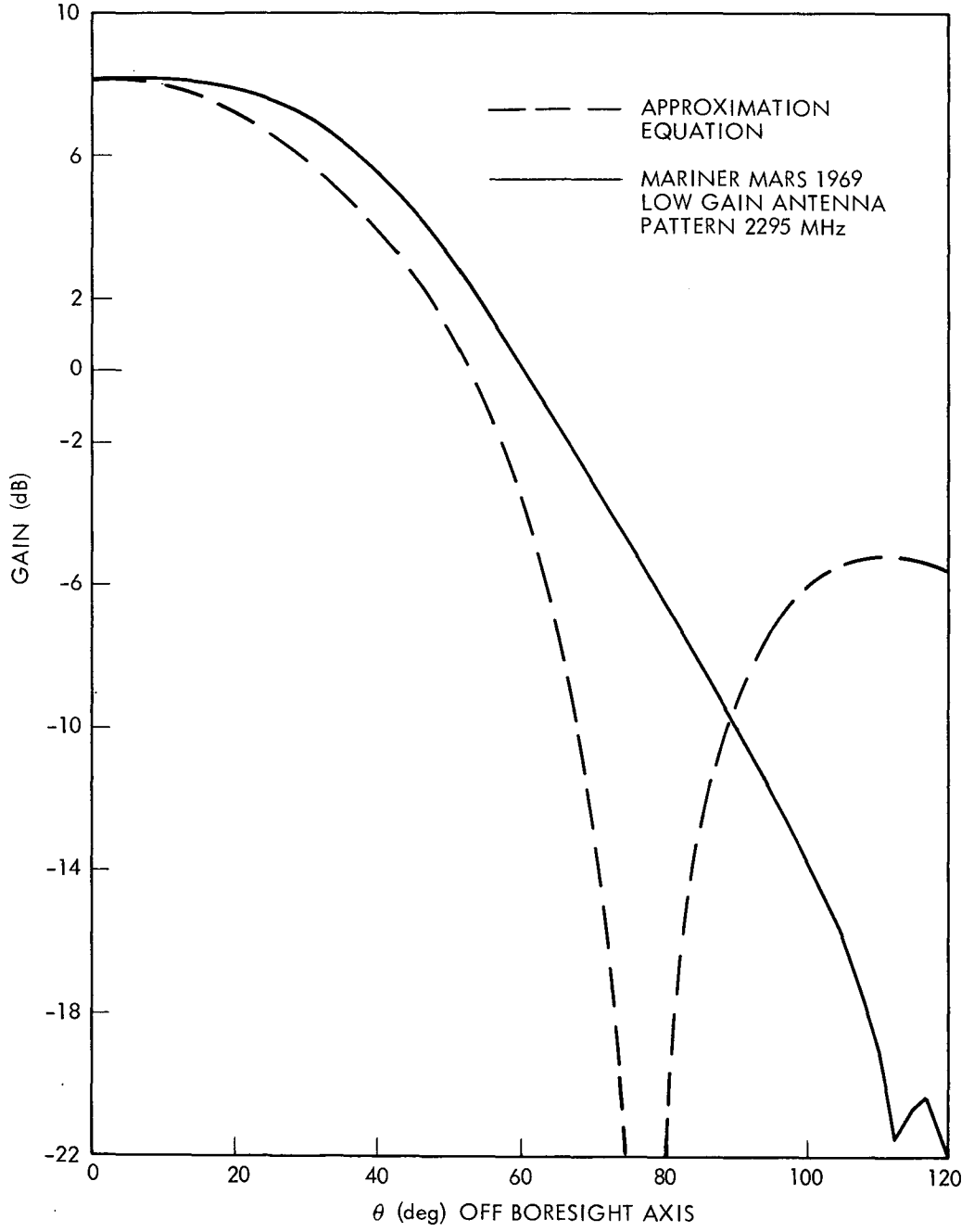

Fig. 7-4. Comparison of actual pattern and approximation equation for the Mariner Mars 1969 low-gain antenna at 2295 MHz

k_3 dB is a constant used to join the linear curve fit to the error at points where k_2 is changed for better fit

$\pm k_1$ is included in the design control table (DCT) as the tolerance on the peak gain

k_2 and k_3 are used to determine pointing loss tolerances as in paragraph 7.3

7.1.3 Gain - Beamwidth Relationships

In equation 7.1-7, we used the parameter θ_o, the 3 db-beamwidth of the antenna. θ_o is defined as the central planar angle over which the antenna gain function remains within 3 db of the peak antenna gain. Depending on the type of antenna, θ_o, the beamwidth may differ in different directions and in different planes. It is used as a measure of the directivity of the antenna, a small beamwidth implying a highly directive antenna, and vice versa. Thus, for increasing gain, the beamwidth decreases, and proper antenna pointing becomes more important. The concept of beamwidth is usually used only for antennas with a single major lobe, but can be useful in other cases if care is used in specification.

7.2 POINTING ERROR

The maximum spacecraft telecommunications performance is obtained when the target is aligned with the maximum-gain point of the spacecraft antenna. It is usually not desirable or necessary to maintain such target tracking and an acceptable tracking error is specified. This determines the positioning requirements for a given antenna.

Further, errors in spacecraft attitude and in antenna alignment prevent perfect pointing and give a range of positions over which one is likely to see the target.

7.2.1 Tracking Error

A variation of target position over the gain pattern of the antenna occurs with mission time due to the basic limitations of the antenna pointing system. For example:

1) For a fixed antenna position, the spacecraft-to-Earth vector is aligned with the peak gain for only short periods of time.

2) For a single-axis pointing system, the antenna does not track Earth exactly.

3) In a discrete pointing system, tracking error will occur because of noncontinuous position updating.

4) Optimizing antenna position for a range of trajectories may result in tracking errors for a particular flight vehicle trajectory.

The tracking error is not an error in the usual sense. It is a planned deviation from peak antenna gain, to lower costs for, and increase the reliability of the antenna subsystem. Tracking error is a function of mission time and is specified by degrees from boresight in antenna cone and clock coordinates.

7.2.2 Limit Cycle

For deep space missions in which a high quantity data return is desired over planetary distances, it is essential that the spacecraft be 3-axis stabilized. This requires the use of an attitude control system using gas jets. In order to keep gas consumption to realistic levels, the attitude control system typically operates in a "bang-bang" mode whereby the restoring torque is of the form shown in Figure 7-5. In the "dead band," no restoring torque is exerted and the spacecraft is free to move within this region. This results in an aiming tolerance for the antenna. The worst-case deadband excursion, transformed into antenna clock and cone coordinates, is entered into the supplementary information of the DCT. The worst case, best case, and the no-limit cycle case are used to find the pointing loss and tolerances as described in paragraph 7.3.

7.2.3 Uncertainty

In addition to the planned errors, there are two types of errors which contribute undesired components to antenna pointing error.

The first type appears in antenna installation. This includes errors in mounting the antenna to the spacecraft, the feed to the antenna, and in fabricating the antenna.

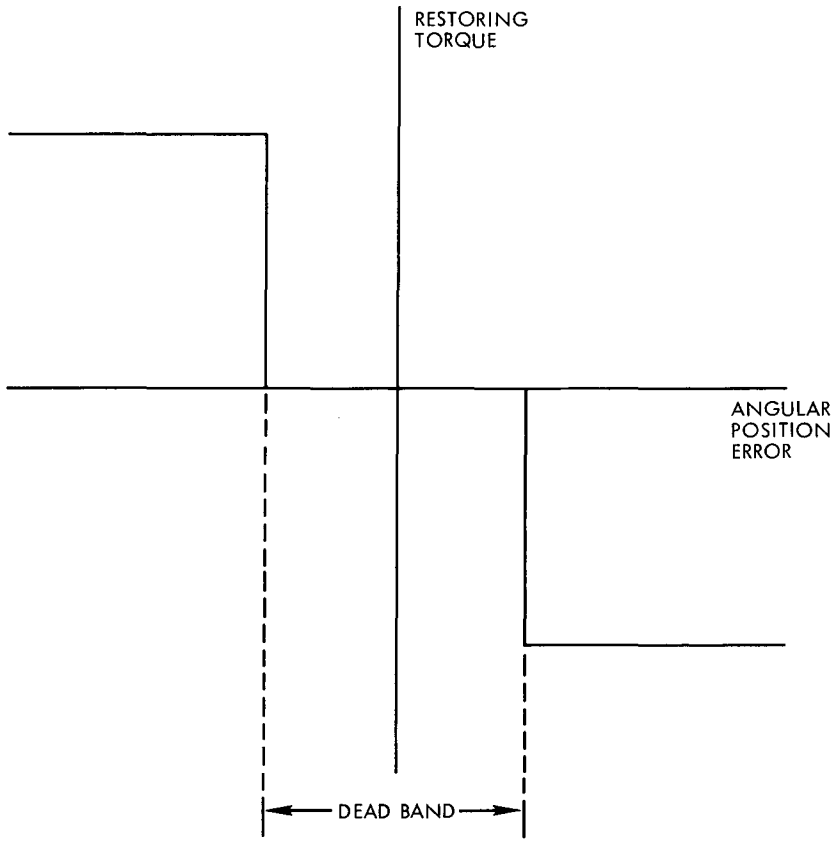

Fig. 7-5. Attitude control system operation

The second type of error occurs because the attitude sensing devices for detecting the correct spacecraft orientation are inaccurately mounted to the spacecraft. This results in the spacecraft attitude differing slightly from the nominal position in an unpredictable way.

For a typical vehicle, these errors are identified as:

1) Mechanical boresight location

2) Electrical boresight location

3) Sun sensor misalignment

4) Canopus sensor misalignment

Each of these uncertainties must have a specification range, which is then converted to antenna clock and cone coordinates. The sum of these angular errors form the uncertainty component of pointing loss tolerances. Table 7-2 gives an example of uncertainty error computation.

Table 7-2. Computation of uncertainty error

Source	Error in Antenna clock (deg)	Error in Antenna cone (deg)
Mechanical Boresight Location	±0.05	±0.05
Electrical Boresight Location	±0.05	±0.05
Sun Sensor Misalignment	±0.20	±0.25
Canopus Sensor Misalignment	±0.05	±0.10
Total Uncertainty Contribution	±0.35	±0.45

7.3 POINTING LOSS

Pointing loss has two components. The nominal pointing loss includes the planned gain loss due to tracking error. The pointing loss tolerances include the worst limit cycle case and the error contribution caused by antenna and sensor mounting inaccuracies. Best and no limit cycle cases are calculated in the same manner as shown below for worst-case pointing loss tolerances, and are provided in the DCT as comparison information.

7.3.1 Nominal Pointing Loss

Nominal pointing loss is found by locating the spacecraft-Earth vector on the antenna pattern. The clock and cone components of this vector are referred to as the tracking error, discussed in paragraph 7.7.1. Nominal pointing loss, usually just called pointing loss, is determined by:

$$P_L = G(\text{clock}, \text{cone}) - G_m \qquad (7.3\text{-}1)$$

where G(clock, cone) is the nominal antenna gain function and G_m is the nominal antenna gain. In some cases, the pointing loss will be referred to the gain at the axis of symmetry rather than the peak antenna gain. The reference to be used must be clearly specified.

7.3.2 Pointing Loss Tolerances

The pointing loss angular tolerances are found by adding the possible cone and clock deviations due to worst-case limit cycling and uncertainty. Let ΔC_{L+} be the positive deviation in clock, and ΔC_{L-} be the negative deviation in clock; ΔC_{c+} be the positive deviation in cone, and ΔC_{c-} be the negative deviation in cone. Also let C_L be the nominal target clock angle, and C_c be the nominal target cone angle. We then find the following antenna gains:

$$G(C_L,\ C_c) \triangleq G_o$$

$$G(C_L + \Delta C_{L+},\ C_c + \Delta C_{c+}) \triangleq G_1$$

$$G(C_L + \Delta C_{L+},\ C_c - \Delta C_{c-}) \triangleq G_2$$

$$G(C_L - \Delta C_{L-},\ C_c - \Delta C_{c-}) \triangleq G_3$$

$$G(C_L - \Delta C_{L-},\ C_c + \Delta C_{c+}) \triangleq G_4$$

The pointing loss tolerances at each of these points are defined by:

$$\pm (k_2 P_{Li} + k_3) \triangleq \pm T_i \qquad (7.3\text{-}2)$$

where

$$P_{Li} = G_i - G_m, i = 0, 1, 2, 3, 4$$

Now if i = k for $G_i + T_i$ a maximum, and i = ℓ for $G_i - T_i$ a minimum, then the favorable tolerance on pointing loss is equal to $k_2 P_{Lk} + k_3$, and the adverse tolerance is equal to $-k_2 P_{L\ell} - k_3$.

7.4 POLARIZATION LOSS

The gain function of an antenna does not completely characterize its performance. $G(\Omega)$ includes information on the magnitude of the electric field vectors of the antenna radiation, but discards information as to their relative phase. An antenna transmits an E field in a preferred way which can be described by the polarization factor, p, of the wave at each point in space,

where $p = E_y/E_x$ in a known coordinate system. By the theory of reciprocity, a receiving antenna will select incoming waves of the polarization of its transmit pattern and discard all others. The antenna is said to have a polarization pattern, and the ratio of the power delivered to the antenna terminals, P_R, to the power, P_{Avail}, which would be received by an antenna matched to the incident polarization, is called the polarization efficiency, ν.

$$\nu = \frac{P_R}{P_{Avail}} \tag{7.4-1}$$

This is referred to as polarization loss, measured in dB, and it must be added to the transmission equation to obtain the true received power.

In general, p is a function of the coordinate system chosen, and is a complex number. In practice, the antenna is usually designed so that orthogonal E-vector components are 90 degrees out-of-phase with one another in time. In this case, the E vector describes an ellipse with major axis R_1 and minor axis R_2. For this case,

$$p = \pm j\frac{R_1}{R_2} \triangleq \pm jAR$$

where $j = \sqrt{-1}$, and AR is called the axial ratio. The sign denotes the direction of E vector rotation. The term ellipticity is used to express the axial ratio in dB, where:

$$\text{ellipticity} = 20 \log_{10} AR \tag{7.4-2}$$

Generally, the antenna is characterized by a gain pattern and an ellipticity pattern.

For AR = 1, the E vector traces a circle and we have circular polarization. If the E vector rotates counterclockwise to an observer looking from the receiver to the source, p = -j and the wave is right-circularly polarized (RCP). For p = j, the wave is left-circularly polarized (LCP). Circular polarization is usually desirable for deep-space communication because ideally, a change in orientation of the spacecraft antenna with respect to the target

antenna, causes no polarization loss. However, for application to landers, or for certain atmospheric experiments, other considerations may dominate. For example, under certain conditions the multipath from a lander transmitting RCP will be almost entirely LCP and may be rejected by an RCP antenna.

All antennas have some ellipticity. It may be shown (reference 7-2) that the power transmission between two stations with generally RCP, can be written:

$$\frac{P(T)}{P_{tr}} = G_r G_t L_S L_C L_A G \left[\frac{\left(1+R_R^2\right)\left(1+R_T^2\right) + 4R_T R_R + \left(1-R_R^2\right)\left(1-R_T^2\right)\cos 2\psi}{2\left(1+R_R^2\right)\left(1+R_T^2\right)} \right] \quad (7.4\text{-}3)$$

(The term in brackets is the polarization loss (gain), L_P.)

where

$P(T)$ = Total received power at the receiver case

P_{tr} = Transmitted power at the transmitting antenna terminals

G_r = Gain of receiver antenna in receiving direction

G_t = Gain of transmitter antenna in transmitting direction

L_S = Space loss

L_C = Receiving circuit loss

L_A = Absorption loss

R_R = Receiving antenna axial ratio

R_T = Transmitting antenna axial ratio

ψ = Angle between the major axes of the polarization ellipses

G = Other system losses and gains.

Equation (7.4-3) applies to the antenna patterns on the digital antenna pattern (DAP) tapes that JPL uses. However, G_r and G_t are frequently given as referenced to an RCP wave. In this case:

$$\frac{P(T)}{P_{tr}} = G_t G_r L_S L_C L_A G \left[\frac{4\left(1 + R_R^2\right)\left(1 + R_T^2\right)}{\left(1 + R_R\right)^2 \left(1 + R_T\right)^2} \right]$$

$$\left[\frac{\left(1 + R_R^2\right)\left(1 + R_T^2\right) + 4R_R R_T + \left(1 - R_R^2\right)\left(1 - R_T^2\right) \cos 2\psi}{2\left(1 + R_R^2\right)\left(1 + R_T^2\right)} \right] \qquad (7.4\text{-}4)$$

7.4.1 Polarization Loss and Tolerances for the DCT

In general, we do not know the relative orientation of the polarization ellipses. Thus, we assume that ψ is random between 0 and 90 degrees (for greater than 90 degrees, the pattern repeats since the angular factor is 2ψ). If we denote polarization loss by the notation $L_P(\psi)$, then L_P (0 degrees) is a maximum (favorable), L_P (90 degrees) is a minimum (adverse), and L_P (45 degrees) is the average value. For DCT purposes, we use the polarization loss equations shown in Table 7-3. Figure 7-6 gives a plot of L_P (45°) versus spacecraft and DSIF antenna ellipticities.

7.5 ANTENNA NOISE TEMPERATURE AND NOISE SPECTRAL DENSITY

The noise power component seen by an antenna is due to electromagnetic radiation generated in the antenna bandwidth by:

1) Celestial bodies within the antenna beam
2) Atmospheric absorption and reradiation
3) Absorption and reradiation by physical bodies surrounding the antenna.

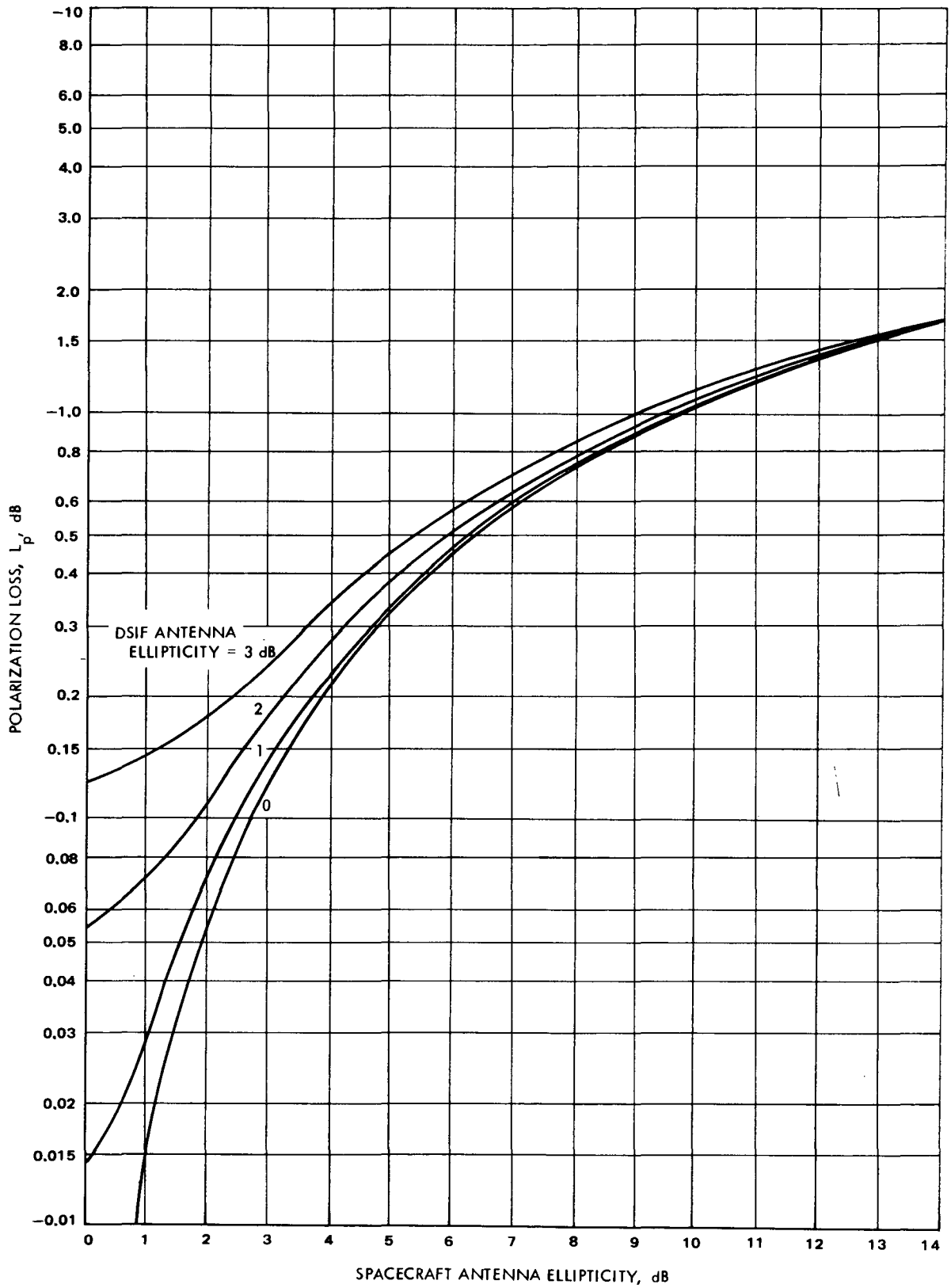

Fig. 7-6. Nominal polarization loss, L_p, versus spacecraft antenna ellipticity and DSIF antenna ellipticity

Table 7-3. Polarization loss equations

Type of Data	Polarization loss components (db)
DAP Tape:	
Nominal	$10 \log_{10}\left[\frac{1}{2} + \frac{2R_R R_T}{\left(1 + R_R^2\right)\left(1 + R_T^2\right)}\right] = L_P\,(45°)$
Adverse Tolerance	$-10 \log_{10}\left[\frac{1}{2} + \frac{2R_R R_T}{\left(1 + R_R^2\right)\left(1 + R_T^2\right)} - \frac{\left(1 - R_R^2\right)\left(1 - R_T^2\right)}{2\left(1 + R_R^2\right)\left(1 + R_T^2\right)}\right] + L_P\,(45°)$
Favorable Tolerance	$-10 \log_{10}\left[\frac{1}{2} + \frac{2R_R R_T}{\left(1 + R_R^2\right)\left(1 + R_T^2\right)} + \frac{\left(1 - R_R^2\right)\left(1 - R_T^2\right)}{2\left(1 + R_R^2\right)\left(1 + R_T^2\right)}\right] + L_P\,(45°)$
RCP Relative Patterns:	
Nominal	$10 \log_{10}\left[\frac{4\left(1 + R_R^2\right)\left(1 + R_T^2\right)}{\left(1 + R_R\right)^2\left(1 + R_T\right)^2}\right] + L_P(45°)$ above (see equation 7.4-4)
Tolerances	Unchanged from above equations

The effective antenna noise temperature is defined by (reference 7-2):

$$T_{ae} = \frac{\int_{4\pi} T(\Omega)G(\Omega)d\Omega}{\int_{4\pi} G(\Omega)d\Omega} \qquad (7.5\text{-}1)$$

where $T(\Omega)$ is the blackbody temperature of the environment in the direction Ω. At 2 GHz, typical spacecraft values of T_{ae}, including noise contributions due to surface finish errors and other antenna generated sources, are (refer to reference 7-4):

T_{ae} = 50°K, no bright noise sources occupying a significant fraction of the beam

T_{ae} = 200°K, entire beam intercepted by the moon

T_{ae} = 290°K, entire beam intercepted by the Earth

$T_{ae} \sim$ 10,000°K, entire beam intercepted by the Sun.

DSN antennas may have noise temperatures at S-band of 15°K or less when aimed at cold sky (no major celestial source) at high elevation angles. At X-band, T_{ae} is greatly increased by the presence of water vapor. Reference 7-5 should be consulted for typical values.

Frequently, the antenna noise temperature is divided into the following two components

$$T_g = \frac{\int_{\text{main lobe}} T(\Omega)G(\Omega)d\Omega}{\int_{4\pi} G(\Omega)d\Omega} \tag{7.5-2}$$

and

$$T_a = \frac{\int_{\text{side lobes}} T(\Omega)G(\Omega)d\Omega}{\int_{4\pi} G(\Omega)d\Omega} \tag{7.5-3}$$

then,

$$T_{ae} = T_g + T_a \tag{7.5-4}$$

This division is particularly useful for ground-based antennas at S-band, since for a cold sky and elevation angles greater than 10 degrees, T_g is constant and T_a is a function of azimuth and elevation of the antenna. At X-band, T_g may be modeled as the sum of an input temperature dependent on celestial sources, and an effective noise temperature $T_{Ae} = (L_A - 1)T_A$ due to atmospheric attenuation. Where T_{Ae} is the effective temperature of the atmosphere, L_A is the total loss due to energy absorption, and T_A is a density averaged temperature of the atmosphere equal to about 280 to 290°K. This is equivalent to regarding the atmosphere as a passive circuit loss as discussed in paragraph 2.6.3.4.1.

For spacecraft antennas, the distinction between T_g and T_a is not usually made, although it might prove useful for steerable antennas if the spacecraft effects are large and variable.

The noise spectral density, N_o, at the antenna terminal is:

$$N_o = kT_{ae} \tag{7.5-5}$$

where k is Boltzmann's constant, 1.38×10^{-20} mW-sec/°K, or -198.6 dBm/Hz°K. By definition 7.5-1, antenna gain is included in the computation of T_{ae}. Frequently, noise contributers such as surface finish errors are lumped into T_{ae}, since there is no effective way to separately measure these sources when measuring T_{ae}.

7.6 CHOICE OF ANTENNA PATTERN

For a telecommunication system, varying the antenna gain is one of the least expensive methods of getting performance per dB, provided proven antenna types are used. The only other method that rivals antenna choice is bit rate, but bit rate is generally set by other system requirements.

(For a given power-gain product, there is a particular combination of antenna gain and transmitter power at which the spacecraft weight is minimized. Thus, in weight-critical vehicles, increasing transmitter power rather than antenna gain may be required despite possibly higher cost (reference 7-6).)

The telecommunications designer must obtain an idea of the minimum antenna gains necessary to accomplish the mission for each mode by using state-of-the-art values for spacecraft parameters and the committed DSN parameters for the mission data. This provides a starting point for antenna choice.

For example, a minimum antenna gain of 2 dB implies one or more low gain antennas of a form dependent on coverage requirements. A minimum gain of 18 dB would require highly directive antennas and perhaps a steerable dish.

7.6.1 Coverage Requirements

The designer begins by mapping the gain requirements for each mission phase and for the range of trajectories on a cone-clock grid referenced to the spacecraft. This gain contour map is combined with other constraints (e.g., roll symmetry in maneuvers) to determine the required gain and beamwidth. The antenna designer and system designer can then work together to determine types of antennas and their articulation. Note that antenna position and motion also impact the mechanical structure, attitude control, and Central Computer and Sequencer Subsystem, the number of commands, and mission operations.

7.7 FLIGHT ENVIRONMENT

Mounting antennas on a spacecraft changes their patterns and introduces interference effects which may be estimated and measured.

7.7.1 Interferometer Effects

A typical spacecraft mounts at least two antennas of the same design frequencies. These are connected by circulator switches to the same receiver. Because of line mismatches and imperfect switches some fraction of power into the receiver comes from the antenna which is not in use. (Similarly in transmission, a fraction of the power transmitted comes from the non-operating antenna.) Since the path length traveled from the antenna to the receiver is different, the signals will not be in phase when they are summed. Thus, an interference and loss of power called the interferometer effect will occur.

Figure 7-7 gives a model for interferometer equations, where:

a_1 = Unknown electrical path length from Antenna 1 phase center to summing point.

a_2 = Unknown electrical path length from Antenna 2 phase center to summing point.

ℓ = Free space distance between antenna phase centers.

θ = Angle between the spacecraft (S/C)-to-Earth vector and the line joining the antenna phase centers.

$d = \ell \cos \theta$ = extra distance the wave travels from Antenna 1 to Antenna 2.

k_1 = Voltage gain (loss) for Antenna 1 signal between Antenna 1 and summing point.

k_2 = Voltage gain (loss) for Antenna 2 signal between Antenna 2 and summing point.

The relative voltages received at Antenna 1 and Antenna 2, respectively, are:

$$V_1 = g_1(\Omega_1) \tag{7.7-1}$$

$$V_2 = g_2(\Omega_2)e^{j\beta d} \tag{7.7-2}$$

where

g_1 = The voltage gain function of Antenna 1

g_2 = The voltage gain function of Antenna 2

Ω_1 = Solid angle from the axis of Antenna 1 to the S/C-to-Earth vector

Ω_2 = Solid angle from the axis of Antenna 2 to the S/C-to-Earth vector

$\beta = 2\pi/\lambda$

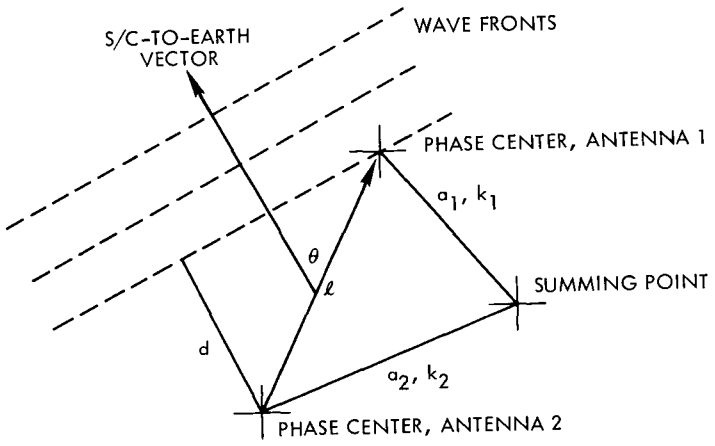

Fig. 7-7. Model for interferometer effect

So that, at the summing point, the received voltage is:

$$V_R = k_1 g_1(\Omega_1) e^{j\beta a_1} + k_2 g_2(\Omega_2) e^{j\beta(d+a_2)} \tag{7.7-3}$$

with average power:

$$P_R = |V_R|^2 = k_1^2 g_1(\Omega_1)^2 + k_2^2 g_2(\Omega_2)^2 + 2k_1 k_2 g_1(\Omega_1) g_2(\Omega_2) \cos\left[\beta(d + a_1 - a_2)\right] \tag{7.7-4}$$

Now if the operating antenna is chosen as Antenna 1, then the received power desired is

$$P_{R1} = k_1^2 g_1(\Omega_1)^2 = k_1^2 P_o G_1(\Omega_1) \tag{7.7-5}$$

where

$G_1(\Omega_1)$ = Power gain of Antenna 1

P_o = Power received at the antenna terminals of an isotropic antenna located at the phase center of Antenna 1 (or at the phase center of Antenna 2 since the range difference is negligible)

So that

$$\frac{P_R}{P_{R1}} = 1 + \left(\frac{k_2}{k_1}\right)^2 \frac{G_2(\Omega_2)}{G_1(\Omega_1)} + 2\frac{k_2}{k_1}\left[\frac{G_2(\Omega_2)}{G_1(\Omega_1)}\right]^{1/2} \cos\left[\beta(d+a_1-a_2)\right] \qquad (7.7\text{-}6)$$

is the power gain (loss) due to the interferometer effect. If the coordinates of an interferometer minimum are known, $a_1 - a_2$ may be found by the relation:

$$\beta(a_1 - a_2 + d_m) = \pi \qquad (7.7\text{-}7)$$

Or,

$$(a_1 - a_2) = \frac{\lambda}{2} - d_m \qquad (7.7\text{-}8)$$

where $d_m = d$ for P_R a minimum due to the interferometer effect.

Equation (7.7-6) can be used to establish interferometer power gain and its tolerances by using the tolerances on $\Omega, G_1, G_2, k_1, k_2$, and $(a_1 - a_2)$, and searching for the worst and best combination. P_R/P_{R1} is very sensitive to $a_1 - a_2$, therefore, for accurate estimation of this quantity, $a_1 - a_2$ must be known to about 0.1λ. If this accuracy is not obtainable, the nominal, adverse, and favorable tolerances may be obtained by setting the cosine term equal to 0, 1, and -1, respectively, and varying Ω, G_1, G_2, k_1, and k_2 within their tolerances.

P_R/P_{R1} is an average effect. The fading should also be examined as a function of time to insure that no fades develop that are deep enough to cause loss of lock. In addition, for a large effect, the assumption of Gaussian noise breaks down, and the statistics of data reception must be re-examined.

The above analysis can be easily extended to more than two antennas by adding the appropriate received voltages.

7.7.2 Spacecraft Obscuration of Antenna Pattern

Although the antenna is usually pointed in the general direction of the target, there are times when, either accidentally or intentionally, the target may be off the main beam. During maneuver, for example, reception may be required off the back side of the spacecraft structure.

The spacecraft does not "block" the radiation as would be predicted by geometrical optics. Rather, the spacecraft structure forms a radiating structure. Thus, some rf may be detected even though the antenna is completely obscured in the target direction.

For the purposes of this handbook, it is sufficient to mention that the system designer may expect very deep nulls (down 50 dB or more from peak gain) due to spacecraft obscuration. These will place limits on spacecraft maneuvering that will become increasingly stringent with increasing range.

REFERENCES

7-1 Silvers, S., ed. Microwave Antenna Theory and Design, Boston Technical Lithographers, Inc., (Lexington, Mass: 1963).

7-2 Rusch, W. V. T., and P. D. Potter, Analysis of Reflector Antennas, Academic Press (New York: 1970).

7-3 Blake, L. V., Antennas, John Wiley & Sons (New York: 1966).

7-4 Kenduck, J. B., ed., TRW Space Data, 3rd Edition, TRW Systems Group (TRW, Inc.: 1967).

7-5 Deep Space Network/Flight Project Interface Design Handbook, DSN Standard Practice, 810-5 (JPL internal document).

7-6 Mathison, R. P., "Spacecraft Telecommunication System Design," October, 1963.

SECTION VIII

CHOICE OF SIGNAL FREQUENCIES

8.1 INTRODUCTION

In considering a signal frequency design for a deep space flight project, the system designer must satisfy his project's requirements for navigational accuracy, command capability, data return and radio-science measurements within the constraints and procedures of the DSN. This section describes these constraints and procedures and discusses signal design within them.

8.2 CHOICE OF CARRIER FREQUENCIES

Out of the entire electromagnetic spectrum, only certain increments are used for deep-space communications. These increments are chosen for various reasons: administrative, technological, and physical.

For purposes of identification, the microwave spectrum is divided into eight lettered bands, as shown in Table 8-1. Within these bands are the ranges permissible for deep-space communication. These are usually referred to by their letter designation even though they occupy only a small portion of the letter band. For example, when referring to deep-space communication through the DSN, S-band includes 2110 to 2120 MHz uplink, and 2290 to 2300 MHz downlink, although in general, S-band represents the spread from 1550 to 5200 MHz. These designations have no official standing, so that caution must be used in their reference to assure mutual understanding.

8.2.1 Spectrum Allocation

In order to manage the use of the electromagnetic frequency spectrum, the International Telecommunication Union (ITU) has established regulations on the use of all frequencies below 275.0 GHz. The United States Government has acted within these regulations to further restrict the purpose for which frequencies can be used. Thus, the DSN is strictly limited in its selection of carrier frequencies and, in general, frequency is not a performance optimization variable.

The DSIF has one operational frequency capability in S-band, and one soon to be operational in X-band. The DSIF frequency capability and status undergo considerable development, and the most up-to-date revision of reference 8-15 should be consulted for frequency band availability.

Table 8-1. Letter designations for microwave bands*

Band	Frequency Range (MHz)	Wavelength (cm)
P	225 - 390	133.3 - 76.9
L	390 - 1550	76.9 - 19.3
S	1550 - 5200	19.3 - 5.77
X	5200 - 10,900	5.77 - 2.75
K	10,900 - 36,000	2.75 - 0.834
Q	36,000 - 46,000	0.834 - 0.652
V	46,000 - 56,000	0.652 - 0.536
W	56,000 - 100,000	0.536 - 0.300
* Source: Reference 8-1, with permission		

8.2.1.1 S-band Limits. The normal frequency allocation for DSIF S-band operation is:

Uplink: 2110 to 2120 MHz

Downlink: 2290 to 2300 MHz

Many deep space projects are constrained to use the DSIF frequencies. Thus, these bands have been divided into frequency channels, one or more of which, to a limit of 3.3 MHz, are assigned for uplink and downlink transmission. Reference 8-15 details the channel center frequencies.

For S-band, these channel allocations have average bandwidths of approximately:

Uplink: .34 MHz

Downlink: .37 MHz

The channel bandwidths are not necessarily equal to these figures for any given channel.

Performance is not completely uniform over the full bandwidth. For example, for the Block IIIC exciter (the present operational system) on the 64-m antenna, performance is down 1 dB at the extremes of the allocation (2110 and 2120 MHz), due to band limiting in the exciter.

8.2.1.2 X-band Limits. The soon-to-be-operational Block IV equipment has an X-band capability in addition to S-band. The full frequency allocation for DSIF X-band operation is:

Uplink: 7145 to 7235 MHz

Downlink: 8400 to 8500 MHz

These channel allocations have average bandwidths of approximately:

Uplink: 1.16 MHz

Downlink: 1.36 MHz

The channel bandwidths are not necessarily equal to these figures for any given channel. At the Jet Propulsion Laboratory, X-band spacecraft capability is considered experimental. It will first be tested operationally by Mariner-Venus-Mercury '73 on the downlink only.

8.2.1.3 Coherent Up and Downlink. For vehicles with stringent navigation requirements, two-way doppler is a necessity. This requires coherency between up and downlink carriers. Coherency is maintained by use of frequency translation of the uplink carrier. For DSN-compatible spacecraft, the translation ratios are shown in Table 8-2.

Since the up and downlink frequency band allocations are not related to each other by these ratios over their whole range, the transponder usable bands are restricted as shown in Table 8-3.

8.2.2 Data Return

As was demonstrated earlier, the data return for a given modulation scheme depends on the ratio of total received power divided by noise spectral

Table 8-2. Coherency ratios

Uplink	Downlink	Nomenclature	Ratio of Frequencies Down/Up
S-band	S-band	S/S	240/221
S-band	X-band	S/X	880/221
X-band	X-band	X/X	27/23

Table 8-3. Available frequency band for coherent operation

Mode	Link	Approximate Usable Frequency Range
S/S	Up	2110-2117.9 MHz
	Down	2291.4 - 2300 MHz
S/X	Up	2110 - 2120 MHz
	Down	8401.8 - 8441.6 MHz
X/X	Up	7155.6 - 7235 MHz
	Down	8400 - 8493.3 MHz

density (P_T/N_o) at the input to the detector. The components of this ratio depend on carrier frequency and phenomena which depend on carrier frequency. The details of this frequency dependence are discussed in Appendix A.8.1. The conclusions are detailed below.

A simple analysis which neglects atmospheric phenomena, indicates improvement in P_T/N_o with increasing frequency.

For a paraboloid-horn antenna pair (the typical command and cruise telemetry situation), $P_T/N_o \propto f$. For a paraboloid - paraboloid pair (typical encounter sequence), $P_T/N_o \propto f^2$.

For clear sky conditions and frequencies from 1 to 10 GHz, the analysis is valid and the above proportionalities apply. Thus, the data return is greatly increased by choice of a higher frequency band. One caution is necessary however; the analysis assumes that phase jitter is independent of frequency. Phase jitter tends to increase with increasing frequency due to hardware design problems. Thus, the performance gain is somewhat, but not substantially, less than shown.

At and above X-band, the atmospheric losses due to oxygen and water resonances limit improvement. These frequencies are thus weather dependent links. Reference 8-2 discusses system considerations for operation in these regions.

For X-band systems, bad weather can make the system inoperable. This problem can be ameliorated by increasing the spacecraft data storage capacity to enable rebroadcast in periods of good weather. Since the DSN sites are located in dry areas of the Earth, the probability of high degradation due to weather is low, giving the X-band system significant data-return advantages where real-time operation is not required over long periods. Reference 8-15 has information as to antenna gain and weather degradation for the X-band system.

8.2.3 Multiple Uplink Transmission

When two or more spacecraft are separated by very small angular increments, it may be possible to transmit uplink signals to them, and receive downlink signals from them, simultaneously. For example, two Mars Orbiters are well within the 3-dB beamwidth of the DSS-14 antenna at either X or S-band.

The small size of the angular increments can be judged from the antenna 3-dB beamwidths shown in Table 8-4.

When the transmitted uplink carriers are in different frequency channels (the usual case), there are two methods of transmission: time multiplexing and frequency multiplexing. Each has certain desirable and undesirable characteristics, as described below. Neither has been used operationally and both must be classified as experimental.

8.2.3.1 Time Multiplexing. The time multiplexing of carriers is known as the switched-carrier mode of operation. The method is to switch on each carrier and its modulation for an equal amount of time, cycling through all carriers. Limiting consideration to the dual-carrier situation, the uplink signal is represented by (reference 8-3):

$$s(t) = \left[\frac{1}{2} + \frac{1}{2}\,\mathrm{sq}\,(\omega_s t)\right] \sqrt{P}\,\sin\left(\omega_1 t + \theta_{c_1} + \theta_{m_1}\, m(t) + \theta_{r_1}\, r(t)\right)$$

$$+ \left[\frac{1}{2} - \frac{1}{2}\,\mathrm{sq}\,(\omega_s t)\right] \sqrt{P}\,\sin\left(\omega_2 t + \theta_{c_2} + \theta_{m_2}\, m(t) + \theta_{r_2}\, r(t)\right)$$

$$= s_1(t) + s_2(t) \qquad (8.2\text{-}1)$$

where $\mathrm{sq}\,(\omega_s t)$ = Square wave of amplitude ±1 (for two carriers)

ω_s = Switching frequency

θ_c = Random carrier phase

$m(t)$ = Command modulation (single-channel, digital command system)

$r(t)$ = Ranging modulation

θ_m = Command modulation angle

θ_r = Ranging modulation angle

and subscript 1 applies to carrier 1, subscript 2 applies to carrier 2.

Equation (8.2-1) may be expanded into the carrier, command, ranging, and intermodulation terms familiar from CW analysis, plus terms

Table 8-4. 3 dB beamwidths of DSN antennas

Antenna Size	Nominal Uplink Beamwidth (deg)	
	S band	X band
64 meter	0.150	0.044
26 meter	0.36	0.11

which depend on the switching frequency. For example,

$$
\begin{aligned}
s_1(t) = {} & \frac{\sqrt{P}}{2} \cos\theta_{m_1} \cos\theta_{r_1} \sin(\omega_1 t + \theta_{c_1}) \\
& + \frac{\sqrt{P}}{2} \cos\theta_{m_1} \sin\theta_{r_1}\, r(t) \cos(\omega_1 t + \theta_{c_1}) \\
& + \frac{\sqrt{P}}{2} \sin\theta_{m_1} \cos\theta_{r_1}\, m(t) \cos(\omega_1 t + \theta_{c_1}) \\
& - \frac{\sqrt{P}}{2} \sin\theta_{m_1} \sin\theta_{r_1}\, m(t)\, r(t) \sin(\omega_1 t + \theta_{c_1}) \\
& + \frac{\sqrt{P}}{2} \cos\theta_{m_1} \cos\theta_{r_1}\, \mathrm{sq}(\omega_s t) \sin(\omega_1 t + \theta_{c_1}) \\
& + \frac{\sqrt{P}}{2} \cos\theta_{m_1} \sin\theta_{r_1}\, r(t)\, \mathrm{sq}(\omega_s t) \cos(\omega_1 t + \theta_{c_1}) \\
& + \frac{\sqrt{P}}{2} \sin\theta_{m_1} \cos\theta_{r_1}\, m(t)\, \mathrm{sq}(\omega_s t) \cos(\omega_1 t + \theta_{c_1}) \\
& - \frac{\sqrt{P}}{2} \sin\theta_{m_1} \sin\theta_{r_1}\, m(t)\, r(t)\, \mathrm{sq}(\omega_s t) \sin(\omega_1 t + \theta_{c_1})
\end{aligned}
\tag{8.2-2}
$$

In general, one-half of the available power is lost in the switching sidebands. In addition, the choice of sq ($\omega_s t$) may produce undesired harmonics which degrade performance. However, the switching harmonic power may be regained in the desired spectrum if sq ($\omega_s t$) is chosen to be m(t), r(t), a combination of m(t) and r(t), or the high frequency or clock component of r(t) (r(t) = c(t) $\oplus$ r'(t)).

Any such choice places constraints on the system and may require hardware changes on the spacecraft. Table 8-5 lists the constraints for several choices of switching signal.

A particularly interesting choice is to use sq ($\omega_s t$) = c(t), the ranging clock. However, if c(t) is chosen to be of frequency $2f_s$, where $f_s = 1/T_B$ and T_B is a ranging code bit time, the combination of switching and modulation will be such that the spacecraft limiter will eliminate every other range bit. This problem can be alleviated by the choice sq ($\omega_s t$) = $4f_s$, or sq ($\omega_s t$) = $2f_s \angle 90°$. This method causes a 3-dB loss in ranging power from that originally sent to each spacecraft and doubles the ranging signal bandwidth.

With this method, the limiter would cause a signal suppression factor of

$$\alpha_\ell = \text{erf} \sqrt{\eta_\ell / 2} \tag{8.2-3}$$

where η_ℓ = Limiter input SNR

The output SNR of the limiter, η_o, would be given by:

$$\eta_o = \frac{\alpha_\ell^2}{1 - \alpha_\ell^2} \tag{8.2-4}$$

(reference 8-4).

The switched-carrier method remains highly experimental, with many theoretical and experimental questions to be answered. The results of some experiments have been published as reference 8-5.

Table 8-5. System constraints for switched-carrier choices of switching waveform

Switching Waveform sq ($\omega_s t$)	Constraints
a. Two-Channel Ranging and Command Modulation.	
r(t)	r(t) signal components in-phase instead of quadrature. Requires shifting S/C carrier reference 90° to demodulate r(t)
m(t)	Same comment as above, but for m(t).
m(t) r(t)	No S/C change needed, but Θ_m and Θ_r are no longer independent variables. Power in signal components depends on $\Theta_{m_1} + \Theta_{r_1}$ and $\Theta_{m_2} - \Theta_{r_2}$.
c(t)	sq ($\omega_s t$) must be twice the frequency of c(t) or shifted 90° from c(t); otherwise the ranging limiter on the S/C destroys the ranging information. The bandwidth of the ranging signal is doubled by this action.
b. Ranging and Command Interplexed	
r(t) or m(t)	Same comment as for sq ($\omega_s t$) = m(t) r(t) above
r(t) m(t)	Power in r(t) and m(t) components is constrained to be equal.

8.2.3.2 Frequency Multiplexing. Frequency multiplexing is operationally simpler than time multiplexing since it does not require highly accurate, extremely fast switching modules. The uplink signal out of the exciter is represented by:

$$\begin{aligned} s(t) &= A_1 \cos\left(\omega_1 t + \theta_{c_1} + \theta_{m_1}\, m(t) + \theta_{r_1}\, r(t)\right) \\ &+ A_2 \cos\left(\omega_2 t + \theta_{c_2} + \theta_{m_2}\, m(t) + \theta_{r_2}\, r(t)\right) \\ &+ \ldots + A_n \cos\left(\omega_n t + \theta_{c_n} + \theta_{m_n}\, m(t) + \theta_{r_n}\, r(t)\right) \end{aligned} \tag{8.2-5}$$

where $\frac{1}{2}\left(A_1^2 + A_2^2 \ldots + + A_n^2\right) = P$, the total power transmitted. (Note the flexibility in power allocation for each carrier.)

Limiting consideration to two carriers, and ignoring modulation,

$$s(t) = A_1 \cos\left(\omega_1 t + \theta_{c_1}\right) + A_2 \cos\left(\omega_2 t + \theta_{c_2}\right) \tag{8.2-6}$$

The problems in frequency multiplexing occur primarily because s(t) is not the transmitted signal. The klystron amplifier is a highly non-linear device, whose output can be represented by:

$$s_T(t) = \sum_{k=0}^{\infty} C_k \left[s(t)\right]^k \tag{8.2-7}$$

Thus, for an S-band signal, possibly interfering harmonics extend past X-band. For example, for the two carrier signals of equation (8.2-6), the frequencies present in $s_T(t)$ to only third order are:

$0,\ \omega_1,\ \omega_2,\ 2\omega_1,\ \omega_1 + \omega_2,\ \omega_1 - \omega_2,\ 2\omega_2,\ 3\omega_1,\ 2\omega_1 + \omega_2,\ 2\omega_1 - \omega_2,$ $2\omega_2 + \omega_1,\ 2\omega_2 - \omega_1,\ 3\omega_2$. Harmonics generated by k = 7 are easily visible in a spectral analyzer, particularly the components at every spacing Δ,

where $\omega_2 - \omega_1 = \Delta$. When modulation is applied to the carriers, it also appears on the intermodulation products (IMP). For time multiplexing, only integer frequency multiples appear as IMP since the klystron sees only one carrier at a time. Switching frequencies are too low for the klystron bandpass characteristic to pass.

With care, carrier frequencies may sometimes be chosen so that the IMP are not directly in a spacecraft's loop bandwidth. Thus, the particular problem is primarily due to interference from the wide spectrum of the ranging. Choosing the carriers further apart does not necessarily eliminate the system problem, since this results in lower order (and hence greater power) harmonics in the ground receiver passband.

This method is also experimental but has the advantage that the analysis methods for determining degradation are well understood. At present, the DSIF limits power per carrier in a dual-carrier configuration to 10 percent of full-scale, single-carrier operation. The klystron tubes were not designed for such operation and there is uncertainty as to how they will be affected. Figure 8-1 shows a sample transmitted signal spectrum for a frequency multiplexing experiment.

8.2.4 Radio Science Factors

The presence of gases in the communication path is generally inimical to telecommunication performance. However, precise measurement of the electromagnetic wave changes caused by their presence gives information as to their physical properties. Thus, it may be desirable to choose frequencies that are better degraded by such effects and system parameters that permit precise measurement. However, radio science investigations in the DSN are limited to the operational frequencies for which DSN equipment is designed. Within this constraint, radio science frequency preferences are one input to determining spacecraft frequency assignments. This section discusses the requirements for two types of measurements: neutral measurements and charged particle measurements. References 8-6 through 8-11 discuss elements of the problems in detail.

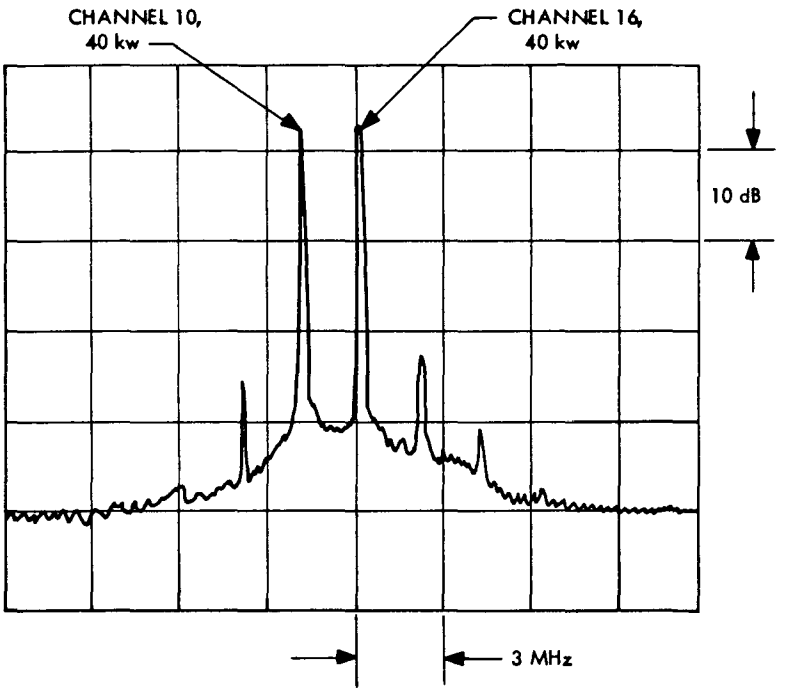

Fig. 8-1. Sample transmitted frequency-multiplexed signal spectrum

8.2.4.1 Neutral Particle Measurements. When an electromagnetic wave passes through the neutral portion of a planet's atmosphere, it is altered in phase, power, and direction in a manner which depends on the atmospheric composition, pressure, and temperature. By measuring the above effects, an atmospheric refractivity profile can be obtained, which, upon processing, can result in knowledge of the atmosphere. Paragraph 2.6.3.5 discusses some of these effects and their impact on telecommunications.

Such measurements can be obtained from a spacecraft carrier signal if other effects which also cause phase, power, and directional changes can be minimized sufficiently. Thus, specifications on the carrier component must reflect radio science requirements. Table 8-6 lists error sources and their trend with frequency selection.

Table 8-6. Neutral atmospheric measurement error sources and the effect of frequency selection

Error Source	Trend with Increasing Frequency
Doppler Inaccuracy	Decreases
Carrier Frequency Instability	Increases
Earth Tropospheric Effects	Increase
Earth and Planetary Ionospheric Effects	Decrease
Solar Corona Bandwidth Spreading	Decreases $\propto 1/f$ (one way) (ref. 8-7)
Interplanetary Plasma Effects	Decrease
Planetary Atmospheric Attenuation	Depends on atmosphere. Small attenuations give information. Highly attenuating atmospheres cut off signal above planetary surface.
Resolution Inaccuracy in Heights	Decreases $\propto 1/\sqrt{f}$ (ref. 8-6)

8.2.4.2 Charged Particle Measurements. A concentration of charged particles changes the same properties of an electromagnetic wave as does a neutral particle concentration. However, where the neutral effect is relatively independent of frequency, the charged particle effect is a function of the inverse of the frequency. Hence, it is desirable to decrease frequency for measurement of these effects. Table 8-6 also applies to charged particle error sources if it is noted that the planetary ionosphere and interplanetary plasma effects are now the variables of interest.

At spacecraft communication frequencies, the effects caused by positively charged particles are negligible because of the particles' relatively large mass. Thus, the measurements of interest concern electron concentrations. For example, solar proton flux is not measurable by its effect on carrier frequency.

Solar coronal and interplanetary plasma measurements can be accomplished by a single S-band carrier frequency spacecraft. To measure the refractivity profile of a planet by this method poses problems, since it is difficult to separate tropospheric and ionospheric effects. With one S-band carrier frequency, this can be done by the altitude diversity of the layers. However, calibration to eliminate the effects of the interplanetary and Earth ionospheric media is difficult. Simultaneous independent measurements of Earth's ionospheric electron concentration and solar activity reduce this form of error.

There are three methods for further reduction. If two spacecraft are in the vicinity of the planet, only one of which is transmitting through the atmosphere, the second vehicle can be used as a calibration source. Reference 8-11 briefly describes this approach.

The second method, termed the "Differenced Range versus Integrated Doppler" or DRVID technique, measures the first time-derivative of total electron content along the ray path. This measurement can be integrated along the spacecraft trajectory and used both to measure charged particle effects, and calibrate for charged particle densities of extraneous phenomena. A brief discussion of the technique will be found in paragraph 2.3.4.

The most accurate method is to use frequency diversity aboard a single spacecraft. If the vehicle transmits two carriers, one at S-band and a coherent frequency at X-band, the X-band transmission will calibrate the S-band charged particle measurements, since X-band is virtually unaffected by the observed electron densities. As a bonus, X-band is generally more accurate in determining neutral atmospheric parameters. This method is discussed in detail in reference 8-10. A brief description will be found in paragraph 4.4.3.

8.2.4.3 Faraday Rotation. When a linearly polarized electromagnetic wave is incident on a plasma in the presence of a magnetic field, the plane of polarization is rotated by an amount:

$$\Omega = \frac{R}{f^2} \int_{\substack{\text{ray} \\ \text{path}}} ||\bar{H}|| \cos \Theta \, n_e(s) \, ds \qquad (8.2\text{-}8)$$

where Ω = Faraday rotation of the plane of polarization, radians.

Θ = Angle between the signal direction and $\bar{H}$, the magnetic field vector

$||\bar{H}|| \cos \Theta$ = Tangential component of the magnetic field above the ray path, A-turns/m.

$n_e(s)$ = Local density of electrons along the ray path, electrons/m^3

f = Signal frequency, Hz

R = 2.97×10^{-2} in mks units.

Thus, Faraday rotation can be used to measure electron density if the magnetic field and the original plane of polarization are known. The effect is used for measurements of the Earth's ionospheric effects during spacecraft measurement by using satellite transponders (see reference 8-8).

8.3 BANDWIDTH CONSIDERATIONS AND CONSTRAINTS

In addition to frequency channel restrictions defined by the spacecraft channel assignments, DSN equipment is limited in the bandwidth it can handle for various types of signals. Within these constraints the designer is free to vary bandwidth to give the optimum performance for his system. In certain cases, the optimum bandwidths are known, for example, the optimum spacecraft ranging signal bandwidth has been derived for the JPL equipment. In other cases, the bandwidth is optimized by using the information in preceding sections of this handbook. This section discusses some of the considerations not mentioned above, and references appropriate design information from the DSN equipment descriptions in reference 8-15.

8.3.1 Total Signal Bandwidth

The total signal bandwidth can be divided into the design signal bandwidth and the total mission occupancy due to doppler shifting of the design bandwidth.

The design bandwidth includes the optimum signal spectrum which the designer wishes the data detection devices to see. It is limited either by equipment constraints or noise constraints. As an example of the latter, there is no point in trying to send a very good square wave if the power in the higher harmonics does not improve the bit error rate more than the noise admitted by a wider bandwidth degrades it. The better solution would be to put more power into the lower harmonics and neglect decreasing the rise and fall times of the wave.

Doppler shifting of the signal can easily move it into another channel during a mission and will also change the nominal signal bandwidth. This effect must be included in requesting a frequency allocation and in designing the system.

8.3.1.1 Signal Harmonics. A signal of the form (see section 5.2.1.1)

$$s(t) = \sin \left[\omega t + \theta (D_1 \oplus SC_1) + \theta_2 (D_2 \oplus SC_2)\right] \qquad (8.3\text{-}1)$$

where D_i = Binary data symbols in the i^{th} channel and

SC_i = Subcarrier waveform in the i^{th} channel, can be rewritten in the form

$$s(t) = \cos(\theta_1 SC_1) \cos(\theta_2 SC_2) \sin \omega t$$

$$+ D_1 \sin(\theta_1 SC_1) \cos(\theta_2 SC_2) \cos \omega t$$

$$+ D_2 \sin(\theta_2 SC_2) \cos(\theta_1 SC_1) \cos \omega t$$

$$+ D_1 \oplus D_2 \sin(\theta_1 SC_1) \sin(\theta_2 SC_2) \sin \omega t \qquad (8.3\text{-}2)$$

The four terms of 8.3-2 can be recognized as: carrier; data 1; data 2; and intermodulation product terms, respectively. The detailed spectrum of the signal depends on the form of the subcarriers. For a sine-wave subcarrier, $SC = \sin \omega_{sc} t$, the data signal is modulated on a baseband spectrum of the form

$$\sin(\theta \sin \omega_{sc} t) = \sum_{n=1}^{\infty} 2 J_n(\theta) \sin n \omega_{sc} t \qquad (8.3\text{-}3)$$

with power at the n^{th} harmonic equal to

$$P_n = 2P_{tr} J_n^2(\theta)$$

A square-wave subcarrier, $SC = sq(\omega_{sc} t)$ modulates the data on

$$\sin(\theta \, sq(\omega_{sc} t)) = sq(\omega_{sc} t) \sin \theta$$

$$= \sum_{k=1}^{\infty} \frac{4}{\pi(2k-1)} \sin \theta \sin((2k-1) \omega_{sc} t) \qquad (8.3\text{-}4)$$

with $P_n = \frac{8P_{tr}}{\pi^2 n^2} \sin^2 \theta$, where now n must be odd.

From the expression above it is seen that more power is concentrated at the subcarrier fundamental frequency for a square-wave subcarrier than for a sine wave, thus giving a higher power reference for the phase-locked-loop of the subcarrier demodulator.

On the other hand, the sine-wave signal can be reproduced with greater fidelity for a given bandwidth, since the even harmonics are absent in the square-wave case.

Care must be exercised in selecting data rates and subcarrier frequencies, as dc baseband harmonic components will degrade carrier tracking by adding phase jitter at the carrier frequency. Similarly, harmonics can cause data channel to data channel (subcarrier and intersymbol) interference. Thus, a selection of subcarriers, data rates, and ranging signals requires development of the rf spectrum to determine the existence of a problem.

8.3.1.2 Doppler Spread. A planned spacecraft will have three or more carrier frequencies of interest for each link, $\omega_{c\ min}$, ω_c, and $\omega_{c\ max}$, where, from paragraph 4.4.1,

$$\omega_{c\ min} = \sqrt{\frac{c - \dot{R}_{max}}{c + \dot{R}_{max}}}\ (\omega_c + \dot{\phi}_1) \qquad (8.3\text{-}5)$$

$$\omega_{c\ max} = \sqrt{\frac{c - \dot{R}_{min}}{c + \dot{R}_{min}}}\ (\omega_c + \dot{\phi}_2) \qquad (8.3\text{-}6)$$

and

ω_c = Design carrier frequency

c = Speed of propagation

$\dot{R}$ = Rate-of-change of spacecraft-to-Earth range

$\dot{\phi}_{1,2}$ = Rate-of-change of link phase delays at the time of "min" and "max", respectively.

(Note that these expressions assume that $\dot{R}$ dominates the received carrier frequency. If $\ddot{\phi}$ is significant, $\omega_{c\ min}$ or $\omega_{c\ max}$ will not necessarily occur at $\dot{R}_{max}$ or $\dot{R}_{min}$, respectively.)

The bandwidth of the designed signal extends from $\omega_c - \omega_-$ to $\omega_c + \omega_+$, where ω_- and ω_+ are defined as those frequencies at which the signal spectral density falls below the receiver threshold. This definition may be relaxed somewhat if the interference requirements of projects in adjacent channels are less stringent.

Just as with carrier frequency, the maximum and minimum spectral components are doppler shifted to give:

$$\omega_{-\ max} = \sqrt{\frac{c - \dot{R}_{max}}{c + \dot{R}_{max}}}\ \omega_- \tag{8.3-7}$$

and

$$\omega_{+\ max} = \sqrt{\frac{c - \dot{R}_{min}}{c + \dot{R}_{min}}}\ \omega_+ \tag{8.3-8}$$

Thus, the operational bandwidth, B_{op} is given by:

$$B_{op} = (\omega_{c\ max} + \omega_{+\ max}) - (\omega_{c\ min} - \omega_{-\ max})$$

$$B_{op} = \sqrt{\frac{c - \dot{R}_{min}}{c + \dot{R}_{min}}}\ (\omega_c + \omega_+ + \dot{\phi}_2) - \sqrt{\frac{c - \dot{R}_{max}}{c + \dot{R}_{max}}}\ (\omega_c - \omega_- + \dot{\phi}_{1.}) \tag{8.3-9}$$

B_{op} determines the number of adjacent channels required for a flight project link. If B_{op} stretches over too many channels, various compromises may have to be made, such as clearing adjacent channels during times of high doppler shift or a change of carrier frequency with mission time. The situation may be ameliorated by the ground antenna pointing direction, since the rapid fall-off of the off-axis gain may effectively eliminate interchannel interference. This is known as space diversity.

Paragraph 8.3.6.2 discusses the effects of interference induced by a spacecraft across the frequency spectrum. This gives a quantitative method of selecting ω_+ and ω_- for interference levels above receiver threshold.

8.3.2 Tracking Bandwidth

For a perfect sine-wave carrier signal of fixed frequency, the optimum carrier tracking loop would be centered at the carrier frequency and have a zero bandwidth. Introducing a finite bandwidth would simply add noise in the loop without increasing the detected signal energy.

In the actual situation, the carrier is neither a perfect sine wave nor fixed in frequency. The spectrum of the carrier is spread by several effects, the most important of which is phase jitter in the spacecraft transponder (two-way) or auxiliary oscillator (one-way). The carrier spectrum is translated in frequency by doppler shift and doppler rate. Thus, for adequate carrier tracking, we need a bandwidth wide enough to include the majority of carrier power and to react to doppler rates within the time for which it is desired to avoid changing the center frequency of the loop, and narrow enough to avoid excess noise power in the tracking loop.

Reference 8-15 lists tracking loop bandwidths and recommended minimum operating carrier signal levels for the DSIF in two-way lock. For a zero doppler rate environment, threshold improvement is in the inverse ratio of loop bandwidths ($2B_{LO}$) down to 12 Hz. Further decrease to a 3 Hz bandwidth produces less than 6 dB improvement because of oscillator phase instability. Future improvement in this parameter may permit operation in a 1 Hz bandwidth.

Section IV presents the equations governing a choice of tracking bandwidth for the spacecraft and ground stations. Reference 8-15 gives the

available bandwidths of the DSIF equipment as well as recommended bandwidths and carrier powers for various acquisition modes which introduce additional doppler. It is important to note that acquisition requirements might be a limiting factor in design and must be kept in mind.

Future developments to permit operation in a small bandwidth even where doppler rate is high, may lead to the use of third-order PLL's and/or programable oscillators.

8.3.3 Ranging Bandwidth

Under present designs, the spacecraft is passive to the receipt of planetary ranging codes. The transponder ranging channel, when commanded "on" from the ground, removes ranging modulation from the uplink carrier, passes it through a hard limiter, and remodulates the firmed-up signal onto the downlink carrier. In order to be compatible with the DSN, the transponder ranging bandwidth must extend from dc to 1.5 MHz minimum or to 3 MHz maximum. The minimum bandwidth was chosen to optimize the tradeoff between channel noise and sideband power. In the future, for missions at ranges of several A.U., it may be necessary to have an active spacecraft transponder, incorporating a ranging clean-up loop.

There are two planetary ranging systems now in use by the DSN. Operationally, the major difference between the two is the acquisition time, T_{acq}, shown below.

T_{acq} is defined as the time for which the system has a probability, P_{acq}, of acquiring the ranging signal. For $P_{acq} = .95$,

$$T_{acq} = 4550\ N_o/P_R \tag{8.3-10}$$

for the "Tau" ranging system, and

$$T_{acq} = 74\ N_o/P_R \tag{8.3-11}$$

for the "Mu" system, where P_R is the ranging sideband power on the downlink in watts, N_o is in watts/Hz, and T_{acq} is in seconds. For both systems, T_{acq} is greater than some minimum value which depends on the particular system implementation (see reference 8-15 for minimum values of T_{acq}).

The Tau system is a composite coded ranging system of the signal form:

$$PN_1 \oplus PN_2 \oplus \cdots \oplus 2f_s \tag{8.3-12}$$

where the clock signal square wave has a fixed frequency $2f_s$ = 500.1 KHz derived from the carrier frequency source, and $1/f_s$ is the bit time of the PN codes. The periods of the PN codes are relatively prime, and the number of codes used depends on the a priori knowledge of the spacecraft range, since increasing the code period decreases the range ambiguity. The mod 2 sum of several codes of relatively prime periods generates a very long code with great similarity to a PN code with a length equal to the product of the periods. The Tau spectrum is nearly continuous (line spacing of 1 KHz or less) and has the approximate power spectral density envelope (reference 8-15):

$$P(f) = \frac{1}{f_s} \frac{\sin^4(\pi f/4fs)}{(\pi f/4fs)^2} \text{ /Hz} \tag{8.3-13}$$

where P(f) = Power in a 1-Hz bandwidth relative to the total ranging power. The spectrum nulls occur at

$$f_n = 4nf_s, \; n = 1, 2, 3, \cdots \tag{8.3-14}$$

Figure 8-2 plots the normalized cumulative power as a function of frequency. Between 0 and $4f_s$ (approximately 1 MHz) the fraction of total power is about 86 percent (see reference 8-12). The phase jitter accuracy limitation is fixed at about ±3.4 meters, independent of P_R/N_o (reference 8-18).

Mu ranging achieves faster acquisition times by employing a binary coded sequential acquisition system which uses rf doppler rate as an aid for range decoder shifting. By sending sequentially a series of square waves,

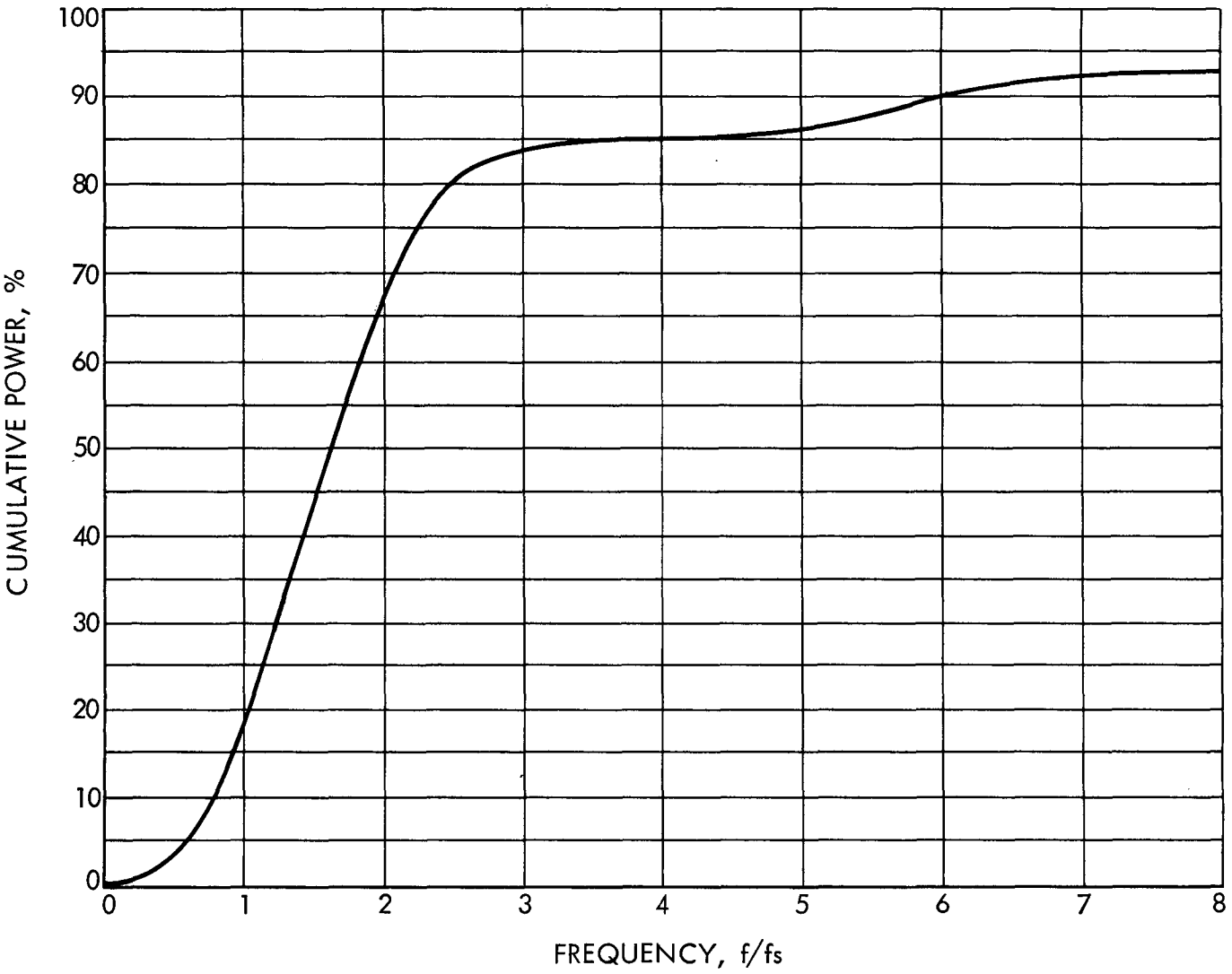

Fig. 8-2. Cumulative power for PN$\oplus 2f_s$

the Mu system can send full power in each component, whereas Tau must divide the available power among simultaneously transmitted components. The period, t_n of the n^{th} square wave component is:

$$t_n = \frac{(2^n)\ 64}{3\ f_s} = \frac{(2^n)(2048)}{f_c} \qquad (8.3\text{-}15)$$

where

f_s = Transmitter VCO frequency (SYN. FREQ.)

and

f_c = Carrier frequency = 96 f_s

n ranges from 1 to a maximum of 18. Actual range accuracy depends on the n = 1 component, whereas the higher period components simply reduce range ambiguity. Thus, it is frequently unnecessary to use all 18 possible frequencies, since a priori knowledge of the range reduces the ambiguity. For example, only ten components are needed to resolve the range to 150 km. Table 8-7 gives the approximate ambiguity resolution for each component. The values are approximate since they depend on carrier frequency.

The frequency of the n^{th} component is

$$f_n = \frac{3f_s}{(2^n)\,64} = \frac{f_c}{(2^n)\ (2048)} \qquad (8.3\text{-}16)$$

and the power spectrum is that of a square wave of frequency f_n at the time that component n is transmitted.

The standard deviation of frequency jitter due to noise in the signal is (reference 8-17):

$$\sigma = \frac{t_1}{8}\sqrt{\frac{N_o}{P_r\ T_I}}\ ,\ \text{seconds} \qquad (8.3\text{-}17)$$

Table 8-7. Code range resolving power for μ ranging.*

Component C_n	Approximate period t_n, μs	Approximate ambiguity resolving power, km
1	1.94	2.85×10^{-1}
2	3.88	5.70×10^{-1}
3	7.76	1.14
4	1.55×10^{1}	2.28
5	3.10×10^{1}	4.56
6	6.21×10^{1}	9.11
7	1.24×10^{2}	1.82×10^{1}
8	2.48×10^{2}	3.65×10^{1}
9	4.97×10^{2}	7.29×10^{1}
10	9.93×10^{2}	1.46×10^{2}
11	1.99×10^{3}	2.92×10^{2}
12	3.97×10^{3}	5.83×10^{2}
13	7.94×10^{3}	1.17×10^{3}
14	1.59×10^{4}	2.33×10^{3}
15	3.18×10^{4}	4.67×10^{3}
16	6.36×10^{4}	9.33×10^{3}
17	1.27×10^{5}	1.87×10^{4}
18	2.54×10^{5}	3.73×10^{4}

*Source: Reference 8-19.

where

P_r = Ranging link power, watts

N_o = Noise spectral density, watts/Hz

T_I = Integration time, seconds.

Reference 8-16 gives a description of the Mu system. Figure 8-3 is a block diagram of the system reproduced from reference 8-16 and shows the generation of frequencies in the system.

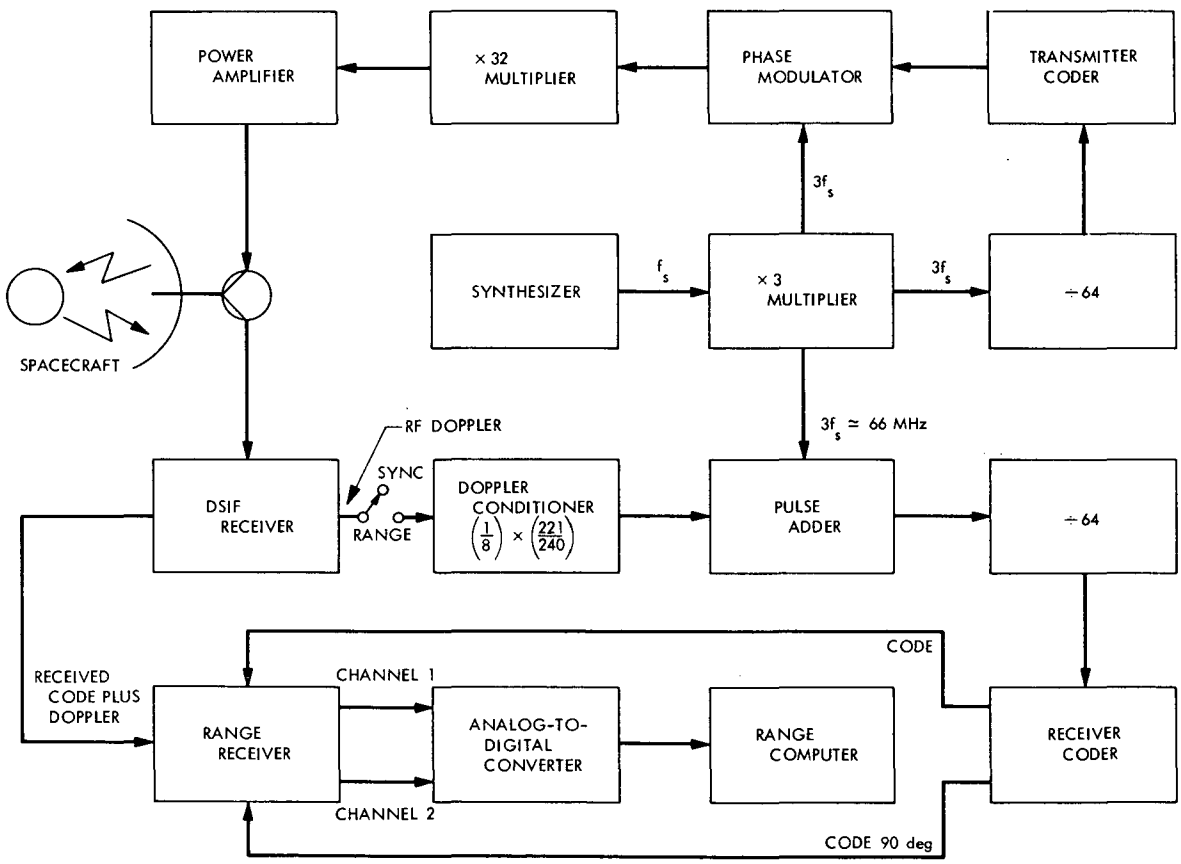

Fig. 8-3. Binary-coded sequential acquisition ranging (mu-ranging) system

8.3.4 Telemetry (PSK)

Binary PCM/PSK/PM data is detected through the DSIF's channel D, or multimission telemetry (MMT) system, the operating parameters of which are described and specified in reference 8-15. There are two related aspects of the telemetry signal which require discussion and are dependent upon one another, subcarrier frequencies and data rates.

8.3.4.1 Subcarrier Frequencies. As mentioned earlier, interference between signal harmonics must be minimized, in particular:

> "The subcarrier frequency and/or the frequency difference between subcarrier frequencies should not be harmonically related to any frequency within the interval of 10 MHz ± n [times] symbol rate ... The value of n should ideally be as large as possible and nonintegral so that any possible interfering signals (due to harmonics) are not within the predemodulation bandwidth of the subcarrier demodulator assembly (SDA). However, should any harmonic fall within the predemodulation bandwidth, measurements should be made to verify that the effect on performance is acceptably small. At high data rates, where the symbol/bit rate is integrally related to the subcarrier frequency, n may be any nonintegral number larger than one " (reference 8-15).

Reference 8-15 contains recommendations for subcarrier frequency ranges for given data rates. For channels near the edge of the allocated frequency band, high frequency subcarrier and data modulation may be degraded by the filter drop-off, particularly under a high doppler environment. Information as to these losses is also contained in reference 8-15, as is the performance expected for various combinations of data rate and subcarrier phase tracking loop noise bandwidth.

8.3.4.2 Data Rates. Reference 8-15 contains DSIF data rate limitations imposed by the ground hardware. Constraints on the data rates which can be returned by the stations in real time may be more stringent than those imposed on data receipt at the stations.

8.3.5 Command

Reference 8-15 lists the DSN compatible bandwidths for command subcarriers and compatible data rates. For channels near the edge of the rf transmission bandwidth, subcarriers may be suppressed due to the filter characteristic.

The limitations on command bit rate capability of the DSIF are due to software restrictions. Below 1 bps, the bit rate is clocked by the TCP software which cannot handle rates below 0.3 bps. Above 1 bps, the rate is hardware clocked, but above 20 bps, the TCP cannot deliver command sequences without some dimunition of telemetry capability.

The appropriate subcarrier bandwidth depends on the command method chosen. Reference 8-15 lists the DSIF constraints. Reference 8-12 examines theoretical considerations as described below.

8.3.5.1 Dual-Channel Command. The dual-channel command signal is characterized by the equation:

$$V_{sync} (PN \oplus 2f_s) + V_{data} D(t) \sin (2\pi f_s t) \qquad (8.3\text{-}18)$$

where

$PN \oplus 2f_s$ = Sync information

V_{sync} and V_{data} = Peak-to-peak voltage values of the sine- and square-wave signals, respectively,

and $D(t)$ = Binary command data.

The wideband characteristics are determined by the sync information, $PN \oplus 2f_s$, which has the same spectrum as shown for the Tau ranging system of paragraph 8.3.3 above. Generally then, the minimum bandwidth

must be $4f_s$ ($8f_s$ double sided). The power spectrum of the composite command signal is plotted in Figure 8-4, where

P_S = Sync power

P_D = Data power

$P_C = P_S + P_D$

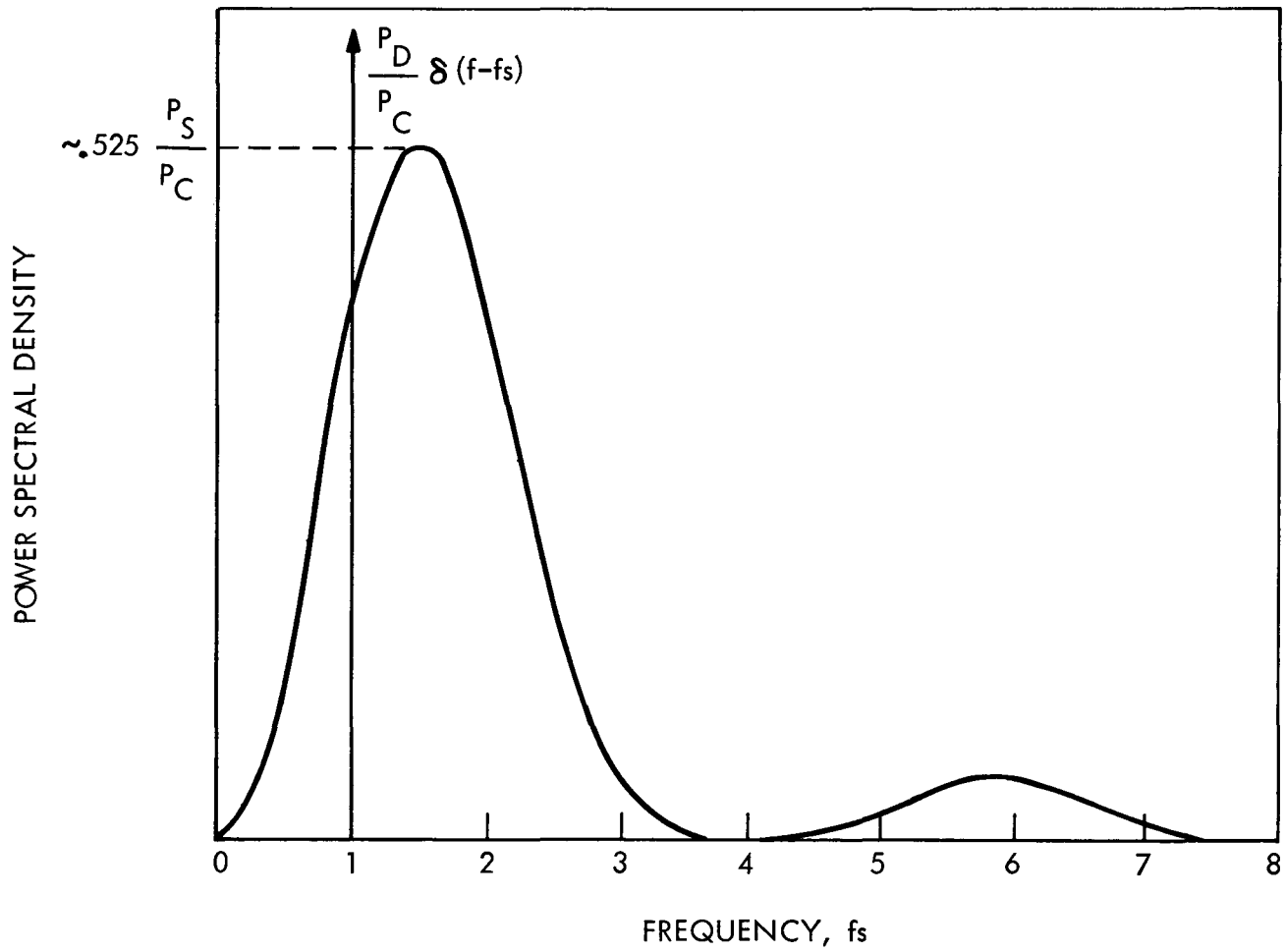

Fig. 8-4. Power spectral density for the two-channel composite command signal

8.3.5.2 Single-Channel Command. The analog single-channel command signal is of the form:

$$D(t) \sin (2\pi f_s t) \tag{8.3-19}$$

which has the data modulated on a baseband spectrum of the form shown in equation (8.3-3) with $\omega_{sc} = 2\pi f_s$.

The digital single-channel command system sends sequential acquisition signals characterized by:

f_s, for subcarrier detection and acquisition modes

and

$BS(t) \oplus f_s$ for bit sync detection and acquisition modes

where

$BS(t)$ is a square wave signal of frequency $2/T_B$ as described in section VI.

Upon completion of acquisition, the uplink carrier may be modulated by a command signal of the form:

$$D(t) \oplus BS(t) \oplus f_s \tag{8.3-20}$$

The data is modulated on a baseband spectrum of the form shown in equation (8.3-4), with $\omega_{sc} = 2\pi f_s$.

8.3.6 Signal Combinations

Degradation in system performance can result from the following three types of signal combinations:

1) Combinations of carrier, subcarrier, data, and ranging signals specified by the system designer
2) Combinations of the desired signal with spurious signals generated by the ground system and/or spacecraft system
3) Combinations with signals generated by spacecraft in adjacent frequency channels.

The first type of signal combinations must be guarded against by careful examination of the rf spectrum, as discussed above. The second type can be eliminated by proper loop design and shielding. The third type is minimized by spectral analysis and proper channel assignment.

Signal combinations of any type can result in degradation by two mechanisms, false lock and interference.

8.3.6.1 False Lock. False lock is the condition in which a tracking loop locks onto a spurious frequency present in the loop. For such an occurrence, the loop must see a highly peaked frequency component within its pull-in range, with a signal-to-noise power greater than loop threshold. Often such a frequency component is generated by the equipment associated with the loop.

Conceptually, this problem admits of easy solution; simply eliminate the offending frequency component. Actually, this requires very careful hardware and spectrum design.

Such a situation can lead to catastrophic failure if the component is generated in the spacecraft hardware. The loop may lock onto this component permanently. Thus, this problem should be anticipated from the earliest stages of hardware design.

8.3.6.2 Interference. The presence of non-white noise on the data signal caused by other signal sources degrades the system error rate performance in a different way than white noise. Appendix A8.2 presents the results of an analysis of the effect of this degradation on an antipodal, binary-valued signal (± 1).

The effect of interference can be treated in a manner similar to radio loss (see paragraph 5.4.5.1). As an example, for uncoded data, the effect can be regarded as a factor (less than one) which relates the ST_B/N_o into the system to the ST_B/N_o which would give the same error rate in a system without interference, thus,

$$\left(\frac{ST_B}{N_o}\right)_{eq.} = \left(\frac{ST_B}{N_o}\right)_{in} \eta_I$$

where

η_I = "Interference efficiency."

Similarly, interference in the tracking loops will degrade tracking performance and increase jitter, reflecting itself in higher system losses.

Approximating interference by increasing $N_o B_n$ by the interference power for the non-gaussian process is an adequate approximation if $(ST_B/N_o)_{in} \gtrsim 5$ dB and the interference-to-signal-power ratio is less than -5 dB.

Because of anticipated interference problems between space vehicles, the NASA now requires that its vehicles have the capability of ceasing transmission at the end of a mission upon ground command.

8.4 OBTAINING A CARRIER FREQUENCY ALLOCATION IN THE DSN

In order to make a carrier frequency allocation, the DSN requires information about the desired spectrum, the methods of modulation, and the spacecraft trajectory. This section describes the information required and the request procedure.

8.4.1 Required Information

The following is the current list of information which must be submitted with frequency assignment requests of users of the DSN:

1) Mission Schedule
   - a) Launch windows
   - b) Mission duration
   - c) Alternate dates
   - d) Number of spacecraft in space at any given time.
2) Mission trajectories and time profile of rf coverage required, including angular separation of multiple spacecraft

3) Doppler Time Profiles

4) Spacecraft Transmitter Characteristics
   a) Accuracy
   b) Stability
   c) Power gain product

5) Functional Requirements
   a) Two-way doppler
   b) Ranging
   c) Telemetry
   d) Command

6) Modulation Characteristics
   a) Modes
   b) Types and indices
   c) Spectrum
   d) Required bandwidths of receiver and other elements

7) Other Peculiarities Which Determine Frequency Choice
   a) Interference characteristics
   b) Other rf sources on spacecraft which do not utilize DSN.

Also included should be an indication of the firmness of the data submitted. This list is not all inclusive and will be updated from time-to-time as new DSN capabilities become available. Thus, any relevant information should be added even though there may be no specific category included in the listing. The latest copy of this information list should be obtained from the manager of the DSN Systems section prior to submitting a request.

8.4.2 Request Procedure

The information discussed above should be submitted to the manager of the DSN Systems section. Since it may not be possible to exactly fulfill the requested capabilities within the frequency constraints of the network, the request must be subject to negotiation. In addition, DSN personnel may have suggestions for frequency band usage, based on their detailed knowledge of the DSN capabilities and plans, which might make a change of request desirable. Thus, early submission is advisable.

REFERENCES

8-1. Reference Data for Radio Engineers, Fifth Edition, Howard W. Sams & Co., Inc (Indianapolis: 1968).

8-2. Potter, P.D., M.S. Shumate, Stelzried, C.T., Wells, W.H., A Study of Weather - Dependent Data Links for Deep Space Applications, Jet Propulsion Laboratory Technical Report 32-1392, October 15, 1969.

8-3. Simon, M.K., Some Preliminary Results on the Problem of Ground Transmitter Multiplexing of Two Carriers, private communication.

8-4. Simon, M.K., A Summary of Progress on the Problem of Ground Transmitter Multiplexing of Two Carriers, private communication.

8-5. Kolbly, R.B., "Switched - Carrier Experiments," Jet Propulsion Laboratory Technical Report 32-1526, Vol. III, The Deep Space Network: Progress Report for March and April 1971, June 15, 1971, pp. 133-146.

8-6. Kliore, A, Cain, D.L., and Hamilton, T.W., Determination of Some Physical Properties of the Atmosphere of Mars from Changes in the Doppler Signal of a Spacecraft on an Earth-Occultation Trajectory, Jet Propulsion Laboratory Technical Report 32-674, October 15, 1964.

8-7. Dutcher, G.L., A Communication Channel Model of the Solar Corona and the Interplanetary Medium, M.I.T. Center for Space Research, CSR T-69-1, January, 1969.

8-8. Mulhall, B.D., et al, Tracking System Analytic Calibration Activities for the Mariner Mars 1969 Mission, Jet Propulsion Laboratory Technical Report 32-1499, November 15, 1970.

8-9. Fjeldbo, G., and Eshleman, V.R., "The Bistatic Radar - Occultation Method for the Study of Planetary Atmospheres," J. of Geophysical Res., Vol. 70, No. 13, July 1, 1965, pp. 3217-3225.

8-10. Fjeldbo, G., et al, "The Two-Frequency Bistatic Radar - Occultation Method for the Study of Planetary Ionospheres," J. of Geophysical Res., Vol. 70, No. 15, August 1, 1965, pp. 3701-3710.

8-11. Fjeldbo, G., Kliore, A., and Seidel, B., "The Mariner 1969 Occultation Measurements of the Upper Atmosphere of Mars," Radio Science, Vol. 5, No. 2, February 1970, pp. 381-386. Reprinted in Stallkamp, J.A., et al, Mariner Mars 1969 Final Project Report: Scientific Investigations, Jet Propulsion Laboratory Technical Report 32-1460, Vol. III, September 15, 1971.

8-12. Springett, J.C., Telemetry and Command Techniques for Planetary Spacecraft, Jet Propulsion Laboratory Technical Report 32-495, January 15, 1965.

8-13. Skolnik, M.I., Introduction to Radar Systems, McGraw-Hill (New York; 1962).

8-14. Koerner, M.A., Effect of Interference on a Binary Communication Channel Using Known Signals, Jet Propulsion Laboratory Technical Report 32-1281, December 1, 1968.

8-15. Deep Space Network/Flight Project Interface Design Handbook, DSN Standard Practice, 810-5 (JPL internal document).

8-16. Mac Doren, P. F., and Martin, W.L., "DRVID Charged-Particle Measurement with a Binary-Coded Sequential Acquisition Ranging System." Jet Propulsion Laboratory Space Programs Summary 37-62, Vol. II, The Deep Space Network, March 31, 1970, pp. 34-41.

8-17. Butman, S., "Coding and Synchronization Studies: The Effect of Amplitude Uncertainty on Estimating Phase of a Square Wave," Jet Propulsion Laboratory Space Programs Summary 37-58, Vol. III, August 31, 1969, pp. 55-57.

8-18. Tappan, R.W., private communication.

8-19. Martin, W. L., "Information Systems: A Binary-Coded Sequential Acquisition Ranging System," Jet Propulsion Laboratory Space Programs Summary 37-57, Vol. II, May 31, 1969, pp. 72-81.

APPENDIX A8.1

FREQUENCY DEPENDENCE OF DATA RETURN

A8.1.1 FREQUENCY DEPENDENCE OF DATA RETURN

The data return for a given modulation scheme depends on the ratio of total received power to noise spectral density (P_T/N_o) at the input to the detector. The components of this ratio depend on the carrier frequency and phenomena which are functions of carrier frequency. It is convenient to consider $P_T(f)$ and $N_o(f)$ separately and combine them to find $P_T/N_o = g(f)$.

A8.1.1.1 Frequency Dependence of Total Received Power

Using the notation of Section II, we have:

$$P_T = P_{tr} G_t G_r L_s L_A L_p L_c G_R \qquad \text{(A8.1-1)}$$

Now P_{tr}, L_p, L_c, and G_R can be chosen independently of the carrier frequency. The space loss, L_s is found from

$$L_s = \left(\frac{\lambda}{4\pi R}\right)^2 \qquad \text{(A8.1-2)}$$

or

$$L_s = \left(\frac{c}{4\pi R}\right)^2 \left(\frac{1}{f^2}\right) \qquad \text{(A8.1-3)}$$

where

c = Speed of electromagnetic wave propagation

f = Carrier frequency.

For the present DSN configurations the ground antenna is a paraboloid. Generally the spacecraft antenna is either a horn or paraboloid.

Thus, from Table 7-1,

$$G_t G_r \propto \begin{cases} f^3 & \text{(paraboloid-horn pair)} \\ f^4 & \text{(paraboloid-paraboloid pair)} \end{cases} \qquad \text{(A8.1-4)}$$

Then

$$\frac{P_T}{L_A} \propto f, \text{ at least}$$

L_A, the atmospheric absorption loss will be considered below, since it is related to the system noise temperature.

A8.1.1.2 Frequency Dependence of Noise Spectral Density

Above 1 GHz, the Earth's atmosphere can be modeled as a passive loss. From Section II, the noise spectral density into the detector will be

$$N_o = kG_R \left[T_g L_A L_c + T_A (1 - L_A) L_c + T (1 - L_c) + T_o (F - 1) \right] \qquad \text{(A8.1-5)}$$

where the symbols have been defined above, except

T_A = Average physical temperature of the atmosphere ~ 260°K

(A8.1-5) can be rewritten as:

$$N_o = kG_R \left[L_c T_{SKY} + T (1 - L_c) + T_o (F - 1) \right] \qquad \text{(A8.1-6)}$$

where

$$T_{SKY} = T_g L_A + T_A (1 - L_A) \qquad \text{(A8.1-7)}$$

or

$$L_A = \frac{T_A - T_{SKY}}{T_A - T_g} \qquad \text{(A8.1-8)}$$

Figures A8.1-1 and A8.1-2 show the frequency dependence of T_{SKY} and L_A respectively for a standard atmosphere. The peak at ~22 GHz is due to absorption by water vapor. The peak at ~60 GHz is caused by absorption by oxygen. Figure A8.1-2 is drawn for a $T_A = 260°K$. As T_{SKY} increases for large frequencies, it approaches this value of T_A. Therefore, T_A must be known very well for these frequencies, to accurately predict L_A. Figure A8.1-2 is thus not reliable in the region above 10 GHz, but does show the absorption trends. Terms in N_o due to circuit loss and receiver noise can be chosen relatively independent of frequency.

A8.1.1.3 Frequency Dependence of P_T/N_o

For signals at X-band and higher frequencies, T_{SKY} and L_A become strongly dependent on atmospheric water vapor content, as discussed in reference 8-2. These frequencies are then weather dependent links.

For clear-sky conditions, however, there is a broad minimum for T_{SKY} and L_A from 1 GHz to 10 GHz so that over this range,

$$\frac{P_T}{N_o} \propto f \text{ at least,}$$

and for typical encounter sequences, with a high-gain spacecraft antenna,

$$\frac{P_T}{N_o} \propto f^2$$

Thus, the data return is greatly increased by choice of a higher frequency band. Above X-band the oxygen and water vapor resonances limit improvement. In addition, the technology is not well advanced. Reference 8-2 discusses the system considerations for frequencies of X-band and higher.

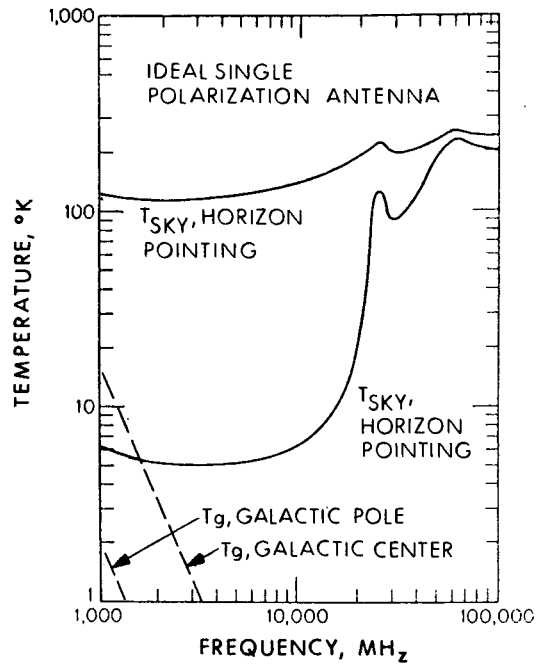

Fig. A8.1-1. T_{SKY} and T_g vs frequency for standard atmospheric conditions

(Ref. 8-13, from Introduction to Radar Systems by M.I. Skolnik. Copyright 1962 by McGraw-Hill Book Company. Used with permission of McGraw-Hill Book Co.)

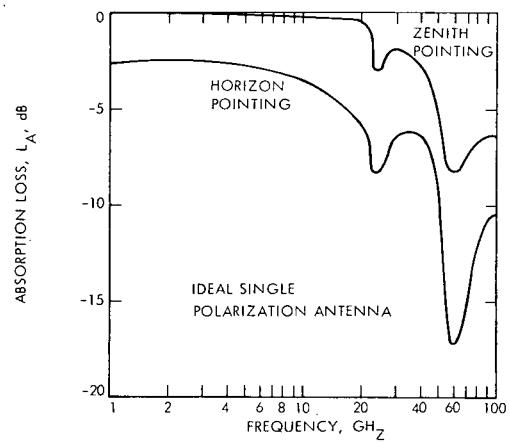

Fig. A8.1-2. Absorption Loss, L_A, vs frequency for T_A = 260°K and standard atmospheric conditions

APPENDIX A8.2

INTERFERENCE

A8.2.1 THE EFFECTS OF INTERFERING SIGNALS ON TELECOMMUNICATION PERFORMANCE

Koerner (reference 8-14) has analyzed "the effects of sinusoidal and gaussian interference on the performance of the maximum-likelihood [correlation] receiver for extracting binary data from a sequence of messages in white gaussian noise when each signal has [a symbol time T_s] and is chosen with equal a priori probability from a dictionary of two messages." This section summarizes Koerner's work for antipodal, binary valued signals (±1).

Let us define the following ratios at the input to the symbol value decision element:

λ = Signal energy-to-noise spectral density ratio for the signal embedded in gaussian white noise only.

η = Interference-to-signal ratio

ξ = Interference-to-noise ratio

Then,

$$\lambda = \frac{ST_s}{N_o}$$

for a sinusoidal interference signal,

$$\eta = \frac{P_i}{S}\left(\frac{\sin(\pi f_i T_s)}{\pi f_i T_s}\right)^2 \qquad \text{(A8.2-1)}$$

$$\xi = \frac{2 P_i T_s}{N_o}\left(\frac{\sin(\pi f_i T_s)}{\pi f_i T_s}\right)^2 \qquad \text{(A8.2-2)}$$

and for a gaussian interference signal,

$$\eta = \frac{P_i}{S} \int_{-\infty}^{\infty} \frac{G_i(f)}{P_i} \left(\frac{\sin(\pi f T_s)}{\pi f T_s} \right)^2 df \qquad \text{(A8.2-3)}$$

$$\xi = 2 \frac{P_i T_s}{N_o} \int_{-\infty}^{\infty} \frac{G_i(f)}{P_i} \left(\frac{\sin(\pi f T_s)}{\pi f T_s} \right)^2 df \qquad \text{(A8.2-4)}$$

where

S = Desired signal power

T_s = Symbol time

N_o = One-sided noise spectral density

P_i = Interference signal power

f_i = Frequency of an interfering sinusoid

and

$G_i(f)$ = Two-sided power spectral density of a gaussian interfering signal

(Note that $\xi = 2 \lambda \eta$.)

With these definitions the probabilities of symbol error are:

$$P_{SE} = p(\lambda) = \frac{1}{2} \left[1 - \mathrm{Erf}(\lambda^{1/2}) \right] \qquad \text{(A8.2-5)}$$

for no interference signal.

$$P_{SE} = p_s(\lambda; \eta) = \frac{1}{\pi} \int_{-\pi/2}^{\pi/2} \frac{1}{2} \left[1 - \mathrm{Erf} \left\{ \lambda^{1/2} \left[1 + (2\eta)^{1/2} \sin u \right] \right\} \right] du$$

$$= p_s(\lambda;\frac{\xi}{2\lambda}) = \frac{1}{\pi}\int_{-\pi/2}^{\pi/2} \frac{1}{2}\left[1 - \mathrm{Erf}\,(\lambda^{1/2} + \xi^{1/2}\sin u)\right] du \quad \text{(A8.2-6)}$$

for a sinusoidal interference signal.

$$P_{SE} = p_G(\lambda;\eta) = \frac{1}{2}\left\{1 - \mathrm{Erf}\left[\lambda^{1/2}(1 + 2\eta\lambda)^{-1/2}\right]\right\}$$

$$= p_G(\lambda, \frac{\xi}{2\lambda}) = \frac{1}{2}\left\{1 - \mathrm{Erf}\left[\lambda^{1/2}(1 + \xi)^{-1/2}\right]\right\} \quad \text{(A8.2-7)}$$

for gaussian interference, where

$$\mathrm{Erf}(x) = \frac{2}{\sqrt{\pi}}\int_0^x \exp(-t^2)\, dt.$$

These expressions assume a perfect correlation detector. The effects of system losses must be added for P_{SE} for the real system (see paragraphs 5.4.5 and 5.4.6 and Appendix A5.1).

Figures A8.2-1 through A8.2-8 plot equations (A8.2-6) and (A8.2-7) for various parametric representations.

Rather than examining the symbol error degradation due to interference, the telecommunication systems designer may find it more useful to determine the additional factor, δ, by which λ must be increased to give symbol error performance equivalent to that obtained in the absence of interference. δ will take on different values, depending on whether η or ξ is held constant. If the receiving system is to be compensated by δ, P_i/S, and therefore η will remain constant. If the transmitting system is adjusted, P_i/N_o, and therefore ξ, will be unchanged. Equations (A8.2-8) through (A8.2-11) give expressions for δ for the conditions cited.

Sinusoidal Interference:

$$n \text{ constant, } p_s(\delta\lambda;\eta) = p(\lambda) \tag{A8.2-8}$$

δ finite for $\eta < \frac{1}{2}$

or $\eta \geq \frac{1}{2}$ and $\lambda < \lambda_o$

where

$$\text{Erf}(\lambda_o^{1/2}) = \frac{2}{\pi} \sin^{-1}\left[(2\eta)^{-1/2}\right]$$

or,

$$\lambda_o = \left[\text{Erf}^{-1}\left(\frac{2}{\pi} \sin^{-1}\left[(2\eta)^{-1/2}\right]\right)\right]^2$$

λ_o versus η is plotted in Figure (A8.2-9)

$$\xi \text{ constant, } p_s\left(\delta\lambda;\frac{\xi}{2\delta\lambda}\right) = p(\lambda) \tag{A8.2-9}$$

Gaussian Interference:

$$\eta \text{ constant, } p_G(\delta\lambda;\eta) = p(\lambda)$$

or

$$\delta = \begin{cases} (1-2\eta\lambda)^{-1}, & \lambda < (2\eta)^{-1} \\ \infty & \lambda > (2\eta)^{-1} \end{cases} \tag{A8.2-10}$$

$$\xi \text{ constant, } p_G\left(\delta\lambda;\frac{\xi}{2\delta\lambda}\right) = p(\lambda)$$

or

$$\delta = 1 + \xi \qquad \text{(A8.2-11)}$$

These relations are plotted as Figures (A8.2-10) through (A8.2-16).

A useful engineering approximation for evaluating the effect of non-gaussian interference on a receiver is to assume it equivalent to that effect caused by a gaussian process of equal power at the receiver output. Koerner shows that a gaussian approximation to sinusoidal interference is adequate for $\lambda \lesssim 5$ dB and $\eta < -5$ dB. The approximation rapidly breaks down above these values.

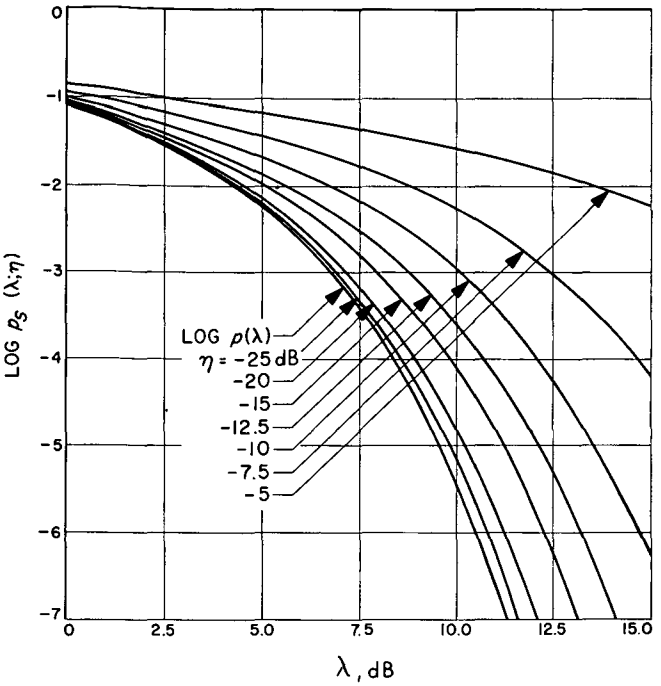

Fig. A8.2-1. Log p_S (λ; η) as a function of λ

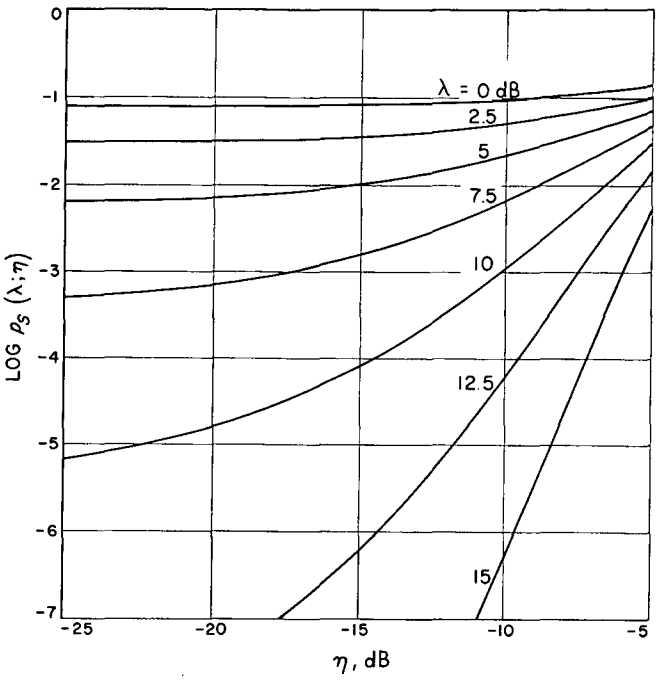

Fig. A8.2-2. Log p_S ($\lambda;\eta$) as a function of η

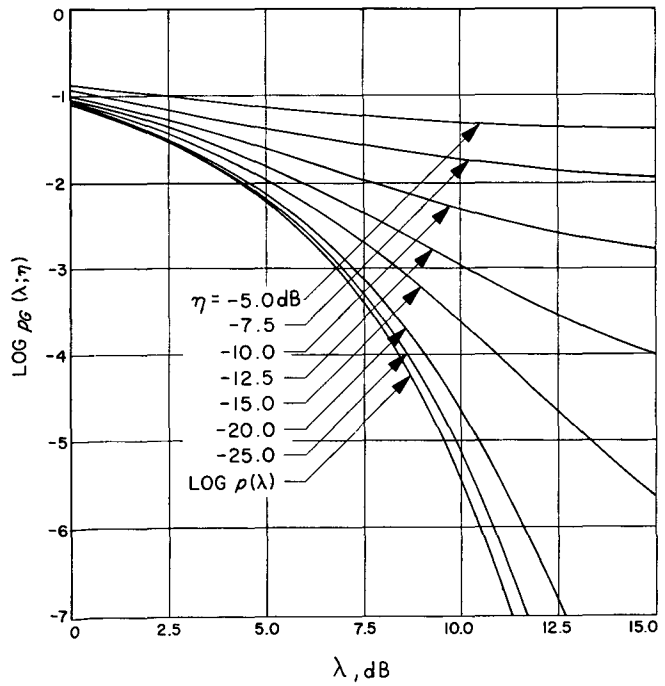

Fig. A8.2-3. Log p_G ($\lambda;\eta$) as a function of λ

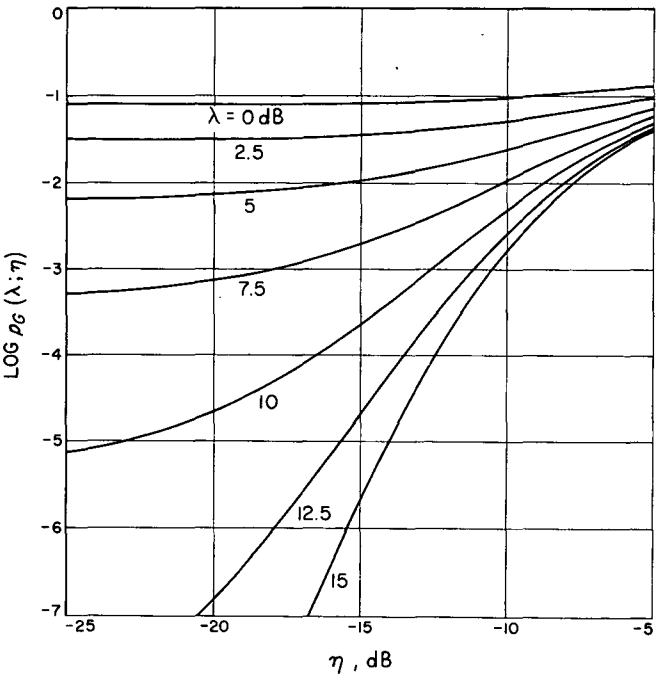

Fig. A8.2-4. Log p_G ($\lambda;\eta$) as a function of η

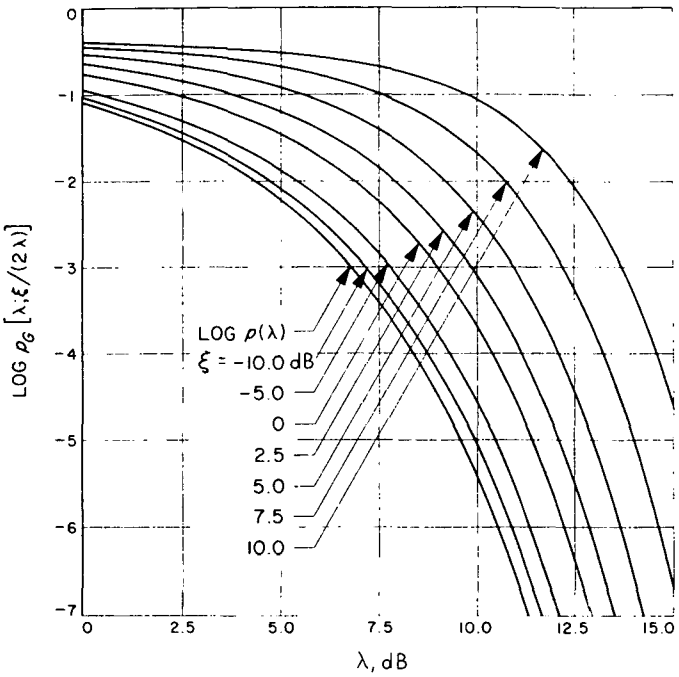

Fig. A8.2-5. Log $p_s\left[\lambda;\xi/(2\lambda)\right]$ as a function of λ

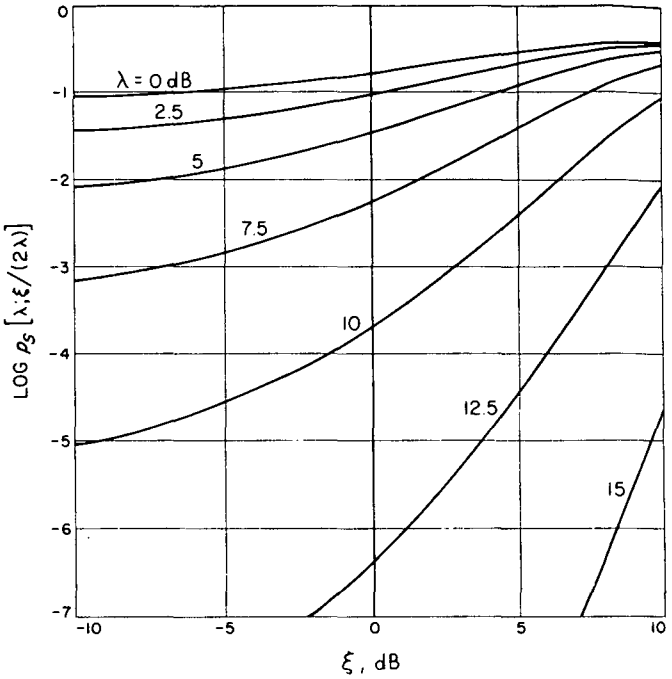

Fig. A8.2-6. Log $p_s\left[\lambda;\xi/(2\lambda)\right]$ as a function of ξ

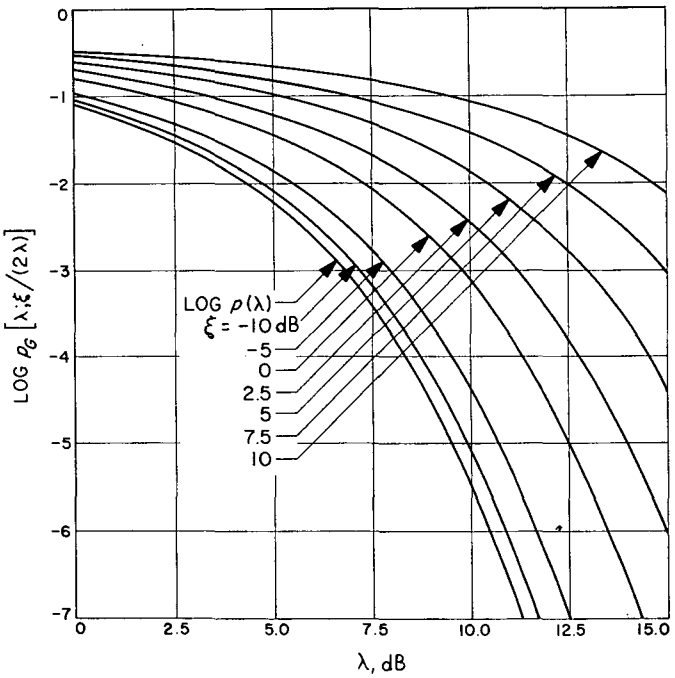

Fig. A8.2-7. Log $p_G\left[\lambda;\xi/(2\lambda)\right]$ as a function of λ

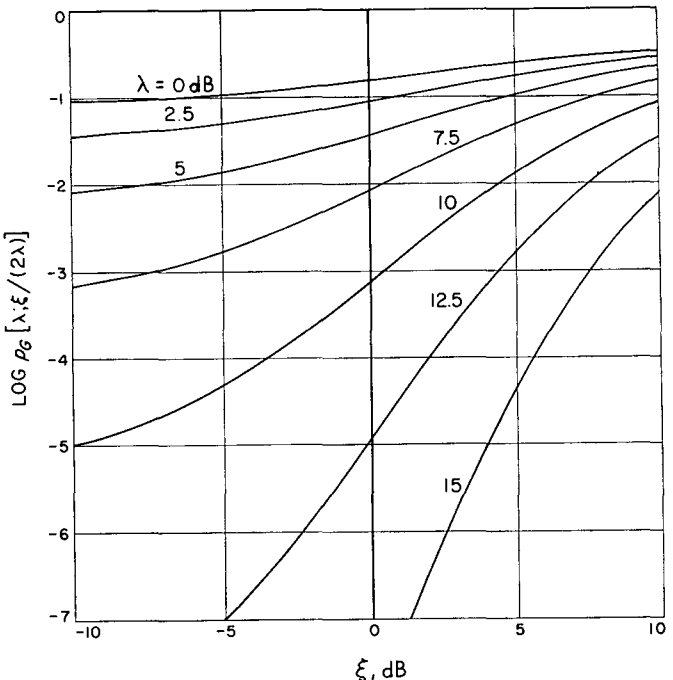

Fig. A8.2-8. Log $p_G\left[\lambda;\xi/(2\lambda)\right]$ as a function of ξ

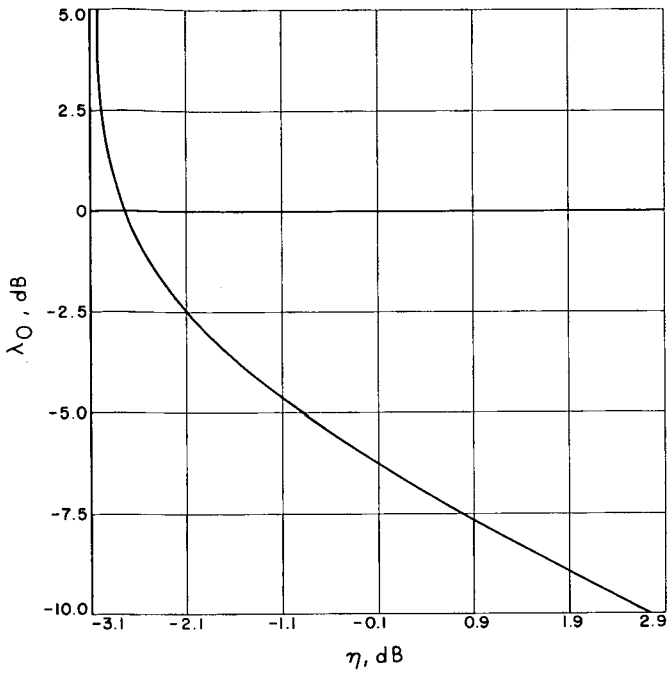

Fig. A8.2-9. λ_O for sinusoidal interference and constant η as a function of η

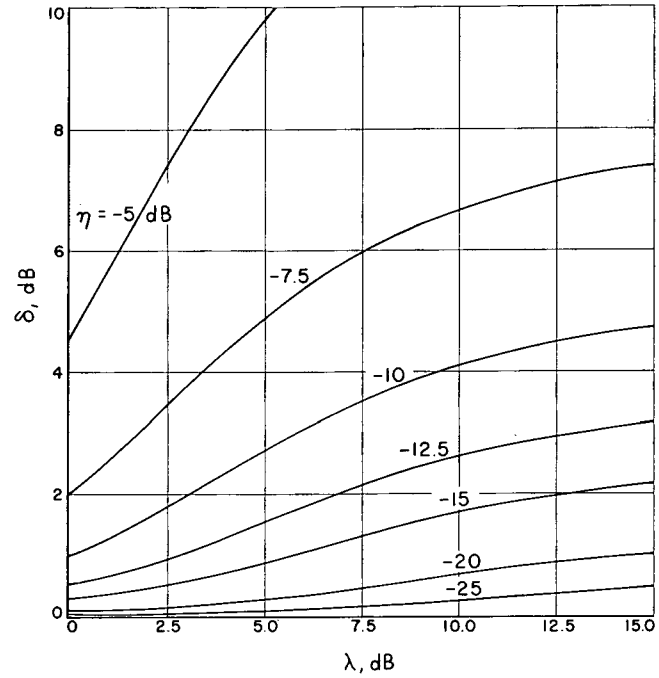

Fig. A8.2-10. δ for sinusoidal interference and constant η as a function of λ

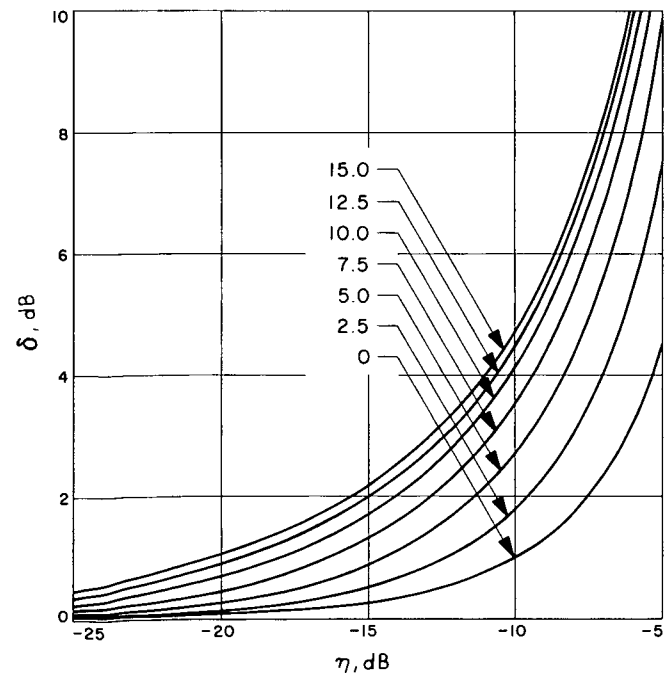

Fig. A8.2-11. δ for sinusoidal interference and constant η as a function of η

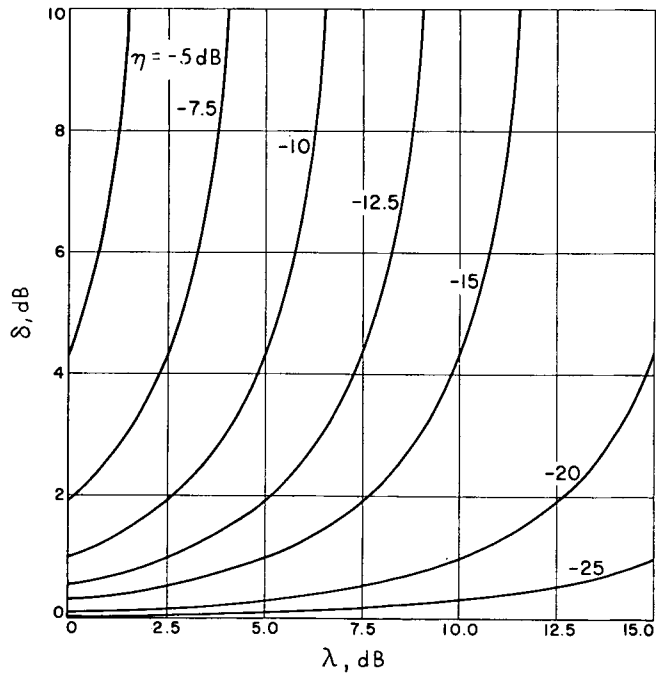

Fig. A8.2-12. δ for gaussian interference and constant η as a function of λ

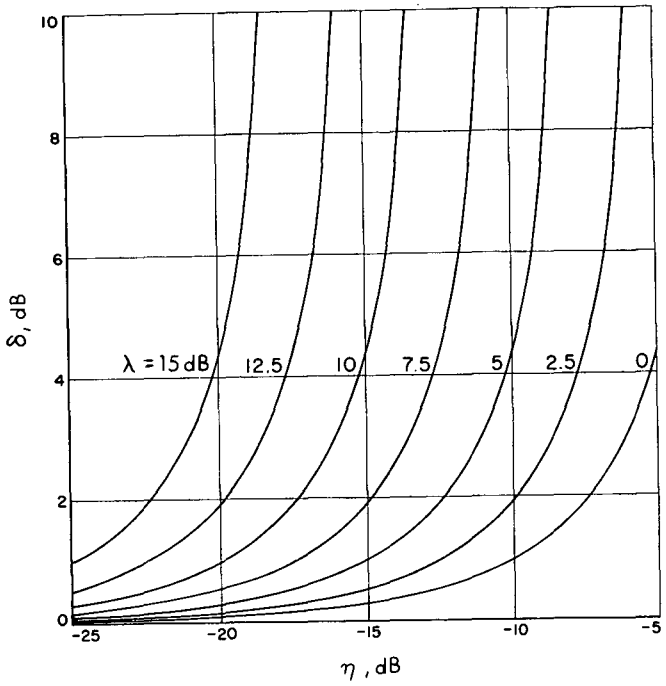

Fig. A8.2-13. δ for gaussian interference and constant η as a function of η

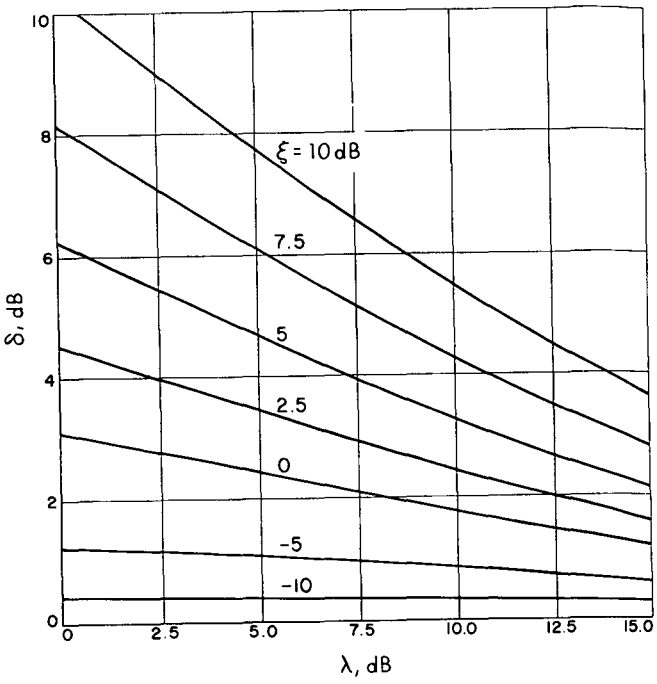

Fig. A8.2-14. δ for sinusoidal interference and constant ξ as a function of λ

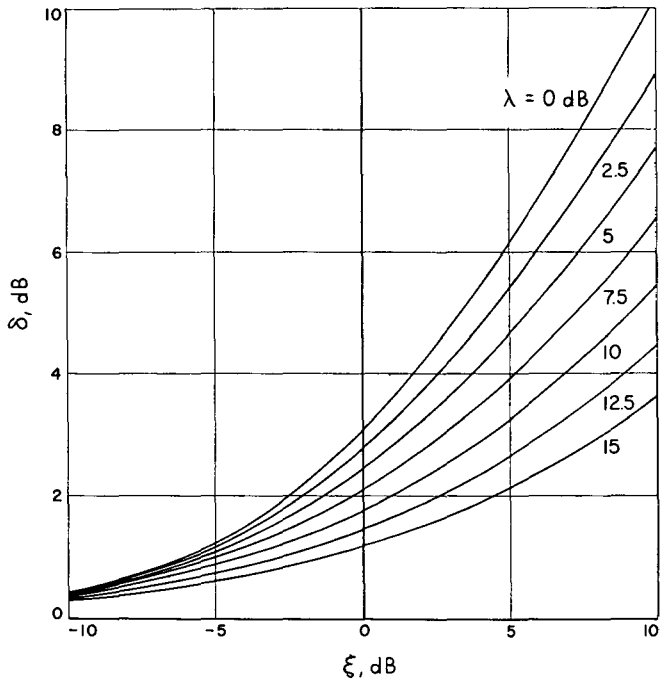

Fig. A8.2-15. δ for sinusoidal interference and constant ξ as a function of ξ

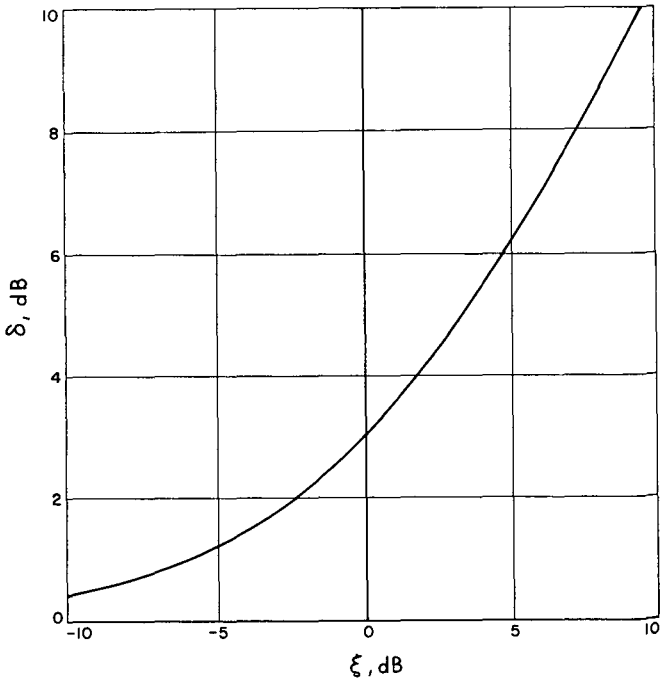

Fig. A8.2-16. δ for gaussian interference and constant ξ as a function of ξ

SECTION IX

TELECOMMUNICATIONS PERFORMANCE PREDICTION AND ANALYSIS

9.1 INTRODUCTION

When individual elements of the telecommunications link have been defined or when tradeoffs between competing implementations are desired, overall link performance predictions must be generated. These predictions consist of two major forms. First, design control tables (DCT's) indicate static performance for given points in time. Second, plots show the variation in performance versus time.

These two outputs allow the system designer to make tradeoffs in the following areas:

1) Value or merit of different system implementations

2) Mission operation decisions, such as when to switch antennas, when to change bit rates, or over what portion of the spacecraft sphere a given bit rate may be supported for a proposed spacecraft maneuver, etc.

The basic tool for performance prediction is a software program called the "Telecommunication Prediction and Analysis Program" (TPAP). "Prediction" and "Analysis" in this title are defined as follows:

1) Prediction is the generation of performance data indicating what is predicted for the link.

2) Analysis is the comparison of the predicted performance with the observed performance.

The prediction portion of TPAP is used throughout the evolution of a flight project, from initial mission studies through in-flight performance generation. The analysis portion of TPAP is used only for in-flight and post-flight performance analysis, to establish how well the system met its predicted capabilities. This comparison gives the Telecom System Engineer the information to keep the project aware of system status, and also provides valuable reference data for future system designs.

9.1.1 Reference Documents

The following documents provide more detail on TPAP structure and operation or illustrate its usage.

MIP-71-3-1240	Software Requirements Document, Mariner Mars '71 Telecommunications Prediction and Analysis Program (TPAP).
MIP-71-5-1240	Division Engineering Planning Document for Telecommunications Prediction and Analysis Program (TPAP).
PD 610-57	Mariner Mars 1971 Project Telecommunications Design Control Document.
PD 615-11	Venus Mercury 1973 Project Telecommunications Design Control Document.

9.2 THE TELECOMMUNICATIONS PREDICTION AND ANALYSIS REPORT

9.2.1 Program Functions

The TPAP will, at the option of the user, perform the following functions:

1) Telemetry performance prediction

2) Command performance prediction

3) Ranging performance prediction

4) Actual versus predicted performance comparisons

Predictions may be run for only one mode at a time. Comparisons are made only for telemetry data since all the mission observables, uplink carrier, downlink carrier, and telemetry signal-to-noise ratios are available from the telemetry predicts run.

A functional block diagram of TPAP is given in Figure 9-1. The figure is largely self-explanatory, however, the details of inputs and outputs will be discussed in the following paragraphs.

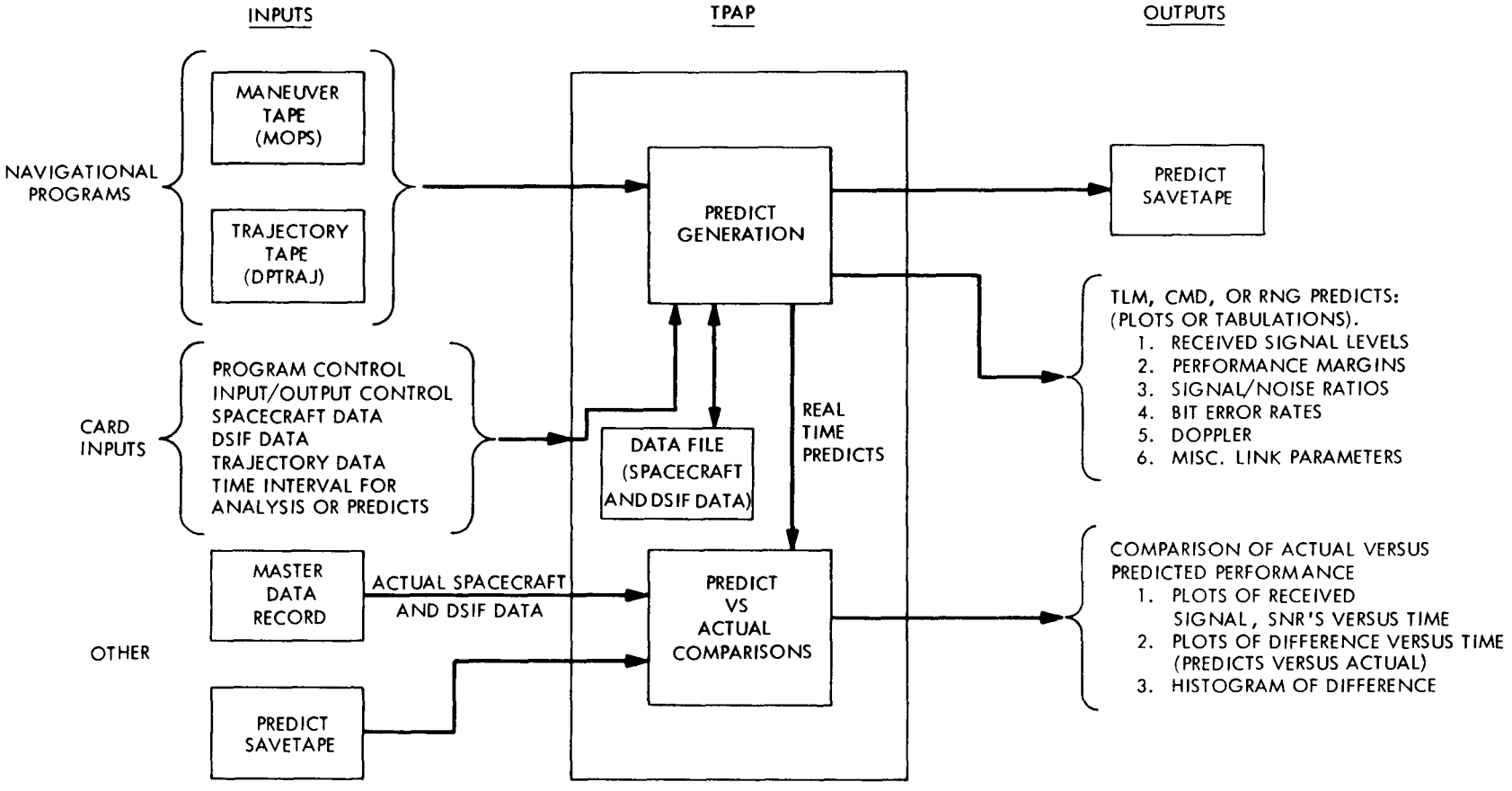

Fig. 9-1. TPAP functional block diagram

9.2.2 Program Use: Predictions

9.2.2.1 Functions. As indicated above, the user can generate predictions for command, telemetry, or ranging links. In all cases, the uplink and downlink carrier performance is provided. For telemetry runs, a PREDICT SAVE TAPE may be generated. This tape is used later as a source for predicted data when making analysis (comparison of predict versus actual) runs. The input requirements and output capabilities are presented below to assist in understanding the program operation.

9.2.2.2 Inputs. The input requirements are listed in Table 9-1. The inputs tell the program what the user wishes to do, provide the necessary data for calculations, and indicate what outputs are required.

Table 9-1. Inputs to prediction portion of TPAP

Data type	Typical information included	Possible data sources
Trajectory data	Earth cone and clock angles, range, range rate, range acceleration, station elevation angles [Data may be station centered or geocentric (Station at earth center)]	1. Input from cards 2. Trajectory save tape 3. Maneuver save tape
Program control	1. Start and stop times 2. Type of output desired 3. Type of run desired	1. Cards
Spacecraft data	1. Antenna patterns, up and down links 2. Power levels and systems losses 3. Data rates and threshold levels	1. Cards 2. From data file on tape
DSIF data	1. Antenna gains, ellipticity and pointing losses 2. Power level and system losses	1. Cards 2. From data file on tape

9.2.2.3 Outputs. Output capabilities are summarized in Table 9-2. For any run, DCT's and/or Summary tables are provided at times requested by the operator. Either performance or trajectory tabulations (and/or plots) may be outputted for each run, and a Predicts Save Tape may be written for telemetry runs.

A complete set of outputs for a telemetry run is given in Figures 9-2 through 9-9 and Tables 9-3 through 9-6. Tables 9-7 and 9-8 illustrate the Design Control Table outputs for command (dual-channel) and ranging runs. For the telemetry case, the outputs illustrate both the performance and trajectory tabulations and plots. Command and ranging outputs are similar.

The notations on the figures convey the following information:

D951 = Trajectory information from Trajectory Tape D951;

85 ft. = 85-foot (26-meter) ground antenna;

GEO. = Geocentric station location assumed;

33 = Engineering bit rate of 33-1/3 bps;

HP = Spacecraft in high-power transmitting mode;

LGAR = Low-gain antenna receiving;

LGAX = Low-gain antenna transmitting;

T2 = Traveling wave tube amplifier number 2 parameters;

X2 = Exciter number 2 parameters;

SC-2 = Parameters for spacecraft number 2;

GMT = Greenwich meridian time, days;

NOM = Design case;

W-C = Worst case;

TOL = |Sum of the adverse tolerances|;

Carrier power = carrier signal power component at the receiver case.

Table 9-2. Outputs of prediction portion of TPAP

Output type	Content	Output control	Examples
1. Summary Tables	Summary of spacecraft, DSIF, and trajectory data for one point in time	Provided at times requested by user	Table 9-4.
2. Design Control Tables	All link parameters and final output performance margins and tolerances	Provided at times requested	Tables 9-3, 9-7, and 9-8.
3. Performance Tabulations and/or Plots	Tabulated performance of uplink and downlink carrier channels, and data channels for each point in time considered	Provided at user request	Tabulations: Table 9-5 Plots: Figures 9-2, 9-3, 9-4, and 9-5.
4. Trajectory Tabulations and/or Plots	Tabulation of trajectory data, plus uplink and downlink doppler shifts	Provided at user request	Tabulations: Table 9-6 Plots: Figures 9-6, 9-7, 9-8, and 9-9.
5. Predicts Save-Tape	Tape tabulation of performance data, to be used for comparison of actual-to-predicted performance	Provided at user request for telemetry runs only	Figures 9-10, 9-11, and 9-12.

The DCT's presented here are somewhat different in format than those shown in Section III. These DCT's are per the present TPAP program implementation. In the future, they may be updated to the section III format.

The output data is felt to be self-explanatory. One possible area of question is in the use of the adverse tolerance for the telemetry performance margin. The absolute value is used so that the plots will illustrate the cross-over point, where the performance margin equals the adverse tolerances, since this point is the definition of minimum satisfactory link performance.

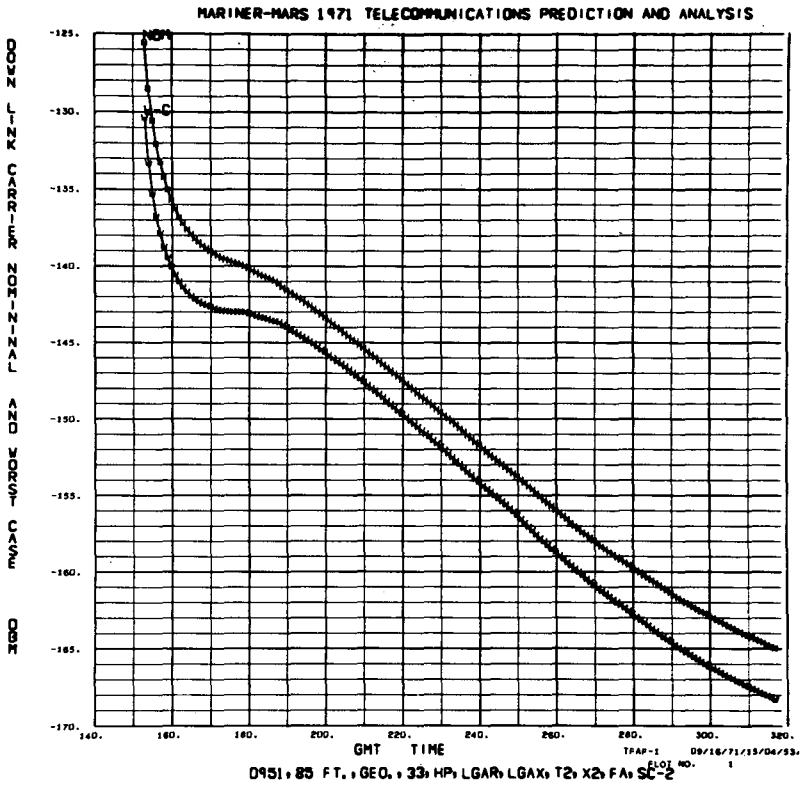

Fig. 9-2. Typical TPAP plot of downlink carrier level vs time

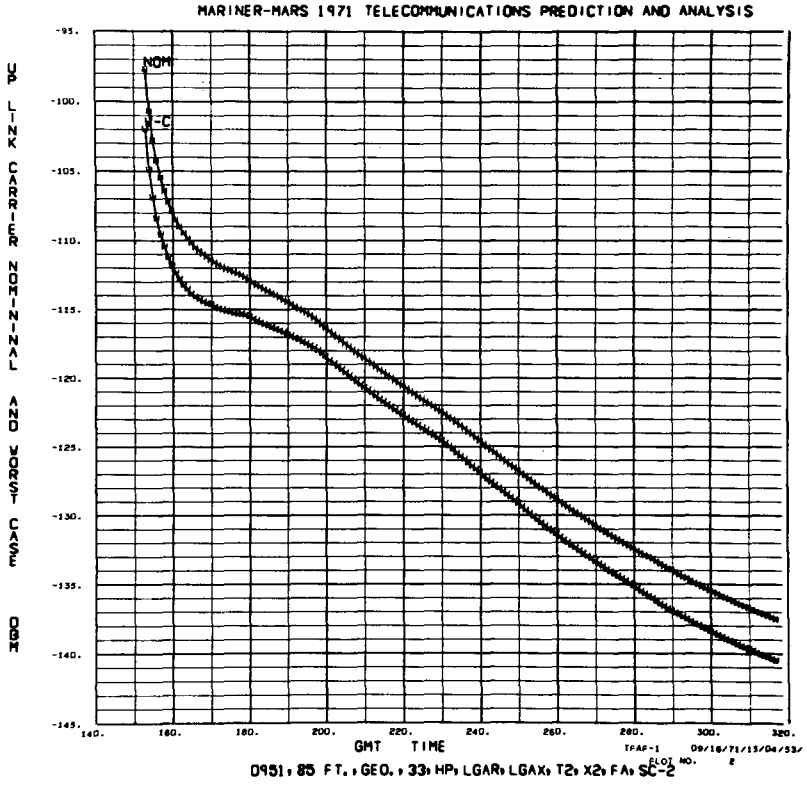

Fig. 9-3. Typical TPAP plot of uplink carrier level vs time

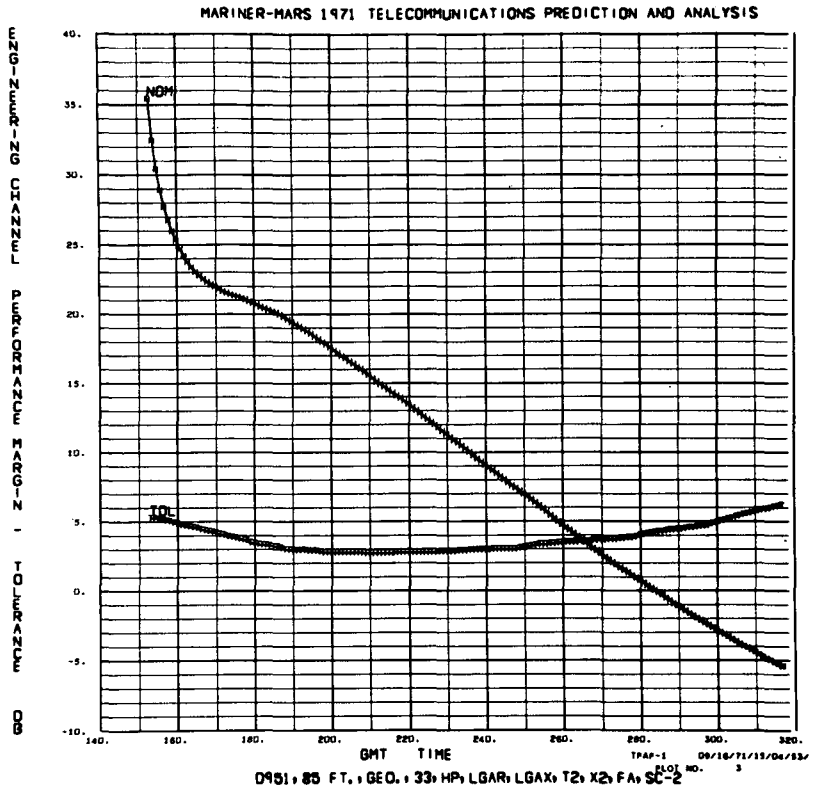

Fig. 9-4. Typical TPAP plot of telemetry performance margin vs time

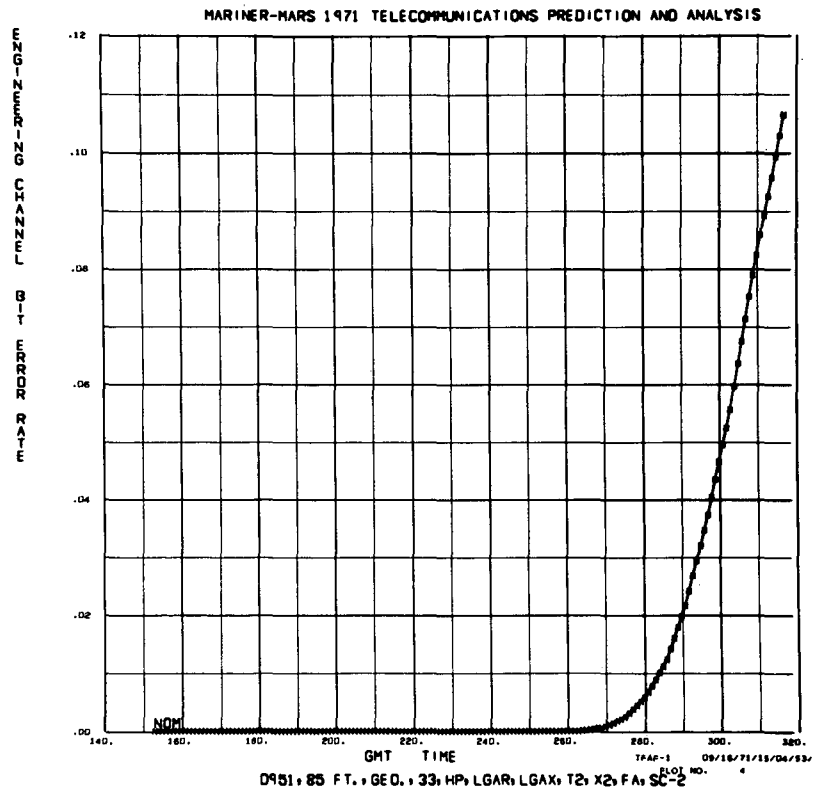

Fig. 9-5. Typical TPAP plot of telemetry bit error rate vs time

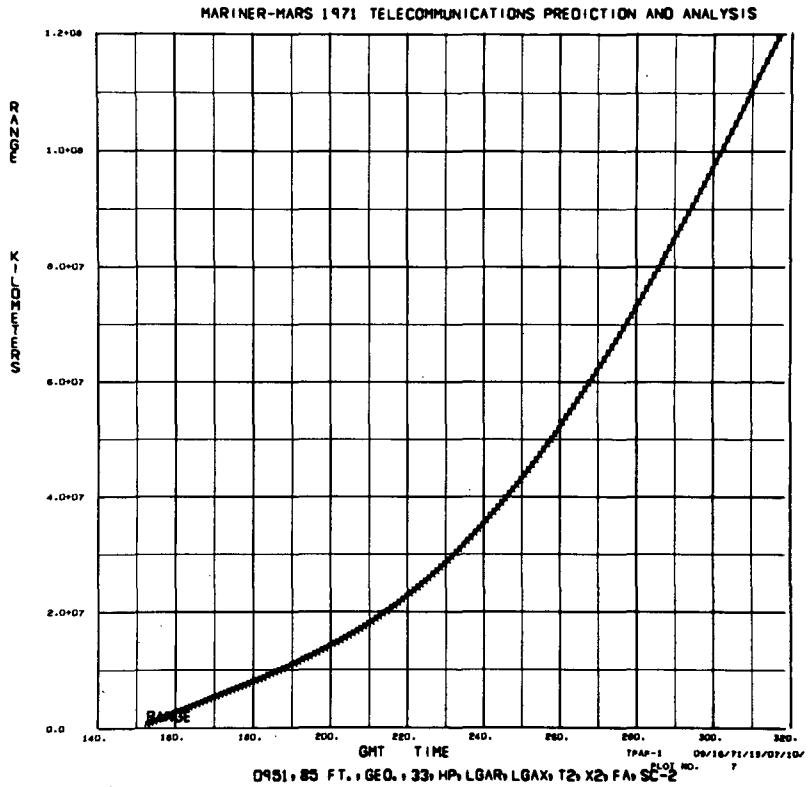

Fig. 9-6. Typical TPAP plot of earth to spacecraft range vs time

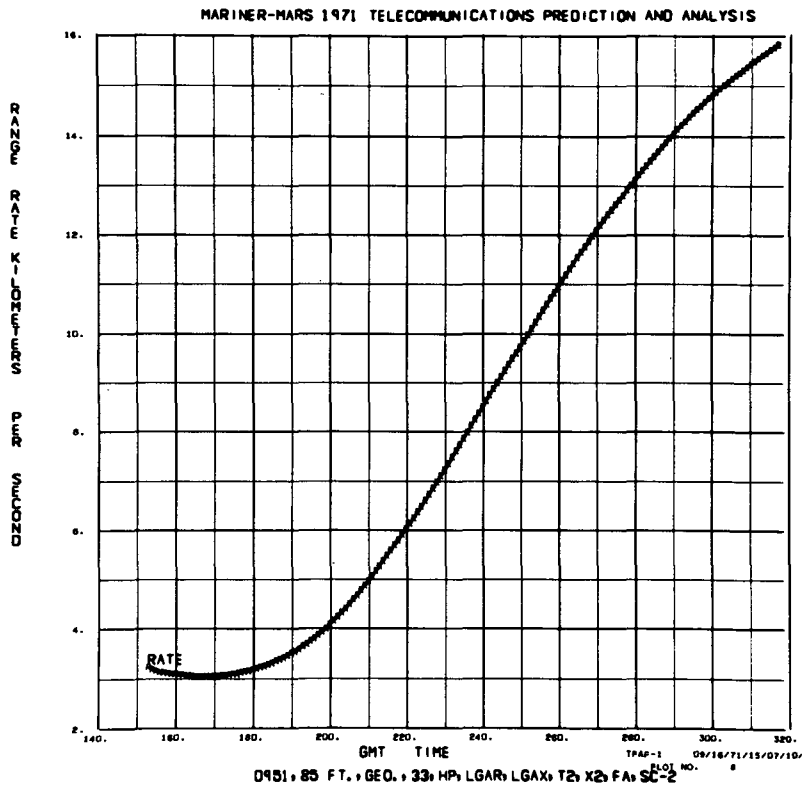

Fig. 9-7. Typical TPAP plot of range rate vs time

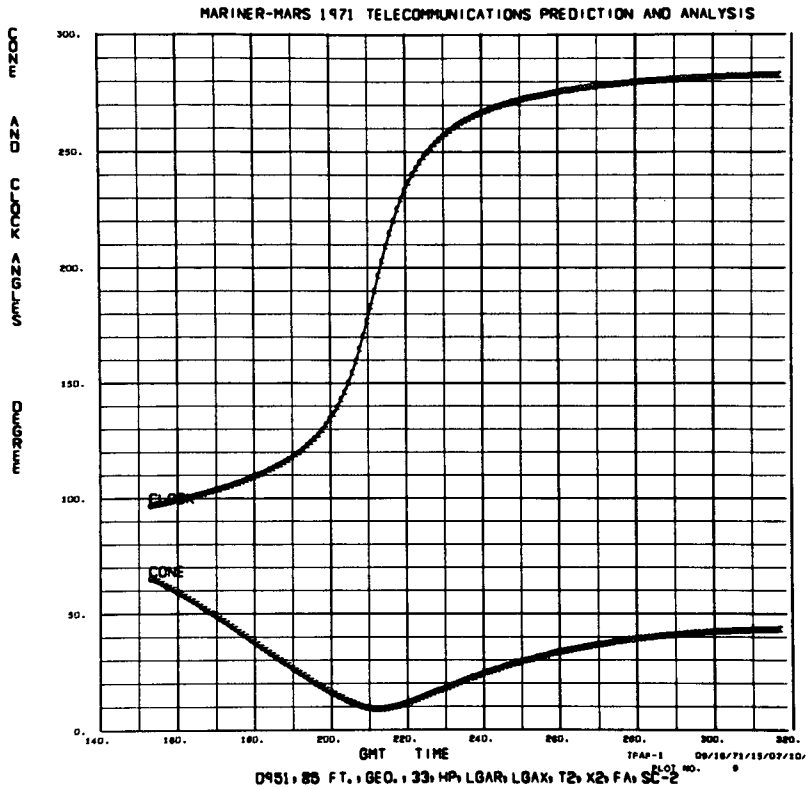

Fig. 9-8. Typical TPAP plot of earth cone and clock angles vs time

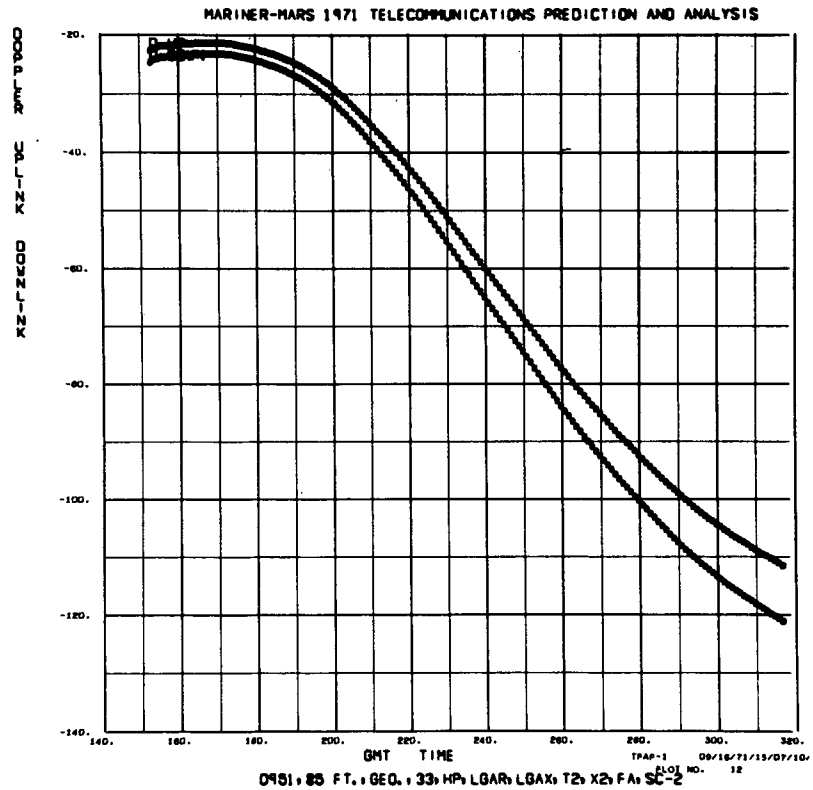

Fig. 9-9. Typical TPAP plot of Doppler shift vs time

Table 9-3. TPAP telemetry design control table

09/13/71/

MM71 DNLINK TELEMETRY DESIGN CONTROL TABLE

D951,85 FT.,GEO.,33,HP,LGAR,LGAX,T2,X2,FA,SC-2

ENGR. CHANNEL 33.30 BPS SCI. CHANNEL .00 BPS

LAUNCH- 5/30/71 STATION- GEOCENTRIC DATA

TIME IN MISSION- L+160.94 DAYS (11/ 9/71) ARRIVAL- 11/14/71

	NOMINAL	FAV.TOL.	ADV.TOL.
TRANSMITTER PARAMETERS			
1) RF POWER, DBM	41.75	.50	-.50
POWER OUTPUT= .15+02 WATTS			
2) CIRCUIT LOSS, DB	-1.03	.11	-.11
3) ANTENNA GAIN, DB	7.71	.73	-.73
4) POINTING LOSS, DB	-2.99	.95	-1.12
PATH PARAMETERS			
5) SPACE LOSS, DB	-260.81		
FREQ= 2296.11 MHZ			
RANGE= 114.022+06 KM			
RECEIVER PARAMETERS			
6) POLARIZATION LOSS, DB	.00	.05	-.05
7) ANTENNA GAIN, DB	53.30	.60	-.60
8) POINTING LOSS, DB	-.04	.00	.00
9) CIRCUIT LOSS, DB	.00	.00	.00
10) SYSTEM NOISE SPEC. DENS., DBM/HZ	-182.47	-.33	.31
SYSTEM NOISE TEMPERATURE, DEG. K	41.00	-3.00	3.00
ZENITH NOISE TEMPERATURE, DEG. K	33.00	-3.00	3.00
ZENITH NOISE SPEC. DENS., DBM/HZ	-183.41	-.41	.38
ELEVATION ANGLE= 25.00 DEGREES.			
11) CARR. THRESHOLD NOISE BW (HZ), DB	10.79	-.97	.00
TOTAL POWER SUMMARY			
12) LINK LOSS, DB (2+3+4+5+6+7+8+9)	-203.86	2.45	-2.61
13) RECEIVED POWER P(T),DBM (1+12)	-162.11	2.95	-3.11
14) CARRIER MODULATION LOSS, DB	-2.42	.12	-.21
15) RECEIVED CARR. POWER, DBM (13+14)	-164.53	3.07	-3.32
CARRIER TRACKING PERFORMANCE (ONE WAY)			
16) THRESHOLD SNR IN 2BLO, DB	8.00	.00	.00
17) THRESHOLD CARR. PWR.,DBM(10+11+16)	-163.68	-1.30	.31
18) PERFORMANCE MARGIN, DB (15-17)	-.85	4.37	-3.63
CARRIER TRACKING PERFORMANCE (TWO WAY)			
19) THRESHOLD SNR IN 2BLO, DB	8.00	.00	.00
20) THRESHOLD CARR. PWR., DBM(10+11+19)	-163.68	-1.30	.31
21) PERFORMANCE MARGIN, DB (15-20)	-.85	4.37	-3.63

Table 9-3. TPAP telemetry design control table (cont'd)

MM71- 1 TELEMETRY DESIGN CONTROL TABLE PAGE 2 OF 3

	ENGR	SCIENCE
22) DATA BIT RATE (BPS), DB	15.22	.00
FAVORABLE TOLERANCE	.00	.00
ADVERSE TOLERANCE	.00	.00
23) MODULATION LOSS, DB	-3.69	.00
FAVORABLE TOLERANCE	.27	.00
ADVERSE TOLERANCE	-.17	.00
24) WAVEFORM DISTORTION LOSS, DB	-.10	.00
FAVORABLE TOLERANCE	.10	.00
ADVERSE TOLERANCE	-.10	.00
25) RADIO SYSTEM LOSS, DB	-1.36	.00
FAVORABLE TOLERANCE	.62	.00
ADVERSE TOLERANCE	-1.81	.00
UPLINK SNR IN 2BLO = 17.4 DB (NOMINAL)		
DOWNLINK SNR IN 2BLO = 6.7 DB (NOMINAL)		
26) SUBCARRIER DEMOD. LOSS, DB	-.43	.00
FAVORABLE TOLERANCE	.15	.00
ADVERSE TOLERANCE	-.27	.00
27) BIT SYNC/DETECTOR LOSS, DB	-.10	.00
FAVORABLE TOLERANCE	.10	.00
ADVERSE TOLERANCE	-.10	.00
28) RECEIVED DATA PWR, DBM (13+23+24+25+26+27)	-167.80	.00
FAVORABLE TOLERANCE	4.19	.00
ADVERSE TOLERANCE	-5.57	.00
29) THRESHOLD PT/N, DB	4.30	.00
FAVORABLE TOLERANCE	.00	.00
ADVERSE TOLERANCE	.00	.00
BIT ERROR RATE (NOMINAL)	3.3-02	1.0-06
30) THRESHOLD DATA PWR, DBM (10+22+29)	-162.95	.00
FAVORABLE TOLERANCE	-.33	.00
ADVERSE TOLERANCE	.31	.00
31) PERFORMANCE MARGIN, DB (29-30)	-4.85	.00
FAVORABLE TOLERANCE	4.51	.00
ADVERSE TOLERANCE	-5.88	.00

Table 9-4. TPAP parameter summary table

T = 3862.49 HOURS FROM LAUNCH — 11 — 9 — 1971 — GMT TIME — 0000 — .000 — SECONDS

TRAJECTORY DATA	GEOCENTRIC DATA	TAPE						
	CONE ANGLE	42.86 DEGREES	CLOCK ANGLE	282.51 DEGREES	RANGE	.114021539+09	KM	
TELEMETRY PERFORMANCE								
	CHANNEL 1 MARGIN	-4.85	4.51	-5.33 DB	CHANNEL 2 MARGIN	.00	.00	.00 DB
TRACKING PERFORMANCE								
	UL ONE-WAY MARGIN	10.34	4.49	-4.72 DB	UL CARRIER LEVEL	-137.06	3.36	-3.00 DB
	DL ONE-WAY MARGIN	-.85	4.37	-3.63 DB	DL CARRIER LEVEL	-164.53	3.07	-3.32 DB
	TWO-WAY MARGIN	-.85	4.37	-3.63 DB				
MISCELLANEOUS LINK DATA								
	REC ANT GAIN	4.739	1.515	-1.643 DB	TX ANT GAIN	4.723	1.683	-1.850 DB
	POLARIZATION LOSS	.001	.107	-.110 DB	POLARIZATION LOSS	.000	.054	-.055 DB
	UL SPACE LOSS	-260.033		DB	DL SPACE LOSS	-260.810		DB
	RADIO LOSS 1	-1.365	.618	-1.809 DB	PBE1	.926-01		
	RADIO LOSS 2	.000	.000	.000 DB	PBE2	.100-05		
	UL SNR IN 2BLO	17.439	4.562	32.831 DB	DL SNR IN 2BLO	6.676	15.325	32.831 DB
	UPLINK DOPPLER	-109.995		KHZ	DOWNLINK DOPPLER	-113.452	KHZ	
	TWO-WAY DOPPLER	-238.887		KHZ	DOPPLER STD DEV	.000		HZ
	GROUND REC TEMP	41.000	-3.000	3.000 DEG K				

* *MM71 * * *MM71 * * *MM71 * * *MM71 * * *MM71 * * *MM71 * * *MM71 * * *MM71 * * *MM71 * * *MM71 *

Table 9-5. TPAP telemetry performance summary table

PAGE 10F 5
RUN DATE DD/MM/YY HH:MM:SS
09/13/71 14:07:23

TELEMETRY PERFORMANCE SUMMARY TABLE
D951,85 FT,,GEC,,33,HP,LGAR,LGAX,T2,X2,FA,SC-2
LAUNCH- 5/30/71 ARRIVAL -11/14/71 GEOCENTRIC DATA

GMT	DOWNLINK CARRIER		UPLINK CARRIER		33.30 BPS ENG			.00 BPS SCI		
DDD HH MM	NOMDBM	WC DBM	NOMDBM	WC DBM	PM DB	TOL DB	BIT ER	PM DB	TOL DB	BIT ER
153/ 0/ 0	-125.99	-130.37	-97.69	-101.95	35.43	5.27	.10-05	.00	.00	.10-05
154/ 0/ 0	-128.54	-133.32	-100.69	-104.92	32.45	5.25	.10-05	.00	.00	.10-05
155/ 0/ 0	-130.59	-135.31	-102.73	-106.93	30.41	5.20	.10-05	.00	.00	.10-05
156/ 0/ 0	-132.10	-136.77	-104.26	-108.41	28.89	5.14	.10-05	.00	.00	.10-05
157/ 0/ 0	-133.28	-137.39	-105.47	-109.55	27.71	5.09	.10-05	.00	.00	.10-05
158/ 0/ 0	-134.24	-138.78	-106.44	-110.49	26.75	5.01	.10-05	.00	.00	.10-05
159/ 0/ 0	-135.02	-139.48	-107.24	-111.23	25.97	4.94	.10-05	.00	.00	.10-05
160/ 0/ 0	-135.71	-140.09	-107.94	-111.85	25.28	4.84	.10-05	.00	.00	.10-05
161/ 0/ 0	-136.30	-140.57	-108.54	-112.37	24.69	4.74	.10-05	.00	.00	.10-05
162/ 0/ 0	-136.80	-141.01	-109.05	-112.83	24.19	4.68	.10-05	.00	.00	.10-05
163/ 0/ 0	-137.23	-141.39	-109.50	-113.22	23.75	4.62	.10-05	.00	.00	.10-05
164/ 0/ 0	-137.61	-141.70	-109.88	-113.55	23.38	4.56	.10-05	.00	.00	.10-05
165/ 0/ 0	-137.93	-141.96	-110.21	-113.83	23.05	4.50	.10-05	.00	.00	.10-05
166/ 0/ 0	-138.21	-142.17	-110.50	-114.07	22.76	4.44	.10-05	.00	.00	.10-05
167/ 0/ 0	-138.45	-142.35	-110.75	-114.27	22.54	4.38	.10-05	.00	.00	.10-05
168/ 0/ 0	-138.66	-142.49	-110.97	-114.43	22.33	4.31	.10-05	.00	.00	.10-05
169/ 0/ 0	-138.84	-142.60	-111.17	-114.55	22.15	4.24	.10-05	.00	.00	.10-05
170/ 0/ 0	-139.03	-142.68	-111.39	-114.66	21.95	4.13	.10-05	.00	.00	.10-05
171/ 0/ 0	-139.20	-142.77	-111.59	-114.79	21.79	4.05	.10-05	.00	.00	.10-05
172/ 0/ 0	-139.34	-142.86	-111.77	-114.92	21.64	4.00	.10-05	.00	.00	.10-05
173/ 0/ 0	-139.47	-142.93	-111.93	-115.04	21.51	3.94	.10-05	.00	.00	.10-05
174/ 0/ 0	-139.58	-142.98	-112.08	-115.13	21.40	3.88	.10-05	.00	.00	.10-05
175/ 0/ 0	-139.67	-143.01	-112.20	-115.21	21.31	3.82	.10-05	.00	.00	.10-05
176/ 0/ 0	-139.75	-143.03	-112.32	-115.28	21.23	3.76	.10-05	.00	.00	.10-05
177/ 0/ 0	-139.82	-143.04	-112.42	-115.33	21.16	3.70	.10-05	.00	.00	.10-05
178/ 0/ 0	-139.90	-143.04	-112.53	-115.38	21.08	3.62	.10-05	.00	.00	.10-05
179/ 0/ 0	-140.05	-143.02	-112.72	-115.41	20.94	3.46	.10-05	.00	.00	.10-05
180/ 0/ 0	-140.19	-143.10	-112.90	-115.54	20.80	3.40	.10-05	.00	.00	.10-05
181/ 0/ 0	-140.32	-143.20	-113.07	-115.63	20.67	3.36	.10-05	.00	.00	.10-05
182/ 0/ 0	-140.44	-143.28	-113.23	-115.62	20.54	3.33	.10-05	.00	.00	.10-05
183/ 0/ 0	-140.56	-143.36	-113.39	-115.95	20.43	3.29	.10-05	.00	.00	.10-05
184/ 0/ 0	-140.67	-143.43	-113.53	-116.07	20.32	3.25	.10-05	.00	.00	.10-05
185/ 0/ 0	-140.77	-143.50	-113.68	-116.19	20.22	3.22	.10-05	.00	.00	.10-05
186/ 0/ 0	-140.87	-143.56	-113.82	-116.30	20.12	3.18	.10-05	.00	.00	.10-05
187/ 0/ 0	-141.00	-143.62	-113.95	-116.41	19.99	3.11	.10-05	.00	.00	.10-05
188/ 0/ 0	-141.19	-143.67	-114.14	-116.51	19.80	2.97	.10-05	.00	.00	.10-05
189/ 0/ 0	-141.37	-143.83	-114.31	-116.65	19.61	2.95	.10-05	.00	.00	.10-05
190/ 0/ 0	-141.55	-144.00	-114.47	-116.80	19.43	2.94	.10-05	.00	.00	.10-05
191/ 0/ 0	-141.73	-144.16	-114.63	-116.94	19.25	2.92	.10-05	.00	.00	.10-05
192/ 0/ 0	-141.91	-144.32	-114.79	-117.08	19.07	2.91	.10-05	.00	.00	.10-05

Table 9-6. TPAP trajectory performance summary table

TRAJECTORY PERFORMANCE SUMMARY TABLE

D951.95 F.T.,SEC.,33,HP,LGAR,LGAX,T2,X2,FA,SC-2

LAUNCH- 5/30/71 ARRIVAL -11/14/71 GEOCENTRIC DATA

GMT DDD HH MM	RANGE KM	R-RATE KM/SEC	CONE DEG.	CLOCK DEG.	ELEV. DEG.	R-ACC M/SEC2	D-UP KHZ	D-DOWN KHZ	D2WAY KHZ
153/ 0/ 0	6.406+05	3.226+00	64.78	96.38	25.00	1.000+00	-22.744	-24.633	-49.339
154/ 0/ 0	9.165+05	3.168+00	64.36	96.82	25.00	1.000+00	-22.341	-24.261	-48.516
155/ 0/ 0	1.189+06	3.136+00	63.68	97.21	25.00	1.000+00	-22.119	-24.021	-48.037
156/ 0/ 0	1.459+06	3.116+00	62.87	97.58	25.00	1.000+00	-21.974	-23.863	-47.695
157/ 0/ 0	1.729+06	3.107+00	61.97	97.95	25.00	1.000+00	-21.912	-23.796	-47.558
158/ 0/ 0	1.996+06	3.095+00	61.04	98.32	25.00	1.000+00	-21.827	-23.703	-47.353
159/ 0/ 0	2.263+06	3.085+00	60.09	98.69	25.00	1.000+00	-21.754	-23.624	-47.216
160/ 0/ 0	2.529+06	3.075+00	59.11	99.07	25.00	1.000+00	-21.689	-23.554	-47.079
161/ 0/ 0	2.794+06	3.067+00	58.11	99.46	25.00	1.000+00	-21.630	-23.489	-46.843
162/ 0/ 0	3.059+06	3.059+00	57.11	99.85	25.00	1.000+00	-21.574	-23.428	-46.806
163/ 0/ 0	3.323+06	3.052+00	56.09	100.25	25.00	1.000+00	-21.523	-23.374	-46.737
164/ 0/ 0	3.586+06	3.045+00	55.06	100.67	25.00	1.000+00	-21.478	-23.324	-46.600
165/ 0/ 0	3.849+06	3.040+00	54.02	101.09	25.00	1.000+00	-21.439	-23.281	-46.532
166/ 0/ 0	4.111+06	3.035+00	52.97	101.52	25.00	1.000+00	-21.405	-23.246	-46.464
167/ 0/ 0	4.373+06	3.032+00	51.91	101.97	25.00	1.000+00	-21.382	-23.221	-46.395
168/ 0/ 0	4.635+06	3.030+00	50.83	102.43	25.00	1.000+00	-21.370	-23.208	-46.355
169/ 0/ 0	4.897+06	3.030+00	49.76	102.90	25.00	1.000+00	-21.370	-23.209	-46.395
170/ 0/ 0	5.159+06	3.032+00	48.67	103.38	25.00	1.000+00	-21.384	-23.223	-46.395
171/ 0/ 0	5.421+06	3.036+00	47.57	103.88	25.00	1.000+00	-21.413	-23.254	-46.464
172/ 0/ 0	5.684+06	3.042+00	46.47	104.39	25.00	1.000+00	-21.456	-23.301	-46.600
173/ 0/ 0	5.947+06	3.051+00	45.36	104.92	25.00	1.000+00	-21.515	-23.365	-46.669
174/ 0/ 0	6.211+06	3.061+00	44.24	105.46	25.00	1.000+00	-21.585	-23.445	-46.874
175/ 0/ 0	6.476+06	3.074+00	43.12	106.02	25.00	1.000+00	-21.678	-23.541	-47.073
176/ 0/ 0	6.742+06	3.088+00	42.00	106.60	25.00	1.000+00	-21.781	-23.653	-47.285
177/ 0/ 0	7.010+06	3.105+00	40.87	107.20	25.00	1.000+00	-21.898	-23.780	-47.558
178/ 0/ 0	7.279+06	3.123+00	39.74	107.82	25.00	1.000+00	-22.028	-23.922	-47.832
179/ 0/ 0	7.549+06	3.144+00	38.61	108.46	25.00	1.000+00	-22.172	-24.078	-48.106
180/ 0/ 0	7.822+06	3.166+00	37.48	109.12	25.00	1.000+00	-22.329	-24.248	-48.448
181/ 0/ 0	8.097+06	3.190+00	36.35	109.81	25.00	1.000+00	-22.498	-24.433	-48.959
182/ 0/ 0	8.373+06	3.216+00	35.22	110.52	25.00	1.000+00	-22.692	-24.632	-49.201
183/ 0/ 0	8.652+06	3.244+00	34.08	111.27	25.00	1.000+00	-22.878	-24.845	-49.580
184/ 0/ 0	8.934+06	3.274+00	32.97	112.05	25.00	1.000+00	-23.087	-25.072	-50.090
185/ 0/ 0	9.219+06	3.305+00	31.84	112.97	25.00	1.000+00	-23.310	-25.314	-50.569
186/ 0/ 0	9.505+06	3.339+00	30.73	113.72	25.00	1.000+00	-23.547	-25.571	-51.117
187/ 0/ 0	9.795+06	3.374+00	29.61	114.62	25.00	1.000+00	-23.797	-25.843	-51.664
188/ 0/ 0	1.009+07	3.412+00	28.50	115.57	25.00	1.000+00	-24.062	-26.131	-52.212
189/ 0/ 0	1.038+07	3.451+00	27.40	116.55	25.00	1.000+00	-24.342	-26.434	-52.829
190/ 0/ 0	1.068+07	3.493+00	26.31	117.64	25.00	1.000+00	-24.638	-26.756	-53.443
191/ 0/ 0	1.098+07	3.538+00	25.22	118.78	25.00	1.000+00	-24.951	-27.096	-54.128
192/ 0/ 0	1.130+07	3.585+00	24.14	119.99	25.00	1.000+00	-25.283	-27.456	-54.880

Table 9-7. TPAP command design control table

09/13/71/

MM71 UPLINK COMMAND DESIGN CONTROL TABLE

D951,85 FT.,GEO.,33,HP,LGAR,LGAX,T2,X2,FA,SC-2

COMMAND CHANNEL 1.00 BPS SYNC CHANNEL 1.00 BPS

LAUNCH- 5/30/71 STATION- GEOCENTRIC DATA

TIME IN MISSION- L+160.34 DAYS (11/ 9/71) ARRIVAL- 11/14/71

	NOMINAL	FAV.TOL.	ADV.TOL.
TRANSMITTER PARAMETERS			
1) RF POWER, DBM	70.00	.50	.00
POWER OUTPUT= .10+05 WATTS			
2) CIRCUIT LOSS, DB	.00	.00	.00
3) ANTENNA GAIN, DB	51.80	.90	-.90
4) POINTING LOSS, DB	-.04	.00	.00
PATH PARAMETERS			
5) SPACE LOSS, DB	-260.09		
FREQ= 2114.33 MHZ			
RANGE= 114.022+06 KM			
RECEIVER PARAMETERS			
6) POLARIZATION LOSS, DB	.00	.11	-.11
7) ANTENNA GAIN, DB	7.00	.81	-.81
8) POINTING LOSS, DB	-2.20	.71	-.84
9) CIRCUIT LOSS, DB	-1.03	.14	-.14
10) SYSTEM NOISE SPEC. DENS., DBM/HZ	-167.46	-.61	1.27
SYSTEM NOISE TEMPERATURE, DEG. K	1300.00	-170.00	440.00
11) CARR. THRESHOLD NOISE BW (HZ), DB	12.55	-.51	.46
TOTAL POWER SUMMARY			
12) LINK LOSS, DB (2+3+4+5+6+7+8+9)	-204.56	2.66	-2.80
13) RECEIVED POWER P(T),DBM (1+12)	-134.56	3.16	-2.80
14) CARRIER MODULATION LOSS, DB	-2.50	.20	-.20
15) RECEIVED CARR. POWER, DBM (13+14)	-137.06	3.36	-3.00
CARRIER TRACKING PERFORMANCE (ONE WAY)			
16) THRESHOLD SNR IN 2BLO, DB	7.00	.00	.00
17) THRESHOLD CARR. PWR.,DBM(10+11+16)	-147.91	-1.12	1.72
18) PERFORMANCE MARGIN, DB (15-17)	10.84	4.48	-4.72
CARRIER TRACKING PERFORMANCE (TWO WAY)			
19) THRESHOLD SNR IN 2BLO, DB	7.00	.00	.00
20) THRESHOLD CARR. PWR.,DBM(10+11+19)	-147.91	-1.12	1.72
21) PERFORMANCE MARGIN, DB (15-20)	10.84	4.48	-4.72

Table 9-7. TPAP command design control table (cont'd)

MM71- 2 COMMAND DESIGN CONTROL TABLE PAGE 2 OF 3

	DATA	SYNC
22) DATA BIT RATE (BPS), DB	.00	.00
FAVORABLE TOLERANCE	.00	.00
ADVERSE TOLERANCE	-.00	.00
23) MODULATION LOSS, DB	-6.99	-6.01
FAVORABLE TOLERANCE	.22	.18
ADVERSE TOLERANCE	-.24	-.19
24) WAVEFORM DISTORTION LOSS, DB	.00	.00
FAVORABLE TOLERANCE	.00	.00
ADVERSE TOLERANCE	.00	.00
25) RADIO SYSTEM LOSS, DB	-.78	-.78
FAVORABLE TOLERANCE	.19	.19
ADVERSE TOLERANCE	-.22	-.22
UPLINK SNR IN 2BLO = 17.4 DB (NOMINAL)		
DOWNLINK SNR IN 2BLO = 9.1 DB (NOMINAL)		
26) SUBCARRIER DEMOD. LOSS, DB	.00	.00
FAVORABLE TOLERANCE	.00	.00
ADVERSE TOLERANCE	.00	.00
27) BIT SYNC/DETECTOR LOSS, DB	.00	.00
FAVORABLE TOLERANCE	.00	.00
ADVERSE TOLERANCE	.00	.00
28) RECEIVED DATA PWR, DBM (13+23+24+25+26+27)	-144.33	-141.35
FAVORABLE TOLERANCE	3.57	3.53
ADVERSE TOLERANCE	-3.26	-3.21
29) THRESHOLD PT/N, DB	11.70	14.70
FAVORABLE TOLERANCE	-.80	-.80
ADVERSE TOLERANCE	.80	.80
BIT ERROR RATE (NOMINAL)	1.0-06	
30) THRESHOLD DATA PWR, DBM (10+22+29)	-155.76	-152.76
FAVORABLE TOLERANCE	-1.41	-1.41
ADVERSE TOLERANCE	2.07	2.07
31) PERFORMANCE MARGIN, DB (28-30)	11.43	11.41
FAVORABLE TOLERANCE	4.98	4.94
ADVERSE TOLERANCE	-5.32	-5.27

Table 9-8. TPAP ranging design control table

09/13/71/

MM71 UPLINK RANGING DESIGN CONTROL TABLE

D951,85 FT.,SEO.,33,HP,LGAR,LGAX,T2,X2,FA,SC-2
LAUNCH- 5/30/71 STATION- GEOCENTRIC DATA

TIME IN MISSION- L+160.94 DAYS (11/ 9/71) ARRIVAL- 11/14/71

	NOMINAL	FAV.TOL.	ADV.TOL.
TRANSMITTER PARAMETERS			
1) RF POWER, DBM	70.00	.50	.00
POWER OUTPUT= .10+05 WATTS			
2) CIRCUIT LOSS, DB	.00	.00	.00
3) ANTENNA GAIN, DB	51.80	.90	-.90
4) POINTING LOSS, DB	-.04	.00	.00
PATH PARAMETERS			
5) SPACE LOSS, DB	-260.09		
FREQ= 2114.33 MHZ			
RANGE= 114.022+06 KM			
RECEIVER PARAMETERS			
6) POLARIZATION LOSS, DB	.00	.11	-.11
7) ANTENNA GAIN, DB	7.00	.81	-.81
8) POINTING LOSS, DB	-2.20	.71	-.84
9) CIRCUIT LOSS, DB	-1.03	.14	-.14
10) SYSTEM NOISE SPEC. DENS., DBM/HZ	-167.46	-.61	1.27
SYSTEM NOISE TEMPERATURE, DEG. K	1300.00	-170.00	440.00
11) CARR. THRESHOLD NOISE BW (HZ), DB	12.55	-.51	.46
TOTAL POWER SUMMARY			
12) LINK LOSS, DB (2+3+4+5+6+7+8+9)	-204.56	2.66	-2.80
13) RECEIVED POWER P(T),DBM (1+12)	-134.56	3.16	-2.80
14) CARRIER MODULATION LOSS, DB	-9.00	.62	-.69
15) RECEIVED CARR. POWER, DBM (13+14)	-143.56	3.78	-3.49
CARRIER TRACKING PERFORMANCE (ONE WAY)			
16) THRESHOLD SNR IN 2BLO, DB	7.00	.00	.00
17) THRESHOLD CARR. PWR.,DBM(10+11+16)	-147.91	-1.12	1.72
18) PERFORMANCE MARGIN, DB (15-17)	4.34	4.90	-5.21
CARRIER TRACKING PERFORMANCE (TWO WAY)			
19) THRESHOLD SNR IN 2BLO, DB	7.00	.00	.00
20) THRESHOLD CARR. PWR., DBM(10+11+19)	-147.91	-1.12	1.72
21) PERFORMANCE MARGIN, DB (15-20)	4.34	4.90	-5.21

Table 9-8. TPAP ranging design control table (cont'd)

09/13/71/

MM71 DNLINK RANGING DESIGN CONTROL TABLE

D951•85 FT.•GEO.•33•HP•LGAR•LGAX•T2•X2•FA•SC-2
LAUNCH- 5/30/71 STATION- GEOCENTRIC DATA

TIME IN MISSION- L+160.34 DAYS (11/ 9/71) ARRIVAL- 11/14/71

	NOMINAL	FAV.TOL.	ADV.TOL.
TRANSMITTER PARAMETERS			
1) RF POWER• DBM	41.75	.50	-.50
POWER OUTPUT= .15+02 WATTS			
2) CIRCUIT LOSS• DB	-1.03	.11	-.11
3) ANTENNA GAIN• DB	7.71	.73	-.73
4) POINTING LOSS• DB	-2.99	.95	-1.12
PATH PARAMETERS			
5) SPACE LOSS• DB	-260.81		
FREQ= 2296.11 MHZ			
RANGE= 114.022+06 KM			
RECEIVER PARAMETERS			
6) POLARIZATION LOSS• DB	.00	.05	-.05
7) ANTENNA GAIN• DB	53.30	.60	-.60
8) POINTING LOSS• DB	-.04	.00	.00
9) CIRCUIT LOSS• DB	.00	.00	.00
10) SYSTEM NOISE SPEC. DENS.• DBM/HZ	-182.47	-.33	.31
SYSTEM NOISE TEMPERATURE• DEG. K	41.00	-3.00	3.00
ZENITH NOISE TEMPERATURE• DEG. K	33.00	-3.00	3.00
ZENITH NOISE SPEC. DENS.• DBM/HZ	-183.41	-.41	.38
ELEVATION ANGLE= 25.00 DEGREES.			
11) CARR. THRESHOLD NOISE BW (HZ)• DB	10.79	-.37	.00
TOTAL POWER SUMMARY			
12) LINK LOSS• DB (2+3+4+5+6+7+8+9)	-203.86	2.45	-2.61
13) RECEIVED POWER P(T)•DBM (1+12)	-162.11	2.95	-3.11
14) CARRIER MODULATION LOSS• DB	-8.62	.26	-1.63
15) RECEIVED CARR. POWER• DBM (13+14)	-170.73	3.21	-4.74
CARRIER TRACKING PERFORMANCE (ONE WAY)			
16) THRESHOLD SNR IN 2BLO• DB	8.00	.00	.00
17) THRESHOLD CARR. PWR.•DBM(10+11+16)	-163.68	-1.30	.31
18) PERFORMANCE MARGIN• DB (15-17)	-7.05	4.51	-5.05
CARRIER TRACKING PERFORMANCE (TWO WAY)			
19) THRESHOLD SNR IN 2BLO• DB	8.00	.00	.00
20) THRESHOLD CARR. PWR.• DBM(10+11+19)	-163.68	-1.30	.31
21) PERFORMANCE MARGIN• DB (15-20)	-7.05	4.51	-5.05

Table 9-8. TPAP ranging design control table (cont'd)

PLANETARY RANGING SYSTEM

22)	UPLINK RANGING MODULATION LOSS (DB)	-.580
	FAVORABLE TOLERANCE	.090
	ADVERSE TOLERANCE	-.100
23)	RANGING SIGNAL POWER (DBM) (10UL+22)	-135.144
	FAVORABLE TOLERANCE	3.253
	ADVERSE TOLERANCE	-2.899
24)	RANGING NOISE BANDWIDTH (DB-HZ)	61.139
	FAVORABLE TOLERANCE	-.348
	ADVERSE TOLERANCE	.322
25)	RANGING NOISE POWER (DB) (10UL+24)	-106.321
	FAVORABLE TOLERANCE	-.956
	ADVERSE TOLERANCE	1.599
26)	SNR AT LIMITER INPUT (DB) (23-25)	-28.823
	FAVORABLE TOLERANCE	4.209
	ADVERSE TOLERANCE	-4.487
27)	RANGING SUPPRESSION (DB)	-30.912
	FAVORABLE TOLERANCE	4.204
	ADVERSE TOLERANCE	-4.481
28)	DOWNLINK RANGING POWER/TOTAL POWER (DB)	-14.850
	FAVORABLE TOLERANCE	.780
	ADVERSE TOLERANCE	-2.280
29)	TOTAL RANGING SUPPRESSION (DB) (27+28)	-45.762
	FAVORABLE TOLERANCE	4.984
	ADVERSE TOLERANCE	-6.761
30)	RANGING SIGNAL LEVEL (DBM) (13DL+29)	-207.868
	FAVORABLE TOLERANCE	7.931
	ADVERSE TOLERANCE	-9.876
31)	RANGING S/NO FOR 10 MINUTE ACQUISITION (DBM)	-9.090
	FAVORABLE TOLERANCE	.000
	ADVERSE TOLERANCE	.000
32)	REQUIRED RANGING SIGNAL POWER (DBM) (10DL+31)	-131.562
	FAVORABLE TOLERANCE	-.330
	ADVERSE TOLERANCE	.307
33)	RANGING PERFORMANCE MARGIN (DB) (30-32)	-16.306
	FAVORABLE TOLERANCE	8.261
	ADVERSE TOLERANCE	-10.182

The computer runs presented are geocentric. For geocentric runs, no range acceleration is available from the trajectory tape, therefore, the program arbitrarily holds range acceleration at one. A ground antenna elevation angle of 25 degrees is used for geocentric runs. For station-centered analysis (not shown), actual range acceleration and antenna elevation angle are used.

9.2.3 Program Use: Analysis (Comparison)

9.2.3.1 Functions. The only function available compares data from a telemetry predicts run with actual spacecraft data. Comparison is made for the uplink carrier, downlink carrier, and telemetry signal-to-noise ratios. The spacecraft configuration must be the same for both the predict and actual data or the comparison will be invalid.

9.2.3.2 Inputs. Input predict data is in the form of a Predicts Save Tape, which must have been previously generated.

Actual data may be from cards or from a mission-dependent data tape previously generated on the telemetry processor.

Both inputs (predict and actual) consist of the uplink carrier level, downlink carrier level, telemetry signal-to-noise ratios, and the time (GMT) of each point.

9.2.3.3 Outputs. The outputs consist of tabulations and plots of the following:

1) Actual and predicted performance of each function
2) The difference between actual and predicted
3) Histograms of the difference between predicted and actual

Sample output plots are shown in Figures 9-10 through 9-12.

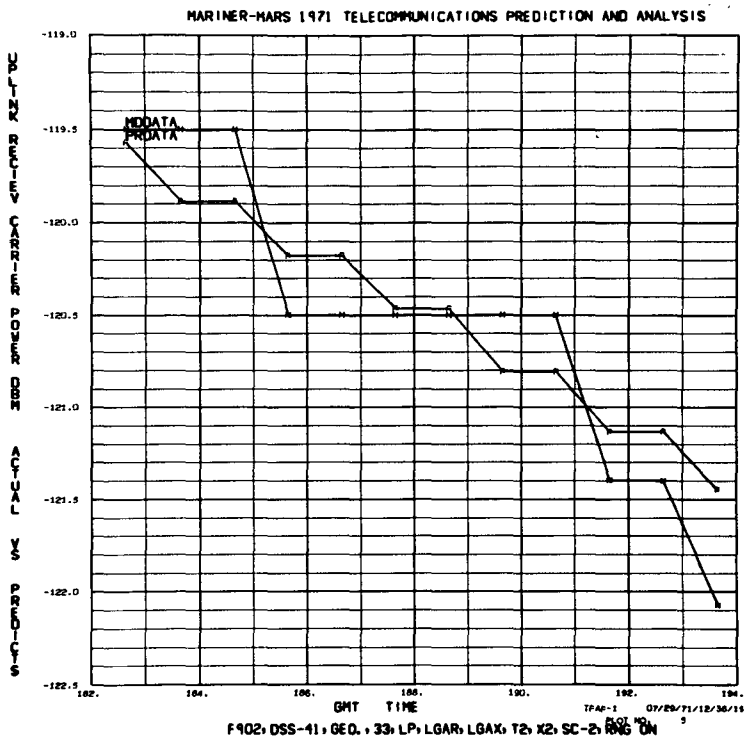

Fig. 9-10. Typical TPAP plot of actual (MDDATA) vs predicted (PRDATA) performance

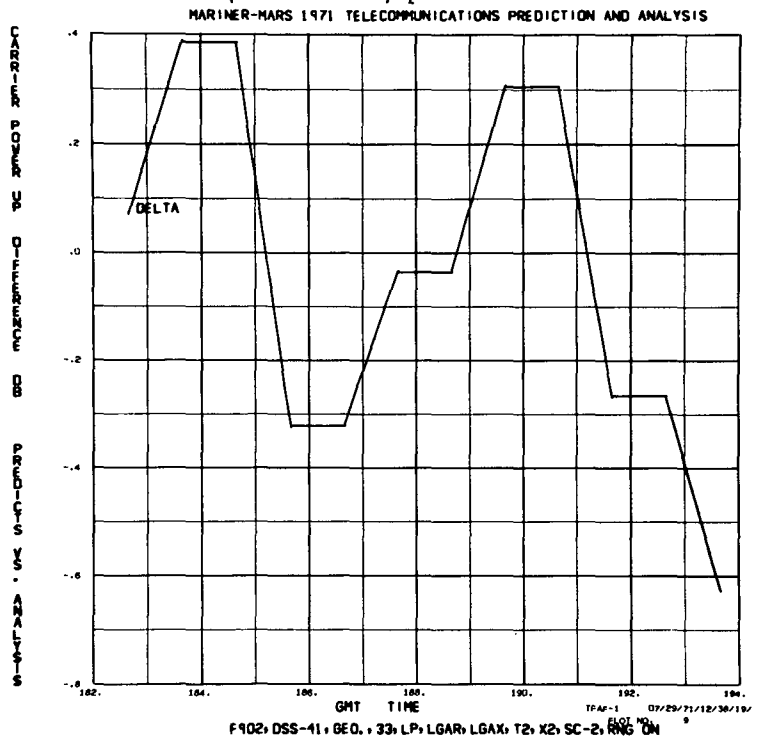

Fig. 9-11. Typical TPAP plot of the difference between actual and predicted performance

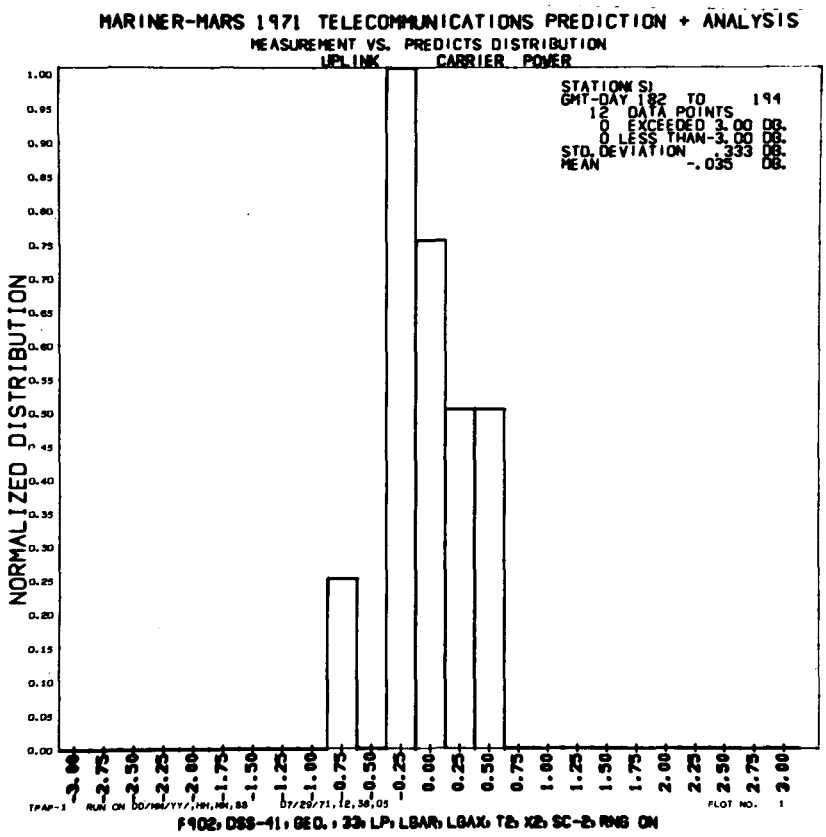

Fig. 9-12. Typical TPAP histogram of difference between actual and predicted performance

SECTION X

CRITICAL SYSTEM INTERFACES

Both the spacecraft and the DSN are composed of a large number of functional subsystems. The correct definition and control of the interfaces between these subsystems is essential to achieve successful missions. This section attempts to define the critical interfaces which inevitably exist between subsystems. These interfaces are all a part of the telecommunication link and as such should be controlled by either the Telecommunication Design Control document, or by the Telecommunication System Functional Requirements.

10.1 SPACECRAFT INTERNAL SUBSYSTEMS AND INTERFACES

Figure 10-1 is a block diagram of a typical spacecraft system showing the subsystem interfaces which affect telecommunications performance. The subsystems shown are presented as examples of how the various hardware functions required for telecommunications may be implemented. Typically, these functions are:

1) Science instrument sensors
2) Spacecraft functional sensors (engineering sensors)
3) A data-handling function (to perform editing and multiplexing)
4) A data-storage function
5) A telemetry modulation function
6) A command demodulation function
7) A Radio Subsystem
8) An Antenna Subsystem
9) Spacecraft structure

In addition to this minimum list of required functions, additional functions may be implemented to increase the capabilities of the telecommunication system. Typical examples are:

10) An on-board computer and central timing source, or sequencer
11) An antenna pointing system

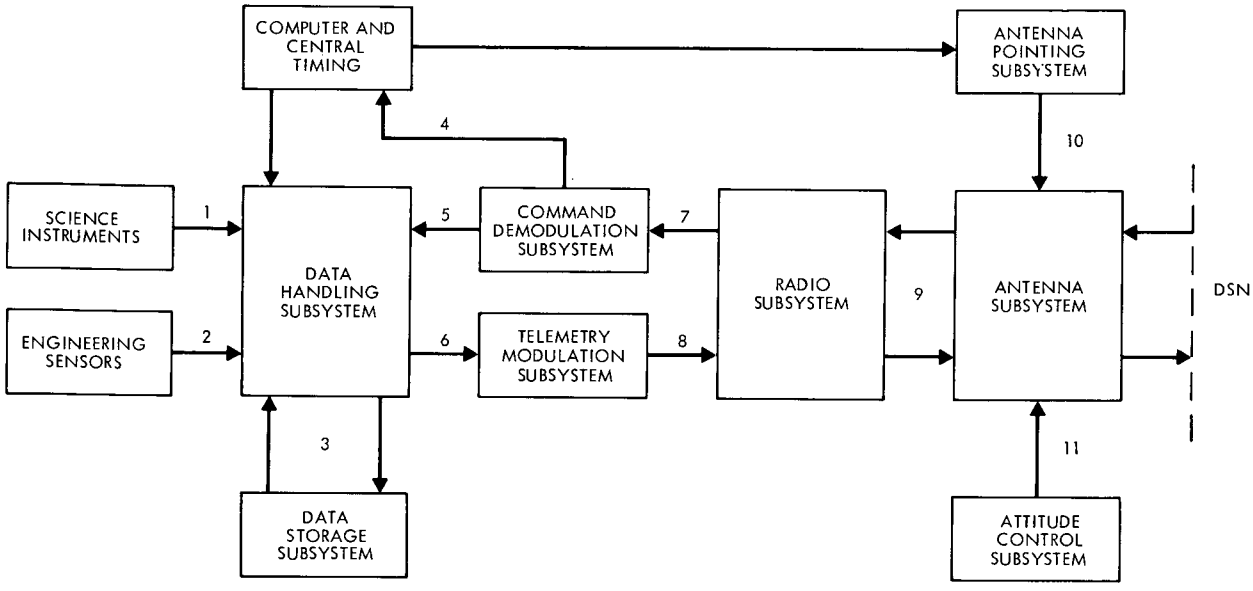

Fig. 10-1. Spacecraft subsystem interfaces

12) Relay radio systems for spacecraft supporting secondary vehicles (e.g., landers, probes, satellites, etc.)

13) A spacecraft attitude control system

The solid numbered lines on Figure 10-1 are the subsystem interfaces. They affect the telecommunication link as follows:

Science Instrument/Data Handling Interface (1)

The science instrument data is sampled and formatted by the Data Handling Subsystem. The data has a data rate associated with it, and there is a data quality measure associated with the data when finally delivered to the user.

Engineering Sensor/Data Handling Interface (2)

The engineering subsystems are monitored by sensors whose outputs are sampled and formatted by the Data Handling Subsystem. The data has a

data rate associated with it, and there is a data quality measure associated with the data when finally delivered to the user.

Data Storage/Data Handling Interface (3)

Data is sometimes stored on-board the spacecraft, usually on a tape recorder for playback at a later time. The tape recorder introduces bit errors into the stored data when played back. Gaps in the data, called dropouts, also occur. The playback data rate is mechanized in the Data Storage Subsystem. Bit errors and dropouts will decrease the quality of data returned to the user.

Command Demodulation Output Interfaces (4) and (5)

The operation of most spacecraft subsystems is affected by ground command. The commands must be decoded with a prescribed quality and provided to appropriate subsystems as discussed in section VI.

Data Handling/Telemetry Modulation Interface (6)

The Data Handling Subsystem supplies formatted data streams to the Telemetry Modulation Subsystem for coding and modulation onto subcarriers. The data rates and their stability are controlled by the Data Handling Subsystem. The subcarriers are generated in the modulation system. The frequencies and stabilities of the subcarriers and the data rates affect telemetry performance. The modulation indices are set in the modulation system, but their selection may be controlled by mode signals sent from the Data Handling Subsystem. The data is encoded in the modulation system, but sync signals for the coders must be provided by the same timing source that generates the data rates. The proper phase relationships among data and sync signals must be specified.

The data must be returned to the users with a prescribed quality as discussed in Section V.

Radio/Command Demodulator Interface (7)

The radio receiver removes the carrier from the uplink signal, and provides the command signal to the Command Demodulator for bit detection and decoding. The bit detection and decoding processes must be performed with a prescribed probability of correct detection and processing.

Radio/Telemetry Modulation Interface (8)

The telemetry modulator modulates data onto the subcarriers, sets the waveform voltage levels to establish modulation indices, and sums these signals in a weighted fashion to obtain a composite telemetry stream. This telemetry stream drives the rf phase modulator in the Radio Subsystem which modulates the telemetry signal onto the rf carrier for transmission to Earth.

The quality of data returned to the user is critically dependent on the telemetry waveforms, voltage levels, rf phase modulator sensitivity, rf phase modulator bandwidth, and the stability and frequency of the rf carrier.

Radio/Antenna Interfaces (9)

The radio receiver receives the rf signal energy from the receiving antennas, and sends rf signal energy to the transmitter and transmitting antennas. The efficiency with which this energy transfer is performed determines the quality of tracking, telemetry, and command.

Antenna Pointing Subsystem/Antenna Interfaces (10)

The Antenna Pointing Subsystem receives commands from the on-board computer, or from the ground, and updates the positions of steerable antennas. The accuracy with which the antenna rf boresight is pointed toward Earth affects the quality of tracking, telemetry and command.

Attitude Control/Antenna Interface (11)

The accuracy with which the attitude of the spacecraft is controlled affects the pointing error of the antennas as discussed in section VII.

10.1.1 Hardware Specifications

Some of the hardware parameters which must be specified in order to control the interfaces just discussed are:

1) Instrument data rate
2) Instrument data quality requirements
3) Engineering data rate
4) Engineering data quality requirements

5) Data formats

6) Synchronization codes

7) Data storage bit error rates and dropouts

8) Channel data rate

9) Channel data rate stability

10) Coding

11) Coding sync signals required

12) Sync signal phase relationships

13) Command data rates

14) Command data formats

15) Command data quality

16) Command synchronizations

17) Subcarrier frequencies

18) Subcarrier frequency stability

19) Telemetry voltage levels and tolerances

20) Telemetry waveform shape and tolerances

21) Rf modulator sensitivity and tolerances

22) Rf modulator bandwidth

23) Auxiliary oscillator frequency

24) Auxiliary oscillator frequency stability

25) Antenna pointing angle resolution

26) Antenna pointing angle accuracy

27) Antenna pointing angle slew rate

28) Antenna mechanical and electrical alignment

29) Rf switching and cabling circuit losses

30) Receiver noise figure

31) Receiver threshold loop bandwidth, $2B_{LO}$

32) Receiver threshold sensitivity ($P_o = 2B_{LO}N_o$)

33) Receiver input and center frequency

34) Receiver input frequency range

35) Receiver phase transfer function H(s)

36) Receiver PLL loop gain

37) Loop filter order and time constants

38) Receiver pull-in range

39) Receiver hold-in range

40) Maximum sweep rate

41) Transmitter output power

42) Antenna patterns

43) Antenna gains

44) Attitude control errors

10.2 SPACECRAFT/DSN INTERFACES

There are three significant interfaces between the spacecraft and the DSN. These interfaces are:

1) The spacecraft tracking functions and the DSN tracking system

2) The spacecraft telemetry functions and the DSN telemetry system

3) The spacecraft command functions and the DSN command system

10.2.1 Tracking Interfaces

The tracking interfaces are characterized by the following:

1) Uplink transmitter frequency and frequency stability

2) Uplink received SNR in $2B_{LO}$

3) Transponder turn-around ratio

4) Downlink transmitter frequency and stability

5) Downlink received SNR in $2B_{LO}$

6) Transponder phase delay

7) Transponder group delays

8) Ground phase delays

9) Ground group delays

10) Spacecraft receiver static phase error

11) Uplink carrier acquisition time

12) Uplink frequency acquisition range

13) Uplink frequency tuning range and maximum sweep rate

14) Spacecraft doppler shifts and doppler rates

15) Downlink carrier acquisition time

16) Ranging acquisition time

17) Ranging resolution

18) Ranging measurement variance

19) Doppler resolver resolution

20) Doppler measurement variance

10.2.2 Command Interfaces

The command interfaces are characterized by the following:

1) Command bit rate

2) Command modulation type

3) Command modulation index

4) Command subcarrier frequency

5) Command transmission delays

6) Command formats

7) Command acquisition times

8) Ground command system reliability

9) Spacecraft command system reliability

10) Command quality measures

10.2.3 Telemetry Interfaces

The telemetry interfaces are characterized by the following:

1) Number of subcarrier channels

2) Modulation type

3) Data rates and modes

4) Data formats

5) Telemetry data quality requirements

6) Subcarrier acquisition times and tracking bandwidths

7) Symbol sync acquisition times and tracking bandwidths

8) Decoder performance

9) DSIF telemetry efficiency (system losses)

10) Ground Communications Facility bit error rates

11) Ground Communications Facility reliability

12) Data rate capacity of the project's data decommutation and presentation scheme.

10.2.4 Hardware Specifications

Some of the hardware parameters which characterize the spacecraft/DSN interfaces are:

1) Spacecraft transmitter output power

2) Spacecraft antenna gain pattern

3) Spacecraft antenna pointing error

4) Spacecraft receiver threshold

5) Spacecraft system noise temperature

6) Spacecraft receiver threshold loop bandwidth

7) Spacecraft modulation indices

8) Spacecraft subcarrier frequencies

9) Spacecraft data rates

10) Spacecraft transponder turn-around ratios

11) Transponder phase and group delays

12) Ground transmitter power

13) Ground antenna gain pattern

14) Ground pointing error

15) Ground receiver threshold

16) Ground receiver threshold loop bandwidth

17) Ground system noise temperature

18) Ground subcarrier frequency (uplink)

19) Command bit rate

20) Command modulation index

21) Ranging modulation indices

22) Ground phase and group delays

23) Ground frequency reference standard stability

10.3 DSN INTERNAL INTERFACES

Interfaces between the three DSN facilities affect the telecommunication performance. These are the DSIF/GCF interface and the GCF/Network Control Center interface.

Tracking and telemetry data are transferred from the DSIF stations to the project through the GCF and the Network Control Center. Command data is transferred from the project to the Network Control Center, through the GCF, and to the DSIF stations.

The interface between the DSIF and the GCF is characterized by:

1) GCF bandwidth for the TTY circuits, high speed data line, wide-band data line, and microwave links which are available for project use

2) Bit error rates introduced by the GCF in data transmission

3) Data formats required by the GCF

Quantitative parameters describing these interface characteristics are provided in the appropriate DSN documents.

The GCF/Network Control Center interface is characterized by:

1) GCF bandwidths

2) Data formats outputted from the GCF

3) Data outages

4) Data quality

10.4 DSN/FLIGHT PROJECT INTERFACES

An interface exists between the DSN (in the Network Control Center) and the Flight Project user. This interface is characterized by

1) Mission-dependent equipment interfaces

2) Mission-dependent software interfaces

3) Data quality input to the project software

4) Data quantity input to the project software

5) Command generation and handling provided for the user

NASA — JPL — Coml., L.A., Calif.